

Fathalla A. Rihan

Delay Differential Equations and Applications to Biology



Springer

Forum for Interdisciplinary Mathematics

Editors-in-Chief

Viswanath Ramakrishna, University of Texas, Richardson, USA

Zhonghai Ding, University of Nevada, Las Vegas, USA

Editorial Board

Ravindra B. Bapat, Indian Statistical Institute, New Delhi, India

Balasubramaniam Jayaram, Indian Institute of Technology Hyderabad, Hyderabad, India

Ashis Sengupta, Indian Statistical Institute, Kolkata, India

Bhu Dev Sharma, Jaypee Institute of Information Technology, Noida, India

P.V. Subrahmanyam, Indian Institute of Technology Madras, Chennai, India

The *Forum for Interdisciplinary Mathematics* is a Scopus-indexed book series. It publishes high-quality textbooks, monographs, contributed volumes and lecture notes in mathematics and interdisciplinary areas where mathematics plays a fundamental role, such as statistics, operations research, computer science, financial mathematics, industrial mathematics, and bio-mathematics. It reflects the increasing demand of researchers working at the interface between mathematics and other scientific disciplines.

More information about this series at <http://www.springer.com/series/13386>

Fathalla A. Rihan

Delay Differential Equations and Applications to Biology



Springer

Fathalla A. Rihan
Department of Mathematical Sciences
United Arab Emirates University
Al-Ain, Abu Dhabi, United Arab Emirates

ISSN 2364-6748

ISSN 2364-6756 (electronic)

Forum for Interdisciplinary Mathematics

ISBN 978-981-16-0625-0

ISBN 978-981-16-0626-7 (eBook)

<https://doi.org/10.1007/978-981-16-0626-7>

© The Editor(s) (if applicable) and The Author(s), under exclusive license to Springer Nature Singapore Pte Ltd. 2021

This work is subject to copyright. All rights are solely and exclusively licensed by the Publisher, whether the whole or part of the material is concerned, specifically the rights of translation, reprinting, reuse of illustrations, recitation, broadcasting, reproduction on microfilms or in any other physical way, and transmission or information storage and retrieval, electronic adaptation, computer software, or by similar or dissimilar methodology now known or hereafter developed.

The use of general descriptive names, registered names, trademarks, service marks, etc. in this publication does not imply, even in the absence of a specific statement, that such names are exempt from the relevant protective laws and regulations and therefore free for general use.

The publisher, the authors and the editors are safe to assume that the advice and information in this book are believed to be true and accurate at the date of publication. Neither the publisher nor the authors or the editors give a warranty, expressed or implied, with respect to the material contained herein or for any errors or omissions that may have been made. The publisher remains neutral with regard to jurisdictional claims in published maps and institutional affiliations.

This Springer imprint is published by the registered company Springer Nature Singapore Pte Ltd.
The registered company address is: 152 Beach Road, #21-01/04 Gateway East, Singapore 189721,
Singapore

Delay differential equations (DDEs) are differential equations having retarded arguments. They arise in many realistic models of problems in science, engineering, and medicine, where there is a time lag or after-effect. Numerical techniques for such problems may be regarded as extensions of dense-output methods for ordinary differential equations (ODEs), but scalar DDEs are inherently infinite dimensional with a richer structure than their ODE counterparts.

Christopher T. H. Baker

Retarded differential equations, Journal of Computational and Applied Mathematics 125 (2000) 309–335.

Preface

Delay differential equations (DDEs) or functional differential equations arise in models representing biological phenomena when the time-delays occurring in these phenomena are considered. Mathematical modeling using such DDEs is widely applied for performing analysis and predictions in various areas of life sciences, such as population dynamics, epidemiology, immunology, physiology, and neural networks. The memory or time-delays in these models are related to the duration of certain hidden processes, such as the stages of a life cycle, the time between the start of a cell infection and the production of new viruses, the infection period, and the immune period. In ordinary differential equations (ODEs), the unknown state and its derivatives are evaluated at the same time instant. In DDEs, however, the evolution of the system at a certain time instant depends on the past history/memory. Introduction of such time-delays in a differential model significantly improves the dynamics of the model and increases the complexity of the system. Therefore, studying qualitative and quantitative behaviors of such class of differential equations is essential.

Here, parts of the theory of differential equations and functional differential equations are discussed that can or have been applied to modeling biological systems. Models with fractional-order derivatives and models with environmental noise (stochastic models) are also investigated. This book is different from other books on this topic; this is because both qualitative and quantitative features of DDEs and their applications in biosciences are studied herein. This book covers various important topics related to DDEs, including numerical methods, stability, inverse problems, parameter estimations, sensitivity analysis, optimal control, and biological systems with memory (time-delays). This book is useful to a wide range of mathematicians and specialists in the fields of mathematical biology, mathematical modeling, life sciences, immunology, and infectious diseases. Thus, it can be recommended as a textbook for graduate and postgraduate students, bridging the gap between mathematics and various areas of bioscience research.

In this monograph, we discuss a wide range of DDEs with integer- and fractional-order derivatives and show how they have a richer mathematical framework for the analysis of dynamical systems (compared with differential equations without memory). This monograph consists of two parts, organized into 13 chapters. Part I (Chaps. 1–7) is devoted to the study of the qualitative and quantitative features of DDEs, whereas Part II (Chaps. 8–13) discusses certain applications of DDEs in biosciences. Chapter I provides a brief introduction and discusses the qualitative features of DDEs. In Chapter II, we study numerical solutions and methods for DDEs. In Chapter III, we investigate stability concepts of the numerical schemes of DDEs. Chapter IV provides unconditionally stable numerical schemes for integro-DDEs, which are suitable for stiff and non-stiff problems. In Chapter V, we explore the inverse problem with DDEs as well as parameter estimation and parameter identifiability of DDEs. In Chapter VI, we estimate sensitivity functions and analysis of DDEs to evaluate how the state variable can vary with respect to small variations in the initial data and parameters (or constant lags) appearing in the model. Chapter VII discusses certain features of stochastic delay differential equations (SDDEs), and we also study some efficient numerical schemes for SDDEs. Chapter VIII shows how DDEs have, prospectively, more interesting dynamics for epidemics and infectious diseases. In Chapter IX, we study DDEs with tumor-immune interaction in presence of external treatment and optimal control. In Chapter X, we investigate DDEs for ecological and predator-prey systems. In Chapter XI, we explore fractional-order DDEs for predator-prey systems. In Chapter XII, we study the dynamics of Hepatitis C viral infection through fractional-order DDEs. In Chapter XIII, we study stochastic delay differential equations for the spread of COVID-19. In the last chapter, we discuss some current challenges related to numerical solutions and mathematical modeling with DDEs.

January 2021

Fathalla A. Rihan
Helwan University
Cairo, Egypt

United Arab Emirates University, Al-Ain, Abu
Dhabi, United Arab Emirates

Acknowledgments

I would like to express my deepest gratitude to the following colleagues, co-authors, Ph.D. students, postdoctoral research fellows, and friends from various institutes for their productive past research works, which created the basis for this monograph: Prof. Gennady A. Bocharov (Moscow), Prof. Eid H. Doha (Egypt), Prof. Abdalla Azamov (Uzbekistan), Dr. Rakkiyappan Rajan (India), Dr. Lakshmanan Shanmugam (India), Prof. Elsayed Ahmed (Egypt), Prof. Yang Kuang (USA), Prof. Adel Hashish (UAE), Prof. Hongjiong Tian (Chaina), Prof. Radouane Yafia (Morocco), Prof. MA Aziz-Alaoui (France) Prof. Eugene Parmuzin (Moscow), Prof. Stefan Turek (Germany), Prof. Fatma Al-Maskari (UAE), Dr. Rajivganthi Chinnathambi (India), Dr. Hebatallah J. Alsakaji (UAE), Dr. Duaa H. Abdolrahman (UAE), Prof. Nasser Sweilam (Egypt), Prof. Ephraim Agyingi (USA), Prof. Cemil Tunc (Turkey), Dr. Nasser Al-Salti (Oman), Prof. M. Naim Anwar (Egypt), Dr. N.M. Kamel (Egypt), Dr. Fatma Ibrahim (Germany), Dr. Velmurugan Ganthi (India), Prof. Mohamed Sheek Hussein (UAE), Prof. Dumitru Baleanu (Turkey), Prof. P. Balasubramaniam (India), Dr. M. Prakash (India), Prof. Neville Ford (UK), Prof. Helmut Maurer (Germany), Dr. R. Raja (India), Dr. V. P. Latha (India), Dr. Abdessamad Tridane (UAE), Dr. Bassel F. Rihan (Egypt), Dr. Nouran F. Rihan (Egypt), Dr. M. Syed Ali (India), and Dr. Ayman Arafa (Egypt).

This work is dedicated to the memory of Prof. Christopher T. H. Baker (1939–2017). He was one of the pioneers in the field of numerical solution of integral equations and functional differential equations.

My special thanks goes to all my colleagues and friends at the Department of Mathematical Sciences, United Arab Emirates University (UAE), and at the Department of Mathematics, Helwan University (Egypt).

Finally, I thank my wife (Prof. Mayada A. Youssef) and my children (Bassel, Nouran, and Ahmed) for their support, patience, and love.

Contents

Part I Qualitative and Quantitative Features of Delay Differential Equations

| | | |
|----------|---|-----------|
| 1 | Qualitative Features of Delay Differential Equations | 3 |
| 1.1 | Introduction | 3 |
| 1.2 | Delay Models in Population Dynamics | 5 |
| 1.2.1 | Logistic Equation with Discrete Delay | 5 |
| 1.2.2 | Logistic Equation with Distributed Delay | 7 |
| 1.2.3 | Delayed Lotka-Volterra System | 7 |
| 1.3 | Stability of DDEs | 8 |
| 1.3.1 | Stability of Linear Constant Coefficient DDEs | 9 |
| 1.3.2 | Asymptotical Stability Region for Linear DDEs | 10 |
| 1.3.3 | Stability of Linear NDDEs | 10 |
| 1.3.4 | Asymptotic Stability Region for Linear NDDEs | 11 |
| 1.4 | Stability of Non-linear DDEs and Contractivity Conditions | 12 |
| 1.5 | Stability of DDEs in Lyapunov Method | 17 |
| 1.5.1 | Lyapunov-Krasovskii Sense | 18 |
| 1.5.2 | Lyapunov-Razumikhin Sense | 18 |
| 1.5.3 | Stability of Linear Systems with Discrete Delays | 19 |
| 1.6 | Concluding Remarks | 20 |
| | References | 21 |
| 2 | Numerical Solutions of Delay Differential Equations | 23 |
| 2.1 | Propagation and Location of Discontinuities in DDEs | 25 |
| 2.2 | Method of Steps for DDEs | 26 |
| 2.3 | Existence and Uniqueness Solution of DDEs | 28 |
| 2.4 | Numerical Approach for DDEs | 28 |
| 2.4.1 | General Approach | 28 |
| 2.4.2 | Θ -Methods for DDEs | 30 |
| 2.4.3 | Continuous One-Step Runge-Kutta Methods for ODE | 31 |
| 2.4.4 | Runge-Kutta Method for DDEs | 34 |

| | | |
|----------|--|-----------|
| 2.5 | More General Classes of DDEs | 36 |
| 2.5.1 | Neutral Delay Differential Equations (NDDEs) | 37 |
| 2.5.2 | Equations with State-Dependent Lags | 37 |
| 2.5.3 | Equation with a Small or Vanishing Lag | 39 |
| 2.6 | Stiffness Problems | 40 |
| 2.7 | Software Aspects | 43 |
| 2.7.1 | Discretization Error | 43 |
| 2.7.2 | Location of Jump Discontinuities | 45 |
| 2.7.3 | Stepsize Control | 45 |
| 2.7.4 | Interpolation to $\tilde{y}(t)$ | 46 |
| 2.7.5 | DDE Solvers and Available Software | 47 |
| 2.8 | Concluding Remarks | 47 |
| | References | 48 |
| 3 | Stability Concepts of Numerical Solutions of Delay Differential Equations | 51 |
| 3.1 | Introduction | 51 |
| 3.2 | Stability of Numerical Methods for DDEs | 51 |
| 3.2.1 | Stability Regions for DDEs: P-stability and GP-stability | 53 |
| 3.2.2 | Stability Regions for Linear NDDEs | 57 |
| 3.3 | Contractivity Concepts and GPN-Stability | 61 |
| 3.3.1 | Contractivity Concepts and GRN-Stability | 64 |
| 3.4 | Concluding Remarks | 66 |
| | References | 67 |
| 4 | Numerical Solutions of Volterra Delay Integro-Differential Equations | 69 |
| 4.1 | Introduction | 69 |
| 4.2 | Analytical Stability | 70 |
| 4.3 | Continuous Mono-Implicit RK Scheme for DDEs | 73 |
| 4.4 | Numerical Treatment of VDIDEs | 75 |
| 4.4.1 | CMIRK Scheme for VDIDEs | 76 |
| 4.4.2 | Numerical Integration Formula and Boole's Quadrature Rule | 77 |
| 4.4.3 | MIDDE Software Aspects | 78 |
| 4.5 | Numerical Stability | 79 |
| 4.6 | Numerical Results and Simulations | 81 |
| 4.7 | Concluding Remarks | 85 |
| | References | 85 |
| 5 | Parameter Estimation with Delay Differential Equations | 87 |
| 5.1 | Introduction | 87 |
| 5.2 | Parameter Estimation with DDEs | 87 |
| 5.2.1 | Non-linearity of Model Predictions | 88 |

| | |
|---|------------|
| Contents | xiii |
| 5.3 Computation of Estimates | 89 |
| 5.3.1 Basic Iteration | 90 |
| 5.3.2 Acceptability | 91 |
| 5.3.3 Convergence | 91 |
| 5.4 Discontinuities Associated with Delay | 92 |
| 5.5 Solving the Minimization Problem | 94 |
| 5.6 Models and Goodness of Fit for Cell Growth | 95 |
| 5.6.1 Problem 1: Fitting DDEs with Growth of Fission Yeast | 96 |
| 5.6.2 Fitting DDEs with Growth of Tetrahymena Pyriformis | 98 |
| 5.7 Concluding Remarks | 101 |
| References | 101 |
| 6 Sensitivity Analysis of Delay Differential Equations | 103 |
| 6.1 Introduction | 103 |
| 6.2 Sensitivity Functions | 104 |
| 6.2.1 Adjoint Equations | 105 |
| 6.3 Variational Approach | 106 |
| 6.4 Direct Approach | 109 |
| 6.5 Sensitivity of Optimum Parameter \hat{p} to Data | 112 |
| 6.5.1 Standard Deviation of Parameter Estimates | 113 |
| 6.5.2 Non-linearity and Indications of Bias | 114 |
| 6.6 Numerical Results | 114 |
| 6.7 Concluding Remarks | 120 |
| References | 122 |
| 7 Stochastic Delay Differential Equations | 123 |
| 7.1 Introduction | 123 |
| 7.1.1 Preliminaries | 124 |
| 7.2 Existence and Uniqueness of Solutions for SDDEs | 127 |
| 7.3 Stability Criteria for SDDEs | 130 |
| 7.4 Numerical Scheme for Autonomous SDDEs | 133 |
| 7.4.1 Convergence and Consistency | 134 |
| 7.5 Numerical Schemes for Non-autonomous SDDE | 135 |
| 7.5.1 Taylor Approximation | 136 |
| 7.5.2 Implicit Strong Approximations | 136 |
| 7.6 Milstein Scheme for SDDEs | 137 |
| 7.6.1 Convergence and Mean-Square Stability of the Milstein Scheme | 138 |
| 7.7 Concluding Remarks | 140 |
| References | 140 |

Part II Applications of Delay Differential Equations in Biosciences

| | |
|---|-----|
| 8 Delay Differential Equations with Infectious Diseases | 145 |
| 8.1 Introduction | 145 |
| 8.2 Time-Delay in Epidemic Models | 146 |
| 8.2.1 Development of SIR Model (8.1) | 147 |
| 8.3 Delay Differential Models with Viral Infection | 148 |
| 8.3.1 DDEs with HIV Infection of CD4+ T-cells | 150 |
| 8.3.2 Steady States | 154 |
| 8.3.3 Stability Analysis of Infected Steady State | 156 |
| 8.3.4 Existence of Hopf Bifurcation | 157 |
| 8.4 Physiology | 160 |
| 8.5 Concluding Remarks | 163 |
| References | 164 |
| 9 Delay Differential Equations of Tumor-Immune System with Treatment and Control | 167 |
| 9.1 Introduction | 167 |
| 9.2 Description of the Model | 168 |
| 9.2.1 Non-negativity and Boundedness Solutions of Model (9.3) | 170 |
| 9.2.2 Model with Chemotherapy | 172 |
| 9.3 Drug-Free Steady States and Their Stability | 173 |
| 9.3.1 Stability of Tumor-Free Steady State | 174 |
| 9.3.2 Stability of Lethal Steady States | 175 |
| 9.3.3 Stability of Coexisting Steady States | 175 |
| 9.4 Optimal Control Problem Governed by DDEs | 177 |
| 9.5 Existence of Optimal Solution | 179 |
| 9.6 Optimality Conditions | 181 |
| 9.7 Immuno-Chemotherapy | 183 |
| 9.8 Numerical Simulations of Optimal Control System | 184 |
| 9.9 Concluding Remarks | 188 |
| References | 188 |
| 10 Delay Differential Equations of Ecological Systems with Allee Effect | 191 |
| 10.1 Introduction | 191 |
| 10.2 Delay Differential Model of Two-Prey One-Predator System | 194 |
| 10.2.1 Positivity and Boundedness of the Solution | 196 |
| 10.3 Local Stability and Hopf Bifurcation | 197 |
| 10.3.1 Existence of Interior Equilibrium Points | 198 |
| 10.3.2 Stability and Bifurcation Analysis of the Interior Equilibrium | 199 |
| 10.4 Global Stability of Interior Steady State \mathcal{E}^* | 203 |

| | | |
|-----------|---|------------|
| 10.5 | Sensitivity to Allee Effect | 205 |
| 10.6 | Numerical Simulations | 206 |
| 10.7 | Concluding Remarks | 209 |
| | References | 209 |
| 11 | Fractional-Order Delay Differential Equations with Predator-Prey Systems | 211 |
| 11.1 | Introduction | 211 |
| 11.1.1 | Preliminaries | 212 |
| 11.2 | Fractional Delayed Predator-Prey Model | 215 |
| 11.3 | Local Stability Analysis and Hopf Bifurcation | 216 |
| 11.3.1 | Trivial and Semi-trivial Equilibria and Their Stabilities | 217 |
| 11.3.2 | Interior Equilibrium and Its Stability | 218 |
| 11.4 | Global Stability Analysis | 220 |
| 11.5 | Implicit Euler's Scheme for FODDEs | 222 |
| 11.5.1 | Stability and Convergence of Implicit Scheme for FODDEs | 225 |
| 11.5.2 | Numerical Simulations | 227 |
| 11.6 | Concluding Remarks | 228 |
| | References | 230 |
| 12 | Fractional-Order Delay Differential Equations of Hepatitis C Virus | 233 |
| 12.1 | Introduction | 233 |
| 12.2 | Mathematical Model of HCV | 235 |
| 12.3 | Local Stability of Infection-Free and Infected Steady States | 237 |
| 12.4 | Global Stability of Infection-Free Steady State \mathcal{E}_0 | 242 |
| 12.5 | Numerical Simulations and Validity of Model | 243 |
| 12.5.1 | Parameter Estimation and Validity of Model | 245 |
| 12.6 | Concluding Remarks | 250 |
| | References | 251 |
| 13 | Stochastic Delay Differential Model for Coronavirus Infection COVID-19 | 253 |
| 13.1 | Introduction | 253 |
| 13.2 | Stochastic SIRC Epidemic Model | 255 |
| 13.3 | Existence and Uniqueness of Positive Solution | 257 |
| 13.4 | Existence of Ergodic Stationary Distribution | 259 |
| 13.5 | Extinction | 266 |
| 13.6 | Numerical Simulations and Discussions | 268 |
| 13.7 | Concluding Remarks | 273 |
| | References | 274 |
| 14 | Remarks and Current Challenges | 277 |
| | Appendix A: Fifth-Order Dormand and Prince RK Method | 281 |

| | |
|---|------------|
| Appendix B: Adams-Bashforth-Moulton Method for Fractional-Order Delay Differential Equations | 283 |
| Appendix C: Matlab Program for Stochastic Delay Differential Equations Using Milstein Scheme | 285 |

About the Author



Fathalla A. Rihan is currently a professor of mathematics at the United Arab Emirates University (UAE) and Helwan University (Egypt). He was awarded his BSc in mathematics from the Faculty of Science, Alexandria University, in 1986. He received his PhD in 2000 from the School of Mathematics, The University of Manchester (UK), in “Numerical Treatment of Delay Differential Equations in Biosciences” and received his Doctor of Science Degree (DSc) in 2018, from National University of Uzbekistan, in the field of “Features of Delay Differential Equations and Their Application.” His research interests include numerical analysis; mathematical biology;mathematical modeling of real-life phenomena with memory, such as cell division, population dynamics, and infectious diseases; parameter estimation; sensitivity analysis; and qualitative and quantitative analysis of delay differential equations. Professor Rihan has published a considerable number of research articles in highly impacted journals and has participated in more than 100 international conferences. Over the course of his career, Prof. Rihan has worked in different institutes, including Manchester University (UK) and Salford University (UK). In addition, he is on the editorial board of many international journals and a reviewer for American Mathematical Society. He has supervised many PhD students and is a principal investigator of many research projects in the field of mathematical biology. Prof. Rihan was among the top 2% of researchers classified by Stanford University for 2019–2020. He has more than 30 years of experience in teaching mathematics to undergraduate and graduate students.

Part I

Qualitative and Quantitative Features of Delay Differential Equations

Delay differential equations (DDEs) are also referred to as time-delay systems, systems with after-effect, memory, time-delay, hereditary systems, equations with deviating argument, or differential-difference equations. They belong to the class of functional differential equations that are infinite-dimensional, as opposed to ordinary differential equations (ODEs).

Recently, this class of differential equations has received considerable attention from researchers because the introduction of memory terms in a differential model significantly increases its complexity. Therefore, studying qualitative and quantitative behavior, numerical treatment of such models, parameter estimation, and sensitivity and stability analyses of delay integro-differential equations as well as stochastic delay differential equations (SDDEs) are essential. In this part (Chaps. 1–7), we will study the qualitative and quantitative features of DDEs, which have not been adequately investigated in the literature until now.

Chapter 1

Qualitative Features of Delay Differential Equations



1.1 Introduction

Ordinary and partial differential equations have long played an important role in *bioscience*, and they are considered to continue to serve as indispensable tools in future investigations as well. However, they frequently provide only a first approximation of the systems under consideration. More realistic models need to include some of the past states of these systems as well; that is, a real system needs to be modeled using differential equations with time-delays (or time-lags). Delay models formulated in mathematical biology include several types of functional differential equations, such as delay differential equations (DDEs), neutral delay differential equations (NDDEs), integro-differential equations, and retarded partial differential equations (RPDEs). Recently, stochastic delay differential equations (SDDEs) have attracted significant attention from researchers.

To create more realistic mathematical models for problems with time-lag or after-effect, we need to consider using retarded functional differential equations (RFDEs) in place of ordinary differential equations (ODEs), such as

$$y'(t) = f \left(t, y(t), y(\alpha(t, y(t))), \int_{-\infty}^t \mathcal{K}(t, s, y(t), y(s)) ds \right), \quad t \geq t_0, \quad (1.1)$$

where $\alpha(t, y(t)) \leq t$ and $y(t) = \psi(t)$, $t \leq t_0$. Such retarded equations form a class of equations that is, in some sense, between ODEs and time-dependent partial differential equations (PDEs), and they generate infinite-dimensional dynamical systems. RFDEs (1.1), where the integral term is absent, are usually called delay differential equations (DDEs) and they assume forms such as

$$y'(t) = f(t, y(t), y(\alpha(t, y(t)))), \quad \alpha(t, y(t)) \leq t. \quad (1.2)$$

Neutral delay differential equations (NDDEs) are defined by equations of the form

$$y'(t) = f(t, y(t), y(\alpha(t, y(t))), y'(\beta(t, y(t)))) , \quad (1.3)$$

where $\alpha(t, y(t)), \beta(t, y(t)) \leq t$. The introduction of the “lagging” or “retarded” arguments $\alpha(t, y(t)), \beta(t, y(t))$ is to reflect an “after-effect”; e.g., the gestation period in population modeling.

Mathematical modeling of several real-life phenomena in bioscience requires “differential equations” that depend partially on the past history rather than only the current state. Such examples occur in population dynamics (taking into account the gestation and the maturation time), infectious diseases (accounting for the incubation periods), physiological and pharmaceutical kinetics (modeling, for example, hematopoiesis and respiration, where the delays are, respectively, due to cell maturation and blood transport between the lung and brain, etc.), chemical and enzyme kinetics (such as mixing reactants), biological immune response (in which the antibody production by the B-cell population depends on the antigenic stimulation at an earlier time), navigational control of ships and aircraft (with large and short lags, respectively), and more general control problems. An early use of DDEs was to describe technical devices such as control circuits. In that context, the delay is a measurable physical quantity; e.g., the time that the signal travels to the controlled object, the reaction time, and the time that the signal takes to return. Similarly, there are parallels in the reaction of the body to pain, for example. Refer to [1–11] for further examples of DDEs in biomathematics.

In many applications in the field of life sciences, a time-delay is introduced when there are certain hidden variables and processes that are not well understood but are known to cause a time-lag [12]. Thus, a delay may, in fact, represent a reaction chain or a transport process. We shall see later that the mathematical properties of DDEs justify such approximations. A well-known example is Cheyne-Stokes respiration (or periodic breathing), discovered in the nineteenth century, wherein some people show periodic oscillations of breathing frequency under constant conditions [13, 14]. This strange phenomenon is due to a delay caused by cardiac insufficiency in the physiological circuit controlling carbon dioxide levels in the blood.

Time-delays occur naturally in biological systems, e.g., in a chemostat (a laboratory device for controlling the supply of nutrients to a growing cell population [15]). The use of ODEs to model a chemostat carries the implication that changes occur instantaneously. This is a potential deficiency of the ODE model. There are two sources of delays in the chemostat model: (i) delays due to the possibility that the organism stores the nutrients (so that the “free” nutrient concentration does not reflect the nutrients available for growth) and (ii) delays due to the cell cycle; see [16–18].

When delays are introduced in first-order non-linear differential equations, or in discrete difference equations, erratic solutions can appear (such a chaotic behavior is also observed in nature); see [19, 20] and Fig. 1.1.

Among the classical references for DDEs are the books by Bellman and Cooke [21] and Elsgol’ts and Norkin [22]. These are rich sources for analytical techniques

and understanding the many interesting examples. Kolmanovskii et al. [23, 24] gave a rigorous treatment for a wide range of problems. The monographs of Hale [25] and Hale and Verduyn Lunel [26] are standard sources for understanding the theory of delay equations. Another important monograph is by Diekmann et al. [27]. Kuang [28] and Banks [29] pay particular attention to problems in population dynamics, wherein the former looked at neutral equations. Gopalsamy [30] and Györi and Ladas [31] addressed the question of oscillations in DDEs. Early books by Cushing [32], Driver [33], Halanay [34], MacDonald [18, 35], May [20], and Waltman [36] have been very stimulating for the development of the field.

Our concern in this chapter is with the qualitative features of DDEs. We show that DDEs have a richer mathematical framework for the analysis of biosystem dynamics compared with ODEs. First, we start from simple real-life problems and formulate them in terms of DDEs; see Sect. 1.2. We then briefly study the stability of delay models described by linear and non-linear DDEs, and the conditions that ensure stable behavior; see Sects. 1.3, 1.4 and 1.5.

1.2 Delay Models in Population Dynamics

In this section, we briefly discuss some simple mathematical models with time-delays of population dynamics. Naturally, the growth of a population subject to maturation delay is modeled by using either a discrete delay or a delay continuously distributed over the population. The use of a discrete delay might be seen as a rough approximation in modeling the delay distribution over a large population size. However, it is much more realistic to assume the delay being continuously distributed by a continuous distribution function, with a mean delay equal to the discrete delay.

1.2.1 Logistic Equation with Discrete Delay

Let $y(t)$ be the population of a certain species that is independent of other species. The simple model of exponential growth is

$$y'(t) = \lambda y(t) \quad (\lambda > 0). \quad (1.4)$$

From the hypothesis that the growth rate will decrease with increasing population $y(t)$ due to lack of resources (food and space), one arrives instead at the deterministic model of Verhulst (1845)

$$y'(t) = ry(t) \left(1 - \frac{y(t)}{K}\right), \quad (1.5)$$

where λ in (1.4) is replaced by $r \left(1 - \frac{y(t)}{K}\right)$, with K representing the level of food availability. The derivative of y is determined by the current value of $y(t)$. All solutions of this equation, with initial value $y(0) > 0$, tend asymptotically to K as $t \rightarrow \infty$.

If we now assume that the growth rate depends on the population of the preceding generation and take into account the hatching and maturation periods, then the above equation is replaced by a delay equation. Hutchinson (1948) [37] was one of the first to introduce a delay in a biological model. He modified the classical logistic equation (1.5) into the form

$$y'(t) = ry(t) \left(1 - \frac{y(t-\tau)}{K}\right). \quad (1.6)$$

Here, the derivative depends on $y(t)$ and the earlier state $y(t-\tau)$, where the lag $\tau > 0$ represents the maturation time of individuals in the population. The non-negative parameters r and K are known as the intrinsic growth rate and the environmental carrying capacity, respectively.

Now, we illustrate how the presence of a delay in a differential equation can lead to a notable increase in the complexity of the observed behavior (stable steady states may be destabilized and consequently large amplitude oscillations can occur [38].) Consider a delayed logistic equation (1.6), which can be changed (by putting $Ky(t) = y(t\tau)$, $\alpha^* = b\tau$) into the form

$$\frac{dy(t)}{dt} = \alpha^* y(t)[1 - y(t-1)]. \quad (1.7)$$

It is observed that the qualitative picture (Fig. 1.1) of the solution set of Eq. (1.7) is significantly dependent upon the delay parameter τ and upon the initial function. For “large” values of τ , the equation possesses undamped oscillatory solutions; whereas for small values of τ , the equation behaves like an ODE. For $0 < \alpha^* < \pi/2$, $x = 1$ is a stable steady state; but for $\alpha^* > \pi/2$, chaotic behavior and periodic solution can

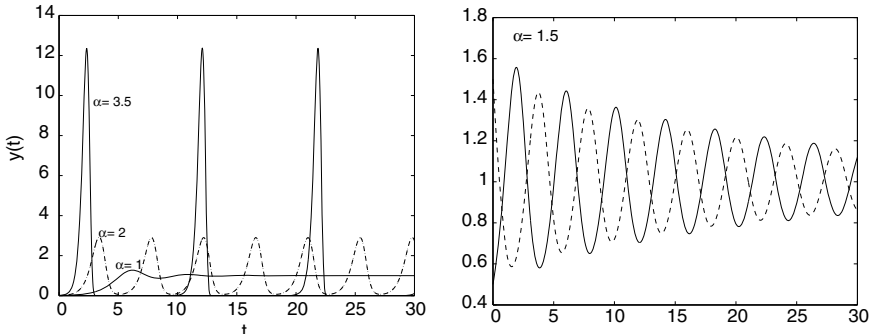


Fig. 1.1 Solutions of DDE $y'(t) = \alpha^* y(t)[1 - y(t-1)]$: **a** for differing α^* , **b** for differing initial functions $\psi(t)$ for $t \leq 0$

arise [39]. For a small $\alpha^* - \pi/2$, Morris [40] proved that the period is approximately $p \sim 4 + 16(\alpha^* - \pi/2)[\pi(3\pi - 2)]$. We note from Fig. 1.1a that the stable periodic solution of (1.7) rapidly acquires a spiky form as α^* increases; see Fowler [38]. The numerical solution at $\alpha^* = 3.5$ consists of a series of well-separated pulses. This simple example illustrates many of the complexities that arise with delays and has the advantage that results may be easily and explicitly worked out.

1.2.2 Logistic Equation with Distributed Delay

Although Hutchinson's approach leading to Eq. (1.6) is quite useful to explain the appearance of sustained oscillations in a single-species population without any predatory interaction of other species, the underlying argument is somewhat questionable. We may ask: How can it be that the present change in population size depends exactly on the population size of time τ units earlier? The question has led people to consider *integro-differential equations* [41]

$$y'(t) = ry(t) \left(1 - \frac{1}{K} \int_{t-\tau}^t y(s)G(t-s)ds \right), \quad t \geq t_0. \quad (1.8)$$

Here, the derivative depends on $y(t)$ and all the previous states after the initial moment t_0 . The delay is continuously distributed and the problem is said to have a fixed time-lag (or finite-memory) and a bounded retardation because the difference between t and $t - \tau$ is fixed and bounded.

MacDonald [35] used the integro-differential equation

$$y'(t) = ry(t) \left\{ 1 - \frac{y(t)}{K} - \int_0^t y(s)G(t-s)ds \right\}, \quad (1.9)$$

for parasite population growth that completes its life cycle within the same host and does not kill the host. (Immunological resistance by the host depends on exposure to the parasite population.) The delay here is continuously distributed and the problem is said to have an unbounded time-lag because the difference between 0 and t is unbounded. The initial time ($t = 0$) represents the start of the experiment or the time at which the naive host ingests the parasite. Here, it is possible to adopt the simple memory function $G(t) = \text{constant}$.

1.2.3 Delayed Lotka-Volterra System

Many mathematical studies using delay models to study ecology are built upon various generalizations of Volterra's integro-differential system with infinite delays, which are motivated by the characteristic nature of predator-prey dynamics, such as

$$\begin{aligned} x'(t) &= b_1 x(t) \left(1 - c_{11} x(t) - c_{12} \int_{-\infty}^t y(s) k_1(t-s) ds \right), \\ y'(t) &= b_2 y(t) \left(-1 + c_{21} \int_{-\infty}^t x(s) k_2(t-s) ds \right), \end{aligned} \quad (1.10)$$

where the variables $x(t)$, $y(t)$ represent the populations of the prey and the predator, and the parameters specifying the birth and interaction rates are non-negative¹ (see [32]).

In studying a similar interaction for predator-prey models, Wanggersky and Cunningham (1975) have used equations such as

$$\begin{aligned} x'(t) &= ax(t) \left(\frac{m-x(t)}{m} \right) - bx(t)y(t), \\ y'(t) &= -cy(t) + dx(t-\tau)y(t-\tau). \end{aligned} \quad (1.11)$$

More general delayed predator-prey models take the form

$$\begin{aligned} x'(t) &= x(t)F(t, x_t, y_t), \\ y'(t) &= y(t)G(t, x_t, y_t), \end{aligned} \quad (1.12)$$

where $x_t(\theta) = x(t+\theta)$, $y_t(\theta) = y(t+\theta)$ for $\theta \leq 0$, and F , G satisfy appropriate conditions (namely, $\partial F/\partial x_t \leq 0$, $\partial F/\partial y_t < 0$; $\partial G/\partial x_t > 0$, and $\partial G/\partial y_t \leq 0$), and (1.12) has positive solutions.

A question of great importance is how does the qualitative behavior depends on the form and magnitude of the delays? In other words, are discrete and continuous delays equivalent from the perspective of the qualitative dynamical properties of the model? The paper by [12] examines certain aspects of this question.

In the next two sections, we discuss the stability of different types of DDEs.

1.3 Stability of DDEs

Time-delay is, in many cases, a source of instability. However, for some systems, the presence of delay can have a stabilizing effect. In the well-known example

$$y''(t) + y(t) - y(t-\tau) = 0, \quad (1.13)$$

the system is unstable for $\tau = 1$, but it is asymptotically stable when $\tau = 1$. The approximation $y'(t) \approx [y(t) - y(t-\tau)]/\tau$ explains the damping effect. The stability analysis and robust control of time-delay systems are, therefore, of theoretical and practical importance.

In the following subsections, we present a brief summary of some theories and analysis about the stability of linear and non-linear DDEs. We should first mention

¹ There are multiple variations of these equations, including forms with differing limits of integration.

the physical and mathematical interpretations of local and global stability. *Local stability* of an equilibrium point means that if you put the system somewhere near the point, then it will move itself to the equilibrium point in some time. However, *global stability* means that the system will come to the equilibrium point from any possible starting point (i.e., there is no “nearby” condition). Moreover, in *local asymptotic stability*, the solutions of the system must approach an equilibrium point under initial conditions close to the equilibrium point. Whereas in *global asymptotic stability*, the solutions must approach an equilibrium point under all initial conditions.

1.3.1 Stability of Linear Constant Coefficient DDEs

Consider a simple delay model of population growth given by the following linear DDE:

$$\begin{aligned} y'(t) &= \lambda y(t) + \mu y(t - \tau), \quad t \geq t_0, \\ y(t_0) &= \psi(t), \quad t \leq t_0. \end{aligned} \tag{1.14}$$

One of the fundamental methods for finding the solution of (1.14) is to build up the solution as a sum of simple exponential terms. Assuming the solution to be of the form $y(t) = ce^{st}$ (where c , and s are constants), it will be a solution of (1.14) if and only if s is a zero of the transcendental function

$$h(s) = s - \lambda - \mu e^{-s\tau}. \tag{1.15}$$

(The equation $h(s) = 0$ is called the characteristic equation of (1.14), and s_r is the characteristic root if it is a zero of this equation.) Bellman and Cooke [21] observed that the roots s_r of (1.15) are infinite in number and complex conjugate and that all lie in the left half-plane $\operatorname{Re}(s) < c$, for some constant c .

Here, we summarize the necessary and sufficient conditions for the “asymptotical” stability of the linear DDEs (1.14). Driver [33], in the following theorem, provided the conditions for DDE (1.14) to be stable:

Theorem 1.1 *A necessary and sufficient condition for all continuous solutions of (1.14) to approach zero as $t \rightarrow \infty$ is that all the characteristic roots have negative real parts.*

The following results impose conditions on λ and μ in (1.15) for the roots of $h(s) = 0$ to have negative real parts ($\operatorname{Re}(s) < 0$):

- When λ and μ are complex. This case is also considered by Barwell [42] and he proved that: A sufficient condition that all the roots of (1.15) have negative real parts is

$$|\mu| \leq -\operatorname{Re}(\lambda). \tag{1.16}$$

- When λ and μ are real, all roots of equation (1.15) have negative real parts if and only if (i) $\lambda < 1$, (ii) $\lambda < -\mu\sqrt{\zeta^2 + \lambda^2}$, where ζ is the root of $\zeta = \lambda \tan(\zeta\tau)$ such that $0 < \zeta\tau < \pi$ (if $\lambda = 0$, take $\zeta = \frac{1}{2}\pi/\tau$); see Bellman and Cooke [21].
- When $\lambda = 0$ and μ is complex. This case has been considered by Barwell [42], and the result is: For $\mu = re^{i\phi}$, a sufficient condition that all the roots of (1.15) have negative real parts is (i) $\operatorname{Re}(\mu) < 0$ ($\frac{1}{2}\pi < \phi < \frac{3}{2}\pi$), (ii) $0 < r\tau < \min(\frac{3}{2}\pi - \phi, \phi - \frac{1}{2}\pi)$.

1.3.2 Asymptotical Stability Region for Linear DDEs

To find the asymptotical stability region [24] (which depends on the lag term τ), suppose, without any loss of generality, that $\tau = 1$ in (1.14). We search for (λ, μ) values for which the first solution s crosses the imaginary axis ($\operatorname{Re}(s) = 0$), i.e., $s = i\theta$ for θ real. If we insert this into (1.15), we obtain

$$\lambda = -\mu \quad \text{for } \theta = 0 \quad (\text{s real}),$$

$$\lambda = i\theta - \mu e^{-i\theta} \quad \text{for } \theta \neq 0.$$

By separating the real and imaginary parts, we get $\lambda = \frac{\theta \cos \theta}{\sin \theta}$, $\mu = -\frac{\theta}{\sin \theta}$ valid for all real λ and μ . Thus, the stability region of $y'(t) = \lambda y(t) + \mu y(t-1)$ is bounded by $\mu = -\lambda$ and the parametrized curve $\lambda = \theta \cot(\theta)$, $\mu = -\theta/\sin(\theta)$; see Fig. 1.2.

A smaller subset of the stability region, which has been classically considered in [42], is given by the set of pairs (λ, μ) such that the solution $y(t)$ of (1.14) asymptotically vanishes *independently* of the lag τ (in the (λ, μ) -plane: $\Sigma = \{(\lambda, \mu) \in \mathbb{R}^2 \mid \lambda + |\mu| < 0\}$).

We next extend this analysis to linear *neutral* DDEs.

1.3.3 Stability of Linear NDDEs

Consider a linear *neutral* delay differential equation of the form

$$\begin{aligned} y'(t) &= \lambda y(t) + \mu y(t-\tau) + v y'(t-\tau), \quad t \geq t_0, \\ y(t_0) &= \psi(t), \quad t \leq t_0. \end{aligned} \tag{1.17}$$

We summarize the necessary and sufficient conditions for the stability of linear NDDEs (1.17) as follows:

Theorem 1.2 *Every solution (of the form $y(t) = ce^{st}$) of (1.17) tends to zero as $t \rightarrow \infty$ if all roots of the characteristic equation*

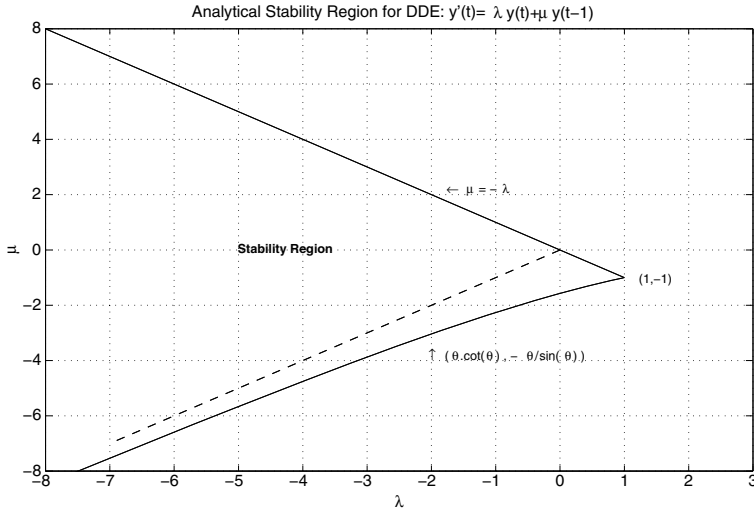


Fig. 1.2 Asymptotical stability region in (λ, μ) -plane when solving DDE: $y'(t) = \lambda y(t) + \mu y(t - 1)$, $t \geq 0$

$$s = \lambda + \mu e^{-\tau s} + \nu s e^{-\tau s} \quad (1.18)$$

have negative real parts and are bounded away from the imaginary axis.

Bellen et al. [43] gave a sufficient condition for the stability of the test equation (1.17) in the following theorem.

Theorem 1.3 *A sufficient condition for all the roots of (1.18) to have negative real parts is*

$$|\lambda \bar{v} - \bar{\mu}| + |\lambda v + \mu| < -2\operatorname{Re}(\lambda).$$

(λ , μ , and v are complex parameters.)

Remark 1.1 If λ , μ , and v are real, then the condition $|\lambda \bar{v} - \bar{\mu}| + |\lambda v + \mu| < -2\operatorname{Re}(\lambda)$ is equivalent to the condition $|\mu| < -\lambda$ and $|\nu| < 1$. If λ and μ are complex and $v = 0$, then the hypothesis of Theorem 1.2 reduces to $|\mu| < -\operatorname{Re}(\lambda)$, which gives a sufficient condition for the stability of the test equation (1.14).

1.3.4 Asymptotic Stability Region for Linear NDDEs

Suppose that $\tau = 1$ in Eq. (1.17). We need to search for the stability regions in terms of parameters (λ, μ) for which the first solution s of (1.18) crosses the imaginary axis ($\operatorname{Re}(s) = 0$), i.e., $s = i\theta$ for θ real. By separating the real and imaginary parts, we obtain

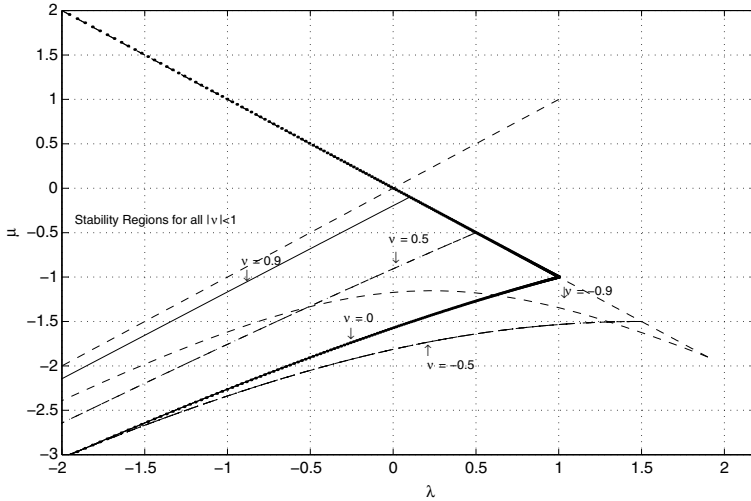


Fig. 1.3 Asymptotical stability regions when solving NDDE: $y'(t) = \lambda y(t) + \mu y(t-1) + \nu y'(t-1)$, $t \geq 0$

$$\mu = \frac{-\theta}{\sin(\theta)} + \theta \nu \cot(\theta) \quad \text{for } \theta \neq 0; \quad (1.19)$$

$$\lambda = -\mu \cos(\theta) - \theta \nu \sin(\theta) \quad \text{for } \theta \neq 0. \quad (1.20)$$

The stability regions for the NDDE (1.17) in the space of parameters (λ, μ) for $\nu = -0.9, -0.5, 0.5, 0.9$ are shown in Fig. 1.3. Equation (1.17) is always unstable for $|\nu| > 1$; see [24].

1.4 Stability of Non-linear DDEs and Contractivity Conditions

Consider a more general, non-linear DDE with a fixed time-lag τ

$$\begin{aligned} y'(t) &= f(t, y(t), y(t-\tau)), \quad t \geq t_0, \\ y(t) &= \psi(t), \quad t \leq t_0, \end{aligned} \quad (1.21)$$

where $y \in [t_0, \infty] \rightarrow \mathbb{C}^n$, $f : [t_0, \infty) \times \mathbb{C}^n \times \mathbb{C}^n \rightarrow \mathbb{C}^n$ and $\psi \in [t_0 - \tau, t_0] \rightarrow \mathbb{C}^n$. We wish to examine the effect that a small change in the initial conditions has on a solution. Thus, we consider another system, defined by the same function $f(t, y, x)$ of (1.21) but with another initial condition:

$$\begin{aligned} z'(t) &= f(t, z(t), z(t - \tau)), \quad t \geq t_0, \\ z(t) &= \phi(t), \quad t \leq t_0. \end{aligned} \quad (1.22)$$

In the sense of Lyapunov [24], the stability of the solution of (1.21) is defined by the following definition:

Definition 1.1 If there exists a norm on \mathbb{C}^n such that for every $t \geq t_0$, the solution of (1.21) is said to be

- (1) stable (with respect to perturbing the initial function), if for each $\varepsilon > 0$ there exists $\delta = \delta(\varepsilon, t_0)$ such that $\|y(t) - z(t)\| \leq \varepsilon$ when $\|\psi(t) - \phi(t)\| \leq \delta$;
- (2) asymptotically stable, if it is stable and $\|y(t) - z(t)\| \rightarrow 0$ as $t \rightarrow \infty$;
- (3) uniformly asymptotically stable, if under condition (ii) the number $\delta = \delta(\varepsilon)$ is independent of t_0 ;
- (4) globally uniformly asymptotically stable, if δ can be an arbitrarily large, finite number;
- (5) ξ -exponentially stable, if it is asymptotically stable and, given t_0 , there exists a finite constant K such that $\|y(t) - z(t)\| \leq K e^{-\xi(t-t_0)}$,

where $y(t)$ and $z(t)$ are solutions of (1.21) and (1.22), respectively, and $\psi(t)$ and $\phi(t)$ are distinct and continuous functions.

Definition 1.2 The problem (1.21) is contractive (with respect to perturbing the initial function) if for every $t \geq t_0$:

$$\|y(t) - z(t)\| \leq \max_{t \leq t_0} \|\psi(t) - \phi(t)\|$$

holds.

Corollary 1.1 The zero solution of (1.21) is stable if there exists a norm on \mathbb{C}^n such that for every $t \geq t_0$:

$$\|y(t)\| \leq \max_{t \leq t_0} \|\psi(t)\|.$$

The following theorem provides sufficient conditions for the contractivity of (1.21) (in the sense described above):

Theorem 1.4 (Contractivity Condition [44]) For a given inner product $\langle ., . \rangle$ in \mathbb{C}^n and the corresponding norm $\|.\|$, let $\sigma(t)$ and $\gamma(t)$ be continuous functions such that

$$\sigma(t) \geq \sup_{\substack{z, y_1, y_2 \in \mathbb{C}^n \\ y_1 \neq y_2}} \frac{\operatorname{Re}\langle (f(t, y_1, z) - f(t, y_2, z), y_1 - y_2) \rangle}{\|y_1 - y_2\|^2} \quad (1.23)$$

and

$$\gamma(t) \geq \sup_{\substack{y, z_1, z_2 \in \mathbb{C}^n \\ z_1 \neq z_2}} \frac{\|f(t, y, z_1) - f(t, y, z_2)\|}{\|z_1 - z_2\|}. \quad (1.24)$$

If

$$\sigma(t) + \gamma(t) \leq 0, \quad \text{for every } t \geq t_0, \quad (1.25)$$

then it holds that

$$\|y(t) - z(t)\| \leq \max_{x \leq t_0} \|\psi(x) - \phi(x)\|, \quad t \geq t_0. \quad (1.26)$$

Corollary 1.2 Suppose that $f(t, y(t), y(t - \tau)) = \lambda y(t) + \mu y(t - \tau)$, as in Eq. (1.14). Then, $\sigma(t) = Re(\lambda)$ and $\gamma(t) = |\mu|$. In this case, if $Re(\lambda) \leq -|\mu|$, using theorem (1.4) we get $|y(t)| \leq \max_{t \leq t_0} |\psi(t)|$ for every $t \geq t_0$.

To prove Theorem 1.4, the following theorems are needed:

Theorem 1.5 Consider the initial value problems of the form

$$\begin{aligned} y'(t) &= \lambda(t)y(t) + g(t), \quad t \geq t_0, \\ y(t_0) &= y_0, \end{aligned} \quad (1.27)$$

with $y, \lambda, g : [t_0, +\infty) \rightarrow \mathbb{C}$ and $Re(\lambda(t)) < 0$ for every $t \geq t_0$. Then, the solution $y(t)$ of the initial value problem (1.27) is such that:

$$|y(t)| \leq \max \left\{ |y_0|; \max_{t_0 \leq x \leq t} |g(x)/(-Re(\lambda(x)))| \right\}.$$

Proof Define $A(t) := \int_{t_0}^t \lambda(x)dx$; we note that $Re(A(t)) < 0$ for every $t \geq t_0$. The solution of (1.27) is

$$y(t) = y_0 e^{A(t)} + e^{A(t)} \int_{t_0}^t e^{-A(x)} g(x) dx.$$

We have that

$$\begin{aligned} \left| \int_{t_0}^t e^{-Re(A(x))} g(x) dx \right| &= \left| \int_{t_0}^t \left[-Re(\lambda(x))e^{-Re(A(x))} g(x)/(-Re(\lambda(x))) \right] dx \right| \\ &\leq \max_{t_0 \leq x \leq t} \{|g(x)/(-Re(\lambda(x)))|\} \left| \int_{t_0}^t -Re(\lambda(x))e^{-Re(A(x))} dx \right|, \end{aligned}$$

and

$$\int_{t_0}^t -Re(\lambda(x))e^{-ReA(x)} dx = e^{-Re(A(t))} - 1.$$

Therefore,

$$\left| \int_{t_0}^t e^{-Re(A(x))} g(x) dx \right| \leq \max_{t_0 \leq x \leq t} \{g(x)/(-Re(\lambda(x)))\} |e^{-Re(A(t))} - 1|.$$

Hence:

$$|y(t)| \leq e^{Re(A(t))} |y_0| + (1 - e^{Re(A(t))}) \max_{t_0 \leq x \leq t} |g(x)/(-Re(\lambda(x)))|,$$

and so, for every $t \geq t_0$:

$$|y(t)| \leq \max \left\{ |y_0|; \max_{t_0 \leq x \leq t} |g(x)/(-Re(\lambda(x)))| \right\}.$$

Theorem 1.6 Consider, two initial value problems,

$$\begin{aligned} y'(t) &= f(t, y(t), u(t)), \quad t \geq t_0, \\ y(t_0) &= y_0, \end{aligned} \tag{1.28}$$

and

$$\begin{aligned} z'(t) &= f(t, z(t), v(t)), \quad t \geq t_0, \\ z(t_0) &= z_0, \end{aligned} \tag{1.29}$$

with $f : [t_0, +\infty) \times \mathbb{C}^n \times \mathbb{C}^n \rightarrow \mathbb{C}^n$ and $y, z, u, v : [t_0, +\infty) \rightarrow \mathbb{C}^n$, and $y_0 \neq z_0$. Assume there exists an inner product $\langle \cdot, \cdot \rangle$ on \mathbb{C}^n such that (1.25) holds ($\|x\| = \langle x, x \rangle$ for every $x \in \mathbb{C}^n$). Then, for every $t \geq t_0$:

$$\|y(t) - z(t)\| \leq \max \left\{ \|y_0 - z_0\|; \max_{t_0 \leq x \leq t} \{\gamma(x) \|u(x) - v(x)\| / (-\sigma(x))\} \right\}.$$

Proof We have

$$\begin{aligned} \frac{1}{2} \frac{d}{dt} \|y(t) - z(t)\|^2 &= Re \langle y'(t) - z'(t), y(t) - z(t) \rangle \\ &= Re \langle f(t, y(t), u(t)) - f(t, z(t), v(t)), y(t) - z(t) \rangle \\ &= Re \langle f(t, y(t), u(t)) - f(t, y(t), v(t)), y(t) - z(t) \rangle + \\ &\quad Re \langle f(t, y(t), v(t)) - f(t, z(t), v(t)), y(t) - z(t) \rangle. \end{aligned}$$

It follows from the definitions of $\sigma(t)$ and $\gamma(t)$ and from Schwartz inequality that

$$\begin{aligned} \frac{1}{2} \frac{d}{dt} \|y(t) - z(t)\|^2 &\leq \|f(t, y(t), u(t)) - f(t, y(t), v(t))\| \|y(t) - z(t)\| + \sigma(t) \|y(t) - z(t)\|^2 \\ &\leq \gamma(t) \|u(t) - v(t)\| \|y(t) - z(t)\| + \sigma(t) \|y(t) - z(t)\|^2. \end{aligned}$$

Define

$$Y(t) := \|y(t) - z(t)\|.$$

Note that $Y(t) > 0$ for every $t > t_0$ because we assume that the function f is such that (1.28) has a unique solution $y(t)$ for every initial condition $y(t_0) = y_0$.

Then,

$$\frac{1}{2} \frac{d}{dt} \|y(t) - z(t)\|^2 = \|y(t) - z(t)\| \frac{d}{dt} \|y(t) - z(t)\| = Y(t)Y'(t),$$

so we have

$$Y(t)Y'(t) \leq \sigma(t)Y^2(t) + \gamma(t)\|u(t) - v(t)\|Y(t),$$

and hence

$$Y'(t) \leq \sigma(t)Y(t) + \gamma(t)\|u(t) - v(t)\|.$$

Define $g(t) := \gamma(t)\|u(t) - v(t)\|$; Therefore,

$$Y'(t) \leq \sigma(t)Y(t) + g(t),$$

and, by Theorem 1.5, for $t \geq t_0$:

$$Y(t) \leq \max \left\{ Y_0; \max_{t_0 \leq x \leq t} g(x)/(-\sigma(x)) \right\},$$

i.e.,

$$\|y(t) - z(t)\| \leq \max \left\{ \|y_0 - z_0\|; \max_{t_0 \leq x \leq t} \{\gamma(x)\|u(x) - v(x)\|/(-\sigma(x))\} \right\}.$$

Proof Theorem 1.4. From Theorem 1.6 we know that, for every $t \geq t_0$, the solutions $y(t)$ and $z(t)$ of (1.21) and (1.22), respectively, are such that

$$\|y(t) - z(t)\| \leq \max \{ \|\psi(t_0) - \phi(t_0)\|; \max_{t_0 \leq x \leq t} \{\gamma(x)\|y(x - \tau) - z(x - \tau)\|/(-\sigma(x))\} \}.$$

Assume that $\gamma(t) \leq -\sigma(t)$ and $\tau > 0$ for every $t \geq t_0$; therefore:

$$\|y(t) - z(t)\| \leq \max \left\{ \|\psi(t_0) - \phi(t_0)\|; \max_{t_0 \leq x \leq t} \|y(x - \tau) - z(x - \tau)\| \right\},$$

i.e.,

$$\|y(t) - z(t)\| \leq \max_{t \leq t_0} \{ \|\psi(t) - \phi(t)\| \}.$$

Therefore, the DDE (1.21) is stable if conditions (1.23)–(1.25) are satisfied. \square

Next, we will study global stability using Lyapunov functionals.

1.5 Stability of DDEs in Lyapunov Method

Lyapunov functions are an essential tool in the stability analysis of dynamical systems, both in theory and applications. As in systems without delay, an efficient method for stability analysis of DDEs is the Lyapunov method. For DDEs, there exist two main Lyapunov methods: the Krasovskii method of Lyapunov functionals [45] and the Razumikhin method of Lyapunov functions [46, 47]. The two Lyapunov methods for linear DDEs result in linear matrix inequalities (LMIs) conditions. The LMI approach to analysis and design of DDEs provides constructive finite-dimensional conditions, despite significant model uncertainties [48].

Consider a simple DDE of the form

$$y'(t) = f(t, y(t - \tau)), \quad t \geq t_0, \quad (1.30)$$

where $f : \mathbb{R} \times C[-\tau, 0] \rightarrow \mathbb{R}^n$ is continuous in both arguments and is locally Lipschitz continuous in the second argument. We assume that $f(t, 0) = 0$, which guarantees that (1.30) possesses a trivial solution $y(t) = 0$. The system is uniformly asymptotically stable if its trivial solution is uniformly asymptotically stable.

The core concept of Lyapunov stability theory is to construct a functional $V(y(t))$ (total energy stored in a system) to be defined and its derivative along the trajectories of the system.

Definition 1.3 Let $V : \mathbb{R}^n \rightarrow \mathbb{R}$ be a Lyapunov function if

- (i) $V(y(t)) \geq 0$ with equality if and only if $y = 0$, and
- (ii) $\frac{d}{dt} V(y(t)) \leq 0$.

Theorem 1.7 (Lyapunov's Second Theorem on \mathbb{R}) *If there exists a Lyapunov function V , then $y = 0$ is Lyapunov stable. Furthermore, if $V(y(t)) < 0$, then equilibrium $y = 0$ is asymptotically stable.*

Given a DDE of the form:

$$y'(t) = f(y(t), y(t - \tau)), \quad f(0, 0) = 0,$$

where $f(., .)$ is locally Lipschitz in its arguments. Let us assume that $V(t) = y^2(t)$, which is a typical Lyapunov function for $n = 1$. Then, we have along the system:

$$V'(t) = 2y(t)y'(t) = 2y(t)f(y(t), y(t - \tau)).$$

For the feasibility of inequality $V'(t) \leq 0$, we need to ensure that $y(t)f(y(t), y(t - \tau)) \leq 0$ for all sufficiently small $|y(t)|$ and $|y(t - \tau)|$. This essentially restricts the class of equations considered. For example, $y'(t) = -y(t)y^2(t - \tau)$ is stable based on the above arguments.

1.5.1 Lyapunov-Krasovskii Sense

Let $V : \mathbb{R} \times C[-\tau, 0] \rightarrow \mathbb{R}$ be a continuous functional, and let $y_s(t, \phi)$ be the solution of (1.30) at time $s \geq t$ with the initial condition $y_t = \phi(t)$. We define the right upper derivative $\dot{V}(t, \phi)$ along (1.30) as follows:

$$\dot{V}(t, \phi) = \lim_{\Delta t \rightarrow 0^+} \sup \frac{1}{\Delta t} [V(t + \Delta t, y_{t+\Delta t}(t, \phi)) - V(t, \phi)].$$

Intuitively, a non-positive $\dot{V}(t, \phi)$ indicates that y_t does not grow with t , meaning that the system under consideration is stable.

Theorem 1.8 (Lyapunov-Krasovskii Theorem, Gu et al. [49]) Suppose that $f : \mathbb{R} \times C[-\tau, 0] \rightarrow \mathbb{R}^n$ maps $\mathbb{R} \times$ (bounded sets) in $C[-\tau, 0]$ into bounded sets of \mathbb{R}^n and that $u; v; w : \mathbb{R}_+ \rightarrow \mathbb{R}_+$ are continuous nondecreasing functions, $u(s)$ and $v(s)$ are positive for $s > 0$, and $u(0) = v(0) = 0$. The trivial solution of (1.30) is uniformly stable if there exists a continuous functional $V : \mathbb{R} \times C[-\tau, 0] \rightarrow \mathbb{R}^+$, which is positive-definite, i.e.,

$$u(|\phi(0)|) \leq V(t, \phi) \leq v(|\phi(0)|), \quad (1.31)$$

and such that its derivative along (1.30) is non-positive in the sense that

$$\dot{V}(t, \phi) \leq -w(\|\phi\|_C). \quad (1.32)$$

If $w(s) > 0$ for $s > 0$, then the trivial solution is uniformly asymptotically stable. If in addition $\lim_{s \rightarrow \infty} u(s) = \infty$, then it is globally uniformly asymptotically stable.

1.5.2 Lyapunov-Razumikhin Sense

In Razumikhin approach, the derivative V along the solution $y(t)$ of (1.30) of a differentiable function $V : \mathbb{R} \times \mathbb{R}^n \rightarrow \mathbb{R}_+$ is defined as follows:

$$\dot{V}(t, y(t)) = \frac{d}{dt} V(t, y(t)) = \frac{\partial V(t, y(t))}{\partial t} + \frac{\partial V(t, y(t))}{\partial y} f(t, y_t). \quad (1.33)$$

Theorem 1.9 (Lyapunov-Razumikhin Theorem, Gu et al. [49]) Suppose that $f : \mathbb{R} \times C[-\tau, 0] \rightarrow \mathbb{R}^n$ maps $\mathbb{R} \times$ (bounded sets) in $C[-\tau, 0]$ into bounded sets of \mathbb{R}^n and that $u; v; w : \mathbb{R}_+ \rightarrow \mathbb{R}_+$ are continuous nondecreasing functions, $u(s)$ and $v(s)$ are positive for $s > 0$, and $u(0) = v(0) = 0$, v is strictly increasing. The trivial solution of (1.30) is uniformly stable if there exists a continuous functional $V : \mathbb{R} \times C[-\tau, 0] \rightarrow \mathbb{R}^+$, which is positive-definite, i.e.,

$$u(|y|) \leq V(t, y) \leq v(|y|), \quad (1.34)$$

and the derivative along (1.30) satisfies

$$\dot{V}(t, y(t)) \leq -w(|y(t)|), \text{ if } V(t + \theta, y(t + \theta)) < V(t, y(t)), \text{ for } \theta \in [0, \tau]. \quad (1.35)$$

If, in addition, $w(s) > 0$ for $s > 0$, and there exists a continuous nondecreasing function $\rho(s) > 0$, for $s > 0$, such that condition (1.35) is strengthened to

$$\dot{V}(t, y(t)) \leq -w(|y(t)|), \text{ if } V(t + \theta, y(t + \theta)) < \rho(V(t, y(t))), \text{ for } \theta \in [0, \tau], \quad (1.36)$$

then the trivial solution is uniformly asymptotically stable. If in addition $\lim_{s \rightarrow \infty} u(s) = \infty$, then it is globally uniformly asymptotically stable.

1.5.3 Stability of Linear Systems with Discrete Delays

Given the linearized system

$$\dot{y}(t) = Ay(t) + By(t - \tau(t)), \quad y(t) = \phi(t), \quad t \in [-\tau_M, 0], \quad (1.37)$$

$\tau(t) \in [0, \tau]$ is abounded. A simple Lyapunov-Krasovskii functional for the above system has the form

$$V(t, y(t)) = y^T(t)Py(t) + \int_{t-\tau(t)}^t y(s)Qy(s)ds,$$

where $P > 0$ and $Q > 0$ are $n \times n$ matrices. Clearly V satisfies the positivity condition $V(t, y(t)) \geq \beta|y(t)|^2$, for $\beta > 0$. Then, differentiating V along the system, we have

$$\dot{V}(t, y(t)) = 2y^T(t)P\dot{y}(t) + y^T(t)Qy(t) - (1 - \dot{\tau})y^T(t - \tau)Qy(t - \tau).$$

If we further substitute $\dot{y}(t)$, the right-hand side of the DDEs system, with $\dot{\tau} \leq d \leq 1$, we arrive at

$$\dot{V}(t, (y(t))) \leq y^T(t)y^T(t - \tau)W \begin{bmatrix} y(t) \\ y(t - \tau) \end{bmatrix} \leq -\varepsilon|y(t)|^2, \text{ for } \varepsilon > 0, \text{ if}$$

$$\begin{bmatrix} A^T P + PA + Q & PB \\ B^T A & -(1 - d)Q \end{bmatrix} < 0. \quad (1.38)$$

The linear matrix inequality (LMI) (1.38) does not depend on τ and it is, therefore, delay-independent (but delay-derivative dependent). The feasibility of LMI (1.38) is a sufficient condition for the delay-independent asymptotic stability of systems with slowly varying delays; see [49].

However, delay-independent conditions cannot be applied for the stabilization of unstable plants through a feedback with delay. For such systems, delay-dependent conditions are then needed. Now, we derive stability conditions by applying Razumikhin's approach and using the Lyapunov function:

$$V(t, y(t)) = y^T(t) P y(t)$$

with $P > 0$ that satisfies the positivity condition (1.34). Consider the derivative of V along (1.37). We will apply the Lyapunov-Razumikhin theorem with $\rho(s) = \bar{\rho} \cdot s > 1$, where the constant $\bar{\rho} > 1$. Whenever Razumikhin's condition:

$$\bar{\rho}y^T(t)Py(t) - y^T(t - \tau(t))Py(t - \tau(t)) > 0$$

holds for $\bar{\rho}\epsilon + 1$, with $\epsilon > 0$. We then conclude that, for any $q > 0$, there exists $\alpha > 0$ such that

$$\begin{aligned} \dot{V}(t, y(t)) &= 2y^T(t)P[Ay(t) + A_1y(t - \tau(T))] \\ &\leq 2y^T(t)P[Ay(t) + A_1y(t - \tau)] + \\ &q[\bar{\rho}y^T(t)Py(t) - y^T(t - \tau(t))Py(t - \tau(t))] \leq -\alpha|y(t)|^2 \end{aligned} \quad (1.39)$$

if

$$\begin{bmatrix} A^T P + PA + qP & PB \\ B^T P & -qP \end{bmatrix} < 0. \quad (1.40)$$

The MLI (1.40) does not depend on τ . Therefore, the feasibility of (1.40) is sufficient for delay-independent uniform asymptotic stability for systems with fast-varying delays (without any constraints on the delay-derivatives); see [49].

1.6 Concluding Remarks

In this chapter, we have provided a general introduction on DDEs and examined the stability of delay models described by linear and non-linear DDEs along with conditions that ensure local and global asymptotic stable behavior. Next, we will study approximation solutions and numerical schemes of DDEs. We will also discuss how the Runge-Kutta methods, which are so popular for ODEs, can be extended to DDEs.

References

1. Balasubramaniam, P., Prakash, M., Rihan, F.A., Lakshmanan, S.: Hopf bifurcation and stability of periodic solutions for delay differential model of HIV infection of CD4⁺ T-cells. *Abstr. Appl. Anal.* **982978**, 1–18 (2014)
2. Bocharov, G.A., Rihan, F.A.: Numerical modelling in biosciences using delay differential equations. *J. Comput. Appl. Math.* **125**, 183–199 (2000)
3. Metz, J..A..J., Diekmann, O.: *The Dynamics of Physiologically Structured Populations*. Lecture Notes in Biomathematics, vol. 68. Springer, NY (1986)
4. Rihan, F.A.: Numerical treatment of delay differential equations in bioscience. PhD. Thesis, University of Manchester, UK (2000)
5. Rihan, F.A., Abdelrahman, D., Al-Maskari, F., Ibrahim, F.: A delay differential model for tumour-immune response and control with chemo-immunotherapy. *Comput. Math. Methods Med.* **2014**, 15 (2014)
6. Rihan, F.A., Abdelrahman, D.H., Lakshmanan, S.: A time delay model of tumour- immune system interactions: Global dynamics, parameter estimation, sensitivity analysis. *Appl. Math. Comput.* **232**, 606–623 (2014)
7. Rihan, F.A., Azamov, A.A., AlSakaji, H.J.: An inverse problem for delay differential equations: parameter estimation, nonlinearity, sensitivity. *Appl. Math. Inform. Sci.* **12**(1), 63–74 (2018)
8. Rihan, F.A., Lakshmanan, S., Maurer, H.: Optimal control of tumour-immune model with time-delay and immuno-chemotherapy. *Appl. Math. Comput.* **353**(7), 147–165 (2019)
9. Rihan, F.A., Rihan, B.F.: Numerical modelling of biological systems with memory using delay differential equations. *Appl. Math. Inf. Sci.* **9**(3), 1615–1658 (2015)
10. Rihan, F.A., Kuang, Y., Bocharov, G.: Delay differential equations: theory, applications and new trends, vol. 13. Editorial: Discrete and Continuous Dynamical Systems - Series S (2018)
11. Rihan, F.A., Tunc, C., Saker, S.H., Lakshmanan, S., Rakkiyappan, R.: Applications of delay differential equations in biological systems, vol. 2018. Editorial: Complexity (2018)
12. Cooke, K., Grossman, Z.: Discrete delays, distributed delays and stability switches. *J. Math. Anal. Appl.* **86**, 592–624 (1982)
13. Mackey, M.C., Glass, L.: Oscillations and chaos in physiological control systems. *Science* **197**, 287–289 (1977)
14. Mackey, M.C., Milton, J.C.: Feedback, delays, and the origin of blood cell dynamics. *Comm. Theor. Biol.* **1**, 299–327 (1990)
15. Smith, H.L., Waltman, P.: *The Theory of the Chemostat*. Cambridge University Press, Cambridge (1994)
16. Bertta, E., Bischi, G., Solimano, F.: Stability in chemostat equations with delayed nutrient recycling. *J. Math. Biol.* **28**, 99–111 (1990)
17. Caperon, R.P.: Time lag in population growth response of *isochrysis galbana* to variable nitrate environment. *Ecology* **50**, 188–192 (1969)
18. Caperon, R.P.: *Biological Delay System: Linear Stability Theory*. Cambridge University Press, Cambridge (1989)
19. Lorenz, E.N.: Deterministic non-periodic flow. *J. Atmos. Sci.* **20**, 130–141
20. May, R.: *Stability and Complexity in Model Ecosystems*. Princeton University Press, Princeton, New Jersey (1974)
21. Bellman, R., Cooke, K.L.: *Differential-Difference Equations*. Academic Press, New York (1963)
22. Elsgolt's, L.E., Norkin, S.B.: *Introduction to the theory and application of differential equations with deviating arguments*
23. Kolmanovskii, V.B., Myshkis, A.: *Applied Theory of Functional Differential Equations* (1992)
24. Kolmanovskii, V.B., Nosov, V.R.: *Stability of Functional Differential Equations*. Academic Press, NY (1986)
25. Hale, J.: *Theory of Functional Differential Equations*. Springer, New York (1997)
26. Hale, J.K., Verduyn Lunel, S.M.: *Introduction to Functional Differential Equations*. Springer, NY (1993)

27. Diekmann, O., van Gils, S., Verduyn Lunel, S., Walter, H.-O.: *Delay Equation, Functional-, Complex-, and Nonlinear Analysis*. Springer, Berlin (1995)
28. Kuang, Y.: *Delay Differential Equations with Applications in Population Dynamics*. Academic Press (1993)
29. Banks, R.B.: *Growth and Diffusion Phenomena. Mathematical Frameworks and Applications. Texts in Applied Mathematics*, vol. 14. Springer, Berlin (1994)
30. Gopalsamy, K.: *Stability and Oscillations in Delay Differential Equations of Population Dynamics*. Kluwer, Dordrecht (1992)
31. Györi, I., Ladas, G.: *Oscillation Theory of Delay Equations with Applications*. Oxford Mathematical Monographs. Clarendon Press, Oxford
32. Cushing, J.M.: *Integro-Differential Equations and Delay Models in Population Dynamics. Lecture Notes in Biomathematics*. Springer, Berlin (1977)
33. Driver, R.D.: *Ordinary and Delay Differential Equations. Applied Mathematics Series* 20. Springer (1977)
34. Halanay, A.: *Differential Equations, Stability, Oscillations, Time Lags*. Academic Press, New York (1966)
35. MacDonald, N.: *Time-Lags in Biological Models. Lecture Notes in Biomathematics*, vol. 27. Springer, Berlin (1978)
36. Waltman, P.: *Deterministic Threshold Models in the Theory of Epidemics. Lecture Notes in Biomathematics*, vol. 1. Springer, Berlin (1974)
37. Hutchinson, G.E.: Circular causal systems in ecology. *Anal. New York Acad. Sci.* **50**, 221–246 (1948)
38. Fowler, A.C.: An asymptotic analysis of the delayed logistic equation when the delay is large. *IMA J. Appl. Math.* **28**(1), 41–47
39. Jones, G.S.: The existence of periodic solutions of $f'(x) = -\alpha f(x - \tau)\{1 + f(x)\}$. *J. Math. Anal. Appl.* **5**, 435–450 (1962)
40. Morris, H.C.: A perturbative approach to periodic solutions of delay-differential equations. *J. Inst. Math. Applics.* **18**, 15–24 (1976)
41. Morris, H.C.: Variations and fluctuations in the numbers of co-existing animal species. In: Scudo, F.M., Ziegler, J.R. (eds.) *The Golden Age of Theoretical Ecology: 1923–1940. Lecture Notes in Biomathematics*, vol. 22. Springer, Berlin (1979)
42. Barwell, V.K.: Special stability problems for functional equations, pp. 130–135 (1975)
43. Bellen, A., Jaciewicz, Z., Zennaro, M.: Stability analysis of one-step methods for neutral delay-differential equations. *Numer. Math.* **52**, 605–619 (1988)
44. Bellen, A., Jaciewicz, Z., Zennaro, M.: Stability of numerical methods for delay differential equations. *J. Comput. Appl. Math.* **25**, 15–26 (1989)
45. Krasovskii, N.: *Stability of Motion*. Stanford University Press (1959)
46. Lyapunov, A.M.: The general problem of the stability of motion. *Int. J. Control* **55**(3), 531–534 (1992)
47. Razumikhin, B.: On the stability of systems with a delay. *Prikl. Math. Mech. (in Russian)* **20**
48. Boyd, S., El Ghaoui, L., Feron, E., Balakrishnan, V.: *Linear matrix inequality in systems and control theory*. SIAM, Studies in Applied Mathematics, vol. 15. Philadelphia (1994)
49. Gu, K., Kharitonov, V., Chen, J.: *Stability of Time-delay Systems*. Birkhauser Boston, USA (2003)

Chapter 2

Numerical Solutions of Delay Differential Equations



In many application areas, one finds evolutionary problems with an after-effect whose numerical solution is based on the use of an integrator for ODEs combined with a suitable continuous extension. Our aim in this chapter is to survey numerical methods for solving DDEs and NDDEs based on modified ODE formulae. Special emphasis is given to continuous Runge-Kutta methods that have been used by the author. We describe, in brief, the theory of accuracy and some issues related to numerical solutions of DDEs and NDDEs.

Many real-life phenomena can be modeled by initial value problems (IVPs) for ODEs of the type

$$\begin{aligned}y'(t) &= f(t, y(t)), \quad t \geq t_0, \\y(t_0) &= y_0,\end{aligned}\tag{2.1}$$

where the function $y(t)$ represents some physical quantity that evolves in time.

We noted earlier that to make the model more consistent with real-life phenomena, it is sometimes necessary to modify the right-hand side of Eq. (2.1) to include the dependence of the derivative y' not only on y at the current value t but also at some past value $t - \tau$. The lag τ , which is always non-negative, may be just a constant (*constant lag*; $\tau = \text{const.}$), a function of t (*variable lag*; $\tau = \tau(t)$), or even a function of t and y itself (*state-dependent lag*; $\tau = \tau(t, y(t))$) according to the complexity of the phenomenon being modeled. In some cases, Eq. (2.1) would be changed to a DDE of the form

$$\begin{aligned}y'(t) &= f(t, y(t), y(t - \tau)), \quad t \geq t_0, \\y(t) &= \psi(t), \quad t \leq t_0.\end{aligned}\tag{2.2}$$

A clear difference between Eqs. (2.1) and (2.2) is that the solution of the latter is determined by an initial function $\psi(t)$ rather than by a simple initial value y_0 as in the former. Consequently (even if the functions $f(t, y, z)$, $\tau(t)$, and $\psi(t)$ are

C^∞ -continuous), if the solution $y(t)$ is not smoothly linked to the initial function $\psi(t)$ at the initial point t_0 , jumps can arise in the derivatives of $y(t)$. (To be precise, this occurs if $\psi'(t_0) \neq f(t_0, y(t_0), \psi(t_0 - \tau))$.) Such jumps spread forward along the integration interval. More precisely, a set of *discontinuity points* is generated, whose location is determined by the delayed argument $t - \tau$. We shall discuss this further in Sect. 2.1.

In most real-life situations, the number of instances where an exact solution can be found by analytical means is very limited. Thus, there is continued interest in the numerical treatment of DDEs and several schemes have been developed in this regard (using ideas embodied in schemes for ODEs). The choice of numerical techniques for the treatment of the DDEs and NDDEs depends mainly on the construction of densely defined *continuous extensions*. The ODE literature contains examples of *continuous RK formulae* that incorporate an inbuilt method to generate dense output. Such formulae are generated by the continuous RK triple $(\mathbf{c}, \mathbf{A}, \mathbf{b}^T(\theta))$ featured in Sect. 2.4.3.

Fourth-order Runge-Kutta methods and two-point Hermite interpolation polynomials have been used by Neves [1] for DDEs, and algorithms based on fourth- and seventh-order Runge-Kutta-Fehlberg methods together with Hermite interpolation polynomials have been presented by Oberle and Pesch [2]. Thompson [3] has developed numerical methods that are based on a continuously embedded Runge-Kutta method of Sarafyan [4]. An algorithm based on a prediction-correction mode of a one-step collocation method at k Gaussian points has been constructed by Bellen and Zennaro [5].

An explicit Runge-Kutta method has been proposed by Paul and Baker [6]. This method is based on the successful Dormand and Prince fifth-order Runge-Kutta method for ODEs by Shampine [7] and a fifth-order Hermite interpolant [2].

In general, in addition to the usual consistency and stability requirements for ODE numerical schemes, the numerical treatment of DDEs has to account for two other difficulties: firstly, the approximation of the delayed term and, secondly, any jump discontinuities in the various derivatives of the solution.

In this chapter, the emphasis is on general concepts and results rather than details and proofs. We shall describe, briefly, some basic features of one-step continuous extensions of Runge-Kutta methods and their application to DDEs (2.2). Propagation and location of discontinuities arising in the solution of DDEs are discussed in Sect. 2.1. In Sect. 2.2, the method of steps for solving DDEs is discussed. In Sect. 2.3, we provide an existence and uniqueness theory for the solution of DDEs. A general strategy for the numerical solution of the DDEs, using θ -methods and Runge-Kutta methods is discussed in Sect. 2.4. More general classes of DDEs are considered in Sect. 2.5. Finally, software aspects are discussed in Sect. 2.7.

2.1 Propagation and Location of Discontinuities in DDEs

In this section, we consider DDEs of the type (2.2), where $f : [t_0, T] \times \mathbb{R} \times \mathbb{R} \rightarrow \mathbb{R}$ is uniformly Lipschitz continuous in the last two variables and the lag τ is either constant or variable but not state dependent. Moreover, if it is variable, we shall assume, for simplicity, that the delayed argument $t - \tau(t)$ is a strictly increasing function and $\tau(t) \geq \tau^*$ for all $t \in [t_0, T]$.

Definition 2.1 A point ξ is called a (point of) derivative jump discontinuity of the solution $y(t)$ of (2.2) if $y(t)$ or some derivative of $y(t)$ has a jump discontinuity at $t = \xi$.

A set of derivative jump discontinuities is propagated from an initial point, which generally is the point $t = t_0$. This set forms the so-called *primary discontinuities* of $y(t)$. If ξ is a point of discontinuity of either ψ or f (e.g., if ψ is discontinuous for $t \in [-\tau, t_0]$), then ξ can generate a set of *secondary discontinuities* in the various derivatives of $y(t)$.

The propagation of discontinuities is intimately related to the lag function and the inter-component coupling in systems of DDEs. For example, from the DDE

$$y'(t) = y(t - \tau), \quad (t \geq 0) \quad y(t) = 1 \text{ for } t \in [-\tau, 0],$$

we can see that $y'_+(0) = y(-\tau) = 1$ while $y'_-(0) = 0$; therefore, a jump occurs in $y'(t)$ at $t = 0$, and this jump propagates to the points $t = \tau, 2\tau, 3\tau, \dots$. Since $y_{\pm}^{(n+1)}(t) = y'_{\pm}(t - n\tau)$, a jump in $y'(t)$ at $t = 0$ propagates to one in $y''(t)$ at $t = \tau$ ($y'_+(\tau) \neq y'_-(\tau)$) and then to one in $y'''(t)$ at $t = 2\tau$. Hence, $y(t)$ becomes smoother as t increases; see [8, 9].

For a scalar equation with a variable lag, we can show, quite simply, how discontinuities propagate. Consider Eq. (2.2), where the value $y'_-(t_0) = f(t_0, y(t_0), \psi(t_0 - \tau(t_0)))$ may differ from the value $\psi'_-(t_0)$; in this case, $y'(t)$ undergoes a jump as the argument traverses the point $\xi_0 = t_0$. Suppose that at a subsequent value of the argument (say, $t = \xi_1$) the delay function $t - \tau(t)$ traverses the point ξ_0 ; then, the jump in the derivative $y'(t)$ at ξ_0 is transmitted through the DDE to produce a discontinuity in one of the derivatives of $y(t)$ at ξ_1 . The precise propagation mechanism is determined by the dependency of $y'(t)$ on lag functions, but it may be noted that, for the propagation to occur, $\xi_0 - \tau(t)$ must undergo a change of sign at the point $t = \xi_1$ (see [10]). Having introduced a discontinuity at ξ_1 , this discontinuity can itself propagate discontinuities to subsequent points. Moreover, if $\psi(t)$ has discontinuities at the initial interval, then the discontinuities will propagate in the same manner as the discontinuity at t_0 .

In general, the discontinuity points ξ_k can be detected recursively by solving the recurrence:

$$\xi_k - \tau(\xi_k) = \xi_{k-1}, \quad k \geq 1, \tag{2.3}$$

where $\xi_0 = t_0$.

Because of the hypotheses made, an increasing sequence $\{\xi_k\}_{k \geq 0}$ can be determined a priori by using (2.3). In this manner, a sequence of intervals $[\xi_k, \xi_{k-1}]$ is also defined. Moreover, every pair of consecutive discontinuity points satisfies $\xi_k - \xi_{k-1} \geq \tau^*$. The above hypotheses yield the existence and uniqueness of the solution quite easily. In fact, this can be proved solely by using induction on the intervals $[\xi_{k-1}, \xi_k]$ and the well-known existence and uniqueness theorem for ODEs (2.1) under the hypotheses of uniform Lipschitz continuity of the right-hand side.

2.2 Method of Steps for DDEs

A solution of (2.2) with fixed time-lag τ on the whole interval $[t_0, t_0 + T]$ can be obtained using the *method of steps* (or the method of successive integrations) [10], i.e., by consecutive continuation from one interval to another (from $[t_0 + (n-1)\tau, t_0 + n\tau]$ to $[t_0 + n\tau, t_0 + (n+1)\tau]$). This approach could be adapted for numerical methods, but it would generally fail in certain kinds of DDEs and may prove to be too expensive.

To simplify the discussion, we confine ourselves to a scalar equation with a *constant lag* τ . Define $\xi_k = t_0 + k\tau$. On the interval $[\xi_0, \xi_1]$, the DDE (2.2) has the form

$$\begin{aligned} y'(t) &= f(t, y(t), \psi(t - \tau)), \quad \xi_0 \leq t \leq \xi_1, \\ y(t_0) &= \psi(t_0), \end{aligned} \tag{2.4}$$

and it is solved by means of a standard method for ODEs. If we assume, by induction, to have solved the DDE up to the defined discontinuity point ξ_{k-1} , then we can rewrite the DDE up to the next discontinuity point ξ_k as the following system of ODEs:

$$\begin{aligned} y'_i(t) &= f(t - (k-i)\tau, y_i(t), y_{i-1}(t)), \quad \xi_{k-1} \leq t \leq \xi_k, \\ y_i(\xi_{i-1}) &= y(\xi_{i-1}), \quad i = 1, 2, \dots, k, \end{aligned} \tag{2.5}$$

where we have set $y_0(t) = \psi(t - k\tau)$ and $y_i(t) = y(t - (k-i)\tau)$ ($i = 1, \dots, k$). As we have already computed approximations to the initial values $y_i(\xi_{i-1})$ ($i = 1, \dots, k$), we can solve the system via a chosen method for ODEs to obtain an approximation in the current interval $[\xi_{k-1}, \xi_k]$. In this manner, we are obliged to solve a system of ever-growing dimension and, in principle, to recompute the same pieces of solution related to the previous intervals many times. On the other hand, the reduction to a system of ODEs avoids the typical complications due to the presence of the delayed argument.

This method allows us the opportunity to simultaneously determine the solution $y(t)$ on several finite intervals and to prove the “existence” and “uniqueness” of the solution in a neighborhood of the point $(t_0, \psi(t_0))$ (if ψ and f are continuous in the

range of the variables and if function f , of Eq. (2.4), satisfies the Lipschitz condition on the second argument).

Example 2.1 Consider:

$$y'(t) = 6y(t - 1), \quad y = t \quad \text{for } 0 \leq t \leq 1.$$

We determine $y(t)$ for $1 \leq t \leq 3$.

Applying the method of steps, we obtain

$$y'(t) = 6(t - 1), \quad 1 \leq t \leq 2, \quad y(1) = 1;$$

integrating, we get

$$y(t) = 3(t - 1)^2 + 1.$$

For $2 \leq t \leq 3$,

$$y'(t) = 6[3(t - 2)^2 + 1], \quad y(2) = 4.$$

Therefore,

$$y(t) = 6(t - 2)^3 + 6t - 8.$$

Example 2.2 Applying the method of steps for

$$y'(t) = ay(t - \tau), \quad t \geq t_0,$$

$$y(t) = c, \quad t_0 - \tau \leq t \leq t_0,$$

(c and τ are constants, and $\tau > 0$), we obtain

$$y(t) = c \sum_{n=0}^{\lceil \frac{t-t_0}{\tau} \rceil + 1} a^n \frac{(t - t_0 - (n - 1)\tau)^n}{n!}, \quad t \geq t_0,$$

where $[t]$ is the integer part of t .

We note that even if the functions ψ and f have continuous derivatives of all orders, the solution of the DDEs will have a *primary discontinuity* (which comes from the initial point t_0) of the k th order derivatives at the point $t_0 + (k - 1)\tau$, but the lower derivatives will be continuous at this point.

The above analysis is based upon a constant lag τ , and it can be readily extended to certain instances of a “non-constant” lag. However, this direct implementation of the method of steps suffers from a limitation inherent in the analysis technique: when a vanishing lag occurs ($\tau(t_*) = 0$), the method encounters a natural barrier at t_* , beyond which the solution cannot proceed; see Sect. 2.5.3.

2.3 Existence and Uniqueness Solution of DDEs

The theory of existence and uniqueness of solutions to (2.2) does not present substantial additional difficulties with respect to the ordinary case (2.1). In this section, we briefly present general concepts, rather than details and proofs, of the existence and uniqueness theory for DDEs.

As already shown in Sect. 2.2, if we apply the method of steps, a DDE can be reduced to an ODE equation without a delay argument to which we may apply known existence and uniqueness theorems for the solution of the initial value problem.

If we consider the DDE (2.2), and apply the method of steps, we obtain Eq. (2.4); consequently, (2.2) has a solution if f and ψ are continuous and this solution is unique near t_0 if function $f(t, y, z)$ satisfies a Lipschitz condition in its second argument, $y(t)$, for t near t_0 , for z near $\psi(t - \tau(t_0))$, and y near y_0 .

For a more general, state-dependent equation, $\tau = \tau(t, y(t))$, the first step gives

$$\begin{aligned} y'(t) &= f(t, y(t), \psi(t - \tau(t, y(t)))), \quad \xi_0 \leq t \leq \xi_1, \\ y(t_0) &= \psi(t_0). \end{aligned} \tag{2.6}$$

If the functions f , ψ , and τ are continuous, then a solution exists; if, in addition in (2.6), the right-hand side $F(t, y(t)) \equiv f(t, y(t), \psi(t - \tau(t, y(t))))$ satisfies a Lipschitz condition with respect to $y(t)$, then the solution is unique. (For this it suffices that $|\frac{\partial f}{\partial y}|$, $|\frac{\partial f(t, y, z)}{\partial z}|$, $|\psi'(t)|$, $|\tau'_y(t, y)|$ be bounded in a neighborhood of the initial values; see [11].)

2.4 Numerical Approach for DDEs

In this section, we briefly describe the theory of Runge-Kutta methods for DDEs (2.2). The discussion will be extended to more general classes of DDEs (such as vanishing lag and state-dependent DDEs) in Sect. 2.5.

2.4.1 General Approach

One general approach to the solution of DDEs is based upon the following strategy:

1. Choose a *discrete* numerical method for solving ODEs;
2. Choose an interpolant $\hat{y}(t)$ (such as a continuous extension, or a Hermite interpolant) to estimate the numerical solution $\tilde{y}(t)$ at non-mesh points. Then, the delayed term $y(t - \tau)$ can be computed at each step;
3. Compute the discontinuity points $\{\xi_k\}$ (one after the other) defined by the recurrence relation (2.3) and, in each interval $[\xi_{k-i}, \xi_k]$, use the chosen numerical

ODE method to approximate the solution of the ODE

$$\begin{aligned} w'(t) &= f(t, w(t), \hat{y}(t - \tau)), \quad \xi_{k-1} \leq t \leq \xi_k, \\ w(\xi_{k-1}) &= \hat{y}(\xi_{k-1}). \end{aligned} \quad (2.7)$$

The first two steps of this procedure may alternatively be replaced by the direct choice of a *continuous* numerical method for ODEs (*discrete* and *continuous* numerical methods mean the approximation of the solution is on the discrete set of points or in the whole interval of integration, respectively).

With regard to stage (3), we may instead seek a method such that the stepsize is determined by the DDE solver (rather than exclusively by the position of the $\{\xi_i\}$). Suppose $\hat{y}(t)$ has been computed by advancing from the initial point t_0 : the approximate solution values, $\{\hat{y}_n\}$, have been computed on the mesh points, then the solutions at non-mesh points $\hat{y}(t)$ can be computed for $t_0 \leq t \leq t_n$ using some approximation formula, and for $t < t_0$ by evaluation of the initial function. *The next step* in the numerical solution consists of choosing a stepsize h_n such that the solution on the interval (t_n, t_{n+1}) contains no discontinuities, or only “small” discontinuities, in its sufficiently low-order derivatives, and then solving

$$\begin{aligned} w'(t) &= f(t, w(t), \hat{y}(t - \tau)), \quad t_n \leq t \leq t_{n+1}, \\ w(t_n) &= \hat{y}(t_n). \end{aligned} \quad (2.8)$$

In the case of constant lag τ , calculating the numerical solution is straightforward, provided that $h_n \leq \tau$. For cases where τ is small relative to the choice of stepsize, or for *state-dependent* delays in which we find that $\tau(t_*, \hat{y}(t_*)) < 0$ at some points t_* , it seems there is a need to evaluate $\hat{y}(t)$ with arguments exceeding the subinterval endpoint t_{n+1} and, possibly, even exceeding t_{n+2} ; see Sect. 2.5.

Given a “discrete” numerical solution, defined on a mesh $\{t_i\}$, there are several methods of extending it to a function of a continuous variable, e.g., by Lagrange interpolation, Hermite interpolation, or by a continuous extension formula provided by the method itself. The order of the accuracy is determined by the error in the interpolation polynomial and the error in mesh-value $\{\hat{y}(t_i)\}$.

A large variety of ODE methods (including methods based on explicit and implicit LM methods, explicit and implicit RK methods, collocation formulae, and linear multi-stage multi-value formulae; see [12]) can be adapted to DDEs. The use of such methods involves adaptation of the formulae for unequal meshsizes, choice of the iterative method for implicit formulae, variation of the choice of the formulae to adapt to error control, local stability, etc.

For the theory of the numerical methods for ODEs, refer to books by Butcher [13], Hairer, Nørsett and Wanner [14] and Hairer and Wanner [15], and Lambert [16]. Let us start our analysis with Θ -methods for DDEs, and later with RK methods.

2.4.2 Θ -Methods for DDEs

We describe a class of methods for DDEs based upon the Θ -methods for ODEs with linear interpolation, which have the following form:

$$\begin{aligned}\tilde{y}_{n+1} &= \tilde{y}_n + h_{n+1}[(1 - \Theta)f(t_n, \tilde{y}_n, \hat{y}(t_n - \tau)) + \Theta f(t_{n+1}, \tilde{y}_{n+1}, \hat{y}(t_{n+1} - \tau))]; \\ \hat{y}(t_n + sh_{n+1}) &= \tilde{y}_n + sh_{n+1}[(1 - \Theta)f(t_n, \tilde{y}_n, \hat{y}(t_n - \tau)) \\ &\quad + \Theta f(t_{n+1}, \tilde{y}_{n+1}, \hat{y}(t_{n+1} - \tau))], \quad 0 \leq s \leq 1,\end{aligned}$$

where Θ is a parameter belonging to $[0, 1]$. Observe that, for $\Theta = 0$, they reduce to the so-called *forward (explicit) Euler method*, whereas, for $\Theta = 1$, they reduce to *backward (or implicit) Euler method* (which are both $1 - stage$ RK methods). The order of the Θ -methods is always 1 but for $\Theta = \frac{1}{2}$, which corresponds to the *trapezium rule method*, the order is 2.

We take, by way of example, the simplest linear DDE:

$$y'(t) = \lambda y(t) + \mu y(t - 1), \quad 0 < t \leq T.$$

Suppose that $\tau = 1 = (m + \theta)h$, $m \in \mathbb{Z}_+$, and $\theta \in [0, 1)$. Then, with constant step-size h and $\tilde{y}_n = y(t_n)$, we have (using linear interpolation)

$$\tilde{y}(t_n - 1) := \tilde{y}(t_{n-m} - \theta h) \approx \theta \tilde{y}_{n-m-1} + (1 - \theta) \tilde{y}_{n-m}.$$

For $\Theta = 0$ (the forward Euler method), we have the recurrence:

$$\tilde{y}_{n+1} = (1 + \frac{\lambda}{m + \theta})\tilde{y}_n + \frac{\mu}{m + \theta} [\theta \tilde{y}_{n-m-1} + (1 - \theta) \tilde{y}_{n-m}].$$

If $\Theta = 1$ (the backward Euler method), the recurrence becomes

$$(1 - \frac{\lambda}{m + \theta})\tilde{y}_{n+1} = \tilde{y}_n + \frac{\mu}{m + \theta} [\theta \tilde{y}_{n-m} + (1 - \theta) \tilde{y}_{n-m+1}].$$

For the trapezium method, $\Theta = \frac{1}{2}$, we have

$$(1 - \frac{\lambda}{2(m + \theta)})\tilde{y}_{n+1} = (1 + \frac{\lambda}{2(m + \theta)})\tilde{y}_n + \frac{\mu}{2(m + \theta)} [(1 - \theta)\tilde{y}_{n-m+1} + \tilde{y}_{n-m} + \theta \tilde{y}_{n-m-1}].$$

In the rest of this section, we extend the analysis from Θ -methods to the RK methods for DDEs.

2.4.3 Continuous One-Step Runge-Kutta Methods for ODE

To modify a class of RK methods for DDEs, we must consider their application to ODEs.

A v -stage Runge-Kutta method for the solution of ODE (2.1) for a given mesh $\Delta = \{t_0 < t_1 \dots < t_N = T\}$, is defined by

$$Y_{n+1}^i = \tilde{y}_n + h_{n+1} \sum_{j=1}^v a_{ij} f(t_{n+1}^j, Y_{n+1}^j), \quad i = 1, \dots, v, \quad (2.9)$$

$$\tilde{y}_{n+1} = \tilde{y}_n + h_{n+1} \sum_{i=1}^v b_i f(t_{n+1}^i, Y_{n+1}^i), \quad (2.10)$$

where

$$\begin{array}{c|cccc} c_1 & a_{11} & a_{12} & \dots & a_{1v} \\ c_2 & a_{21} & a_{22} & \dots & a_{2v} \\ \vdots & \vdots & \vdots & & \vdots \\ c_v & a_{v1} & a_{v2} & \dots & a_{vv} \\ \hline & b_1 & b_2 & \dots & b_v \end{array} \equiv \frac{\mathbf{c} | \mathbf{A}}{\mathbf{b}^T},$$

$$c_i = \sum_{j=1}^v a_{ij}, \quad (i = 1, \dots, v), \quad t_{n+1}^i = t_n + c_i h_{n+1} \quad \text{and} \quad h_{n+1} = t_{n+1} - t_n.$$

The values $\{c_i\}$ are called *abscissae* and, for many common methods, they belong to $[0, 1]$.

The computational complexity of the method is determined mainly by the number v of *stages* and by the form of the coefficient matrix $\mathbf{A} = [a_{ij}]$, $(i, j = 1, \dots, v)$. It is well known that when the matrix \mathbf{A} is lower triangular with zero diagonal elements, the formula is called formally *explicit* and the computational cost (per-step) is lower, whereas when the matrix \mathbf{A} is full, the method is called *implicit* and the computational cost (per-step) is higher. However, we may be able to take fewer steps by using an implicit method.

We need to impose some additional requirements into the ODE solver to be able to solve DDEs. For example, we need the dense output of the solution to obtain an approximant $\hat{y}(t)$ to the numerical solution \tilde{y}_n at non-meshpoints.

The one-step interpolants are constructed step-by-step by making use of information from the underlying step $[t_n, t_{n+1}]$, possibly by including some additional stages. On the other hand, *multistep* interpolants can also be used to determine the approximation at the underlying step, using information from more than one step. A *continuous extension* $\hat{y}(t + \theta h_{n+1})$ of the numerical solution \tilde{y}_n , in each subinterval determined by the mesh points, can be used to get dense output. Later in this section,

we show that Hermite interpolation, in specific cases, can take the form of continuous extension with support points $t_n + r_i h_{n+1}$ with, e.g., $r_i = \{0, \frac{1}{2}, 1\}$, in the underlying step $[t_n, t_{n+1}]$.

Definition 2.2 (*Continuous Extension*) The continuous extension $\hat{y}(t + \theta h_{n+1})$ of the numerical solution \tilde{y}_n in (2.9)–(2.10) is defined, in each subinterval determined by the mesh Δ , by a one-step continuous quadrature rule of the form

$$\hat{y}(t_n + \theta h_{n+1}) = \tilde{y}_n + h_{n+1} \sum_{i=1}^s b_i(\theta) f(t_{n+1}^i, Y_{n+1}^i), \quad 0 \leq \theta \leq 1, \quad (2.11)$$

where

$$Y_{n+1}^i = \tilde{y}_n + h_{n+1} \sum_{j=1}^s a_{ij} f(t_{n+1}^i, Y_{n+1}^i) \approx y(t_{n+1}^i), \quad i = 1, \dots, v, \dots, s. \quad (2.12)$$

The terms $b_i(\theta)$'s are polynomials, and the number of stages involved is $s \geq v$. To assure the continuity of the interpolant, i.e.,

$$\hat{y}(t_n) = \tilde{y}_n \quad \text{and} \quad \hat{y}(t_{n+1}) = \tilde{y}_{n+1}, \quad (2.13)$$

and the polynomials $b_i(\theta)$ satisfy $b_i(0) = 0$ and $b_i(1) = b_i$, $i = 1, 2, \dots, s$.

Formulae (2.11)–(2.12) produce a *continuous* RK method, whereas, in contrast, the set (2.9)–(2.10) is called a *discrete* RK method.

To orient the reader, we introduce, e.g., a continuous trapezium rule:

$$\frac{\mathbf{c} | \mathbf{A}}{\theta | \mathbf{b}^T(\theta)} \equiv \begin{array}{c|cc} 0 & 0 \\ \hline 1 & \frac{1}{2} & \frac{1}{2} \\ \hline \theta & \theta(1 - \frac{1}{2}\theta) & \frac{1}{2}\theta^2 \end{array}, \quad \theta \geq 0. \quad (2.14)$$

Definition 2.3 (*Local Order*) The RK method (2.9)–(2.10) has (nodal or discrete) order p if p is the largest integer such that, for all C^p -continuous right-hand side functions $f(t, y(t))$ in (2.1) and for all mesh points,

$$\|z_{n+1}(t_{n+1}) - \tilde{y}_{n+1}\| = O(h_{n+1}^{p+1}), \quad (2.15)$$

where $z_{n+1}(t)$ is the local solution to the local problem

$$\begin{aligned} z'_{n+1}(t) &= f(t, z_{n+1}(t)), \quad t \geq t_n, \\ z_{n+1}(t_n) &= \tilde{y}_n. \end{aligned} \quad (2.16)$$

Definition 2.4 (*Continuous Local Order*) The one-step interpolant (2.11) has uniform order q if q is the largest integer such that

$$\max_{t_n \leq t \leq t_{n+1}} \|z_{n+1}(t) - \hat{y}(t)\| = O(h_{n+1}^{q+1}). \quad (2.17)$$

The uniform order q of the interpolant, which clearly does not exceed p , is also the uniform order of the *continuous* RK method (2.11)–(2.12), such that

$$\sum_i b_i(\theta) c_i^s = \frac{\theta^{s+1}}{s+1} \quad \text{for } s = 0, \dots, q-1.$$

Remark 2.1 A necessary condition for the RK method (2.9)–(2.10) to actually perform with order p is that the right-hand side function $f(t, y)$ in (2.16) must be sufficiently smooth, namely, at least C^p -continuous.

The additional $(s - v)$ stages in the continuous extension formula (2.11) are assumed to raise its order q to order p (or at least $p - 1$) of the discrete RK methods (2.9)–(2.10). On the other hand, in some applications (e.g., in case of solving NDDEs), we may need to differentiate the continuous extension formula, and then the uniform order can be less than $p - 1$. In that case, the interpolant must satisfy certain *asymptotic orthogonality* conditions (2.20) which define the so-called *Natural Continuous Extension* (NCEs) for ODE RK methods, introduced by Zennaro [17].

Definition 2.5 (*Natural Continuous Extension*) The RK method (2.9)–(2.10) of order p has an NCE $\hat{y}(t)$ of degree d if there exist v polynomials $b_i(\theta)$, $i = 1, \dots, v$, of degree $\leq d$, such that for the function defined by (2.11) (with $s = v$), condition (2.13) holds and

$$\max_{t_n \leq t \leq t_{n+1}} \|z_{n+1}(t) - \hat{y}(t)\| = O(h_{n+1}^{d+1}), \quad (2.18)$$

$$\max_{t_n \leq t \leq t_{n+1}} \|z'_{n+1}(t) - \hat{y}'(t)\| = O(h_{n+1}^d), \quad (2.19)$$

$$\left\| \int_{t_n}^{t_{n+1}} G(t) [z'_{n+1}(t) - \hat{y}'(t)] dt \right\| = O(h_{n+1}^{p+1}), \quad (2.20)$$

for every sufficiently smooth function $G(t)$, where $z_{n+1}(t)$ is the local solution to (2.16).

Theorem 2.1 (Error in Derivatives) [18] Given an NCE $\hat{y}(t)$, then condition (2.19) implies the following error bounds for higher derivatives of the NCEs:

$$\max_{t_n \leq t \leq t_{n+1}} \|z_{n+1}^{(k)}(t) - \hat{y}^{(k)}(t)\| = O(h_{n+1}^{d-k+1}), \quad k = 2, 3, \dots, d, \quad (2.21)$$

and, clearly, $\hat{y}^{(k)} \equiv 0$ for $k \geq d + 1$.

It has also been proved in [18] that every RK formula has at least an NCE of minimal degree $\left\lceil \frac{p+1}{2} \right\rceil$, where $[x]$ is the integer part of x .

In the underlying step $[t_n, t_{n+1}]$, it is quite common to approximate $y(t)$ at $t = t_n + \theta h_{n+1}$, using the formulae based on Hermite interpolation, because the derivatives of $\tilde{y}(t)$ at the integration points are known. Moreover, it is possible to prove that more specific Hermite-type interpolant for an explicit RK method with abscissae $\{c_i\}$ can, in some cases, take the form of continuous extension; see [7] and [19]. The Hermite approximation $H(t)$, with support points $t_n + r_i h_{n+1}$ with $r_i \in [0, 1]$ and derivative function $\tilde{F}(t) \equiv f(t, y(t))$, can be expressed in the form:

$$H(t_n + \theta h_{n+1}) = \sum_i p_i(\theta) \tilde{y}(t_n + r_i h_{n+1}) + h_{n+1} \sum_i q_i(\theta) \tilde{F}(t_n + r_i h_{n+1}), \quad (2.22)$$

where the solution value $\tilde{y}(t_n + r_i h_{n+1})$ (with abscissae $\{c_i\}$) takes the form:

$$\tilde{y}(t_n + r_i h_{n+1}) = \tilde{y}_n + h_{n+1} \sum_j a_{ij} \tilde{F}(t_n + c_j h_{n+1}).$$

Thus (with $\sum_i p_i(\theta) = 1$), Eq. (2.22) can be rewritten in the form

$$H(t_n + \theta h_{n+1}) = \tilde{y}_n + h_{n+1} \sum_i p_i(\theta) \sum_j a_{ij} \tilde{F}(t_n + c_j h_{n+1}) + h_{n+1} \sum_i q_i(\theta) \tilde{F}(t_n + r_i h_{n+1}).$$

It should also be noted that the interpolation order and, thereby, the number of support points have to be adapted to the order of the numerical method; we shall discuss this further in Sect. 2.7.4 and in Appendix A.

In the following subsection, we illustrate one of the main applications of interpolants to DDEs.

2.4.4 Runge-Kutta Method for DDEs

Given a mesh $\Delta = \{t_0 < t_1 \cdots < t_N = T\}$, the numerical methods we consider for solution of DDEs (2.2) are obtained by applying the continuous RK method (2.11)–(2.12) to the ODE (2.7) in the interval $[t_n, t_{n+1}]$. They have the form

$$Y_{n+1}^i = \tilde{y}_n + h_{n+1} \sum_{j=1}^s a_{ij} f(t_{n+1}^j, Y_{n+1}^j, \hat{y}(t_{n+1}^j - \tau)), \quad i = 1, \dots, s, \quad (2.23)$$

$$\hat{y}(t_n + \theta h_{n+1}) = \tilde{y}_n + h_{n+1} \sum_{i=1}^s b_i(\theta) f(t_{n+1}^i, Y_{n+1}^i, \hat{y}(t_{n+1}^i - \tau)), \quad 0 \leq \theta \leq 1. \quad (2.24)$$

If the lag τ is a function of t , it must be evaluated at the relevant points t_{n+1}^j . For $t \leq t_0$, we define $\widehat{y}(t) = \psi(t)$. Furthermore, we assume, for simplicity, that the abscissae c_i lie in $[0, 1]$, $i = 1, \dots, s$.

This method is called the RK method for DDEs. The pair formed by the underlying discrete RK method (2.9)–(2.10) and by the underlying interpolant (2.11) is called the underlying *continuous RK method* for the DDE.

Clearly, it would be desirable for the nodal order p of the underlying discrete RK method to be inherited by the RK method for DDEs. Therefore, in view of Remark 2.1, it is necessary to include at least the first p discontinuity points ξ_k in mesh Δ . Moreover, the interpolant (2.24) should have a uniform order of accuracy of at least $p - 1$.

In fact, an adaptive ODE solver is implemented in a variable stepsize mode. In such an approach, it is not possible to predict a priori where the retarded term $\widehat{y}(t - \tau)$ will be computed at each step, and a uniform high order accuracy is consequently required. The following theorem gives the order of the convergence of the numerical method for DDEs.

Theorem 2.2 (Order of Convergence of DDE Methods) [18] *If the RK method for DDEs (2.23)–(2.24) is applied to (2.2) with a mesh Δ that includes the discontinuity points ξ_k , if the underlying discrete RK method has nodal order p and if the underlying interpolant has order $q \geq p - 1$, then the continuous numerical solution $\widehat{y}(t)$ is such that*

$$\max_{t_0 \leq t \leq T} \|y(t) - \widehat{y}(t)\| = O(h^p),$$

where

$$h = \max_{1 \leq n \leq N} h_n.$$

The variable stepsize strategy is adopted to ensure, as much as possible, the proportionality of the global error to a given tolerance and to minimize the computational cost. We may do this by estimating the local error of the advancing method via another higher order method (of order $p + 1$).

It is easy to prove (in the underlying step $[t_n, t_{n+1}]$) that the local problem

$$\begin{aligned} z'_{n+1}(t) &= f(t, z_{n+1}(t), \widehat{y}(t - \tau)), & t_n \leq t \leq t_{n+1}, \\ z_{n+1}(t_n) &= \widetilde{y}_n. \end{aligned} \tag{2.25}$$

(which is actually solved numerically) is a perturbation of the smooth problem

$$\begin{aligned} \check{z}'_{n+1}(t) &= f(t, \check{z}_{n+1}(t), \widehat{y}_{n+1}(t - \tau)), & t_n \leq t \leq t_{n+1}, \\ \check{z}_{n+1}(t_n) &= \check{y}_n, \end{aligned} \tag{2.26}$$

where $\widehat{y}_{n+1}(t - \tau)$ is a suitable *delayed local solution* that satisfies

$$\max_{t_n \leq t \leq t_{n+1}} \|\widehat{y}_{n+1}(t - \tau) - \widehat{y}(t - \tau)\| = O(h^{q+1}),$$

where q is the uniform order of accuracy of the interpolant $\hat{y}(t)$. This implies that

$$\|\check{z}_{n+1}(t_{n+1}) - z_{n+1}(t_{n+1})\| = O(h^{q+2}).$$

Now, given a discrete RK method, let \tilde{w}_{n+1} and $\tilde{\check{w}}_{n+1}$ be the numerical solutions of (2.25) and (2.26), respectively. Since the numerical solution depends on the data, we also have

$$\|\tilde{\check{w}}_{n+1} - \tilde{w}_{n+1}\| = O(h^{q+2}).$$

Therefore, in view of Remark 2.1, it is easy to prove that, in order to preserve the order p of the advancing method, $q \geq p$ is required for successful implementation of the higher order method used to estimate the local error; see [5].

If the solution of DDE does not change its behavior significantly along the integration interval, a less robust ODE code may be successfully implemented, which does not perform the stepsize selection at each step. In this case, even a constant stepsize might prove to be a reasonable choice.

Corollary 2.1 (Order of Convergence of NCE) *If an RK method of order p for solving DDEs (2.23)–(2.24) is applied to (2.2) with a constrained mesh Δ and the underlying interpolant is NCE of degree d , then continuous numerical solution $\hat{y}(t)$ is such that*

$$\max_{t_0 \leq t \leq T} \|y(t) - \hat{y}(t)\| = O(h^{d'}), \quad (2.27)$$

where $d' = \min\{d + 1, p\}$.

Observe that, if $d \geq p - 1$, then we (naturally) again find the result stated by Theorem 2.2.

2.5 More General Classes of DDEs

In this section, we consider more general DDEs of the form (2.2) but of *neutral* type as well as DDEs that are not subject to the restrictions on the lag τ imposed in the above sections, such as *state-dependent* DDEs. We also consider the possibilities (i) $\tau(t) < h$, (ii) $\tau(t) \rightarrow 0$ as $t \rightarrow t^*$ (with small or vanishing lag DDEs). In these cases, the lag term $t_{n+1}^i - \tau(t_{n+1}^i) > t_n$ for some t_{n+1}^i , and when we are at the stage of finding an approximation $\tilde{y}(t)$ for $t \in [t_n, t_{n+1}]$, no approximation to $y(t_{n+1}^i - \tau(t_{n+1}^i))$ is available. Of course, if one relaxes these assumptions, there is a risk of explicit equations becoming implicit. In this case, one can get an accumulation of discontinuity points and then the method of steps would fail for certain DDEs.

2.5.1 Neutral Delay Differential Equations (NDDEs)

Definition 2.6 If f in (2.2) contains a derivative component with deviation τ , the DDE is called *neutral* delay differential equation (NDDE) and may take the form

$$\begin{aligned} y'(t) &= f(t, y(t), y(t - \tau), y'(t - \tau)), \quad t \geq t_0, \\ y(t) &= \psi(t), \quad t \leq t_0. \end{aligned} \quad (2.28)$$

If the two hypotheses of positivity and monotonicity of the delayed argument hold (for constant or variable lag with $\tau(t) \geq \tau^*$), then it is easily seen that the existence and uniqueness of the solution are guaranteed if the right-hand side function $f(t, y, x, w)$ is sufficiently smooth. Moreover, the problem of the location of the discontinuity points is clearly unchanged. Nevertheless, the presence of the neutral term $y'(t - \tau)$ prevents the smoothing of the solution at the discontinuity points ξ_k as the index k increases.

From a numerical perspective, one can use the derivative of the interpolant (or another type of approximation) to approximate the derivative of the delayed term. Formulae (2.23)–(2.24) can be modified to be suitable for NDDEs as follows:

$$\begin{aligned} Y_{n+1}^i &= \tilde{y}_n + h_{n+1} \sum_{j=1}^s a_{ij} f(t_{n+1}^j, Y_{n+1}^j, \hat{y}(t_{n+1}^j - \tau), \phi(t_{n+1}^j - \tau)), \quad i = 1, \dots, s, \\ \hat{y}(t_n + \theta h_{n+1}) &= \tilde{y}_n + h_{n+1} \sum_{i=1}^s b_i(\theta) f(t_{n+1}^i, Y_{n+1}^i, \hat{y}(t_{n+1}^i - \tau), \phi(t_{n+1}^i - \tau)), \quad 0 \leq \theta \leq 1, \end{aligned}$$

where $\phi(t - \tau)$ is an approximation to $y'(t - \tau)$, possibly being $\phi(t) = \hat{y}'(t)$. Of course, for $t \leq t_0$ we define $\hat{y}(t) = \psi(t)$ and $\phi(t) = \psi'(t)$.

We should note that we may create a problem by using the derivative of the interpolant $\hat{y}'(t)$ because we lose one order accuracy whenever we differentiate the interpolant.

If the delayed argument $t - \tau(t)$ does not satisfy the hypotheses of positivity and monotonicity, then we have problems for the location of the discontinuity points ξ_k as the index increases; the eventual accumulation of discontinuity points is a serious problem for the maintenance of the order of the accuracy of the numerical methods. Moreover, the existence and uniqueness of the solution is no longer such a trivial matter and, in general, may not be guaranteed. For numerical and theoretical analysis of NDDEs, we may refer to [20].

2.5.2 Equations with State-Dependent Lags

Definition 2.7 A DDE is *state dependent* if the lag τ is dependent on the solution $y(t)$; then, $\tau \equiv \tau(t, y(t))$. The DDE (2.2) then takes the form:

$$\begin{aligned} y'(t) &= f(t, y(t), y(t - \tau(t, y(t)))), \quad t \geq t_0, \\ y(t) &= \psi(t), \quad t \leq t_0. \end{aligned} \tag{2.29}$$

The difficulty in such a situation is that the locations of the jump discontinuities (which are characterized as the zeros of switching non-linear functions) depend on the (unknown) solution $y(t)$. Consequently, it is not possible to locate the discontinuity points a priori without any knowledge of the solution; see [21] and [8]. The difficulty of detecting the discontinuity points a priori makes the numerical solution of (2.29) a rather complicated task because it becomes very hard to include the discontinuity points in mesh Δ , which is important for accuracy requirements.

Consider, in some more detail, the case of strictly positive lag $\tau(t, y(t)) \geq \tau^* > 0$. It is convenient to choose the stepsize $h_{n+1} \leq \tau^*$, as the delayed term is previously known. A first adaptation of RK formulae (2.23)–(2.24) is

$$Y_{n+1}^i = \tilde{y}_n + h_{n+1} \sum_{j=1}^s a_{ij} f(t_{n+1}^j, Y_{n+1}^j, \hat{y}(t_{n+1}^j - \tau(t_{n+1}^j, Y_{n+1}^j))), \quad i = 1, \dots, s,$$

$$\hat{y}(t_n + \theta h_{n+1}) = \tilde{y}_n + h_{n+1} \sum_{i=1}^s b_i(\theta) f(t_{n+1}^i, Y_{n+1}^i, \hat{y}(t_{n+1}^i - \tau(t_{n+1}^i, Y_{n+1}^i))), \quad 0 \leq \theta \leq 1.$$

Along with the above RK formulae, to approximate the discontinuity points, we can use a root-finding routine (see Sect. 2.7.2) to solve in sequence the equation:

$$\xi_k - \tau(\xi_k, \hat{y}(\xi_k)) = \xi_{k-1}, \quad k \geq 1, \tag{2.30}$$

making use of the already computed continuous (extrapolation) approximation $\hat{y}(t)$ to the solution $y(t)$. However, apart from the possible non-uniqueness of the solution, in case the delayed argument $t - \tau(t, \hat{y}(t))$ is not monotonic, there is another problem to face: whenever we have a solved Eq. (2.30) and have found the approximation to the next discontinuity point ξ_k , we have necessarily already passed such a point ξ_k with our numerical integration. Therefore, unless it has been accidentally included in mesh Δ , a loss of accuracy has possibly occurred. To overcome this difficulty, more sophisticated strategies are necessary; see Willé and Baker [22].

Sometimes, in real-life applications, we may find DDEs or NDDEs with several delays. In this case, there are no particular additional difficulties with respect to (2.2) and (2.28). If all the lags are of the same type, the existence and uniqueness theorem as well as stability results can be easily modified to the more general situation; see [21].

2.5.3 Equation with a Small or Vanishing Lag

Consider DDE (2.2), where the lag $\tau(t)$ is variable and may vanish for some $t \in [t_0, T]$. Of course, $\tau(t)$ small is also a problem.

Definition 2.8 A DDE has vanishing lag $\tau(t)$, or a singular DDE, at point t^* if the lag satisfies $\tau(t^*) = 0$ (such that $\tau(t) > 0$ for all $t \neq t^*$).

To illustrate the previous definition, consider the simple *initial value delay differential equations* (IVDDEs):

$$\begin{aligned} y'(t) &= y(t - |t - 1|) \quad (t \geq 0), \\ y(0) &= \psi(0). \end{aligned} \tag{2.31}$$

Since $\tau(t) = |t - 1|$, this is a *varying-lag* and the point at which the lag vanishes is $\{t^*\} = \{1\}$.

Under the assumptions of positivity and monotonicity of the delayed argument $t - \tau(t)$, and for vanishing lag, there is one main problem for the numerical treatment of (2.2). We illustrate this problem through DDE (2.31): as the integration proceeds toward t^* , the discontinuity points become increasingly closer (they are at $0, \frac{1}{2}, \frac{3}{4}, \frac{15}{16}, \frac{31}{32}, \dots$) so that, at some points, the distance between each two successive points becomes smaller than the stepsize used by the numerical method. If $[t_n, t_{n+1}]$ is the underlying step of integration, an approximation $\hat{y}(t - \tau(t))$ of the delayed part $y(t - \tau(t))$ is already known only in the first part of the step and unknown in the rest of the step (with reference to RK method for DDEs (2.23)–(2.24), some of the quantities $\hat{y}(t_{i+1}^j - \tau(t_{i+1}^j))$ might be unknown and should be computed together with the stage values Y_{n+1}^i). Thus, if we assume that $0 \leq c_1 \leq c_2 \leq \dots \leq c_s \leq 1$ and if we define $c_0 = 0$ and the integer r , $0 \leq r \leq s - 1$, such that $t_{n+1}^r - \tau(t_{n+1}^r) \leq t_n < t_{n+1}^{r+1} - \tau(t_{n+1}^{r+1})$, then (2.23)–(2.24) could be modified into (see [23])

$$\begin{aligned} Y_{n+1}^i &= \tilde{y}_n + h_{n+1} \sum_{j=1}^r a_{ij} f(y_{n+1}^j, Y_{n+1}^j, \hat{y}(t_{n+1}^j - \tau(t_{n+1}^j))) \\ &\quad + h_{n+1} \sum_{j=r+1}^s a_{ij} f(t_{n+1}^j, Y_{n+1}^j, Z_{n+1}^j), \quad i = 1, \dots, s, \end{aligned} \tag{2.32}$$

$$\begin{aligned} Z_{n+1}^i &= \tilde{y}_n + h_{n+1} \sum_{j=1}^r b_j(\theta_{n+1}^i) f(t_{n+1}^j, Y_{n+1}^j, \hat{y}(t_{n+1}^j - \tau(t_{n+1}^j))) \\ &\quad + h_{n+1} \sum_{j=r+1}^s b_j(\theta_{n+1}^i) f(t_{n+1}^j, Y_{n+1}^j, Z_{n+1}^j), \quad i = r + 1, \dots, s, \end{aligned} \tag{2.33}$$

$$\begin{aligned}\widehat{y}(t_n + \theta h_{n+1}) &= \widetilde{y}_n + h_{n+1} \sum_{i=1}^r b_i(\theta) f(t_{n+1}^i, Y_{n+1}^i, \widehat{y}(t_{n+1}^i - \tau(t_{n+1}^i))) \quad (2.34) \\ &\quad + h_{n+1} \sum_{i=r+1}^s b_i(\theta) f(t_{n+1}^i, Y_{n+1}^i, Z_{n+1}^i), \quad 0 \leq \theta \leq 1.\end{aligned}$$

Here:

$$\theta_{n+1}^i = \frac{t_{n+1}^i - \tau(t_{n+1}^i) - t_n}{h_{n+1}}, \quad i = r+1, \dots, s,$$

and the unknown quantities $Z_{n+1}^i = \widehat{y}(t_{n+1}^i - \tau(t_{n+1}^i))$ play the role of additional stage values related to the delayed term. Clearly, even if the underlying RK method (2.9)–(2.10) is explicit, the resulting method (2.32)–(2.33)–(2.34) is implicit in the additional stage values Z_{n+1}^i .

Another problem, wherein one or more (or even infinitely many) discontinuity points ξ_k may lie inside the underlying step $[t_n, t_{n+1}]$, can also arise. This may breakdown the order p of the accuracy of the method.

In some cases, the lag $\tau(t)$ vanishes already at t_0 and it is strictly positive later. Thus, no discontinuity points are spread ahead and the solution $y(t)$ is determined solely by the initial value at t_0 . In this situation we have problems only in the first step of integration.

In case the retarded argument $t - \tau(t)$ is not monotone, the situation will become more difficult. The difference from the monotone case consists of the possible non-uniqueness of the solution of (2.3). Moreover, if the lag vanishes for some t^* , then we also have the phenomenon of the accumulation of discontinuity points. Thus, a priori control of the location of the discontinuity points becomes very difficult.

From the numerical point of view, it is quite clear that a constrained mesh strategy is almost always not possible, and the method of steps would fail for all kinds of DDEs with vanishing lag. For a deeper analysis for DDEs of this type, refer to Rihan [10] and Paul and Baker [6].

2.6 Stiffness Problems

Initial value problems (IVPs) with strongly decreasing and increasing solution components are called *stiff*, which exist in many real-life and bioscience problems [24]. Usually, a DDE is considered *stiff* when it contains processes of widely different time scale. From a computational perspective, stiffness implies that while solving numerically the corresponding IVP using a given method with assigned tolerance, the stepsize is restricted by stability requirements rather than accuracy demands. In [25], a DDE is classified as a stiff equation when certain implicit methods perform better than explicit ones. Reliable and suitable numerical schemes for treating stiff DDEs include *implicit*, *singly implicit* RK methods, and [26], *mono-implicit* RK methods

[27]. Moreover, a suitable routine is necessary to decide whether a given problem should be treated as stiff or as non-stiff. This routine is considered as an automatic stiffness detection and stepsize control for the two different algorithms: one of them to treat the stiff part and the other one for non-stiff part; see [28].

Example 2.3 Consider a singularly perturbed DDE, which is considered as a stiff problem,

$$\varepsilon y'(t, \varepsilon) = \lambda y(t, \varepsilon) + \mu y(t - \tau, \varepsilon), \quad t \geq 0, \quad y(t, \varepsilon) = \psi(t), \quad t \in [-\tau, 0]. \quad (2.35)$$

Suppose that the initial function $\psi(t)$ is smooth and $\lambda < 0$. Using method of steps, when $\psi(t) = c$ yields

$$y(t, \varepsilon) = \begin{cases} R_2 e^{\frac{\lambda}{\varepsilon} t} - cR_1, & 0 < t \leq \tau, \\ R_2 e^{\frac{\lambda}{\varepsilon} t} + R_2 \left[\frac{\mu}{\varepsilon} (t - \tau) - R_1 \right] e^{\frac{\lambda}{\varepsilon} (t - \tau)} + cR_1^2, & \tau < t \leq 2\tau, \\ R_2 e^{\frac{\lambda}{\varepsilon} t} + R_2 \left[\frac{\mu}{\varepsilon} (t - \tau) - R_1 \right] e^{\frac{\lambda}{\varepsilon} (t - \tau)} + \\ R_2 \left[\frac{\mu}{\varepsilon} \left(\frac{\mu}{2\varepsilon} (t - 2\tau)^2 - R_1(t - 2\tau) \right) + R_1^2 \right] e^{\frac{\lambda}{\varepsilon} (t - 2\tau)} - cR_1^3, & 2\tau < t \leq 3\tau, \\ R_2 e^{\frac{\lambda}{\varepsilon} t} + R_2 \left[\frac{\mu}{\varepsilon} (t - \tau) - R_1 \right] e^{\frac{\lambda}{\varepsilon} (t - \tau)} + \\ R_2 \left[\frac{\mu}{\varepsilon} \left(\frac{\mu}{2\varepsilon} (t - 2\tau)^2 - R_1(t - 2\tau) \right) + R_1^2 \right] e^{\frac{\lambda}{\varepsilon} (t - 2\tau)} + \\ R_2 \left\{ \frac{\mu}{\varepsilon} \left[\frac{2\mu}{2\varepsilon} \left(\frac{\mu}{3\varepsilon} (t - 3\tau)^3 - R_1(t - 3\tau)^2 \right) + R_1^2(t - 3\tau) \right] - R_1^3 \right\} e^{\frac{\lambda}{\varepsilon} (t - 3\tau)} + \\ cR_1^4, & 3\tau < t \leq 4\tau, \\ \vdots & \vdots \\ R_2 e^{\frac{\lambda}{\varepsilon} t} + R_2 R_1^5 e^{\frac{\lambda}{\varepsilon} (t - \tau)} + R_2 R_2^5 e^{\frac{\lambda}{\varepsilon} (t - 2\tau)} + R_2 R_3^5 e^{\frac{\lambda}{\varepsilon} (t - 3\tau)} + \\ R_2 R_4^5 e^{\frac{\lambda}{\varepsilon} (t - 4\tau)} + \cdots + R_2 R_{(n-1)}^5 e^{\frac{\lambda}{\varepsilon} (t - (n-1)\tau)} + (-1)^n cR_1^n, & (n-1)\tau < t \leq n\tau \end{cases} \quad (2.36)$$

where, for $\lambda < 0$, $R_1 = \frac{\mu}{\lambda}$, $R_2 = c(1 + R_1)$, and

$$R_n^5 = \left(\frac{\mu}{\varepsilon} \right)^n \frac{1}{n!} (t - n\tau)^n - \left(\frac{\mu}{\varepsilon} \right)^{(n-1)} \frac{R_1}{(n-1)!} (t - n\tau)^{(n-1)} + \left(\frac{\mu}{\varepsilon} \right)^{(n-2)} \frac{R_1^2}{(n-2)!} (t - n\tau)^{(n-2)} + \cdots + (-1)^n R_1^n.$$

When ε is very small, then the difference equation

$$y(t, 0) = -\frac{\mu}{\lambda} y(t - \tau, 0), \quad t > 0, \quad y(t, 0) = c, \quad t \in [-\tau, 0] \quad (2.37)$$

has the solution $y(t, 0) = \left(-\frac{\mu}{\lambda} \right)^n c$ for $t \in [(n-1)\tau, n\tau]$, $n = 1, 2, 3, \dots$, which is ascending if $|\mu| > |\lambda|$, and descending if $|\mu| < |\lambda|$.

We notice from (2.36) at $t = k\tau$, $k = 0, 1, 2, \dots$ that

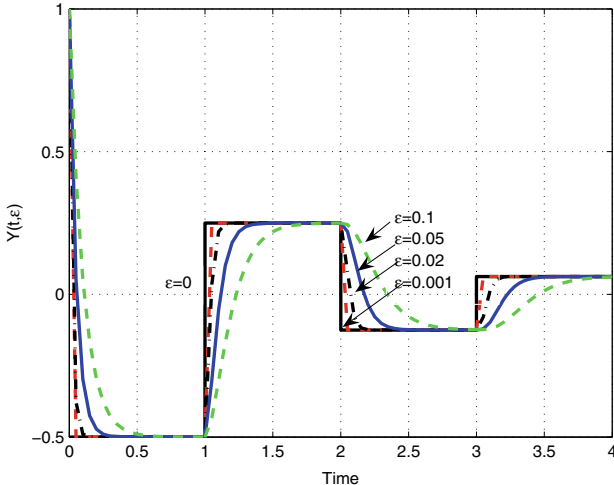


Fig. 2.1 Exact solutions $y(t, \varepsilon)$ of DDE $\varepsilon y'(t, \varepsilon) = \lambda y(t, \varepsilon) + \mu y(t - \tau, \varepsilon)$, $t \geq 0$; $y(t, \varepsilon) = 1$ when $t \leq 0$ for different values of ε compared with the degenerate solution $y(t, 0)$

$$\lim_{t \rightarrow (k\tau)_-} \left(\lim_{\varepsilon \rightarrow 0} y(t, \varepsilon) \right) \neq \lim_{\varepsilon \rightarrow 0} \left(\lim_{t \rightarrow (k\tau)_+} y(t, \varepsilon) \right). \quad (2.38)$$

Such non-uniform behavior usually occurs and propagates at $t = n\tau$ ($n = 0, 1, 2, \dots$) whenever the initial function $\psi(t)$ is not smooth at the initial points.

Therefore, the degenerate solution $y(t, 0)$ of (2.37) provides a very close approximation to $y(t, \varepsilon)$ for sufficiently small $\varepsilon > 0$. We also note from (2.36) and (2.37) that $\lim_{\varepsilon \rightarrow 0} y(t, \varepsilon) = y(t, 0)$ only when $\lambda < 0$ and $\psi(t) = c$ (any constant). However, if $\lambda > 0$ $\lim_{\varepsilon \rightarrow 0} y(t, \varepsilon) = y(t, 0)$ if and only if $\lambda = -\mu$. The true solution $y(t, \varepsilon)$ does not possess discontinuities for $t > 0$ and may smooth out, while the degenerate Eq. (2.37) only possesses a piecewise continuous solution. However, the true solution $y(t, \varepsilon)$ shows a boundary layer at the right side of each interval that gives rise to large derivatives (in the time) of the solution for small ε .

Figure 2.1 shows the exact solution of the stiff problem (2.35) compared with the solution of the degenerated equation,; while Fig. 2.2 displays the numerical solutions by using explicit and implicit schemes. The plots have a kink at $t = n\tau$ ($n = 1, 2, \dots$) because of the existence of the time-delay term.

In Chap. 4, we provide a subclass of implicit Runge-Kutta (IRK), called Mono-Implicit Runge-Kutta (MIRK) method for stiff DDEs and Volterra delay integro-differential equations. These schemes combine the accuracy of implicit method and efficient implementation. The schemes have been developed to reduce the computational cost of the fully implicit method, and they are efficient for both stiff and non-stiff initial value problems.

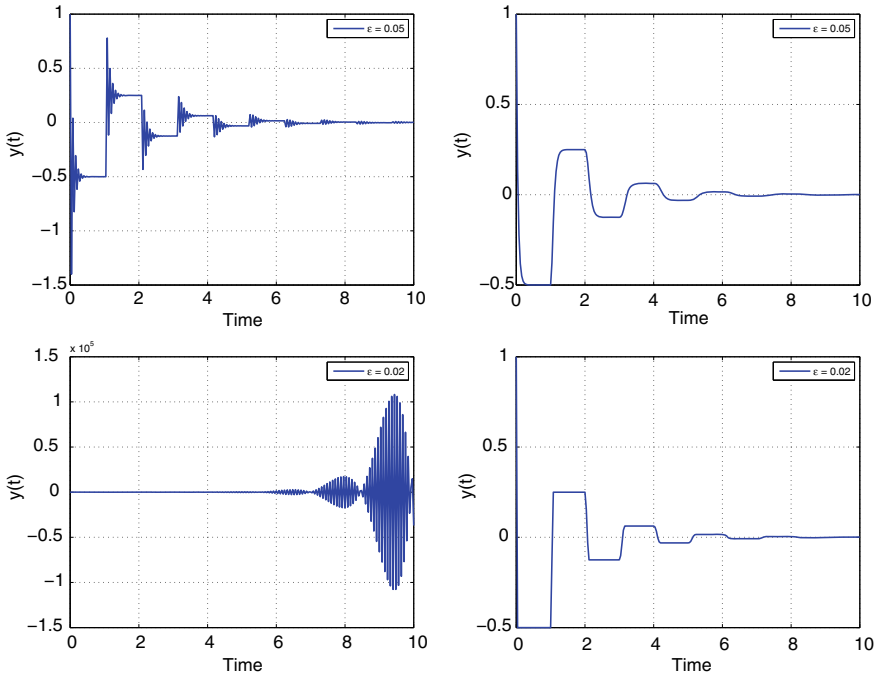


Fig. 2.2 Numerical simulations of DDE: $\varepsilon y'(t) = \lambda y(t) + \mu y(t - \tau)$, $t \geq 0$; $y(t) = 1$ for $t \leq 0$, using explicit scheme (left) of order 2 and implicit scheme (right) for the same order, with $\tau = 1 = mh$; $\lambda = -1$, $\mu = -0.5$, $m = 25$. when $\varepsilon = 0.05$ and 0.02 , respectively

2.7 Software Aspects

For numerical proposes, DDEs are replaced by ODEs along with an appropriate interpolation scheme to approximate $y(t - \tau)$. Then, software codes cannot be taken over from the theory of ODEs without any change. Stepsize must be adjusted to control the growth of the global error through local error estimates. Software codes should also be able to determine the location of the derivative jump discontinuities. In addition, numerical schemes must handle some details about the types of output desired, stiffness, etc.

2.7.1 Discretization Error

Software code must be able to approximate the desired solution values with reasonable accuracy. Since the exact solution is generally not known and cannot be calculated, the discretization error is usually estimated or bounded. There are two measures of the discretization error: (1) global error, and (2) local error.

Global error is the difference between the computed solution and the true solution determined by the original data at t_0 , i.e.,

$$e(t) = y(t) - \tilde{y}_h(t).$$

Here $y(t)$ is the exact solution of (2.2), and \tilde{y}_h is any numerical approximation of $y(t)$. Error estimates for (2.2) are then given by

$$\|y(t) - \tilde{y}_h(t)\| \leq C \cdot [|E_1(h)| + |E_2(h)|],$$

where $E_1(h)$ is the norm of the local error of the integration method, $E_2(h)$ is the norm of the interpolation error, and C is a constant. Consequently, if

$$E_1(h) = O(h^p) \quad \text{and} \quad E_2(h) = O(h^q), \quad \text{then}$$

$$\|y(t) - \tilde{y}_h(t)\| = O(h^{\min(p,q)}). \quad (2.39)$$

The orders p and q depend on how the primary discontinuities are treated; see [29].

Local error in ODEs is the error that would be produced in one step if the previous values were exact and if there were no roundoff errors. A local error consists of the local integration error and the local approximation (interpolation) error. More precisely, let $\tilde{y}_n(t)$ be the function of (2.2) so that *the local error* is then defined to be

$$d_n = z_{n+1} - \tilde{y}_h(t_{n+1}),$$

where z is the local solution of

$$\begin{aligned} z(t) &= f(t, z(t), \hat{u}(t - \tau)), \quad t \geq t_0, \\ z(t) &= \psi(t), \quad t \leq t_0, \end{aligned}$$

where \hat{u} is the numerical solution computed in advance. For further illustration, we consider local error of the form

$$\|d_n\| = O(h^{p+1}) + O(h^{q+1}), \quad (2.40)$$

where $O(h^{p+1})$ is the local error of the RK method of order p , and $O(h^{q+1})$ is the local approximation error.

2.7.2 Location of Jump Discontinuities

Consider the more general recurrence Eq. (2.30) and define $\alpha(t, y(t)) := t - \tau(t, y(t))$, then we have a switching function:

$$g(t) = \alpha(t, y(t)) - Z, \quad (2.41)$$

where $Z \in \{\xi_k\}$ is the location of the previous jump. The derivative jump discontinuities are the zeros of the non-linear switching function (2.41). We now describe the switching function method to determine the derivative jump discontinuities in the following algorithm:

Algorithm ([8]) The switching function algorithm finds the next derivative jump discontinuity that is used as a next grid point. If t_{n+1} is the most recent grid point, \tilde{y}_{n+1} is a numerical approximation to $y(t_{n+1})$, and ξ_h is a numerical approximation to an exact previous derivative jump discontinuity, then the algorithm is as follows:

1. If $[\alpha(t_n, \tilde{y}_n) - \xi_h] \times [\alpha(t_{n+1}, \tilde{y}_{n+1}) - \xi_h] > 0$, then proceed to the next jump integration step.
2. If $[\alpha(t_n, \tilde{y}_n) - \xi_h] \times [\alpha(t_{n+1}, \tilde{y}_{n+1}) - \xi_h] \leq 0$, then there is a derivative jump discontinuity in $[t_n, t_{n+1}]$. To locate this jump:
 - 2.1 Construct an interpolation polynomial $g_h(t)$ from $q + 1$ previous values of the discrete switching function:

$$g_h(t_i) = \alpha(t_i, y_i) - \xi_h, \quad i = n - q, \dots, n.$$

- 2.2 Use the bisection method to find the zero ξ_h of this polynomial in the extrapolated interval (t_n, t_{n+1}) and take ξ_h as an approximation to the exact root z of the continuous switching function $\alpha(t, y(t)) - \xi$.
- 2.3 Take $t_{n+1} = \xi_h$ as the next grid point.

□

2.7.3 Stepsize Control

Using an RK formula pair provides a practical way to estimate local error of a numerical method and to control the stepsize.

If \hat{y}_n and \tilde{y}_n denote the numerical approximations of the $(p + 1)$ th- and the p th-order formulae, respectively, then the difference $EST = \|\hat{y}_n - \tilde{y}_n\|$ estimates the local error of the integration process.

The strategy adapted for the stepsize control is to bind the local discretization error by a tolerance (TOL) per unit step. If $\|\cdot\|$ is the maximum norm, h_{old} is the

most recent stepsize, h_{new} is the next step to be taken, and h_{min} is the minimum step allowed by the routine, then the stepsize control algorithm¹ is as follows:

Algorithm This algorithm controls the stepsize for the Runge-Kutta (5,4) formulae. After each integration step:

1. Compute the estimate EST per unit step, i.e., $\|\tilde{y}_n - \tilde{y}_n\|$,
2. If $EST \leq TOL$, then

$factor = \min\{1.5, 0.9 * (TOL/EST)^{1/5}\}$,

$h_{new} = h_{old} * factor$,

$n = n + 1$,

go to start.
3. If $TOL < EST$, then

If the number of successive failures is less than three, then

$factor = \min\{1.5, 0.9 * (TOL/EST)^{1/5}\}$,

$h_{new} = h_{old} * factor$,

if $h_{new} < h_{min}$ user must increase TOL to continue

else

go to start.

If the number of successive failures is greater than or equal to three, then if

$h_{old} * 0.5 > h_{min}$, then

$h_{new} = h_{old} * 0.5$,

go to start

if $h_{old} * 0.5 \leq h_{min}$, user must increase TOL to continue.

□

2.7.4 Interpolation to $\tilde{y}(t)$

The value $y(t - \tau)$, of $y(t)$ at the delay $t - \tau$ (with all cases of the time-lag τ) can be computed from the dense output of the solution $\hat{y}(t)$ using the continuous extension process. The one-step interpolant can be constructed step-by-step by utilizing information from the underlying step $[t_n, t_{n+1}]$, possibly by including some additional stages. One can use Hermite interpolation [2], where the interpolant polynomial passes through the numerical solution $\tilde{y}(t)$, as well as its derivatives agree with $\tilde{y}'(t)$ at the support points, $t_n + r_i h_{n+1}$, $r_i \in [0, 1]$. A three-point² Hermite interpolation polynomial of degree ‘five’ can be considered to make the formula (2.39) of the same order as the (5,4) Runge-Kutta pair formulae (see Appendix A).

¹Restrictions are imposed on the rate at which the stepsize is allowed to decrease and increase: In Archi code, the stepsize is not allowed to increase if an accepted step was immediately proceeded by a rejected step.

²The best choice of fixed Hermite support points r_i is $\{0, \frac{1}{2}, 1\}$. We may require extra RK stages to get $\tilde{y}_{n+1/2}$ at $t = t_n + \frac{1}{2}h_{n+1}$; see [7].

2.7.5 DDE Solvers and Available Software

From a modeler's viewpoint, two historical periods in the production of numerical codes for delay equations can be distinguished. During the first period, a number of experimental codes were developed by modelers or numerical analysts. The second period can be characterized by the availability of more sophisticated DDE solvers. The major problems that the designers of such codes try to accommodate are automatic location or tracking of the discontinuities in the solution or its derivatives, efficient handling of any "stiffness" (if possible), dense output requirements, control strategy for the local and global error underlying the stepsize selection, the cost and consistency of interpolation technique for evaluating delayed terms.

The earliest, simple numerical methods for DDEs (2.2) utilized the *Euler* or classical fourth-order *RK* methods with a constant stepsize, supplemented with linear interpolation schemes for the retarded terms. Such adaptations provided minimally effective means for solving models numerically: they had no error control, used fixed stepsize, and had problems coping with "stiffness." Numerical analysts are now able to cite published algorithms for the numerical solution of DDEs. Several packages and software are available for the numerical integration and/or the study of bifurcations in DDEs. The following is a short list of available software:

- Archi (Paul [30]) simulates a large class of functional differential equations.
- DDE23 (Shampine, S. Thompson [31]) simulates retarded differential equations with several fixed discrete delays.
- RADAR5 (Guglielmi, Hairer [32]) simulates stiff problems, including differential-algebraic and neutral delay equations with constant or state-dependent (eventually vanishing) delay.
- DLAG6 (Thompson [33]) simulates retarded and neutral differential equations with state-dependent delays.
- MIDDE (Rihan, et al. [27]) simulates stiff and non-stiff delay differential equations and Volterra delay integro-differential equations using mono-implicit RK methods.
- BIFDD (Hassard [34]) (Fortran 77) allows normal form analysis of Hopf bifurcations of differential equations with several fixed discrete delays.
- DDE-BIFTOOL (Engelborghs [35]) (MATLAB) allows computation and stability analysis of steady-state solutions, their fold and Hopf bifurcations, and periodic solutions of differential equations with several fixed discrete delays.

2.8 Concluding Remarks

We have discussed how formulae for ODEs can be adapted to solve various types of DDEs. Next, we describe some concepts of the stability of various schemes for linear and non-linear delay differential models and sufficient conditions for contractivity of the solutions.

References

1. Neves, K.W.: Automatic integration of functional differential equations: an approach. *ACM Trans. Math. Softw.* **1**, 369–371 (1975)
2. Oberle, H.J., Pesch, H.J.: Numerical treatment of delay differential equations by Hermite interpolation. *Numer. Math.* **37**, 235–255 (1981)
3. Oberle, H.J., Pesch, H.J.: Stepsize control for delay differential equations using continuously imbedded Runge-Kutta methods of Sarafyan. *J. Comput. Appl. Math.* **31**(2), 267–275 (1990)
4. Thompson, S.: Root-finding and interpolation with Runge-Kutta-Sarafyan methods. *Trans. Soc. Comput. Simul.* **2**(3), 207–218 (1985)
5. Bellen, A., Zennaro, M.: Numerical solution of delay differential equations by uniform corrections to an implicit Runge-Kutta method. *Numer. Math.* **47**
6. Bellen, A., Zennaro, M.: Explicit Runge-Kutta methods for numerical solution of singular delay differential equations. In: Numerical Analysis Report MCCM report No. 212, University of Manchester (1992)
7. Bellen, A., Zennaro, M.: Some practical Runge-Kutta formulas. *Math. Comput.* **46**, 135–150 (1986)
8. Neves, K.W., Feldstein, A.: High order methods for state-dependent delay differential equations with non-smooth solutions. *SIAM J. Numer. Anal.* **21**, 339–343 (1984)
9. Neves, K.W., Feldstein, A.: Characterization of jump discontinuities for state dependent delay differential equations. *J. Math. Anal.* **56**, 689–707 (1976)
10. Rihan, F.A.: Numerical Treatment of Delay Differential Equations in Bioscience. University of Manchester, UK (2000).Ph.D. Thesis
11. Elsgolt's, L.E., Norkin, S.B.: Introduction to the theory and application of differential equations with deviating arguments
12. Cryer, C.W.: Numerical methods for functional differential equations. In: Schmitt, K. (ed.) *Delay and Functional Differential Equations*
13. Butcher, J.C.: *The Numerical Analysis of Ordinary Differential Equations*. Wiley, London (1987)
14. Hairer, E., Nørsett, S.P., Wanner, G.: *Solving Ordinary Differential Equations i, Nonstiff Problems*. Springer, Berlin (1993)
15. Hairer, E., Wanner, G.: *Solving Ordinary Differential Equations ii, Stiff Problems*. Springer, New York (1997)
16. Lambert, J.D.: *Numerical Methods for Ordinary Differential Systems*. Wiley, Chichester (1991)
17. Lambert, J.D.: Natural Runge-Kutta and projection methods. *Numer. Math.* **53**, 423–438 (1989)
18. Zennaro, M.: Natural continuous extensions of Runge-Kutta methods delays. *Math. Comp. Appl.* **46** (1986)
19. Shampine, L.F.: Interpolation for Runge-Kutta methods **22**, 1014–1026 (1985)
20. Bellen, A., Jaciewicz, Z., Zennaro, M.: Stability analysis of one-step methods for neutral delay-differential equations. *Numer. Math.* **52**, 605–619 (1988)
21. Baker, C.T.H., Paul, C.A.H., Willé, D.R.: Issues in the numerical solution of evolutionary delay differential equations. *Adv. Comp. Math.* **3**, 171–196 (1995)
22. Willé, D.R., Baker, C.T.H.: The tracking of derivative discontinuities in system of delay differential equations. *Appl. Numer. Math.* **9**, 209–222 (1992)
23. Willé, D.R., Baker, C.T.H.: *Delay Differential Equations: Theory and Numerics*. OUP, Oxford (1995)
24. Bocharov, G.A., Marchuk, G.I., Romanyukha, A.A.: Numerical solution by LMMs of stiff delay differential systems modelling an immune responses. *Numer. Math.* **73**, 131–148 (1996)
25. Faroogi, Z.H., Mohler, R.: Distribution models of recirculating lymphocytes. *IEEE. Trans. Biomed. Eng.* **36**, 355–362 (1999)
26. Faroogi, Z.H., Mohler, R.: The adaptation of STRIDE to delay differential equations. *Appl. Numer. Math.* **9**, 415–425 (1992)

27. Rihan, F.A., Doha, E.H., Hassan, M.I., Kamel, N.M.: Mono-implicit Runge-Kutta method for delay differential equations. *J. Egypt. Math. Soc.* **17**(2), 213–232 (2009)
28. Rihan, F.A., Doha, E.H., Hassan, M.I., Kamel, N.M.: Numerical treatments for Volterra delay integro-differential equations. *Comput. Methods Appl. Math. (CMAM)* **9**(3), 292–308 (2009)
29. Arndt, H.: Numerical solution of retarded initial value problems: local and global error and stepsize control. *Numer. Math.* **34**, 343–360 (1984)
30. Paul, C.A.H.: A user-guide to archi: An explicit runge-kutta code for solving delay and neutral differential equations and parameter estimation problems. In: MCCM Technical Report 283, University of Manchester (1997)
31. Shampine, L.F., Thompson, S.: Solving ddes in matlab. *Appl. Numer. Math.* **37**, 441–458 (2001)
32. Guglielmi, N., Hairer, E.: Implementing radau ii-a methods for stiff delay differential equations. *J. Comput. Math.* **67**, 1–12 (2001)
33. Corwin, S.P., Sarafyan, D., Thompson, S.: DKLAG6: a code based on continuously embedded sixth-order runge-kutta methods for the solution of state-dependent functional differential equations. *Appl. Numer. Math.* **24**, 317–330 (1997)
34. Hassard, B.D., Kazarinoff, N.D., Wan, Y.H.: Theory and Applications of Hopf Bifurcation. London Mathematical Society Lecture Note Series 41. Cambridge University Press, Cambridge (1981)
35. Engelborghs, K., Luzyanina, T., Samaey, G.: DDE-BIFTOOL v. 2.00: a Matlab package for bifurcation analysis of delay differential equations (2001)

Chapter 3

Stability Concepts of Numerical Solutions of Delay Differential Equations



3.1 Introduction

In this chapter, we discuss the stability properties of the numerical methods described in the previous chapter. In particular, we derive the stability regions of the solutions (Sect. 3.2). Sufficient conditions for the contractivity of the solutions are also discussed (Sect. 3.3).

The classical stability analysis of a differential equation with constant coefficients requires testing a *characteristic polynomial* to see if all its roots have a negative real part. Polynomials with this property are commonly termed *Hurwitz polynomials* and they correspond to stable systems. From the numerical analysis perspective, the stability of a difference equation (which may come from the approximation of a differential equation) is governed by an associated characteristic polynomial. The solutions of a difference equation decay to zero as the index tends to infinity if all the roots of the characteristic polynomial are (absolute value) smaller than *unity*. Polynomials of this type are termed *Schur polynomials*. It is quite possible that the difference equation may be unstable even though the differential equation is stable. In any case, it is important to know the stability properties of both the differential and the difference equations.

3.2 Stability of Numerical Methods for DDEs

In this section, we briefly describe the theory of stability of the step-by-step numerical methods of DDEs that have been discussed in Chap. 2. A special emphasis is given to stability regions and contractivity concepts of Runge-Kutta (RK) methods for DDEs and NDDEs. There are many concepts of stability of DDEs, which are based on different test equations (see, e.g., [1–4]). Equation (1.21) can be solved by a

step-by-step ODE integrator provided that the solution is unknown up to the current integration point. We need the dense output of the continuous ODE integrator for the standard initial value problem:

$$\begin{aligned} y'(t) &= f(t, y(t)), \quad t \geq t_0, \\ y(t_0) &= y_0. \end{aligned} \quad (3.1)$$

(The discontinuity points ξ_i of the DDE (1.21) can be recursively detected by solving $\xi_i - \tau(\xi_i) = \xi_{i-1}$, $\xi_0 = t_0$.)

The standard form of the RK method for the initial value problem (3.1) is

$$Y_{n+1}^i = \tilde{y}_n + h_{n+1} \sum_{j=1}^v a_{ij} f(t_{n+1}^j, Y_{n+1}^j), \quad i = 1, \dots, v, \quad (3.2)$$

$$\tilde{y}_{n+1} = \tilde{y}_n + h_{n+1} \sum_{i=1}^v b_i f(t_{n+1}^i, Y_{n+1}^i), \quad (3.3)$$

where

$$t_{n+1}^i = t_n + c_i h_{n+1}, \quad \frac{\mathbf{c} | \mathbf{A}}{\mathbf{b}}, \quad c_i = \sum_{j=1}^v a_{ij}, \quad i = 1, \dots, v, \quad \text{and} \quad h_{n+1} = t_{n+1} - t_n.$$

The *abscissae* c_i for most common methods belong to $[0, 1]$.

We recall that the *continuous* extension $\hat{y}(t + \theta h_{n+1})$ of a numerical solution \tilde{y}_n is defined, in each subinterval determined by mesh Δ , by a one-step continuous quadrature rule of the form

$$\hat{y}(t_n + \theta h_{n+1}) = \tilde{y}_n + h_{n+1} \sum_{i=1}^s b_i(\theta) f(t_{n+1}^i, Y_{n+1}^i), \quad 0 \leq \theta \leq 1, \quad (3.4)$$

where

$$Y_{n+1}^i = \tilde{y}_n + h_{n+1} \sum_{j=1}^s a_{ij} f(t_{n+1}^j, Y_{n+1}^j), \quad i = 1, \dots, v, \dots, s. \quad (3.5)$$

The polynomials $b_i(\theta)$ satisfy $b_i(0) = 0$ and $b_i(1) = b_i$, $i = 1, 2, \dots, s$.

The standard adaptation of a *continuous* RK method to DDE (1.21) has the form

$$Y_{n+1}^i = \tilde{y}_n + h_{n+1} \sum_{j=1}^s a_{ij} f(t_{n+1}^j, Y_{n+1}^j, \hat{y}(t_{n+1}^j - \tau)), \quad i = 1, \dots, s, \quad (3.6)$$

$$\widehat{y}(t_n + \theta h_{n+1}) = \widetilde{y}_n + h_{n+1} \sum_{i=1}^s b_i(\theta) f(t_{n+1}^i, Y_{n+1}^i, \widehat{y}(t_{n+1}^j - \tau)), \quad 0 \leq \theta \leq 1. \quad (3.7)$$

3.2.1 Stability Regions for DDEs: P-stability and GP-stability

Consider a simple delay model of the form

$$\begin{aligned} y'(t) &= \lambda y(t) + \mu y(t - \tau), \quad t \geq t_0, \\ y(t_0) &= \psi(t), \quad t \leq t_0. \end{aligned} \quad (3.8)$$

We start our analysis with some definitions of stability based on the simplest test equations (3.8), with “constant” delay, which leads to the concepts of *P-stability* and *GP-stability* (defined by Barwell [5]) as a generalization of the concept of *A-stability* of ODEs.

Definition 3.1 [5] The *P-stability region* of a numerical step-by-step method for the linear DDE (3.8) is the set S_P of the pairs of complex (α, β) , $\alpha = h\lambda$, $\beta = h\mu$, such that the discrete solution $\{\widetilde{y}_n\}_{n \geq 0}$ of (3.8) is uniformly bounded for all constant lags τ and all initial functions $\psi(t)$ and for any constant stepsize $h > 0$ under the constraint

$$h = \tau/m, \quad m \in \mathbb{N}. \quad (3.9)$$

A sufficient condition of P-stability is given in the following definition:

Definition 3.2 A numerical step-by-step method for DDEs is P-stable if

$$S_P \supseteq \{(\alpha, \beta) \in \mathbb{C}^2 \mid Re(\alpha) + |\beta| < 0\}.$$

If we drop the restriction (3.9), then we obtain the definition of *GP-stability*:

Definition 3.3 A numerical method for linear DDEs (3.8) is called GP-stable if $\{\widetilde{y}_n\}_{n \geq 0}$ of (3.8) is uniformly bounded for all constant lag τ , for all initial functions $\psi(t)$, and for any constant stepsize $h > 0$.

It is obvious that $S_{GP} \subseteq S_P$; thus, *GP-stable* is *P-stable* as well. Furthermore, the *P-stable* method for DDEs is *A-stable* for ODEs.

To study the stability of the RK method for DDEs such as (3.8) with constant lag τ , we consider two cases here:

- (i) When we do not require a separate continuous extension formulae to approximate the retarded term $y(t - \tau)$. In this case, under condition (3.9) (i.e., $\tau = mh$), when $\widetilde{y}(nh + c_i h - \tau)$ is required, it is possible to refer to it as the previous internal stage value \widetilde{y}_{n-m} such that $c_i \in [0, 1]$. Let us, for simplicity, use K's formulae of the RK method for solving DDEs:

$$\begin{aligned} K_{n+1}^i &= f(t_n + c_n h, \tilde{y}_n + h \sum_{j=1}^s a_{ij} K_{n+1}^j, \tilde{y}_{n-m+1}), \quad i = 1, \dots, s, \\ \tilde{y}_{n+1} &= \tilde{y}_n + h \sum_{i=1}^s b_i K_{n+1}^i. \end{aligned} \quad (3.10)$$

Applying this method for Eq. (3.8), we get the recurrence form

$$\tilde{y}_{n+1} = [1 + \lambda h \mathbf{b}^T (\mathbf{I} - \lambda h \mathbf{A})^{-1} \mathbf{e}] \tilde{y}_n + \mu h \mathbf{b}^T (\mathbf{I} - \lambda h \mathbf{A})^{-1} \tilde{\mathbf{y}}_{n-m}, \quad (3.11)$$

in which $\tilde{\mathbf{y}}_{n-m}$ is a vector consisting of “back-values” $\tilde{y}(nh + c_i h - \tau)$. Equation (3.11) can be written in the form

$$\tilde{y}_{n+1} = r(\lambda h) \tilde{y}_n + \mu h \mathbf{b}^T \mathbf{S} \tilde{\mathbf{y}}_{n-m}, \quad (3.12)$$

where $r(z) := 1 + z \mathbf{b}^T \mathbf{S} \mathbf{e}$, $\mathbf{S} \equiv \mathbf{S}(\lambda h) = (\mathbf{I} - \lambda h \mathbf{A})^{-1}$, and $\mathbf{e} = [1, \dots, 1]^T \in \mathbb{R}^s$.

Corollary 3.1 *The improved Euler method for Eq. (3.8), defined by $\mathbf{b} = [1/2, 1/2]^T$, $\mathbf{A} = \begin{bmatrix} 0 & 0 \\ 1 & 0 \end{bmatrix}$, with $\tau = mh$ gives*

$$\tilde{y}_{n+1} = \left(1 + \alpha + \frac{\alpha^2}{2}\right) \tilde{y}_n + \frac{\beta}{2} \tilde{y}_{n-m+1} + \frac{\beta(1 + \alpha)}{2} \tilde{y}_{n-m}, \quad (3.13)$$

which is asymptotically stable, provided that all the roots of the characteristic equation

$$\xi^{m+1} - \left(1 + \alpha + \frac{\alpha^2}{2}\right) \xi^m - \frac{\beta}{2} \xi - \frac{\beta}{2} (1 + \alpha) = 0$$

are in the unit circle, where $\alpha = \lambda h$ and $\beta = \mu h$.

Corollary 3.2 *If we drop condition (3.9) and suppose that $\tau = (m + \theta)h$, $m \in \mathbb{N}$ and $\theta \in [0, 1]$, then Eq. (3.11) (with the linear interpolation $\tilde{y}(t_{n-m} - \theta h) = \theta \tilde{y}_{n-m-1} + (1 - \theta) \tilde{y}_{n-m}$) takes the form:*

$$\begin{aligned} \tilde{y}_{n+1} &= \left[1 + \frac{\lambda \tau}{m + \theta} \mathbf{b}^T \left(\mathbf{I} - \frac{\lambda \tau}{m + \theta} \mathbf{A}\right)^{-1}\right] \tilde{y}_n + \\ &\quad \frac{\mu \tau}{m + \theta} \mathbf{b}^T \left(\mathbf{I} - \frac{\lambda \tau}{m + \theta} \mathbf{A}\right)^{-1} [\theta \tilde{y}_{n-m-1} + (1 - \theta) \tilde{y}_{n-m}]. \end{aligned} \quad (3.14)$$

By way of example, the explicit Euler method for the simple DDE,

$$y'(t) = \lambda y(t) + \mu y(t - 1), \quad t \geq 0, \quad (3.15)$$

gives ($\tau = 1 = (m + \theta)h$)

$$\tilde{y}_{n+1} = \left\{ 1 + \frac{\lambda}{m + \theta} \right\} \tilde{y}_n + \frac{\mu}{m + \theta} \left\{ \theta \tilde{y}_{n-m-1} + (1 - \theta) \tilde{y}_{n-m} \right\}.$$

Then, stability conditions can be determined from the characteristic equation

$$\xi^{m+2} - \left(1 + \frac{\lambda}{m + \theta} \right) \xi^{m+1} - \frac{\mu(1 - \theta)}{m + \theta} \xi - \frac{\mu\theta}{m + \theta} = 0,$$

whereas the characteristic equation (with $\alpha = \lambda h$, $\beta = \mu h$, and $h = \tau/(m + \theta)$) due to application of implicit Euler method into (3.15) is

$$\xi^{m+1} - \frac{1}{1 - \alpha} \xi^m - \frac{\beta(1 + \theta)}{1 - \alpha} \xi - \frac{\theta\beta}{1 - \alpha} = 0.$$

The characteristic equation arising from the application of the improved Euler method for solving (3.15) is

$$\xi^{m+1} - \left(1 + \alpha + \frac{\alpha^2}{2} \right) \xi^m + \frac{\beta}{2} \xi^2 - \frac{\beta}{2} (1 - \alpha\theta) \xi - \frac{\beta}{2} (1 + \alpha)(1 + \theta) = 0.$$

Applying the trapezium rule to (3.15) produces the characteristic equation

$$\left(1 - \frac{\alpha}{2} \right) \xi^{m+2} - \left(1 + \frac{\alpha}{2} \right) \xi^{m+1} - \frac{\beta}{2} (1 - \theta) \xi^2 - \frac{\beta}{2} \xi - \frac{\beta}{2} \theta = 0.$$

In practice, derivation of the stability regions of the DDEs, depending on lag τ , is very useful. Graphs in Figs. 3.1, 3.3, 3.4, and 3.5 show the stability regions of the DDEs (3.15), with stepsize $h = \tau/(m + \theta)$, in the (λ, μ) -plane for different methods (such as explicit, implicit, and improved Euler methods as well as the trapezium rule method), using the boundary locus technique [6]. The degree of sensitivity to θ can also be noted from the same graphs. On the other hand, Fig. 3.2 illustrates the behavior of the solutions of the DDE (3.15) using explicit and implicit Euler methods.

- (ii) When relying on the internal stage values to approximate the retarded term $y(t - \tau)$. In this case, under the condition (3.9), we use the *natural continuous extension NCE* for the approximation of the retarded part $\tilde{y}(nh + c_i h - \tau) := \hat{y}(t_{n-m} + c_i h)$:

$$\hat{y}(t_{n-m} + c_i h) = \tilde{y}_{n-m} + h \sum_{j=1}^s b_j(c_i) K_{n-m+1}^j, \quad 0 \leq c_i \leq 1. \quad (3.16)$$

By putting $b_{ij} = b_j(c_i)$, we get the $s \times s$ matrix $\mathbf{B} = \{b_{ij}\}$ and we can conclude that the RK method for DDEs, applied to the test problem (3.8) with constant stepsize h satisfying the constrain (3.9), is

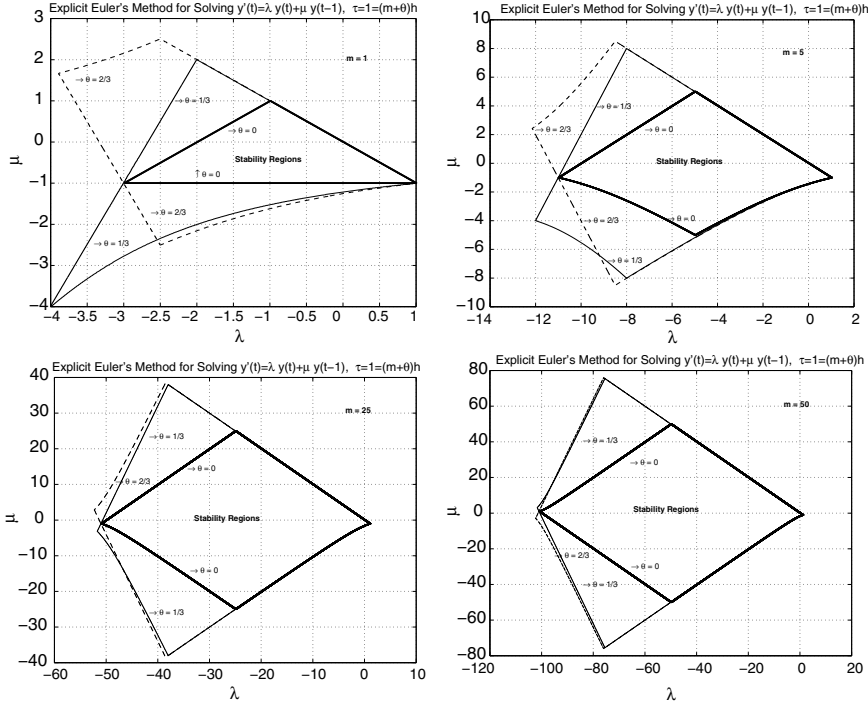


Fig. 3.1 Stability regions in the (λ, μ) -plane for the explicit Euler method when solving $y'(t) = \lambda y(t) + \mu y(t - 1)$ with $h = 1/(m + \theta)$

$$\begin{aligned} K_{n+1}^i &= \lambda \left(\tilde{y}_n + h \sum_{j=1}^s a_{ij} K_{n+1}^j \right) + \mu \left(\tilde{y}_{n-m} + h \sum_{j=1}^s b_{ij} K_{n-m+1}^j \right), \quad i = 1, \dots, s, \\ \tilde{y}_{n+1} &= \tilde{y}_n + h \sum_{i=1}^s b_i K_{n+1}^i. \end{aligned} \tag{3.17}$$

Put $\mathbf{K}_i = [K_i^1, \dots, K_i^s]^T$; hence, (3.17) takes the form

$$\begin{aligned} \mathbf{K}_{n+1} &= \lambda (\tilde{y}_n \mathbf{e} + h \mathbf{A} \mathbf{K}_{n+1}) + \mu (\tilde{y}_{n-m} \mathbf{e} + h \mathbf{B} \mathbf{K}_{n-m+1}), \\ \tilde{y}_{n+1} &= \tilde{y}_n + h \mathbf{b}^T \mathbf{K}_{n+1}. \end{aligned} \tag{3.18}$$

Then, by putting $\Phi_n = [\tilde{y}_n, h \mathbf{K}_n^T]^T$, this pair of equations can be reduced to the following recurrence relation with constant coefficients for the sequences of $(s + 1)$ -dimensional vectors:

$$\Phi_{n+1} = \mathbf{P}(\alpha) \Phi_n + \beta \mathbf{Q}(\alpha) \Phi_{n-m+1} + \beta \mathbf{R}(\alpha) \Phi_{n-m}, \tag{3.19}$$

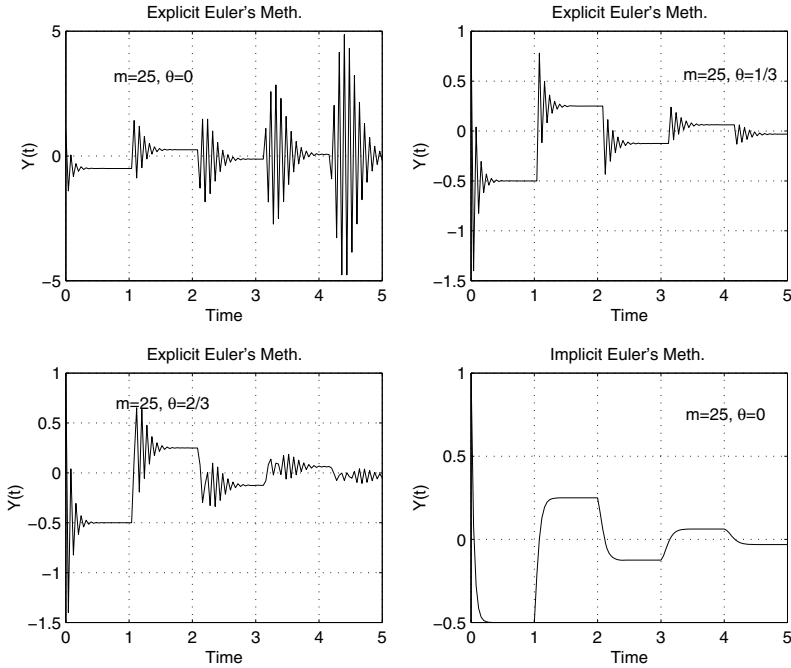


Fig. 3.2 Numerical solutions of DDE $y'(t) = \lambda y(t) + \mu y(t - 1)$, $t \geq 0$; $y(t) = 1$ for $t \leq 0$ and with $\tau = 1 = (m + \theta)h$; $\lambda = -40$, $\mu = -20$

where

$$\mathbf{P}(\alpha) = \begin{bmatrix} r(\alpha) & 0 \\ \alpha \mathbf{Se} & \mathbf{O} \end{bmatrix}, \quad \mathbf{Q}(\alpha) = \begin{bmatrix} 0 & \mathbf{b}^T \mathbf{S} \mathbf{B} \\ \mathbf{O} & \mathbf{S} \mathbf{B} \end{bmatrix}, \quad \mathbf{R}(\alpha) = \begin{bmatrix} \mathbf{b}^T \mathbf{S} \mathbf{e} & 0 \\ \mathbf{S} \mathbf{e} & \mathbf{O} \end{bmatrix},$$

$\mathbf{B} = [b_j(c_i)]_{i,j=1}^s$, $\mathbf{e} = [1, \dots, 1]^T \in \mathbb{R}^s$ and \mathbf{O} is the zero matrix $\in \mathbb{R}^{s \times s}$.

The asymptotic behavior of the solution of (3.19) is determined by the roots ξ of its characteristic equation:

$$\det[\xi^{m+1} \mathbf{I} - \xi^m \mathbf{P}(\alpha) - \xi \beta \mathbf{Q}(\alpha) - \beta \mathbf{R}(\alpha)] = 0. \quad (3.20)$$

For stability of (3.19), we require the zeros $\{\xi_i\}$ of (3.20) to satisfy the Neumann root condition ($|\xi_i| \leq 1$).

3.2.2 Stability Regions for Linear NDDEs

The above analysis of the stability of the numerical method can be extended to the NDDE (1.17).

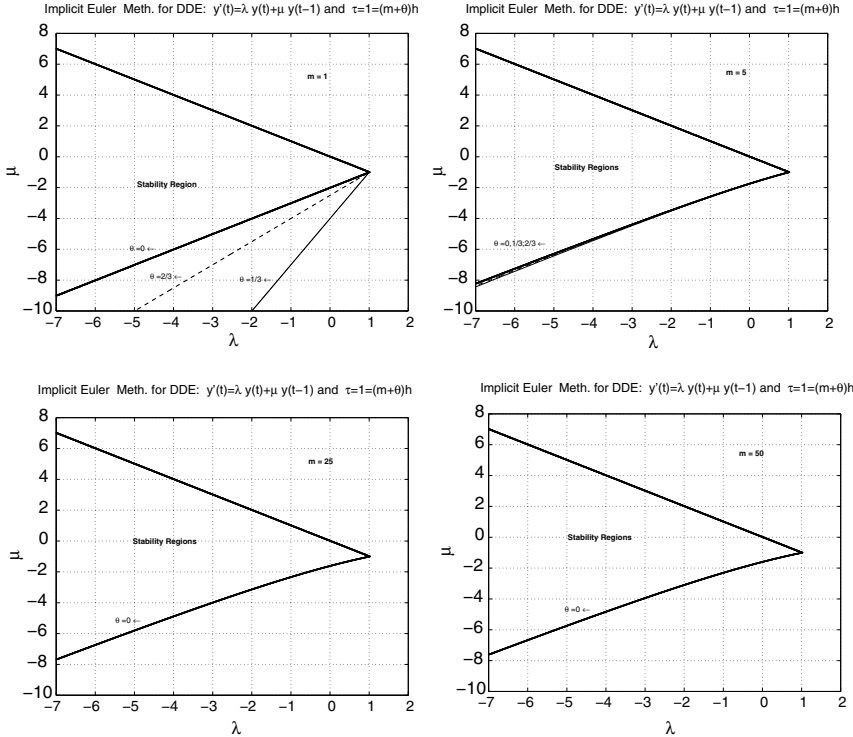


Fig. 3.3 Stability regions in the (λ, μ) -plane for the implicit Euler method when solving the DDE $y'(t) = \lambda y(t) + \mu y(t - 1)$ with $h = 1/(m + \theta)$

Let $\alpha = \lambda h$, $\beta = \mu h$, and $\gamma = vh$, where $\{\tilde{y}_n\}_{n \geq 0}$ denotes the discrete solution obtained from application of RK method to the NDDE (1.17) with $\tau = mh$ for some $m \in \mathbb{N}$. We now introduce the following definition:

Definition 3.4 Suppose $\tau = mh$ for some $m \in \mathbb{N}$. RK method for NDDE (1.17) with stepsize h is said to be stable for given (α, β, γ) if $\{\tilde{y}_n\}_{n \geq 0}$ is uniformly bounded. The region of stability of (1.17) is the set of all values (α, β, γ) for which (1.17) is stable. The method is said to be NP-stable if the region of stability contains the set:

$$S_{NP} \supseteq \{(\alpha, \beta, \gamma) : |\alpha\bar{\gamma} - \bar{\beta}| + |\alpha\gamma + \beta| < -2Re(\alpha)\}.$$

Applying the RK method for the test equation (1.17), with constant stepsize h satisfying the constraint (3.9), gives

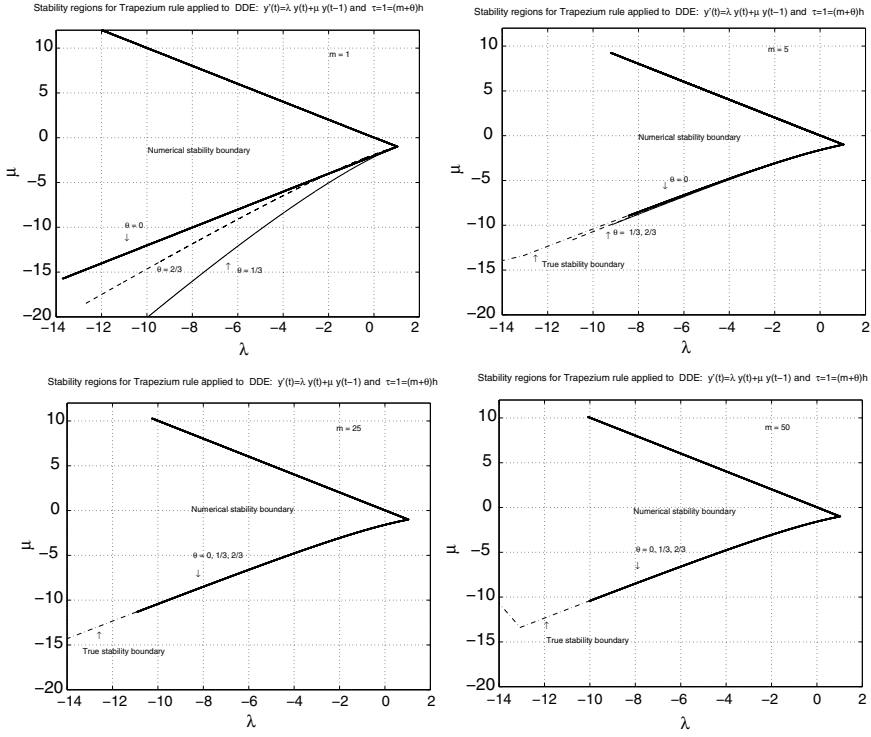


Fig. 3.4 Stability regions in the (λ, μ) -plane for the trapezium method when solving the DDE $y'(t) = \lambda y(t) + \mu y(t-1)$ with $h = 1/(m+\theta)$

$$\begin{aligned} K_{n+1}^i &= \lambda \left(\tilde{y}_n + h \sum_{j=1}^s a_{ij} K_{n+1}^j \right) + \mu \left(\tilde{y}_{n-m} + h \sum_{j=1}^s b_{ij} K_{n-m+1}^j \right) + v \left(h \sum_{j=1}^s c_{ij} K_{n-m+1}^j \right), \\ \tilde{y}_{n+1} &= \tilde{y}_n + h \sum_{i=1}^s b_i K_{n+1}^i. \end{aligned} \quad (3.21)$$

Using the notation of the above section, (3.21) takes the form

$$\begin{aligned} \mathbf{K}_{n+1} &= \lambda (\tilde{\mathbf{y}}_n \mathbf{e} + h \mathbf{A} \mathbf{K}_{n+1}) + \mu (\tilde{\mathbf{y}}_{n-m} \mathbf{e} + h \mathbf{B} \mathbf{K}_{n-m+1}) + v (h \mathbf{C} \mathbf{K}_{n-m+1}), \\ \tilde{y}_{n+1} &= \tilde{y}_n + h \mathbf{b}^T \mathbf{K}_{n+1}, \end{aligned} \quad (3.22)$$

where $\mathbf{C} := \{c_{ij}\} = [b_j'(c_i)]_{i,j=1}^s$. Then, these equations can be reduced to the recurrence:

$$\Phi_{n+1} = \mathfrak{P} \Phi_n + \mathfrak{Q} \Phi_{n-m+1} + \beta \mathfrak{R} \Phi_{n-m}, \quad (3.23)$$

where

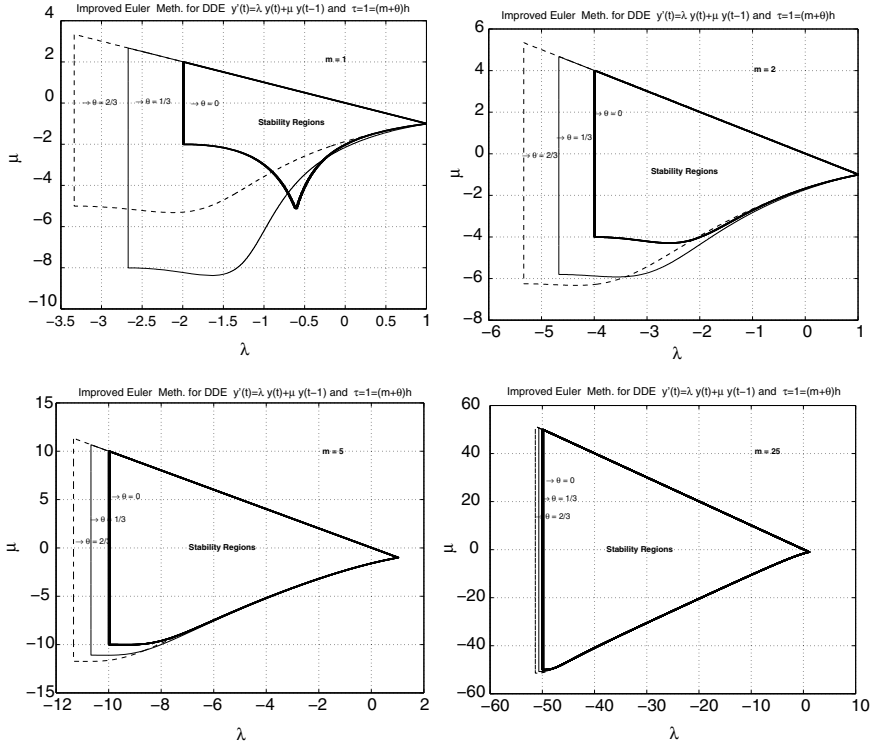


Fig. 3.5 Stability regions on the (λ, μ) -plane for the improved Euler method when solving the DDE $y'(t) = \lambda y(t) + \mu y(t-1)$ with $h = 1/(m+\theta)$

$$\mathfrak{P} = \begin{bmatrix} r(\alpha) & 0 \\ \alpha \mathbf{S} \mathbf{e} & \mathbf{O} \end{bmatrix}, \quad \mathfrak{Q} = \begin{bmatrix} 0 & \mathbf{b}^T \mathbf{S} (\beta \mathbf{B} + \gamma \mathbf{C}) \\ \mathbf{O} & \mathbf{S} (\beta \mathbf{B} + \gamma \mathbf{C}) \end{bmatrix}, \quad \mathfrak{R} = \begin{bmatrix} \mathbf{b}^T \mathbf{S} \mathbf{e} & 0 \\ \mathbf{S} \mathbf{e} & \mathbf{O} \end{bmatrix}.$$

Then, the asymptotic behavior of the solution of (3.23) is determined by the roots ξ of its characteristic equation:

$$\det[\xi^{m+1} \mathbf{I} - \xi^m \mathbf{P} - \xi \mathfrak{Q} - \beta \mathbf{R}] = 0. \quad (3.24)$$

Regions of stability can be computed using the boundary locus (or grid-search) technique, where one seeks the loci on which the characteristic polynomial (3.24) has a zero of modulus unity. Such a region can be obtained in the (λ, μ) -plane for each parameter ν of the test equation (1.17). Graphs in Figs. 3.6 and 3.7 show the stability regions for the Euler method applied to the test equation (1.17).

3.3 Contractivity Concepts and GPN-Stability

The linear test DDEs (3.8) with variable coefficients

$$\begin{aligned} y'(t) &= \lambda(t)y(t) + \mu(t)y(t - \tau), & t \geq t_0, \\ y(t) &= \psi(t), & t \leq t_0 \end{aligned} \quad (3.25)$$

lead to the concepts of *PN*-stability and *GPN*-stability. Recall the definition of $\sigma(t)$ and $\gamma(t)$ defined by (1.23) and (1.24). Here, $\sigma(t) = \operatorname{Re}(\lambda(t))$, $\gamma(t) = |\mu(t)|$. Hence, by Theorem 1.4, the solution of (3.25) is bounded by $\psi(t)$ ($|y(t)| \leq \max_{t \leq t_0} |\psi(t)|$), provided that, for every $t \geq t_0$,

$$|\mu(t)| \leq -\operatorname{Re}(\lambda(t)). \quad (3.26)$$

Definition 3.5 A numerical method for DDEs is said to be PN-stable (see [7], [8], and [3]) if the discrete numerical solution \tilde{y}_k of (3.25) under the condition (3.26) is such that

$$|\tilde{y}_k| \leq \max_{t \leq t_0} |\psi(t)|, \quad (3.27)$$

for all constant lags τ , $k \geq 0$, and under the constraint (3.9).

Definition 3.6 [8] A numerical method for DDEs is said to be GPN-stable if under condition (3.26) the numerical solution of (3.25) satisfies (3.27) for every $k \geq 0$ and for every stepsize $h > 0$.

Torelli [4] gave a sufficient condition for GPN-stability by using the contractivity properties of the ODE solver and for interpolant with respect to the test equation:

$$y'(t) = \lambda(t)y(t) + g(t), \quad y(t_0) = y_0, \quad (3.28)$$

whenever

$$\operatorname{Re}(\lambda(t)) < 0, \quad \text{for } t \geq t_0. \quad (3.29)$$

Assume that the functions $\lambda(t)$ and $g(t)$ are such that Eq. (3.28) has a unique solution of the form:

$$y(t) = e^{A(t)}y_0 + e^{A(t)} \int_{t_0}^t e^{-A(x)}g(x)dx,$$

where $A(t) = \int_{t_0}^t \lambda(x)dx$.

One can see from Theorem 1.5 that the contractivity property of the ODE (3.28) with respect to y_0 and $g(t)$ is

$$|y(t)| \leq \max \left\{ |y_0|; \max_{t_0 \leq x \leq t} \frac{|g(x)|}{-Re(\lambda(x))} \right\}, \quad \text{for } t \geq t_0. \quad (3.30)$$

With regard to the numerical methods for (3.28), we need the following definitions of AN_g -stability, for the numerical method and interpolant, respectively.

Definition 3.7 [4] An RK method (3.2)–(3.3) is said to be AN_g -stable if for all coefficients $\lambda(t)$ satisfying (3.29), the numerical solution \tilde{y}_n of the ODE (3.28) satisfies

$$|\tilde{y}_{n+1}| \leq \max \left\{ |\tilde{y}_n|; \max_{1 \leq i \leq v} \frac{|g(t_n + c_i h)|}{-Re(\lambda(t_n + c_i h))} \right\}, \quad (3.31)$$

for every stepsize $h > 0$ and for every function g .

Definition 3.8 [4] Consider an AN_g -stable RK method for the test problem (3.28). An interpolant \hat{y} defined by (3.4) is said to be an AN_g -stable interpolant to the RK method if there exists a constant $M \geq 1$ such that

$$\max_{0 \leq \theta \leq 1} |\hat{y}(t_n + \theta h)| \leq M \max \left\{ |\tilde{y}_n|; \max_{1 \leq i \leq v} \frac{|g(t_n + c_i h)|}{-Re(\lambda(t_n + c_i h))} \right\}, \quad (3.32)$$

for every $n \geq 0$ such that condition (3.29) holds for every g .

Remark 3.1 One can observe that a linear interpolant related to an AN_g -stable RK method is an AN_g -stable interpolant with $M = 1$.

A sufficient condition for GPN-stability is given by the following theorem [4]:

Theorem 3.1 *If we apply an AN_g -stable RK method together with an AN_g -stable interpolant to the DDE (3.25), then the numerical approximation \tilde{y}_k at the point t_k is such that $|\tilde{y}_k| \leq \max_{t_0 - \tau \leq t \leq t_0} |\psi(t)|$ for $k \geq 0$, for every τ , for every ψ , and for every step stepsize $h > 0$ such that*

$$M|\mu(t)| \leq -Re(\lambda(t))$$

for every $t \geq t_0$, where M is the constant in (3.32).

This means that an RK method for DDE is GPN-stable if both the RK method (3.2)–(3.3) and the interpolant (3.4) are AN_g -stable.

To translate the stability properties of the continuous RK method (3.6)–(3.7) for DDEs with respect to the test problem (3.25) in terms of the coefficients, we must obtain the necessary and sufficient condition of the underlying continuous RK method for its AN_g stability. Applying the RK method (3.4)–(3.5) to the test equation (3.28) under condition (3.29) yields

$$Y_{n+1}^i = \tilde{y}_n + h_{n+1} \sum_{j=1}^s a_{ij} \left(\lambda(t_{n+1}^j) Y_{n+1}^j + g(t_{n+1}^j) \right), \quad i = 1, \dots, s,$$

$$\hat{y}(t_n + \theta h_{n+1}) = \tilde{y}_n + h_{n+1} \sum_{i=1}^s b_i(\theta) \left(\lambda(t_{n+1}^i) Y_{n+1}^i + g(t_{n+1}^i) \right), \quad 0 \leq \theta \leq 1.$$

We put for every $i \in \{1, \dots, s\}$:

$$a_i = \lambda(t_{n+1}^i), \quad z_i = ha_i; \quad g_i = g(t_{n+1}^i),$$

$$\phi_i = \frac{g_i}{-Re(a_i)} \quad (\text{hence, } hg_i = -Re(z_i)\phi_i),$$

$$Y^i = Y_{n+1}^i.$$

Note that $Re(z_i) < 0$ for every i because $Re(\lambda(t)) < 0$ for every $t \geq t_0$. With this notation, we can write

$$Y^i = \tilde{y}_n + \sum_{j=1}^s a_{ij} z_j Y^j + \sum_{j=1}^s a_{ij} h g_j, \quad i = 1, \dots, s,$$

$$\hat{y}(t_n + \theta h_{n+1}) = \tilde{y}_n + \sum_{i=1}^s b_i(\theta) z_i Y^i + \sum_{i=1}^s b_i(\theta) z_i g_i, \quad 0 \leq \theta \leq 1.$$

Define the $s \times s$ matrix $\mathbf{Z} = \text{diag}(z_1, \dots, z_s)$ and the vectors $\mathbf{Y} = (Y^1, \dots, Y^s)^T$, $\mathbf{g} = (g_1, \dots, g_s)^T$, and $\Phi = (\phi_1, \dots, \phi_s)^T$, so that the RK method takes the compact form

$$\begin{aligned} \mathbf{Y} &= (I - \mathbf{ZA})^{-1} \mathbf{e} \tilde{y}_n - (I - \mathbf{ZA})^{-1} \mathbf{A} Re(\mathbf{Z}) \Phi, \\ \hat{y}(t_n + \theta h_{n+1}) &= \tilde{y}_n + \mathbf{b}(\theta)^T \mathbf{ZY} - \mathbf{b}(\theta)^T Re(\mathbf{Z}) \Phi. \end{aligned}$$

Then, the numerical approximation is

$$\hat{y}(t_n + \theta h_{n+1}) = (1 + \mathbf{b}(\theta)^T (I - \mathbf{ZA})^{-1} \mathbf{Ze}) \tilde{y}_n - \mathbf{b}(\theta)^T (I - \mathbf{ZA})^{-1} Re(\mathbf{Z}) \Phi, \quad (3.33)$$

where I is the identity matrix and \mathbf{e} is the unity s -vector.

The contractivity conditions of the numerical solution of DDEs have been given by Torelli [4] in the following theorem:

Theorem 3.2 Assume that Eq. (3.25) satisfies (3.26). If the RK method (3.6)–(3.7) for DDEs satisfies the following conditions:

(1) If $(I - \mathbf{ZA})$ is nonsingular, and

$$|1 + \mathbf{b}(\theta)^T (I - \mathbf{ZA})^{-1} \mathbf{Ze}| + \|\mathbf{b}(\theta)^T (I - \mathbf{ZA})^{-1} Re(\mathbf{Z})\|_1 \leq 1 \quad (3.34)$$

Table 3.1 Important stability concepts in the literature

| Test equation | Conditions | Type of stability | ODE concept |
|---|--|-------------------------------|--------------|
| $y'(t) = \lambda y(t) + \mu y(t - \tau),$ $ \mu < -Re(\lambda)$ | $\tau/h \in \mathbb{N}$ arbitrary h | P-stability GP-stability | A-stability |
| $y'(t) = \lambda y(t) + \mu y(t - \tau) + v y'(t - \tau),$ $ \lambda\bar{v} - \bar{\mu} + \lambda v + \mu < -Re(\lambda)$ | $\tau/h \in \mathbb{N}$ arbitrary h | NP-stability NGP-stability | - |
| $y'(t) = \lambda(t)y(t) + \mu(t)y(t - \tau),$ $ \mu(t) < -Re(\lambda(t))$ | $\tau/h \in \mathbb{N}$ arbitrary h | PN-stability GPN-stability | AN-stability |
| $y'(t) = f(t, y(t), y(t - \tau)),$ subject to (3.38)–(3.40) | $\tau/h \in \mathbb{N}$ arbitrary h | RN-stability GRN-stability | BN-stability |

for every \mathbf{Z} , and all $\theta \in [0, 1]$, then

$$(2) \quad \max_{0 \leq \theta \leq 1} |\hat{y}(t_n + \theta h_{n+1})| \leq \max_{t \leq t_0} |\psi(t)| \text{ holds for all } n \text{ and all } \psi,$$

where $\|x\|_1 = \sum_{i=1}^s |x_i|$ for any s -dimensional row-vector x .

From the above, we can say that a GPN-stable method is also PN-stable and that a PN-stable method is AN-stable for ODEs. We also note that PN-stability and GPN-stability are stronger concepts than P-stability and GP-stability because they are based on a more general test equation, to the same extent that AN-stability is a stronger stability concept than A-stability for ODEs; see Table 3.1 for a summary of numerical stability of DDEs.

A more extensive stability analysis of numerical methods based on a more general non-linear test problem (1.21) is considered in the next section.

3.3.1 Contractivity Concepts and GRN-Stability

Now, we analyze the stability properties of the RK methods for DDEs with respect to the general non-linear system (1.21) under condition (1.25). This gives rise to the concepts of *RN*-stability and *GRN*-stability [9]. Here, to be more suitable, we reiterate (1.21) and (1.22):

$$\begin{aligned} y'(t) &= f(t, y(t), y(t - \tau)), & t \geq t_0, \\ y(t) &= \psi(t), & t \leq t_0, \end{aligned} \tag{3.35}$$

$$\begin{aligned} z'(t) &= f(t, z(t), z(t - \tau)), & t \geq t_0, \\ z(t) &= \phi(t), & t \leq t_0. \end{aligned} \tag{3.36}$$

For the particular case of constant lag $\tau > 0$, Torelli [4] gave the following definitions:

Definition 3.9 A numerical method for DDEs is called RN-stable if, under the condition (1.25), the discrete numerical solutions \tilde{y}_k and \tilde{z}_k of (3.35) and (3.36), respectively, satisfy the condition:

$$\|\tilde{y}_k - \tilde{z}_k\| \leq \max_{t \leq t_0} \|\psi(t) - \phi(t)\|, \quad k \geq 0 \quad (3.37)$$

for all constant lag τ and every $k \geq 0$ and for every stepsize and any constant stepsize $h > 0$ under the condition (3.9).

Definition 3.10 A numerical method for DDEs is called GRN-stable if the discrete numerical solutions $\{\tilde{y}_k\}$ and $\{\tilde{z}_k\}$ of the pairs of the systems (3.35) and (3.36) satisfying (1.25) are such that (3.37) holds, for every $k \geq 0$ and for every stepsize $h > 0$.

The above definitions reflect demands for the discrete numerical solutions to preserve the contractivity properties of the solution. Bellen and Zennaro [10] introduced the sufficient conditions for *RN*-stability and *GRN*-stability by the contractivity concepts of ODE solvers. Results of Theorem 3.2 can be extended to the non-linear equation (3.35) for a variable delay and free mesh points. For convenience, we reiterate the definitions of $\sigma(t)$ and $\gamma(t)$ given by (1.23)–(1.24):

$$\sigma(t_{n+1}^i) \geq \sup_{\substack{z, y_1, y_2 \in \mathbb{C}^n \\ y_1 \neq y_2}} \frac{\operatorname{Re}\left(f(t_{n+1}^i, y_1, z) - f(t_{n+1}^i, y_2, z), y_1 - y_2\right)}{\|y_1 - y_2\|^2} \quad (3.38)$$

and

$$\gamma(t_{n+1}^i) \geq \sup_{\substack{y, z_1, z_2 \in \mathbb{C}^n \\ z_1 \neq z_2}} \frac{\|f(t_{n+1}^i, y, z_1) - f(t_{n+1}^i, y, z_2)\|}{\|z_1 - z_2\|}, \quad (3.39)$$

under the condition

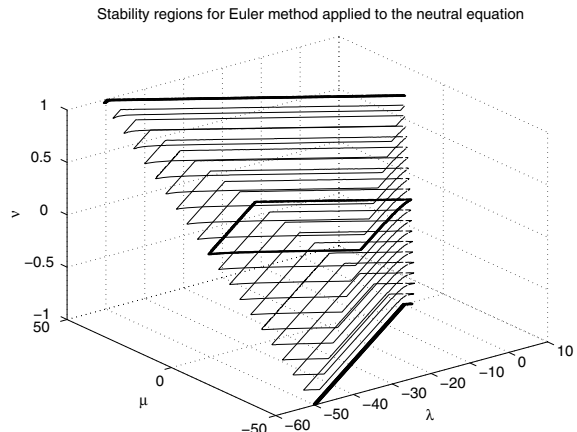
$$\gamma(t) \leq -\sigma(t), \quad \text{for all } t \geq t_0. \quad (3.40)$$

Assume that the numerical solution of (3.35) is in the form (3.6)–(3.7), so the solution of (3.36) takes the form

$$Z_{n+1}^i = \tilde{z}_n + h_{n+1} \sum_{j=1}^s a_{ij} f(t_{n+1}^j, Z_{n+1}^j, \hat{\rho}(t_{n+1}^j - \tau)), \quad i = 1, \dots, s, \quad (3.41)$$

$$\hat{\rho}(t_n + \theta h_{n+1}) = \tilde{z}_n + h_{n+1} \sum_{i=1}^s b_i(\theta) f(t_{n+1}^i, Z_{n+1}^i, \hat{\rho}(t_{n+1}^i - \tau)), \quad 0 \leq \theta \leq 1. \quad (3.42)$$

Fig. 3.6 Stability regions in the space of parameters (λ, μ, v) for the explicit Euler method when solving the NDDE $y'(t) = \lambda y(t) + \mu y(t - 1) + v y'(t - 1)$ with $\tau = 1 = mh$ ($m = 25$); the middle bold one is for $v = 0$



The following theorem provides the conditions of contractivity of the RK methods for DDEs (3.35):

Theorem 3.3 [9] Assume that the function f in (3.35) and (3.36) satisfies the condition (3.40). If the continuous RK method satisfies the conditions (i) in Theorem 3.2, then the result for the DDE method $|\hat{y}(t) - \hat{\rho}(t))| \leq \max_{s \leq t_0} |\psi(s) - \phi(s)|$ holds for all $t \geq t_0$, for any integration mesh points and for any pair of functions $\psi(t), \phi(t)$.

3.4 Concluding Remarks

In this chapter, we have examined the stability of numerical methods of DDEs. Specifically, we have derived some stability regions for certain numerical methods applied to linear constant coefficient DDEs. New results for numerical stability regions were obtained by choosing $\tau = (m + \theta)h$, with $\theta \in [0, 1)$ and $m \in \mathbb{N}$. We observed interesting stability regions (for various methods) that are sensitive to θ (Figs. 3.1, 3.3, 3.4, and 3.5). Such a sensitivity is much less pronounced for implicit formulae. From the graph in Fig. 3.1, it may also be observed that the intercept with the $\mu = 0$ axis is consistent with results for ODE stability (e.g., in case of explicit method, $\lambda h \in (-2, 0)$). Implicit formulae give unbounded stability regions which, for $m \geq 5$, are the same as the true stability regions. The technique has been extended to find the stability regions of the solutions of linear NDDEs; see Figs. 1.3, 3.6, and 3.7. We get an unstable area for $|v| > 1$.

In the next chapter, we shall introduce a numerical technique for Volterra delay integro-differential equations.

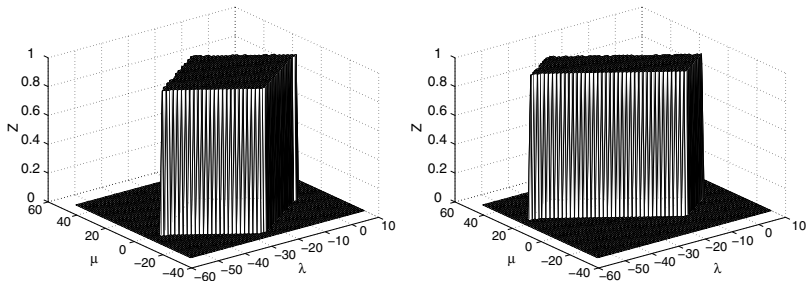


Fig. 3.7 Numerical stability areas, using grid-search technique, of the explicit Euler method when solving the NDDE $y'(t) = \lambda y(t) + \mu y(t-1) + \nu y'(t-1)$, with $\tau = mh$, $m = 25$. The first graph corresponds to $v = 0$, and the second one is to $v = 0.5$

References

1. Rihan, F.A.: Stability conditions for singularly perturbed delay differential equations. *Comput. Math. Model.* **19**(3), 292–303 (2008)
2. Ibrahim, F., Rihan, F.A., Turek, S.: Stability analysis of extended one-step schemes for stiff and non-stiff delay differential equations. *Appl. Math. Inf. Sci.* **10**(5), 1705–1717 (2016)
3. Thompson, S.: Stability of numerical methods for delay differential equations. *J. Comput. Appl. Math.* **25**, 15–26 (1989)
4. Torelli, L.: A sufficient condition for gpn-stability for delay differential equations. *J. Comput. Appl. Math.* **59**
5. Barwell, V.K.: Special stability problems for functional equations, pp. 130–135 (1975)
6. Paul, C.A.H., Baker, C.T.H.: Stability boundaries revisited- Runge-Kutta methods delay differential equations. Numerical Analysis Report MCCM report No. 205, University of Manchester (1991)
7. in 't Hout, K.J.: The stability of a class of Runge-Kutta methods for delay differential equations. *Appl. Numer. Math.* **9**, 347–355 (1992)
8. in 't Hout, K.J., Spijker, M.N.: Stability analysis of numerical methods for delay differential equations. *Numer. Math.* **59**, 807–814 (1991)
9. Bellen, A.: Contractivity of continuous Runge-Kutta methods for delay differential equations. *Appl. Numer. Math.* **24**, 219–232 (1997)
10. Bellen, A., Zennaro, M.: Strong contractivity properties of numerical methods for ordinary and delay differential equations. *Appl. Numer. Math.* **9**, 321–346 (1992)

Chapter 4

Numerical Solutions of Volterra Delay Integro-Differential Equations



4.1 Introduction

In this chapter, we introduce a numerical technique for Volterra delay integro-differential equations. The technique is based on the mono-implicit Runge-Kutta method and collocation method for the integral part. In the following pages, the efficiency and stability properties of this technique are examined. Later, numerical results are presented to demonstrate the effectiveness of the methodology.

The mono-implicit Runge-Kutta (MIRK) method is a subclass of the well-known family of implicit Runge-Kutta methods [1] and has many applications for the efficient numerical solution of systems of initial and boundary value ODEs. These methods are suitable for stiff problems (where the global accuracy of the numerical solution is determined by stability rather than local error and implicit methods are more appropriate; see, e.g., [2]). In [3], the authors adapted MIRK methods for stiff and non-stiff DDEs and studied the efficiency and stability properties of this class of methods. In this chapter, we extend the technique to solve Volterra delay integro-differential equations of the form

$$\begin{aligned} y'(t) &= f(t, y(t), y(\alpha(t, y(t)))), \int_{a(t)}^t g(t, s, y(s))ds, \quad \text{for } t \geq 0, \\ y(t) &= \psi(t), \quad t \leq 0, \end{aligned} \tag{4.1}$$

where $\alpha(t, y(t)) < t$. The integral part in (4.1) introduces *continuously distributed delay*. If $a(t) = t - \tau$, with fixed $\tau > 0$, then (4.1) has a fixed time-lag and bounded retardation since the difference between $t - \tau$ and t is fixed and bounded. If $a(t) = 0$, then (4.1) has unbounded time-lag since the difference between 0 and t is unbounded. However, if $a(t) \rightarrow -\infty$, then (4.1) has infinite time-lag; see [4, 5].

The absence of the integral term in Eq. (4.1) reduces it to the DDE

$$\begin{aligned} y'(t) &= f(t, y(t), y(\alpha(t, y(t)))), \quad \text{for } t \geq 0, \\ y(t) &= \psi(t), \quad t \leq 0. \end{aligned} \tag{4.2}$$

Here, if $\alpha(t, y(t)) \equiv t - \tau$, with fixed $\tau > 0$, then Eq. (4.2) has *discretely distributed delay* and the time-lag or retardation is bounded. However, if $\alpha(t, y(t)) = \mu t$, $\mu \in [0, 1)$, then Eq. (4.2) has unbounded time-lag.

For simplicity, consider a scalar VDIDE of the form:

$$\begin{aligned} y'(t) &= f(t, y(t), y(t - \tau), \int_{a(t)}^t g(t, s, y(s))ds), \quad \text{for } t \geq 0, \\ y(t) &= \psi(t), \quad t \leq 0, \end{aligned} \quad (4.3)$$

with fixed $\tau > 0$ and the integral term in (4.3) introduces either unbounded time-lag, i.e., $a(t) = 0$ or bounded time-lag, i.e., $a(t) = t - \tau$. The functions f, g are assumed to be sufficiently smooth with respect to their arguments, and $\psi(t)$ is an initial function that is assumed to be continuous. To solve (4.3) numerically, we not only need an approximation to the solution at the proposed mesh points but also need to create the solution at the non-mesh points to produce dense output of the solution in order to approximate the delay term $y(t - \tau)$ and the integral term $\int_{a(t)}^t g(t, s, y(s))ds$. The proposed technique is based on continuous mono-implicit Runge-Kutta (CMIRK) method (see [6]) to treat the differential part, and Boole's quadrature rule (see [7]) to treat the integral part.

This chapter is organized as follows: In Sect. 4.2, we briefly discuss the analytical stability of VDIDEs and review MIRK methods for initial value problems in Sect. 4.3. In Sect. 4.4, we present the numerical technique and the numerical algorithm for VDIDEs that are based on CMIRK methods of fourth order along with Boole's quadrature rule. The numerical stability regions of the underlying methods are presented in Sect. 4.5. The numerical results are presented in Sect. 4.6, and some concluding remarks are given in Sect. 4.7.

4.2 Analytical Stability

Consider the test problem of scalar VDIDE of the form

$$\begin{aligned} y'(t) &= \lambda y(t) + \mu y(t - \tau) + \gamma \int_{t-\tau}^t y(v)dv, \quad t > 0 \\ y(t) &= \psi(t), \quad -\tau \leq t \leq 0, \end{aligned} \quad (4.4)$$

where λ, μ and γ are complex and $\tau > 0$ is a constant delay. Looking for solutions of (4.4) of the form $y(t) = \exp(st)$, we are led to the characteristic equation

$$\mathcal{H}(s) \equiv s - \lambda - \mu \exp(-\tau s) - \frac{\gamma}{s}(1 - \exp(-\tau s)) = 0. \quad (4.5)$$

The asymptotic stability of the zero solution to (4.4) is equivalent to the condition that all the roots of the characteristic equation (4.5) have negative real parts and are bounded away from the imaginary axis [8].

The analytical stability region \mathcal{S}_a of (4.4) is determined by the set of (λ, μ, γ) values for which all the roots s of (4.5) have negative real parts:

$$\mathcal{S}_a = \{(\lambda, \mu, \gamma) : \operatorname{Re}(s) < 0 \quad \forall s\}.$$

To find the boundary of the analytical stability region for which $\operatorname{Re}(s) = 0$, we assume that $\lambda, \beta, \gamma \in \mathbb{R}$ and $s \in \mathbb{C}$ is pure complex, i.e., $s = i\theta$; then, Eq. (4.5) takes the form

$$\mathcal{H}(i\theta) = i\theta - \lambda - \mu \exp(-i\theta\tau) - \frac{\gamma}{i\theta} (1 - \exp(-i\theta\tau)) = 0. \quad (4.6)$$

Separating the real and complex parts of (4.6) and writing μ and γ in terms of λ and θ , we obtain

$$\mathcal{S}_a(\lambda, \theta) = \left\{ \mu(\lambda, \theta) = \lambda - \frac{\theta \sin \theta \tau}{(1 - \cos \theta \tau)}, \gamma(\lambda, \theta) = \frac{\theta(\theta \cos \theta \tau - \lambda \sin \theta \tau)}{(1 - \cos \theta \tau)} \right\}, \quad (4.7)$$

for any $\tau > 0$ and $\theta \in (0, 2\pi)$. If $\theta = 0$, then relations in (4.7) reduce to the straight line

$$\mu + \tau \gamma = -\lambda. \quad (4.8)$$

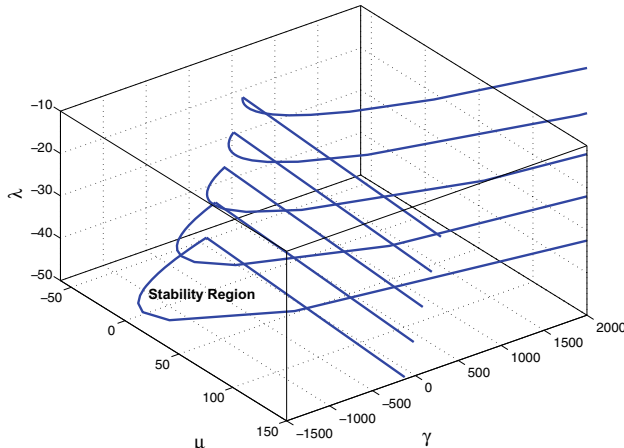


Fig. 4.1 Analytical stability region of VDIDE (4.4) with different values of $\lambda = -10, -20, -30, -40, -50$. The asymptotic stability region getting larger with more negative values of λ

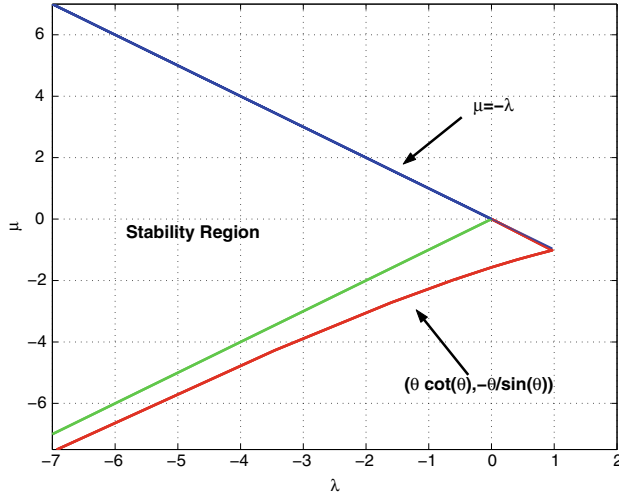


Fig. 4.2 Analytical stability region for Eq. (4.9)

The graphs of Fig. 4.1 show the analytical stability regions of (4.4) that are determined by the parametrized curves in (4.7) and the line of (4.8). The asymptotic stability region becomes wider as λ becomes more negative.

Note that when $\gamma = 0$, VDIDE (4.4) coincides with the test DDE

$$\begin{aligned} y'(t) &= \lambda y(t) + \mu y(t - \tau), t > 0 \\ y(t) &= \psi(t), \quad -\tau \leq t \leq 0, \end{aligned} \tag{4.9}$$

and the boundary (4.7) of the analytical stability region reduces to

$$\mathcal{S}_a(\lambda, \theta) = \left\{ \mu(\lambda, \theta) = \lambda - \frac{\theta \sin \theta \tau}{(1 - \cos \theta \tau)}, \quad 0 = (\theta \cos \theta \tau - \lambda \sin \theta \tau) \right\}, \quad \theta \neq 0 \tag{4.10}$$

that can be simplified to

$$\mathcal{S}_a(\theta) = \left\{ \mu(\theta) = -\theta / \sin \theta \tau, \quad \lambda(\theta) = \theta \cot \theta \tau, \right\}, \quad \theta \neq 0. \tag{4.11}$$

This equation provides the same bounding below the curve of the analytical stability region for the DDE (4.9). Equation (4.8) for $\gamma = 0$ reduces immediately to the line $\mu = -\lambda$, which is the same boundary line of (4.9); see Fig. 4.2.

The necessary conditions imposed on the coefficients to guarantee the asymptotic stability of (4.4) are given by the following theorem:

Theorem 4.1 *The zero solution of (4.4) is delay-independent asymptotically stable if and only if the following three conditions are satisfied:*

$$\begin{aligned} & \lambda + \mu + \gamma\tau \neq 0 \text{ for any } \tau \geq 0, \\ & Re(\lambda) < 0 \& (Re(\lambda)Re(\lambda\bar{\gamma}) + (Im(\gamma))^2 < 0, \text{ or } \gamma = 0) \\ & m((\lambda + \mu)\bar{\gamma}) = 0 \& \{|\mu|^2 < (Re(\lambda))^2 + 2Re(\gamma), \text{ or} \\ & Im(\lambda) = 0, |\mu|^2 = (Re(\lambda))^2 + 2Re(\gamma)\}. \end{aligned} \quad (4.12)$$

When $\gamma = 0$, the above conditions are reduced to $|\mu| < -Re(\lambda)$. However, when λ , μ , and γ are all real and $\gamma \neq 0$, these conditions are reduced to $\lambda < 0$, $\gamma < 0$, and $\mu^2 \leq \lambda^2 + 2\gamma$; see [9] for the proof and more discussions.

4.3 Continuous Mono-Implicit RK Scheme for DDEs

Mono-implicit Runge-Kutta (MIRK) methods are a subclass of the well-known implicit Runge-Kutta methods and have application in the efficient numerical solution of systems of initial and boundary value ordinary differential equations; see [6]. MIRK schemes are developed to reduce the computational cost of the fully implicit method which combines the accuracy of implicit method and efficient implementation. In this section, we briefly review the MIRK method for initial value problems (IVPs)

$$y'(t) = f(t, y(t)), \quad 0 < t \leq T, \quad y(0) = y_0. \quad (4.13)$$

Given the mesh points $\Delta = \{0 < t_1 < \dots < t_N = T\}$ with stepsize $h_n = t_{n+1} - t_n$, and $y_n \approx y(nh_n)$, one gets

$$y_{n+1} = y_n + h_n \sum_{r=1}^s b_r \mathcal{K}_{n+1}^r, \quad (4.14)$$

with stages, defined by

$$\mathcal{K}_{n+1}^r = f \left(t_n^r, (1 - v_r)y_n + v_r y_{n+1} + h_n \sum_{j=1}^{r-1} a_{rj} \mathcal{K}_{n+1}^j \right). \quad (4.15)$$

Here, \mathcal{K}_n^r is the r th stage, b_r , v_r , c_r , and a_{rj} are the parameters of the MIRK method that are defined by the tableau (with $1 \leq r, j \leq s$):

| | | | | | | |
|----------|----------|-----------|-----------|----------|-------------|----------|
| c_1 | v_1 | 0 | 0 | ... | 0 | 0 |
| c_2 | v_2 | $a_{2,1}$ | 0 | ... | 0 | 0 |
| \vdots | \vdots | \vdots | \vdots | \vdots | \vdots | \vdots |
| c_s | v_s | $a_{s,1}$ | $a_{s,2}$ | ... | $a_{s,s-1}$ | 0 |
| | | b_1 | b_2 | b_3 | ... | b_s |

\equiv

$$\begin{array}{c|c|c} \mathbf{C} & \mathbf{V} & \mathbf{A} \\ \hline & & \mathbf{b}^T \end{array}$$

The abscissae $c_i \in [0, 1]$ ($i = 1, 2, \dots, s$), $\mathbf{b}^T = [b_1, b_2, \dots, b_s]$, $\sum_{i=1}^s b_i = 1$, $\mathbf{V} = [v_1, v_2, \dots, v_s]^T$, $\mathbf{C} = [c_1, c_2, \dots, c_s]^T$, and $\mathbf{A} = \{a_{ij}\}_{i,j=1}^{s,s-1}$. The abscissae c_r relate b_r and v_r by the form $c_r = v_r + \sum_{i=1}^s a_{ri}$, and $t_n^r = t_n + v_r h_n$.

The stability function of this scheme is defined by (see [6])

$$\mathcal{R}(z) = \frac{P(z, \mathbf{e} \cdot \mathbf{V})}{P(z, -\mathbf{V})}, \quad P(z, \mathbf{w}) = 1 + z \mathbf{b}^T (\mathbf{I} - z \mathbf{A})^{-1} \mathbf{w},$$

where $\mathbf{w} \in \mathbb{R}^s$ and $\mathbf{e} = [1, 1, \dots, 1]^T$ is $s \times 1$ vector. The MIRK scheme is of order p (i.e., it has local error of order $p+1$) if for the local problem, $y'(t_i) = f(t_i, y(t_i))$, $y(t_{i-1}) = y_{i-1}$, the numerical solution y_n given by solving (4.14) and (4.15) satisfies $|y(t_n) - y_n| = O(h_n^{p+1})$.

We can then utilize the above scheme to solve the DDE, see [3], by using continuous extension to find the solution at non-mesh points. Given a DDE of the form:

$$\begin{aligned} y'(t) &= f(t, y(t), y(t-\tau)), \quad \text{for } t \geq 0, \\ y(t) &= \psi(t), \quad -\tau \leq t \leq 0, \end{aligned} \tag{4.16}$$

where $\tau > 0$ is the delay in time, the function f is assumed to be sufficiently smooth with respect to its arguments, and $\psi(t)$ is an initial function which is assumed to be continuous. Applying the s -stages MIRK scheme to (4.16) yields

$$\mathcal{K}_{n+1}^r = f \left(t_n^r, (1 - v_r)y_n + v_r y_{n+1} + h_n \sum_{j=1}^{r-1} a_{rj} \mathcal{K}_{n+1}^j, y(t_n^r - \tau) \right). \tag{4.17}$$

Of course, the complexity of the scheme depends on the coefficients $\{v_r\}_{r=1}^s$, $\{a_{ij}\}_{i,j=1}^{s,s-1}$, the weights $\{b_r\}_{r=1}^s$, and the number of stages s . Due to the nature of DDEs, the numerical solution obtained by the discrete MIRK scheme at mesh points is not sufficient as in the earlier described ODE case. The presence of the delay

term $y(t_n^r - \tau)$ in Eq. (4.17) requires the availability of an approximation to the solution at any point $t_n^r - \tau$ that is not always a mesh point. Continuous Mono-Implicit RK (CMIRK) scheme provides continuous approximate solution $u(t)$ at any point between the two mesh points t_n and t_{n+1} using the equation

$$u(t_n + \vartheta h_n) = y_n + h_n \sum_{r=1}^{s^*} b_r(\vartheta) \mathcal{K}_{n+1}^r, \quad 0 \leq \vartheta \leq 1, \quad (4.18)$$

where $s^* \geq s$ is the number of stages for CMIRK scheme, and $\mathcal{K}_{n+1}^r, r = 1, \dots, s^*$ are defined by the same equation (4.17) as in the discrete scheme to reduce extra computations. $b_r(\vartheta), r = 1, \dots, s^*$ are polynomials in $\vartheta, 0 \leq \vartheta \leq 1$, of degree $d \leq p$, where p is the order of accuracy of the Runge-Kutta method [10]. The additional $s^* - s$ stages in the continuous extension formula (4.18) are assumed to raise its uniform order to the order of the discrete Runge-Kutta methods.

The parameters of the CMIRK scheme are then defined by the tableau:

| | | | | | | |
|-----------|-----------|------------------|------------------|------------------|-----------------|----------------------|
| c_1 | v_1 | 0 | 0 | ... | 0 | 0 |
| c_2 | v_2 | $a_{2,1}$ | 0 | ... | 0 | 0 |
| \vdots | \vdots | \vdots | \vdots | \vdots | \vdots | \vdots |
| c_{s^*} | v_{s^*} | $a_{s^*,1}$ | $a_{s^*,2}$ | ... | a_{s^*,s^*-1} | 0 |
| | | $b_1(\vartheta)$ | $b_2(\vartheta)$ | $b_3(\vartheta)$ | ... | $b_{s^*}(\vartheta)$ |

 \equiv

| C | V | A |
|---|---|---------------------------|
| | | $\mathbf{b}^T(\vartheta)$ |

The polynomials $b_r(\vartheta)$ and s^* are chosen to satisfy some continuity and order conditions (see [1, 10, 11] for more details). Numerical stability analysis of CMIRK schemes for DDEs is discussed in [3]. Next, we extend CMIRK scheme to numerically solve VDIDEs.

4.4 Numerical Treatment of VDIDEs

To utilize ODEs' solvers for solving VDIDEs, we should consider the propagation of derivative jump discontinuities and the dependence of the solution on past conditions. These two special features coincide with those of DDEs, under the assumption that the integrated function is smooth. The former means that a jump in the first derivative of the solution at $t = 0$ can cause a jump in the second derivative at $t = \tau$ and a jump in the third derivative at $t = 2\tau$, and so on, till the n^{th} derivative, which will have a jump at $t = (n-1)\tau$. The dependence of the solution on past conditions, through the delay term $y(t - \tau)$ and the integral term $\int_{a(t)}^t g(t, s, y(s))ds$, requires the availability of a dense output solution [5].

4.4.1 CMIRK Scheme for VDIDEs

The MIRK scheme defined by equations (4.14) and (4.17) is extended to solve the VDIDE (4.3) on the defined mesh $\Delta = \{0 < t_1 < \dots < t_n < \dots < t_i = T\}$ as follows:

$$y(t_n + \vartheta h_n) = y_n + h_n \sum_{r=1}^{s^*} b_r(\vartheta) \mathcal{K}_{n+1}^r, \quad 0 \leq \vartheta \leq 1, \quad (4.19)$$

with stages

$$\mathcal{K}_{n+1}^r = f \left(t_n^r, (1 - v_r)y_n + v_r y_{n+1} + h_n \sum_{j=1}^{r-1} a_{rj} \mathcal{K}_{n+1}^j, y(t_n^r - \tau), I_n \right). \quad (4.20)$$

The integral part, $I_n = \int_{a(t_n^r)}^{t_n^r} g(t, s, y(s))ds$, is evaluated numerically using Boole's quadrature rule. To find an approximation to the integral I_n in (4.20), we subdivide its integration interval as follows:

If $a(t) = t - \tau$:

$$I_n = \int_{t_n - \tau}^{t_n} g(t, s, y(s))ds + \int_{t_n}^{t_n^r} g(t, s, y(s))ds - \int_{t_n - \tau}^{t_n - \tau + c_r h_n} g(t, s, y(s))ds.$$

When $a(t) = 0$:

$$I_n = \int_0^{t_n} g(t, s, y(s))ds + \int_{t_n}^{t_n^r} g(t, s, y(s))ds.$$

The fourth-order ($s = 5$) discrete MIRK scheme is defined by the following tableau:

| 0 | 0 | 0 | 0 | 0 | 0 | 0 |
|-----------------|---------------------|--------------------|---------------------|------------------|------------------|---------------|
| 1 | 1 | 0 | 0 | 0 | 0 | 0 |
| $\frac{1}{20}$ | $\frac{29}{4000}$ | $\frac{361}{8000}$ | $-\frac{19}{8000}$ | 0 | 0 | 0 |
| $\frac{19}{20}$ | $\frac{3971}{4000}$ | $\frac{19}{8000}$ | $-\frac{361}{8000}$ | 0 | 0 | 0 |
| $\frac{1}{2}$ | $\frac{11}{16}$ | $\frac{1}{32}$ | $\frac{267}{608}$ | $\frac{25}{684}$ | $-\frac{25}{36}$ | 0 |
| | | $-\frac{43}{228}$ | $-\frac{43}{228}$ | $\frac{25}{57}$ | $\frac{25}{57}$ | $\frac{1}{2}$ |

The discrete solution at the mesh points obtained using the discrete MIRK scheme is insufficient to solve the VDIDEs. A dense output solution is needed at non-mesh

points as explained earlier, using Eq. (4.18) of the fourth-order CMIRK scheme (see [3]) (with $s^* = 5$), such that

| | | | | | | |
|----------------|---------------------|---------------------|---------------------|------------------|------------------|------------------|
| 0 | 0 | 0 | 0 | 0 | 0 | 0 |
| 1 | 1 | 0 | 0 | 0 | 0 | 0 |
| $\frac{1}{18}$ | $\frac{29}{3991}$ | $\frac{361}{8000}$ | $-\frac{19}{8000}$ | 0 | 0 | 0 |
| $\frac{1}{20}$ | $\frac{4000}{4000}$ | $\frac{8000}{8000}$ | $-\frac{361}{8000}$ | 0 | 0 | 0 |
| $\frac{1}{2}$ | $\frac{11}{16}$ | $\frac{1}{32}$ | $\frac{267}{608}$ | $\frac{25}{684}$ | $-\frac{25}{36}$ | 0 |
| | | $b_1(\vartheta)$ | $b_2(\vartheta)$ | $b_3(\vartheta)$ | $b_4(\vartheta)$ | $b_5(\vartheta)$ |

where

$$\begin{aligned} b_1(\vartheta) &= -\frac{1}{228}\vartheta(1200\vartheta^3 - 2714\vartheta^2 + 1785\vartheta - 228), \\ b_2(\vartheta) &= \frac{1}{228}\vartheta^2(1200\vartheta^2 - 2086\vartheta + 843), \\ b_3(\vartheta) &= \frac{25}{171}\vartheta^2(40\vartheta^2 - 86\vartheta + 49), \\ b_4(\vartheta) &= -\frac{25}{171}\vartheta^2(40\vartheta^2 - 74\vartheta + 31), \\ b_5(\vartheta) &= -\frac{1}{2}\vartheta^2(2\vartheta - 3). \end{aligned} \quad (4.21)$$

4.4.2 Numerical Integration Formula and Boole's Quadrature Rule

To find an approximation to the definite integral

$$\int_a^b z(x)dx \quad (4.22)$$

with known tabulated data of $z(x)$ at some mesh points $a = a_1 < a_2 < \dots < a_N = b$, a *quadrature rule* is needed. A quadrature rule approximates the integral by

$$\int_a^b z(x)dx \simeq \sum_{k=1}^N w_k f(a_k), \quad (4.23)$$

where $w_k, k = 1, 2, \dots, N$ and $a_k, k = 1, 2, \dots, N$ are called *weights* and *nodes*, respectively. Of course, the quadrature rules differ in the choice of *weights* and *nodes*.

Newton-Cotes quadrature (NCQ) rules are very popular numerical integration techniques. In NCQ rules, the nodes are equally spaced. The N -nodes NCQ technique finds a Lagrange polynomial P_N that passes through the N nodes and then the integral of $z(x)$ is approximated by the integral of P_N . NCQ is classified into closed NCQ, if a_1, a_N are used, and open NCQ, if a_1, a_N are not used [12].

Many well-known quadrature rules are NCQ rules, such as the trapezoidal rule (which is a 2-node closed NCQ), Simpson's $\frac{1}{3}$ rule (which is a 3-node closed NCQ), Simpson's $\frac{3}{8}$ rule (which is a 4-node closed NCQ), and Boole's rule (which is a 5-node closed NCQ).

Boole's rule is a 5-node closed NCQ that approximates the integral by the following formula:

$$\int_{a_1}^{a_5} z(s)ds \simeq \frac{2}{45}h(7z_1 + 32z_2 + 12z_3 + 32z_4 + 7z_5), \quad (4.24)$$

where $h = a_i - a_{i-1}$, $i = 2, \dots, 5$ and with an error of order h^7 . If the number of points used in the evaluation of the integral is greater than 5, then Boole's rule is applied repeatedly, which results in the composite Boole's rule. For example, if we have 9 points, then the composite Boole's rule takes the form

$$\int_{a_1}^{a_9} z(s)ds \simeq \frac{2}{45}h(7z_1 + 32z_2 + 12z_3 + 32z_4 + 14z_5 + 32z_6 + 12z_7 + 32z_8 + 7z_9). \quad (4.25)$$

Therefore, the approximation of the integral I_n in (4.20) is defined by

$$I_n = \int_{t_n-\tau}^{t_n} g(t, s, y(s))ds + \int_{t_n}^{t_n^r} g(t, s, y(s))ds - \int_{t_n-\tau}^{t_n-\tau+c_r h_n} g(t, s, y(s))ds$$

for $a(t) = t - \tau$. However, for $a(t) = 0$,

$$I_n = \int_0^{t_n} g(t, s, y(s))ds + \int_{t_n}^{t_n^r} g(t, s, y(s))ds.$$

Each of the above integrals is approximated by applying Boole's rule (4.24). For previous intervals, CMIRK scheme provides the solution at any non-mesh point needed by Boole's rule. However, for the current mesh, cubic spline interpolation is used to obtain the solution at any non-mesh point needed by Boole's rule.

4.4.3 MIDDE Software Aspects

The suggested numerical technique in this work is implemented in a MATLAB code “MIDDE” which is based on the CMIRK schemes to treat the differential part and Boole's quadrature rule to treat the integral part. The code MIDDE is designed to solve both systems of DDEs and VDIDEs.

The MIDDE code has the following aspects:

- The points of jump discontinuities are located and taken as mesh points.
- The dense output solution is obtained inside the MIDDE code using the CMIRK method.
- A stepsize control strategy is implemented inside the code to maintain the defect in the numerical solution within a specified tolerance.

In the following, we briefly introduce the numerical algorithm and stepsize control in MIDDE code.

4.4.3.1 Numerical Algorithm and Stepsize Control

The general steps of the numerical algorithm implemented in MIDDE code for solving VDIDEs (4.3) can be briefly summarized as follows:

1. Derivative jump discontinuity points are located and taken as mesh points. For each interval $[t_n, t_{n+1}]$, the next steps are repeated.
2. The interval is divided into equally spaced points $t_n = t_1, t_2, \dots, t_m, t_{m+1} = t_{n+1}$ with stepsize $h_n = t_{n+1} - t_n$, where $\tau = mh_n$. Delay terms $y(t_n^r - \tau)$ are calculated either by $\psi(t)$ in (4.3) (in the first interval), then by CMIRK formula (4.18) otherwise.
3. Approximations to the solution $\mathbf{Y} = \{y_i\}_{i=1}^{m+1}$ and the continuous record of the previous mesh are used by Boole's rule to evaluate I_n (see Sect. 4.4.2). Then, delay terms $y(t_n^r - \tau)$ as well as integral terms I_n and \mathbf{Y} are used to calculate stages $\{\mathcal{K}_{n+1}^r\}_{r=1}^s$ by (4.20).
4. The residual function is $\Psi(\mathbf{Y})$, whose n th component $\Psi_n = y_{n+1} - y_n - h_n \sum_{r=1}^s b_r \mathcal{K}_{n+1}^r$ is evaluated. Then, the system of equations $\Psi(\mathbf{Y}) = 0$ is solved using Newton's iteration.
5. Newton's iteration is terminated when the numerical solution \mathbf{Y} causes $\Psi(\mathbf{Y})$ to be within a defined tolerance, otherwise \mathbf{Y} is updated and steps 3 – 5 are repeated.
6. The CMIRK scheme is then used to obtain the continuous solution $u(t)$ (4.18). Then, an estimate to the defect [11] is calculated by

$$\text{Defect}_i = \frac{|u'(t_i) - f(t_i, u(t_i), u(t_i - \tau), I_i)|}{1 + |f(t_i, u(t_i), u(t_i - \tau), I_i)|}. \quad (4.26)$$

7. An adaptive algorithm is used to control the stepsize in order to keep the defect (4.26) within a specified tolerance. If the defect is not within tolerance, then the step size is halved and the iteration steps 2–7 are repeated.

4.5 Numerical Stability

In this section, we investigate the numerical stability of the underlying schemes for the scalar test problem VDIDE (4.4). For simplicity, we assume that $\tau = mh$ is constant and $m \in \mathbb{I}$, so we do not need internal stages to estimate $y(t - \tau)$ (i.e., $y(t - \tau) = y_{n-m}$). The numerical approximations are then given by

$$y_{n+1} = y_n + h \sum_{r=1}^s b_r \mathcal{K}_{n+1}^r, \quad (4.27)$$

with stages

$$\mathcal{K}_{n+1}^r = \lambda \left((1 - v_r) y_n + v_r y_{n+1} + h \sum_{j=1}^{r-1} a_{rj} \mathcal{K}_{n+1}^j \right) + \mu y_{n-m} + \gamma h \sum_{l=0}^m w_l y_{n-l}. \quad (4.28)$$

Combining the two Eqs. (4.27) and (4.28) yields

$$y_{n+1} = (1 + \alpha \mathbf{b}^T \mathbf{Se}) y_n + \beta \mathbf{b}^T \mathbf{Se} y_{n-m} + \kappa \mathbf{b}^T \mathbf{Se} \sum_{l=0}^m w_l y_{n-l}, \quad (4.29)$$

where $\alpha = h\lambda$, $\beta = h\mu$, $\kappa = h^2\gamma$, $\mathbf{S} = [\mathbf{I} - \alpha(\mathbf{V}\mathbf{b}^T + \mathbf{A})]^{-1}$, and $\mathbf{e} = (1, 1, \dots, 1)^T$ is $s \times 1$ vector.

Letting $\xi^{-1} = y_n$, we get a characteristic equation of the form

$$1 - (1 + \alpha \mathbf{b}^T \mathbf{Se}) \xi^{-1} - \beta \mathbf{b}^T \mathbf{Se} \xi^{-1-m} - \kappa \mathbf{b}^T \mathbf{Se} \sum_{l=0}^m w_l \xi^{-1-l} = 0. \quad (4.30)$$

Put $\xi^{-1} = e^{i\theta}$ in (4.30) and separate real and imaginary parts to have

$$\begin{aligned} 1 - \cos \theta &= \mathbf{b}^T \mathbf{Se} \left(\alpha \cos \theta + \beta \cos(m+1)\theta + \kappa \sum_{l=0}^m w_l \cos(l+1)\theta \right), \\ -\sin \theta &= \mathbf{b}^T \mathbf{Se} \left(\alpha \sin \theta + \beta \sin(m+1)\theta + \kappa \sum_{l=0}^m w_l \sin(l+1)\theta \right). \end{aligned} \quad (4.31)$$

When $\theta = 0$, these equations reduce to $\alpha + \beta + \kappa \sum_{l=0}^m w_l = 0 \equiv \lambda + \mu + \gamma \tau = 0$,

because Boole's quadrature rule is exact for constants, i.e., $\int_{t-\tau}^t ds = h \sum_{l=0}^m w_l = \tau$.

This is the same straight line bounding the analytical stability region obtained earlier in Sect. 4.2.

For $\theta \in (0, 2\pi)$, the boundary of the stability region is defined by (4.31). To plot this curve, we write β , G in terms of α , and after some manipulation, we have

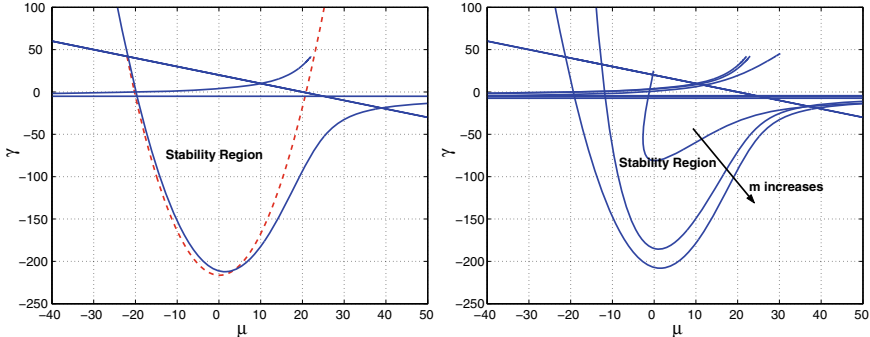


Fig. 4.3 The left banner shows the numerical stability region (solid curve) with $\lambda = -20$ and $m = 128$ compared with the boundary of the analytical stability region (dashed curve) for the same value of λ . The right banner displays the stability regions (when $\tau/h = m$) with $\lambda = -20$ and various values of $m = 8; 64; 128$. As m increases, the stability region becomes wider

$$\begin{aligned} \kappa &= (1/\sum_{l=0}^m w_l \sin(m-l)\theta) \left\{ -\alpha \sin m\theta + \frac{\sin(m+1)\theta - \sin m\theta}{\mathbf{b}^T \mathbf{S}\mathbf{e}} \right\}, \\ \beta &= -(1/(\sin(m+1)\theta - \sin m\theta)) \left\{ \alpha \sin \theta + \kappa \sum_{l=0}^m w_l (\sin(l+1)\theta + \sin l\theta) \right\}. \end{aligned} \quad (4.32)$$

Since κ and β are even functions of θ , we consider Eq. (4.32) for $\theta \in (0, 2\pi)$. Figure 4.3 shows the numerical stability regions for three values of $m=8, 64$, and 128 and fixed $\lambda = -20$. It also shows a comparison of numerical stability region with analytical stability region for fixed $\lambda = -20$ and $m = 128$. The numerical stability region becomes bigger as stepsize decreases.

4.6 Numerical Results and Simulations

In this section, we provide some numerical examples of various types of Volterra delay integro-differential equations [13] to show the effectiveness of the underlying technique.

Example 4.1 First, we consider a scalar VDIDE with continuously distributed delay of the form

$$\begin{aligned} y'(t) &= y(t-1) + \int_{t-1}^t y(s)ds, \quad t \geq 0, \\ \psi(t) &= \exp(t), \quad t \leq 0. \end{aligned} \quad (4.33)$$

The exact solution of (4.33) is $\exp(t)$. With tolerance 10^{-10} , the obtained numerical solution, using the underlying method, is plotted in Fig. 4.4 and the error function. The error is of order 10^{-5} at $t_f = 10$.

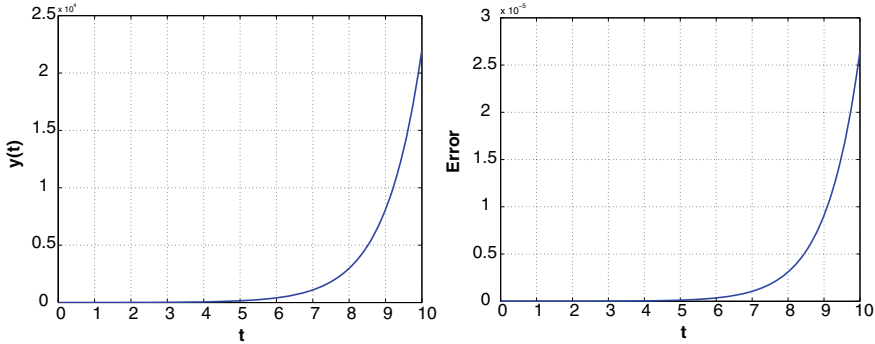


Fig. 4.4 Numerical simulation of VDIDE (4.33) (left) and the error function (right) at the mesh points

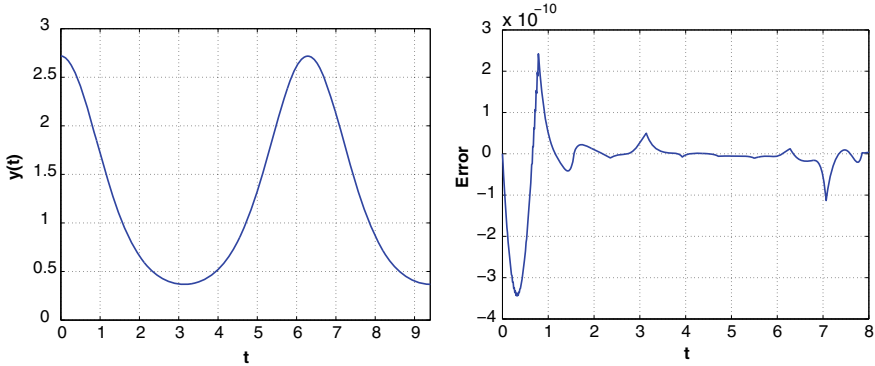


Fig. 4.5 Numerical solution of VDIDE (4.34) (left) and the error function (right) at the mesh points

Example 4.2 Now, we consider a VDIDE with variable coefficients

$$\begin{aligned} y'(t) &= -(6 + \sin t)y(t) + y(t - \pi/4) - \int_{t-\pi/4}^t \sin s y(s) ds + 5 \exp(\cos t), \quad t \geq 0 \\ \psi(t) &= \exp(\cos t), \quad t \leq 0. \end{aligned} \quad (4.34)$$

The exact solution of (4.34) is $y(t) = e^{\cos t}$. Figure 4.5 shows the numerical solution of (4.34), and corresponding error in the numerical solution which is decaying to zero, with tolerance 10^{-10} .

Example 4.3 We can also utilize CMIRK scheme to solve the non-linear system of VDIDEs of the form

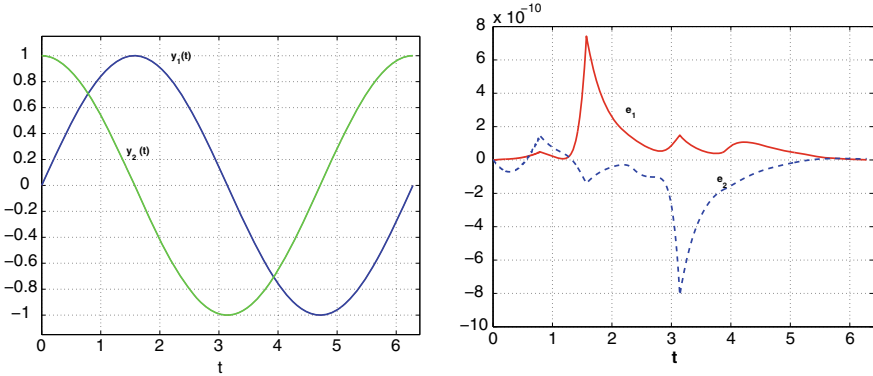


Fig. 4.6 Numerical simulations of VDIDEs (4.35) on the interval $[0, 2\pi]$ (left) and the error function (right) at the mesh points

$$\begin{aligned} \frac{d}{dt} \begin{pmatrix} y_1(t) \\ y_2(t) \end{pmatrix} = & -3 \begin{pmatrix} y_1(t) \\ y_2(t) \end{pmatrix} + \begin{pmatrix} 0 & \sin t \\ \cos t & 0 \end{pmatrix} \begin{pmatrix} y_1(t - \pi/4) \\ y_2(t - \pi/4) \end{pmatrix} \\ & + \frac{1}{\sqrt{2}} \int_{t-\pi/4}^t \begin{pmatrix} \frac{(1 + \sin^2 t)y_1^2(s)}{1 + y_1^2(s)} \\ \frac{(1 + \cos^2 t)y_2^2(s)}{1 + y_2^2(s)} + \end{pmatrix} ds + \\ & \frac{\sqrt{2}}{16} \begin{pmatrix} 16 \sin(t + \pi/4) - 2 \sin 2t + 6 \cos 2t - \pi - 4 + 16\sqrt{2} \sin t \\ 16 \cos(t + \pi/4) - 2 \sin 2t + 6 \cos 2t + \pi + 4 + 16\sqrt{2} \cos t \end{pmatrix}, \quad t \geq 0, \end{aligned} \quad (4.35)$$

$$\psi(t) = \begin{pmatrix} \sin t \\ \cos t \end{pmatrix}, \quad t \leq 0,$$

with both discretely and continuously distributed delays and bounded time-lag. This system has exact solutions $(\sin t, \cos t)$. Figure 4.6 shows the numerical solution of (4.35) with tolerance 10^{-10} and the error components e_1 and e_2 .

Example 4.4 Consider the Lotka-Volterra system of the form

$$\begin{aligned} u'(t) &= u(t) \left(1 - 0.5 v(t) - \int_0^t \exp((1.5)(s-t)) v(s) ds \right), \quad t \geq 0 \\ v'(t) &= -v(t) \left(0.75 - 0.25 u(t) - \int_0^t \exp((3.5)(s-t)) u(s) ds \right), \quad t \geq 0, \\ u(0) &= v(0) = 1. \end{aligned} \quad (4.36)$$

This system represents predator-prey population dynamics in which $u(t)$ represents the prey population size while $v(t)$ represents the predator population size. This system has continuously distributed delay and the time-lag is unbounded. Figure 4.7 shows the numerical solution for (4.36) by using CMIRK scheme with tolerance 10^{-4} .

Fig. 4.7 Numerical solution of Lotka-Volterra system (4.36)

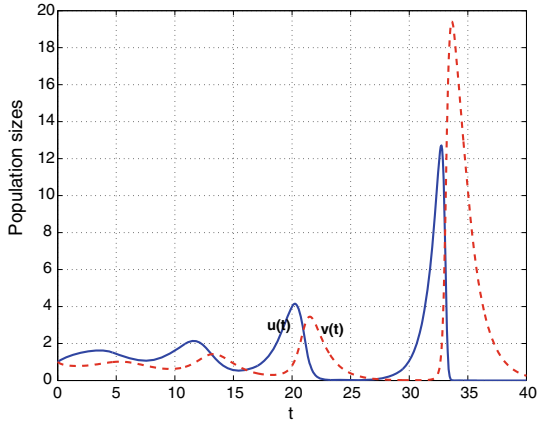
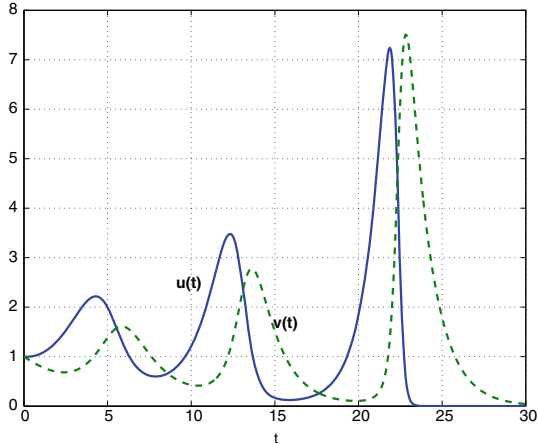


Fig. 4.8 Numerical simulation of Lotka-Volterra system (4.37), with $\tau = 1$



Now, if we change the lower bound of integration from $0 \rightarrow (t - \tau)$ where $\tau > 0$ is fixed, then Eq. (4.36) takes the form

$$\begin{aligned} u'(t) &= u(t) \left(1 - 0.5 v(t) - \int_{t-\tau}^t \exp((1.5)(s-t)) v(s) ds \right), \quad t \geq 0 \\ v'(t) &= -v(t) \left(0.75 - 0.25 u(t) - \int_{t-\tau}^t \exp((3.5)(s-t)) u(s) ds \right), \quad t \geq 0, \\ u(t) &= v(t) = 1, \quad t \leq 0. \end{aligned} \tag{4.37}$$

The oscillatory behaviors of numerical solution of the Lotka-Volterra system (4.37) are shown in Fig. 4.8, when $\tau = 1$.

4.7 Concluding Remarks

In this chapter, we have presented an efficient numerical technique for solving Volterra delay integro-differential equations. The scheme is based on continuous mono-implicit RK formulae for the differential part and Boole's quadrature rule for the integral part. Analytical and numerical stability regions have been deduced. The numerical simulations show the effectiveness of the underlying numerical technique for solving various types of VDIDEs and are also suitable for stiff as well as non-stiff problems.

In the next chapter, we shall produce a numerical view for parameter estimations with DDEs using a least squares approach.

References

1. Butcher, J.C., Chartier, P.: A generalization of singly-implicit Runge-Kutta methods. *J. Appl. Num. Math.* **24**, 343–350 (1997)
2. Cash, J.R., Singhal, A.: Mono-implicit Runge-Kutta formula for the numerical integration of stiff differential systems. *IMA J. Num. Anal.* **2**, 211–227 (1982)
3. Rihan, F.A., Doha, E.H., Hassan, M.I., Kamel, N.M.: Mono-implicit Runge-Kutta method for delay differential equations. *J. Egypt. Math. Soc.* **17**(2), 213–232 (2009)
4. Baker, C.T.H., Bocharov, G.A., Filiz, A., Ford, N.J., Paul, C.A.H., Rihan, F.A.: RM Thomas A Tang, H Tian, and DR Wille, pp. 113–137. Topics in Computer Mathematics and its Applications, LEA Athens, Hellas, Numerical modelling by delay and volterra functional differential equations (2006)
5. Brunner, H.: Collocation methods for Volterra integral and related functional differential (Cambridge Monographs on Applied and Computational Mathematics). Cambridge University Press, Cambridge (2004)
6. Muir, P.H.: Optimal discrete and continuous mono-implicit Runge-Kutta schemes for BVODEs. *J. Adv. Comput. Math.* **10**, 135–167 (1999)
7. Forsythe, G.E., Malcolm, M.A., Moler, C.B.: Computer methods for mathematical computations. Prentice-Hall Inc., Englewood Cliffs, The NJ (1977)
8. Baker, C.T.H., Ford, N.J.: Stability properties of a scheme for the approximate solution of delay-integro-differential equation. *Appl. Num. Math.* **9**, 357–370 (1992)
9. Koto, T.: Stability of θ -methods for delay integro-differential equations. *Comput. Appl. Math.* **161**
10. Muir, P.H., Owren, B.: Order barriers and characterizations for continuous mono-implicit Runge-Kutta schemes, Technical Report, 258, University of Toronto (1991)
11. Enright, W.E., Muir, P.H.: A Runge-Kutta Boundary Value ODE Solver With Defect Control, Technical Report 267/93. University of Toronto, Department of Computer Science (1993)
12. Mathews, J.H., Fink, K.K.: he Prentice-Hall Inc. Upper Saddle River, New Jersey, USA (2004)
13. Mathews, J.H., Fink, K.K.: A test set of functional differential equations. MCCM Technical Report 243, University of Manchester (1994)

Chapter 5

Parameter Estimation with Delay Differential Equations



5.1 Introduction

Estimation of model parameters is generally performed via minimization of an objective function, which represents a selected fitting criterion. It is known that observations are usually inexact, i.e., contain an uncertainty related to the measurement errors, random effects, non-linearity effects, and unknown process contribution. If the data display statistically regular features, then the standard criteria of the optimal estimation can be applied for parameter identification (e.g., the maximum likelihood method and Bayesian analysis) [1–3]. The essential points for the correct use of an approach are the availability of a sufficient amount of data and the stochastic nature of the data; see [4].

Our aim in this chapter is to estimate the unknown parameters that occur in delay differential models by using a *least squares* (LS) approach, combined with the Runge-Kutta methods (see Chap. 2) to evaluate the objective function. Some related problems associated with parameter estimation in DDEs due to the delay terms are addressed; see Sects. 5.2–5.5. Numerical results are illustrated by fitting some numerical models for different patterns of cell growth; see Sect. 5.6.

5.2 Parameter Estimation with DDEs

Consider an N-dimensional system of DDEs with multiple delays in the form

$$\begin{aligned}\mathbf{y}'(t, \mathbf{p}) &= \mathbf{f}(t, \mathbf{y}(t, \mathbf{p}), \mathbf{y}(t - \boldsymbol{\tau}, \mathbf{p}); \mathbf{p}), \quad t \in [t_0, t_0 + T], \\ \mathbf{y}(t, \mathbf{p}) &= \boldsymbol{\psi}(t; \mathbf{p}), \quad t \in [t_0 - \tau_{\min}, t_0] \quad (\tau_{\min} = \max_i \tau_i)\end{aligned}\tag{5.1}$$

where $\mathbf{y} \in \mathbb{R}^N$, $\mathbf{p} \in \mathbb{R}^L$, and $\boldsymbol{\tau} \in \mathbb{R}^{L_p}$, $L_p < L$. (The initial function as well as the initial values often contain unknown parameters.)

The classical *LS* criterion is commonly utilized for fitting a model to data. If the difference between the model predictions $\mathbf{y}(t_j, \mathbf{p})$ and the observed data \mathbf{Y}_j specified at certain points $\{t_j\}$ is expressed via the residuals, then the objective function $\Phi(\mathbf{p})$ has the following form:

$$\Phi(\mathbf{p}) := \sum_{j=1}^M w_j [F(\mathbf{Y}_j, \mathbf{y}(t_j, \mathbf{p}))]^2 = \sum_{j=1}^M w_j [\mathbf{Y}_j - \mathbf{y}(t_j, \mathbf{p})]^2 \quad (5.2)$$

where the positive weights w_j are defined by a weighting procedure, M is the total number of different observation times, and $F(\cdot)$ meets the symmetry condition $F(\mathbf{y}(\mathbf{p}), Y) = F(Y, \mathbf{y}(\mathbf{p}))$.

We should mention that some limitations of the *LS* approach have been observed in several applications. It is known that non-linear *LS* fitting can lead to several local minima, unlike the linear *LS* case where $\Phi(\mathbf{p})$ has only one minimum. To confront this problem, a non-linear Chebyshev fitting was suggested by Williams and Kalogirato [5] to increase the possibility of unique global fits. Moreover, the functional $\Phi(\mathbf{p})$ possesses different sensitivity: firstly, to the deviation of different signs of the values of $\mathbf{y}(t_i, \mathbf{p})$ from \mathbf{Y}_i ; secondly, to the choice of measurement units for $\mathbf{y}(t, \mathbf{p})$; thirdly, to the scattering of the absolute values of the observed data; and fourthly, to non-linearities of the model solutions. For these reasons, other objective functions are sometimes employed with regard to the nature of particular observation data, and the parametric non-linearities of the model solutions (see [6]) such as (in the scalar case)

$$\Phi(\mathbf{p}) = \sum_{j=1}^M w_j \left[\left(\frac{\mathbf{Y}_j - \mathbf{y}(t_j, \mathbf{p})}{\mathbf{Y}_j} \right)^2 + \left(\frac{\mathbf{Y}_j - \mathbf{y}(t_j, \mathbf{p})}{\mathbf{y}(t_j, \mathbf{p})} \right)^2 \right], \quad (5.3)$$

and

$$\Phi(\mathbf{p}) = \sum_{j=1}^M w_j \left[\log \left(\frac{\mathbf{Y}_j}{\mathbf{y}(t_j, \mathbf{p})} \right) \right]^2. \quad (5.4)$$

5.2.1 Non-linearity of Model Predictions

When the predictions are governed by differential equation models, then the *LS* approach (even for models linear in their parameters) generally yields a non-linear minimization problem. (This non-linearity comes from a combination of the quadratic transformation $[.]^2$, the ratios scaling function $F(\cdot)$, and the solution function $\mathbf{y}(t, \mathbf{p})$ of the mathematical model formulated as a parameter-dependent differential system.) The non-linearity of the fitness function $\Phi(\mathbf{p})$ with respect to \mathbf{p} can lead to several local minima. To decrease the non-linearity of $\Phi(\mathbf{p})$, the function F should be selected with this behavior of $\mathbf{y}(t, \mathbf{p})$ in mind.

To illustrate the above ideas, we consider the simplest case of the linear ODE model: $y'(t) = py(t)$. Let the model be exactly related to the observed process, and let p^* be the “true” parameter, i.e., observations are described by $Y(t) = y_0 e^{p^* t}$. The solution of the model for a perturbed p value is $y_0 e^{pt}$ (with $y(0) = y_0$). Then, the classical residual of *LS* approach leads to the non-linear minimization problem for p :

$$\Phi(\mathbf{p}) = \sum_{j=1}^M y_0^2 \left(e^{pt_j} - e^{\hat{p}t_j} \right)^2,$$

and the relative distance *LS* approach results in the problem:

$$\Phi(\mathbf{p}) = \sum_{j=1}^M \left(e^{(p-\hat{p})t_j} \right)^2.$$

Selecting the scaling function $F(.)$ as the logarithm formula (5.4) decreases the exponential non-linearity of model predictions with respect to \mathbf{p} . With this choice, one arrives at the following minimization problem:

$$\Phi(\mathbf{p}) = \sum_{j=1}^M (p - \hat{p})^2 t_j^2.$$

The last formulation is the common linear *LS* problem corresponding to the linear ODE model, $y'(t) = py(t)$.

The real situations may become much more complicated due to inexactness of models, non-linearity of the differential system, noisy observation data, and non-exponential behavior of the solution. Nevertheless, the *LS* criterion for relative distance can be scaled by a logarithmic transformation [7]:

$$\Phi(\mathbf{p}) = \sum_{j=1}^M w_j \left[\log \left(\frac{\mathbf{y}_j}{\mathbf{y}(t_j, \mathbf{p})} \right) \right]^2.$$

In the next chapter, we estimate the biases in the values of the parameter estimates due to non-linearity of the parameters, with the *LS* estimator.

5.3 Computation of Estimates

Many algorithms have been suggested for the iterative techniques for minimization of a *non-linear* objective function $\Phi(\mathbf{p})$. The Gauss-Newton iterative algorithm and the Newton-Raphson methods are employed for non-linear least squares. The Levenberg-

Marquardt algorithm is an alternative method to the Gauss-Newton method suggested by Moré [8]. For more details and references, refer to Bard [1].

5.3.1 Basic Iteration

The methods we consider for minimizing $\Phi(\mathbf{p})$ are iterative in nature. We start with a given point \mathbf{p}_1 , known as the initial guess, and proceed to generate a sequence of points $\mathbf{p}_2, \mathbf{p}_3, \dots$ that we hope converge to the point $\widehat{\mathbf{p}}$ at which $\Phi(\widehat{\mathbf{p}})$ is minimum. (The computation of \mathbf{p}_{i+1} is called the i th iteration.) In practice, one terminates the sequence after a finite number k of iterations and one accepts \mathbf{p}_k as an approximation to $\widehat{\mathbf{p}}$. The vector

$$\boldsymbol{\sigma}_i = \mathbf{p}_{i+1} - \mathbf{p}_i \quad (5.5)$$

is called the i th step. We wish each step to bring us closer to the minimum. Since we do not know where the minimum is, we cannot test for this condition directly. In a sense, however, we may consider the i th step to have “improved” our situation if

$$\Phi_{i+1} < \Phi_i, \quad (5.6)$$

where $\Phi_j = \Phi(\mathbf{p}_j)$ ($j = 1, 2, \dots$). We call the i th step *acceptable* if Eq. (5.6) holds. An iterative method is acceptable if all the steps of its procedures are acceptable. We shall only consider acceptable methods.

The methods we consider are based on the following scheme:

1. Set $i = 1$. An initial guess \mathbf{p}_1 must be provided.
2. The model solution values $\{\mathbf{y}(t_j, \mathbf{p}_1)\}$ are obtained numerically.
3. Determine a vector \mathbf{v}_i (see Theorem 1) in the direction of the proposed i th step.
4. Determine a scalar ρ_i such that the step

$$\boldsymbol{\sigma}_i = \rho_i \mathbf{v}_i$$

is acceptable. That is, we take

$$\mathbf{p}_{i+1} = \mathbf{p}_i + \rho_i \mathbf{v}_i \quad (5.7)$$

and require that ρ_i be chosen so that Eq. (5.6) holds.

5. Test whether the termination criterion

$$|\mathbf{p}_{i+1,j} - \mathbf{p}_{i,j}| \leq \epsilon_j \quad (j = 1, 2, \dots, L),$$

where $\mathbf{p}_{i,j}$ is the j th component of \mathbf{p}_i . If not, increase i by one and return to step 3. Otherwise, accept \mathbf{p}_{i+1} as the value of $\widehat{\mathbf{p}}$.

5.3.2 Acceptability

Consider the i th iteration of a minimization procedure. Suppose we strike out from \mathbf{p}_i along some direction \mathbf{v} , generating the ray

$$\mathbf{p}(\rho) \equiv \mathbf{p}_i + \rho\mathbf{v}, \quad (\rho \in \mathbb{R}).$$

Along this ray, the objective function varies as ρ is changed, thus becoming a function of ρ alone. We designate this function as

$$\Psi_{i\mathbf{v}}(\rho) \equiv \Phi(\mathbf{p}(\rho)) = \Phi(\mathbf{p}_i + \rho\mathbf{v}),$$

and its derivative is given by

$$d\Psi_{i\mathbf{v}}/d\rho = (\partial\Phi/\partial\mathbf{p})^T(\partial\mathbf{p}/\partial\rho) = (\partial\Phi/\partial\mathbf{p})^T\mathbf{v}.$$

The gradient vector of $\Phi(\mathbf{p})$ is $\partial\Phi/\partial\mathbf{p} := \mathbf{q}(\mathbf{p})$. Denoting the gradient vector evaluated at $\mathbf{p} = \mathbf{p}_i$ by \mathbf{q}_i , we have

$$\Psi'_{i\mathbf{v}} \equiv d\Psi_i/d\rho|_{\rho=0} = \mathbf{q}_i^T\mathbf{v}.$$

In the sequel, we assume $\mathbf{q}_i \neq 0$.

The quantity $\Psi'_{i\mathbf{v}}$ is called the *directional derivative* of Φ relative to \mathbf{p}_i . If $\Psi'_{i\mathbf{v}} < 0$, then $\Phi(\mathbf{p})$ decreases in value when one starts moving away from \mathbf{p}_i in the direction of \mathbf{v} . Therefore, if ρ is a sufficiently small positive number, the step $\rho\mathbf{v}$ is acceptable. On the other hand, if $\Psi'_{i\mathbf{v}} \geq 0$, a positive value of ρ for which $\rho\mathbf{v}$ is an acceptable step may not exist. We call \mathbf{v} an *acceptable direction* if $\Psi'_{i\mathbf{v}} < 0$.

Theorem 1 A direction \mathbf{v} is acceptable if and only if there exists a positive definite matrix R such that $\mathbf{v}_i = -R\mathbf{q}_i$.

For the proof, see Bard [1].

Therefore, the basic equation of the i th iteration in any gradient method is

$$\mathbf{p}_{i+1} = \mathbf{p}_i - \rho_i R_i \mathbf{q}_i, \tag{5.8}$$

and various gradient methods differ in the manner of choosing R_i and ρ_i . If $\rho_i = 1$ and $R_i = H_i^{-1}$ (where $H := \partial^2\Phi(\mathbf{p})/\partial\mathbf{p}\partial\mathbf{p}^T$ is the Hessian matrix), then Eq. (5.8) defines the i th iteration of the Newton (or Newton-Raphson) method.

5.3.3 Convergence

The main aim is that the selected method converges to a true global minimum of the objective function. Convergence proofs usually require certain assumptions to

be made concerning the nature of the objective function, and the validity of these assumptions is difficult to verify for any given problem. A method may converge in theory and yet may take an excessive number of iterations or require computations to be carried out with a reasonable number of significant digits.

Suppose $\Phi(\mathbf{p})$ is smooth as a function of \mathbf{p} in the neighborhood of the optimal parameter $\hat{\mathbf{p}}$, and let Φ_i denote the value of $\Phi(\mathbf{p}_i)$. If we select (at each iteration) an acceptable point, then the sequence $\{\Phi_i\} \equiv \{\Phi_0, \Phi_1, \Phi_2, \dots\}$ is monotone decreasing. If the values of the objective function possess a lower bound, and the sequence $\{\mathbf{p}_i\}$ is bounded, then this sequence must converge to a limit Φ_∞ . It follows from the assumption of continuity of Φ that $\Phi(\mathbf{p}_\infty) = \Phi_\infty$, where \mathbf{p}_∞ is any limit point of $\{\mathbf{p}_i\}$. In all practical cases, the sequence $\{\mathbf{p}_i\}$ is either unbounded (and has more than one limit point) or converges to a point \mathbf{p}_∞ . The rate of convergence, however, may be so slow that the sequence appears non-convergent.

A *stationary point* of the objective function is one at which $\mathbf{q}(\mathbf{p}) = 0$. If \mathbf{p}_i is stationary, i.e., $\mathbf{q}_i = 0$, then Eq.(5.8) shows that all $\mathbf{p}_j (j \geq i)$ coincide with \mathbf{p}_i . Convergence to the true minimum can be guaranteed only if it can be shown that the objective function has no other stationary points. To obtain a true minimum, the initial guess of the parameter values should be sufficiently close to the global minimum. The graphs in Sect. 6 show the stationary points of the objective functions corresponding to some related cell division examples with experimental data points. The graphs also show the sensitivity of the objective function $\Phi(\mathbf{p})$ to the variations of the parameters in the neighborhood of minimum points.

5.4 Discontinuities Associated with Delay

One obvious difficulty with such procedures (from both practical and theoretical viewpoints) is that solutions of DDEs are not generally differentiable with respect to the lag τ .¹ In addition, some discontinuities can arise and propagate in the solution of DDE. Such discontinuities, when arising from the initial point $t_0(\mathbf{p})$ (and the initial function $\psi(t, \mathbf{p})$), may propagate into $\Phi(\mathbf{p})$ via the solution $y(t, \mathbf{p})$ if it has a jump at one of the data points $\{\zeta_i\}$. Let us explain this further.

From the fact that

$$\left(\frac{\partial \Phi(t_i; \mathbf{p})}{\partial p_l} \right)_\pm = -2 \sum_{i=1}^M [Y(t_i) - y(t_i; \mathbf{p})] \left(\frac{\partial y(t_i; \mathbf{p})}{\partial p_l} \right)_\pm, \quad (5.9)$$

¹ τ need not be a parameter but could depend on the parameters.

$$\begin{aligned} \left(\frac{\partial^2 \Phi(t_i; \mathbf{p})}{\partial p_l \partial p_m} \right)_{\pm\pm} &= 2 \sum_{i=1}^M \left[\left(\frac{\partial y(t_i; \mathbf{p})}{\partial p_l} \right)_+ \left(\frac{\partial y(t_i; \mathbf{p})}{\partial p_m} \right)_+ \right. \\ &\quad \left. - [Y(t_i) - y(t_i; \mathbf{p})] \left(\frac{\partial^2 y(t_i; \mathbf{p})}{\partial p_l \partial p_m} \right)_{\pm\pm} \right], \end{aligned} \quad (5.10)$$

$$\frac{\partial}{\partial \tau} y(t_i - \tau; \mathbf{p}) = -y'(t_i - \tau; \mathbf{p}). \quad (5.11)$$

It is clear from Eqs. (5.9), (5.10), and (5.11) that, unless $Y(t_i) = y(t_i; \mathbf{p})$, jumps can arise in the first or the second partial derivative of $\Phi(\mathbf{p})$, with respect to p_l , if the first or the second partial derivatives of $y(t; \mathbf{p})$ with respect to p_l has a jump at $t = t_i$ (one of the data points). These jumps can propagate into the second derivative of $\Phi(\mathbf{p})$ if the first derivative of $y(t; \mathbf{p})$, with respect to p_l , has a jump at one of the data points $t = t_i$ even when $Y(t_i) = y(t_i; \mathbf{p})$. Jumps can also arise in the derivatives of $\Phi(\mathbf{p})$ if lag τ is considered as a parameter to be estimated and the derivative of $y(t; \mathbf{p})$ (with respect to t) has a jump at one of the data points. For further discussion about these issues, refer to [6].

As a result of the above remarks, we see that parameter estimation in DDEs (5.1) mainly depends on

- differentiability of the solution $y(t; \mathbf{p})$ of the DDEs with respect to parameter \mathbf{p} ;
- the existence and uniqueness of the solution y , which depends on the initial function ψ and parameter \mathbf{p} ;
- existence and position of the jump discontinuity points depending on τ ;
- the statistical nature of the observed data points $\{t_i, Y(t_i)\}_{i=1}^M$.

One can also establish the connection between jumps in the derivatives of $y(t; \mathbf{p})$ with respect to t and the partial derivatives (in $\Phi(\mathbf{p})$) of $y(t; \mathbf{p})$ with respect to some p_l . Let us rewrite the scalar case of (5.1) in the form

$$\begin{aligned} y'(t, \mathbf{p}) &= f(t, y(t, \mathbf{p}), y(\sigma(t), \mathbf{p}); \mathbf{p}), \quad t \geq t_0, \\ y(t, \mathbf{p}) &= \psi(t; \mathbf{p}), \quad t \leq t_0, \end{aligned} \quad (5.12)$$

where $\sigma(t) = t - \tau$. Differentiating both sides of (5.12) with respect to p_l gives the variational system of the form

$$\begin{aligned} \frac{d}{dt} y_l(t; \mathbf{p}) &= \frac{\partial f}{\partial y(t, \mathbf{p})} (t, y(t, \mathbf{p}), y(\sigma(t), \mathbf{p}); \mathbf{p}) \frac{\partial y(t, \mathbf{p})}{\partial p_l} + \\ &\quad \frac{\partial f}{\partial y(\sigma(t), \mathbf{p})} (t, y(t, \mathbf{p}), y(\sigma(t), \mathbf{p}); \mathbf{p}) y'(\sigma(t), \mathbf{p}) \frac{\partial \sigma(t)}{\partial p_l} + \\ &\quad \frac{\partial f}{\partial p_l} (t, y(t, \mathbf{p}), y(\sigma(t), \mathbf{p}); \mathbf{p}), \end{aligned} \quad (5.13)$$

$$y_l(t; \mathbf{p}) = \psi_l(t; \mathbf{p}), \quad t \leq t_0,$$

where $y_l(t; \mathbf{p}) \equiv \frac{\partial y(t; \mathbf{p})}{\partial p_l}$. Note that Eqs. (5.12) and (5.13) together give a system of *neutral* delay differential equations (NDDEs). The jumps in the solution of this system are clearly intimately related to the jumps in the derivatives $y(t, \mathbf{p})$ with respect to t in the delay differential system. Such jumps can spread forward along the integration interval; see Sect. 2.1.

In the case of state-dependent DDEs, the problem may become more complicated. In this case, Hartung and Turi [9] provided the sufficient conditions of differentiability of the solutions with respect to the parameters in the following theorem:

Theorem 2 *In case of state-dependent DDEs ($\tau = \tau(t, y(t); \mathbf{p})$), the derivatives of $\Phi(\mathbf{p})$ in (5.9)–(5.10) and $y'_l(t; \mathbf{p})$ in (5.13) exist if*

- A1. *$f(t, u, v; p)$ is (i) continuous; (ii) locally Lipschitz continuous in u , v , and \mathbf{p} ; and (iii) continuously differentiable with respect to u , v , and \mathbf{p} .*
- A2. *$\tau(t, \psi; \mathbf{p})$ is (i) continuous; (ii) locally Lipschitz continuous in ψ and \mathbf{p} ; (iii) continuously differentiable with respect to t , ψ , and \mathbf{p} ; and (iv) the derivatives $\frac{\partial \tau}{\partial t}$, $\frac{\partial \tau}{\partial \psi}$, and $\frac{\partial \tau}{\partial \mathbf{p}}$ are locally Lipschitz continuous in ψ and \mathbf{p} .*
- A3. *$\psi(t; \mathbf{p})$ is (i) continuous, (ii) locally Lipschitz continuous in \mathbf{p} , and (iii) continuously differentiable with respect to t and \mathbf{p} .*

The following two examples indicate how jumps can arise into the objective function $\Phi(\mathbf{p})$ and into the system (5.13), via the solution $y(t; \mathbf{p})$.

Example 1 Consider a DDE

$$\begin{aligned} y'(t; \mathbf{p}) &= \lambda y(t - \tau) \text{ for } t \geq 0, \\ y(t, \mathbf{p}) &= \beta, \quad t \leq 0. \end{aligned}$$

In this case, $\mathbf{p} = [\lambda, \tau, \beta]^T$ and we note that $y^{(n-1)}(t; \mathbf{p})$ has jumps at $n\tau$ $n \in \mathbb{N}$. However, no jumps occur in the partial derivative of $\Phi(\mathbf{p})$ with respect to λ , or β . If the lag τ is to be estimated, then $\partial \Phi / \partial \tau$ may have jumps at $\tau = t_i/n$.

5.5 Solving the Minimization Problem

The task of parameter estimation is one of minimizing a suitable Objective function $\Phi(\mathbf{p})$, e.g., one given by (5.2), defined by the unknown parameters and based on the observed data. In the case of parameter estimation for DDEs, this can include not only estimating parameters appearing in the DDEs but also estimating the position of the initial point, the initial function, and the delayed arguments.

For example, consider the problem of estimating the parameters ρ_0 , ρ_1 , ρ_2 , and τ in the model (5.14). The optimum parameter $\hat{\mathbf{p}} \equiv [\hat{\rho}_0, \hat{\rho}_1, \hat{\rho}_2, \hat{\tau}]^T$ is taken to be the value such that

$$\Phi(\hat{\mathbf{p}}) \leq \Phi(\mathbf{p})$$

for all physically meaningful values of \mathbf{p} and $\hat{\mathbf{p}}$.

Given a set of experimental data $\{\mathbf{Y}_j\}_{j=1}^N$, the technique for finding the best-fit parameter values for a given mathematical model and objective function involves

1. Providing an initial guess for the parameter estimates.
2. Solving the model equations at the current values of the parameters to compute $\Phi(\mathbf{p})$.
3. The parameter values are then adjusted (by using a suitable minimization routine, such as EO4UPF² in the NAG library, LMDIF from³ NETLIB, and FMINS in MATLAB) so as to reduce the value of the objective function.
4. When no further reduction in the value of $\Phi(\mathbf{p})$ is possible, the (*local*) best-fit parameter values have been found.

To find the *global* best-fit parameter values, the initial estimate of the parameter values should be sufficiently close to the global minimum. Thus, good starting estimates for the parameter values can be of great assistance, both in speeding up the minimization process and finding the global minimum.

5.6 Models and Goodness of Fit for Cell Growth

As mentioned in the introduction, cell division, as well as cell differentiation and cell maturation, is not an instantaneous process but takes a finite time to occur. Our aim here is to demonstrate how a mathematical model of cell growth that incorporated a time-lag in the cell division phase provides both a qualitatively and quantitatively better fit to certain reported data than the classical exponential ODE growth model.

The models that we consider here are selected from a hierarchy of NDDEs, the most complex linear model being

$$\begin{aligned} \frac{dy}{dt} &= \rho_0 y(t) + \rho_1 y(t - \tau_{cell}) + \rho_2 y'(t - \tau_{cell}) \quad (t \geq 0), \\ y(t) &= \Psi(t) \quad (-\tau_{cell} \leq t < 0), \end{aligned} \tag{5.14}$$

where $y'(t)$ is the right-hand derivative of $y(t)$ with respect to t and $y(0) = y_0$ is given. This equation is a linear NDDE with four scalar parameters ρ_0 , ρ_1 , ρ_2 , and τ_{cell} . An additional parameter β may be introduced to model the fraction of cells that divide over the first step, so that $y(t) = \beta\Psi(t)$ for $t \in [-\tau_{cell}, 0]$. One possible biological interpretation of these parameters is given in Table 5.1.

By instantaneous cell growth, we mean that the rate of growth is dependent on the *current* cell populations. Similarly, by “delayed” cell growth, we mean that the rate

² EO4UPF is designed to minimize an arbitrary smooth sum of squares function subject to constraints (which may include simple bounds on the variables, linear constraints, and smooth non-linear constraints) using a sequential quadratic programming (SQP) method [10].

³ LMDIF is an unconstrained minimization routine (used in Archi-1 code [11]) based on the Levenberg-Marquardt algorithm [8].

Table 5.1 One possible biological meaning of the parameters in the NDDE (5.14)

| Parameter | Biological interpretation |
|------------------------|--|
| $\tau_{cell} > 0$ | The average cell-division time |
| $\rho_0 \geq 0$ | The proportionate rate of instantaneous asynchronous cell growth |
| $\rho_1 \geq 0$ | The proportionate rate of delayed asynchronous cell growth |
| $0 \leq \rho_2 \leq 2$ | A measure of the proportionate rate of delayed synchronous cell growth |

of growth is dependent on some *previous* cell population. In the case of idealized synchronous growth, $\rho_0 = 0$, $\rho_1 = 0$, and $\rho_2 = 2$, the degree of synchronization of cells in the cell population remains constant. However, it should be noted that the effects of synchronizing a cell culture are usually only temporary; see [12].

The simplest model based on (5.14) is the *exponential growth model*:

$$\frac{dy}{dt} = \rho_0 y(t) \quad (t \geq 0), \quad (5.15)$$

with $y(t) = y_0 \exp(\rho_0 t)$ for $t \geq 0$. Another model based on (5.14) is the *time-lag growth model*

$$\begin{aligned} \frac{dy}{dt} &= \rho_1 y(t - \tau_{cell}) \quad (t \geq 0), \\ y(t) &= \Psi(t) \quad (-\tau_{cell} \leq t < 0). \end{aligned} \quad (5.16)$$

One of our aims is to demonstrate the *qualitative* and *quantitative* differences between different models based on (5.14). In practice, approximate solutions of (5.14) are obtained numerically (see Chap. 2), and so a hierarchy of that model can be considered.

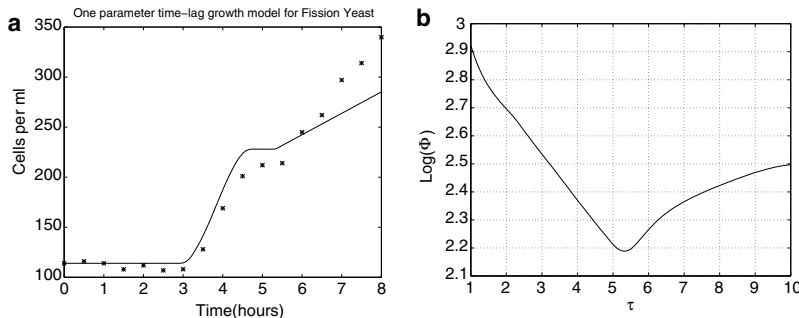
Nest, we analyze two different patterns of cell growth to demonstrate the *qualitative* and *quantitative* differences between various models in our hierarchy. The qualitative fit is indicated by a graph of the best-fit solution and the experimental data, while the quantitative fit is indicated by the norm of the residual vector $\|\text{Err}\|_2 = \sqrt{\Phi(\mathbf{p}^*)}$ and the standard deviations of the best-fit parameter values.

5.6.1 Problem 1: Fitting DDEs with Growth of Fission Yeast

We analyze the growth of *fission yeast* using data that does not exhibit exponential growth [13]. The data for yeast growth are given in Table 5.2 (see [13, Fig. 4f]). The features of the model are given in [14] as (i) the cell growth is not exponential, and (ii) the cells are synchronized at time zero.

Table 5.2 Data for non-exponential fission yeast growth

| | | | | | | | | | |
|--------------|-----|-----|-----|-----|-----|-----|-----|-----|-----|
| Time (hours) | 0.0 | 0.5 | 1.0 | 1.5 | 2.0 | 2.5 | 3.0 | 3.5 | 4.0 |
| Cells per ml | 114 | 116 | 114 | 108 | 112 | 107 | 108 | 128 | 169 |
| Time (hours) | 4.5 | 5.0 | 5.5 | 6.0 | 6.5 | 7.0 | 7.5 | 8.0 | |
| Cells per ml | 201 | 212 | 214 | 245 | 262 | 297 | 314 | 340 | |

**Fig. 5.1** a The best-fit solution of a one-parameter time-lag model to the observed data in Table 5.2. b Local uniqueness of the best fit and the dependence of Φ values on parameter τ **Table 5.3** Least squares estimates and standard deviations of the parameters for fission yeast growth models

| Exponential Model | | Time-Lag Model | | | | | | | |
|--------------------|----------------------|--------------------|---------------------|-----------------------|---------------------------|------------------|---------|-----------------|--------------------|
| τ_{cal} (hrs) | $\sigma(\tau_{cal})$ | $ \text{Err} _2$ | τ_{cell} (hrs) | $\sigma(\tau_{cell})$ | $\rho_1 (\text{hr}^{-1})$ | $\sigma(\rho_1)$ | β | $\sigma(\beta)$ | $ \text{Err} _2$ |
| 5.44 | 0.241 | 113 | 5.33 | 0.163 | — | — | — | — | 86 |
| — | — | — | 5.58 | 0.054 | 0.399 | 0.018 | — | — | 28 |
| — | — | — | 5.45 | 0.038 | 0.443 | 0.014 | 0.864 | 0.019 | 15 |

The exponential growth model can only provide an estimate of the culture-doubling time $\tau_{culture}$. However, the time-lag growth model (5.16) can provide estimates of the average cell-division time τ_{cell} , the fraction β of cells dividing over the first step, and the rate of commitment of cells ρ_1 to cell division (see Table 5.3).

It may be noted that the quantitative consistency of the exponential model is worse than that of the time-lag model (as measured by $||\text{Err}||_2$). Results in Table 5.3 indicate that, as the number of parameters being estimated in the time-lag model increases, the quantitative consistency of the model with the data improves significantly. However, the standard deviations (in Table 5.3) also indicate that, as the number of parameters being estimated in the time-lag model increases, the accuracy of the parameter estimates improves. It may also be observed that the values of $\tau_{culture}$ and τ_{cell} for the three-parameter time-lag model are the same, although their standard deviations differ by a factor of 6. The qualitative consistency of the models is indicated by the graphs in Figs. 5.1, 5.2a, and 5.3a., while Figs. 5.1b, 5.2b, and 5.4 show the local

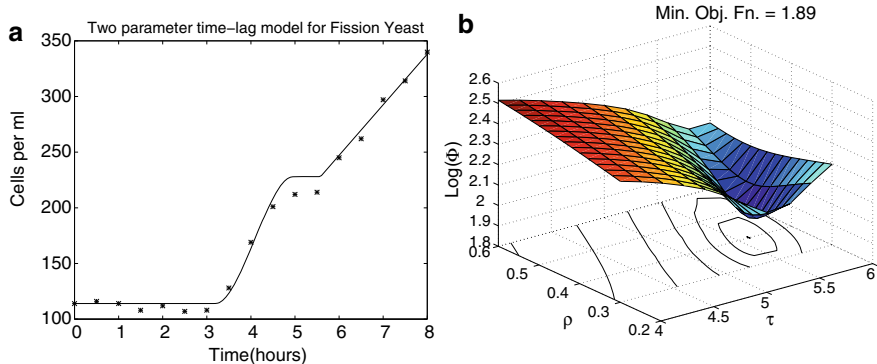


Fig. 5.2 **a** The best-fit solution of a two-parameter time-lag model to the observed data in Table 5.2.
b The local uniqueness of the best fit and the dependence of Φ values on parameter τ/ρ_1

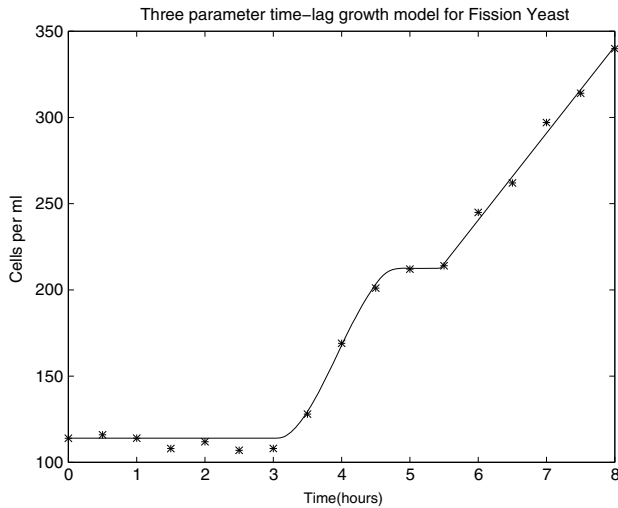


Fig. 5.3 The best-fit solution of a three-parameter time-lag model to the observed data in Table 5.2

uniqueness of the best fit at the concerned range of estimate and dependence of Φ on the parameter estimates for time-lag growth models.

5.6.2 Fitting DDEs with Growth of *Tetrahymena Pyriformis*

Given a general form of linear NDDE (5.14) and experimental data given in Table 5.4 of a non-monotone cell growth, provided by the in vitro system of synchronized *Tetrahymena pyriformis* cells [15], we demonstrate how the above mathematical

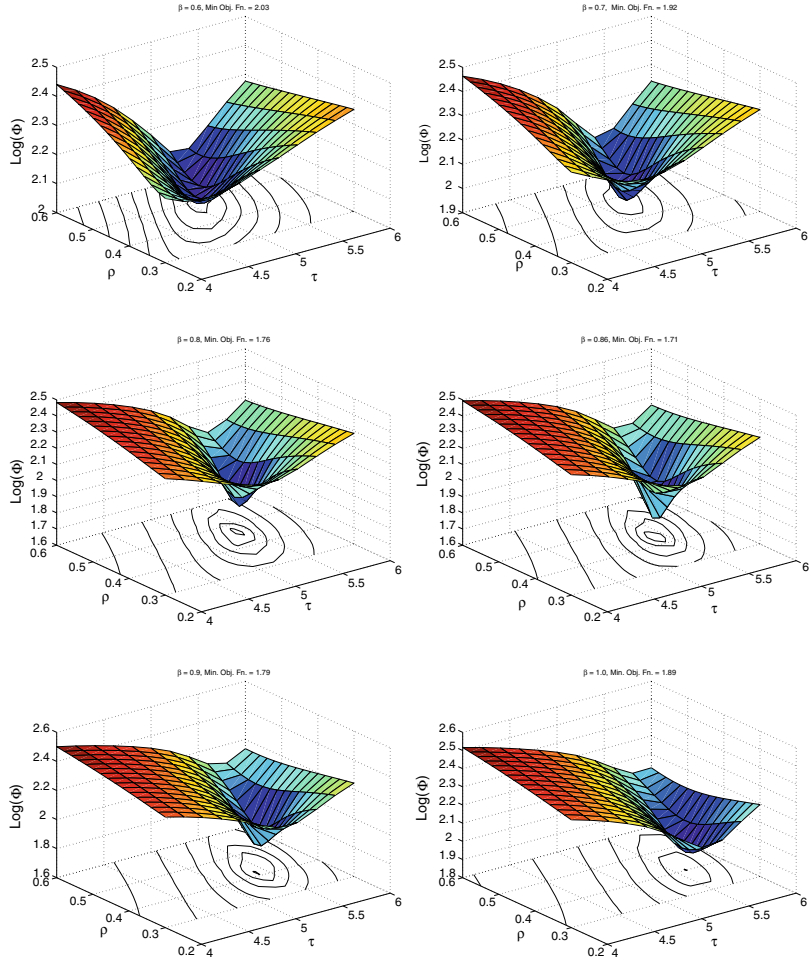


Fig. 5.4 a → f The local uniqueness of the best fit and the dependence of Φ values on parameters τ , ρ_1 , and β . Each point in the grid was calculated for fixed values of $\beta = 0.5 : 0.1 : 1$.

model of cell growth that incorporated a time-lag in the cell-division phase provides both a qualitative and quantitative consistency with the reality. We adopt the LS approach to fit the observations to model (5.14) to evaluate the unknown parameters of the model. We consider here a uniform initial function $\psi(t) = 25$ for $t \in [-\tau, 0]$, and initial value $y(0) = 50$. The graph of Fig. 5.5 displays model prediction for the best-fit parameters given in Table 5.5. Prescott (1959) [15] measured the *generation times*⁴ of a population of *Tetrahymena pyriformis* cells under uniform conditions. The distribution of generation times in the cell population was displayed for a sub-

⁴ *Generation time*, which varies from cell to cell, is defined as the age at which a cell divides, where age is time measured from birth of a cell.

Table 5.4 Data for growth of a population of ciliates (*Tetrahymena pyriformis*) (see Fig. 2 in Prescott (1959))

| Time (mins) | 0.0 | 22.2 | 42.5 | 59.2 | 83.3 | 90.7 | 98.1 | 101.8 | 105.5 | 109.2 | 111.1 |
|-------------|-------|-------|-------|-------|-------|-------|-------|-------|-------|-------|-------|
| Cell no. | 50 | 49 | 49 | 48 | 49 | 53 | 61 | 66 | 71 | 79 | 85 |
| Time (mins) | 114.8 | 118.5 | 122.2 | 125.9 | 133.3 | 138.8 | 151.8 | 168.5 | 181.4 | 190.7 | 196.2 |
| Cell no. | 90 | 93 | 96 | 99 | 102 | 101 | 100 | 101 | 101 | 102 | 105 |
| Time (mins) | 201.8 | 205.5 | 209.2 | 211.1 | 214.8 | 216.6 | 220.3 | 222.2 | 225.5 | 228.8 | 232.5 |
| Cell no. | 110 | 115 | 119 | 125 | 132 | 137 | 144 | 150 | 157 | 162 | 170 |
| Time (mins) | 235.1 | 238.8 | 243.7 | 248.1 | 254.8 | 259.2 | 266.6 | 274 | 279.6 | 288.8 | 296.2 |
| Cell no. | 175 | 179 | 184 | 187 | 191 | 194 | 197 | 197 | 198 | 200 | 215 |
| Time (mins) | 302.9 | 312.2 | 322.2 | 331.4 | 339.9 | 351.8 | 359 | 370.3 | 379.6 | 388.8 | 398.1 |
| Cell no. | 230 | 250 | 275 | 305 | 325 | 350 | 365 | 380 | 395 | 410 | 425 |

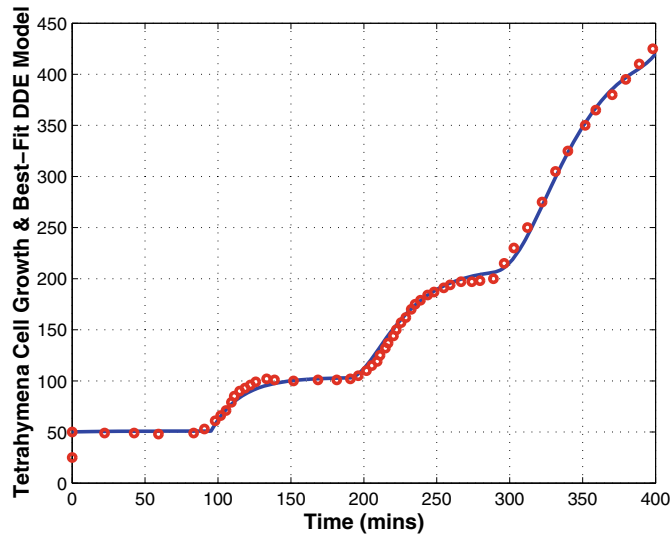


Fig. 5.5 The circles, Y_i , represent the data for growth of a population of $Y_0 = 50$ of newborn cells of *Tetrahymena pyriformis*. This data represents the multiplication of 25 cells in perfect division synchrony at first population doubling. The line $y(t, p)$ shows the prediction of the perfect model that is based on the DDE (5.14), with $y(0) = 50$, $y(t) = 25$ for $t < 0$, and best-fit parameters given in Table 5.5. The initially synchronized cell population becomes desynchronized over time

population of newborn cells at a given time from the *synchronized* cell population, all of age zero. The mean generation time $\tilde{\tau}$ was 111 min, which is close to the estimated value of the best fit, $\tau = 96.33$; see Table 5.5. The parameters are estimated and displayed in Table 5.5. A MATLAB program and Archi code are utilized to estimate the parameters and simulate the best-fit solutions. Fitting of the parametric growth models to the given experimental data is obtained using the a MATLAB program and Archi code [11].

Table 5.5 Parameter estimates, STD $\sigma(\cdot)$, errors of the growth model (5.14) that best fits data of Table 5.4

Parameter estimates for *Tetrahymena pyriformis* growth model

| Model | ρ_0 | ρ_1 | ρ_2 | τ | $\ Err\ _2$ |
|-----------------|----------|----------|----------|--------|-------------|
| Parameters | -0.0518 | 0.1054 | - | 96.33 | 34.41 |
| $\sigma(\cdot)$ | 0.0034 | 0.0082 | - | 0.0168 | |

5.7 Concluding Remarks

In this chapter, we have discussed some numerical techniques for parameter identification in DDEs as well as some problems associated with the delay term. We have seen from the numerical results that a mathematical model of cell growth that incorporated a time-lag in the cell-division phase provides both a qualitatively and quantitatively better fit to certain reported data than the classical exponential ODE growth model.

Additionally, the use of DDE models can give a direct estimate of some relevant growth parameters of synchronous cultures, such as (i) the cell-division time, (ii) the fraction of cells that are dividing, (iii) the rate of commitment of cells to cell division, (iv) the degree of synchronization of cells in the population, and (v) the death rate of cells. While using ODE models gives an indirect estimate of the culture-doubling time, $\tau_{culture} = \ln(2)/\rho_0$. Jumps can arise in the derivatives of $\Phi(\mathbf{p})$ due to the delay terms, especially if the lag τ is considered as a parameter to be estimated.

The question that arises here is the following: How does the parameters' uncertainty affect the model predictions? In the next chapter, we shall examine the sensitivity analysis (the effect of perturbing the optimal parameters and changes due to noisy data) and estimate the biases in the values of the parameters due to the non-linearity.

References

1. Bard, Y.: Nonlinear parameter estimation. Academic, New York (1974)
2. Bates, D.M., Watts, D.G.: Nonlinear regression analysis and its applications. Wiley, New York (1988)
3. Ratkowsky, D.A.: Nonlinear Regression Modelling, a Unified Practical Approach. Marcel Dekker, New York (1983)
4. Bertuzzi, A., Bruni, C., Grandolfi, A., Koch, G.: Maximum likelihood identification of an immune response model, in marchuk, ed., modelling optimization of complex systems
5. William, J., Kalogiratou, Z.: Least squares and chebyshev fitting for parameter estimation in ODE's. Adv. Comput. Math. **1**, 357–366 (1993)
6. Rihan, F.A.: Numerical treatment of delay differential equations in bioscience. University of Manchester, UK Ph.D. Thesis (2000)
7. Bocharov, G.A., Romanyukha, A.A.: Numerical treatment of parameter identification problem for delay differential systems arising in immune response modelling. Appl. Num. Math. **15**, 307–326 (1994b)

8. Moré, J.J.: The levenberge-marquardt algorithm, in: (g.a. watson ed.), numerical analysis: proceedings of the binnial conference held at dundee. Lecture Notes in Mathematics, vol. 630. Springer (1977)
9. Hartung, F., Turi, J.: On differentiability of solutions with respect to parameters in state-dependent delay equations. *J. Diff. Equ.* **135**, 192–237 (1997)
10. Gill, P.E., Murray, W., Saunders, M.A., Wright, M.H.: Practical Optimization. Academic, London and New York (1981)
11. Paul, C.A.H.: A user-guide to archi: An explicit runge-kutta code for solving delay and neutral differential equations and parameter estimation problems, MCCM Technical Report 283, University of Manchester (1997)
12. Chiu, C., Hoppensteinadt, F.C.: A particle method for population shock waves with application to synchronization of bacterial culture growth
13. Moreno, S., Nurse, P.: Regulation of progression through the G1 phase of the cell-cycle by the rum1(+) gene. *Nature* **367**, 236–242 (1994)
14. Baker, C.T.H., Bocharov, G.A., Paul, C.A.H., Rihan, F.A.: Modelling and analysis of time-lags in cell proliferation. *J. Math. Biol.* **37**(4), 341–371 (1998)
15. Prescott, D.M.: Variations in th individual generation times of Tetrahymena geleii HS. *Exp. Cell Res.* **16**, 279–284 (1959)

Chapter 6

Sensitivity Analysis of Delay Differential Equations



6.1 Introduction

Delay differential equations can be used to model many problems in biosciences and are parameterized by meaningful constant parameters p or/and variable parameters (e.g., control functions) $u(t)$. It is often desirable to have information about the effect on the solution of the dynamic system of perturbing the initial data, control functions, time-lags, and other parameters appearing in the model. The main purpose of this chapter is to derive a general theory for the sensitivity analysis of mathematical models that contain time-lags. In this chapter, we use *adjoint equations* and *direct methods* to estimate the sensitivity functions when the parameters that appear in the model are not only constants but also variables of time. To illustrate the results, the methodology is applied numerically to an example of a delay differential model.

Many studies in the sensitivity analysis of models without delay have been done (see, e.g., [1–4]); however, there are few results on sensitivity analysis for time-lag systems. A knowledge of how the state variable can vary with respect to small variations in the initial data, parameters (or constant lags) appearing in the model, and the control functions can yield insights into the behavior of the model and can actually assist the modeling process. Sensitivity analysis may provide some guidelines for the reduction of complex models by indicating those variables and parameters that determine the essential behavior of the system and, hence, must be retained in any simpler model. For example, if it can be seen that a particular parameter has no effect on the solution, it may be possible to eliminate it, at some stages, from the modeling process.

In this chapter, we evaluate sensitivity functionals of DDEs with constant and variable parameters. We estimate general sensitivity coefficients for the constant parameters appearing in the model, and functional derivative sensitivity coefficients for variable coefficients such as initial and control functions. We utilize variational method in Sect. 6.3 and direct method in Sect. 6.4. In the variational approach, the

sensitivity coefficients are calculated based on the introduction of adjoint variables to solve state and adjoint equations. The direct methods are based on consideration of all parameters as constants and then the sensitivity coefficients are estimated by solving a variational system simultaneously with the original system. We also investigate the sensitivity of the best estimates to small noise in the data/observations in Sect. 6.5.

6.2 Sensitivity Functions

Let us consider a class of systems modeled by DDEs of the form [5]

$$\mathbf{y}'(t) = \mathbf{f}(t, \mathbf{y}(t), \mathbf{y}(t - \tau), \mathbf{u}(t), \mathbf{u}(t - \sigma), \mathbf{p}), \quad 0 \leq t \leq T, \quad (6.1a)$$

$$\mathbf{y}(t) = \Psi(t, \mathbf{p}), \quad t \in [-\tau, 0], \quad \mathbf{y}(0) = \mathbf{y}_0 \in \mathbb{R}^n \quad (6.1b)$$

$$\mathbf{u}(t) = \Phi(t), \quad t \in [-\sigma, 0], \quad \mathbf{u}(0) = \mathbf{u}_0 \in \mathbb{R}^m, \quad (6.1c)$$

where the vector function \mathbf{f} in the right-hand side is sufficiently smooth with respect to each of arguments; and $\mathbf{y}(t) \in \mathbb{R}^n$, $\mathbf{y}(t - \tau) \in \mathbb{R}^{n'}$, $\mathbf{u}(t) \in \mathbb{R}^m$, $\mathbf{u}(t - \sigma) \in \mathbb{R}^{m'}$, $\mathbf{p} \in \mathbb{R}^r$, and $\tau \in \mathbb{R}^{r'}$ and $\sigma \in \mathbb{R}^{r''}$ are positive constant lags ($r', r'' \leq r$, $n' \leq n$, $m' \leq m$). $\Psi(t)$ and $\Phi(t)$ are given continuous functions. We note that $\mathbf{u}(t)$ in (6.1a) can be viewed as a control variable, defined on $[-\sigma, T]$, which gives a minimum to the objective functional

$$J(\mathbf{u}) = F_0(\mathbf{y}(T)) + \int_0^T F_1(t, \mathbf{y}(t), \mathbf{y}(t - \tau), \mathbf{u}(t), \mathbf{u}(t - \sigma), \mathbf{p}) dt, \quad (6.2)$$

where F_0 and F_1 are continuous functionals.

We also note that the system model involves both lags in the state variable $\mathbf{y}(t)$ and the control variable $\mathbf{u}(t)$. In this chapter, we estimate the sensitivity functions for the system (6.1a)–(6.1c) rather than the computational aspects of optimal control problems. (For the computational treatment of time-delayed optimal control problems, refer to the monograph by Kolmanovskii et al. [6].)

To examine the effect of parameter uncertainty on a model, it is necessary to test the sensitivity of the predicted model responses to numerical values of the parameters. In this manner, possible deficiencies in the model can be revealed if, e.g., small changes in a parameter from its nominal value result in large, improbable changes in patterns of model prediction. Equally, sensitivity analysis can indicate the most informative data points for a specific parameter. We start our analysis with the definitions of sensitivity functions of a dynamic system, including constant and variable parameters, as follows:

Definition 6.1 For the given DDEs (6.1a)–(6.1c):

1. The sensitivity functions, when the parameters are constants, are defined by the partial derivatives

$$S_{ij}(t) = \frac{\partial y_i(t)}{\partial \alpha_j}, \quad (6.3)$$

where α_j represent the parameters p_j , the constant lags τ_j , or the initial values $y_j(0)$. Then, the total variation in $y_i(t)$ due to small variations in the parameters α_j is such that

$$\delta y_i(t) = \sum_j \frac{\partial y_i(t)}{\partial \alpha_j} \delta \alpha_j + O(|\alpha|^2). \quad (6.4)$$

Thus, Eq. (6.3) estimates the sensitivity of the state variable to small variations in parameters α_j .

2. The functional derivative sensitivity coefficients, when the parameters are functions of time, are defined by

$$\beta_{ij}(t, t^*) = \frac{\partial y_i(t^*)}{\partial u_j(t)}, \quad t < t^*. \quad (6.5)$$

Then, the total variation in $y_i(t^*)$ due to any perturbation in the parameters $u_j(t)$ is denoted by $\delta y_i(t^*)$, such that

$$\delta y_i(t^*) = \int_0^{t^*} \frac{\partial y_i(t^*)}{\partial u_j(t)} \delta u_j(t) dt, \quad t < t^*. \quad (6.6)$$

Thus, the functional derivative sensitivity density function $\frac{\partial y_i(t^*)}{\partial u_j(t)}$ measures the sensitivity of $y_i(t)$ at location t^* to variation in $u_j(t)$ at any location $t < t^*$. It is then noted that the sensitivity density functions inherently contain and provide more information than the sensitivity coefficients.

6.2.1 Adjoint Equations

Adjoint equations have been used by Marchuk [7, 8] to study sensitivity analysis of non-linear functionals $J(\mathbf{y})$ depending on the solution of the delay differential models:

$$\mathbf{y}'(t) = \mathbf{f}(t, \mathbf{y}(t), \mathbf{y}(t - \tau), \mathbf{p}), \quad t \geq t_0; \quad \mathbf{y}(t) = \psi(t, \mathbf{p}), \quad t \in [t_0 - \tau, t_0]. \quad (6.7)$$

He considered the quadratic functional and its first-order variation caused by perturbations of the basic parameter set \mathbf{p} (where $\mathbf{y} \equiv \mathbf{y}(t, \mathbf{p})$)

$$J(\mathbf{y}) = \int_0^T \langle \mathbf{y}, \mathbf{y} \rangle dt, \quad \delta J(\mathbf{y}) = 2 \int_0^T \langle \mathbf{y}, \delta \mathbf{y} \rangle dt = 2 \sum_i \int_0^T \langle \mathbf{y}, \mathbf{s}_i(t, \mathbf{p}) \delta p_i \rangle dt,$$

where $\mathbf{s}_i(t, \mathbf{p})$ is a solution of the sensitivity equation

$$\mathcal{A}(\mathbf{y}(t, \mathbf{p}), \mathbf{p}) \mathbf{s}_i(t, \mathbf{p}) = \frac{\partial \mathbf{f}}{\partial p_i}, \quad t \geq 0, \quad \mathbf{s}_i(t, \mathbf{p}) = \frac{\partial \psi}{\partial p_i}, \quad t \in [-\tau, 0]. \quad (6.8)$$

The operator $\mathcal{A} \equiv \frac{d}{dt} - \frac{\partial \mathbf{f}(t)}{\partial \mathbf{y}} - \frac{\partial \mathbf{f}(t + \tau)}{\partial \mathbf{y}_\tau} D_\tau$, where $\mathbf{f}(t)$ denotes the value of \mathbf{f} at time t , $\mathbf{y}_\tau = \mathbf{y}(t - \tau)$, and D_τ is a backward shift operator. The linear operator \mathcal{A} in (6.8) acts on some Hilbert space H with domain $\mathcal{D}(\mathcal{A})$. Given \mathcal{A} , the adjoint operator \mathcal{A}^* can be introduced satisfying the Lagrange identity $\langle \mathcal{A}(\mathbf{y}, \mathbf{p}) \mathbf{s}, \mathbf{w} \rangle = \langle \mathbf{s}, \mathcal{A}^*(\mathbf{y}, \mathbf{p}) \mathbf{w} \rangle$, where $\langle \cdot, \cdot \rangle$ is an inner product in H , $\mathbf{s} \in \mathcal{D}(\mathcal{A})$, $\mathbf{w} \in \mathcal{D}(\mathcal{A}^*)$. Using the solution $\mathbf{w}(t)$ of the adjoint problem

$$\begin{aligned} \mathcal{A}^*(\mathbf{y}, \mathbf{p}) \mathbf{w}(t) &\equiv -\frac{d\mathbf{w}(t)}{dt} - \frac{\partial \mathbf{f}^T(t)}{\partial \mathbf{y}} \mathbf{w}(t) - \frac{\partial \mathbf{f}^T(t + \tau)}{\partial \mathbf{y}_\tau} \mathbf{w}(t + \tau) = \mathbf{y}(t, \mathbf{p}), \\ 0 \leq t \leq T, \quad \mathbf{w}(t) &= 0, \quad t \in [T, T + \tau] \end{aligned} \quad (6.9)$$

enables one to estimate the first-order variation of $J(\mathbf{y})$, due to perturbations of the parameters p_i , via the following formula:

$$\delta J(\mathbf{y}) = \sum_{i=1}^r 2 \int_0^T \left\langle \mathbf{w}, \frac{\partial \mathbf{f}}{\partial p_i} \delta p_i \right\rangle dt = \sum_{i=1}^r \frac{\partial J}{\partial p_i} \delta p_i, \quad (6.10)$$

where $\frac{\partial J}{\partial p_i} \equiv 2 \int_0^T \left\langle \mathbf{w}, \frac{\partial \mathbf{f}}{\partial p_i} \right\rangle dt$ is the gradient of the functional with respect to the parameters.

To estimate the sensitivity of the functional $J(\mathbf{y})$ to variations in all parameters appearing in the model (6.7), we need to solve this system model together with the adjoint problem (6.9). In the next section, we extend the use of adjoint equations to investigate the sensitivity analysis for a more general system (6.1a)–(6.1c), including constant and variable parameters.

6.3 Variational Approach

In this section, we use adjoint equations to formulate systematically formulae for the sensitivities of the state variable to small variations in the initial data, delays, parameters, and the control function appearing in the model. Then, the main object

here is to derive equations for the sensitivity coefficients $\frac{\partial y_i(t)}{\partial \alpha_j}$ and the sensitivity density functions $\frac{\partial y_i(t^*)}{\partial u_j(t)}$.

Theorem 6.1 *If $\mathbf{W}(t)$ is an n -dimensional adjoint function that satisfies the differential equation*

$$\begin{aligned} \mathbf{W}'(t) &\equiv \frac{d\mathbf{W}(t)}{dt} = -\frac{\partial \mathbf{f}^T(t)}{\partial \mathbf{y}} \mathbf{W}(t) - \frac{\partial \mathbf{f}^T(t+\tau)}{\partial \mathbf{y}_\tau} \mathbf{W}(t+\tau), \quad t \leq t^*, \\ \mathbf{W}(t) &= 0, \quad t > t^*; \quad \mathbf{W}(t^*) = [0, \dots, 0, 1_{ith}, 0, \dots, 0]^T, \end{aligned} \quad (6.11)$$

then

1. The sensitivity coefficients for the DDEs (6.1a)–(6.1c) can be expressed by the formulae

$$\frac{\partial y_i(t^*)}{\partial \mathbf{y}_0} = \mathbf{W}(0), \quad (6.12a)$$

$$\frac{\partial y_i(t^*)}{\partial \mathbf{p}} = \int_0^{t^*} \mathbf{W}^T(t) \frac{\partial \mathbf{f}}{\partial \mathbf{p}} dt, \quad t \leq t^*, \quad (6.12b)$$

$$\frac{\partial y_i(t^*)}{\partial \tau} = - \int_{-\tau}^{t^*-\tau} \mathbf{W}^T(t+\tau) \frac{\partial \mathbf{f}(t+\tau)}{\partial \mathbf{y}_\tau} \mathbf{y}'(t) dt, \quad (6.12c)$$

$$\frac{\partial y_i(t^*)}{\partial \sigma} = - \int_{-\sigma}^{t^*-\sigma} \mathbf{W}^T(t+\sigma) \frac{\partial \mathbf{f}(t+\sigma)}{\partial \mathbf{u}_\sigma} \mathbf{u}'(t) dt. \quad (6.12d)$$

2. The functional derivative sensitivity coefficients can also be expressed by

$$\frac{\partial y_i(t^*)}{\partial \Psi(t)} = \frac{\partial \mathbf{f}^T(t+\tau)}{\partial \mathbf{y}} \mathbf{W}(t+\tau), \quad t \in [-\tau, 0] \quad (6.13a)$$

$$\frac{\partial y_i(t^*)}{\partial \Phi(t)} = \frac{\partial \mathbf{f}^T(t+\sigma)}{\partial \mathbf{u}_\sigma} \mathbf{W}(t+\sigma), \quad t \in [-\sigma, 0] \quad (6.13b)$$

$$\frac{\partial y_i(t^*)}{\partial \mathbf{u}(t)} = \frac{\partial \mathbf{f}^T}{\partial \mathbf{u}} \mathbf{W}(t) + \frac{\partial \mathbf{f}^T(t+\sigma)}{\partial \mathbf{u}_\sigma} \mathbf{W}(t+\sigma), \quad t \in (0, t^*]. \quad (6.13c)$$

Proof For simplicity in Eq. (6.1a), we write

$$\mathbf{f}(t, \mathbf{y}, \mathbf{y}_\tau, \mathbf{u}, \mathbf{u}_\sigma, \mathbf{p}) = \mathbf{f}(t, \mathbf{y}(t), \mathbf{y}(t-\tau), \mathbf{u}(t), \mathbf{u}(t-\sigma), \mathbf{p}).$$

Small variations in the initial data, control, and system parameters cause a perturbation in the system state in (6.1a)–(6.1c). Then, small variations $\delta\Psi$, $\delta\Phi$, $\delta\mathbf{y}_0$, $\delta\mathbf{u}$, $\delta\mathbf{p}$, $\delta\tau$, and $\delta\sigma$ result in a variation $\delta\mathbf{y}$ that satisfies (for first order) the equation

$$\begin{aligned}\delta \mathbf{y}'(t) &= \frac{\partial \mathbf{f}}{\partial \mathbf{y}} \delta \mathbf{y}(t) + \frac{\partial \mathbf{f}}{\partial \mathbf{y}_\tau} \delta \mathbf{y}(t - \tau) + \frac{\partial \mathbf{f}}{\partial \mathbf{u}} \delta \mathbf{u}(t) + \frac{\partial \mathbf{f}}{\partial \mathbf{u}_\sigma} \delta \mathbf{u}(t - \sigma) + \frac{\partial \mathbf{f}}{\partial \mathbf{p}} \delta \mathbf{p} + \\ &\quad \frac{\partial \mathbf{f}}{\partial \mathbf{y}} \frac{\partial \mathbf{y}(t - \tau)}{\partial \tau} \delta \tau + \frac{\partial \mathbf{f}}{\partial \mathbf{u}} \frac{\partial \mathbf{u}(t - \sigma)}{\partial \sigma} \delta \sigma,\end{aligned}\tag{6.14a}$$

$$\delta \mathbf{y}(t) = \delta \Psi(t), \quad t \in [-\tau, 0]; \quad \delta \mathbf{y}(0) = \delta \mathbf{y}_0 \in \mathbb{R}^n, \tag{6.14b}$$

$$\delta \mathbf{u}(t) = \delta \Phi(t), \quad t \in [-\sigma, 0]. \tag{6.14c}$$

If we multiply both sides of (6.14a) by $\mathbf{W}^T(t)$ (the transpose of the function $\mathbf{W}(t)$) and integrate both sides with respect to t over the interval $[0, t^*]$, we obtain

$$\begin{aligned}\mathbf{W}^T(t^*) \delta \mathbf{y}(t^*) - \mathbf{W}^T(0) \delta \mathbf{y}(0) - \int_0^{t^*} \mathbf{W}'^T(t) \delta \mathbf{y}(t) dt = \\ \int_0^{t^*} \mathbf{W}^T(t) \left[\frac{\partial \mathbf{f}}{\partial \mathbf{y}} \delta \mathbf{y}(t) + \frac{\partial \mathbf{f}}{\partial \mathbf{y}_\tau} \delta \mathbf{y}(t - \tau) \right] dt + \\ \int_0^{t^*} \mathbf{W}^T(t) \left[\frac{\partial \mathbf{f}}{\partial \mathbf{u}} \delta \mathbf{u}(t) + \frac{\partial \mathbf{f}}{\partial \mathbf{u}_\sigma} \delta \mathbf{u}(t - \sigma) \right] dt + \\ \int_0^{t^*} \mathbf{W}^T(t) \left[\frac{\partial \mathbf{f}}{\partial \mathbf{p}} \delta \mathbf{p} + \frac{\partial \mathbf{f}}{\partial \mathbf{y}_\tau} \frac{\partial \mathbf{y}(t - \tau)}{\partial \tau} \delta \tau + \frac{\partial \mathbf{f}}{\partial \mathbf{u}_\sigma} \frac{\partial \mathbf{u}(t - \sigma)}{\partial \sigma} \delta \sigma \right] dt.\end{aligned}\tag{6.15}$$

Equation (6.15), after some manipulations, can be rewritten in the form

$$\begin{aligned}\mathbf{W}^T(t^*) \delta \mathbf{y}(t^*) - \mathbf{W}^T(0) \delta \mathbf{y}(0) &= \int_{-\tau}^0 \mathbf{W}^T(t + \tau) \frac{\partial \mathbf{f}(t + \tau)}{\partial \mathbf{y}_\tau} \delta \Psi(t) dt \\ &\quad + \int_0^{t^* - \tau} \left[\mathbf{W}'^T(t) + \frac{\partial \mathbf{f}^T}{\partial \mathbf{y}} \mathbf{W}(t) + \frac{\partial \mathbf{f}^T(t + \tau)}{\partial \mathbf{y}_\tau} \mathbf{W}(t + \tau) \right]^T \delta \mathbf{y}(t) dt \\ &\quad + \int_{t^* - \tau}^{t^*} \left[\mathbf{W}'^T(t) + \frac{\partial \mathbf{f}}{\partial \mathbf{y}} \mathbf{W}(t) \right]^T \delta \mathbf{y}(t) dt + \int_{-\sigma}^0 \mathbf{W}^T(t + \sigma) \frac{\partial \mathbf{f}(t + \sigma)}{\partial \mathbf{u}_\sigma} \delta \Phi(t) dt \\ &\quad + \int_0^{t^* - \sigma} \left[\mathbf{W}^T(t) \frac{\partial \mathbf{f}}{\partial \mathbf{u}} + \mathbf{W}^T(t + \sigma) \frac{\partial \mathbf{f}(t + \sigma)}{\partial \mathbf{u}_\sigma} \right] \delta \mathbf{u}(t) dt + \int_{t^* - \sigma}^{t^*} \mathbf{W}^T(t) \frac{\partial \mathbf{f}}{\partial \mathbf{u}} \delta \mathbf{u}(t) dt \\ &\quad + \int_0^{t^*} \mathbf{W}^T(t) \frac{\partial \mathbf{f}}{\partial \mathbf{p}} \delta \mathbf{p} dt - \int_{-\tau}^{t^* - \tau} \mathbf{W}^T(t + \tau) \frac{\partial \mathbf{f}(t + \tau)}{\partial \mathbf{y}_\tau} \mathbf{y}'(t) \delta \tau dt \\ &\quad - \int_{-\sigma}^{t^* - \sigma} \mathbf{W}^T(t + \sigma) \frac{\partial \mathbf{f}(t + \sigma)}{\partial \mathbf{u}_\sigma} \mathbf{u}'(t) \delta \sigma dt, \quad t \leq t^*.\end{aligned}\tag{6.16}$$

Under the assumptions given in (6.11), the above equation takes the form

$$\begin{aligned}
\delta y_i(t^*) &= \mathbf{W}^T(0)\delta\mathbf{y}(0) + \int_{-\tau}^0 \mathbf{W}^T(t+\tau) \frac{\partial \mathbf{f}(t+\tau)}{\partial \mathbf{y}_\tau} \delta\Psi(t) dt \\
&\quad + \int_{-\sigma}^0 \mathbf{W}^T(t+\sigma) \frac{\partial \mathbf{f}(t+\sigma)}{\partial \mathbf{u}_\sigma} \delta\Phi(t) dt \\
&\quad + \int_0^{t^*} \left[\mathbf{W}^T(t) \frac{\partial \mathbf{f}}{\partial \mathbf{u}} + \mathbf{W}^T(t+\sigma) \frac{\partial \mathbf{f}(t+\sigma)}{\partial \mathbf{u}_\sigma} \right] \delta\mathbf{u}(t) dt \\
&\quad + \int_0^{t^*} \mathbf{W}^T(t) \frac{\partial \mathbf{f}}{\partial \mathbf{p}} \delta\mathbf{p} dt - \int_{-\tau}^{t^*-\tau} \mathbf{W}^T(t+\tau) \frac{\partial \mathbf{f}(t+\tau)}{\partial \mathbf{y}_\tau} \mathbf{y}'(t) \delta\tau dt \\
&\quad - \int_{-\sigma}^{t^*-\sigma} \mathbf{W}^T(t+\sigma) \frac{\partial \mathbf{f}(t+\sigma)}{\partial \mathbf{u}_\sigma} \mathbf{u}'(t) \delta\sigma dt, \quad t \leq t^*; \tag{6.17}
\end{aligned}$$

or

$$\begin{aligned}
\delta y_i(t^*) &= \mathbf{W}^T(0)\delta\mathbf{y}(0) + \int_0^{t^*} \mathbf{W}^T(t) \frac{\partial \mathbf{f}}{\partial \mathbf{p}} \delta\mathbf{p} dt \\
&\quad - \int_{-\tau}^{t^*-\tau} \mathbf{W}^T(t+\tau) \frac{\partial \mathbf{f}(t+\tau)}{\partial \mathbf{y}_\tau} \mathbf{y}'(t) \delta\tau dt - \int_{-\sigma}^{t^*-\sigma} \mathbf{W}^T(t+\sigma) \frac{\partial \mathbf{f}(t+\sigma)}{\partial \mathbf{u}_\sigma} \mathbf{u}'(t) \delta\sigma dt \\
&\quad + \int_{-\tau}^0 \mathbf{W}^T(t+\tau) \frac{\partial \mathbf{f}(t+\tau)}{\partial \mathbf{y}_\tau} \delta\Psi(t) dt + \int_{-\tau}^0 \mathbf{W}^T(t+\sigma) \frac{\partial \mathbf{f}(t+\sigma)}{\partial \mathbf{u}_\sigma} \delta\Phi(t) dt \\
&\quad + \int_0^{t^*} \left[\mathbf{W}^T(t) \frac{\partial \mathbf{f}}{\partial \mathbf{u}} + \mathbf{W}^T(t+\sigma) \frac{\partial \mathbf{f}(t+\sigma)}{\partial \mathbf{u}_\sigma} \right] \delta\mathbf{u}(t) dt, \quad t \leq t^*. \tag{6.18}
\end{aligned}$$

Functional derivative sensitivity coefficients, for constant parameters, are equivalent to the partial derivative sensitivity coefficients defined by (6.3). When $\delta\mathbf{y}(0) \rightarrow 0$, $\delta\mathbf{p} \rightarrow 0$, $\delta\tau \rightarrow 0$, and $\delta\sigma \rightarrow 0$, we, respectively, obtain the sensitivity coefficients (6.12a)–(6.12d) from the first four terms of Eq. (6.18). Then, the first part of Theorem 6.1 is proved.

From the definition of the functional derivative sensitivity coefficients in (6.6), we then obtain the formulae (6.13a)–(6.13c) from the last three terms of Eq. (6.18). Thus, the second part of Theorem 6.1 is proved.

6.4 Direct Approach

If we take all the parameters appearing in the system model (6.1a)–(6.1c) to be constants, then sensitivity analysis, in this case, may just entail finding the partial derivatives of the solution with respect to each parameter.

We denote by $\mathbf{S}(t)$ the $n \times \tilde{n}$ matrix $\mathbf{S}(t, \alpha)$ of the sensitivity functions

$$\mathbf{S}(t) \equiv \mathbf{S}(t, \alpha) := \left[\frac{\partial y^i(t, \alpha)}{\partial \alpha_j} \right]_{\substack{i=1, \dots, n \\ j=1, \dots, \tilde{n}}}, \quad \tilde{n} = r + r'.$$

If we introduce the notation $\left\{ \frac{\partial}{\partial \alpha} \right\}^T$, the matrix of *sensitivity functions* takes the form

$$\mathbf{S}(t, \alpha) \equiv \left\{ \frac{\partial}{\partial \alpha} \right\}^T \mathbf{y}(t, \alpha) \in \mathbb{R}^{n \times \tilde{n}}. \quad (6.19)$$

Its i th column is

$$S_i(t, \alpha) = \left[\frac{\partial y_i(t, \alpha)}{\partial \alpha_1}, \frac{\partial y_i(t, \alpha)}{\partial \alpha_2}, \dots, \frac{\partial y_i(t, \alpha)}{\partial \alpha_{\tilde{n}}} \right]^T.$$

Thus, $S_i(t, \alpha)$ is a vector whose components denote the sensitivity of the solution $y_i(t, \alpha)$ of the model to small variations in the parameters α_j , $j = 1, 2, \dots, \tilde{n}$.

Theorem 6.2 $\mathbf{S}(t)$ satisfies the DDE:

$$\mathbf{S}'(t) = \mathbf{J}(t)\mathbf{S}(t) + \mathbf{J}_\tau(t)\mathbf{S}(t - \tau) + \mathbf{B}(t), \quad t \geq 0, \quad (6.20)$$

where

$$\mathbf{J}(t) := \frac{\partial}{\partial \mathbf{y}} \mathbf{f}(t, \mathbf{y}, \mathbf{y}_\tau, \mathbf{u}, \mathbf{u}_\sigma; \mathbf{p}) \in \mathbb{R}^{n \times n} \quad (6.21a)$$

$$\mathbf{J}_\tau(t) := \frac{\partial}{\partial \mathbf{y}_\tau} \mathbf{f}(t, \mathbf{y}, \mathbf{y}_\tau, \mathbf{u}, \mathbf{u}_\sigma; \mathbf{p}) \in \mathbb{R}^{n \times r'}; \quad (6.21b)$$

$$\mathbf{B}(t) := \frac{\partial}{\partial \alpha} \mathbf{f}(t, \mathbf{y}, \mathbf{y}_\tau, \mathbf{u}, \mathbf{u}_\sigma; \mathbf{p}) \in \mathbb{R}^{n \times \tilde{n}}. \quad (6.21c)$$

Proof Assuming appropriate differentiability of $\mathbf{y}(t, \alpha)$ with respect to α , we have

$$\mathbf{y}(t, \alpha + \delta\alpha) = \mathbf{y}(t, \alpha) + \sum_{j=1}^{\tilde{n}} \frac{\partial \mathbf{y}(t, \alpha)}{\partial \alpha_j} \delta\alpha_j + O(\|\delta\alpha\|^2), \quad \text{or, using (6.19),}$$

$$\delta\mathbf{y}(t, \alpha) = \mathbf{S}(t, \alpha)\delta\alpha + O(\|\delta\alpha\|^2).$$

Thus, the $n \times \tilde{n}$ matrix $\mathbf{S}(t, \alpha)$ may be regarded as the *local* sensitivity of the solution $\mathbf{y}(t, \alpha)$ to small variations in α . (The term *local* refers to the fact that these sensitivities describe the system around a given set of values for the parameters α .)

By differentiating equations (6.1a)–(6.1b) with respect to the vector of parameters α , we obtain the variational system

$$\begin{aligned}\mathbf{S}'(t, \alpha) &= \frac{\partial \mathbf{f}}{\partial \mathbf{y}}(t, \mathbf{y}, \mathbf{y}_\tau, \mathbf{u}, \mathbf{u}_\sigma; \mathbf{p}) \mathbf{S}(t, \alpha) + \frac{\partial \mathbf{f}}{\partial \mathbf{y}_\tau}(t, \mathbf{y}, \mathbf{y}_\tau, \mathbf{u}, \mathbf{u}_\sigma; \mathbf{p}) \mathbf{S}(t - \tau, \alpha) \\ &\quad + \frac{\partial \mathbf{f}}{\partial \alpha}(t, \mathbf{y}, \mathbf{y}_\tau, \mathbf{u}, \mathbf{u}_\sigma; \mathbf{p}) \quad t \geq 0, \\ \mathbf{S}'(t, \alpha) &= \frac{\partial \Psi(t, \alpha)}{\partial \alpha}, \quad t \leq 0.\end{aligned}$$

Our result is as follows. \square

To estimate the sensitivity functions $\mathbf{S}(t)$, we must solve the $n \times \tilde{n}$ sensitivity Eq. (6.20) together with the original system (6.1a)–(6.1c). We should mention here that solving such systems can be a difficult and costly numerical problem when the number of states and parameters is large, or when the sensitivities must be computed repeatedly.

Remark 6.1 We apply the direct method to the linear DDE model:

$$\begin{aligned}y'(t, \alpha) &= p_1 y(t, \alpha) + p_2 y(t - \tau, \alpha) + p_3 u(t), \quad t \geq 0 \\ y(t, \alpha) &= \psi(t, \alpha), \quad t \leq 0,\end{aligned}\tag{6.22}$$

as an example. Here $\alpha = [p_1, p_2, p_3, \tau]^T$. The equations for $S(t)$ cannot be solved in isolation; they require the solution $y(t)$. We obtain, in the present model, a system of *neutral delay differential equations* (NDDEs) expressed as

$$\begin{aligned}\mathbf{x}'(t, \alpha) &= \mathbf{A}\mathbf{x}(t, \alpha) + \mathbf{B}\mathbf{x}(t - \tau, \alpha) + \mathbf{C}\mathbf{x}'(t - \tau, \alpha) + \mathbf{D}(t), \quad t > 0, \\ \mathbf{x}(t, \alpha) &= \Psi(t, \alpha), \quad t \in [-\tau, 0],\end{aligned}\tag{6.23}$$

where

$$\mathbf{A} = \begin{bmatrix} p_1 & 0 & 0 & 0 & 0 \\ 1 & p_1 & 0 & 0 & 0 \\ 0 & 0 & p_1 & 0 & 0 \\ 0 & 0 & 0 & p_1 & 0 \\ 0 & 0 & 0 & 0 & p_1 \end{bmatrix}, \quad \mathbf{B} = \begin{bmatrix} p_2 & 0 & 0 & 0 & 0 \\ 0 & p_2 & 0 & 0 & 0 \\ 1 & 0 & p_2 & 0 & 0 \\ 0 & 0 & 0 & p_2 & 0 \\ 0 & 0 & 0 & 0 & p_2 \end{bmatrix}, \quad \mathbf{C} = \begin{bmatrix} 0 & 0 & 0 & 0 & 0 \\ 0 & 0 & 0 & 0 & 0 \\ 0 & 0 & 0 & 0 & 0 \\ 0 & 0 & 0 & 0 & 0 \\ 0 & 0 & 0 & 0 & -p_2 \end{bmatrix},$$

$$\mathbf{D}(t) = \begin{bmatrix} p_3 u(t) \\ 0 \\ 0 \\ u(t) \\ 0 \end{bmatrix}, \quad \mathbf{x}(t, \alpha) = \begin{bmatrix} y(t, \mathbf{p}) \\ s_{p_1}(t, \alpha) \\ s_{p_2}(t, \alpha) \\ s_{p_3}(t, \alpha) \\ s_\tau(t, \alpha) \end{bmatrix}, \quad \text{and } \Psi(t, \alpha) = \begin{bmatrix} \psi(t, \alpha) \\ \frac{\partial}{\partial p_1} \psi(t, \alpha) \\ \frac{\partial}{\partial p_2} \psi(t, \alpha) \\ \frac{\partial}{\partial p_3} \psi(t, \alpha) \\ \frac{\partial}{\partial \tau} \psi(t, \alpha) \end{bmatrix}.$$

Here, $s_{\alpha_i} \equiv \frac{\partial y(t, \alpha)}{\partial \alpha_i}$, and some terms $\frac{\partial}{\partial \alpha_i} \psi(t, \alpha)$ are non-vanishing in the case where the initial function ψ depends non-trivially upon p_1, p_2, p_3 , and τ .

6.5 Sensitivity of Optimum Parameter $\hat{\mathbf{p}}$ to Data

To compute $\frac{\partial \hat{\mathbf{p}}}{\partial \mathbf{Y}_j}$, the sensitivity of the parameter estimate $\hat{\mathbf{p}}$ to the observed data \mathbf{Y}_j , assume that the unweighted objective function

$$\Phi(\mathbf{p}) \equiv \Phi(\mathbf{p}, \mathbf{Y}) := \sum_i \left[y(t_i, \mathbf{p}) - \mathbf{Y}_i \right]^2 \quad (6.24)$$

is smooth as a function of \mathbf{p} in the neighborhood of the optimal parameter $\hat{\mathbf{p}}$. Then we have

$$\frac{\partial}{\partial p_k} \Phi(\mathbf{p}, \mathbf{Y}) = 2 \sum_i \left[y(t_i, \mathbf{p}) - \mathbf{Y}_i \right] \frac{\partial y(t_i, \mathbf{p})}{\partial p_k}, \quad (6.25)$$

$$\frac{\partial^2}{\partial p_l \partial p_k} \Phi(\mathbf{p}, \mathbf{Y}) = 2 \sum_i \frac{\partial y(t_i, \mathbf{p})}{\partial p_l} \frac{\partial y(t_i, \mathbf{p})}{\partial p_k} + 2 \sum_i \left[y(t_i, \mathbf{p}) - \mathbf{Y}_i \right] \frac{\partial^2 y(t_i, \mathbf{p})}{\partial p_l \partial p_k}. \quad (6.26)$$

To minimize the objective function (6.24), the right-hand side of Eq. (6.25) vanishes at $\mathbf{p} = \hat{\mathbf{p}}$ (where $\hat{\mathbf{p}} \equiv \hat{\mathbf{p}}(\mathbf{Y})$); therefore,

$$\sum_i [y(t_i, \hat{\mathbf{p}}(\mathbf{Y})) \mathbf{Y}_i] s_k(t_i, \hat{\mathbf{p}}(\mathbf{Y})) = 0. \quad (6.27)$$

Now, the left-hand side of Eq. (6.27) is a function of $\hat{\mathbf{p}}$ and \mathbf{Y} ; differentiating both sides with respect to \mathbf{Y}_j yields, for $k = 1, \dots, L$,

$$\sum_{i=1}^N \sum_{l=1}^L \left[s_k(t_i, \hat{\mathbf{p}}) s_l(t_i, \hat{\mathbf{p}}) + [y(t_i, \hat{\mathbf{p}}) - \mathbf{Y}_i] r_{lk}(t_i, \hat{\mathbf{p}}) \right] \frac{\partial \hat{p}_l}{\partial \mathbf{Y}_j} = s_k(t_j, \hat{\mathbf{p}}). \quad (6.28)$$

If we assume that $y(t_i, \hat{\mathbf{p}})$ is close to the observed value \mathbf{Y}_i , so that the second term in the left-hand side of Eq. (6.28) can be neglected, then the above system can be approximated by

$$\sum_{i=1}^N \sum_{l=1}^L s_k(t_i, \hat{\mathbf{p}}) s_l(t_i, \hat{\mathbf{p}}) \frac{\partial \hat{p}_l}{\partial \mathbf{Y}_j} \approx s_k(t_j, \hat{\mathbf{p}}), \quad k = 1, \dots, L,$$

or

$$\sum_{i=1}^N s_k(t_i, \hat{\mathbf{p}}) \left(\sum_{l=1}^L s_l(t_i, \hat{\mathbf{p}}) \frac{\partial p_l}{\partial \mathbf{Y}_j} \right) \approx s_k(t_j, \hat{\mathbf{p}}), \quad k = 1, \dots, L. \quad (6.29)$$

This equation can be written in a compact form:

$$\left[\sum_{i=1}^N \mathbf{s}(t_i, \hat{\mathbf{p}}) \mathbf{s}^T(t_i, \hat{\mathbf{p}}) \right] \frac{\partial \hat{\mathbf{p}}}{\partial b f Y_j} \approx \mathbf{s}(t_j, \hat{\mathbf{p}}). \quad (6.30)$$

Then, the sensitivity of the best-fit parameter estimate $\hat{\mathbf{p}}$ to observations $\mathbf{Y}_j (j = 1, 2, \dots, N)$ can be estimated by

$$\frac{\partial \hat{\mathbf{p}}}{\partial \mathbf{Y}_j} \approx \left[\mathfrak{B}(\hat{\mathbf{p}}) \right]^{-1} \mathbf{s}(t_j, \hat{\mathbf{p}}), \quad (6.31)$$

where \mathbf{s} is $L \times 1$ vector and $\mathfrak{B}(\hat{\mathbf{p}}) := \left[\sum_{i=1}^N \mathbf{s}(t_i, \hat{\mathbf{p}}) \mathbf{s}^T(t_i, \hat{\mathbf{p}}) \right]$ is a $L \times L$ nonsingular matrix.

A desirable property of the model is that the sensitivity of the parameter estimate to the observation $\frac{\partial \hat{\mathbf{p}}}{\partial \mathbf{Y}_j}$ should be small to minimize the effect of observation noise on the parameter estimate. Equation (6.31) suggests that increasing $\mathbf{s}(t, \hat{\mathbf{p}})$ (the sensitivity of the state variable with respect to the unknown parameter) decreases the sensitivity of the parameter estimation to observation.

6.5.1 Standard Deviation of Parameter Estimates

We can use the sensitivity coefficients ($s_i, i = 1, \dots, L$) to determine the covariance matrix $[\varsigma_{ij}]$ of the estimates as follows [9]:

$$\begin{bmatrix} \varsigma_{11} & \varsigma_{12} & \dots & \varsigma_{1L} \\ \varsigma_{21} & \varsigma_{22} & \dots & \varsigma_{2L} \\ \varsigma_{31} & \varsigma_{32} & \dots & \varsigma_{3L} \\ \dots & \dots & \dots & \dots \\ \varsigma_{R1} & \varsigma_{R2} & \dots & \varsigma_{RL} \end{bmatrix} = 2 \frac{\Phi(\hat{\mathbf{p}})}{N - L} \left[H(\hat{\mathbf{p}}) \right]^{-1},$$

where $(N - L)$ is the number of degrees of freedom and $H(\hat{\mathbf{p}})$ is the Hessian matrix of the objective function $\Phi(\hat{\mathbf{p}})$. Using the notation $\frac{\partial}{\partial \mathbf{p}}$ and $\frac{\partial}{\partial \mathbf{p}^T}$, the Hessian matrix can be written in the form

$$H(\hat{\mathbf{p}}) = \left[\frac{\partial^2}{\partial \mathbf{p} \partial \mathbf{p}^T} \Phi(\hat{\mathbf{p}}) \right].$$

This matrix can be approximated, in terms of (6.26) and using the sensitivity coefficients, as

$$H(\hat{\mathbf{p}}) \approx \tilde{H}(\hat{\mathbf{p}}) := 2 \left[\sum_{k=1}^N s_i(t_k, \hat{\mathbf{p}}) s_j(t_k, \hat{\mathbf{p}}) \right]_{i,j=1,\dots,L}.$$

Hence, the standard deviations for the parameter estimates are the quantities $\sigma_i \equiv \sigma(\hat{p}_i) = \sqrt{\varsigma_{ii}}$ ($i = 1, \dots, L$).

6.5.2 Non-linearity and Indications of Bias

We remarked earlier that percentage *bias* in the values of the parameter estimates is a good indicator of the quantitative effect of non-linearity [10]. To examine the *biases* in the values of the parameter estimates due to the non-linearity of the parameters, we proceed as follows:

- (1) Perturb the obtained solution of the model corresponding to the best-fit parameters $\hat{\mathbf{p}}$ with normally distributed random errors of zero mean and variance (see [9]):

$$s^2 = \frac{\Phi(\hat{\mathbf{p}})}{N - L}.$$

- (2) Find new best-fit parameters $\tilde{\mathbf{p}}$ to the perturbed data from (1).
- (3) Repeat this process a large number of times (500, or preferably 1000 times) to generate a statistically significant estimate of the mean value of $\tilde{\mathbf{p}}$.
- (4) If the *relative biases* satisfy the relation

$$\|\hat{\mathbf{p}} - \text{mean}\{\tilde{\mathbf{p}}\}\| < 0.01\|\hat{\mathbf{p}}\|,$$

then the effect of non-linearity is not regarded as significant and the experimenter can have confidence in the parameter estimates and their standard deviations.

In other words, if the *LS* estimator of a non-linear regression model is only *slightly biased* (the relative biases $< 1\%$) with a distribution close to that of a normal distribution and with a variance only slightly in excess of the minimum variance bound, it seems reasonable to consider the estimator as behaving *close to a linear* regression model. If, on the other hand, the *LS* estimator has a large non-linear bias, with a distribution far from normal and variance greatly in excess of the minimum variance bound, the non-linear regression model might be far from a linear model in its behavior. For more details about the non-linearity effect and issues related to parameter estimations, refer to [9–12].

6.6 Numerical Results

In this section, we apply the results obtained in the above sections, to an example of linear DDE:

$$\begin{aligned} y'(t) &= p_1 y(t) + p_2 y(t - \tau) + p_3, \quad t \geq 0, \\ y(t) &= \psi(t), \quad t \in [-\tau, 0]. \end{aligned} \quad (6.32)$$

We have chosen this model because it has many applications in cell-growth dynamics, as the behavior of its solution (for particular parameters) is consistent with the step-like growth pattern; see [12]. A knowledge of how the solution can vary with respect to small changes in the initial data or the parameters can yield insights into the behavior of the model and can assist the modeling process. The observation interval is often divided into subintervals, each of which could be informative about a specific parameter. Knowledge of these intervals is not only important for understanding the role of the model but also for an enhanced experiment design for estimating selected parameters. Thus, sensitivity functions can allow one to qualitatively assess which data points have the most effect on a particular parameter.

According the above analysis, we wish to find (analytically and numerically) the sensitivity density function $\frac{\partial y(t^*)}{\partial \psi(t)}$ (where $t \leq t^*$) and the sensitivity coefficients $\frac{\partial y(t)}{\partial \alpha}$. The sensitivity coefficients (for constant parameters) can be obtained by using both variational and direct methods. However, the functional derivative sensitivity coefficients can only be computed by using the variational method.

- First, we apply the variational approach.

In (6.32), $\alpha = [p_1, p_2, p_3, \tau]^T$ and the control is chosen to be $u(t) = p_3 = 1$. The adjoint equation for this case is

$$\begin{aligned} W'(t) &= -p_1 W(t) - p_2 W(t + \tau), \quad t \leq t^*, \\ W(t) &= 0, \quad t > t^*, \quad W(t^*) = 1. \end{aligned} \quad (6.33)$$

The analytical solution of the adjoint Eq. (6.33) is as follows:

$$(1) \quad 0 < t^* \leq \tau$$

$$W(t) = e^{-p_1(t-t^*)}, \quad t \leq t^*, \quad (6.34)$$

$$(2) \quad \tau < t^* \leq 2\tau$$

$$W(t) = \begin{cases} e^{-p_1(t-t^*)} - p_2(t - t^* + \tau)e^{-p_1(t-t^*+\tau)}, & 0 < t \leq t^* - \tau, \\ e^{-p_1(t-t^*)}, & t^* - \tau < t \leq t^*. \end{cases} \quad (6.35)$$

(Here, $W(t + \tau) = 0$ for $t^* - \tau < t \leq t^*$ and $W(t + \tau) = e^{-p_1(t-t^*+\tau)}$ for $0 < t \leq t^* - \tau$.)

The solution of the DDE (6.32), with an initial function $\psi(t) = 0$ with $t \leq 0$, is

$$y(t) = \begin{cases} \xi(e^{p_1 t} - 1), & 0 < t \leq \tau, \\ \xi^2 p_2 - \xi + \xi e^{p_1 t} + \xi p_2(t - \tau - \xi)e^{p_1(t-\tau)}, & \tau < t \leq 2\tau, \end{cases} \quad (6.36)$$

where $\xi = \frac{1}{p_1}$.

Thus, the functional derivative sensitivity density function to the initial function, by using (6.13a), becomes

$$(1) \quad 0 < t^* \leq \tau$$

$$\frac{\partial y(t^*)}{\partial \psi(t)} = p_2 W(t + \tau) = \begin{cases} p_2 e^{-p_1(t-t^*+\tau)}, & -\tau < t \leq t^* - \tau, \\ 0, & t^* - \tau < t \leq 0. \end{cases} \quad (6.37)$$

$$(2) \quad \tau < t^* \leq 2\tau$$

$$\frac{\partial y(t^*)}{\partial \psi(t)} = \begin{cases} p_2 e^{-p_1(t-t^*+\tau)} - p_2^2(t - t^* + 2\tau)e^{-p_1(t-t^*+2\tau)}, & -\tau < t \leq t^* - 2\tau, \\ p_2 e^{-p_1(t-t^*+\tau)}, & t^* - 2\tau < t \leq 0. \end{cases} \quad (6.38)$$

On the other hand, the sensitivity functional to the control variable $u(t)$, as depicted in (6.13c), becomes

$$\frac{\partial y(t^*)}{\partial u(t)} = W(t). \quad (6.39)$$

The sensitivity function of $y(t)$ to the constant parameter p_1 , by using (6.12b), takes the form

$$\frac{\partial y(t^*)}{\partial p_1} = \int_0^{t^*} W(t) \frac{\partial f}{\partial p_1} dt = \begin{cases} \xi^2 + \xi(t^* - \xi)e^{p_1 t^*}, & 0 < t^* \leq \tau, \\ I_1 + I_2, & \tau < t^* \leq 2\tau, \end{cases} \quad (6.40)$$

where

$$\begin{aligned} I_1 &= \int_0^{t^* - \tau} W(t) \frac{\partial f}{\partial p_1} dt \\ &= \xi(t^* - \tau)e^{p_1 t^*} + \xi^2(e^{p_1 \tau} - e^{p_1 t^*}) + \frac{1}{2}\xi p_2(t^* - \tau)^2 e^{p_1(t^* - \tau)} \\ &\quad - \xi^2 p_2(t^* - \tau)e^{p_1(t^* - \tau)} - \xi^3 p_2(1 - e^{p_1(t^* - \tau)}), \end{aligned} \quad (6.41)$$

and

$$I_2 = \int_{t^* - \tau}^{t^*} W(t) \frac{\partial f}{\partial p_1} dt = I_1 + \xi^2 + \xi(t^* - \xi)e^{p_1 t^*}. \quad (6.42)$$

The sensitivity of $y(t)$ to the parameter p_3 is given by

$$\frac{\partial y(t^*)}{\partial p_3} = \int_0^{t^*} W(t) \frac{\partial f}{\partial p_3} dt \quad (6.43)$$

$$= \begin{cases} \xi(e^{p_1 t^*} - 1), & 0 < t^* \leq \tau \\ \xi^2 p_2 - \xi + \xi e^{p_1 t^*} + \xi p_2(t^* - \tau - \xi)e^{p_1(t^*-\tau)}, & \tau < t^* \leq 2\tau \end{cases} \quad (6.44)$$

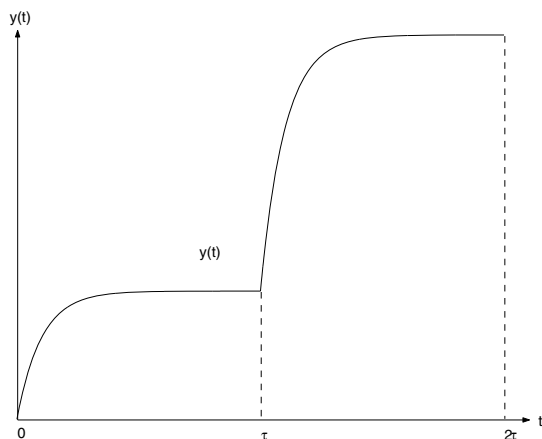
It is clear that $\frac{\partial y(t^*)}{\partial p_3} = y(t^*)$, as it is satisfying Eq.(6.32).

By using (6.12c), we obtain the sensitivity coefficient of $y(t)$ to the constant parameter τ as

$$\begin{aligned} \frac{\partial y(t^*)}{\partial \tau} &= - \int_{-\tau}^{t^*-\tau} W(t+\tau) \frac{\partial f(t+\tau)}{\partial y_\tau} y'(t) dt \\ &= \begin{cases} 0, & 0 < t^* \leq \tau, \\ -p_2(t^* - \tau)e^{p_1(t^*-\tau)}, & \tau < t^* \leq 2\tau, \end{cases} \end{aligned} \quad (6.45)$$

Numerical results using the variational approach are presented in Figs. 6.1, 6.2, 6.3, 6.4, 6.5, and 6.6. Figure 6.1 plots the analytical solution of DDE (6.32) in the interval $[0, 2\tau]$. Figures 6.2 and 6.3 show the sensitivity of the state variable to the initial function $\frac{\partial y(t^*)}{\partial \psi(t)}$ ($t < t^*$) as a function of t for (i) $0 < t^* \leq \tau$ and (ii) $\tau < t^* \leq 2\tau$, respectively. For case (i), $\frac{\partial y(t^*)}{\partial \psi(t)}$ is positive and increases monotonically in the interval $[-\tau, t^* - \tau]$ and attains maximum value at $t = t^* - \tau$ and vanishes for $t^* - \tau < t \leq 0$. In case (ii), $\frac{\partial y(t^*)}{\partial \psi(t)}$ monotonically increases and then decreases to attain the minimum at $t = t^* - 2\tau$. We note that $t = t^* - 2\tau$ is the time when the initial data stops to affect the state delay in the system dynamic. The functional

Fig. 6.1 Analytical solution of DDE (6.32) in the interval $0 \leq t \leq 2\tau$ with $p_1 = -2$, $p_2 = 4$, and $p_3 = 1$



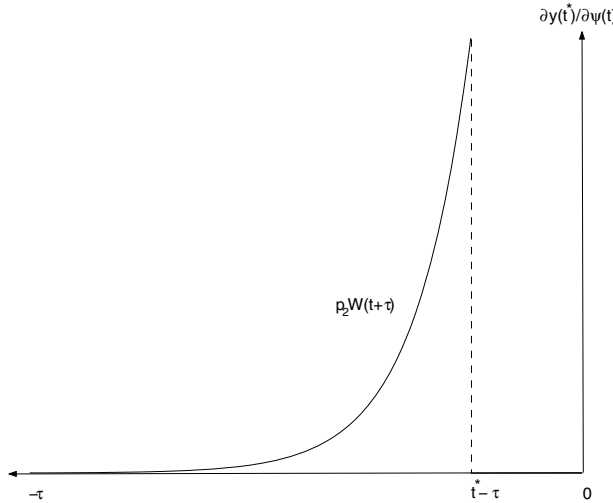


Fig. 6.2 Functional derivative sensitivity density function $\frac{\partial y(t^*)}{\partial \psi(t)}$, (6.37), when $0 < t^* \leq \tau$

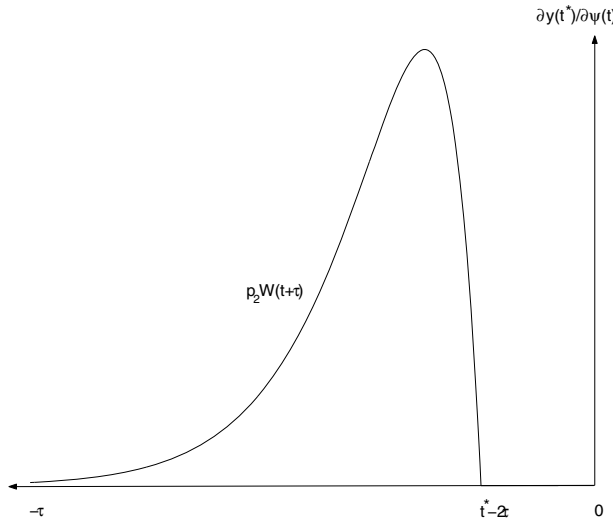


Fig. 6.3 Functional derivative sensitivity density function $\frac{\partial y(t^*)}{\partial \psi(t)}$, (6.38), when $\tau < t^* \leq 2\tau$

derivative sensitivity density function $\frac{\partial y(t^*)}{\partial u(t)}$ is shown in Fig. 6.4 as a function of t for $t^* = 2\tau$.

Figure 6.5 shows the plot of the sensitivity coefficient $\frac{\partial y(t)}{\partial p_1}$. We note that $\frac{\partial y(t)}{\partial p_1}$ is positive and increases as t increases. Figure 6.6 shows the sensitivity of the state

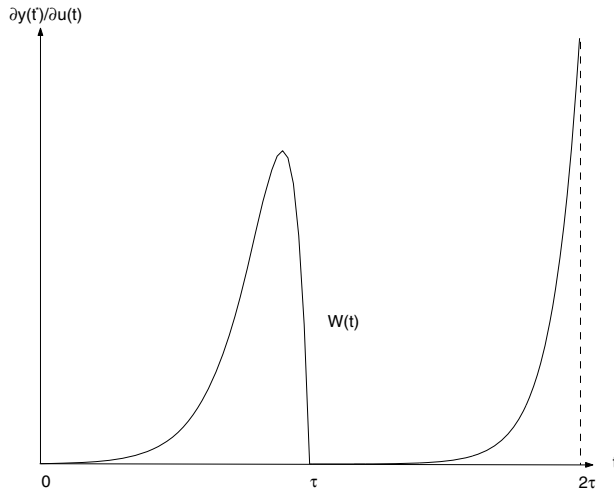


Fig. 6.4 Functional derivative sensitivity density function $\frac{\partial y(t^*)}{\partial u(t)}$, (6.39), for $t^* = 2\tau$

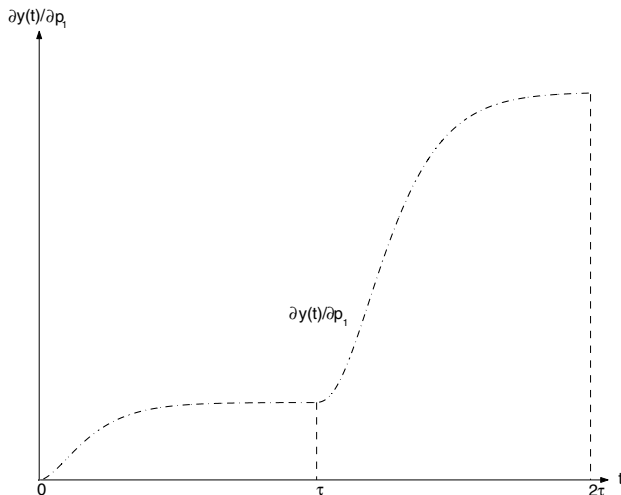


Fig. 6.5 Sensitivity function $\frac{\partial y(t)}{\partial p_1}$, (6.40)

variable to lag τ , $\frac{\partial y(t)}{\partial \tau}$. We note that $\frac{\partial y(t)}{\partial \tau}$ is negative and, as expected, $y(t)$ is very sensitive to changes in τ in the time interval $\tau < t \leq 2\tau$ and is insensitive to changes in the constant lag τ in the time interval $[0, \tau]$. The plots have a kink at $t = \tau$ as a result of existence of the delay in the system state.

- Secondly, if we apply *the direct approach* in the example being considered (6.32), we can simply use the results obtained in Remark 6.1 to obtain a variational

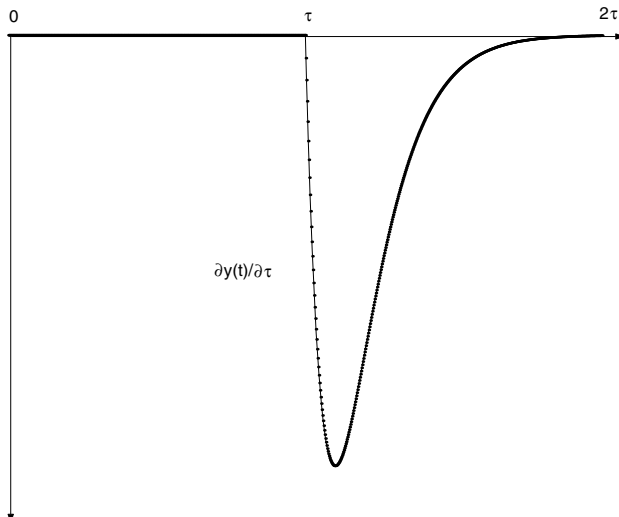


Fig. 6.6 Sensitivity function $\frac{\partial y(t)}{\partial \tau}$, (6.45)

system of NDDEs in the unknown functions of the sensitivity coefficients. We solve this system numerically, as discussed in the previous section, using Archi code [13] together with the original equations. The numerical results are displayed in Fig. 6.7. We note that this approach provides the same results provided by the variational approach.

6.7 Concluding Remarks

In this chapter, we have investigated the sensitivity of model solutions by perturbing the parameters appearing in delay differential systems, using variational and direct approaches. The theory is applied to a linear DDE. Either of the two approaches is capable, in principle, of providing the same information concerning the system. It has been shown that adjoint equations need to be solved to estimate the sensitivity coefficients via the variational approach. In models consisting of parameters that are varying or temporally varying, the functional derivative sensitivity coefficients can only be computed via the variational method. The direct method is based only on considering all parameters as constants (those independent of time or location) and then the sensitivity coefficients are estimated by solving a variational system simultaneously with the original system. The variational approach can provide a rigorous sensitivity measure that gives a precise interpretation of the results because sensitivity density functions contain more information than the sensitivity coefficients.

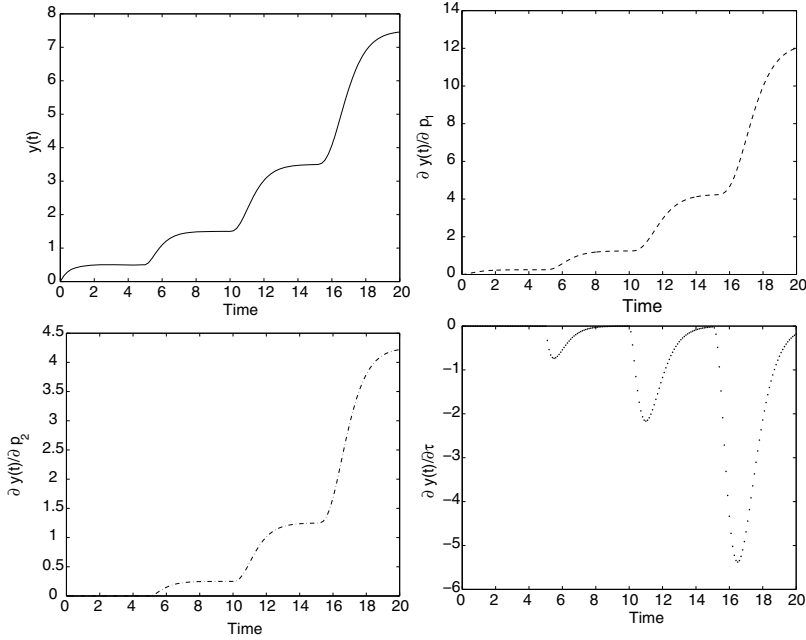


Fig. 6.7 Numerical results for (6.32). The first graph (from left to right, up to down) plots the numerical solution. The second shows the sensitivity function $\frac{\partial y(t)}{\partial p_1}$, the third $\frac{\partial y(t)}{\partial p_2}$, and the fourth $\frac{\partial y(t)}{\partial \tau}$

We have discussed how sensitivity analysis can be used to evaluate which parameters have a significant effect on uncertainty. Sensitivity functions of the solution $y(t)$ for the given DDE model are shown in Figs. 6.2, 6.3, 6.4, 6.5, and 6.6 (by using the variational approach), and in Fig. 6.7 (by using the direct method). These functions are useful in simulation studies for assessing the sensitivity of the solutions with respect to assigned model parameters. We have seen how the sensitivity functions enable one to assess the relevant time intervals for the identification of specific parameters and improve the understanding of the role played by specific model parameters in describing experimental data. We noted, e.g., from Figs. 6.6 and 6.7, that the experimental points in the subinterval $[\tau, 2\tau]$ are informative data points for the estimation of parameter τ , while the state variable is insensitive to a change in the constant parameter τ through the time interval $[0, \tau]$. The oscillation accompanied by the sensitivity of $y(t)$ to τ (in Fig. 6.7) indicates that the solution is sensitive to changes in the parameter τ , and this parameter plays an important role in the model.

In the next chapter, we extend the analysis to study stochastic delay differential equations (SDDEs) which play a prominent role in many application areas including biology, epidemiology, and population dynamics. SDDEs mostly can offer a more sophisticated insight through physical phenomena than their deterministic counterparts do.

References

1. Büskens, C., Maurer, H.: Sqp-methods for solving optimal control problems with control and state constraints: adjoint variables, sensitivity analysis and real-time control. *J. Comput. Appl. Math.* **120**(1–2), 85–108 (2000)
2. Eno, L., Beumee, J.G., Rabitz, H.: Sensitivity analysis of experimental data. *Appl. Math. Comput.* **16** (1985)
3. Leis, J.R., Kramer, M.A.: The simultaneous solution and sensitivity analysis of systems of described by ordinary differential equations. *ACM. Trans. Math. Softw.* **14**, 45–60 (1988)
4. Thomaseseth, K., Cobelli, C.: Generalized sensitivity in physiological system identification. *Ann. Biomed. Engin.* **27**, 607–616 (1999)
5. Thomaseseth, K., Cobelli, C.: Sensitivity analysis of dynamic systems with time lags. *J. Comput. Appl. Math.* **151**, 445–462 (2003)
6. Kolmanovskii, V.B., Shaikhet, L.E.: Control of systems with aftereffect. *Amer. Math. Soc.* (1996)
7. Kolmanovskii, V.B., Shaikhet, L.E.: Mathematical Modelling of Immune Response in Infectious Diseases, MIA, vol. 395. Kluwer Academic Publishers, Dordrecht (1997)
8. Marchuk, G.I.: Adjoint Equations and Analysis of Complex Systems, MIA, vol. 295. Kluwer Academic Publishers, Dordrecht (1994)
9. Bard, Y.: Nonlinear Parameter Estimation. Academic, New York (1974)
10. Ratkowsky, D.A.: Nonlinear Regression Modelling, a Unified Practical Approach. Marcel Dekker, New York (1983)
11. Bates, D.M., Watts, D.G.: Nonlinear Regression Analysis and Its Applications. Wiley, New York (1988)
12. Rihan, F.A.: Numerical treatment of delay differential equations in bioscience. Ph.D. Thesis University of Manchester, UK (2000)
13. Paul, C.A.H.: A user-guide to archi: an explicit runge-kutta code for solving delay and neutral differential equations and parameter estimation problems. MCCM Technical Report 283, University of Manchester (1997)

Chapter 7

Stochastic Delay Differential Equations



7.1 Introduction

Real biological systems are always exposed to influences that are not completely understood or not feasible to model explicitly, and therefore, there is an increasing need to extend the deterministic models to models that embrace more complex variations in the dynamics. A way of modeling these elements is by including stochastic influences or noise. A natural extension of a deterministic differential equations model is a system of stochastic differential equations (SDEs), where relevant parameters are modeled as suitable stochastic processes, or stochastic processes are added to the driving system equations. Therefore, stochastic delay differential equations (SDDEs) are crucial in ecology, epidemiology, and many other fields. SDDEs are also considered as a generalization of both deterministic delay differential equations (DDEs) and stochastic ordinary differential equations (SODEs). Some basic concepts about stochastic differential equations are discussed in [1–3]. The fundamental theory of existence and uniqueness of the solution of SDDEs has been studied by Mao [4] and Mohammed [5]. Some stability properties of numerical schemes of SDDEs are also studied in [6–8].

An important characteristic of environmental noise is its spectrum, which describes variance as a sum of sinusoidal waves of different frequencies. The spectrum of frequencies in noise is particularly important to the dynamics and persistence of systems [9]. However, Brownian motion with normally distributed errors is commonly used in the continuous differential models of dynamical systems. In this monograph, we consider white noise type. In white noise, the variance is the same at all frequencies. Therefore, this is the most thoroughly studied and applied form of noise. The reason for this is that, it is a simple and easily articulated model for noise. From an observational perspective, the random effect of Brownian motion is more visualized with normally distributed errors [1, 6].

In the literature, many numerical schemes for SDDEs have been investigated, such as Euler-type schemes [10, 11], drift-implicit Euler scheme [12, 13], Milstein

schemes [14, 15], split-step schemes [16, 17], and multistep schemes [18]. The extension of numerical approaches for SODEs to SDDEs is non-trivial, particularly since the time-delays may induce instabilities in the basic SDDEs, while their corresponding SODEs are stable [12]. In addition, the presence of time-delays influences the convergence order and computational complexity of the numerical schemes [19]. In general, there is no analytical closed-form solution of the models considered in this dissertation, and we usually require numerical techniques to investigate the models quantitatively.

In this chapter, we briefly study qualitative features of SDDEs (see Sects. 7.2 and 7.3). We also introduce some numerical schemes for their approximate solutions. We investigate local and global errors; convergence and consistency of the scheme. We discuss strong discrete time approximations of solutions of non-autonomous SDDEs, including Euler and Taylor schemes and implicit schemes. The proposed schemes converge in a strong sense. The mean-square stability of the Milstein scheme is also discussed; see Sects. 7.4 and 7.5.

7.1.1 Preliminaries

Definition 7.1 ([20]) Let $(\Omega, \mathcal{A}, \mathbb{P})$ be a probability space with a filtration $\{\mathcal{A}_t\}_{t \geq 0}$. A one-dimensional (standard) Brownian motion is a real-valued continuous $\{\mathcal{A}_t\}$ -adapted process $\{W_t\}_{t \geq 0}$ satisfying the following properties:

1. $W(0) = 0$ a.s. (with probability 1).
2. For $0 \leq s < t \leq T$, the random variable given by the increment $W(t) - W(s)$ is normally distributed with mean zero and variance $t - s$; equivalently, $W(t) - W(s) \sim \sqrt{t - s} N(0, 1)$, where $N(0, 1)$ denotes a normally distributed random variable with zero mean and unit variance.
3. For $0 \leq s < t < u < v \leq T$, the increments $W(t) - W(s)$ and $W(v) - W(u)$ are independent.

Example 7.1 Let us consider the Hutchinson equation

$$\frac{dy(t)}{dt} = ry(t) \left(1 - \frac{y(t - \tau)}{K}\right). \quad (7.1)$$

Here, $r > 0$ is the intrinsic growth rate, $K > 0$ is the carrying capacity of the population, and time-delay τ is considered as hatching time. We can add a small random perturbation σdW , usually referred to as the noise term in Eq. (7.1), which then becomes

$$dy(t) = \left[ry(t) \left(1 - \frac{y(t - \tau)}{K}\right)\right] dt + \sigma dW. \quad (7.2)$$

In Eq. (7.2), the noise term does not include the dependent variable y , and hence, the equation is referred to as an SDDE with additive noise. However, it may be

more natural to consider our extension from the Hutchinson equation by looking at the proportionate population change $\frac{dy(t)}{y(t)}$ and adding our stochastic term to this quantity. This gives us

$$\frac{dy(t)}{y(t)} = \left[\left(1 - \frac{y(t-\tau)}{K} \right) \right] dt. \quad (7.3)$$

Therefore, Eq. (7.3) becomes

$$\frac{dy(t)}{y(t)} = \left[r \left(1 - \frac{y(t-\tau)}{K} \right) \right] dt + \sigma dW. \quad (7.4)$$

Multiplying by $y(t)$ gives us the following SDDE with multiplicative noise:

$$dy = \left[r \left(1 - \frac{y(t-\tau)}{K} \right) y(t) \right] dt + \sigma y(t) dW. \quad (7.5)$$

This implies a more natural procedure, and we will only consider equations with multiplicative noise in this thesis. Figure 7.1 shows the effect of environmental fluctuations on a Hutchinson equation, such that $r = 0.15$ and $k = 1$. The figures at the top show simulation results for $\tau = 5.6$, which indicates that the population attains its steady state value of 1 regardless of the external noise. Hence, it fluctuates within the interval $[0.95, 1.15]$ as $\sigma^2 = 0.01$ (top-left), and as the intensities of white noise increases to $\sigma^2 = 0.05$, it fluctuates within $[0.65, 1.5]$ (top-right). When the magnitude of time-delay is increased to a threshold value $\tau = 11$ (periodic oscillations) and taking $\sigma^2 = 0.01$, the stochastic fluctuations disappears (bottom-left). As $\sigma^2 = 0.05$, we observe abrupt oscillation in population (bottom-right).

Remark 7.1 An important fact about the impact of environmental noise is that, it can suppress a potential population explosion [21]; see Fig. 7.2.

To illustrate this phenomenon, let us consider DDE with pure delay

$$\frac{dy}{dt} = \mu_1 y(t-\tau). \quad (7.6)$$

Equation (7.6) with multiplicative noise takes the form

$$dy = \mu_1 y(t-\tau) dt + \sigma y(t) dW. \quad (7.7)$$

As $\mu_1 > 0$, the solution of (7.6) increases exponentially to infinity as $t \rightarrow \infty$. However, Fig. 7.2 shows the effect of environmental fluctuations on (7.6), with $\mu_1 = 0.06$, $\tau = 0.4$, and $\sigma^2 = 0.16$.

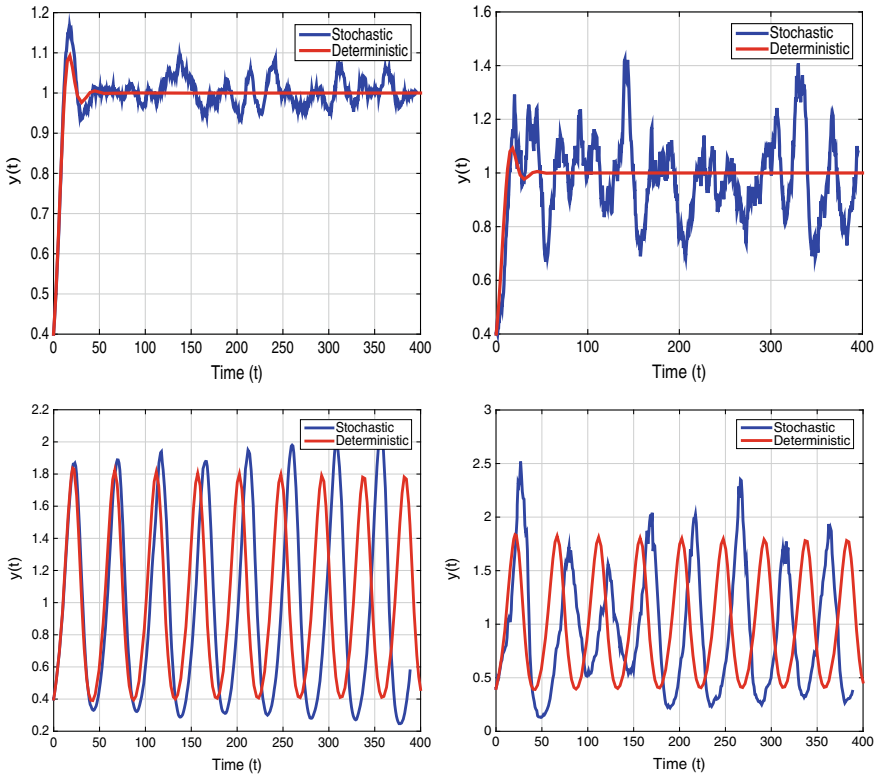


Fig. 7.1 Numerical simulations of deterministic Hutchinson DDE (7.1) and its corresponding SDDE (7.5) when $r = 0.15$ and $k = 1$

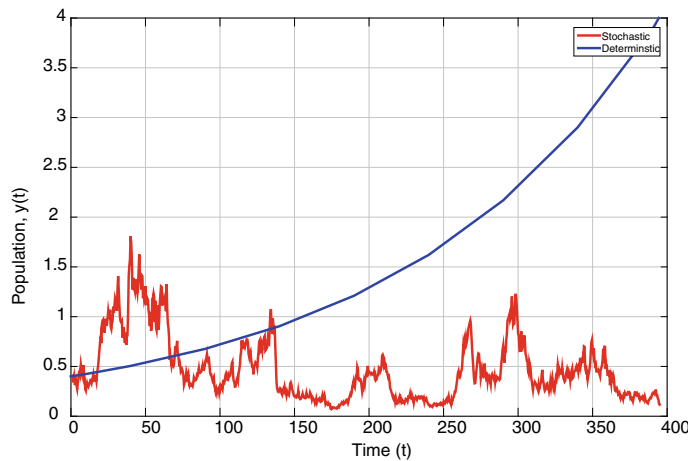


Fig. 7.2 How environmental Brownian noise suppresses explosions in population dynamics, described by $dy = \mu_1 y(t - \tau) dt + \sigma y(t) dW$ and its corresponding deterministic Eq.(7.6)

7.2 Existence and Uniqueness of Solutions for SDDEs

Let us consider d -dimensional SDDEs with r -dimensional standard Wiener processes on the filtered probability space $(\mathcal{Q}, \mathcal{A}, \mathcal{A}_{t_0}, \mathbb{P})$. Therefore, we have equations of the form

$$\begin{aligned} d\mathbf{y}(t) &= \underbrace{\mathbf{f}(t, \mathbf{y}(t), \mathbf{y}(t-\tau)) dt}_{\text{drift coefficient}} + \underbrace{\sum_{j=1}^r \mathbf{g}_j(t, \mathbf{y}(t), \mathbf{y}(t-\tau)) d\mathbf{W}_j(t)}_{\text{diffusion coefficient}}, \quad t \in [0, T], \\ \mathbf{y}(t) &= \psi(t), \quad t \in [-\tau, 0]. \end{aligned} \tag{7.8}$$

With one fixed delay τ , where $\psi(t)$ is an \mathcal{A}_{t_0} -measurable $C([- \tau, 0], \mathbb{R}^d)$ -valued random variable. The drift coefficient $\mathbf{f} : [0, T] \times \mathbb{R}^d \times \mathbb{R}^d \rightarrow \mathbb{R}^d$ and the diffusion coefficient $\mathbf{g}_j : [0, T] \times \mathbb{R}^d \times \mathbb{R}^d \rightarrow \mathbb{R}^d$, $j = 1, 2, \dots, r$ are d -dimensional. Equation (7.8) can be formulated as

$$\mathbf{y}(t) = \mathbf{y}(0) + \int_0^t \mathbf{f}(s, \mathbf{y}(s), \mathbf{y}(s-\tau)) ds + \sum_{j=1}^r \int_0^t \mathbf{g}(s, \mathbf{y}(s), \mathbf{y}(s-\tau)) d\mathbf{W}_j(s), \tag{7.9}$$

for $t \in [0, T]$ and with $\mathbf{y}(t) = \psi(t)$ for $t \in [-\tau, 0]$.

Definition 7.2 (*Strong solution*) A d -dimensional stochastic process $\mathbf{y} = \{\mathbf{y}(t) : [-\tau, T]\}$ is called a strong solution of (7.8), if it has the following properties:

- $\{\mathbf{y}(t)\}$ is measurable, sample continuous process and $(\mathcal{A}_t)_{0 \leq t \leq T}$ -adapted;
- Equations (7.8) and (7.9) hold for every $t \in [0, T]$ almost definitely.

Definition 7.3 (*Path-wise unique solution*) Let the set \mathcal{X} denote some class of stochastic processes that solve (7.8). If any two processes $\mathbf{y}^{(i)} = \{y^{(i)}(t), t \in [-\tau, T]\}$, $i = 1, 2$ from \mathcal{X} with the same initial functions have the same path on $[0, T]$, almost definitely, i.e.,

$$\mathbb{P}\left(\sup_{0 \leq t \leq T} |y^{(1)}(t) - y^{(2)}(t)| > 0\right) = 0, \tag{7.10}$$

then the solution of (7.8) is path-wise unique within \mathcal{X} .

Herein, we formulate the Lipschitz condition (L_1) and growth condition (L_2) to guarantee the existence of a unique solution of (7.8). Assuming that $|\cdot|$ denotes the Euclidian norm, we have

(L_1) *Lipschitz condition:* There exists a constant $K \in (0, \infty)$, such that

$$\begin{aligned} |\mathbf{f}(t, x_1, y_1) - \mathbf{f}(t, x_2, y_2)| + |\mathbf{g}_1(t, x_1, y_1) - \mathbf{g}_1(t, x_2, y_2)| + \cdots + \\ |\mathbf{g}_r(t, x_1, y_1) - \mathbf{g}_r(t, x_2, y_2)| \leq K(|x_2 - x_1| + |y_2 - y_1|), \end{aligned}$$

for $t \in [0, T]$ and $x_1, x_2, y_1, y_2 \in \mathbb{R}^d$.

(L₂) Growth condition: There exists a constant $G \in (0, \infty)$, such that

$$|\mathbf{f}(t, x, y)|^2 + |\mathbf{g}_1(t, x, y)|^2 + \cdots + |\mathbf{g}_r(t, x, y)|^2 \leq G(1 + |x|^2 + |y|^2),$$

for $t \in [0, T]$ and $x, y \in \mathbb{R}^d$.

Let $C = C([-\tau, 0], \mathbb{R}^d)$ be the Banach space of all d -dimensional continuous functions η on $[-\tau, 0]$ equipped with the sup-norm $\|\eta\|_C = \sup_{s \in [-\tau, 0]} |\eta(s)|$. For every function $\xi|[-\tau, T] \rightarrow \mathbb{R}^d$ and every $t \in [0, T]$, so that

$$\xi_t = \{\eta(s) := \xi(t + s), s \in [-\tau, 0]\},$$

a function defined on $[-\tau, 0]$, the segment of ξ at t . In the same manner, the segment-valued function $t \rightarrow \xi_t$ for $t \in [0, T]$ is obtained. Additionally, we denote $\mathcal{L}_2(\Omega, C, \mathcal{A}_0)$, the set of \mathbb{R}^d -valued continuous processes $\eta = \{\eta(s), s \in [-\tau, 0]\}$ with $\eta(s)$ being \mathcal{A}_0 -measurable for all $s \in [-\tau, 0]$ and

$$\mathbb{E}\|\eta\|_C^2 = \mathbb{E} \sup_{s \in [-\tau, 0]} |\eta(s)|^2 < \infty. \quad (7.11)$$

Note that the initial function ψ can be considered as a square integrable $C = C([-\tau, 0], \mathbb{R}^d)$ -valued random variable on $(\Omega, \mathcal{A}_0, \mathbb{P})$. Hence, the above assumptions lead to the following theorem:

Theorem 7.1 ([11]) Assume that (L₁) and (L₂) hold, and ψ be in $\mathcal{L}_2(\Omega, C, \mathcal{A}_0)$. Then the SDDE (7.8), with initial segment ψ , has a path-wise unique strong solution $\mathbf{y} = \{\mathbf{y}(t), t \in [-\tau, T]\}$ in $\mathcal{L}_2(\Omega, C, \mathcal{A}_0)$. Moreover

$$\mathbb{E} \sup_{t \in [-\tau, t]} |\mathbf{y}(t)|^2 < \infty, \quad (7.12)$$

and for each $t \in [0, T]$, the segment $\mathbf{y}_t = \{\mathbf{y}(t + s), s \in [-\tau, 0]\}$ is a $C([-\tau, 0], \mathbb{R}^d)$ -valued process having continuous paths. Additionally, if we have $\mathbb{E}\|\psi\|_C^{2k} < \infty$ for some $k \geq 1$, then

$$\mathbb{E}\|\mathbf{y}_t\|_C^{2k} = \mathbb{E} \sup_{s \in [-\tau, 0]} |\mathbf{y}(t + s)|^{2k} < \infty \quad (7.13)$$

and

$$\mathbb{E}\|\mathbf{y}_t\|_C^{2k} \leq C_k [1 + \mathbb{E}\|\psi\|_C^{2k}]. \quad (7.14)$$

For the proof of the above theorem, refer to [5].

Consider $W(t)$ to be a one-dimensional Wiener process, an autonomous scalar stochastic delay differential equation of the form

$$\begin{aligned} dy(t) &= f(y(t), y(t - \tau))dt + g(y(t), y(t - \tau))dW(t), \quad t \in [0, T], \\ y(t) &= \psi(t), \quad t \in [-\tau, 0]. \end{aligned} \quad (7.15)$$

Equation (7.15) can be formulated as

$$y(t) = y(0) + \int_0^t f(y(s), y(s - \tau))ds + \int_0^t g(y(s), y(s - \tau))dW(s), \quad (7.16)$$

for $t \in [0, T]$ and with $y(t) = \psi(t)$ for $t \in [-\tau, 0]$. The second integral in (7.16) is a stochastic integral in the Itô sense. If it is taken as a Stratonovich integral, we will use notation of the form $\int_0^t g(s, y(s)) \circ dW(s)$. Let us consider $f : \mathbb{R} \times \mathbb{R} \rightarrow \mathbb{R}$, $g : \mathbb{R} \times \mathbb{R} \rightarrow \mathbb{R}$, and $\psi : [-\tau, 0] \rightarrow \mathbb{R}$. Now, we introduce the following theorem for Eq. (7.15) [10, 22]:

Theorem 7.2 *Problem (7.15) has a unique strong solution, provided that the uniform Lipschitz condition and a linear growth bound are satisfied for both f and g .*

Example 7.2 Consider the stochastic delay differential equation

$$\begin{aligned} dy(t) &= \mu_1 y(t - \tau)dt + \sigma dW(t), \quad t \geq 0, \\ y(t) &= t + 1, \quad t \in [-\tau, 0]. \end{aligned} \quad (7.17)$$

Assume that $\mu_1 = -1$ and $\tau = 1$; we can easily verify the conditions of Theorem 7.2. Thus, we solve (7.17) using Itô's formula in the interval $[0, 1]$, so that

$$y_1(t) = y(0) - \int_0^t s ds + \int_0^t \sigma dW(s) = 1 - \frac{t^2}{2} + \sigma W(t).$$

In the interval $[1, 2]$, we have

$$\begin{aligned} y_2(t) &= y(1) + \sigma W(1) + \int_1^t \left(-1 + \frac{(s-1)^2}{2} + \sigma W(s-1)\right)ds + \int_1^t \sigma dW(s) \\ &= \frac{(t-1)^3}{6} - t + \frac{3}{2} + \int_1^t \sigma W(s-1)ds + \sigma W(t). \end{aligned}$$

Similarly, in the interval $[2, 3]$, the solution is

$$\begin{aligned} y_3(t) &= -\frac{1}{3} - \int_2^t \left(\frac{(t-2)^3}{6} - t + \frac{5}{2}\right)ds + \int_1^2 \sigma W(s-1)ds + \sigma W(2) \\ &\quad + \int_2^t \int_1^{s_1-1} \sigma W(s-1)ds ds_1 + \int_2^t \sigma W(s-1)ds + \int_2^t \sigma dW(s) \\ &= \frac{8}{3} - \frac{(t-2)^4}{24} + \frac{t^2}{2} - \frac{5}{2}t + \int_1^2 \sigma W(s-1)ds + \int_2^t \int_1^{s_1-1} \sigma W(s-1)ds ds_1 \\ &\quad + \int_2^t \sigma W(s-1)ds + \sigma W(t). \end{aligned}$$

Note that $\int_0^t \sigma dW(s)$ is a martingale. Hence, $\mathbb{E}\left(\int_0^t \sigma dW(s)\right) = 0$. To find the mean function of $y(t)$, we can take the expectation of the solutions on their intervals as follows:

$$\mathbb{E}(y(t)) = \begin{cases} 1 - \frac{t^2}{2}, & t \in [0, 1]; \\ \frac{(t-1)^3}{6} - t + \frac{3}{2}, & t \in [1, 2]; \\ \frac{8}{3} - \frac{(t-2)^4}{24} + \frac{t^2}{2} - \frac{5}{2}t, & t \in [2, 3]. \end{cases}$$

Numerical methods for SDDEs are currently being actively studied and developed. Hence, they should be used carefully for deterministic DDEs and Stochastic Ordinary Differential Equations (SODEs).

7.3 Stability Criteria for SDDEs

There are at least three different types of stability for SDDEs [6]. Consider the following scalar SDDE with $W(t)$ being a one-dimensional Wiener process:

$$\begin{aligned} dy(t) &= f(t, y(t), y(t-\tau))dt + g(t, y(t), y(t-\tau))dW(t), \quad t \in [0, T], \\ y(t) &= \psi(t), \quad t \in [-\tau, 0]. \end{aligned} \tag{7.18}$$

Hence, Eq. (7.18) can be formulated as

$$y(t) = y(0) + \int_0^t f(s, y(s), y(s-\tau))ds + \int_0^t g(s, y(s), y(s-\tau))dW(s). \tag{7.19}$$

We are supposed to be concerned with the main ideas of the p th mean stability of the trivial solution of Eq. (7.19) with respect to perturbations in $\psi(\cdot)$ (for $1 \leq p < \infty$), and also with mean-square stability when $p = 2$.

Definition 7.4 ([23]) For some $p > 0$, the trivial solution of the SDDE (7.19) is called

- Locally stable in the p th mean, if for each $\epsilon > 0$, there exists a $\delta \geq 0$ such that $\mathbb{E}(|y(t; t_0, \psi)|^p) < \epsilon$ whenever $t \geq t_0$ and $\mathbb{E}(\sup_{t \in [t_0-\tau, t_0]} |\psi(t)|^p) < \delta$;
- Locally asymptotically stable in the p th mean if it is stable in the p th mean and if there exists a $\delta \geq 0$ such that whenever $\mathbb{E}(\sup_{t \in [t_0-\tau, t_0]} |\psi(t)|^p) < \delta$, then $\mathbb{E}(|y(t; t_0, \psi)|^p) \rightarrow 0$ for $t \rightarrow \infty$;
- Locally exponentially stable in the p th mean if it is stable in the p th mean and if there exists a $\delta \geq 0$ such that whenever $\mathbb{E}(\sup_{t \in [t_0-\tau, t_0]} |\psi(t)|^p) < \delta$, there exists some finite constant C and a $u^* > 0$ such that $\mathbb{E}(|y(t; t_0, \psi)|^p) \leq C \mathbb{E}(\sup_{s \in [t_0-\tau, t_0]} |\psi(s)|^p) \exp(-u^*(t - t_0))$ ($t_0 \leq t < \infty$). If δ is arbitrarily large, then the stability in the above, in each case, is global rather than local.

A different approach to stability for SDDEs, that of stochastic stability or stability in probability, is as follows:

- The trivial solution of the SDDE (7.19) is termed stochastically stable in probability if for each $e \in (0, 1)$ and $\epsilon > 0$, there exists a $\delta \equiv \delta(e, \epsilon) \geq 0$, such that

$$\mathbb{P}(|y(t; t_0, \psi)| \leq \epsilon \text{ for all } t \geq t_0) \geq 1 - e,$$

whenever $t \geq t_0$ and $\sup_{t \in [t_0 - \tau, t_0]} |\psi(t)|^p < \delta$ with probability 1.

Certain stability conditions for SDDEs can be stated in terms of Lyapunov functionals, similar to the theorems for DDEs. Now, we present the Lyapunov theory approach for SDDEs. Let us consider a more general type for (7.8) with one delay. Thus, an Itô type SDDE is given by

$$\begin{aligned} d\mathbf{y}(t) &= \mathbf{f}(t, \mathbf{y}_t)dt + \mathbf{g}(t, \mathbf{y}_t)dW(t), \quad t \geq t_0, \\ \mathbf{y}_t(\theta) &= \mathbf{y}(t + \theta), \quad -\tau \leq \theta \leq 0, \\ \mathbf{f}(t, 0) &\equiv 0, \quad \mathbf{y}_{t_0} = \psi. \end{aligned} \tag{7.20}$$

Define $\mathbf{y}_t \in C_n$ by $\mathbf{y}_t(\theta) = \mathbf{y}(t + \theta)$ for $\theta \in [-\tau, 0]$, where $\psi \in C_n$, such that when we consider the existence and uniqueness of solutions, without loss of generality, the solution $\mathbf{y}_t = 0$ is an equilibrium.

Theorem 7.3 ([24]) Suppose there is a continuous functional $V : [t_0, \infty] \times C[-\tau, 0] \rightarrow \mathbb{R}$ such that for any solution of (7.20), where $\mathbf{y}_t(\theta) = \mathbf{y}(t + \theta)$ such that $-\tau \leq \theta \leq 0$, the following inequalities hold, such that C_i $i = 1, 2, 3$ are positive constants:

$$\begin{aligned} V(t, \mathbf{y}_t) &\geq C_1 |\mathbf{y}(t)|^2 \\ \mathbb{E}V(t, \mathbf{y}_t) &\leq C_2 \sup_{-\tau \leq \theta \leq 0} \mathbb{E}|\mathbf{y}(t + \theta)|^2, \end{aligned} \tag{7.21}$$

for arbitrary $t \geq t_0$, $s \geq t$

$$\mathbb{E}[V(s, \mathbf{y}_s) - V(t, \mathbf{y}_t)] \leq -C_3 \int_t^s \mathbb{E}|\mathbf{y}(h)|^2 dh. \tag{7.22}$$

Then, the trivial solution of (7.20) is asymptotically mean-square stable.

Example 7.3 Consider an SDDE of the form

$$dy(t) = -\mu_1 y(t - \tau)dt + \mu_2 y(t)dW(t), \quad t > t_0, \tag{7.23}$$

where μ_1, μ_2 are positive constants. Sufficient conditions for asymptotic mean-square stability of (7.23) are

$$0 < \mu_1 \tau < 1, \quad \mu_1(1 - \mu_1 \tau) > \frac{\mu_2^2}{2}.$$

To prove this, consider the functional

$$V(\psi) = \left[\psi(0) - \mu_1 \int_{-\tau}^0 \psi(\theta) d\theta \right]^2 + \mu_1^2 \int_{-\tau}^0 ds \int_s^0 \psi^2(\theta) d\theta. \quad (7.24)$$

Using Itô formula, we obtain

$$\begin{aligned} dV(y_t) &= 2 \left[y(t) - \mu_1 \int_{t-\tau}^t y(\theta) d\theta \right] (dy(t) - \mu_1 y(t) dt + \mu_1 y(t-\tau) dt) \\ &\quad + \left[\mu_2^2 y^2(t) + \mu_1^2 \tau y^2(t) - \mu_1^2 \int_{t-\tau}^t y^2(\theta) d\theta \right] dt, \\ &= 2 \left[y(t) - \mu_1 \int_{t-\tau}^t y(\theta) d\theta \right] (\mu_2 y(t) dW(t) - \mu_1 y(t) dt) \\ &\quad + \left[\mu_2^2 y^2(t) + \mu_1^2 \tau y^2(t) - \mu_1^2 \int_{t-\tau}^t y^2(\theta) d\theta \right] dt. \end{aligned}$$

Note that

$$2\mu_1^2 y(t) \int_{t-\tau}^t y(\theta) d\theta \leq \mu_1^2 \left[\tau y^2(t) + \int_{t-\tau}^t y^2(\theta) d\theta \right].$$

Hence

$$dV(y_t) \leq 2\mu_2 \left[y(t) - \mu_1 \int_{t-\tau}^t y(\theta) d\theta \right] y(t) dW(t) - [2\mu_1(1 - \mu_1 \tau) - \mu_2^2] y^2(t). \quad (7.25)$$

Integration of both parts of (7.25) from $s \in [t_0, t]$ to t , and then taking the expectation yields

$$\mathbb{E}[V(y_t) - V(y_s)] \leq -[2\mu_1(1 - \mu_1 \tau) - \mu_2^2] \int_s^t \mathbb{E}y^2(h) dh. \quad (7.26)$$

From inequality (7.26), we have

$$\mathbb{E}V(y_t) \leq \mathbb{E}V(y_{t_0}), \quad t \geq t_0. \quad (7.27)$$

Therefore,

$$\mathbb{E} \left[y(t) - \mu_1 \int_{t-\tau}^t y(\theta) d\theta \right]^2 \leq \mathbb{E}V(y_{t_0}), \quad \int_{t_0}^{\infty} \mathbb{E}y^2(s) ds < \infty. \quad (7.28)$$

Inequalities (7.28) and condition $\mu_1 \tau < 1$ imply mean-square stability, since

$$\sup_{t \geq t_0} \mathbb{E}y^2(t) \leq C_1 \sup_{-\tau \leq \theta \leq 0} \mathbb{E}\psi^2(\theta). \quad (7.29)$$

Therefore, asymptotic mean-square stability is implied based on inequalities (7.28) and the fact that $\lim_{t \rightarrow \infty} \mathbb{E}y^2(t) = 0$.

Next, we introduce a numerical scheme for an autonomous SDDE.

7.4 Numerical Scheme for Autonomous SDDEs

Given a scalar autonomous SDDE of the form

$$\begin{aligned} dy(t) &= f(y(t), y(t - \tau))dt + g(y(t), y(t - \tau))dW(t), \quad t \in [0, T], \\ y(t) &= \psi(t), \quad t \in [-\tau, 0]. \end{aligned} \quad (7.30)$$

which can be formulated as

$$y(t) = y(0) + \int_0^t f(y(s), y(s - \tau))ds + \int_0^t g(y(s), y(s - \tau))dW(s), \quad (7.31)$$

for $t \in [0, T]$ and with $y(t) = \psi(t)$ for $t \in [-\tau, 0]$. The second integral in (7.31) is a stochastic integral in the Itô sense.

We define mesh points with a uniform step on the interval $[0, T]$, so that $h = T/N$, $t_n = nh$, where $n = 0, \dots, N$. We also assume that, for the given h , there is a corresponding integer m , where the time-delay can be expressed in terms of the stepsize as $\tau = mh$. For all indices $n - m \leq 0$, we have $\tilde{y}_{n-m} := \psi(t_n - \tau)$; otherwise, the numerical approximation of (7.30) takes the form

$$\tilde{y}_{n+1} = \tilde{y}_n + \phi(h, \tilde{y}_n, \tilde{y}_{n-m}, I_\phi), \quad n = 0, \dots, N-1. \quad (7.32)$$

The increment function $\phi(h, \tilde{y}_n, \tilde{y}_{n-m}, I_\phi) : \mathbb{R} \times \mathbb{R} \rightarrow \mathbb{R}$ includes a finite number of multiple Itô-integrals (see [25, 26]) of the form

$$I_{(j_1, \dots, j_l), h} = \int_t^{t+h} \int_t^{s_1} \dots \int_t^{s_2} dW^{j_1}(s_1) \dots dW^{j_{l-1}}(s_{l-1}) dW^{j_l}(s_l),$$

where $j_i \in \{0, 1\}$ and $dW^0(t) = dt$, and with $t = t_n$ for (7.32), we denote I_ϕ the collection of Itô-integrals required to compute the increment function ϕ .

To guarantee the existence of the numerical solution, some assumptions should be given to the increment function ϕ of (7.32). Suppose that there exist positive constants V_1 , V_2 , and V_3 , such that for all $\kappa, \kappa', \omega, \omega' \in \mathbb{R}$, we have

$$\begin{aligned} \left| \mathbb{E}(\phi(h, \kappa, \omega, I_\phi) - \phi(h, \kappa', \omega', I_\phi)) \right| &\leq V_1 h(|\kappa - \kappa'| + |\omega - \omega'|), \\ \mathbb{E}(|\phi(h, \kappa, \omega, I_\phi) - \phi(h, \kappa', \omega', I_\phi)|^2) &\leq V_2 h(|\kappa - \kappa'|^2 + |\omega - \omega'|^2), \end{aligned} \quad (7.33)$$

and

$$\mathbb{E}(|\phi(h, \kappa, \omega, I_\phi)|^2) \leq V_3 h (1 + |\kappa|^2 + |\omega|^2). \quad (7.34)$$

Lemma 7.1 ([10]) *If the increment function ϕ in Eq. (7.32) satisfies condition (7.34), then $\mathbb{E}|\tilde{y}_n|^2 < \infty$ for all $n \leq N$.*

Let $y(t_{n+1})$ be the exact solution of (7.30) at mesh point t_{n+1} . \tilde{y}_{n+1} is the value of the approximate solution given by (7.32), and $\tilde{y}(t_{n+1})$ is the solution of (7.32) after just one step, so that

$$\tilde{y}(t_{n+1}) = y(t_n) + \phi(h, y(t_n), y(t_n - \tau), I_\phi).$$

Definition 7.5 (*Local and global errors*) The local error that occurs in one step of the above approximation $\{\tilde{y}_n\}$ is the sequence of random variables

$$\delta_{n+1} = y(t_{n+1}) - \tilde{y}(t_{n+1}), \quad n = 0, \dots, N-1. \quad (7.35)$$

However, the global error is the amount of error that occurs in the use of a numerical approximation to solve a problem, which is the sequence of random variables

$$\epsilon_n := y(t_n) - \tilde{y}_n, \quad n = 1, \dots, N. \quad (7.36)$$

Note that ϵ_n is \mathcal{A}_{t_n} -measurable since both $y(t_n)$ and \tilde{y}_n are \mathcal{A}_{t_n} -measurable random variable, such that $(\mathbb{E}|\epsilon_n|^2)^{1/2}$ is the \mathcal{L}^2 -norm of (7.36).

7.4.1 Convergence and Consistency

Definition 7.6 Assume that

$$\delta_{n+1} = y(t_{n+1}) - \tilde{y}(t_{n+1}), \quad n = 0, \dots, N-1. \quad (7.37)$$

The numerical scheme (7.32) is said to be consistent with order p_1 in the mean and with order p_2 in the mean square if, with

$$p_2 \geq \frac{1}{2} \quad \text{and} \quad p_1 \geq p_2 + \frac{1}{2}, \quad (7.38)$$

the estimates

$$\max_{0 \leq n \leq N-1} |\mathbb{E}(\delta_{n+1})| \leq Ch^{p_1} \quad \text{as } h \rightarrow 0, \quad (7.39)$$

and

$$\max_{0 \leq n \leq N-1} \left(|\mathbb{E}(\delta_{n+1})|^2 \right)^{1/2} \leq Ch^{p_2} \quad \text{as } h \rightarrow 0, \quad (7.40)$$

hold, where constant C does not depend on h , but may depend on T , and on the initial data.

Therefore, we can now introduce the basic theorem about the convergence of method (7.32).

Theorem 7.4 ([10]) *Assume that the conditions of Theorem 7.1 are satisfied. Suppose that the method defined by Eq. (7.32) is consistent with order p_1 in the mean and order p_2 in the mean-square sense, such that p_1, p_2 fulfilling (7.38), and the increment function ϕ on Eq. (7.32) satisfies the estimates (7.33). Then, the approximation (7.32) for Eq. (7.30) is convergent in L^2 (as $h \rightarrow 0$ with $\tau/h \in \mathbb{N}$) with order $p = p_2 - 1/2$. That is, convergent is in the mean-square sense, such that*

$$\max_{0 \leq n \leq N-1} \left(|\mathbb{E}(\delta_{n+1})|^2 \right)^{1/2} \leq Ch^p \quad \text{as } h \rightarrow 0, \quad (7.41)$$

Theorem 7.5 ([10]) *If the increment function ϕ of the approximation (7.32) satisfies the estimates (7.33), then the one-step method (7.32) is zero stable in the quadratic mean-square sense.*

Next, we extend our analysis to non-autonomous system of SDDEs (7.8).

7.5 Numerical Schemes for Non-autonomous SDDE

There are some specific discrete time approximations for (7.8). The simplest scheme, which is defined by stochastic difference equation, is represented by Euler approximation as

$$\tilde{\mathbf{y}}_{n+1} = \tilde{\mathbf{y}}_n + \mathbf{f}(t_n, \tilde{\mathbf{y}}_n, \tilde{\mathbf{y}}_{n-m})h + \sum_{j=1}^r \mathbf{g}_j(t_n, \tilde{\mathbf{y}}_n, \tilde{\mathbf{y}}_{n-m})\Delta W_n^j, \quad (7.42)$$

where $\tilde{\mathbf{y}} = \{\tilde{\mathbf{y}}(t), t \in [-\tau, T]\}$ is right continuous with left-hand limits, a discrete time approximation with stepsize h , such that for each $n \in \{1, \dots, N\}$. The random variable $\tilde{\mathbf{y}}(t_n)$ is \mathcal{A}_{t_n} -measurable and $\tilde{\mathbf{y}}(t_{n+1})$ can be expressed as a function of $\tilde{\mathbf{y}}(t_{-m})$, $\tilde{\mathbf{y}}(t_{-m+1}), \dots, \tilde{\mathbf{y}}(t_n)$, discretization time t_n , and a finite number of $\mathcal{A}_{t_{n+1}}$ -measurable random variable. With $\Delta W_n^j = W^j(t_{n+1}) - W^j(t_n)$, for $n = 0, 1, \dots, N-1$ and $j = 0, 1, \dots, r$. By more general assumptions, we can check that Euler approximation strongly converges with order 1/2 [11].

7.5.1 Taylor Approximation

For stochastic differential equations, it is common that by application of the Wagner-Platen stochastic Taylor expansion [27], we can construct discrete time approximations that converge with a given order of strong convergence, which involve in each time step certain multiple integrals. For the general multi-dimensional case $d, r = 1, 2, \dots$ the order-one strong Taylor approximation has the form

$$\begin{aligned} \tilde{\mathbf{y}}_{n+1} &= \tilde{\mathbf{y}}_n + \mathbf{f}(t_n, \tilde{\mathbf{y}}_n, \tilde{\mathbf{y}}_{n-m})h + \sum_{j=1}^r \mathbf{g}_j(t_n, \tilde{\mathbf{y}}_n, \tilde{\mathbf{y}}_{n-m})\Delta W_n^j \\ &+ \sum_{j_1, j_2=1}^r \sum_{i=1}^d g_{i, j_1}(t_n, \tilde{\mathbf{y}}_n, \tilde{\mathbf{y}}_{n-m}) \frac{\partial}{\partial \tilde{y}_n^i} g_{i, j_2}(t_n, \tilde{\mathbf{y}}_n, \tilde{\mathbf{y}}_{n-m}) \int_{t_n}^{t_{n+1}} \int_{t_n}^{s_1} dW^{j_1}(s_2) dW^{j_2}(s_1) \\ &+ \sum_{j_1, j_2=1}^r \sum_{l_1=1}^d g_{i, j_1}(t_{n-m}, \tilde{\mathbf{y}}_{n-m}, \tilde{\mathbf{y}}_{n-2m}) \frac{\partial}{\partial \tilde{y}_{n-m}^i} g_{i, j_2}(t_n, \tilde{\mathbf{y}}_n, \tilde{\mathbf{y}}_{n-m}) \\ &\times \int_{t_n}^{t_{n+1}} \int_{t_n}^{s_1} dW^{j_1}(s_2 - \tau) dW^{j_2}(s_1), \end{aligned} \tag{7.43}$$

for $n = 0, 1, \dots, N-1, i = 1, 2, \dots, d$. One can check that approximation (7.43) converges under suitable assumptions with strong-order-one Taylor approximation [11]. In the one-dimensional case, when $\tau = 0$, scheme (7.43) coincides with the well-known Milstein Scheme for SDEs. However, the time-delay in (7.43) generates an extra term, which describes a double Wiener integral that integrates an earlier segment of the Wiener path with respect to the actual Wiener path.

7.5.2 Implicit Strong Approximations

In practice, explicit schemes not only have smaller computational costs, but also have lower accuracy compared to implicit methods. It is sometimes recommended to use implicit schemes to have numerically stable approximate solutions for SDDEs, as in the case of stiff problem¹

For the general multi-dimensional case (7.8), the family of implicit Euler approximations are

$$\tilde{\mathbf{y}}_{n+1} = \tilde{\mathbf{y}}_n + [\theta \mathbf{f}(t_{n+1}, \tilde{\mathbf{y}}_{n+1}, \tilde{\mathbf{y}}_{n-m+1}) + (1 - \theta) \mathbf{f}(t_n, \tilde{\mathbf{y}}_n, \tilde{\mathbf{y}}_{n-m})]h + \sum_{j=1}^r \mathbf{g}_j(t_n, \tilde{\mathbf{y}}_n, \tilde{\mathbf{y}}_{n-m})\Delta W_n^j, \tag{7.44}$$

for $n = 0, 1, \dots, N-1$, such that $\theta \in [0, 1]$ stands for the degree of implicitness. If $\theta = 0$, we have the explicit Euler approximation (7.42). For $\theta = 1$, we obtain the

¹ A stiff problem is defined as that in which the global accuracy of the numerical solution is determined by stability rather than local error, and implicit methods are more appropriate for it.

fully implicit Euler approximation. The approximation (7.44) converges with strong order $1\backslash 2$ [13].

In the same manner, we can establish an order-one strong implicit Taylor approximation with

$$\begin{aligned}\tilde{\mathbf{y}}_{n+1} = & \tilde{\mathbf{y}}_n + [\theta \mathbf{f}(t_{n+1}, \tilde{\mathbf{y}}_{n+1}, \tilde{\mathbf{y}}_{n-m+1}) + (1 - \theta) \mathbf{f}(t_n, \tilde{\mathbf{y}}_n, \tilde{\mathbf{y}}_{n-m})]h + \sum_{j=1}^r \mathbf{g}_j(t_n, \tilde{\mathbf{y}}_n, \tilde{\mathbf{y}}_{n-m}) \Delta W_n^j \\ & + \sum_{j_1, j_2=1}^r \sum_{i=1}^d g_{i, j_1}(t_n, \tilde{\mathbf{y}}_n, \tilde{\mathbf{y}}_{n-m}) \frac{\partial}{\partial \tilde{y}_n^i} g_{i, j_2}(t_n, \tilde{\mathbf{y}}_n, \tilde{\mathbf{y}}_{n-m}) \int_{t_n}^{t_{n+1}} \int_{t_n}^{s_1} dW^{j_1}(s_2) dW^{j_2}(s_1) \\ & + \sum_{j_1, j_2=1}^r \sum_{i=1}^d g_{i, j_1}(t_{n-m}, \tilde{\mathbf{y}}_{n-m}, \tilde{\mathbf{y}}_{n-2m}) \frac{\partial}{\partial \tilde{y}_{n-m}^i} g_{i, j_2}(t_n, \tilde{\mathbf{y}}_n, \tilde{\mathbf{y}}_{n-m}) \\ & \times \int_{t_n}^{t_{n+1}} \int_{t_n}^{s_1} dW^{j_1}(s_2 - \tau) dW^{j_2}(s_1),\end{aligned}\tag{7.45}$$

Next, we will discuss in detail the mean-square stability of Milstein method since we have used this scheme in the numerical simulations for SDDEs models.

7.6 Milstein Scheme for SDDEs

In this section, we introduce the Milstein scheme for SDDEs and show that the numerical method is mean-square stable under suitable conditions.

Given the one-dimensional version of (7.8), $r = d = 1$, of the following form:

$$\begin{aligned}dy(t) = & f(t, y(t), y(t - \tau))dt + g(t, y(t), y(t - \tau))dW, \quad t \in [0, T], \\ y(t) = & \psi(t), \quad t \in [-\tau, 0].\end{aligned}\tag{7.46}$$

The order one strong Taylor approximation for (7.46) the one-dimensional case is defined by

$$\begin{aligned}\tilde{y}_{n+1} = & \tilde{y}_n + f(t_n, \tilde{y}_n, \tilde{y}_{n-m}) \int_{t_n}^{t_{n+1}} ds_1 + g(t_n, \tilde{y}_n, \tilde{y}_{n-m}) \int_{t_n}^{t_{n+1}} dW(s_1) \\ & + g(t_n, \tilde{y}_n, \tilde{y}_{n-m}) \frac{\partial}{\partial \tilde{y}_n} g(t_n, \tilde{y}_n, \tilde{y}_{n-m}) \int_{t_n}^{t_{n+1}} \int_{t_n}^{s_1} dW(s_2) dW(s_1) \\ & + g(t_{n-m}, \tilde{y}_{n-m}, \tilde{y}_{n-2m}) \frac{\partial}{\partial \tilde{y}_{n-m}} g(t_n, \tilde{y}_n, \tilde{y}_{n-m}) \\ & \times \int_{t_n}^{t_{n+1}} \int_{t_n}^{s_1} dW(s_2 - \tau) dW(s_1).\end{aligned}\tag{7.47}$$

Once we have the Taylor approximation, we can construct the Milstein scheme for (7.46)

$$\begin{aligned}\tilde{y}_{n+1} = & \tilde{y}_n + hf(t_n, \tilde{y}_n, \tilde{y}_{n-m}) + g(t_n, \tilde{y}_n, \tilde{y}_{n-m})\Delta W_n + \frac{1}{2}g(t_n, \tilde{y}_n, \tilde{y}_{n-m})g'(t_n, \tilde{y}_n, \tilde{y}_{n-m})[(\Delta W_n)^2 - h] \\ & + g(t_{n-m}, \tilde{y}_{n-m}, \tilde{y}_{n-2m})\frac{\partial}{\partial \tilde{y}_{n-m}}g(t_n, \tilde{y}_n, \tilde{y}_{n-m})I,\end{aligned}\quad (7.48)$$

where $I = \int_{t_n}^{t_{n+1}} \int_{t_n}^{s_1} dW(s_2 - \tau) dW(s_1)$.

7.6.1 Convergence and Mean-Square Stability of the Milstein Scheme

Consider the linear scalar SDDE of the form

$$\begin{aligned}dy(t) = & [\rho_0 y(t) + \rho_1 y(t - \tau)]dt + [\rho_2 y(t) + \rho_3 y(t - \tau)]dW(t), \quad t \in [0, T], \\ y(t) = & \psi(t), \quad t \in [-\tau, 0],\end{aligned}\quad (7.49)$$

where $\rho_0, \rho_1, \rho_2, \rho_3 \in \mathbb{R}$, $W(t)$ is a one-dimensional standard Wiener process, and $\psi(t)$ is continuous and bounded function with $\mathbb{E}[\|\psi\|^2] < \infty$, where $\|\psi\| = \sup_{-\tau \leq t \leq 0} |\psi(t)|$.

Theorem 7.6 ([11]) Suppose that

$$\rho_0 < -|\rho_1| - \frac{(|\rho_2| + |\rho_3|)^2}{2}, \quad (7.50)$$

then the solution of (7.49) satisfies $\lim_{t \rightarrow \infty} \mathbb{E}[|y(t)|^2] = 0$, i.e., the solution is mean-square stable.

Using order one strong Taylor approximation formula to the linear one delay system (7.49), we have

$$\begin{aligned}y_{n+1} = & y_n + h(\rho_0 y_n + \rho_1 y_{n-m}) + (\rho_2 y_n + \rho_3 y_{n-m})\Delta W_n \\ & + \rho_3(\rho_2 y_{n-m} + \rho_3 y_{n-2m})I_1 + \rho_2(\rho_2 y_n + \rho_3 y_{n-m})I_2,\end{aligned}\quad (7.51)$$

where y_n is an approximation to $y(t_n)$, such that $I_1 = \int_{t_n}^{t_{n+1}} \int_{t_n}^s dW(t - \tau) dW(s)$, $I_2 = \int_{t_n}^{t_{n+1}} \int_{t_n}^s dW(t) dW(s)$. The convergence order of (7.51) can be obtained by Theorem 10.2 in [11], since the coefficients of (7.51) satisfy the Lipschitz condition and growth condition. Thus, the Milstein scheme (7.51) is strongly convergent of order 1.

Theorem 7.7 The Milstein scheme (7.51) is mean-square stable, if condition (7.50) is satisfied [28].

Proof By reorganizing the terms of (7.51), we get

$$\begin{aligned} y_{n+1} = & (1 + \rho_0 h + \rho_2 \Delta W_n) y_n + (\rho_1 h + \rho_3 \Delta W_n) y_{n-m} + \rho_3 (\rho_2 y_{n-m} + \rho_3 y_{n-2m}) I_1 \\ & + \rho_2 (\rho_2 y_n + \rho_3 y_{n-m}) I_2. \end{aligned} \quad (7.52)$$

Squaring both sides of (7.52), it follows from $2ab \leq a^2 + b^2$ ($\forall a, b \in \mathcal{R}$), we have

$$\begin{aligned} y_{n+1}^2 \leq & (1 + \rho_1 h + \rho_2 \Delta W_n)^2 y_n^2 + (\rho_1 h + \rho_3 \Delta W_n)^2 y_{n-m}^2 + \rho_2^2 [(\rho_2^2 + |\rho_2 \rho_3|) y_n^2 + (\rho_3^2 + |\rho_2 \rho_3|) y_{n-m}^2] I_1^2 \\ & + \rho_3^2 [(\rho_2^2 + |\rho_2 \rho_3|) y_{n-m}^2 + (\rho_3^2 + |\rho_2 \rho_3|) y_{n-2m}^2] I_1^2 + |1 + \rho_0 h| |\rho_1| h (y_n^2 + y_{n-m}^2) \\ & + |\rho_2 \rho_3| |\Delta W_n|^2 (y_n^2 + y_{n-m}^2) + 2[(1 + \rho_0 h) \rho_3 + \rho_1 \rho_2 h] \Delta W_n y_n y_{n-m} \\ & + 2\rho_2 \rho_3 (\rho_2 y_n + \rho_3 y_{n-m}) (\rho_2 y_{n-m} + \rho_3 y_{n-2m}) I_1 I_2 \\ & + 2\rho_2 (1 + \rho_0 h + \rho_2 \Delta_n) (\rho_2 y_n + \rho_3 y_{n-m}) y_n I_2 \\ & + 2\rho_3 (1 + \rho_0 h + \rho_2 \Delta_n) (\rho_2 y_{n-m} + \rho_3 y_{n-2m}) y_n I_1 \\ & + 2\rho_2 (\rho_1 h + \rho_3 \Delta W_n) (\rho_2 y_n + \rho_3 y_{n-m}) y_{n-m} I_2 \\ & + 2\rho_3 (\rho_1 h + \rho_3 \Delta W_n) (\rho_2 y_{n-m} + \rho_3 y_{n-2m}) y_{n-m} I_1 \end{aligned} \quad (7.53)$$

Assume that $x_n = \mathbb{E}[y_n^2]$, then take expectation for both sides of (7.53), which yields the following:

$$x_{n+1} \leq A_1 x_n + A_2 x_{n-m} + A_3 x_{n-2m}, \quad (7.54)$$

where

$$\begin{aligned} A_1 &= (1 + \rho_0 h)^2 + \rho_2^2 h + |1 + \rho_0 h| |\rho_1| h + |\rho_2 \rho_3| h + \frac{h^2}{2} \rho_2^2 (\rho_2^2 + |\rho_2 \rho_3|), \\ A_2 &= \rho_1^2 h^2 + \rho_3^2 h + |1 + \rho_0 h| |\rho_1| h + |\rho_2 \rho_3| h + \frac{h^2}{2} \rho_2^2 (\rho_3^2 + |\rho_2 \rho_3|) \\ &\quad + \frac{h^2}{2} \rho_3^2 (\rho_2^2 + |\rho_2 \rho_3|), \quad A_3 = \frac{h^2}{2} \rho_3^2 (\rho_2^2 + |\rho_2 \rho_3|). \end{aligned} \quad (7.55)$$

Therefore

$$\begin{aligned} (1 + \rho_0 h)^2 + \rho_1^2 h^2 + (\rho_2^2 + \rho_3^2 + 2|\rho_2 \rho_3|) h + 2|1 + \rho_0 h| |\rho_1| h \\ + \frac{h^2}{2} (\rho_2^2 + \rho_3^2) (|\rho_2| + |\rho_3|)^2 < 1. \end{aligned} \quad (7.56)$$

Consider

$$\begin{aligned} h_1 &= \frac{-[2\rho_0 + 2|\rho_1| + (|\rho_2| + |\rho_3|)^2]}{(|\rho_0| + |\rho_1|)^2 + \frac{1}{2}(\rho_2^2 + \rho_3^2)(|\rho_2| + |\rho_3|)^2} > 0, \\ h_2 &= \min \left\{ \frac{1}{|\rho_0|}, \frac{-[2\rho_0 + 2|\rho_1| + (|\rho_2| + |\rho_3|)^2]}{(|\rho_0| + |\rho_1|)^2 + \frac{1}{2}(\rho_2^2 + \rho_3^2)(|\rho_2| + |\rho_3|)^2} \right\} > 0, \end{aligned} \quad (7.57)$$

- If $h \in (0, h_1)$, inequality (7.56) holds;

- If $h \in (0, h_2)$, then $1 + \rho_0 h > 0$ (wider range of stable stepsize values) and inequality (7.56) holds;
- Let $h_0 = \max\{h_1, h_2\}$; thus, the Milstein scheme is MS-stable whenever $h \in (0, h_0)$.

□

7.7 Concluding Remarks

In this chapter, we have briefly introduced some features of SDDEs. We have also discussed some numerical schemes for SDDEs. Convergence and consistency of such schemes have been investigated as well. The mean-square stability of the Milstein scheme has been discussed and the obtained result shows that the method preserves the stability property of a class of linear scalar SDDEs. In this monograph, we adopted the above discussed Milstein scheme for solving different examples and models of SDDEs; See Appendix C.

References

1. Oksendal, B.: *Stochastic Differential Equations: An Introduction with Applications*. Springer Science & Business Media, Berlin (2013)
2. Williams, D.: *Probability with Martingales*. Cambridge University Press, Cambridge (1991)
3. Saito, Y., Mitsui, T.: Stability analysis of numerical schemes for stochastic differential equations. *SIAM J. Numer. Anal.* **33**(6), 2254–2267 (1996)
4. Mao, X.: *Exponential Stability of Stochastic Differential Equations*. Marcel Dekker, New York (1994)
5. Mohammed, S.A.: *Stochastic Functional Differential Equations*, vol. 99. Pitman Advanced Publishing Program (1984)
6. Mohammed, S.A.: *Stochastic Differential Equations and Their Applications*. Horwood, Chichester (1997)
7. Hasminskii, R.Z.: *Stochastic Stability of Differential Equations*. Sijthoff & Noordhoff, Alphen aan den Rijn (1980)
8. Kolmanovskii, V., Nosov, V.: *Stability of Functional Differential Equations*, vol. 180. Elsevier, Amsterdam (1986)
9. Vasseur, D.A., Yodzis, P.: The color of environmental noise. *Ecology* **85**(4), 1146–1152 (2004)
10. Baker, C., Buckwar, E.: Numerical analysis of explicit one-step methods for stochastic delay differential equations. *LMS J. Comput. Math.* **3**, 315–335 (2000)
11. Küchler, U., Platen, E.: Strong discrete time approximation of stochastic differential equations with time delay. *Math. Comput. Simul.* **54**(1–3), 189–205 (2000)
12. Huang, C., Gan, S., Wang, D.: Delay-dependent stability analysis of numerical methods for stochastic delay differential equations. *J. Comput. Appl. Math.* **236**(14), 3514–3527 (2012)
13. Liu, M., Cao, W., Fan, Z.: Convergence and stability of the semi-implicit Euler method for a linear stochastic differential delay equation. *J. Comput. Appl. Math.* **170**(2), 255–268 (2004)
14. Buckwar, E., Sickenberger, T.: A comparative linear mean-square stability analysis of Maruyama-and Milstein-type methods. *Math. Comput. Simul.* **81**(6), 1110–1127 (2011)

15. Hofmann, N., Müller-Gronbach, T.: A modified Milstein scheme for approximation of stochastic delay differential equations with constant time lag. *J. Comput. Appl. Math.* **197**(1), 89–121 (2006)
16. Guo, Q., Xie, W., Mitsui, T.: Convergence and stability of the split-step-Milstein method for stochastic delay hopfield neural networks. *Abstr. Appl. Anal.* **2013**, Hindawi (2013)
17. Xiaojie, W., Wang, X., Gan, S.: B-convergence of split-step one-leg theta methods for stochastic differential equations. *J. Appl. Math. Comput.* **38**(1–2), 489–503 (2012)
18. Buckwar, E., Winkler, R.: Multistep methods for SDEs and their application to problems with small noise. *SIAM J. Numer. Anal.* **44**(2), 779–803 (2006)
19. Cao, W., Zhang, Z., Karniadakis, G.: Numerical methods for stochastic delay differential equations via the Wong-Zakai approximation. *SIAM J. Comput.* **37**(1), A295–A318 (2015)
20. Higham, D.J.: An algorithmic introduction to numerical simulation of stochastic differential equations. *SIAM Rev.* **43**, 525–546 (2001)
21. Mao, X., Marion, G., Renshaw, E.: Environmental brownian noise suppresses explosions in population dynamics. *Stoch. Proc. Appl.* **97**(1), 95–110 (2002)
22. Buckwar, E.: Introduction to the numerical analysis of stochastic delay differential equations. *J. Comput. Appl. Math.* **125**(1–2), 297–307 (2000)
23. Baker, C.T.H., Ford, N.J.: Bifurcations in approximate solutions of stochastic delay differential equations. *Int. J. Bifur. Chaos* **14**(09), 2999–3021 (2004)
24. Kolmanovskii, V., Myshkis, A.: Applied Theory of Functional Differential Equations, vol. 85. Springer Science & Business Media, Berlin (2012)
25. Kloeden, P., Platen, E.: Higher-order implicit strong numerical schemes for stochastic differential equations. *J. Stat. Phys.* **66**(1–2), 283–314 (1992)
26. Milstein, G.: Numerical Integration of Stochastic Differential Equations, vol. 313. Springer Science & Business Media, Berlin (1994)
27. Milstein, G.: Numerical Solution of Stochastic Differential Equations, vol. 23. Springer Science & Business Media, Berlin (2013)
28. Wang, Z., Zhang, C.: An analysis of stability of Milstein method for stochastic differential equations with delay. *Comput. Math. with Appl.* **51**(9–10), 1445–1452 (2006)

Part II

Applications of Delay Differential Equations in Biosciences

In this part, we discuss the role of DDEs in modeling biological systems with memory. This involves an understanding of the underlying science and qualitative features of DDEs in dynamical systems. In the following Chaps. (8–13), we discuss a wide range of DDEs with integer- and fractional-order derivatives in biological systems and infectious diseases.

This part is important due to the following reasons: (i) many real-life phenomena involve a delayed, rather than instantaneous, reaction with a dependence on a memory of past events; (ii) DDEs are more consistent with real-life phenomena than differential models with no time-lag; (iii) a single DDE represents an infinite-dimensional dynamical system; (vi) most biological, physical, and engineering systems have long-range temporal memory and/or long-range space interactions; and (v) the presence of memory (time-lag or fractional-order) leads to a notable increase in the complexity of the observed behavior.

The discussion in the following chapters will help biologists to improve the properties of models and experimental data. Similarly, these chapters will also prove to be useful to researchers in the fields of life sciences and medicine (specialists in immunology and infectious diseases) as well as mathematical modelers (in particular, mathematical biologists). These chapters cover the theoretical framework of differential equations with memory as well as their practical applications in biosciences, dynamical systems, medicine, and neural networks. They also bridge the gap between research in mathematics and that in biosciences.

Chapter 8

Delay Differential Equations with Infectious Diseases



8.1 Introduction

Infectious diseases are among the most prominent threats to mankind. Mathematical modeling of infectious diseases, by using delay differential equations, has an important role in the epidemiological aspect of disease control [1, 2]. Mathematical modeling of infectious diseases has an important role in the epidemiological aspect of disease control [1]. Several epidemic models, with various characteristics, have been described and investigated in the literature. Most of these models are based on the susceptible-infected-removed (SIR) model. Casagrandi et al. [3] introduced the SIRC model to describe the dynamical behavior of influenza A by inserting a new compartment, namely, the Cross-Immunity (C) component¹ of people who have recovered after being infected by different strains of the same viral subtype in previous years. Rihan et al. [4] investigated the qualitative behavior of the fractional-order SIRC model for Salmonella bacterial infection. Recently, in [5], the authors provided a deterministic SEIR epidemic model of fractional-order to describe the dynamics of COVID-19. In other descriptions, quarantine state (Q) may be including in the presence of subjects, such as SIRQ models [6].

Introducing the time-delays or time-lags in the mathematical models may, in fact, represent a reaction chain or a transport process, gestation times, incubation periods, transport delays, or can simply lump complicated biological processes together, accounting only for the time required for these processes to occur. Delays also occur naturally in a chemostat (a laboratory device for controlling the supply of nutrients to a growing cell population).

The main concern of the present chapter is to show that DDEs have interesting dynamics and provide potentially more flexible tools for modeling infectious diseases

¹Cross-immunity (or cross-reactivity) is a major evolutionary force that affects pathogen diversity (i.e., it drives viruses and microbes to be as distinct as possible from one another in order to avoid immunity detection, memory recognition, and clearance).

among groups or in cell levels. This chapter is organized as follows. We provide different SIR epidemic models to describe transmission of disease among groups (Sect. 8.2). We show the impact of time delay in the transmission terms. In Sect. 8.3, we introduce delay differential models for the dynamics of viral infection in one host and cell level. Stability of the steady states and existence of Hopf bifurcations due to time-delays are also discussed. In Sect. 8.4, we discuss DDEs with physiology. Some numerical simulations are provided to show that DDEs are qualitatively consistent with dynamic diseases and biological systems with memory.

8.2 Time-Delay in Epidemic Models

Epidemics have always been a great concern of human kind. This concern is now increased, especially with the spread of new stain of coronavirus COVID-19 [7], MERS-CoV and SARS-CoV [8], swine flu viruses H1N1² [9] and, H5N1, which have sparked a deadly outbreak in some countries and spread into other parts of the world. Mathematical modeling is an essential tool in studying a diverse range of such diseases. The basic elements for the description of infectious diseases are mainly based on the Kermack-McKendrick SIR model [10]: $S(t)$ measures the *susceptible*³ portion of population; $I(t)$ represents *infected*⁴; and $R(t)$ denotes the *removed*⁵ ones. It is natural to assume that the number of newly infected people per time unit is proportional to the product $S(t)I(t)$. It is also assumed that the number of newly removed persons is proportional to the infected ones, and the total population is a constant $N = S + I + R$ (except death from the disease). The standard SIR epidemic model is

$$\dot{S}(t) = -\beta S(t)I(t), \quad \dot{I}(t) = \beta S(t)I(t) - \alpha I(t), \quad \dot{R}(t) = \alpha I(t). \quad (8.1)$$

Here, β is rate of infected individuals per unit time (pairwise rate of infection) and α is the fraction of the population that leaves the infective class (removal rate of infectives). The qualitative analysis is displayed as follows: If $S(0) < \alpha/\beta$, then $I(t)$ is a decreasing function that tends to 0, and $S(t)$ is also decreasing and tends to a constant level greater than 0. However, if $S(0) > \alpha/\beta$, $S(t)$ is also decreasing and tends to a constant level greater than 0, but $I(t)$ will first increase in a time period $(0, T_0)$, then decrease and tends to 0 after T_0 .

²Influenza viruses are defined by two different protein components, known as antigens, on the surface of the virus. They are spike-like features called haemagglutinin (H) and neuraminidase (N) components.

³Susceptible: who are not yet infected

⁴Infected: who are infected at time t and are able to spread the disease via contact with susceptible

⁵Removed: who have been infected and then removed from the possibility of being infected again or spreading (Methods of removal: isolation, immunization, recovery, or death)

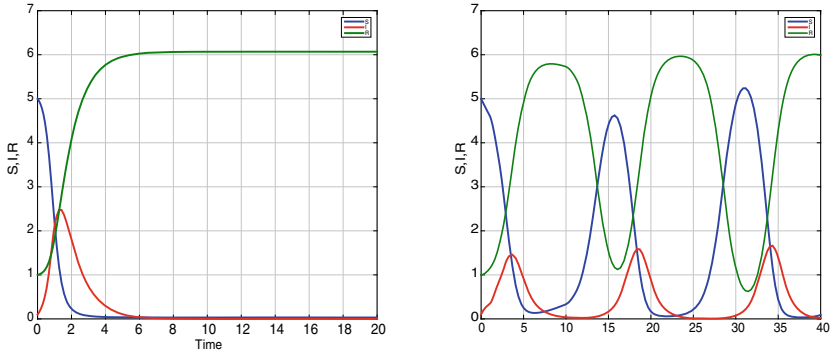


Fig. 8.1 (left) Solution of the SIR model (8.1), which illustrates the spread of an infectious disease in a population. (right) Solution of model (8.2) with time-delays, displaying the periodic outbreak of the disease

Define a dimensionless quantity $\bar{\mathcal{R}}_0 = \frac{\beta S(0)}{\alpha}$ that is a threshold quantity. If we introduce a small number of infectives $I(0)$ into the susceptible population, then an epidemic will occur if $\bar{\mathcal{R}}_0 > 1$. As an example, the solution (with all constants equal to one) of (8.1) (with initial values $S(0) = 5$, $I(0) = 0.1$, $R(0) = 0$) is plotted in Fig. 8.1. We note that an epidemic breaks out, everybody finally becomes “removed,” and nothing further happens.

To prevent an epidemic, we reduce $\bar{\mathcal{R}}_0 = \frac{\beta S(0)}{\alpha}$ and maximize the immunization by reducing $I(0)$ and transferring $S(t)$ to $R(t)$ (removed ones). Suppose that p percent of the population is successfully immunized; then, $S(0)$ is replaced by $(1 - p)S(0)$ and then $p > 1 - \frac{\alpha}{\beta S(0)}$. (For a practical study to estimate the epidemiological parameters, refer to [9, 11]). We note that the occurrence of an epidemic depends on the number of susceptibles, transmission rate, and recovery rate. In other words, the initial number of infectives plays no role in whether there is an epidemic. Other considerations, such as vital dynamics (births and deaths), length of immunity, the incubation period of the disease, and disease induced mortality can all have large influences on the course of an outbreak.

8.2.1 Development of SIR Model (8.1)

The nonautonomous phenomenon occurs mainly due to the seasonal variety, which makes the population behave periodically [12, 13]. To investigate this type of phenomenon in the model, the coefficients should be periodic functions; then, the system is called a periodic system. Assume that the immunized people become susceptible again, say after time τ_1 (say, $\tau_1 = 10$) (see [14, 15]). If we also introduce an incubation period τ_2 between exposure to infection and becoming infected (say, $\tau_2 = 1$), we can arrive at the model

$$\begin{aligned}\dot{S}(t) &= -\beta S(t)I(t - \tau_2) + \gamma I(t - \tau_1), \quad t \geq 0, \\ \dot{I}(t) &= \beta S(t)I(t - \tau_2) - \alpha I(t), \quad t \geq 0, \\ \dot{R}(t) &= \alpha I(t) - \gamma I(t - \tau_1), \quad t \geq 0.\end{aligned}\tag{8.2}$$

The solutions of (8.2) are shown (with initial functions $[S(t), I(t), R(t)]^T = [5, 0.1, 1]^T$ for $t \leq 0$) in Fig. 8.1; we note a periodic outbreak of the disease.

If the model allows for a loss of immunity that causes recovered individuals to become susceptible again, we may also consider the more general nonautonomous SIRS epidemic model, with variable periodic coefficients, with distributed delays

$$\begin{aligned}\dot{S}(t) &= \Lambda(t) - \beta(t)S(t) \int_0^\infty k(\tau)I(t - \tau)d\tau - \mu_1(t)S(t) + \xi(t)R(t), \\ \dot{I}(t) &= \beta(t)S(t) \int_0^\infty k(\tau)I(t - \tau)d\tau - (\mu_2(t) + \alpha(t))I(t), \\ \dot{R}(t) &= \alpha(t)I(t) - (\mu_3(t) + \xi(t))R(t).\end{aligned}\tag{8.3}$$

Here $N(t) = S(t) + I(t) + R(t)$ denotes the total number of the population at time t . The function $\Lambda(t)$ is the growth rate of the population; function $\beta(t)$ is the daily contact rate, that is the average number of contacts per day; functions $\mu_1(t)$, $\mu_2(t)$, and $\mu_3(t)$ are the instantaneous pro capita mortality rates of susceptible, infective, and recovered population, respectively; functions $\alpha(t)$ and $\xi(t)$ are the instantaneous pro capita rates of leaving the infection stage and removed stage, respectively. $k(\tau)$ is the fraction of vector population in which the time taken to become infectious is τ , is assumed to be a nonnegative function on $[0, \infty)$ and satisfies $\int_0^\infty k(\tau)d\tau = 1$ and $\int_0^\infty \tau k(\tau)d\tau < \infty$.

8.3 Delay Differential Models with Viral Infection

The interactions between viruses and cells in an infection process can be seen as an ecological system within the infected host. In past decades, many simple mathematical approaches have been developed to explore the relation between target cells, infected cells producing viruses, and virus load [16]. The response of an immune response (IS) cannot be represented correctly without the hereditary phenomena being considered: cell division, differentiation, etc. (the time needed for immune cells to divide, mature, or die). Moreover, the healthy cell infected with a virus and the virus reproduction cell, there is an intracellular time delay between infection of a cell and production of new virus particles called the latent period. Therefore, DDEs have a particularly important role to play in understanding the dynamics and tracking viral infections and immune populations over time. Many mathematical models for virus dynamics [17–19] explicitly consider delay terms to represent the needed time between the infection of a cell and the production of new viruses of human immunodeficiency virus (HIV) in infected patients.

Most of the mathematical models of immune response with viral infections are mainly based on Marchuk's model [20]

$$\begin{aligned}\dot{V}(t) &= (p_1 - p_2 F(t))V(t), \\ \dot{C}(t) &= \xi(m)p_3 F(t - \tau)V(t - \tau) - p_5(C(t) - C^*), \\ \dot{F}(t) &= p_4(C(t) - F(t)) - p_8 F(t)V(t), \\ \dot{m}(t) &= p_6 V(t) - p_7 m(t),\end{aligned}\tag{8.4}$$

with $t \geq 0$ and $\xi(m)$ is defined by

$$\xi(m) = \begin{cases} 1 & \text{if } m \leq 0.1, \\ (1-m)\frac{10}{9} & \text{if } 0.1 \leq m \leq 1. \end{cases}$$

This model describes the interaction of viruses, $V(t)$; antibodies, $F(t)$; plasma cells, $C(t)$; and the relative characteristics of the affected organs, $m(t)$, of a person infected by a viral disease. This model is formulated as a system of four non-linear DDEs: The *first equation* describes the change in the number of antigens in an organism (similar to a Volterra-Lotka predator-prey equation). The *second equation* describes the creation of new plasma cells with time-lag due to infection (in the absence of infection, the second term creates an equilibrium at $C(t) = C^*$). The *third equation* models the balance of the number of antibodies reacting with antigens: the generation of antibodies from plasma cells is described by $p_4 C(t)$, their decrease due to aging is described by $(-p_4 F(t))$, and binding with antigens by $(-p_8 F(t)V(t))$. The relative characteristic $m(t)$ of damaging organism is given by the *fourth equation* of which the first term expresses the degree of damage to an organ and the second term describes the recuperation due to the recovery activity of the organism. Finally, the $\xi(m)$ represents the fact that the creation of plasma cells slows down when the organism is infected by the viral infection. The time-delay τ is incorporated in the functional terms describing the proliferation and differentiation of lymphocytes, and it represents the time needed for cells to divide, mature (i.e., express certain genes), or to die.

The model (8.4) has been used to study the relationships between the pathogen and the host IS parameters determining the stability of various steady states. It can also be used to understand the basic types of infectious disease dynamics: subclinical, acute with recovery, chronic and lethal, or predicting the results of external manipulations with the IS. In other words, this model allows us, by changing the coefficients $p_1, p_2 \dots, p_8$, to capture all types of behaviors, including stable health, unstable health, acute form of a disease, chronic form, etc. (see Marchuk [20]). One of the stationary solutions of (8.4), which describes the healthy state of an organism is

$$V(t) = 0, \quad C(t) = C^*, \quad F(t) = F^* = C^* \quad \text{and} \quad m(t) = 0.$$

Figures 8.2 and 8.3 show the solutions of the model (8.4) (with different parameters) for $\tau = 0.5$, with the following initial values:

$$V(0) = 0.5 \times 10^{-6}, \quad C(0) = 1, \quad F(0) = 1 \quad \text{and} \quad m(0) = 0$$

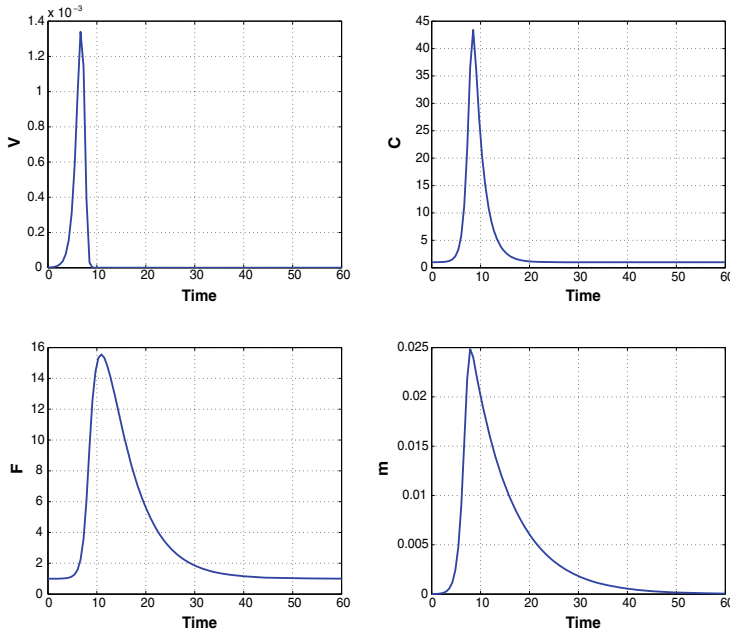


Fig. 8.2 Numerical simulations of model (8.4) for $\tau = 0.5$ and $p_1 = 2$, $p_2 = 0.8$, $p_3 = 10^4$, $p_4 = 0.17$, $p_5 = 0.5$, $p_6 = 10$, $p_7 = 0.12$, and $p_8 = 8$.

and with the following initial functions:

$$V(t) = \max(0, 10^{-6} + t), \quad F(t) = 1, \quad t \leq 0.$$

It may also be noted from the graphs that there is either a complete recovery, as in Fig. 8.2, or periodic outbreak of the disease, as shown in Fig. 8.3.

The above basic model of an infectious disease has only one time-lag. More sophisticated mathematical models for viral/bacterial infections in lungs or T-cell division, incorporate about 10 delays; see [21]. Another example of generic time-lag equations in immunology is provided by Mohler et al. [22], who developed compartmental models for lymphocyte migration. The delays represent the time that cells reside in a particular compartment, or the transit times through compartments, or the duration of inter-compartmental transfer; see [20].

8.3.1 DDEs with HIV Infection of CD4+ T-cells

Herein, we extend the analysis and study the stability and Hopf bifurcation analysis of a DDEs model of HIV infection of CD4⁺ T-cells. The model is based on a system

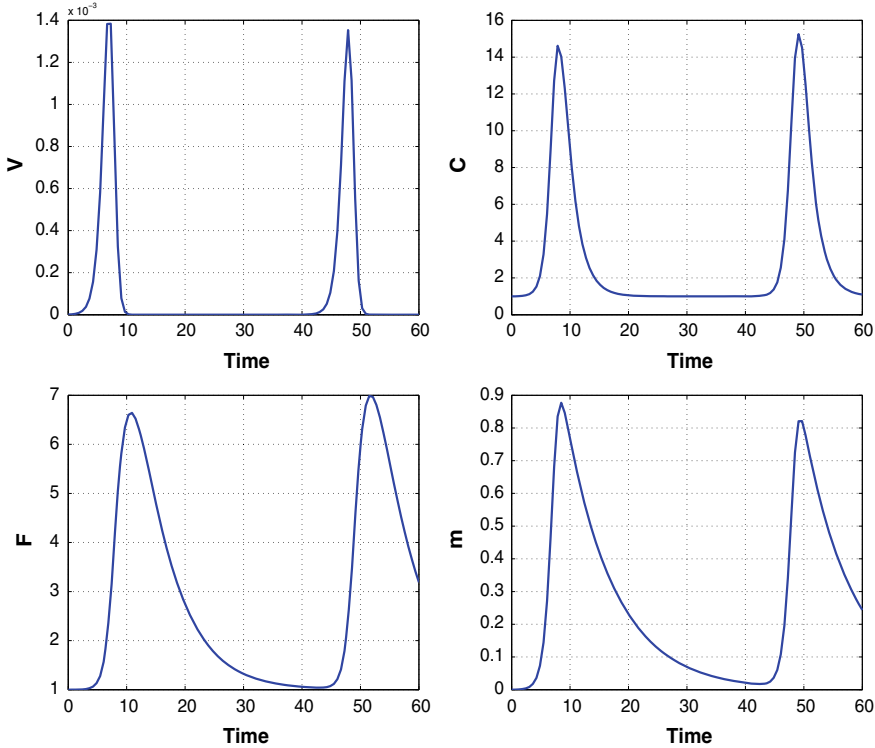


Fig. 8.3 Simulations of model (8.4) with the same parameters of Fig. 8.2, except for $p_6 = 300$. The graphs illustrate the periodic outbreak of the disease

of DDEs with a logistic growth term and antiretroviral treatment with a discrete time-delay, which plays the main role in changing the stability of each steady state. By fixing the time-delay as a bifurcation parameter, we get a limit cycle bifurcation about the infected steady state. We study the effect of the time-delay on the stability of the endemically infected equilibrium.

Let us start the analysis with some basic models of the dynamics of target (uninfected) cells and infected CD4⁺ T-cells by HIV. As a first approximation, the dynamics between HIV and the macrophage population was described by the simplest model of infection dynamics presented in [23–25]. Denoting uninfected cells by $x(t)$, infected cells by $y(t)$, and assuming that viruses are transmitted mainly by cell-to-cell contact, the model is given by

$$\begin{aligned}\dot{x}(t) &= \Lambda - \delta_1 x(t) - \beta x(t)y(t), \\ \dot{y}(t) &= \beta x(t)y(t) - \delta_2 y(t).\end{aligned}\tag{8.5}$$

The target (uninfected) $CD4^+$ T-cells are produced at a rate Λ , die at a rate δ_1 , and become dead at a rate δ_2 . The basic reproductive ratio of the virus is then given by $\mathcal{R}_0 = \frac{\Lambda\beta}{\delta_1\delta_2}$. If there is no infection or if $\mathcal{R}_0 < 1$, there is only trivial equilibrium $(\mathcal{E}_0 = (\Lambda/\delta_1, 0))$ with no virus-producing cells. In contrast, if $\mathcal{R}_0 > 1$, the virus can establish an infection and the system converges to the equilibrium with both uninfected cells and infected cells, $\mathcal{E}_1 = (\delta_2/\beta, \Lambda/\delta_2 - \delta_1/\beta)$.

However, in most viral infections, the CTL response plays a crucial part in antiviral defense by attacking viral infected cells [26, 27]. As the cytotoxic T-lymphocyte (CTL) immune response is necessary to eliminate or control the viral infection, we incorporated the antiviral CTL immune response into the basic model (8.5). Therefore, if we add CTL response, which is denoted by $z(t)$, into model (8.5) (see [25]), then the extended model becomes

$$\begin{aligned}\dot{x}(t) &= \Lambda - \delta_1 x(t) - \beta x(t)y(t), \\ \dot{y}(t) &= \beta x(t)y(t) - \delta_2 y(t) - py(t)z(t), \\ \dot{z}(t) &= cqy(t)z(t) - hz(t).\end{aligned}\tag{8.6}$$

Thus, CTLS proliferate in response to antigens at a rate c , die at a rate h , and lyse infected cells at a rate p . We assume that the CTL pool consists of two populations: the precursors $w(t)$ and the effectors $z(t)$. In other words, we assume that there are primary and secondary responses to viral infections. Then, the model (8.6) becomes

$$\begin{aligned}\dot{x}(t) &= \Lambda - \delta_1 x(t) - \beta x(t)y(t), \\ \dot{y}(t) &= \beta x(t)y(t) - \delta_2 y(t) - py(t)z(t), \\ \dot{w}(t) &= c(1-q)y(t)w(t) - bw(t), \\ \dot{z}(t) &= cqy(t)w(t) - hz(t).\end{aligned}\tag{8.7}$$

The infected cells are killed by CTL effector cells at a rate pyz . Upon contact with antigens, CTLp proliferate at a rate $cy(t)w(t)$ and differentiate into effector cells CTLe at a rate $cqy(t)w(t)$. CTL precursors die at a rate bw , and effectors die at a rate $hz(t)$; see Fig. 8.4.

Since the proliferation of $CD4^+$ T-cells is density dependent, i.e., the rate of proliferation decreases as T-cells increase and reach the carrying capacity. We then extend the above basic viral infection model to include the density dependent growth of the $CD4^+$ T-cell population (see [28–30]). It is also known that HIV infection leads to low levels of $CD4^+$ T-cells via three main mechanisms: direct viral killing of infected cells, increased rates of apoptosis in infected cells, and killing of infected $CD4^+$ T-cells by cytotoxic T-lymphocytes [30]. Hence, it is reasonable to include apoptosis of infected cells. An average of 10^{10} viral particles are produced by infected cells per day. Treatment with a single antiviral drug is considered to be ineffective; hence, a combination of antiviral drugs is needed for the treatment [29]. Therefore, in the below revised model, we combine the antiretroviral drugs, namely, reverse transcriptase inhibitor (RTI) and protease inhibitor (PI), to make the model more

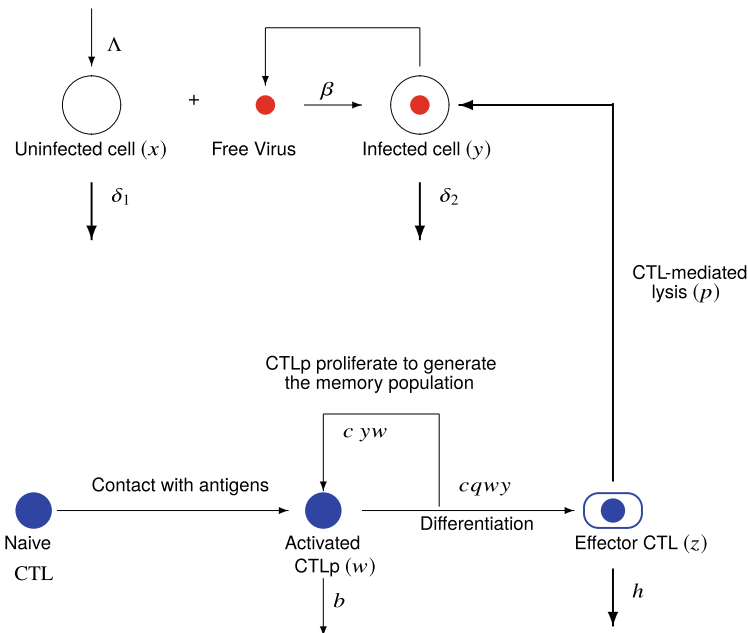


Fig. 8.4 A simplified model of virus-CTL interaction. The virus dynamics are described by the basic model of Nowak & Bangham [34]. The uninfected target cells are produced at a rate Λ and die at a rate $\delta_1 x$. They become infected by the virus at a rate βxy . The infected cells produce new virus particles and die at a rate $\delta_2 y$. When CTL_p recognize antigens on the surface of infected cells, they become activated and expand at a rate $c y w$, decay at a rate $b w$, and differentiate into effector cells at a rate $c q w y$. The effector cells lyse the infected cells at a rate $p y z$

realistic (see [31–33]). RTIs can block the infection of target T-cells by infectious viruses, and PIs cause infected cells to produce noninfectious virus particles. The modified model takes the form

$$\begin{aligned}\dot{x}(t) &= \Lambda - \delta_1 x(t) + r \left(1 - \frac{x(t) + y(t)}{T_{max}}\right) x(t) - (1 - \epsilon)(1 - \eta)\beta x(t)y(t), \\ \dot{y}(t) &= (1 - \epsilon)(1 - \eta)\beta x(t)y(t) - \delta_2 y(t) - e_1 y(t) - p y(t)z(t), \\ \dot{w}(t) &= c y(t)w(t) - c q y(t)w(t) - b w(t), \\ \dot{z}(t) &= c q y(t)w(t) - h z(t).\end{aligned}\quad (8.8)$$

The first equation of model (8.8) represents the rate of change in the count of healthy CD4⁺ T-cells that are produced at rate Λ and become infected at rate β , with the mortality being represented by δ_1 . We assume that the uninfected CD4⁺ T-cells proliferate logistically; thus, the growth rate r is multiplied by the term $\left(1 - \frac{x+y}{T_{max}}\right)$ and this term approaches zero when the total number of T-cells approaches the carrying capacity T_{max} . The effect of combination of RTI and PI antiviral drugs is

represented by the term $(1 - \epsilon)(1 - \eta)\beta xy$, where $(1 - \epsilon), 0 < \epsilon < 1$ represents the effect of RTI and $(1 - \eta), 0 < \eta < 1$ represents the effect of PI. The second equation of model (8.8) denotes the rate of change in the count of infected CD4⁺ T-cells. The infected CD4⁺ T-cells decay at a rate δ_2 , apoptosis rate of infected cells is denoted by e_1 , and infected cells are killed by CTL effectors at a rate p . The third equation of the model denotes the rate of change in the CTLp population. Proliferation rate of the CTLp is given by c and is proportional to the infected cells y . CTLp die at a rate b and differentiate into CTL effectors at a rate cq . The last equation of the model represents the concentration of CTL effectors, which die at a rate h . In reality, the specific IS is not immediately effective following invasion by a novel pathogen. There may be an explicit time-delay between infection and immune initiation, and there may be a gradual build-up in immune efficacy during which the immune response develops, before reaching maximal specificity to the pathogen ([35–37]). To make the model (8.8) more realistic, time-delay in the immune response should be included in the following model:

$$\begin{aligned}\dot{x}(t) &= \Lambda - (1 - \epsilon)(1 - \eta)\beta x(t)y(t) + r\left(1 - \frac{x(t) + y(t)}{T_{max}}\right)x(t) - \delta_1 x(t), \\ \dot{y}(t) &= (1 - \epsilon)(1 - \eta)\beta x(t)y(t) - (\delta_2 + e_1)y(t) - py(t)z(t), \\ \dot{w}(t) &= c(1 - q)y(t - \tau)w(t - \tau) - bw(t), \\ \dot{z}(t) &= cqy(t - \tau)w(t - \tau) - hz(t).\end{aligned}\quad (8.9)$$

We start our analysis by presenting some notations that will be used in the sequel. Let $C = C([-\tau, 0], \mathbb{R}_+^4)$ be the Banach space of continuous functions mapping the interval $[-\tau, 0]$ into \mathbb{R}_+^4 , where $\mathbb{R}_+^4 = (x, y, w, z)$. The initial conditions are given by

$$x(\theta) = \varphi_1(\theta) \geq 0, \quad y(\theta) = \varphi_2(\theta) \geq 0, \quad w(\theta) = \varphi_3(\theta) \geq 0, \quad z(\theta) = \varphi_4(\theta) \geq 0, \quad \theta \in [-\tau, 0],$$

where $\varphi_i(\theta) \in C^1$ are smooth functions for all $i = 1, 2, 3, 4$. From the fundamental theory of functional differential equations (see [38]), it is easy to see that the solution $(x(t), y(t), w(t), \text{and } z(t))$ of system (8.9) with the initial conditions as stated above exist for all $t \geq 0$ and are unique. It can be shown that these solutions exist for all $t > 0$ and stay nonnegative. In fact, if $x(0) > 0$, then $x(t) > 0$ for all $t > 0$. The same argument is true for the y, w and v components. Hence, the interior \mathbb{R}_+^4 is invariant for system (8.9).

8.3.2 Steady States

We can obtain the steady state values by setting $\dot{x} = \dot{y} = \dot{w} = \dot{z} = 0$. The steady state value of the infection-free steady state \mathcal{E}_0 is given by

Table 8.1 Parameter definitions and estimations used in the underlying model

| Parameter | Notes | Estimated | Range | Source |
|------------|---|-----------|---------------|----------|
| Λ | Source of uninfected CD4 ⁺ T-cells | 10 | 0–10 | [30] |
| β | Rate of infection | 0.1 | 0.00001 – 0.5 | [30] |
| T_{max} | Total carrying capacity | 1500 | 1500 | [30] |
| r | Logistic growth term | 0.03 | 0.03–3 | [30] |
| δ_1 | Mortality rate of CD4 ⁺ T-cells | 0.06 | 0.007–0.1 | [30] |
| ϵ | Antiretroviral (RTI) therapy | 0.9 | [0, 1] | See text |
| δ_2 | Infected cells died out naturally | 0.3 | 0.2–1.4 | [30] |
| e_1 | Apoptosis rate of infected cells | 0.2 | 0.2 | [30] |
| p | Clearance rate of infected cells | 1 | 0.001–1 | [30] |
| η | Protease inhibitor therapy | 0.9 | [0, 1] | See text |
| q | Rate of differentiation of CTLs | 0.02 | Assumed | – |
| b | Death rate of CTL precursors | 0.02 | 0.005–0.15 | [30] |
| c | Proliferation of CTLs responsiveness | 0.1 | 0.001–1 | [30] |
| h | Mortality rate or CTL effectors | 0.1 | 0.005–0.15 | [30] |

$$\mathcal{E}_0 = \left(\frac{T_{max}}{2r} \left(r - \delta_1 + \sqrt{(r - \delta_1)^2 + \frac{4r\Lambda}{T_{max}}} \right), 0, 0, 0 \right),$$

while the infected steady state $\mathcal{E}_+ = (x^*, y^*, w^*, z^*)$ is given by

$$y^* = \frac{b}{c(1-q)}, \quad w^* = \frac{h(1-q)z^*}{qb}, \quad z^* = \frac{(1-\epsilon)(1-\eta)\beta x^* - (\delta_2 + e_1)}{p},$$

and x^* is given by the following quadratic equation:

$$c_1 x^2 + c_2 x - c_3 = 0,$$

where $c_1 = c(1 - q)r$, $c_2 = T_{max}b\beta(1 - \epsilon)(1 - \eta) + br - c(1 - q)T_{max}(r - \delta_1)$, $c_3 = c(1 - q)\Lambda T_{max}$.

8.3.3 Stability Analysis of Infected Steady State

To study the full dynamics of model (8.8) by using time-delay as a bifurcation parameter, we need to linearize the model around the steady state \mathcal{E}_+ and determine the characteristic equation of the Jacobian matrix. The roots of the characteristic equation determine the asymptotic stability and existence of Hopf bifurcation for the model. The characteristic equation of the linearized system is given by

$$\begin{vmatrix} -A_1y^* + r - \frac{2r}{T_{max}}x^* - \frac{r}{T_{max}}y^* - \delta_1 - \lambda & -A_1x^* - \frac{r}{T_{max}}x^* & 0 & 0 \\ A_1y^* & A_1x^* - (\delta_2 + e_1) - pz^* - \lambda & 0 & -py^* \\ 0 & c(1 - q)e^{-\lambda\tau}w^* & c(1 - q)e^{-\lambda\tau}y^* - b - \lambda & 0 \\ 0 & cq e^{-\lambda\tau}w^* & cq e^{-\lambda\tau}y^* & -h - \lambda \end{vmatrix} = 0$$

which is equivalent to the equation

$$\lambda^4 + p_1\lambda^3 + p_2\lambda^2 + p_3\lambda + p_4 + e^{-\lambda\tau}(q_1\lambda^3 + q_2\lambda^2 + q_3\lambda + q_4) = 0 \quad (8.10)$$

where $A_1 = (1 - \epsilon)(1 - \eta)\beta$, and

$$\begin{aligned} p_1 &= -a_1 - a_4 - a_8 - a_{11}, \quad p_2 = a_1a_8 + a_8a_{11} + a_1a_{11} + a_4a_8 + a_4a_{11} + a_1a_4 - a_2a_3, \\ p_3 &= a_2a_3a_8 + a_2a_3a_{11} - a_1a_8a_{11} - a_4a_8a_{11} - a_1a_4a_8 - a_1a_4a_{11}, \quad p_4 = a_1a_4a_8a_{11} - a_2a_3a_8a_{11}, \quad q_1 = -a_7, \\ q_2 &= a_1a_7 + a_7a_{11} + a_4a_7 - a_5a_9, \quad q_3 = a_5a_8a_9 + a_1a_5a_9 + a_2a_3a_7 - a_1a_7a_{11} - a_4a_7a_{11} - a_1a_4a_7, \\ q_4 &= a_1a_4a_7a_{11} - a_1a_5a_8a_9 - a_2a_3a_7a_{11}. \end{aligned}$$

and

$$\begin{aligned} a_1 &= -(1 - \epsilon)(1 - \eta)\beta y^* + r - \frac{2rx^*}{T_{max}} - \frac{ry^*}{T_{max}} - \delta_1, \quad a_2 = -(1 - \epsilon)(1 - \eta)\beta x^* - \frac{rx^*}{T_{max}} \\ a_3 &= (1 - \epsilon)(1 - \eta)\beta y^*, \quad a_4 = (1 - \epsilon)(1 - \eta)\beta x^* - (\delta_2 + e_1) - pz^*, \quad a_5 = -py^* \\ a_6 &= c(1 - q)w^*, \quad a_7 = c(1 - q)y^*, \quad a_8 = -b, \quad a_9 = cq w^*, \quad a_{10} = cq y^*, \quad a_{11} = -h. \end{aligned}$$

Let us consider the following equation:

$$\varphi(\lambda, \tau) = \lambda^4 + p_1\lambda^3 + p_2\lambda^2 + p_3\lambda + p_4 + (q_1\lambda^3 + q_2\lambda^2 + q_3\lambda + q_4)e^{-\lambda\tau}.$$

For the non-delayed model (say $\tau = 0$), from Eq. (8.10), we have

$$\lambda^4 + D_1\lambda^3 + D_2\lambda^2 + D_3\lambda + D_4 = 0 \quad (8.11)$$

where

$$D_1 = p_1 + q_1, \quad D_2 = p_2 + q_2, \quad D_3 = p_3 + q_3, \quad D_4 = p_4 + q_4.$$

Lemma 8.1 For $\tau = 0$, the unique non-trivial equilibrium is locally asymptotically stable, if the real parts of all the roots of Equation (8.11) are negative.

Proof The proof of the above Lemma is based on holding the following conditions: $D_1 > 0$, $D_3 > 0$, $D_4 > 0$ and $D_1 D_2 D_3 > D_1^2 D_4 + D_3^2$ as proposed by Routh-Hurwitz criterion. We conclude that equilibrium \mathcal{E}_+ is locally asymptotically stable, if and only if, all the roots of the characteristic equation (8.11) have negative real parts, which depends on the numerical values of parameters that are shown in the numerical exploration. \square

8.3.4 Existence of Hopf Bifurcation

Here, we study the impact of the time-delay parameter on the stability of HIV infection of CD4⁺ T-cells. We deduce the criteria that ensure that the asymptotic stability of infected steady state \mathcal{E}_+ for all $\tau > 0$, and arrive at the following theorem:

Theorem 8.1 Necessary and sufficient conditions for the infected equilibrium \mathcal{E}_+ to be asymptotically stable for all delay $\tau \geq 0$ are

- (1) The real parts of all the roots of $\varphi(\lambda, \tau) = 0$ are negative.
- (2) For all ω , and $\tau \geq 0$, $\varphi(i\omega, \tau) \neq 0$, where $i = \sqrt{-1}$:

Proof Assume that Lemma 8.1 is true. Now for $\omega = 0$, we have

$$\varphi(0, \tau) = D_4 = p_4 + q_4 \neq 0.$$

Substituting $\lambda = i\omega$ ($\omega > 0$) into Eq. (8.9) and separating the real and imaginary parts of the equations yields:

$$\begin{aligned} (\omega^4 - p_2\omega^2 + p_4) + (-q_2\omega^2 + q_4) \cos(\omega\tau) + (-q_1\omega^3 + q_3\omega) \sin(\omega\tau) &= 0 \\ (-p_1\omega^3 + p_3\omega) + (-q_1\omega^3 + q_3\omega) \cos(\omega\tau) - (-q_2\omega^2 + q_4) \sin(\omega\tau) &= 0. \end{aligned} \quad (8.12)$$

After some mathematical manipulations, we obtain the following equations:

$$\begin{aligned} \cos(\omega\tau) &= \frac{(q_2 - p_1 q_1)\omega^6 + (p_3 q_1 - q_4 - p_2 q_2 + p_1 q_3)\omega^4 + (p_2 q_4 + p_4 q_2 - p_3 q_3)\omega^2 - p_4 q_4}{q_1^2 \omega^6 + (q_2^2 - 2q_1 q_3)\omega^4 + (q_3^2 - 2q_2 q_4)\omega^2 + q_4^2}, \\ \sin(\omega\tau) &= \frac{q_1 \omega^7 + (p_1 q_2 - q_3 - p_2 q_1)\omega^5 + (p_2 q_3 + p_4 q_1 - p_3 q_2 - p_1 q_4)\omega^3 + (p_3 q_4 - p_4 q_3)\omega}{q_1^2 \omega^6 + (q_2^2 - 2q_1 q_3)\omega^4 + (q_3^2 - 2q_2 q_4)\omega^2 + q_4^2}. \end{aligned} \quad (8.13)$$

Let

$$\begin{aligned} b_1 &= q_2 - p_1 q_1, \quad b_2 = p_3 q_1 - q_4 - p_2 q_2 + p_1 q_3, \quad b_3 = p_2 q_4 + p_4 q_2 - p_3 q_3, \quad b_4 = -p_4 q_4, \\ b_5 &= q_1^2, \quad b_6 = q_2^2 - 2q_1 q_3, \quad b_7 = q_3^2 - 2q_2 q_4, \quad b_8 = q_4^2, \quad b_9 = q_1, \quad b_{10} = p_1 q_2 - q_3 - p_2 q_1, \\ b_{11} &= p_2 q_3 + p_4 q_1 - p_3 q_2 - p_1 q_4, \quad b_{12} = p_3 q_4 - p_4 q_3. \end{aligned}$$

From Eq. (8.12), we have

$$\omega^8 + c_1 \omega^6 + c_2 \omega^4 + c_3 \omega^2 + c_4 = 0 \quad (8.14)$$

where

$$c_1 = p_1^2 - 2p_2 - q_1^2, \quad c_2 = p_2^2 - 2p_1 p_3 + 2q_1 q_3 + 2p_4 - q_2^2, \quad c_3 = p_3^2 - 2p_2 p_4 + 2q_2 q_4 - q_3^2, \quad c_4 = p_4^2 - q_4^2.$$

Conditions (1) and (2) of Theorem 8.1 hold if and only if Eq. (8.14) has no real positive root. \square

Let $m = \omega^2$; then, Eq. (8.14) takes the form

$$m^4 + c_1 m^3 + c_2 m^2 + c_3 m + c_4 = 0. \quad (8.15)$$

If $c_4 < 0$, then Eq. (8.14) has at least one positive root. In the case when Eq. (8.14) has four positive roots, we have

$$\omega_1 = \sqrt{m_1}, \quad \omega_2 = \sqrt{m_2}, \quad \omega_3 = \sqrt{m_3}, \quad \omega_4 = \sqrt{m_4}.$$

From Eq. (8.12), we have

$$\tau_k^{(j)} = \frac{1}{\omega_k} \left\{ \arcsin \frac{b_9 \omega_k^7 + b_{10} \omega_k^5 + b_{11} \omega_k^3 + b_{12} \omega_k}{b_5 \omega_k^6 + b_6 \omega_k^4 + b_7 \omega_k^2 + b_8} + 2j\pi \right\} \quad (8.16)$$

where $k = 1, 2, 3, 4$ and $j = 0, 1, 2, \dots$; we choose $\tau_0 = \min(\tau_k^{(j)})$.

To establish Hopf bifurcation at $\tau = \tau_0$, we need to show that

$$\Re \left(\frac{d\lambda}{d\tau} \right)_{\tau=\tau_0} \neq 0.$$

By differentiating Equation (8.10) with respect to τ , we can get

$$\frac{d\lambda}{d\tau} = \frac{\lambda e^{-\lambda\tau} (q_1 \lambda^3 + q_2 \lambda^2 + q_3 \lambda + q_4)}{(4\lambda^3 + 3p_1 \lambda^2 + 2p_2 \lambda + p_3) + e^{-\lambda\tau} [(3q_1 \lambda^2 + 2q_2 \lambda + q_3) - \tau(q_1 \lambda^3 + q_2 \lambda^2 + q_3 \lambda + q_4)]}.$$

It follows that

$$\left(\frac{d\lambda}{d\tau} \right)^{-1} = \frac{(4\lambda^3 + 3p_1 \lambda^2 + 2p_2 \lambda + p_3) + e^{-\lambda\tau} [(3q_1 \lambda^2 + 2q_2 \lambda + q_3) - \tau(q_1 \lambda^3 + q_2 \lambda^2 + q_3 \lambda + q_4)]}{\lambda e^{-\lambda\tau} (q_1 \lambda^3 + q_2 \lambda^2 + q_3 \lambda + q_4)}.$$

Then, by combining Eq. (8.10), we get

$$\left(\frac{d\lambda}{d\tau}\right)^{-1} = \frac{(4\lambda^3 + 3p_1\lambda^2 + 2p_2\lambda + p_3) + e^{-\lambda\tau}(3q_1\lambda^2 + 2q_2\lambda + q_3)}{\lambda e^{-\lambda\tau}(q_1\lambda^3 + q_2\lambda^2 + q_3\lambda + q_4)} - \frac{\tau}{\lambda}. \quad (8.17)$$

Substituting $\lambda = i\omega_0$ in Eq. (8.17) (where $\omega_0 > 0$ and $i = \sqrt{-1}$) yields

$$\left.\left(\frac{d\lambda}{d\tau}\right)^{-1}\right|_{\tau=\tau_0} = \frac{d_1 + id_2}{d_3 + id_4} - \frac{\tau}{\lambda}$$

where

$$\begin{aligned} d_1 &= (p_3 - 3p_1\omega_0^2) + (q_3 - 3q_1\omega_0^2) \cos(\omega_0\tau_0) + 2q_2\omega_0 \sin(\omega_0\tau_0), \\ d_2 &= (2p_2\omega_0 - 4\omega^3) + 2q_2\omega_0 \cos(\omega_0\tau_0) - (q_3 - 3q_1\omega_0^2) \sin(\omega_0\tau_0), \\ d_3 &= (q_1\omega_0^4 - q_3\omega_0^2) \cos(\omega_0\tau_0) + (q_4\omega_0 - q_2\omega_0^3) \sin(\omega_0\tau_0), \\ d_4 &= (q_4\omega_0 - q_2\omega_0^3) \cos(\omega_0\tau_0) - (q_1\omega_0^4 - q_3\omega_0^2) \sin(\omega_0\tau_0). \end{aligned}$$

Thus

$$\Re\left(\left.\left(\frac{d\lambda}{d\tau}\right)^{-1}\right|_{\tau=\tau_0}\right) = \frac{d_1d_3 + d_2d_4}{d_3^2 + d_4^2}.$$

Notice that

$$\text{sign}\left(\Re\left.\frac{d\lambda(t)}{d\tau}\right|_{\tau=\tau_0}\right) = \text{sign}\left(\Re\left.\left(\frac{d\lambda}{d\tau}\right)^{-1}\right|_{\tau=\tau_0}\right).$$

By summarizing the above analysis, we arrive at the following theorem:

Theorem 8.2 *The infected equilibrium \mathcal{E}_+ of the system (8.9) is asymptotically stable for $\tau \in [0, \tau_0)$ and it undergoes Hopf bifurcation at $\tau = \tau_0$.*

We provide some simulations of model (8.8) to exhibit the impact of discrete time-delay in the model. We consider the following parameters values: $\lambda = 10$, $\delta_1 = 0.06$, $\delta_2 = 0.3$, $e_1 = 0.2$, $\beta = 0.1$, $p = 1$, $c = 0.1$, $b = 0.02$, $q = 0.02$, $\eta \in [0, 1]$, $h = 0.1$, $r = 0.03$, $\epsilon \in [0, 1]$, $T_{max} = 1500$. According to the given parameter values, the threshold critical value $\tau_0 = 0.4957$ from formula (8.15) exists. The steady state \mathcal{E}_+ exists and is asymptotically stable (see Fig. 8.1). We may notice that the solution converges to the equilibrium \mathcal{E}_+ with damping oscillations as the value of τ increases. Once the delay τ crosses the critical value τ_0 , then the model shows the existence of Hopf bifurcation, which is depicted in Fig. 8.2. In Fig. 8.3, we consider the efficacy of antiretroviral treatment, which may be responsible for loss of stability, by considering the effectiveness of treatment $\epsilon = 0.9$ and fixed time-delay $\tau = 0.4$. The asymptotic behavior to the infection-free steady state, when we consider antiviral treatment (with $\epsilon = 0.9$, $\eta = 0.9$ and time-delay $\tau = 15$) is shown in Fig. 8.4.

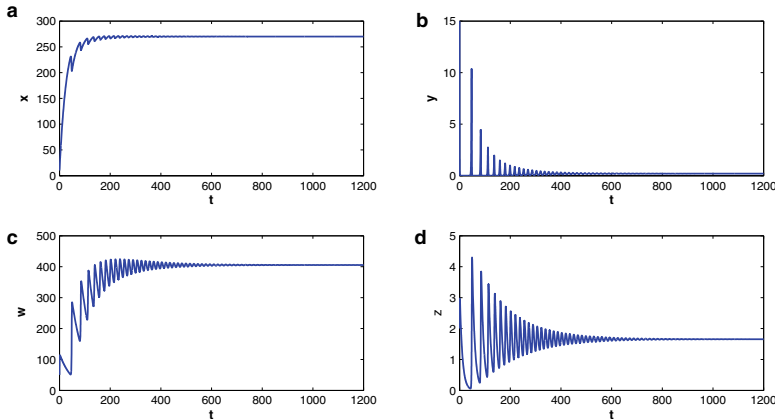


Fig. 8.5 a–d, each panel shows the time evolution and trajectory of model (8.8) when $\tau (= 0.4) < \tau_0$ (critical value) and the effect of therapies is considered to be $\epsilon = 0.9$ and $\eta = 0.2$. It shows that the endemic steady state \mathcal{E}_+ of the model is asymptotically stable

We have seen that if time-delay exceeds the critical value τ_0 , model (8.8) undergoes a Hopf bifurcation. The direction and stability of bifurcating periodic solutions are deduced in explicit formulae using center manifold and normal forms. We also presented some numerical simulations to the underlying model to investigate the obtained results and theory. We have also seen that the antiretroviral treatments help to increase the level of uninfected CD4+ T-cells. The theoretical results that have been confirmed by the numerical simulations show that the delayed CTL response can lead to complex bifurcations and, in particular, the coexistence of multiple stable periodic solutions. When the time-delay exceeds the critical (threshold) value, we may get subcritical behavior that leads to a loss of uninfected CD4+ T-cells (Figs. 8.5, 8.6, 8.7, 8.8).

8.4 Physiology

The great potential of simple DDEs for capturing complex dynamics observed in physiological systems was shown in a series of related works by an der Heiden, Mackey et al. [2, 39]. DDEs were used to model unstable patterns of (i) the human respiratory system and regulation of blood concentration of CO_2 (periodic breathing and prediction of low- and large-amplitude oscillations), (ii) the production of blood cells (periodic and chaotic regimes), and (iii) hormone regulation in the endocrine system (period-doubling bifurcations and chaotic solutions); see [40].

As an illustrative example, let $c(t)$ be the concentration of cells (the population species) in the circulating blood. We assume that the cells are lost (i.e., die) at a rate proportional to their concentration, which is like $\gamma c(t)$, where the parameter γ

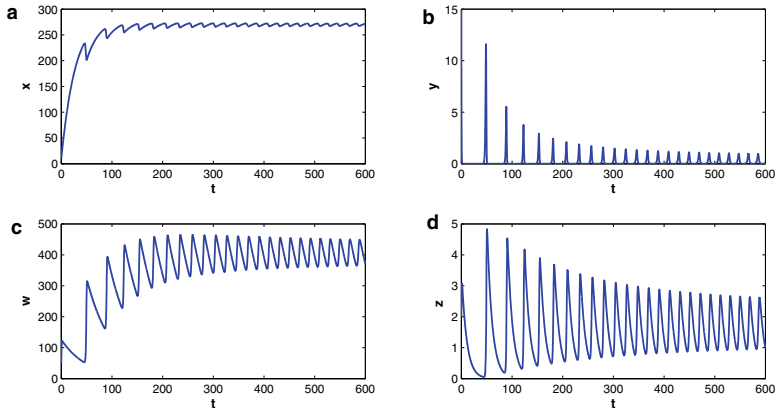


Fig. 8.6 The numerical simulations of model (8.8) when the time-delay of immune activation exceeds the critical value, $\tau = 0.5 > \tau_0$. The endemic steady state \mathcal{E}_+ of the model undergoes Hopf Bifurcation, stability switch and periodic solutions appear

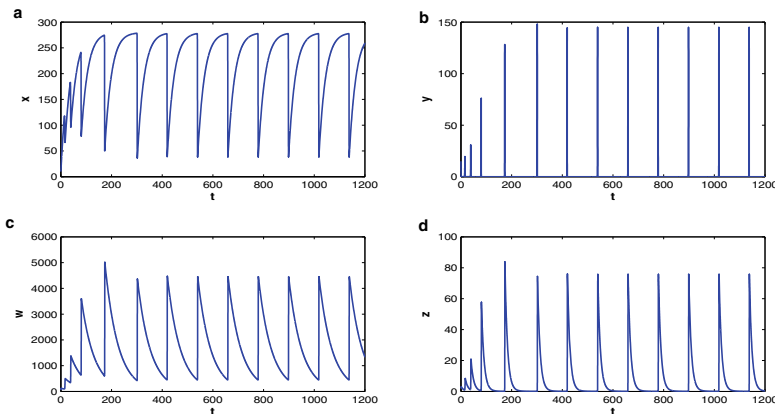


Fig. 8.7 The numerical simulations of model (8.8) when the efficacy rate of antiretroviral treatments is considered to be low, i.e., $\epsilon = 0.2$ and $\eta = 0.2$. It shows that the endemic steady state \mathcal{E}_+ of the model undergoes Hopf bifurcation with oscillatory behavior in solutions even though the delay value is less than the critical value ($\tau = 0.4 < \tau_0$)

has dimensions $(\text{day})^{-1}$. After the reduction in cells in the blood stream, there is an approximately 6-day delay before the bone marrow releases further cells to replenish the deficiency (see [2]). We thus assume that the flux λ of cells into the blood stream depends on the cell concentration at an earlier time, namely, $c(t - \tau)$, where τ is the delay. Such assumptions suggest a model equation of the form

$$\frac{dc(t)}{dt} = \lambda c(t - \tau) - \gamma c(t).$$

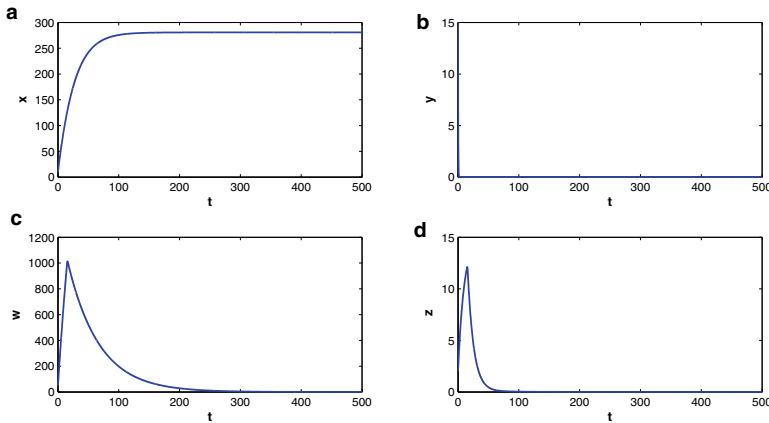
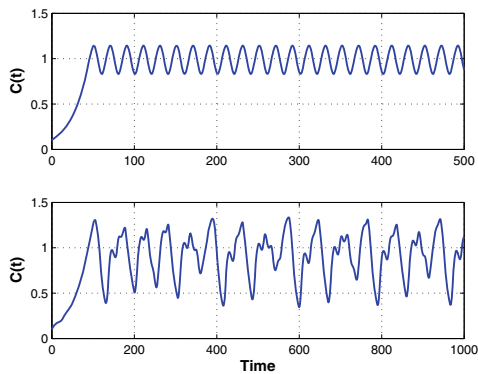


Fig. 8.8 The numerical simulations model (8.8) when the efficacy rate of antiretroviral treatment is at expected level, $\epsilon = 0.9$ and $\eta = 0.9$, and the delay value exceeds the critical value $\tau = 15 > \tau_0$. The solution always lies within the feasible region and the infection-free steady state \mathcal{E}_0 is asymptotically stable

Fig. 8.9 (top) The numerical solution of (8.18) with parameter values $\alpha = 0.1$, $\gamma = 0.1 \text{ days}^{-1}$, $\lambda = 0.2 \text{ days}^{-1}$, $m = 10$ and $\tau = 6 \text{ days}$; (bottom) The numerical simulation with the same parameter values as in **a** except an increase in the delay to $\tau = 20 \text{ days}$



Glass & Mackey [41] proposed a possible replacement in the form of the non-linear DDE:

$$\begin{aligned} \frac{dc(t)}{dt} &= \frac{\lambda a^m c(t - \tau)}{a^m + c^m(t - \tau)} - \gamma c(t), \quad t \geq 0, \\ c(t) &= \alpha, \quad t \leq 0, \end{aligned} \quad (8.18)$$

where λ , a , m , g , τ and α are positive constants. Graphs in Fig. 8.9 show the numerical solutions of (8.18) for two values of delay-time τ . In addition, Fig. 8.10 displays the graphs of $c(t) \times c(t - \tau)$ for different values of the parameter m , a sequence of period doubling leading to a chaotic limit cycle are observed.

It is observed that a chaotic pattern begins around $\tau = 6$, with parameter values $\alpha = 0.1$, $\gamma = 0.1 \text{ days}^{-1}$, $\lambda = 0.2 \text{ days}^{-1}$, $m = 10$. The dynamics give a period

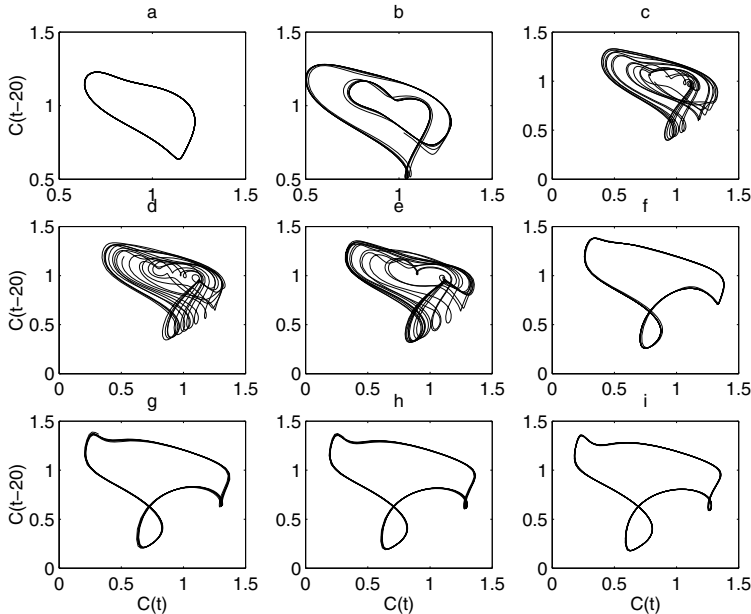


Fig. 8.10 **a** to **i** show the numerical solutions of bifurcating periodic solutions of model (8.18) with $\gamma = 0.1$, $\lambda = 2$, $a = 1$, $\tau = 20$ and $m = 7, 8, 9, 10, 11, 12, 15, 17, 20$. Note the progression from a simple periodic solution to a complex chaotic behavior and turn again to a simple periodic, as indicated in **a** to **i**

pattern, but when $\tau \geq 10$, a chaotic pattern is obtained. According to Hematology and Beutler (2011), normal human red blood cells have a fixed life span with an average of 120 days with a very low random destruction rate (corresponding to the removal of approximately 1% s per day); see [42–44].

8.5 Concluding Remarks

In this chapter, a class of delay differential equation models is developed to consider the memory impact in the transmission dynamics of these diseases in a population. We show that DDEs with infectious diseases are consistent with the real phenomena and rationally reflect the reality.

Including control variables in the model is desirable to determine the best strategy of treatment, control, and elimination of the infection, which will be considered in the next chapter. We next examine DDE models with optimal control.

References

- Wu, G.C., Baleanu, D.: Discrete fractional logistic map and its chaos. *Nonlinear Dyn.* **75**, 283–287
- Mackey, M.C., Glass, L.: Oscillations and chaos in physiological control systems. *Science* **197**, 287–289 (1977)
- Casagrandi, R., Bolzoni, L., Levin, S., Andreasen, V.: The SIRC model and influenza A. *Math. Biosci.* **200**, 152–169 (2006)
- Rihan F.A., Baleanu, D., Lakshmanan, S., Rakkiyappan, R.: On fractional SIRC model with salmonella bacterial infection. *Abstr. Appl. Anal.* **2014**, 9 pages (2014)
- Khan, M.A., Atangana, A.: Modeling the dynamics of novel coronavirus (2019-nCov) with fractional derivative. *Alexandria Eng. J.*, I11 (2020)
- Hethcote, H., Zhien, M., Shengbing, L.: Effects of quarantine in six endemic models for infectious diseases. *Math. Biosci.* **180**, 141–160 (2002)
- Hui, D. et al.: The continuing 2019-ncov epidemic threat of novel coronavirus to global health - the latest: novel coronavirus outbreak in Wuhan, China. *Int. J. Infect. Dis.* **91**(2020), 264–266 (2019)
- Grifoni, A., Weiskopf, D., et al.: Targets of T cell responses to SARS-CoV-2 coronavirus in humans with COVID-19 disease and unexposed individuals. *Cell* **181**, 1–13 (2020)
- Rihan, F.A., Naim Anwar, M., Sheek-Hussein, M., Denic, S.: SIR model of swine influenza epidemic in Abu Dhabi: estimation of vaccination requirement. *J. Pub. Health Frontier (PHF)* **1**(4), 85–89 (2012)
- Kermack, W.O., McKendrick, A.G.: Contributions to the mathematical theory epidemics. *Proc. R. Soc. A* **115**(Part I) (1927)
- Arino, J., Bowman, C.S., Moghadas, S.M.: Antiviral resistance during pandemic influenza: implications for stockpiling and drug use. *BMC Infec. Diseases* (2009)
- Zhang, T., Teng, Z.: On a nonautonomous seirs model in epidemiology. *Bull. Math. Biol.* **69**, 2537–2559 (2007)
- Rihan, F.A., Naim Anwar, M.: Qualitative analysis of delayed SIR epidemic model with a saturated incidence rate. *Int. J. Diff. Equ.* **2012**, 13 pages (2012)
- McCluskey, C.C.: Complete global stability for an SIR epidemic model with delay-distributed or discrete. *Nonlinear Anal. Real World Appl.* **11**, 55–59 (2010)
- Takeuchi, Y., Ma, W., Beretta, E.: Global asymptotic properties of a delay sir epidemic model with finite incubation times. *Nonl. Anal.* **42**, 931–947 (2000)
- Bocharov, G.A., Volpert, V., Ludewig, B., Meyehans, A.: Mathematical Immunology of Virus Infections. Springer, Berlin (2018)
- Balasubramaniam, P., Prakash, M., Rihan, F.A., Lakshmanan, S.: Hopf bifurcation and stability of periodic solutions for delay differential model of HIV infection of CD4⁺ T-cells. *Abstr. Appl. Anal.* ID 982978, 1–18 (2014)
- Pawelek, K.A., Liu, S., Pahlevani, F., Rong, L.: A model of HIV-1 infection with two time delays: mathematical analysis and comparison with patient data. *Math. Biosci.* **235**, 98–109 (2012)
- Lv, C., Yuana, Z.: Stability analysis of delay differential equation models of HIV-1 therapy for fighting a virus with another virus. *J. Math. Anal. Appl.* **352**, 672–683 (2009)
- Marchuk, G.: Mathematical Modelling of Immune Response in Infectious Diseases. Kluwer Academic Publishers, Dordrecht (1997)
- Sidorov, I.A., Romanyukha, A.A.: Mathematical modelling of T-cell proliferation. *Math. Biosci.* **115**, 187–232 (1993)
- Faroogi, Z.H., Mohler, R.: Distribution models of recirculating lymphocytes. *IEEE Trans. Biomed. Eng.* **36**, 355–362 (1999)
- Anderson, R.M., May, R.M.: Population biology of infectious diseases: Part 1. *Nature* **128**, 361–367 (1979)
- Deboer, R.J., Perelson, A.S.: Target cell limited and immune control models of hiv infection: a comparison. *J. Theor. Biol.* **190**, 201–214 (1998)

25. Nowak, M.A., Bangham, C.R.M.: Population dynamics of immune responses to persistent viruses. *Science* **272**, 74–79 (1996)
26. Wodarz, D., Nowak, M.A.: Specific therapy regimes could lead to long-term immunological control of HIV. *Proc. Natl. Acad. Sci.* **96**(25), 14464–14469 (1999)
27. Wodarz, D., Page, K., Arnaout, R., Thomsen, A.R., Lifson, J.D., Nowak, M.A.: A new theory of cytotoxic t-lymphocyte memory: implications for HIV treatment. *Philos. Trans. R. Soc. Lond. B* **355**(1395), 329–343 (2000)
28. Lv, C.: Lihong Huang, and Zhaozhui Yuan, Global stability for an hiv-1 infection model with beddington-deangelis incidence rate and CTL immune response. *Commun. Nonlinear Sci. Numer. Simul.* **19**(1), 121–127 (2014)
29. Perelson, A.S., Nelson, P.: Mathematical analysis of HIV-1 dynamics in vivo. *SIAM Rev.* **41**(1), 3–44 (1999)
30. Wang, Y., Zhou, Y., Brauer, F., Heffernan, J.: Viral dynamics model with ctl immune response incorporating antiretroviral therapy. *J. Math. Biol.* **67**(4), 901–934 (2013)
31. Pitchaimani, M., Monica, C., Divya, M.: Stability analysis for hiv infection delay model with protease inhibitor. *Biosystems* **114**(2), 118–124 (2013)
32. Shu, H., Wang, L.: Role of cd4+ t-cell proliferation in HIV infection under antiretroviral therapy. *J. Math. Anal. Appl.* **394**(2), 529–544 (2012)
33. Wang, S., Zhou, Y.: Global dynamics of an in-host HIV-1 infection model with the long-lived infected cells and four intracellular delays. *Int. J. Biomath.* **05**(06), 1250058 (2012)
34. Nowak, M.A., Bangham, C.R.M.: Population dynamics of immune responses to persistent viruses. *Science* **272**(5258), 74–79 (1996)
35. Beretta, E., Carletti, M., Kirschner, D.E., Marino, S.: Stability analysis of a mathematical model of the immune response with delays. In: *Mathematics for Life Science and Medicine*, pp. 177–206. Springer, Berlin (2007)
36. Fenton, A., Lello, J., Bonsall, M.B.: Pathogen responses to host immunity: the impact of time delays and memory on the evolution of virulence. *Proc. R. Soc. Biol. Sci. Ser. B* **273**(1597), 2083–2090 (2006)
37. Nowak, M.A., May, R.M., Sigmund, K.: Immune responses against multiple epitopes. *J. Theor. Biol.* **175**(3), 325–353 (1995)
38. Hale, J.: *Theory of Functional Differential Equations*. Springer, New York (1997)
39. an der Heiden, U., Mackey, M.C.: The dynamics of production and destruction: analytic insight into complex behaviour. *J. Math. Biol.* **16**, 75–101 (1982)
40. Batzel, J.J., Tran, H.T.: Modelling variation delay in the control system for human respiration: medical applications. *Appl. Math. Comput. J.* **110**(1), 1–51 (2000)
41. Glass, L., Mackey, M.C.: Pathological conditions resulting from instabilities in physiological control systems. *Ann. A.Y. Acad. Sci.* **316**, 214–1235 (1979)
42. Mackey, M.C.: Unified hypothesis for the origin of aplastic anemia and periodic hematopoiesis. *Blood* **51**(5), 941–956 (1978)
43. Colijn, C., Mackey, M.C.: A mathematical model of hematopoiesis: II. cyclical neutropenia. *J. Theor. Biol.* **237**, 133–146 (2005)
44. Zhou, Y., Weis, T.L., Liu, H., Ulaszek, J., Satgurunathan, N. et al., Kang, J.A.: Osteopontin regulates actin cytoskeleton and contributes to cell proliferation in primary erythroblasts. *J. Biol. Chem.* **283**, 6997–7006 (2008)

Chapter 9

Delay Differential Equations of Tumor-Immune System with Treatment and Control



9.1 Introduction

In this chapter, we present a delay differential model with optimal control that describes the interactions of tumor cells (TCs) and immune response cells with external therapy. The intracellular delay is incorporated into the model to justify the time required to stimulate the effector cells (ECs). The optimal control variables are incorporated to identify the best treatment strategy with minimum side effects by blocking the production of new TCs and keeping the number of normal cells above 75% of its carrying capacity. The existence of the optimal control pair and optimality system have been established. Pontryagin's maximum principle is applicable to characterize the optimal controls. The model displays a tumor-free steady state and up to three coexisting steady states. The numerical results show that the optimal treatment strategies reduce the tumor cell load and increase the ECs after a few days of therapy. The performance of combination therapy protocol of immuno-chemotherapy is better than the standard protocol of chemotherapy alone.

Cancer is a major cause of death globally, and it has been considered as one of the most complicated diseases to be treated clinically. Hence, significant research efforts are being devoted to understand the interaction between the tumor cells and the immune system. Indeed, the treatment of cancer is one of the most challenging problems of modern medicine. Any effective cancer treatment needs to kill cancer cells in the entire body while simultaneously keeping healthy cells above the minimum level. Chemotherapy is one of the most prominent cancer treatment modalities. However, it is not always a comprehensive solution for tumor regression. Other treatment options, including surgery, immunotherapy, and radiation, are often able to force the cancer into remission; however, better and suitable treatments are needed [1, 2].

Chemotherapy has been used in combination with immunotherapy to protect the patient from opportunistic infections as well as fighting the cancer itself [3, 4]. This is because, chemotherapy treatment kills both cancerous and healthy cells, and there-

fore, it depletes the patient's immune system, making the patient prone to dangerous infections. For this and other reasons, it is desirable to strengthen the immune system after a course of chemotherapy. Additionally, however, the ability to recruit the body's own defenses to fight the cancer can be a powerful treatment strategy. Therefore, maintaining a strong immune system, by combining immunotherapy during chemotherapy, may be essential to successfully fight this disease. However, what is the most effective way to combine cancer immunotherapy and chemotherapy?

Mathematical models, using ordinary, partial, and delay differential equations, play an important role in understanding the dynamics and tracking tumor and immune cell populations over time (see e.g. [5–12]). Kuznetsov et al. [2] modeled the interactions of cytotoxic T lymphocyte (CTL) response and the growth of an immunogenic tumor. In the contributions of [13–15], the authors take into account the penetration of tumor cells by the ECs, which simultaneously causes the inactivation of ECs. Recently, in [16], the authors adopted a predator-prey formulation of the tumor immunity problem as a battle between immune cells and tumor cells (predators and prey, respectively). Many mathematical models have been reported that describe the interaction between tumor cells and immune cells alone, between tumor cells and normal cells alone, and between tumor cells and chemotherapy treatment alone [17]. We should mention here that the application of the optimal control theory requires the boundedness of the solutions of the model populations; see also [18].

The objective of this chapter is to adopt a delay differential model, and analyze and computationally provide an optimal way to combine chemotherapy and immunotherapy treatment strategies that identify the best treatment strategy that can minimize tumor load while maximizing the strength of the immune system. We formulate and analyze a delay differential model describing immune response and tumor cells under the influence of chemotherapy alone and under the combination of chemotherapy and immunotherapy. In Sect. 9.2, we describe the model. In Sect. 9.3, we study the qualitative behavior of the model without external therapy. In Sect. 9.4, we describe the optimal control problem governed by DDEs with only a chemotherapy control variable. The existence of the solution and optimality conditions are discussed in Sects. 9.5 and 9.6. In Sect. 9.7, we extend the control problem to include a combination of chemotherapy and immunotherapy treatments with two contrail variables. Numerical simulations and a conclusion are included in Sects. 9.8 and 9.9.

9.2 Description of the Model

Let us recall Kuznetsov et al.'s model [2], which describes the dynamics of tumor-immune system interactions by incorporating a system of five ODEs, which we then reduce into two equations but with time-delays. The model describes the response of the effector cells (ECs) to the growth of tumor cells (TCs). The penetration of TCs by ECs, which simultaneously causes the inactivation of ECs, has also been accounted for. It is assumed that interactions between the ECs and TCs are *in vitro*, such that $E(t)$, $T(t)$, $C(t)$, $E^*(t)$, and $T^*(t)$ denote the local concentrations of ECs,

TCs, EC-TC conjugates, inactivated ECs, and “lethally hit” TCs, respectively. The total population of unattacked TCs is $T_{tot}(t) = T(t) + C(t)$. The rate of binding of ECs to TCs and the rate of separation of ECs from TCs without damaging them are denoted by k_1 and k_{-1} , respectively. The rate at which EC-TC interact for lysis is denoted by k_2 while the rate at which EC-TC interaction inactivate ECs is denoted by k_3 . The model takes the form

$$\begin{aligned}\frac{dE(t)}{dt} &= \sigma + F(C(t), T(t)) - d_1 E(t) - k_1 E(t)T(t) + (k_{-1} + k_2)C(t), \\ \frac{dT(t)}{dt} &= \alpha T(t)(1 - \beta T_{tot}(t)) - k_1 E(t)T(t) + (k_{-1} + k_3)C(t), \\ \frac{dC(t)}{dt} &= k_1 E(t)T(t) - (k_{-1} + k_2 + k_3)C(t), \\ \frac{dE^*(t)}{dt} &= k_3 C(t) - d_2 E^*(t), \\ \frac{dT^*(t)}{dt} &= k_2 C(t) - d_3 T^*(t).\end{aligned}\tag{9.1}$$

Here, parameter σ represents the normal rate (not increased by the presence of the tumor) of the flow of adult ECs into the tumor side (region), $F(C(t), T(t)) = F(E(t), T(t)) > 0$ (when $T(t) > 0$) describes the accumulation of ECs in the tumor side due to the presence of the tumor. d_1, d_2 , and d_3 are the coefficients of the processes of destruction and migration of E , E^* , and T^* , respectively. The maximal growth of the tumor is represented by the coefficient α , and β^{-1} is the environment capacity. If we assume that $\frac{dC(t)}{dt} \approx 0$, then $C(t) \approx K E(t)T(t)$ where $K = k_1/(k_{-1} + k_2 + k_3)$, and the model can be reduced to two equations that describe the behavior of ECs and TCs only [1, 2]. That leads to the fact that the rate of stimulated accumulation has some maximum value as TCs get large.

The interaction between TCs and ECs can be regarded as an analog of the “predator-prey” interaction, where the ECs are the predator and TCs represent the prey. Thus, the reduced model that describes the interactions between the two populations, namely TCs $T(t)$ and activated ECs $E(t)$ (such as cytotoxic T-cells or natural killer cells), is of the form

$$\begin{aligned}\frac{dE(t)}{dt} &= \sigma + F(E(t), T(t)) - \mu E(t)T(t) - \delta E(t), \\ \frac{dT(t)}{dt} &= \alpha T(t)(1 - \beta T(t)) - n E(t)T(t),\end{aligned}\tag{9.2}$$

with initial conditions: $E(0) = E_0$, $T(0) = T_0$. The interaction between the ECs and TCs can reduce the size of both populations with different rates. This is expressed as $-\mu E(t)T(t)$ and $-n E(t)T(t)$ to illustrate the interaction between the TCs and ECs. As a result of this interaction, the immune ECs decrease the population of TCs at a rate of n . Additionally, TCs infect some of the ECs, and therefore, the population of uninfected ECs decreases at the rate of μ .

If one considers $T(t)$ as prey and $E(t)$ as predator, then $\mathcal{F}(E, T)$ may take the form $\mathcal{F}(E, T) = \frac{\rho E(t)T(t)}{\eta + T(t)}$, which is the Michaelis-Menton form. In this term, ρ is the maximum immune response rate and η is the steepness of the immune response. The presence of the TCs virtually initiates the proliferation of tumor-specific ECs to reach a saturation level parallel to the increase in the tumor population. Hence, the recruitment function should be zero in the absence of the TCs, whereas it should increase monotonically toward a horizontal asymptote [19]. We also incorporate a discrete time-delay τ into the model to describe the time needed by the immune system to develop a suitable response after recognizing the TCs. Accordingly, the model with discrete time-delay takes the form

$$\begin{aligned} \frac{dE(t)}{dt} &= \sigma + \frac{\rho E(t - \tau)T(t - \tau)}{\eta + T(t - \tau)} - \mu E(t - \tau)T(t - \tau) - \delta E(t), \\ \frac{dT(t)}{dt} &= r_2 T(t)(1 - \beta T(t)) - n E(t)T(t), \end{aligned} \quad t \geq 0 \quad (9.3)$$

with initial functions $E(t) = \psi_1(t)$ and $T(t) = \psi_2(t)$, for all $t \in [-\tau, 0]$. Here, σ represents the normal rate (not increased by the presence of the tumor) of the flow of adult ECs into the tumor side (region). The source of the immune cells is considered to be outside of the system; therefore, it is reasonable to assume a constant influx rate σ . Furthermore, in the absence of any tumor, the cells will die at a rate δ . The presence of TCs stimulates the immune response, represented by the positive non-linear growth term for the immune cells $\rho E(t - \tau)T(t - \tau)/(\eta + T(t - \tau))$, where ρ and η are positive constants and $\tau \geq 0$ is the time-delay that presents the time needed by the immune system to develop a suitable response after recognizing the TCs. The saturation term (Michaelis-Menton form) with the $E(t)$ compartment and logistic term with the $T(t)$ compartment are consoled. Let us first prove the non-negativity and boundedness solutions of the underlying DDEs model (9.3) (see [20]).

9.2.1 Non-negativity and Boundedness Solutions of Model (9.3)

To show that the solutions of model (9.3) are bounded and remain non-negative in the domain of its application for sufficiently large values of time t , we recall the following lemma:

Lemma 9.1 (Gronwall's Lemma [21, p. 9]) *Let x , ψ , and χ be real continuous functions defined in $[a, b]$, $\chi \geq 0$ for $t \in [a, b]$. We suppose that on $[a, b]$ we have the inequality $x(t) \leq \psi(t) + \int_a^t \chi(s)x(s)ds$. Then, $x(t) \leq \psi(t) + \int_a^T \chi(s)\psi(s)e^{\left(\int_s^t \chi(\xi)d\xi\right)}ds$ in $[a, b]$.*

Therefore, we arrive at the following proposition:

Proposition 9.1 *Let (E, T) be a solution of the DDE model (9.3); then, $E(t) < M_1$ and $T(t) < M_2$ for all sufficiently large time t , where*

$$\begin{aligned} M_1 &= E(0) + \frac{\sigma}{\delta} \exp(\delta t) + \int_0^t \left[\rho e^{\delta(\tau+s)} \left(E(0) + \frac{\sigma}{\delta} e^{\delta s} \right) \exp \left(\int_s^\tau \rho e^{\delta(\xi+\xi)} d\xi \right) \right] ds, \quad M_2 \\ &= \max \left(\frac{1}{\beta}, T(0) \right). \end{aligned} \quad (9.4)$$

Proof Let (E, T) denote the solution of model (9.3). From the second equation of system (9.3), we have $\frac{dT}{dt} \leq r_2 T(t)(1 - \beta T(t))$. Thus, $T(t)$ may be compared with the solution of

$$\frac{dX}{dt} = r_2 X(t)(1 - \beta X(t)), \quad \text{with } X(0) = T(0)$$

This proves that $T(t) < M_2$. From the first equation of system (9.3), we obtain

$$E(t) = \exp(-\delta t) \left\{ E(0) + \int_0^t \left[\sigma + \frac{\rho E(s-\tau)T(s-\tau)}{\eta + T(s-\tau)} - \mu E(s-\tau)T(s-\tau) \right] \exp(\delta s) ds \right\}.$$

To show that $E(t)$ is bounded, we use the generalized Gronwall lemma. Since $\frac{T}{\eta + T} < 1$ and $\exp(-\delta t) \in (0, 1]$, we have

$$E(t) \leq E_0 + \frac{\sigma}{\delta} \exp(\delta t) + \int_0^t \rho E(s-\tau) \exp(\delta s) ds.$$

The generalized Gronwall lemma gives $E(t) < M_1$, where M_1 is uniformly bounded. It follows that if (E, T) is a solution of (9.3), then $(E, T) < (M_1, M_2)$ for all t . This shows that the solutions of model (9.3) are uniformly bounded. This completes the proof. \square

From Eq. (9.2) and solution $T(t) = T(0) \exp \left(\int_0^t [r_2(1 - \beta T(s)) - E(s)] ds \right)$, we arrive at the following result:

Corollary 9.1 *If $\frac{\rho}{\eta + T} \geq \mu$, then the solutions (E, T) for model (9.3) are non-negative for any non-negative initial condition. However, if $\frac{\rho}{\eta + T} < \mu$, then there exist non-negative initial conditions such that $E(t)$ becomes negative in a finite time interval.*

9.2.2 Model with Chemotherapy

We extend model (9.3) to consider two extra variables: amount of chemotherapy $u(t)$ and normal cells $N(t)$ (see Fig. 9.1). We also assume a homogeneity of the TCs. The modified model is

$$\begin{aligned}\frac{dE(t)}{dt} &= \sigma + \frac{\rho E(t - \tau)T(t - \tau)}{\eta + T(t - \tau)} - \mu E(t - \tau)T(t - \tau) - \delta E(t) - a_1(1 - e^{-u(t)})E(t), \\ \frac{dT(t)}{dt} &= r_2 T(t)(1 - \beta T(t)) - nE(t)T(t) - c_1 N(t)T(t) - a_2(1 - e^{-u})T(t), \\ \frac{dN(t)}{dt} &= r_3 N(t)(1 - \beta_2 N(t)) - c_2 T(t)N(t) - a_3(1 - e^{-u})N(t), \\ \frac{du(t)}{dt} &= v(t) - d_1 u(t).\end{aligned}\quad (9.5)$$

We assume that the drug kills all types of cells but that the killing rate differs for each type of cell. $F(u) = a_i(1 - e^{-u})$ is the fraction of cells killed for a given amount of drug $u(t)$ at the tumor site. We denote by a_1 , a_2 , and a_3 , the three different response coefficients. $v(t)$ represents the amount of dose that is injected into the system, while d_1 is the decay rate of the drug once it is injected. In this case, the quantity we will control directly is not $u(t)$, but $v(t)$. The TCs and normal cells are modeled by a logistic growth law, with parameters r_i representing the growth rate of two types of cells: $i = 2$ identifies the parameter associated with the tumor, $i = 3$ identifies the parameter associated with the normal tissue, and β and β_2 are the reciprocal carrying capacities of TCs and host cells, respectively. In addition, there are two terms representing the competition between the tumor and host cells $-c_1 NT$ and $-c_2 NT$.

Let $C = C([-\tau, 0], \mathbb{R}^4)$ be the Banach space of continuous functions mapping the interval $[-\tau, 0]$ into \mathbb{R}^4 with the topology of uniform convergence. It is easy to

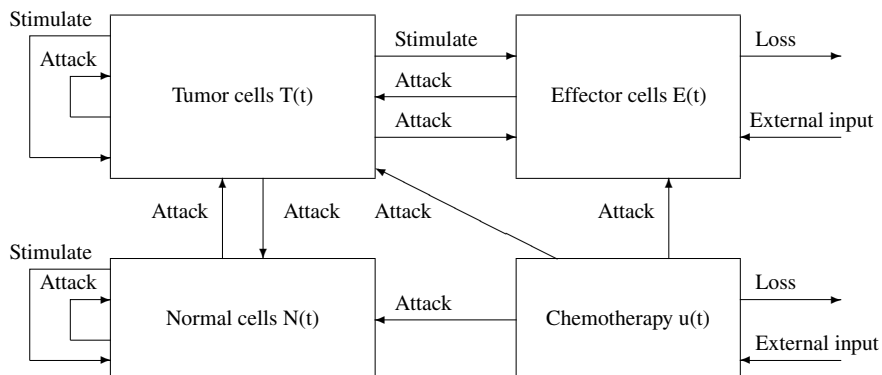


Fig. 9.1 The interaction of TCs, immune cells, and normal cells in the presence of chemotherapy drug

show that there exists a unique solution $(E(t), T(t), N(t), u(t))$ of system (9.5) with initial data $(E_0, T_0, N_0, u_0) \in C$. For biological reasons, we assume that the initial data of system (9.5) satisfy $E_0 \geq 0, T_0 \geq 0, N_0 \geq 0, u_0 \geq 0$. For $\tau = 0$, the model is reduced to the ODE model developed by de Pillis and Radunskaya in [22].

Remark 9.1 We consider the units of the model cells as normalized, so that $\beta_2 = 1$.

The main objective in developing chemotherapy treatment in system (9.5) is to reach either tumor-free steady state or coexisting steady state in which the TCs' size is small, while the normal cells' size is close to its normalized carrying capacity. We next start the analysis by studying the stability of the system when there is no drug (treatment) input, i.e., $u(t) = 0$, for all t .

9.3 Drug-Free Steady States and Their Stability

In the absence of chemotherapy ($u(t) = 0$), the (9.5) model has the following types of steady states:

- Tumor-free steady state, where the tumor cell population is zero, while the normal cells survive. This steady state has the form $\mathcal{E}_0 = (\sigma/\delta, 0, 1)$.
- Dead (lethal) steady state, where the normal cells population is zero, which has the forms
 - (1) $(\sigma/\delta, 0, 0)$ in which the normal and tumor cell populations have died off,
 - (2) $(f(T^*), T^*, 0)$ where the normal cells alone have died off and the TCs have survived, where

$$f(T) = \frac{\sigma(\eta + T)}{\mu T(\eta + T) + \delta(\eta + T) - \rho T},$$

and T^* is a non-negative solution for

$$T^* + (n/r_2\beta)f(T^*) - 1/\beta = 0.$$

- Coexisting steady state, where both normal and TCs coexist with non-zero populations. The steady state is given by $\mathcal{E}_+ = (f(T^*), T^*, g(T^*))$ where $g(T^*) = 1 - (c_2/r_3)T^*$, and T^* is a non-negative solution of

$$C_3T^3 + C_2T^2 + C_1T + C_0 = 0, \text{ where} \quad (9.6)$$

$$\begin{aligned} C_3 &= -\mu r_2\beta + \mu c_1 c_2 / r_3, \\ C_2 &= -\mu \eta r_2\beta + \mu \eta c_1 c_2 / r_3 + \mu r_2 - \mu c_1 - \delta r_2\beta + \delta c_1 c_2 / r_3 + \rho r_2\beta - \rho c_1 c_2 / r_3, \\ C_1 &= \mu \eta r_2 - \mu \eta c_1 - \delta \eta r_2\beta + \delta \eta c_1 c_2 / r_3 + \delta r_2 - \delta c_1 - \rho r_2 + \rho c_1 - \sigma n, \\ C_0 &= \delta \eta r_2 - \delta \eta c_1 - \sigma n \eta. \end{aligned}$$

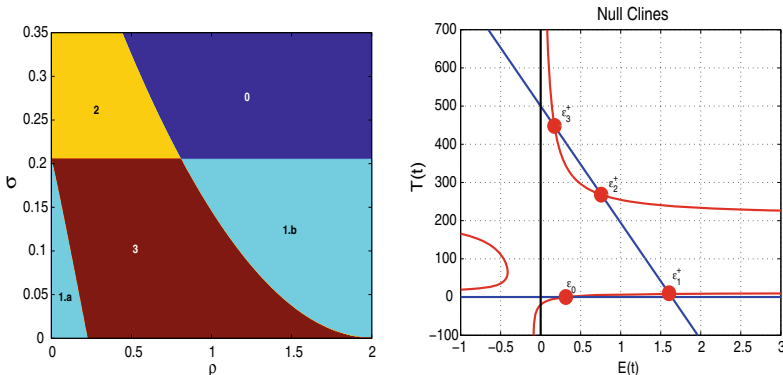


Fig. 9.2 The left panel shows the regions of existence of coexisting equilibria of model (9.3) in (ρ, σ) -plane with parameter values $\delta = 0.2$, $\eta = 0.3$, $\mu = 0.003611$, $r_2 = 1.03$, $r_3 = 1$, $\beta = 2 \times 10^{-3}$, $n = 1$, $c_1 = 0.00003$, and $c_2 = 3 \times 10^{-9}$. The dark blue region (0) represents the case where there is no equilibria, the light blue regions (1.a, 1.b) represent the case where there is a unique equilibrium, the orange region (2) represents the case where there are two steady states, and the brown region (3) represents the case where there are three equilibria. The right panel shows the null clines of the model, which has up to four steady states: tumor-free steady state " \mathcal{E}_0 "; tumor dormancy steady state " \mathcal{E}_1^+ "; medium concentration tumor steady state " \mathcal{E}_2^+ "; and escape tumor steady state " \mathcal{E}_3^+ "

The number of coexisting steady states mainly depends on the parameter values. This could be zero, one, two, or three of these steady states (see Fig. 9.2). We next study the stability of the above-mentioned steady states.

9.3.1 Stability of Tumor-Free Steady State

In this subsection, we investigate the parameter ranges for which the tumor-free steady state \mathcal{E}_0 is locally asymptotically stable. The Jacobian matrix of the linearized system at the tumor-free steady state is given by

$$J_{\mathcal{E}_0} = \begin{pmatrix} -\delta \frac{\rho\sigma}{\eta\delta} e^{-\lambda\tau} - \frac{\mu\sigma}{\delta} e^{-\lambda\tau} & 0 \\ 0 & r_2 - \frac{n\sigma}{\delta} - c_1 \\ 0 & -c_2 & -r_3 \end{pmatrix}$$

with the eigenvalues $\lambda_1 = -\delta < 0$, $\lambda_2 = r_2 - \frac{n\sigma}{\delta} - c_1$, and $\lambda_3 = -r_3 < 0$. Hence, the tumor-free steady state \mathcal{E}_0 is locally stable if $\lambda_2 < 0$ if and only if

$$r_2 < \frac{n\sigma}{\delta} + c_1, \quad \forall \tau \geq 0.$$

This relates r_2 (the growth rate of the TCs) to $n\sigma/\delta$ (the resistance coefficient), which measures how efficiently the immune system competes with the TCs. If this tumor-free steady state is unstable, then no amount of chemotherapy will be able to completely eradicate the TCs.

9.3.2 *Stability of Lethal Steady States*

The same analysis done above shows that the deadly steady state $(\sigma/\delta, 0, 0)$ has the eigenvalues $\lambda_1 = -\delta < 0$, $\lambda_2 = r_2 - n\sigma/\delta$, and $\lambda_3 = r_3 > 0$; hence it is unstable saddle point. Whereas the other deadly steady state $(f(T^*), T^*, 0)$ can be either stable or unstable depending on the model parameters and the value of the time-delay τ . This can be shown by using Routh Harwatz test and Rouche's theorem, as shown in detail in the previous chapters. Since the stability of this steady state is not needed for the developing treatment therapy, we will not delve into further details regarding this part.

9.3.3 *Stability of Coexisting Steady States*

To study the stability of the coexisting steady states, we vary the two parameters ρ (the immune cell growth rate) and σ (the normal flow rate of immune cells), by fixing the other parameters: $\delta = 0.2$, $\eta = 0.3$, $\mu = 0.003611$, $r_2 = 1.03$, $r_3 = 1$, $\beta = 2 \times 10^{-3}$, $n = 1$, $c_1 = 0.00003$, and $c_2 = 3 \times 10^{-9}$. Table 9.1 summarizes the existence and stability results of the coexisting steady states, as present in different regions of Fig. 9.2. It shows that the light blue region (1a) represents the “scape” case where there is a unique stable node steady state with high tumor size, while the light blue region (1b) represents the case where there is a unique steady state with low tumor size. It is a stable spiral for $\tau < \tau^*$, while at $\tau = \tau^*$ the limit cycle occurs due to Hopf bifurcation. Furthermore, the orange region (2) represents the case where there are two steady states: one is a stable node and the other is an unstable saddle node. To this end, the brown region (3) represents the case where there are three steady states: one is a stable node, another is an unstable node, and the last steady state is a spiral stable for $\tau < \tau^*$, while the limit cycle occurs at $\tau = \tau^*$. Of interest are the existence and stability of steady states, where a small tumor population size might coexist with a large number of normal cells. Figure 9.3 presents the phase space for the cell populations in the case where $\rho = 1.4$ and $\sigma = 0.1$. It shows that for $\tau = 0.8$, the steady state is asymptotically stable (left), while for $\tau = 1.2$, a limit cycle is born around the steady state (right). We utilize MIDDE code [23]), which is suitable for simulating stiff and non-stiff problems, to solve the DDEs model using mono-implicit RK methods. Figure 9.4 provides the numerical simulations for $\sigma = 0.182$ and $\delta = 0.545$ that belong to “BR” region of Fig. 9.2, where there are four steady states. We can conclude (see Fig. 9.4 (left)) that for this particular set

Table 9.1 The stability results for the coexisting steady states by using the functions ρ and σ , while fixing the rest of the parameters as mentioned in the text

| Region in Fig. 9.2 | ρ | σ | Steady state (E^*, T^*, N^*) | Eigenvalues $\lambda_1, \lambda_2, \lambda_3$ | Stability for $\tau \geq 0$ |
|--------------------|--------|----------|---|--|--|
| Light blue (1a) | 0.1 | 0.05 | (0.0269, 486.9244, 0.9999) | -0.9509, -1.9105, -1 | Stable node |
| Light blue (1b) | 1.4 | 0.1 | (1.0299, 0.0238, 0.9999) | -1, -0.0486-0.3096i, -0.0486+0.3096i | Stable spiral for $\tau < \tau^*$, Stable limit cycles at $\tau = \tau^*$ |
| Orange (2) | 0.2 | 0.23 | (0.1648, 419.9672, 0.9999) (0.8656, 79.7712, 0.99) | -0.5942, -1, -1.7876 0.276, -1, -0.7291 | Stable node Unstable saddle node |
| Brown (3) | 0.6 | 0.1 | (0.0789, 461.688, 0.99) (0.7236, 148.7078, 0.99) (1.0298, 0.0623, 0.99) | -0.7137, -1.5050, -1 0.4060, -1, -0.8506 -1, -0.0486-0.2922i, -0.0486+0.2922i | Stable node Unstable saddle node Stable spiral for $\tau < \tau^*$, Stable limit cycles at $\tau = \tau^*$ |

of parameters and $\tau = 0.2$, the tumor-free steady state is unstable (saddle node), while the dormant tumor steady state is spirally stable. The medium tumor state is unstable, while the highly tumor state is stable. In this case, it is possible that the tumor will result in either a steady state with dormancy or escape from the immune system. However, Fig. 9.4 (right) shows that for $\tau = 0.86$, the dormant steady state is unstable where there is a limit cycle occurring around the dormant steady state (see Chap. 2), while the escaped tumor steady state remains stable.

Next, we consider chemotherapy treatment ($u(t) > 0$) in the underlying model and establish the existence of an optimal control for the model and provide necessary conditions for optimal control.

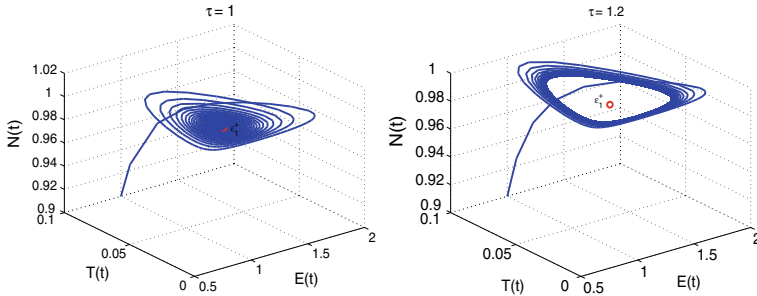


Fig. 9.3 The phase space for the cell population in the case where $\rho = 1.4$ and $\sigma = 0.1$. (left) For $\tau = 1$, the steady state is asymptotically stable. (right) For $\tau = 1.2$, a limit cycle is born around the steady state

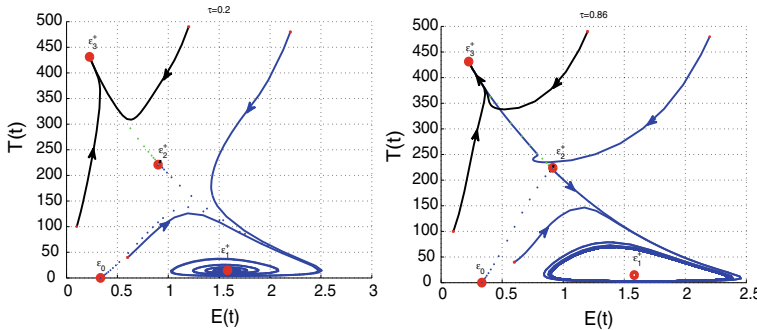


Fig. 9.4 The solutions of model (9.3) with the same set of parameters of Fig. 9.2 and with different values of τ . (Left) For $\tau = 0.2$ both \mathcal{E}_0 and \mathcal{E}_2^+ are unstable, while both \mathcal{E}_1^+ and \mathcal{E}_3^+ are stable. (Right) For $\tau = 0.86$, there exists a limit cycle around \mathcal{E}_1^+ , while the stability of the other steady states does not change

9.4 Optimal Control Problem Governed by DDEs

Once a suitable model of interacting cell populations is constructed, we then focus on the design of an efficient treatment protocol, where we employ the tools of optimal control theory.

Consider the optimal control problem with pure state constraints and control bounds as follows:

$$\max_{x,v} J(x, v) = \Psi(x(t_f)) + \int_0^{t_f} L(t, x(t), v(t)) dt, \quad (9.7a)$$

subject to the DDEs

$$x'(t) = f(t, x(t), x(t - \tau), v(t)), \quad t \in [0, t_f] \quad (9.7b)$$

$$x(t) = \phi(t), \quad t \in [-\tau, 0], \quad (9.7c)$$

with the control constraint

$$a \leq v(t) \leq b \quad t \in [0, t_f]. \quad (9.7d)$$

and state constraint

$$x(t) \geq c \quad t \in [0, t_f]. \quad (9.7e)$$

J is called an objective functional and the integrand $L(\cdot)$ is called the Lagrangian of objective functional. Furthermore, a and b are called the lower and upper bounds. The function $v(t)$ is called an admissible control, if it fulfills the inequality constraints (9.7d). The set of all admissible controls is called the admissible set, and we refer to it as V_{ad} (where “ad” stands for the admissible). The state $x(\cdot)$ enters with a delay τ as $x(t - \tau)$ in the system of the state equations (9.7b), while it is evaluated at the time t as $x(t)$ in the objective functional (9.7a). The set of all admissible states X_{ad} , which satisfies the state equations and the state constraint, is called the set of admissible state.

The goal of chemotherapy is to eradicate the TCs while maintaining adequate amounts of healthy tissue. From a mathematical point of view, adequate destruction of TCs might mean forcing the system out of the basin of an unhealthy spiral node, out of a limit cycle, and into a basin of attraction of a stable tumor-free equilibrium. Alternatively, if the therapy pushes the system into a limit cycle in which the size of the tumor is small for a long period of time (as long as the life of the patient, for example), this could also be considered as a “cure.”

Optimality in treatment might be defined in a variety of ways. Some studies have been done in which the total amount of drug administered is minimized, or the number of TCs is minimized. The general goal is to keep the patient healthy while killing the tumor. Since our model takes into account the toxicity of the drug to all types of cells, our control problem consists of determining the function $v(t)$ that will maximize the amount of ECs and minimize the number of tumor cells and the cost of the control with the constraint that we do not kill too many normal cells. If the units of cells are normalized, so that the carrying capacity of normal cells is 1, we then require that the number of normal cells stay above three-fourth of the carrying capacity. Therefore, our main objective is to optimize the functional

$$\max_{v \in V_{ad}} J(v) = \int_0^{t_f} \left(E(t) - T(t) - \frac{B_v}{2}[v(t)]^2 \right) dt \quad (9.8a)$$

which is subjected to the following underlying DDEs:

$$\frac{dE(t)}{dt} = \sigma + \frac{\rho E(t-\tau)T(t-\tau)}{\eta + T(t-\tau)} - \mu E(t-\tau)T(t-\tau) - \delta E(t) - a_1(1 - e^{-u(t)})E(t), \quad (9.8b)$$

$$\frac{dT(t)}{dt} = r_2 T(t)(1 - \beta T(t)) - n E(t)T(t) - c_1 N(t)T(t) - a_2(1 - e^{-u})T(t), \quad (9.8c)$$

$$\frac{dN(t)}{dt} = r_3 N(t)(1 - \beta_2 N(t)) - c_2 T(t)N(t) - a_3(1 - e^{-u})N(t), \quad (9.8d)$$

$$\frac{du(t)}{dt} = v(t) - d_1 u(t) \quad (9.8e)$$

with control constraint

$$0 \leq v(t) \leq v_{max} < \infty \quad t \in [0, t_f], \quad (9.8f)$$

and state constraint

$$k(N) = N - 0.75 \geq 0, \quad t \in [0, t_f]. \quad (9.8g)$$

Here, B_v is a weight factor that describes the patient's acceptance level of chemotherapy. We choose the control parameter as a class of piecewise continuous functions defined for all t such that $0 \leq v(t) \leq v_{max} < \infty$, where $v(t) = v_{max}$ represents the maximum chemotherapy, while $v(t) = 0$ represents the case where there is no chemotherapy. Thus, we depict the class of admissible controls as

$$V_{ad} = \{v \in L^\infty([0, t_f], \mathbb{R}), \mid 0 \leq v(t) \leq v_{max} < \infty, \forall t \in [0, t_f]\}.$$

We next prove the existence of the optimal solution of the underlying system (9.8).

9.5 Existence of Optimal Solution

To prove the existence of the optimal solution of (9.8), we use the results of Fleming and Rishel [24, Theorem 4.1, p. 68–69] and Lukes [25, Theorem 9.2.1, p. 182].

Theorem 9.1 *There exists an optimal solution $(x^*, v^*) \in W^{1,\infty}([0, t_f], \mathbb{R}^4) \times L^\infty([0, t_f], \mathbb{R})$ for the optimal control problem (9.8), such that*

$$J(v^*) = \max_{v \in V_{ad}} J(v) \quad (9.9)$$

where $x^* = [E^*, T^*, N^*, u^*]^T$ if the following conditions are satisfied:

1. The set of admissible state is nonempty.
2. The admissible set V_{ad} is nonempty, convex, and closed.
3. The right-hand side of the state system is bounded by a linear combination of the state and control variables.

4. The integrand $L(E, T, v) = (E(t) - T(t) - \frac{B_v}{2}[v(t)]^2)$ of the objective functional is concave on V_{ad} .
5. There exist constants $h_2, h_3 > 0$, and $b > 1$, such that $L(E, T, v) \leq h_2 - h_3(|v|)^b$.

Proof To verify the above conditions, we should first prove the existence of the solution for the system of the state equations (9.8b)–(9.8e). Since $\frac{\rho T(t-\tau)}{\eta+T(t-\tau)} < \rho$, $v_{max} < \infty$ and by neglecting the negative terms in the model, we have

$$\frac{dE(t)}{dt} < \sigma + \rho E(t-\tau), \quad \frac{dT(t)}{dt} < r_2 T, \quad \frac{dN(t)}{dt} < r_3 N, \quad \frac{du(t)}{dt} < v_{max}. \quad (9.10)$$

System (9.10) can be rewritten in the form

$$\begin{pmatrix} E(t) \\ T(t) \\ N(t) \\ u(t) \end{pmatrix}' < \begin{pmatrix} 0 & 0 & 0 & 0 \\ 0 & r_2 & 0 & 0 \\ 0 & 0 & r_3 & 0 \\ 0 & 0 & 0 & 0 \end{pmatrix} \begin{pmatrix} E(t) \\ T(t) \\ N(t) \\ u(t) \end{pmatrix} + \begin{pmatrix} \rho & 0 & 0 & 0 \\ 0 & 0 & 0 & 0 \\ 0 & 0 & 0 & 0 \\ 0 & 0 & 0 & 0 \end{pmatrix} \begin{pmatrix} E(t-\tau) \\ T(t-\tau) \\ N(t-\tau) \\ u(t-\tau) \end{pmatrix} + \begin{pmatrix} \sigma \\ 0 \\ 0 \\ v_{max} \end{pmatrix}$$

where $' = d/dt$. This system is linear in finite time with bounded coefficients. Then, the solutions of this linear system are uniformly bounded. Therefore, the solution of the non-linear system (9.8b)–(9.8e) is bounded and exists [25]. Hence, condition one is satisfied.

Clearly, the second condition is satisfied by the definition of V_{ad} . System (9.8b)–(9.8e) is bilinear in the control variable v and can be rewritten as

$$\mathbf{F}(t, \mathbf{X}(t), \mathbf{X}(t-\tau), v) = \boldsymbol{\alpha}(t, \mathbf{X}) + \boldsymbol{\beta}(t, \mathbf{X}(t-\tau)) + \sigma + v \quad (9.11)$$

where $\mathbf{X}(t) = (E, T, N, u)$, $\mathbf{X}(t-\tau) = (E(t-\tau), T(t-\tau), N(t-\tau), u(t-\tau))$, $\boldsymbol{\alpha}$ and $\boldsymbol{\beta}$ are the vector valued functions of $\mathbf{X}(t)$ and $\mathbf{X}(t-\tau)$, respectively. Using that the solutions are bounded, we have

$$|\mathbf{F}(t, \mathbf{X}(t), \mathbf{X}(t-\tau), v)| \leq |F_1 X(t)| + |F_2 X(t-\tau)| + |F_3| + |F_4| \leq h_1 |\mathbf{X}| + |\sigma| + |v|,$$

where h_1 depends on the coefficients of the system, and

$$F_1 = \begin{pmatrix} 0 & 0 & 0 & 0 \\ 0 & r_2 & 0 & 0 \\ 0 & 0 & r_3 & 0 \\ 0 & 0 & 0 & 0 \end{pmatrix}, \quad F_2 = \begin{pmatrix} \rho & 0 & 0 & 0 \\ 0 & 0 & 0 & 0 \\ 0 & 0 & 0 & 0 \\ 0 & 0 & 0 & 0 \end{pmatrix}, \quad F_3 = \begin{pmatrix} \sigma \\ 0 \\ 0 \\ 0 \end{pmatrix}, \quad F_4 = \begin{pmatrix} 0 \\ 0 \\ 0 \\ v \end{pmatrix}.$$

We also note that the integrand of $J(v)$ is concave in V_{ad} . Finally,

$$E(t) - T(t) - B_v/2[v(t)]^2 < E - B_v/2[v(t)]^2 \leq h_2 - h_3|v(t)|^2,$$

where h_2 depends on the upper bounds of $E(t)$ and $T(t)$, and $h_3 = B_v/2$. This completes the proof. \square

We also conclude that there exists an optimal control variable v^* .

9.6 Optimality Conditions

In this section, we establish the necessary conditions for the optimal solution of the optimization problem (9.8). We use Pontryagin's minimum (maximum) principle derived by Göllmann et al. [26] for the retarded optimal control problem with mixed control—state constraints. To this end, we define the augmented Hamiltonian function involving the inequality constraints by

$$\begin{aligned} \mathcal{H}(t, E, T, E_\tau, T_\tau, u, v, \lambda) = & E(t) - T(t) - \frac{B_v}{2} [v(t)]^2 + \lambda_1(T) \frac{dE(t)}{dt} \\ & + \lambda_2(t) \frac{dT(t)}{dt} + \lambda_3(t) \frac{dN(t)}{dt} + \lambda_4 \frac{du(t)}{dt} + \gamma(t)k(N), \end{aligned} \quad (9.12)$$

where

$$\gamma(t) = \begin{cases} 1 & \text{if } N(t) \leq 0.75, \\ 0 & \text{otherwise} \end{cases}$$

and λ_i ($i = 1, 2, 3, 4$) are the adjoint variables satisfy

$$\begin{aligned} \lambda'_1(t) &= -\frac{\partial \mathcal{H}}{\partial E}(t) - \chi_{[0, t_f - \tau]}(t) \frac{\partial \mathcal{H}}{\partial E_\tau}(t + \tau), \quad \lambda_1(t_f) = 0, \\ \lambda'_2(t) &= -\frac{\partial \mathcal{H}}{\partial T}(t) - \chi_{[0, t_f - \tau]}(t) \frac{\partial \mathcal{H}}{\partial T_\tau}(t + \tau), \quad \lambda_2(t_f) = 0, \\ \lambda'_3(t) &= -\frac{\partial \mathcal{H}}{\partial N}(t), \quad \lambda_3(t_f) = 0, \\ \lambda'_4(t) &= -\frac{\partial \mathcal{H}}{\partial u}(t), \quad \lambda_4(t_f) = 0. \end{aligned} \quad (9.13)$$

Here $\chi_{[0, t_f - \tau]}$ denotes the indicator function of the interval $[0, t_f - \tau]$ and is defined by

$$\chi_{[0, t_f - \tau]} = \begin{cases} 1 & \text{if } t \in [0, t_f - \tau], \\ 0 & \text{otherwise.} \end{cases}$$

To minimize the Hamiltonian functional, Pontryagin's minimum principle [26] is used. Thus, we arrive at the following theorem:

Theorem 9.2 Let $(x^*, v^*) \in W^{1,\infty}([0, t_f], \mathbb{R}^4) \times L^\infty([0, t_f], \mathbb{R})$ be the optimal solutions of (9.8a)–(9.8g), where $x^* = [E^*, T^*, N^*, u^*]^T$. Then, there exist an adjoint state $\lambda(t) \in W^{1,\infty}([0, t_f], \mathbb{R}^4)$, defined by (9.13), such that the triple (x^*, v^*, λ) satisfies the state equation

$$\begin{aligned}\frac{dE^*(t)}{dt} &= \sigma + \frac{\rho E^*(t - \tau)T^*(t - \tau)}{\eta + T^*(t - \tau)} - \mu E^*(t - \tau)T^*(t - \tau) - \delta E^*(t) - a_1(1 - e^{-u^*})E^*(t), \\ \frac{dT^*(t)}{dt} &= r_2 T^*(t)(1 - \beta T^*(t)) - \mu E^*(t)T^*(t) - c_1 N^*(t)T^*(t) - a_2(1 - e^{-u^*(t)})T^*(t), \\ \frac{dN^*(t)}{dt} &= r_3 N^*(t)(1 - \beta_2 N^*(t)) - c_2 T^*(t)N^*(t) - a_3(1 - e^{-u^*(t)})N^*(t), \\ \frac{du^*(t)}{dt} &= v^*(t) - d_1 u^*(t),\end{aligned}\tag{9.14}$$

with the initial conditions

$$E^*(t) = \phi_1(t), \quad T^*(t) = \phi_2(t), \quad N^*(t) = \phi_3(t), \quad u(t) = \phi_4(t), \quad t \in [-\tau, 0],$$

the adjoint state equations

$$\begin{aligned}\lambda'_1(t) &= -1 + \lambda_1(t) \left[\delta + a_1(1 - e^{-u^*}) \right] + \lambda_2(t)nT^* + \lambda_1(t + \tau)\chi_{[0,t_f-\tau]} \left[\mu T^* - \frac{\rho T^*}{\eta + T^*} \right], \\ \lambda'_2(t) &= 1 + \lambda_2 \left[-r_2 + 2r_2\beta T^* + nE^* + c_1 N^* + a_2(1 - e^{-u^*}) \right] + \lambda_3 c_2 N^* \\ &\quad + \chi_{[0,t_f-\tau]}\lambda_1(t + \tau) \left[\frac{\rho E^* T^*}{(\eta + T^*)^2} - \frac{\rho E^*}{\eta + T^*} + \mu E^* \right], \\ \lambda'_3(t) &= \lambda_2 c_1 T^* - \lambda_3 \left(r_3 - 2r_3\beta_2 N^* - c_2 T^* - a_3(1 - e^{-u^*}) \right) - \gamma, \\ \lambda'_4(t) &= -\lambda_1(t)a_1 e^{-u^*} E^* + \lambda_2(t)a_2 e^{-u^*} T^* + \lambda_3(t)a_3 e^{-u^*} N^* + \lambda_4(t)d_1,\end{aligned}\tag{9.15}$$

with transversality conditions

$$\lambda_i(t_f) = 0, \quad i = 1, 2, 3, 4\tag{9.16}$$

and the optimal control

$$v^* = \min \left(v_{\max}, \frac{\lambda_4}{B_v} \right).\tag{9.17}$$

Proof The optimal control v^* can be solved from the optimality condition $\frac{\partial \mathcal{H}}{\partial v}(t) = 0$, i.e., $-B_v v + \lambda_4 = 0$. By using the handedness of the control set V_{ad} , it is easy to obtain v^* in the form of (9.17). \square

9.7 Immuno-Chemotherapy

Model (9.5) is extended to include an external source of immunotherapy treatment of the ECs such as ACI. We then add the term $w(t)s_1$ to represent the input rate of externally administered anti-tumor ECs, where $w(t)$ is the control parameter. Our goal is to maximize an objective functional J subject to the new model with a combination of chemotherapy and ACI and constraints on the control and the state

$$\max_{v, w \in W_{ad}} J(v, w) = \int_0^{t_f} \left(E(t) - T(t) - \left[\frac{B_v}{2}[v(t)]^2 + \frac{B_w}{2}[w(t)]^2 \right] \right) dt, \quad (9.18a)$$

subject to DDEs

$$\frac{dE(t)}{dt} = \sigma + \frac{\rho E(t-\tau)T(t-\tau)}{\eta + T(t-\tau)} - \mu E(t-\tau)T(t-\tau) - \delta E(t) - a_1(1 - e^{-u(t)})E(t) + w(t)s_1, \quad (9.18b)$$

$$\frac{dT(t)}{dt} = r_2 T(t)(1 - \beta T(t)) - n E(t)T(t) - c_1 N(t)T(t) - a_2(1 - e^{-u(t)})T(t), \quad (9.18c)$$

$$\frac{dN(t)}{dt} = r_3 N(t)(1 - \beta_2 N(t)) - c_2 T(t)N(t) - a_3(1 - e^{-u(t)})N(t), \quad (9.18d)$$

$$\frac{du(t)}{dt} = v(t) - d_1 u(t) \quad (9.18e)$$

and control constraints

$$0 \leq v(t) \leq v_{max} < \infty, \quad 0 \leq w(t) \leq w_{max} < \infty, \quad t \in [0, t_f], \quad (9.18f)$$

and the state constraint

$$k(N) = N - 0.75 \geq 0, \quad t \in [0, t_f], \quad (9.18g)$$

where B_w is a weight factor that describes a patient's acceptance level of immunotherapy and the set of all admissible controls W_{ad} is defined by

$$W_{ad} = \{(v, w) : (v, w) \text{ piecewise continuous, such that}$$

$$0 \leq v(t) \leq v_{max} < \infty, \quad 0 \leq w(t) \leq w_{max} < \infty, \quad \forall t \in [0, t_f]\}.$$

Similarly, the optimal solution of the optimization problem (9.18) satisfies the state equations

$$\begin{aligned}
\frac{dE^*(t)}{dt} &= \sigma + \frac{\rho E^*(t-\tau)T^*(t-\tau)}{\eta + T^*(t-\tau)} - \mu E^*(t-\tau)T^*(t-\tau) - \\
&\quad \delta E^*(t) - a_1(1-e^{-u^*})E^*(t) + w^*(t)s_1, \\
\frac{dT^*(t)}{dt} &= r_2 T^*(t)(1-\beta T^*(t)) - \mu E^*(t)T^*(t) - c_1 N^*(t)T^*(t) - a_2(1-e^{-u^*(t)})T^*(t), \\
\frac{dN^*(t)}{dt} &= r_3 N^*(t)(1-\beta_2 N^*(t)) - c_2 T^*(t)N^*(t) - a_3(1-e^{-u^*(t)})N^*(t), \\
\frac{du^*(t)}{dt} &= v^*(t) - d_1 u^*(t), \\
E^*(t) &= \phi_1(t), \quad T^*(t) = \phi_2(t), \quad N^*(t) = \phi_3(t), \quad u(t) = \phi_4(t), \quad t \in [-\tau, 0],
\end{aligned} \tag{9.19}$$

The adjoint state equations are

$$\begin{aligned}
\lambda'_1(t) &= -1 + \lambda_1(t) \left[\delta + a_1(1-e^{-u^*(t)}) \right] + \lambda_2(t)nT^*(t) + \lambda_1(t+\tau)\chi_{[0,t_f-\tau]} \left[\mu T^*(t) - \frac{\rho T^*(t)}{\eta + T^*(t)} \right] \\
\lambda'_2(t) &= 1 + \lambda_2 \left[-r_2 + 2r_2\beta T^*(t) + nE^*(t) + c_1 N^*(t) + a_2(1-e^{-u^*}) \right] + \lambda_3 c_2 N^*(t) \\
&\quad + \chi_{[0,t_f-\tau]}\lambda_1(t+\tau) \left[\frac{\rho E^*(t)T^*(t)}{(\eta + T^*(t))^2} - \frac{\rho E^*(t)}{\eta + T^*(t)} + \mu E^*(t) \right] \\
\lambda'_3(t) &= \lambda_2 c_1 T^*(t) - \lambda_3(t) \left(r_3 - 2r_3\beta_2 N^*(t) - c_2 T^*(t) - a_3(1-e^{-u^*(t)}) \right) - \gamma \\
\lambda'_4(t) &= -\lambda_1(t)a_1 e^{-u^*(t)}E^*(t) + \lambda_2(t)a_2 e^{-u^*(t)}T^*(t) + \lambda_3(t)a_3 e^{-u^*(t)}N^*(t) + \lambda_4(t)d_1,
\end{aligned} \tag{9.20}$$

with transversality conditions $\lambda_i(t_f) = 0$, $i = \{1, 2, 3, 4\}$ and the minimum condition

$$v^* = \min \left(v_{max}, \frac{\lambda_4}{B_v} \right), \quad w^* = \min \left(w_{max}, \frac{\lambda_1 s_1}{B_w} \right). \tag{9.21}$$

When $s_1 = 0$ (without immunotherapy), the system (9.19)–(9.21) reduces to system (9.14)–(9.17).

Remark 9.2 In the case of immunotherapy alone ($u(t) = 0$), the objective functional becomes

$$J(w) = \int_0^{t_f} \left(E(t) - T(t) - \frac{B_w}{2}[w(t)]^2 \right) dt. \tag{9.22}$$

9.8 Numerical Simulations of Optimal Control System

Numerical simulations leading to the approximation of the optimal controls (9.19)–(9.21) are carried out using the forward Euler method for the state system and backward difference approximation for the adjoint system. We assume a step-size h such that $\tau = mh$ and $t_f - t_0 = nh$, where $(m, b) \in \mathbb{N}^2$. We define the state, adjoint, and control variables at the mesh points. An initial guess is given for the controls v and w , which are then updated continuously until the objective functional satisfies the

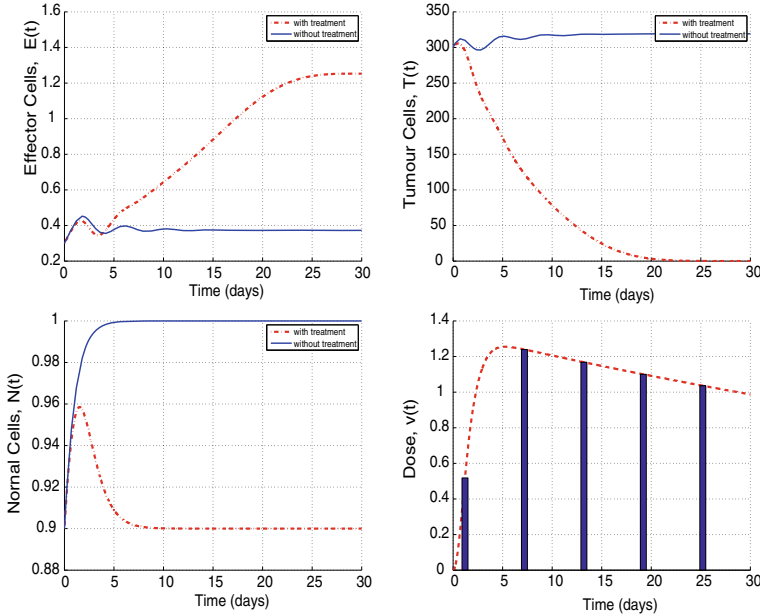


Fig. 9.5 Simulations of the system (9.14)–(9.17) in the stable region before and after the treatment with control with initial conditions $E_0 = 0.3$, $T_0 = 300$, and $N_0 = 0.9$; the parameter values are given in the text

conditions. However, there are several major problems to overcome when solving DDEs. These include stability, stiffness, and discontinuities in the right-hand side of the equation. Stability and stiffness can be handled by using the correct choice of implicit solvers [23]. The delay terms can create a whole suite of discontinuities; see [27, 28].

We choose a different set of parameter values (in stable and unstable regions). In the current simulations, we vary the three parameters σ , ρ , and τ , and fix the other parameters:

$$\delta = 0.2, \eta = 0.3, \mu = 0.003611, s_1 = 0.3, r_2 = 1.03, r_3 = 1, \beta = 2 \times 10^{-3}, \beta_2 = 1, n = 1,$$

$$c_1 = 0.00003, c_2 = 0.00000003, a_1 = 0.2, a_2 = 0.4, a_3 = 0.1, d_1 = 0.01, B = 100.$$

We then solve the optimality system to determine the optimal control situation (i.e., the drug strategy) and to predict the evolution of the tumor cells, ECs, and normal cells of each control strategy in 30 days.

Figure 9.5 shows the numerical simulations of the state system before and after chemotherapy treatment using the optimality system (9.14)–(9.17) when $\sigma = 0.5$, $\rho = 0.01$, and $\tau = 1.2$ (in the stable region). We note that in the presence of chemotherapy with optimal control, the effector cell population grows significantly,

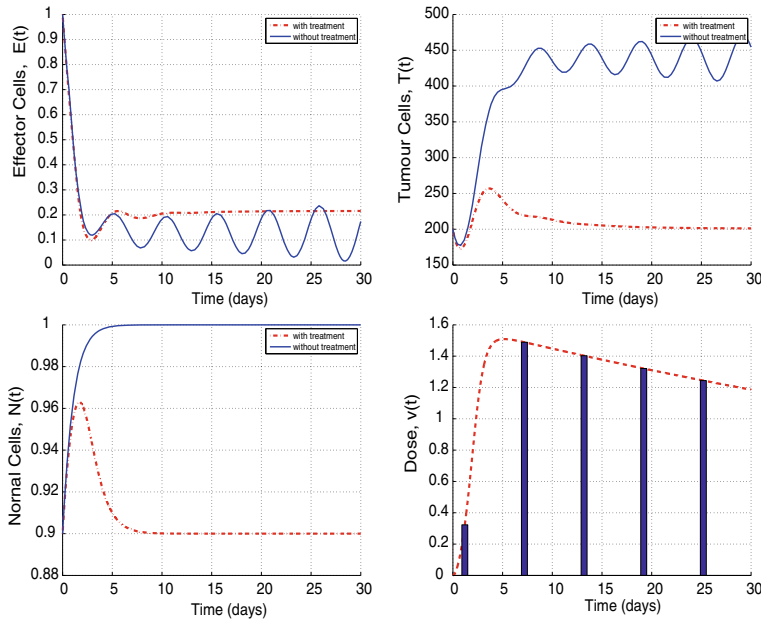


Fig. 9.6 Simulations of the system (9.14)–(9.17) in the unstable region before and after the treatment with control and initial conditions $E_0 = 1$, $T_0 = 200$, and $N_0 = 0.9$; the parameter values are given in the text

while the tumor cell population decreases and is totally eradicated after 20 days. In the meantime, the normal cell population remains over 75%. Figure 9.6 shows the impact of chemotherapy treatment (with optimal control) when we choose the parameter values in an unstable region ($\sigma = 0.2$, $\rho = 0.2$, and $\tau = 1.5$). The tumor and ECs populations are oscillating over time in the absence of chemotherapy, while the presence of treatment helps the immune system keep the growth of the tumor cells under its control.

Figure 9.7 presents the evolution of system (9.19)–(9.21) in the case of combination of chemotherapy and ACI. The parameter values are chosen to be in the stable region. We notice that the tumor cell population can be eradicated after day 12, which is faster compared to the results of Fig. 9.5 (when we used the chemotherapy alone). In other words, the numerical results show that using the combination immuno-chemotherapy is more effective than using chemotherapy treatment alone.

However, Fig. 9.8 shows the evolution of the system with only immunotherapy (i.e., without chemotherapy). We can notice from the figure that this case reflects the best therapeutic strategies for the treatment of tumor, where recovery becomes faster with a high dosage of immunotherapy and where $w(t)$ can reach a value of 3.5, compared to the combination therapy that only reached 2.

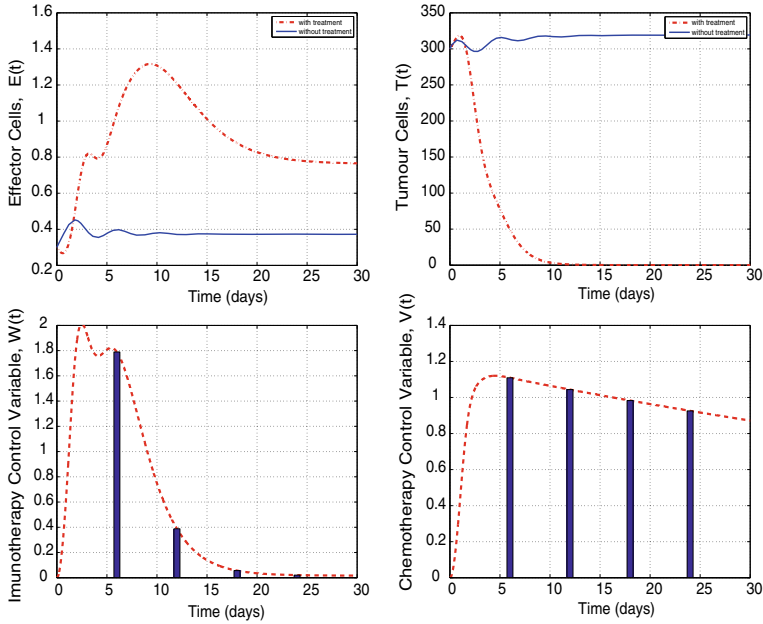


Fig. 9.7 Simulations of system (9.19)–(9.21), in the stable region, before and after the immunotherapy treatments with controls. It shows that the tumor cell population can be eradicated in day 12

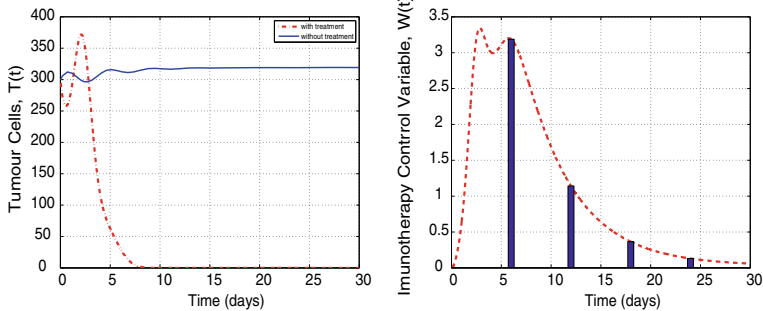


Fig. 9.8 Simulations of the tumor cells population of system (9.19)–(9.21), before and after immunotherapy with control. It shows that the tumor cells can be eradicated at day 7 with high immunotherapy dosage where the control value $w(t)$ reaches to the value of 3.5

9.9 Concluding Remarks

In this chapter, we have provided a delay differential model with control variables that describes the interactions of immune cells, tumor cells, normal cells, and immunotherapy treatment with control variables. A Pontryagin-type maximum principle is derived for retarded optimal control problems with delays in the state variable when the control system is subject to mixed control state constraints in order to minimize the cost of treatment, reduce the tumor cell load, and keep the number of normal cells above 75% of its carrying capacity. We presented an efficient numerical technique, based on forward difference approximation to the state system and backward difference scheme to the adjoint system, to solve the optimal control problem and identify the best treatment strategy when we adopt the chemotherapy treatment alone or a combination of chemo-immunotherapy, with minimum side effects. The numerical results show and confirm that the optimal treatment strategies reduce the tumor cell load and increase the population of ECs after a few days of therapy. The performance of combination therapy protocol was better than the standard protocol of chemotherapy alone. The numerical simulations show the rationality of the model presented, which, in some degree, reflects the practical scenario.

In the next chapter, we will study DDEs with ecological systems.

References

1. Kirschner, D., Panetta, J.: Modelling immunotherapy of the tumour-immune system interaction. *J. Math. Biol.* **38**, 235–252 (1998)
2. Kuznetsov, V.A., Makalkin, I.A., Taylor, M.A., Perelson, A.S.: Nonlinear dynamics of immunogenic tumors: parameter estimation and global bifurcation analysis. *Bull. Math. Biol.* **56**, 295–321 (1994)
3. de Pillis, L.G., Gu, W., Radunskaya, A.E.: Mixed immunotherapy and chemotherapy of tumors: modeling, applications and biological interpretations. *J. Theoret. Biol.* **238**(4), 841–862 (2006)
4. de Pillis, L.G., et al.: Optimal control of mixed immunotherapy and chemotherapy of tumors. *J. Biol. Syst.* **16**(1), 51–80 (2008)
5. Araujo, R., McElwain, D.: A history of the study of solid tumor growth: the contribution of mathematical modeling. *Bull. Math. Biol.* **66**, 1039–1091 (2004)
6. Bellomo, N., Li, N., Maini, P.: On the foundations of cancer modeling: selected topics, speculations, and perspectives. *Math. Mod. Methods Appl. Sci.* **18**, 593–646 (2008)
7. Byrne, H., Alarcon, T., Owen, M., Webb, S., Maini, P.: Modeling aspects of cancer dynamics: a review. *Philos. Trans. R. Soc. A* **364**, 1563–1578 (2006)
8. Chaplain, M.: Modelling aspects of cancer growth: insight from mathematical and numerical analysis and computational simulation. In: *Lecture Notes in Mathematics: Vol. 1940. Multiscale Problems in the Life Sciences*, pp. 147–200. Springer, Berlin (2008)
9. Martins, M., Ferreira, Jr, S.C., Vilela, M.: Multiscale models for the growth of avascular tumors. *Phys. Life Rev.* **4**, 128–156 (2007)
10. Nagy, J.: The ecology and evolutionary biology of cancer: a review of mathematical models of necrosis and tumor cells diversity. *Math. Biosci. Eng.* **2**, 381–418 (2005)
11. Roose, T., Chapman, S., Maini, P.: Mathematical models of avascular tumor growth. *SIAM Rev.* **49**, 179–208 (2007)

12. Yafia, R.: Dynamics analysis and limit cycle in a delayed model for tumor growth with quiescence. *Nonlinear Anal. Model. Contr.* **11**, 95–110 (2006)
13. Eftimie, R.: Interactions between the immune system and cancer: a brief review of non-spatial mathematical models. *Bull. Math. Biol.* **73**, 2–32 (2011)
14. Rihan, F.A., Abdelrahman, D.H.: Delay differential model for tumor-immune dynamics with HIV infection of CD4+ T-cells. *Int. J. Comput. Math.* **90**(3), 594–614 (2013)
15. Rihan, F.A., Muntaser, S., Abdeen, M.A., Abdelrahman, D.H.: Qualitative and computational analysis of a mathematical model for tumour-immune interactions. *J. Appl. Math.* **2012**, 19 (2012)
16. Rihan, F.A., Abdelrahman, D.H., Al-Maskari, F., Ibrahim, F., Abdeen, M.A.: Delay differential model for tumour-immune response with chemoimmunotherapy and optimal control. *Comput. Math. Methods Med.* **2014**, 15 (2014)
17. Rihan, F.A., Lakshmanan, S., Maurer, H.: Optimal control of tumour-immune model with time-delay and immuno-chemotherapy. *Appl. Math. Comput.* **353**, 147–165 (2019)
18. Castiglione, F., Piccoli, B.: Cancer immunotherapy, mathematical modeling and optimal control. *J. Theor. Biol.* **247**, 723–732 (2007)
19. Villasana, M., Radunskaya, A.: A delay differential equation model for tumour growth. *J. Math. Biol.* **47**, 270–294 (2003)
20. Bodnar, M., Forys, U., Poleszczuk, J.: Analysis of biochemical reactions models with delays. *J. Math. Anal. Appl.* **376**(1), 74–83 (2011)
21. Halanay, A.: Differential Equations, Stability, Oscillations, Time Lags. Academic, New York (1966)
22. de Pillis, L.G., Radunskaya, A.: A mathematical tumor model with immune resistance and drug therapy: an optimal control approach. *Comput. Math. Methods Med.* **3**, 78–100 (2001)
23. Rihan, F.A., Doha, E.H., Hassan, M.I., Kamel, N.M.: Mono-implicit Runge-Kutta method for delay differential equations. *J. Egypt. Math. Soc.* **17**(2), 213–232 (2009)
24. Meng, X., Jiao, J., Chen, L.: The dynamics of an age structured predator-prey model with disturbing pulse and time delays. *Nonlinear Anal.: Real World Appl.* **9**, 547–561 (2008)
25. Lukes, D.L.: Differential Equations: Classical to Controlled. Academic, New York (1982)
26. Onofrio, A.D., Manfredi, P., Salinelli, E.: Bifurcation thresholds in SIR model with information dependent vaccination. *Math. Model. Nat. Phenomena, Epidemiol.* **2**(1), 23 (2007)
27. Rihan, F.A.: Numerical Treatment of Delay Differential Equations in Bioscience. University of Manchester, UK (2000). PhD. Thesis
28. Rihan, F.A., Rihan, B.F.: Numerical modelling of biological systems with memory using delay differential equations. *Appl. Math. Inf. Sci.* **9**(3), 1615–1658 (2015)

Chapter 10

Delay Differential Equations of Ecological Systems with Allee Effect



10.1 Introduction

As it has been seen in previous chapters, delay differential equations exhibit much more complicated dynamics than ordinary differential equations since a time-delay could cause a stable equilibrium to become unstable and cause the populations to fluctuate. In this chapter, we study delay differential equations of prey-predator systems with the Allee effect. The dynamic relationship between the prey and their predators has long been and will continue to be one of the dominant themes in ecology due to its universal existence and importance (see, e.g., [1–4]). This relationship/interaction between two or more species has been essential in theoretical ecology since the famous Lotka-Volterra equations [5, 6], which are a system of first-order, non-linear differential equations that describe the dynamics and interactions between two or more species of biological systems. Of course, the qualitative properties of a prey-predator system, such as stability of the steady states, bifurcations analysis, and oscillation of the solutions usually depends on the system parameters; see [7].

Suppose that $N(t)$ is the size of prey population and let $P(t)$ be the size of the predator population at time t , then the Lotka-Volterra model is given by the following equations:

$$\frac{dN(t)}{dt} = N(t)[\beta_1 - \gamma_1 - g_1 N(t)] - eN(t)P(t), \quad \frac{dP(t)}{dt} = P(t)[- \gamma + eN(t)], \quad (10.1)$$

with $N(0) > 0$ and $P(0) > 0$. Here, β_1 is the per-capita maximum filtering rate, γ_1 is the death rate of the prey $N(t)$, and parameter g_1 denotes the strength of intra-specific competition. The predator death rate and predation rate are, respectively, denoted by γ and e . In the above model, it is assumed that prey population is subject to logistic growth rate and the exponential-type functional response. Of course, the response of predators to different prey densities depends on the feeding behavior of individual predators. In [8], Holling discussed three different types of functional responses:

Holling type I (linear), type II, type III, etc. These responses are used to model the phenomena of predation, which captures the usual properties, e.g., positivity and increasing; see also [9–11].

Allee effect and time-delays greatly increase the likelihood of local and global extinction and can produce a rich variety of dynamic effects. But how does the introduction of the Allee effect in the prey growth function change the system dynamics of prey-predator system? Before we introduce the final model, we provide brief preliminaries about the Allee effect and time-delays in the prey-predator model; see [12, 13]. The Allee effect was firstly reported by the American ecologist Allee [14] when he asked “*what minimal numbers are necessary if a species is to maintain itself in nature?*” Allee, in [14], shows that the growth rate is not always positive for small densities, and it may not be decreasing as in the logistic model either. In general, Allee effect mechanisms arise from cooperation or facilitation among individuals in the species [15]. A population is said to show an Allee effect if the growth rate per capita is initially an increasing function for the low density. The effect can be classified into two types: strong and weak. A strong Allee effect takes place when the population density is less than the specified threshold population considered, resulting in the species dying out. However, if the population density is greater than the threshold, the growth rate will remain positive [16]. A weak Allee effect means that the per-capita growth rate cannot go below zero and remains positive.

Now, we show how an Allee effect can be modeled and how the per-capita growth rate is affected by a weak Allee effect or a strong Allee effect using simple examples:

$$\frac{dN}{dt} = rN^2 \left(1 - \frac{N}{K}\right) \text{ for a weak Allee effect, and } \frac{dN}{dt} = rN \left(1 - \frac{N}{K}\right) \left(\frac{N}{A} - 1\right) \text{ for a strong.}$$

Figure 10.1 shows the per-capita growth rate $\frac{1}{N} \frac{dN}{dt}$ of the population with strong and weak Allee effects. The straight line shows the logistic growth, the red curve shows the weak Allee effect, and the blue curve shows the strong Allee effect. The negative density dependence at low population sizes is described as a strong Allee effect, where there exists a threshold population level A , such that for $N < A$, $\frac{1}{N} \frac{dN}{dt} < 0$ (the species will die out) and for $N > A$, $\frac{1}{N} \frac{dN}{dt} > 0$, the growth will remain positive [16]. However, when the growth rate remains positive at low population densities, it is considered as a weak Allee effect.

For multi-species models, there are flexible ways to formulate the Allee effect. For example, due to difficulties in finding mates when prey population density becomes low, the Allee effect takes place in prey species. Herein, we propose and incorporate an additive Allee effect of the form $b(N) \equiv \frac{N}{\alpha_1 + N}$ in the prey growth function of model (10.1), which is considered as the probability of finding a mate (see [17]) so that

$$\frac{dN(t)}{dt} = N(t) \left[\frac{\beta_1 N(t)}{\alpha_1 + N(t)} - \gamma_1 - gN(t) \right] - eN(t)P(t), \quad \frac{dP(t)}{dt} = P(t)[- \gamma + eN(t)]. \quad (10.2)$$

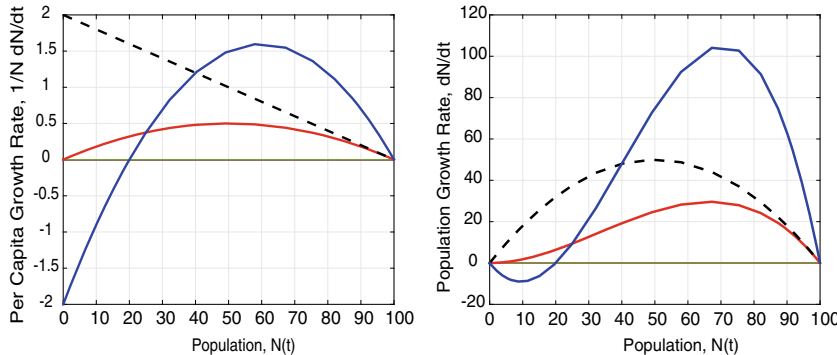


Fig. 10.1 (left) Per-capita growth rate $\frac{1}{N} \frac{dN}{dt}$ versus population $N(t)$ with logistic (black dashes), strong (blue curve), and weak (red curve) Allee effect. (right) Population growth rate $\frac{dN}{dt}$ versus population $N(t)$. For the strong Allee effect, the y-intercept of the per-capita growth rate is less than zero at zero density, while in the weak Allee effect, the y-intercept cannot go below zero

The parameter α_1 is the strength of the Allee effect, $\alpha_1 = 1/R$, where R is the average area that can be searched by an individual [18]. We may notice that $b(0) = 0, b'(N) > 0$ if $N \in [0, \infty)$, i.e., the Allee effect decreases as density increases. $\lim_{N \rightarrow \infty} b(N) = 1$ means that the Allee effect disappears at high densities. Therefore, the term $b(N)$ is considered as a weak Allee effect function in a rectangular hyperbola form, known as Michaelis-Menten-like function [19].

Usually, the individuals of the prey and predator species pass through various stages during their entire life span and the morphology involved differs from one stage to another. Construction of DDE models is a well-known modeling strategy to take care of the stage-specific activities, which are responsible for significant changes in the dynamics of interacting populations. In various existing literature, biological processes such as incubation, gestation, maturation, reaction time, etc., are taken care of by introducing relevant time-delay parameters to the models for prey-predator and other types of interacting populations. Incorporating time-lags (or time-delays) in biological models makes the systems much more realistic, as it can destabilize the equilibrium points and give rise to a stable limit cycle, causing oscillations to grow and enriching the dynamics of the model. Time-delays have been actively studied by many authors in prey-predator models and biological systems; see [19–22].

Thus, it is interesting and important to study the impact of time-delays and the Allee effect on the dynamics of three-species prey-predator models. In this chapter, we extend the work of [23] and study the dynamics of a two-prey one-predator system, where the growth of both prey populations is subject to the Allee effect, and there exists direct competition between the two-prey species having a common predator. Two discrete time-delays τ_1, τ_2 are incorporated into the predator growth equation to represent the reaction time with each prey. Sensitivity analysis to evaluate the uncertainty of the state variables to small changes in the Allee parameters

is also considered. Model formulation is presented in Sect. 10.2. Local stability and bifurcation analysis of the steady states are discussed in Section 10.3, and global asymptotic stability of interior steady state is discussed in Section 10.4. We also utilize sensitivity functions to evaluate the sensitivity (uncertainty) of the state variables (prey and predator populations) to small changes in the severity Allee parameters through Section 10.5. Some numerical simulations are presented in Section 10.6, and we conclude the chapter in Section 10.7.

10.2 Delay Differential Model of Two-Prey One-Predator System

Many studies have been performed in modeling the dynamics of multi-species prey-predator systems, including local and global bifurcations and different types of chaos (see e.g., [23–26]). Sen et al. [23] discussed the Allee effect on the growth function of two preys, where the predator is generalized. They explained how the Allee effect can suppress the chaotic dynamics and the route to chaos in prey growth by comparing it with a model without the Allee effect. In [24], the authors studied the dynamics of a three-species (two preys and one predator) delayed prey-predator model with cooperation among the preys against predation. The growth rate for preys is thought to be logistic. Delays are taken only in the growth components for each of the species. Takeuchi et al. [25] considered two preys with logistic growth rates and an exponential functional response, where the predator survives on two-prey populations. Their results showed that the apparent chaotic behavior is a result of the periodic solution when one of the two preys has greater competitive strength compared to the other. Song et al. [26] explored the dynamic behavior of a Holling II two-prey one-predator system by introducing constant periodic releases of predators via periodically spraying a pesticide on the prey. They were then able to show that the system remains permanent under certain conditions.

Herein, we generalize model (10.2) to multi-species prey-predator system (two-prey one-predator). The model consists of two teams of preys with densities $x(t)$, $y(t)$, interacting with one team of predators with density $z(t)$. We also incorporate the Allee effect in the growth functions of the two-prey populations, and there exists a direct competition between the two-prey species having a common predator. The model takes the general form

$$\begin{aligned} \frac{dx(t)}{dt} &= x(t) \left[\frac{\beta_1 x(t)}{\alpha_1 + x(t)} - \gamma_1 - g_1 x(t) \right] - \alpha x(t)y(t) - ex(t)z(t) \\ \frac{dy(t)}{dt} &= y(t) \left[\frac{\beta_2 y(t)}{\alpha_2 + y(t)} - \gamma_2 - g_2 y(t) \right] - \beta x(t)y(t) - \frac{\delta y(t)z(t)}{1 + cy(t)} \\ \frac{dz(t)}{dt} &= -\beta_3 z(t) + \epsilon ex(t - \tau_1)z(t - \tau_1) + \frac{\epsilon \delta y(t - \tau_2)z(t - \tau_2)}{1 + cy(t - \tau_2)} \end{aligned} \quad (10.3)$$

with initial conditions

Table 10.1 One biological meaning for the parameters of model (10.3)

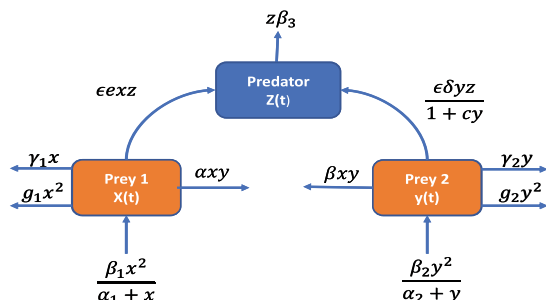
| Parameter | Description |
|----------------------|---|
| α_1, α_2 | Strength of Allee effect |
| β_1, β_2 | Per-capita maximum filtering rate of population |
| g_1, g_2 | Strength of intra competition |
| γ_1, γ_2 | Death rate for preys |
| α, β | Coefficient of competition |
| e, δ | Decrease rate of $x(t)$ and $y(t)$ due to predation by $z(t)$ |
| β_3 | Predator death rate |
| c | Magnitude of interference between the second type of prey |
| ϵ | An equal transformation rate of predator to preys $x(t)$ and $y(t)$ |

$$x(\theta) = \phi_1(\theta) > 0, \quad y(\theta) = \phi_2(\theta) > 0, \quad z(\theta) = \phi_3(\theta) > 0, \quad \theta \in [-\tau, 0], \quad \tau = \max\{\tau_1, \tau_2\}. \quad (10.4)$$

Here, $\phi_i(\theta)$ ($i = 1, 2, 3$) are smooth initial functions. The coefficients α and β represent the coefficients of competition of two preys x and y in the absence of a predator. The description of the rest of model parameters along with their symbols is presented in Table 10.1.

It is reasonable to assume that the death (predation) of preys is instantaneous when attacked by their predator, but their contribution to the growth of predator population must be delayed by some time-delay. Therefore, we incorporated two discrete time-delays τ_1 and τ_2 in the reaction response functionals in the predator growth to represent the reaction time. The interaction between the first species of prey and predator is assumed to be governed by Holling type I. While the interaction between the second species of prey and predator is assumed to be governed by Holling type II (cytoid functional) $\delta y(t)z(t)/(1 + cy(t))$, the response indicates that it is a hard-to-capture prey compared to the first species; see Fig. 10.2.

To investigate the role of the time-delay and Allee effect on the dynamics of the system, we first discuss the boundedness and positivity of the solutions of the system (10.3) with the given positive initial conditions (10.4).

Fig. 10.2 Mathematical scheme of the three-species predator-prey system (10.3)

10.2.1 Positivity and Boundedness of the Solution

The positivity of the solutions indicates the existence of the population, while the boundedness explains the natural control of growth due to the restriction of resources. We arrive at the following lemma:

Lemma 10.1 *Every solution of system (10.3) corresponding to initial conditions (10.4) defined on $[0, \infty)$ remains positive for all $t \geq 0$, which satisfies*

$$\limsup_{t \rightarrow \infty} (x(t) + y(t)) \leq \kappa, \quad \limsup_{t \rightarrow \infty} z(t) \leq N,$$

where $\kappa = \min\{\beta_1, \beta_2\}$ and $N > 0$.

Proof Model (10.3) can be represented in a matrix form:

$$\dot{U}(t) = F(U) \quad (10.5)$$

where $U = (x, y, z)^T \in \mathbb{R}^3$, and

$$F(U) = \begin{bmatrix} F_1(U) \\ F_2(U) \\ F_3(U) \end{bmatrix} = \begin{bmatrix} x \left(\frac{\beta_1 x}{\alpha_1 + x} - \gamma_1 - g_1 x \right) - \alpha x y - e x z \\ y \left(\frac{\beta_2 y}{\alpha_2 + y} - \gamma_2 - g_2 y \right) - \beta x y - \frac{\delta y z}{1 + c y} \\ -\beta_3 z + e x (t - \tau_1) z (t - \tau_1) + \frac{\epsilon \delta y (t - \tau_2) z (t - \tau_2)}{1 + c y (t - \tau_2)} \end{bmatrix}.$$

Let $\mathbb{R}_+^3 = [0, \infty)^3$, since the right-hand side of system (10.3) is locally Lipschitz on $C : \mathbb{R}_+^{3+1} \rightarrow \mathbb{R}^3$, such that $F_i(U)|_{u_i(t)=0, U \in \mathbb{R}_+^3} \geq 0$, where $u_1 = x$, $u_2 = y$, and $u_3 = z$. According to [27], the solutions of (10.5) with initial conditions (10.4) exist uniquely on the interval $[0, \xi]$, where $0 < \xi \leq \infty$; therefore, all solutions exist on the first quadrant of the xyz -plane.

To prove the boundedness of solutions for system (10.3), let us first consider the case when the predator is absent so that

$$\begin{aligned} \frac{dx}{dt} &= x \left(\frac{\beta_1 x}{\alpha_1 + x} - \gamma_1 - g_1 x \right) - \alpha x y \equiv G_1(x, y), \\ \frac{dy}{dt} &= y \left(\frac{\beta_2 y}{\alpha_2 + y} - \gamma_2 - g_2 y \right) - \beta x y \equiv G_2(x, y). \end{aligned} \quad (10.6)$$

With initial conditions $x(0) > 0$ and $y(0) > 0$, we can easily show that $G_1(x, y) \geq 0$ for $y = 0$ and $x < \frac{\beta_1 - \gamma_1}{g_1}$, such that $\beta_1 > \gamma_1$ and $G_2(x, y) \geq 0$ for $x = 0$ and $y < \frac{\beta_2 - \gamma_2}{g_2}$, where $\beta_2 > \gamma_2$. Adding the two equations of (10.6) yields

$$\begin{aligned}
\frac{d}{dt}(x+y) &= x\left(\frac{\beta_1 x}{\alpha_1 + x} - \gamma_1 - g_1 x\right) + y\left(\frac{\beta_2 y}{\alpha_2 + y} - \gamma_2 - g_2 y\right) - xy(\alpha + \beta) \\
&\leq x(\beta_1 - \gamma_1 - g_1 x) + y(\beta_2 - \gamma_2 - g_2 y) \\
&\leq \beta_1 x + \beta_2 y \leq \kappa(x+y)
\end{aligned} \tag{10.7}$$

where $\kappa = \min\{\beta_1, \beta_2\}$. If we integrate both sides of (10.7), we get

$$(x(t) + y(t)) \leq (x(0) + y(0))e^{-\kappa t}.$$

Since $(x(0) + y(0)) > 0$, the solutions are bounded, which clearly shows that $\lim_{t \rightarrow \infty} \sup(x(t) + y(t)) \leq \kappa$.

To extend the analysis to (10.3), let us consider $0 < \phi_1(\theta) + \phi_2(\theta) + \phi_3(0) < M$, $\theta \in [-\tau, 0]$. Additionally, assume that $W(t) = \epsilon x(t - \tau_1) + \epsilon \delta y(t - \tau_2) + z$ and choose $0 < \rho < \beta_3$. By considering the derivative of W , for $t > T + \tau$ for some fixed positive time T , we have

$$\frac{dW}{dt} + \rho W \leq \epsilon x(t - \tau_1)(\beta_1 + \rho - x(t - \tau_1)) + \epsilon \delta y(t - \tau_2)(\beta_2 + \rho - y(t - \tau_2)) + (\rho - \beta_3)z.$$

Since x and y are non-negative and bounded by κ ,

$$\frac{dW}{dt} + \rho W \leq (\epsilon + \epsilon \delta) \kappa + (\rho - \beta_3)z \leq M.$$

Due to the positivity of z and the parametric condition exists for ρ , the differential inequality is bounded above, such that $\frac{dW}{dt} \leq M - \rho W$, i.e., there exists N where $0 < W(t) < N$ for all $t > T$, which implies the boundedness of z , such that $\lim_{t \rightarrow \infty} \sup z(t) \leq N$. \square

10.3 Local Stability and Hopf Bifurcation

In this section, we investigate the qualitative behavior of system (10.3) by studying the local stability of positive equilibria points and Hopf bifurcation analysis, which provides a deeper insight into the model to address the behavioral change of solutions as a response to changes in a particular parameter. Since time-lags τ_1 and τ_2 have a significant impact on the complexity and dynamics of the model, we consider them as bifurcation parameters.

10.3.1 Existence of Interior Equilibrium Points

System (10.3) has some boundary and interior equilibrium points. However, we only focus on the dynamic analysis of interior equilibrium points. To obtain the attainable equilibrium points for the system (10.3), the zero growth isolines of the system are given by $x \left(\frac{\beta_1 x}{\alpha_1 + x} - \gamma_1 - g_1 x \right) - \alpha x y - e x z = 0$, $y \left(\frac{\beta_2 y}{\alpha_2 + y} - \gamma_2 - g_2 y \right) - \beta x y - \frac{\delta y z}{1 + c y} = 0$ and $-\beta_3 z + \epsilon e x z + \frac{\epsilon \delta y z}{1 + c y} = 0$, in $\mathbb{R}_+^3 = \{(x, y, z) \in \mathbb{R}^3 : x, y, z \geq 0\}$. Therefore, the equilibria are the points of intersection of these zero growth isolines regardless of the parameter values.

An interior equilibrium point $\mathcal{E}^* \equiv (x^*, y^*, z^*)$ exists with $\left(\frac{\beta_1 x^*}{\alpha_1 + x^*} - \gamma_1 - g_1 x^* \right) - \alpha y^* - e z^* = 0$, $\left(\frac{\beta_2 y^*}{\alpha_2 + y^*} - \gamma_2 - g_2 y^* \right) - \beta x^* - \frac{\delta z^*}{1 + c y^*} = 0$, $-\beta_3 + \epsilon e x^* + \frac{\epsilon \delta y^*}{1 + c y^*} = 0$, such that $x^* = \frac{1}{\epsilon e} (\beta_3 - \frac{\epsilon \delta y^*}{1 + c y^*}) > 0$, $z^* = \frac{1}{e} \left(\frac{\beta_1 (\beta_3 (1 + c y^*) - \epsilon \delta y^*)}{(1 + c y^*)(\epsilon e + \beta_3)} + g_1 (\beta_3 - \frac{\epsilon \delta y^*}{1 + c y^*}) - \gamma_1 - \alpha y^* \right) > 0$, where y^* is the root(s) to the following equation:

$$G(y) = \sigma_1 y^4 + \sigma_2 y^3 + \sigma_3 y^2 + \sigma_4 y + \sigma_5 = 0. \quad (10.8)$$

The coefficients σ_i , $i = 1, \dots, 5$ are defined by

$$\begin{aligned} \sigma_1 &= \alpha_2 c^2, \quad \sigma_2 = c(2\alpha_2 + \alpha_2 c g_2 + \frac{\beta \beta_2 c}{\epsilon e} - \frac{\beta \delta}{e} - \delta \alpha + c \gamma_2), \\ \sigma_3 &= \frac{\beta_1 \delta^2 \epsilon - c \delta \beta_1 \beta_2}{\epsilon e + \beta_3} + \frac{\alpha_2 \beta \delta \epsilon c - \beta \beta_2 \alpha_2 c^2 - \beta \delta \epsilon}{\epsilon e} - \delta^2 \epsilon g_1 + c \beta_2 \\ &\quad + c^2 \beta_2 + c g_1 \delta \beta_3 + c \delta \gamma_1 + \alpha_2 - \delta \alpha, \\ \sigma_4 &= \frac{\beta \beta_2 - \alpha_2 \beta \delta \epsilon}{\epsilon e} + \frac{\delta \beta_1 \beta_2 + c \delta \beta_1 \beta_3 \alpha_2 + \beta_1 \alpha_2 \delta^2}{\epsilon e + \beta_3} - g_1 \alpha_2 \delta^2 \epsilon \\ &\quad + c \alpha_2 \delta \beta_3 g_1 + c \alpha_2 \delta \gamma_1 + c \alpha_2 \gamma_2 - \beta_2 - \beta_2 c + \alpha_2 g_2 - \delta \beta_2 g_1 - \delta \gamma_1 + \gamma_2, \\ \sigma_5 &= \frac{\delta \beta_1 \beta_3 \alpha_2}{\epsilon e + \beta_3} - \frac{\alpha_2 \beta_2 \beta}{\epsilon e} - \alpha_2 \delta \beta_3 g_1 - \alpha_2 \delta \gamma_1 + \alpha_2 \gamma_2. \end{aligned}$$

The nature of the roots for (10.8) is determined by noting the sign of its discriminant [28]. Therefore, a sufficient condition that guarantees that (10.8) has at least one positive root is $\sigma_5 < 0$, which leads to $\frac{\delta \beta_1 \beta_3 \alpha_2}{\epsilon e + \beta_3} + \alpha_2 \gamma_2 < \frac{\alpha_2 \beta_2 \beta}{\epsilon e} + \alpha_2 \delta \beta_3 g_1 + \alpha_2 \delta \gamma_1$. Thus, system (10.3) can have, at most, four interior equilibria in the presence of an Allee effect. However, in the absence of an Allee effect, we arrive at the following remark.

Remark 10.1 In the absence of an Allee effect ($\alpha_1 = \alpha_2 = 0$), the interior equilibria for system (10.3) are reduced to, at most, three interior equilibria. Consequently, an Allee effect can generate or eradicate interior equilibria. It may stabilize or destabilize the system.

10.3.2 Stability and Bifurcation Analysis of the Interior Equilibrium

Now, we examine the stability of the interior equilibrium $\mathcal{E}^* \equiv (x^*, y^*, z^*)$ at which the Jacobian matrix is

$$J = \begin{bmatrix} F_1 & F_2 & F_3 \\ F_4 & F_5 & F_6 \\ I_1 e^{-\lambda \tau_1} & I_2 e^{-\lambda \tau_2} & F_7 + I_3 e^{-\lambda \tau_1} + I_4 e^{-\lambda \tau_2} \end{bmatrix}.$$

Here,

$$\begin{aligned} F_1 &= \frac{\beta_1 x^*}{(\alpha_1 + x^*)} \left(1 + \frac{\alpha_1}{(\alpha_1 + x^*)} \right) - 2g_1 x^* - \gamma_1 - \alpha y^* - \epsilon z^* < 0, \quad F_2 = -\alpha x^*, \quad F_3 = -\epsilon x^*, \\ F_4 &= -\beta y^*, \quad F_5 = \frac{\beta_2 y^*}{(\alpha_2 + y^*)} \left(1 + \frac{\alpha_2}{(\alpha_2 + y^*)} \right) - 2g_2 y^* - \gamma_2 - \beta x^* - \frac{\delta z^*}{(1 + c y^*)^2} < 0, \\ F_6 &= -\frac{\delta y^*}{1 + c y^*}, \quad F_7 = -\beta_3, \quad I_1 = \epsilon \epsilon z^*, \quad I_2 = \frac{\epsilon \delta z^*}{(1 + c y^*)^2}, \quad I_3 = \epsilon \epsilon x^*, \quad I_4 = \frac{\epsilon \delta y^*}{1 + c y^*}. \end{aligned}$$

The characteristic equation for the interior point $\mathcal{E}^* \equiv (x^*, y^*, z^*)$ is then given by

$$A(\lambda) + B(\lambda)e^{-\lambda \tau_1} + C(\lambda)e^{-\lambda \tau_2} = 0. \quad (10.9)$$

Here,

$$\begin{aligned} A(\lambda) &= \lambda^3 + R_1 \lambda^2 + R_2 \lambda + R_3 \\ B(\lambda) &= N_1 \lambda^2 + N_2 \lambda + N_3 \\ C(\lambda) &= M_1 \lambda^2 + M_2 \lambda + M_3, \end{aligned}$$

such that

$$\begin{aligned} R_1 &= -F_1 - F_5 - F_7, \quad R_2 = F_1 F_5 + F_1 F_7 + F_5 F_7 - F_2 F_4, \quad R_3 = F_2 F_4 F_7 - F_1 F_5 F_7, \\ N_1 &= -I_3, \quad N_2 = (F_1 + F_5)I_3 - F_3 I_1, \quad N_3 = F_2 F_4 I_3 + F_3 F_5 I_1 - F_2 F_6 I_1 - F_1 F_5 I_3, \\ M_1 &= -I_4, \quad M_2 = (F_1 + F_5)I_4 - F_6 I_2, \quad M_3 = F_2 F_4 I_4 + F_1 F_6 I_2 - F_3 F_4 I_2 - F_1 F_5 I_4. \end{aligned}$$

To gain an insight into the interior equilibrium \mathcal{E}^* , we discuss the stability of interior steady states and Hopf bifurcation conditions of the threshold parameters τ_1 and τ_2 by considering the following different cases:

Case (1): When $\tau_1 = \tau_2 = 0$, Eq. (10.9) becomes

$$\lambda^3 + (R_1 + N_1 + M_1)\lambda^2 + (R_2 + N_2 + M_2)\lambda + (R_3 + N_3 + M_3) = 0. \quad (10.10)$$

Therefore, the interior equilibrium \mathcal{E}^* is locally asymptotically stable if

- $(H_1) \quad R_1 + N_1 + M_1 > 0, \quad R_3 + N_3 + M_3 > 0 \quad \& \quad (R_1 + N_1 + M_1)(R_2 + N_2 + M_2) > R_3 + N_3 + M_3$ hold.

Thus, based on Routh-Hurwitz Criteria, all the roots of (10.10) have negative real parts.

Case (2): For $\tau_1 = 0, \tau_2 > 0$, then Eq. (10.9) becomes

$$\lambda^3 + (R_1 + N_1)\lambda^2 + (R_2 + N_2)\lambda + (R_3 + N_3) + (M_1\lambda^2 + M_2\lambda + M_3)e^{-\lambda\tau_2} = 0. \quad (10.11)$$

We assume for some values of ($\tau_2 > 0$) that there exists a real number ω such that $\lambda = i\omega$ is a root of (10.11); then, we obtain

$$\begin{aligned} -(R_1 + M_1)\omega^2 + (R_3 + N_3) &= (M_1\omega^2 - M_3) \cos \omega\tau_2 - M_2\omega \sin \omega\tau_2 \\ -\omega^3 + (R_2 + N_2)\omega &= (M_3 - M_1\omega^2) \sin \omega\tau_2 - M_2\omega \cos \omega\tau_2. \end{aligned} \quad (10.12)$$

Squaring and adding both of the equations yields the following:

$$\omega^6 + a_1\omega^4 + a_2\omega^2 + a_3 = 0, \quad (10.13)$$

where

$$\begin{aligned} a_1 &= (R_1 + M_1)^2 - 2(R_2 + N_2) - M_1^2, \\ a_2 &= (R_2 + N_2)^2 - 2(R_1 + M_1)(R_3 + N_3) + 2M_1M_3 - M_2^2, \quad a_3 = (R_3 + N_3)^2 - M_3^2. \end{aligned} \quad (10.14)$$

By Descartes' rule of signs, Eq.(10.13) has at least one positive root ω_1 if

- $(H_2) \quad R_1^2 + 2R_1M_1 > 2(R_2 + N_2) \quad \text{and} \quad (R_3 + N_3)^2 < M_3^2$ hold.
Eliminating $\sin \omega_1 \tau_2$ from (10.12) yields the following:

$$\tau_{2,j} = \frac{1}{\omega_1} \arccos \left[\frac{((R_3 + N_3) - (R_1 + N_1)\omega_1^2)(M_1\omega_1^2 - M_3) + M_2(R_2 + N_2)\omega_1^2 - M_2\omega_1^4}{(M_3 - M_1\omega_1^2)^2 - (M_2\omega_1)^2} \right] + \frac{2j\pi}{\omega_1} \quad (10.15)$$

where $j = 0, 1, 2, \dots$

By differentiating (10.11) with respect to τ_2 , such that $\omega = \omega_1$ and $\tau_2 = \tau_{2,j}$, the transversality condition can be obtained in this form:

$$\operatorname{Re}\left(\frac{d\lambda}{d\tau_2}\right)^{-1} = \frac{A_1A_4 - A_2A_3}{A_2A_4}. \quad (10.16)$$

Here,

$$\begin{aligned} A_1 &= [(R_2 + N_2) - 3\omega_1^2][(R_2 + N_2)\omega_1^2 - \omega_1^4] + 2(R_1 + N_1)\omega_1[(R_3 + N_3)\omega_1 - (R_1 + N_1)\omega_1^3], \\ A_2 &= (\omega_1^4 - (R_2 + N_2)\omega_1^2)^2 + ((R_3 + N_3)\omega_1 - (R_1 + N_1)\omega_1^3)^2, \\ A_3 &= M_2^2\omega_1^2 + 2(M_1\omega_1^3 - M_3\omega_1)M_1\omega_1, \\ A_4 &= (M_2\omega_1^2)^2 + (M_3\omega_1 - M_1\omega_1^3)^2. \end{aligned}$$

Then, a Hopf bifurcation occurs for τ_2 if $\operatorname{Re}(\frac{d\lambda}{d\tau_2})^{-1} > 0$; i.e., $A_1 A_4 > A_2 A_3$. We arrive at the following theorem:

Theorem 10.1 *Let (H_1) – (H_2) hold, where $\tau_1 = 0$, then there exists $\tau_2 > 0$ such that \mathcal{E}^* remains stable for $\tau_2 < \tau'_2$ and unstable for $\tau_2 > \tau'_2$, where $\tau'_2 = \min\{\tau_{2,j}\}$ defined by (10.15). Moreover, system (10.3) undergoes a Hopf bifurcation at \mathcal{E}^* when $\tau_2 = \tau'_2$.*

Case (3): When $\tau_2 = 0$, $\tau_1 > 0$, in the same manner as that of the previous case, we arrive at the following theorem:

Theorem 10.2 *For system (10.3), with $\tau_2 = 0$, there exists a positive number τ_1 , such that the equilibrium point \mathcal{E}^* is locally asymptotically stable for $\tau_1 < \tau'_1$ and unstable for $\tau_1 > \tau'_1$, where $\tau'_1 = \min\{\tau_{1,j}\}$. Furthermore, Hopf bifurcation occurs at $\tau_1 = \tau'_1$.*

$$\tau_{1,j} = \frac{1}{w_0} \arccos \left[\frac{((R_3 + M_3) - (R_1 + M_1)w_2^2)(N_1 w_2^2 - N_3) - N_2(R_2 + M_2)w_2^2 + N_2 w_2^4}{(N_1 w_2^2 - N_3)^2 + (N_2 w_2)^2} \right] + \frac{2j\pi}{w_2} \quad (10.17)$$

where $j = 0, 1, 2, \dots$.

Case (4): When $\tau_1 > 0$ and $\tau_2 > 0$, we assume that τ_1 is a variable parameter and τ_2 is fixed on its stable interval. Let $\lambda = iw$ as a root of (10.9). Separating the real and imaginary parts,

$$\begin{aligned} -w^3 + R_2 w + (M_1 w^2 - M_3) \sin w\tau_2 + M_2 w \cos w\tau_2 \\ = (N_3 - N_1 w^2) \sin w\tau_1 - N_2 w \cos w\tau_1, \end{aligned} \quad (10.18)$$

$$\begin{aligned} -R_1 w^2 + R_3 + (M_3 - M_1 w^2) \cos w\tau_2 + M_2 w \sin w\tau_2 \\ = (N_1 w^2 - N_3) \cos w\tau_1 - N_2 w \sin w\tau_1. \end{aligned} \quad (10.19)$$

Thus, eliminating the trigonometric functions ($\sin w\tau_1$ and $\cos w\tau_1$) from (10.18) and (10.19) yields the following:

$$w^6 + \xi_4 w^5 + \xi_3 w^4 + \xi_2 w^3 + \xi_1 w^2 + \xi_0 = 0, \quad (10.20)$$

where

$$\begin{aligned} \xi_4 &= -2M_1 \sin w\tau_2, \\ \xi_3 &= R_1 + M_1^2 - 2R_2 - N_1^2 - 2M_2 \cos w\tau_2, \\ \xi_2 &= 2(M_1 R_2 + M_3) \sin w\tau_2 - 2M_3 R_1 \cos w\tau_2, \\ \xi_1 &= -2M_3 R_2 \sin w\tau_2, \\ \xi_0 &= R_3^2 + M_3^2 - N_3^2 + (2M_3 R_3 + R_1 M_1) \cos w\tau_2. \end{aligned}$$

Equation (10.20) is a preternatural equation in a complicated form, and it is quite difficult to predict the nature of its roots. Thus, by applying Descartes' rule of signs we can say that (10.20) has at least one positive root ω_0 if

- (H_3) $\xi_4 > 0$ since $M_1 < 0$ & $\xi_0 < 0$; therefore, we have

$$\tau_{1,j} = \frac{1}{w_0} \arccos \left[\frac{AD + CB}{A^2 + C^2} \right] + \frac{2j\pi}{w_0}, \quad j = 0, 1, 2, \dots \quad (10.21)$$

Here,

$$\begin{aligned} A &= N_1 w_0^2 - N_3, \quad B = -w_0^3 + R_2 w_0 + (M_3 - M_1 w_0^2) \sin w_0 \tau_2 + \cos w_0 \tau_2, \\ C &= N_2 w_0, \quad D = -R_1 w_0^2 + R_3 + (M_1 w_0^2 - M_3) \cos w_0 \tau_2 + M_2 w_0 \sin w_0 \tau_2. \end{aligned}$$

To study the Hopf bifurcation analysis, we fix τ_2 in its stable interval and differentiate Equations (10.18) and (10.19) with respect to τ_1 . Substituting $\tau_1 = \tau_{1,0}$ and $w = w_0$, we have

$$\begin{aligned} Q_2 \left(\frac{d(\Re \lambda)}{d\tau_1} \right) \Big|_{\tau_1=\tau_{1,0}} + Q_1 \left(\frac{d(w)}{d\tau_1} \right) \Big|_{\tau_1=\tau_{1,0}} &= Q_3 \\ -Q_1 \left(\frac{d(\Re \lambda)}{d\tau_1} \right) \Big|_{\tau_1=\tau_{1,0}} + Q_2 \left(\frac{d(w)}{d\tau_1} \right) \Big|_{\tau_1=\tau_{1,0}} &= Q_4, \end{aligned} \quad (10.22)$$

where

$$\begin{aligned} Q_1 &= -3w_0^2 + R_2 + (2N_1 w_0 - N_2 w_0 \tau_{1,0}) \sin w_0 \tau_{1,0} + (N_2 + N_1 \tau_1 w_0^2 - N_3 \tau_{1,0}) \cos w_0 \tau_{1,0} \\ &\quad + (2w_0 M_1 - M_2 \tau_2 w_0) \sin w_0 \tau_2 + (M_1 \tau_2 w_0^2 - M_3 \tau_2 + M_2) \cos w_0 \tau_2, \\ Q_2 &= -2R_1 w_0 + (N_1 w_0^2 \tau_{1,0} - N_3 \tau_{1,0} + N_2) \sin w_0 \tau_{1,0} + (N_2 w_0 \tau_1 - 2N_1 w_0) \cos w_0 \tau_{1,0} \\ &\quad + (M_2 + M_1 w_0^2 \tau_2 - M_3 \tau_2) \sin w_0 \tau_2 + (M_2 w_0 \tau_2 - 2M_1 w_0) \cos w_0 \tau_2, \\ Q_3 &= N_2 w_0^2 \sin w_0 \tau_{1,0} + (N_3 w_0 - N_1 w_0^3) \cos w_0 \tau_{1,0}, \\ Q_4 &= N_2 w_0^2 \cos w_0 \tau_{1,0} + (N_1 w_0^3 - N_3 w_0) \sin w_0 \tau_{1,0}. \end{aligned}$$

From (10.22), we get

$$\left(\frac{d(\Re \lambda)}{d\tau_1} \right) \Big|_{\tau_1=\tau_{1,0}} = \frac{Q_2 Q_3 - Q_1 Q_4}{Q_2^2 + Q_1^2}. \quad (10.23)$$

As $Q_2 Q_3 > Q_1 Q_4$, Hopf bifurcation occurs for $\tau_1 = \tau_{1,0}$.

Therefore, we arrive at the following theorem:

Theorem 10.3 *If \mathcal{E}^* exists, such that (H_1) and (H_3) hold, with $\tau_2 \in (0, \tau_2')$, then there exists a positive threshold parameter τ_1^* , such that the interior equilibrium \mathcal{E}^* is locally asymptotically stable for $\tau_1 < \tau_1^*$ and unstable for $\tau_1 > \tau_1^*$, where*

$\tau_1^* = \min\{\tau_{1,j}\}$ as in (10.21). Additionally, system (10.3) undergoes Hopf bifurcation at \mathcal{E}^* when $\tau_1 = \tau_1^*$.

Remark 10.2 Similarly, for $\tau_1 \in (0, \tau_1')$, there exists a threshold parameter τ_2^* such that the interior equilibrium \mathcal{E}^* is locally asymptotically stable for $\tau_2 < \tau_2^*$ and unstable for $\tau_2 > \tau_2^*$. Also, Hopf bifurcation occurs for system (10.3) as $\tau_2 = \tau_2^*$, where $\tau_2^* = \min\{\tau_{2,j}\}$ is given by

$$\tau_{2,j} = \frac{1}{w_3} \arccos \left[\frac{A_1 D_1 + C_1 B_1}{A_1^2 + C_1^2} \right] + \frac{2j\pi}{w_3}, \quad j = 0, 1, 2, \dots, \quad (10.24)$$

with

$$\begin{aligned} A_1 &= M_1 w_3^2 - M_3, & B_1 &= w_3^3 - R_2 w_3 + (N_3 - N_1 w_3^2) \sin w_3 \tau_1 - N_2 w_3 \cos w_3 \tau_1, \\ C_1 &= M_2 w_3, & D_1 &= -R_1 w_3^2 + R_3 + \cos w_3 \tau_1 + N_2 w_3 \sin w_3 \tau_1. \end{aligned}$$

The proofs are obtained in the same manner as the above analysis.

Remark 10.3 The coexistence between two stable attractors can be determined by increasing or decreasing the value of some control parameters [29]. Therefore, the system pursues one branch of equilibrium points when increasing a control parameter until a threshold limit point is reached at which the system jumps to another branch of stable equilibrium points. The underlying model (10.3) displays bistability of two interior equilibrium, which is based on the variation of the coefficient of competition α ; see Figure 10.5. Both equilibria are locally asymptotically stable.

10.4 Global Stability of Interior Steady State \mathcal{E}^*

Now, we study the global stability of system (10.3) around interior steady state $\mathcal{E}^* \equiv (x^*, y^*, z^*)$.

Theorem 10.4 If $\beta_1 \alpha_1 < g_1(\alpha_1 + x^*)(\alpha_1 + x)$ and $\beta_2 \alpha_2(1 + cy^*)(1 + cy) + \delta c z^*(\alpha_2 + y^*)(\alpha_2 + y) < g_2(\alpha_2 + y^*)(\alpha_2 + y)(1 + cy^*)(1 + cy)$, then system (10.3) is globally asymptotically stable at the interior equilibrium point \mathcal{E}^* .

Proof We suggest the Lyapunov function at $\mathcal{E}^* \equiv (x^*, y^*, z^*)$ of the form

$$V(t) = \varrho_1 \left(x(t) - x^* - x^* \ln \frac{x(t)}{x^*} \right) + \varrho_2 \left(y(t) - y^* - y^* \ln \frac{y(t)}{y^*} \right) + \varrho_3 \left(z(t) - z^* - z^* \ln \frac{z(t)}{z^*} \right)$$

where ϱ_1 , ϱ_2 , and ϱ_3 are non-negative constants. Take derivative V with respect to time t yielding

$$\begin{aligned}
\dot{V}(t) &= \varrho_1 \frac{x - x^*}{x} \dot{x}(t) + \varrho_2 \frac{y - y^*}{y} \dot{y}(t) + \varrho_3 \frac{z - z^*}{z} \dot{z}(t) \\
&= \varrho_1(x - x^*) \left(\frac{\beta_1 x}{\alpha_1 + x} - \gamma_1 - g_1 x - \alpha y - e z \right) \\
&\quad + \varrho_2(y - y^*) \left(\frac{\beta_2 y}{\alpha_2 + y} - \gamma_2 - g_2 y - \beta x - \frac{\delta y z}{y(1 + cy)} \right) \\
&\quad + \varrho_3(z - z^*) \left(-\beta_3 + \frac{\epsilon e x(t - \tau_1) z(t - \tau_1)}{z} + \frac{\epsilon \delta y(t - \tau_2) z(t - \tau_2)}{z(1 + cy(t - \tau_2))} \right) \\
&\leq \varrho_1(x - x^*) \left(\frac{\beta_1 x}{\alpha_1 + x} - \frac{\beta_1 x^*}{\alpha_1 + x^*} - g_1(x - x^*) - \alpha(y - y^*) - e(z - z^*) \right) \\
&\quad + \varrho_2(y - y^*) \left(\frac{\beta_2 y}{\alpha_2 + y} - \frac{\beta_2 y^*}{\alpha_2 + y^*} - g_2(y - y^*) - \beta(x - x^*) + \frac{\delta y^* z^*}{y^*(1 + cy^*)} - \frac{\delta y z}{y(1 + cy)} \right) \\
&\quad + \varrho_3(z - z^*) \left(\frac{\epsilon e x(t - \tau_1) z(t - \tau_1)}{z} + \frac{\epsilon \delta y(t - \tau_2) z(t - \tau_2)}{z(1 + cy(t - \tau_2))} - (\epsilon e x^* + \frac{\epsilon \delta y^*}{1 + cy^*}) \right) \\
&\leq -\varrho_1 g_1(x - x^*)^2 - \varrho_2 g_2(y - y^*)^2 - (\varrho_1 \alpha + \varrho_2 \beta)(x - x^*)(y - y^*) \\
&\quad + (\epsilon e \varrho_3 - e \varrho_1)(x - x^*)(z - z^*) + \varrho_1(x - x^*) \left(\frac{\beta_1 x}{\alpha_1 + x} - \frac{\beta_1 x^*}{\alpha_1 + x^*} \right) \\
&\quad + \varrho_2(y - y^*) \left(\frac{\beta_2 y}{\alpha_2 + y} - \frac{\beta_2 y^*}{\alpha_2 + y^*} \right) + \varrho_2(y - y^*) \left(\frac{\delta y^* z^*}{y^*(1 + cy^*)} - \frac{\delta y z}{y(1 + cy)} \right) \\
&\quad + \varrho_3(z - z^*) \left(\frac{\epsilon \delta y}{1 + cy} - \frac{\epsilon \delta y^*}{1 + cy^*} \right) \\
&\leq -\varrho_1 g_1(x - x^*)^2 - \varrho_2 g_2(y - y^*)^2 - (\varrho_1 \alpha + \varrho_2 \beta)(x - x^*)(y - y^*) \\
&\quad + (\epsilon e \varrho_3 - e \varrho_1)(x - x^*)(z - z^*) + \beta_1 \varrho_1(x - x^*)^2 \left(\frac{\alpha_1}{(\alpha_1 + x^*)(\alpha_1 + x)} \right) \\
&\quad + \beta_2 \varrho_2(y - y^*)^2 \left(\frac{\alpha_2}{(\alpha_2 + y^*)(\alpha_2 + y)} \right) + \delta \varrho_2(y - y^*) \left(\frac{-(z - z^*)}{1 + cy} + \frac{c z^* (y - y^*)}{(1 + cy^*)(1 + cy)} \right) \\
&\quad + \epsilon \delta \varrho_3(y - y^*)(z - z^*) \left(\frac{1}{1 + cy} - \frac{c y}{(1 + cy^*)(1 + cy)} \right).
\end{aligned}$$

Thus, based on the assumptions $\beta_1 \alpha_1 < g_1(\alpha_1 + x^*)(\alpha_1 + x)$, $\beta_2 \alpha_2(1 + cy^*)(1 + cy) + \delta c z^*(\alpha_2 + y^*)(\alpha_2 + y) < g_2(\alpha_2 + y^*)(\alpha_2 + y)(1 + cy^*)(1 + cy)$, $\epsilon \varrho_3 < \max\{\varrho_1, \varrho_2\}$, we can get

$$\begin{aligned}
\dot{V}(t) &\leq \left(\frac{\varrho_1 \alpha_1 \beta_1}{(\alpha_1 + x^*)(\alpha_1 + x)} - \varrho_1 g_1 \right) (x - x^*)^2 + \left(\frac{\epsilon \delta \varrho_3 - \delta \varrho_2}{1 + cy} \right) (y - y^*)(z - z^*) \\
&\quad + \left(\frac{\delta \varrho_2 c z^*}{(1 + cy^*)(1 + cy)} + \frac{\varrho_2 \alpha_2 \beta_2}{(\alpha_2 + y^*)(\alpha_2 + y)} - \varrho_2 g_2 \right) (y - y^*)^2 + (\epsilon e \varrho_3 - \varrho_1 e)(x - x^*)(z - z^*) \\
&\quad - (\varrho_1 \alpha + \varrho_2 \beta)(x - x^*)(y - y^*) - \frac{\epsilon \delta \varrho_3 c y}{(1 + cy^*)(1 + cy)} (z - z^*)(y - y^*) \leq 0.
\end{aligned}$$

Hence, the proof is complete. \square

10.5 Sensitivity to Allee Effect

Here, we study the sensitivity of the model solution of (10.3) with respect to the parameters α_1 and α_2 (strength of the Allee effect). Sensitivity functions of the model solution to small changes in Allee parameters $\alpha_i (i = 1, 2)$ are denoted by

$$S_{x_{\alpha_i}}(t) := \frac{\partial}{\partial \alpha_i} x(t), \quad S_{y_{\alpha_i}}(t) := \frac{\partial}{\partial \alpha_i} y(t), \quad S_{z_{\alpha_i}}(t) := \frac{\partial}{\partial \alpha_i} z(t). \quad (10.25)$$

Using the direct method, discussed in Chap. 2, the sensitivity functions due to small perturbations in α_1 are estimated by solving the following system of DDEs:

$$\begin{aligned} S'_{x_{\alpha_1}}(t) &= S_{x\alpha_1}(t) \left[\frac{\beta_1 x(t)}{\alpha_1 + x(t)} - \gamma_1 - 2g_1 x(t) - \alpha y(t) - e z(t) \right] - \alpha S_{y\alpha_1}(t) x(t) \\ &\quad - e S_{z\alpha_1}(t) x(t) + \beta_1 x(t) \left(\frac{\alpha_1 S_{x\alpha_1}(t) - x(t)}{(\alpha_1 + x(t))^2} \right), \\ S'_{y_{\alpha_1}}(t) &= S_{y\alpha_1}(t) \left[\frac{\beta_2 y(t)}{\alpha_2 + y(t)} - \gamma_2 - 2g_2 y(t) - \beta x(t) \right] + y(t) \left[-\beta S_{x\alpha_1}(t) + \frac{\alpha_2 \beta_2 S_{y\alpha_1}(t)}{(\alpha_2 + y(t))^2} \right] \\ &\quad - \delta \left[\frac{S_{y\alpha_1}(t) z(t)}{(1 + c y(t))^2} + \frac{S_{z\alpha_1}(t) y(t)}{1 + c y(t)} \right], \\ S'_{z_{\alpha_1}}(t) &= -\beta_3 S_{z\alpha_1}(t) + \epsilon e [S_{x\alpha_1}(t - \tau_1) z(t - \tau_1) + S_{z\alpha_1}(t - \tau_1) x(t - \tau_1)] \\ &\quad + \epsilon \delta \left[\frac{S_{y\alpha_1}(t - \tau_2) z(t - \tau_2)}{(1 + c y(t - \tau_2))^2} + \frac{S_{z\alpha_1}(t - \tau_2) y(t - \tau_2)}{1 + c y(t - \tau_2)} \right]. \end{aligned} \quad (10.26)$$

To estimate the sensitivity functions $S_{x_{\alpha_1}}(t)$, $S_{y_{\alpha_1}}(t)$ and $S_{z_{\alpha_1}}(t)$, we have to solve the system of sensitivity equations (10.26), together with the original system (10.3).

Similarly, the sensitivity functions due to small changes in Allee coefficient α_2 satisfy the system of DDEs

$$\begin{aligned} S'_{x_{\alpha_2}}(t) &= S_{x\alpha_2}(t) \left[\frac{\beta_1 x(t)}{\alpha_1 + x(t)} - \gamma_1 - 2g_1 x(t) - \alpha y(t) - e z(t) \right] \\ &\quad + \beta_1 x(t) \left(\frac{\alpha_1 S_{x\alpha_2}(t)}{(\alpha_1 + x(t))^2} \right) - \alpha S_{y\alpha_2}(t) x(t) - e S_{z\alpha_2}(t) x(t), \\ S'_{y_{\alpha_2}}(t) &= S_{y\alpha_2}(t) \left[\frac{\beta_2 y(t)}{\alpha_2 + y(t)} - \gamma_2 - 2g_2 y(t) - \beta x(t) \right] - \beta S_{x\alpha_2}(t) y(t) \\ &\quad + \beta_2 y(t) \left[\frac{\alpha_2 S_{y\alpha_2}(t) - y(t)}{(\alpha_2 + y(t))^2} \right] - \delta \left[\frac{S_{y\alpha_2}(t) z(t)}{(1 + c y(t))^2} + \frac{S_{z\alpha_2}(t) y(t)}{1 + c y(t)} \right], \\ S'_{z_{\alpha_2}}(t) &= -\beta_3 S_{z\alpha_2}(t) + \epsilon e [S_{x\alpha_2}(t - \tau_1) z(t - \tau_1) + S_{z\alpha_2}(t - \tau_1) x(t - \tau_1)] \\ &\quad + \epsilon \delta \left[\frac{S_{y\alpha_2}(t - \tau_2) z(t - \tau_2)}{(1 + c y(t - \tau_2))^2} + \frac{S_{z\alpha_2}(t - \tau_2) y(t - \tau_2)}{1 + c y(t - \tau_2)} \right]. \end{aligned} \quad (10.27)$$

We then solve (10.27) along with (10.3) to evaluate $S_{x_{\alpha_2}}(t)$, $S_{y_{\alpha_2}}(t)$, and $S_{z_{\alpha_3}}(t)$; see Fig. 10.7.

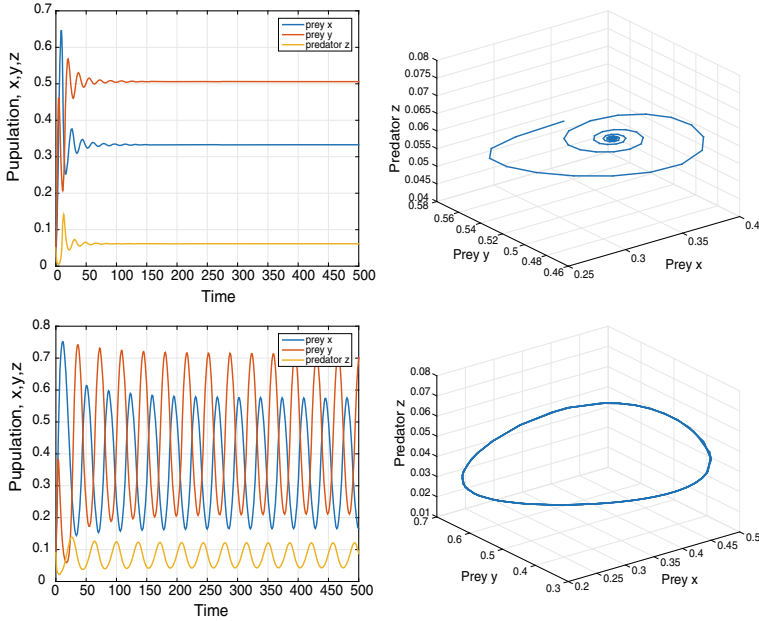


Fig. 10.3 Numerical simulations of system (10.3) around the steady state \mathcal{E}^* . (top) \mathcal{E}^* is asymptotically stable when $\tau_1 = 5.54 < \tau_1^*$ and $\tau_2 \in (0, \tau_2^*)$. (bottom) Hopf bifurcation when $\tau_1 = \tau_1^* = 4.34$ and $\tau_2 < \tau_2^* = 5.34$; the other parameter values are given in (10.28)

10.6 Numerical Simulations

Some numerical simulations of system (10.3) are carried out, in this section, to confirm the obtained theoretical results. We first investigate the behavior of the model around \mathcal{E}^* with parameter values

$$\begin{aligned} \alpha &= 0.9, \alpha_1 = 0.001, \alpha_2 = 0.001, \beta = 1.35, \gamma_2 = 1, \gamma_1 = 1, \\ \beta_1 &= 2, \beta_2 = 2, \beta_3 = 1, \epsilon = 0.5, e = 5, \delta = 1. \end{aligned} \quad (10.28)$$

Figure 10.3 shows the numerical simulations of the delayed system (10.3) around the steady state \mathcal{E}^* . The interior steady state \mathcal{E}^* is asymptotically stable when $\tau_1 < \tau_1^*$ and $\tau_2 \in (0, \tau_2^*)$. The model undergoes a Hopf bifurcation when $\tau_1 = \tau_1^* = 4.34$ and $\tau_2 < \tau_2^* = 5.33$. Figure 10.4 displays the Hopf bifurcation diagrams of τ_1 & τ_2 , which are obtained numerically by the maximum and minimum amplitudes of $z(t)$. (left) Threshold parameter $\tau_1^* = 4.34$ with $\tau_2 < \tau_2^*$. (right) Threshold parameter $\tau_2^* = 5.54$ with $\tau_1 < \tau_1^*$.

Figure 10.5 shows a bistability of two interior equilibrium points, for the DDEs model (10.3) when parameter α varies from $\alpha = 0.5$ to $\alpha = 0.9$. If the interior equi-

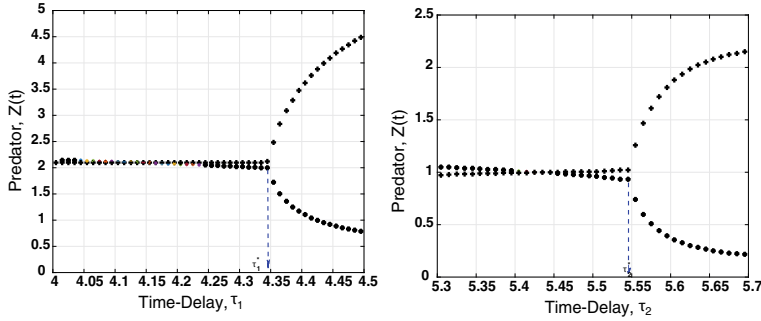


Fig. 10.4 Hopf bifurcation diagrams of τ_1 and τ_2 , which are obtained numerically by maximum and minimum amplitude of $z(t)$. (left) The threshold parameter $\tau_1^* = 4.34$ with $\tau_2 < \tau_1^*$. (right) The threshold parameter $\tau_2^* = 5.54$ with $\tau_1 < \tau_2^*$

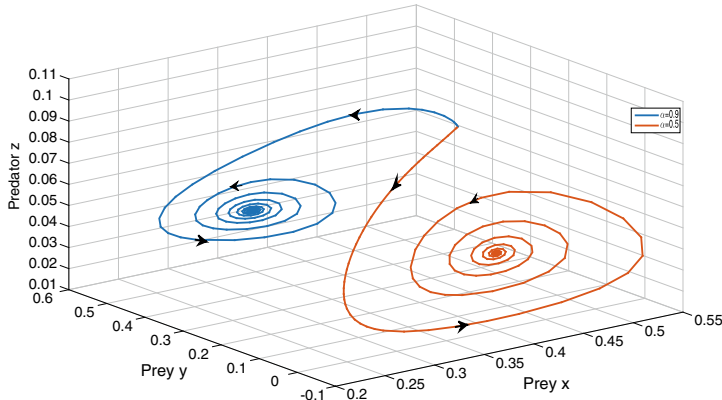


Fig. 10.5 Bistability of two interior equilibria for the delayed system (10.3), with $\alpha = 0.9$ and $\alpha = 0.5$. Both equilibria are locally asymptotically stable, other parameter values are given in (10.28)

libria exist, any trajectory starting from the interior of \mathcal{R}_+^3 converges to one of the interior equilibria.

Figure 10.6 shows the sensitivity of the dynamics of the system (10.3) due to small changes in the severity of the Allee effect α_1 and α_2 . The figures on the left show the numerical simulations with different values of α_1 ($0.001 \leq \alpha_1 \leq 0.02$) and fixed value of $\alpha_2 = 0.001$, while the figures on the right show the simulations with different values of α_2 ($0.01 \leq \alpha_2 \leq 0.02$) and fixed value of $\alpha_1 = 0.01$. The phase portrait gets stretched over time as α_1 reduces, while low values of α_2 increase the oscillations over time. The presence of an Allee effect in the model enriches the dynamics of the system. Figure 10.7 exhibits the absolute values of sensitivity functions: $|\partial x(t)/\partial \alpha_{1,2}|$, $|\partial y(t)/\partial \alpha_{1,2}|$, and $|\partial z(t)/\partial \alpha_{1,2}|$ to evaluate the sensitivity of the state variables due to small perturbations in α_1 and α_2 . The oscillation behav-

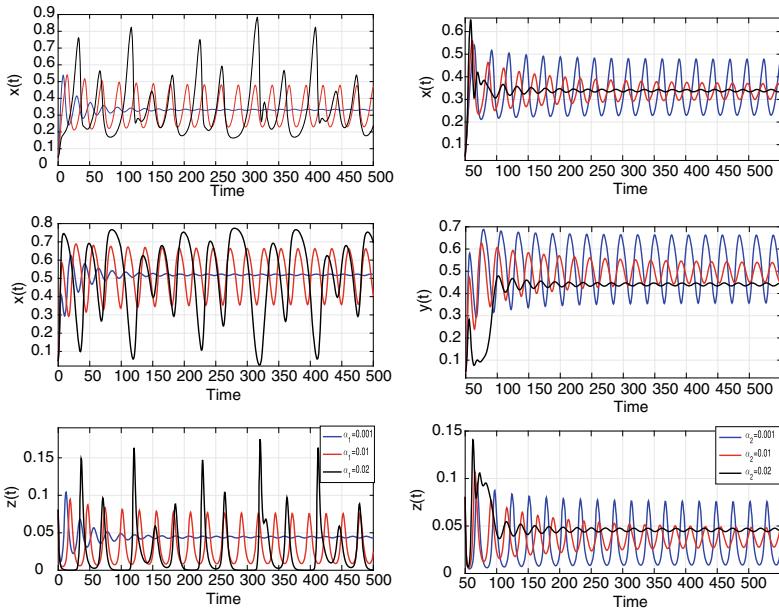


Fig. 10.6 Sensitivity of the dynamics of the system (10.3) due to small changes in the severity of the Allee effect α_1 and α_2 . (left) Numerical simulations with different values of α_1 ($0.001 \leq \alpha_1 \leq 0.02$) and fixed value of $\alpha_2 = 0.001$. (right) Simulations with different values of α_2 ($0.01 \leq \alpha_2 \leq 0.02$) and fixed value of $\alpha_1 = 0.01$. The phase portrait gets stretched over time as α_1 reduces, while low values of α_2 increase the oscillations over time

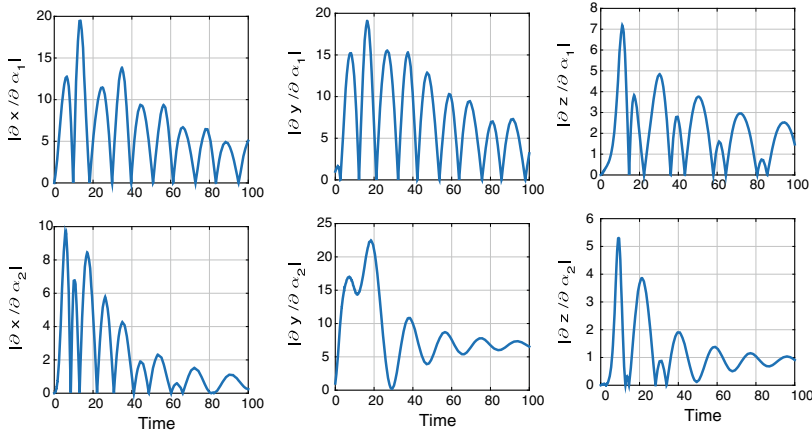


Fig. 10.7 Sensitivity functions of the model solution of the system (10.3) with respect to Allee parameters α_1 and α_2 . (top) Sensitivity functions for $x(t)$, $y(t)$, and $z(t)$ with respect to small changes in Allee parameter α_1 . (bottom) Sensitivity with respect to α_2 . The figures show that the model is very sensitive to the small perturbations of Allee parameters in early time intervals and that the sensitivity decreases with time. The two parameters α_1 and α_2 are significant in the model and have a significant impact in the early stages of interactions

ior indicates that the species population is very sensitive to small changes in the parameter. It is clear that α_1 and α_2 are important in the model and have a significant impact on the dynamics, especially in the early stages of interaction. However, the sensitivity to these parameters decreases with time.

10.7 Concluding Remarks

In this chapter, we have established a two-prey one-predator model with time-delays and a weak Allee effect in the preys' growth functions, where there is a direct competition between prey populations. Although the model is simple, the system exhibits rich dynamic behavior such as bistability of equilibria, Hopf bifurcation, period-doubling chaos, etc. Non-negativity and boundedness of the solutions have been investigated. Some new sufficient conditions for local and global asymptotic stability of interior steady states have been deduced. In addition, Hopf bifurcation with respect to time-delays threshold parameters τ_1^* and τ_2^* have been studied. The model undergoes a Hopf bifurcation when time-delays pass through its critical values. We also investigated the sensitivity of model solutions to small perturbations in the severity of the Allee effect α_1 and α_2 . The obtained results confirm that the Allee effect has a significant impact on the system dynamics in the early stages of interaction. It has been seen by the numerical simulations that time-delay and Allee effect play an important role in the dynamics of prey-predator systems. Introducing time-delay and Allee effect in the model improves the stability results and enriches the dynamics of the system, keeps the population densities in balance, and brings the model closer to reality.

In the next two chapters, we extend the analysis and consider DDEs with fractional-order derivatives to represent long-range temporal memory in the model.

References

1. Kot, M.: *Elements of Mathematical Ecology*. Cambridge University Press, Cambridge (2001)
2. Li, S., Liu, W.: A delayed Holling type III functional response predator-prey system with impulsive perturbation on the prey. *Adv. Differ. Equ.* **2016**(1), 42 (2016)
3. Liu, Z., Tan, R.: Impulsive harvesting and stocking in a monod-Haldane functional response predator-prey system. *Chaos, Solitons Fractals* **34**(2), 454–464 (2007)
4. Murray, J.D.: *Mathematical Biology II*. Springer, Berlin (2003)
5. Lotka, A.: *Elements of Physical Biology*. Williams and Wilkins, Baltimore (1925)
6. Volterra, V.: Fluctuations in the abundance of a species considered mathematically. *Nature* **118**, 558–560 (1926)
7. Kuang, Y.: *Delay Differential Equations with Applications in Population Dynamics*. Academic, New York (1993)
8. Holling, C.S.: The components of predation as revealed by a study of small-mammal predation of the European pine sawfly. *Can. Entomol.* **91**(5), 293–320 (1959)
9. Bandyopadhyay, M., Chakrabarti, C.G.: Deterministic and stochastic analysis of a nonlinear prey-predator system. *J. Biol. Syst.* **11**(02), 161–172 (2003)

10. Nosrati, K., Shafiee, M.: Dynamic analysis of fractional-order singular Holling type-II predator-prey system. *Appl. Math. Comput.* **313**, 159–179 (2017)
11. Srinivasu, P.D.N., Prasad, B.S.R.V., Venkatesulu, M.: Biological control through provision of additional food to predators: a theoretical study. *Theor. Popul. Biol.* **72**(1), 111–120 (2007)
12. Cai, Y., Zhao, C., Wang, W., Wang, J.: Dynamics of a Leslie-Gower predator-prey model with additive Allee effect. *Appl. Math. Model.: Simul. Comput. Eng. Environ. Syst.* **39**(7), 2092–2106 (2015)
13. Liu, H., Li, Z., Gao, M., Dai, H., Liu, Z.: Dynamics of a hostparasitoid model with Allee effect for the host and parasitoid aggregation. *Ecol. Complex.* **6**(3), 337–345 (2009)
14. Allee, W.C.: Animal aggregations: a study in general sociology. *Q. Rev. Biol.* **2**, 367–398 (1927)
15. Hadjivgousti, D., Ichtiarogliou, S.: Allee effect in a prey-predator system. *Chaos, Solitons Fractals* **36**(2), 334–342 (2008)
16. Pal, P.J., Saha, T., Sen, M., Banerjee, M.: A delayed predator-prey model with strong Allee effect in prey population growth. *Nonlinear Dyn.* **68**(1–2), 23–42 (2012)
17. Zu, J., Mimura, M.: The impact of Allee effect on a predator-prey system with Holling type II functional response. *Appl. Math. Comput.* **217**(7), 3542–3556 (2010)
18. Scheuring, I.: Allee effect increases the dynamical stability of populations. *J. Theor. Biol.* **199**(4), 407–414 (1999)
19. Rihan, F.A., Lakshmanan, S., Hashish, A.H., Rakkiyappan, R., Ahmed, E.: Fractional-order delayed predator-prey systems with Holling type-II functional response. *Nonlinear Dyn.* **80**(1–2), 777–789 (2015)
20. Bocharov, G.A., Rihan, F.A.: Numerical modelling in biosciences using delay differential equations. *J. Comput. Appl. Math.* **125**, 183–199 (2000)
21. Batzel, J.J., Tran, H.T.: Stability of the human respiratory control system I. analysis of a two-dimensional delay state-space model. *J. Math. Biol.* **41**, 45–79 (2000)
22. Banerjee, M., Takeuchi, Y.: Maturation delay for the predators can enhance stable coexistence for a class of prey-predator models. *J. Theor. Biol.* **412**, 154–171 (2017)
23. Sen, M., Banerjee, M., Takeuchi, Y.: Influence of Allee effect in prey populations on the dynamics of two-prey-one-predator model. *MBE* **15**(4), 883–904 (2018)
24. Kundu, S., Maitra, S.: Dynamical behaviour of a delayed three species predator-prey model with cooperation among the prey species. *Nonlinear Dyn.* **92**(2), 627–643 (2018)
25. Takeuchi, Y., Adachi, N.: Existence and bifurcation of stable equilibrium in two-prey, one-predator communities. *Bull. Math. Biol.* **45**(6), 877–900 (1983)
26. Song, X.Y., Li, Y.F.: Dynamical complexities of a Holling II two-prey one predator system with impulsive effect. *Chaos, Solitons Fractals* **33**, 463–478 (2007)
27. Huo, H.: Permanence and global attractivity of delay diffusive prey-predator systems with the michaelis-menten functional response. *Comput. Math. with Appl.* **49**(2–3), 407–416 (2005)
28. Garver, R.: On the nature of the roots of a quartic equation. *Math. News Lett.* 6–8 (1933)
29. Goldbeter, A.: Dissipative structures in biological systems: bistability, oscillations, spatial patterns and waves. *Philos. Trans. R. Soc. A* **376**(2124), 20170376 (2018)

Chapter 11

Fractional-Order Delay Differential Equations with Predator-Prey Systems



11.1 Introduction

Mathematical models using differential equations with integer order have proved valuable in understanding the dynamics of biological systems. However, most biological, physical, and engineering systems have long-range temporal memory [1–4] and/or long-range space interactions [5–7]. Modeling such systems using fractional-order differential equations is more advantageous than classical integer-order mathematical modeling, in which the effects of existence of time memory or long-range space interactions are neglected. Moreover, the fractional-order derivative is related to the whole space for a physical process, whereas the integer-order derivative describes the local properties of a certain position. Accordingly, the subject of fractional calculus (i.e., calculus of integral and derivatives of arbitrary order) has gained popularity and importance, mainly due to its demonstrated applications in numerous diverse and widespread fields of science and engineering. It has been successfully applied to system biology [3, 8–11], physics [12–15], chemistry and biochemistry [16], hydrology [17, 18], engineering [19, 20], medicine [21–23], and finance [24]. Examples of fractional-order systems in modeling and control can be found in [25–27]. In most cases, the *fractional-order differential equations* (FODEs) models seem more consistent with the real phenomena than integer-order models. This is because fractional derivatives and integrals enable the description of the memory and hereditary properties inherent in various materials and processes that exist within most biological systems.

In most biological systems time-lags or -delays exist intrinsically, such as predator-prey (PP) systems, where the predator needs time to mature [28–32]. Considerable attention has been given to study and investigate the different types of PP models due to their universal existence and importance. However, most such models have been either studied using integer-order equations with delays or using fractional order without delays [33, 34]. In this work, we combine the fractional-order with the delay terms in the model to describe the complex systems of PP interactions with memory effects. We also study the stability properties of such models.

In [28], the authors addressed the existence and global stability of a periodic solution for a discrete PP system with the functional response and predator cannibalism, whereas a global analysis of Holling type II PP model with a constant prey refuge is presented in [30]. In [32], a Holling-Tanner PP model with time-delay is considered. By regarding the delay as the bifurcation parameter, the local asymptotic stability of the positive equilibrium is investigated. In [31], a delayed stage-structured PP model with non-monotone functional responses is proposed. It is assumed that immature individuals and mature individuals of the predator are divided by a fixed age and that immature predators do not have the ability to attack prey. In [29], the main feature is that the authors introduce time-delay and pulse into the PP (natural enemy-pest) model with age structure, exhibit a new modeling method that is applied to investigate impulsive DDEs, and give some reasonable suggestions for pest management. Next, we present fractional-order with time-delay in the system that allows greater degrees of freedom in the model and in describing systems with long-time memory, such as PP dynamics.

Despite these various applications of fractional calculus, there are some important challenges, such as numerical approximation and the physical interpretation, for the fractional derivative. Fractional differential equations are integro-differential equations and their numerical solution requires large computer memory and long runs of numerical simulations; this makes it very difficult to investigate the general properties of fractional dynamical systems. As a consequence, accurate approximation and a suitable numerical technique play an important role in identifying the solution behavior of such fractional equations and in exploring their applications (see, e.g., [35–37] and the references therein). Recently, an increasing number of investigators have been studying the qualitative properties and numerical solutions of fractional-order biological models [38, 39].

Motivated by the above, in this chapter, we suggest a fractional-order PP model with a feeding rate of delayed saturated form for the prey population. We study the qualitative behavior of the model using local and global stability of the equilibrium points and present conditions in the time-delay τ in which the model is stable. Hopf bifurcation analysis is also addressed and the results of simulation scenarios are presented. We also present suitable implicit schemes for the numerical treatments of such types of *fractional-order delay differential equations* (FODDEs). The organization of this chapter is as follows. In Sect. 11.2, we describe the model. In Sects. 11.3 and 11.4, we present local and global stability of equilibrium states, respectively. In Sect. 11.5, we provide an unconditional stable numerical method for FODDEs along with some numerical examples. Section 11.6 provides a brief discussion and concluding remarks about the obtained results.

11.1.1 Preliminaries

The different definitions of fractional order are Riemann-Liouville, Grunwald-Letnikov, Weyle, Marchaud, Jumarie, Hadamard, and Caputo sense. The Caputo frac-

tional operator provides flexibility to the physical, biological models to attain the different considerable dynamical behaviors and chance to know the better understanding for the model dynamics. Moreover, the Caputo fractional-order system allows the local initial values to be included in a proper way, well understandable features of physical situations, frequently applied to tackle real-world problems.

Definition 11.1 ([40]) Caputo derivative of fractional-order α for a function $f(t)$ is defined by

$$D^\alpha f(t) = \frac{1}{\Gamma(n-\alpha)} \int_0^t (t-\tau)^{n-\alpha-1} f^n(\tau) d\tau, \quad (11.1)$$

where $n-1 < \alpha < n \in \mathbb{Z}^+$, $\Gamma(\cdot)$ is the Gamma function.

The Laplace transform of Caputo fractional-order derivative is defined as follows:

$$\mathcal{L}\{D^\alpha f(t); s\} = s^\alpha \mathcal{F}(s) - \sum_{i=1}^{n-1} s^{\alpha-i-1} f^{(i)}(0) \quad (11.2)$$

where $\mathcal{F}(s) = \mathcal{L}\{f(t)\}$. In particular, when $f^{(i)}(0) = 0, i = 1, 2, \dots, n-1$, then $\mathcal{L}\{D^\alpha f(t); s\} = s^\alpha \mathcal{F}(s)$.

Remark 11.1 For $0 < \alpha \leq 1$, the fractional-order derivative defined based on Caputo sense (see Definition 11.1), the memory effects in dynamical systems is described by using a convolution integral with power-law memory kernel. The memory kernel (time correlation function) decaying rate depends on fractional order α . The lower value of α corresponds to more slowly decaying long memory (time-correlation functions). Then, $\alpha \rightarrow 1$, the influence of memory decreases.

For given the following m-dimensional fractional-order system

$$\begin{aligned} D^{\alpha_1} x_1(t) &= a_{11}x_1(t - \tau_{11}) + a_{12}x_2(t - \tau_{12}) + \dots + a_{1m}x_m(t - \tau_{1m}) \\ D^{\alpha_2} x_2(t) &= a_{21}x_1(t - \tau_{21}) + a_{22}x_2(t - \tau_{22}) + \dots + a_{2m}x_m(t - \tau_{2m}) \\ &\vdots \\ D^{\alpha_m} x_m(t) &= a_{m1}x_1(t - \tau_{m1}) + a_{m2}x_2(t - \tau_{m2}) + \dots + a_{mm}x_m(t - \tau_{mm}) \end{aligned} \quad (11.3)$$

where $0 < \alpha_i < 1$ ($i = 1, 2, \dots, m$). The smooth initial conditions $x_i(t) = \psi_i(t)$, $t \in [-\max_{i,j} \tau_{ij}, 0]$, $i, j = 1, 2, \dots, m$. The state variables $x(t), x(t - \tau_{ij}) \in \mathbb{R}$. Taking Laplace transform for both sides of (11.3), yields

$$\begin{aligned}
s^{\alpha_1} X_1(s) - s^{\alpha_1-1} \psi_1(0) &= a_{11} e^{-s\tau_{11}} \left(X_1(s) + \int_{-\tau_{11}}^0 e^{-st} \psi_1(t) dt \right) + a_{12} e^{-s\tau_{12}} \left(X_2(s) \right. \\
&\quad \left. + \int_{-\tau_{12}}^0 e^{-st} \psi_2(t) dt \right) + \cdots + a_{1m} e^{-s\tau_{1m}} \left(X_m(s) + \int_{-\tau_{1m}}^0 e^{-st} \psi_m(t) dt \right) \\
s^{\alpha_2} X_2(s) - s^{\alpha_2-1} \psi_2(0) &= a_{21} e^{-s\tau_{21}} \left(X_1(s) + \int_{-\tau_{21}}^0 e^{-st} \psi_1(t) dt \right) + a_{22} e^{-s\tau_{22}} \left(X_2(s) \right. \\
&\quad \left. + \int_{-\tau_{22}}^0 e^{-st} \psi_2(t) dt \right) + \cdots + a_{2m} e^{-s\tau_{2m}} \left(X_m(s) + \int_{-\tau_{2m}}^0 e^{-st} \psi_m(t) dt \right) \\
&\vdots \\
s^{\alpha_m} X_m(s) - s^{\alpha_m-1} \psi_m(0) &= a_{m1} e^{-s\tau_{m1}} \left(X_1(s) + \int_{-\tau_{m1}}^0 e^{-st} \psi_1(t) dt \right) + a_{m2} e^{-s\tau_{m2}} \left(X_2(s) \right. \\
&\quad \left. + \int_{-\tau_{m2}}^0 e^{-st} \psi_2(t) dt \right) + \cdots + a_{mm} e^{-s\tau_{mm}} \left(X_m(s) + \int_{-\tau_{mm}}^0 e^{-st} \psi_m(t) dt \right)
\end{aligned} \tag{11.4}$$

where $X_i(s)$ is the Laplace transform of $x_i(t)$. This system can be written in a matrix form

$$\Delta(s) \cdot \begin{bmatrix} X_1(s) \\ X_2(s) \\ \vdots \\ X_m(s) \end{bmatrix} = \begin{bmatrix} b_1(s) \\ b_2(s) \\ \vdots \\ b_m(s) \end{bmatrix}. \tag{11.5}$$

We call $\Delta(s)$ a characteristic matrix of the system

$$\Delta(s) = \begin{bmatrix} s^{\alpha_1} - a_{11} e^{-s\tau_{11}} & -a_{12} e^{-s\tau_{12}} & \dots & -a_{1m} e^{-s\tau_{1m}} \\ -a_{21} e^{-s\tau_{21}} & s^{\alpha_2} - a_{22} e^{-s\tau_{22}} & \dots & -a_{2m} e^{-s\tau_{2m}} \\ \vdots & \vdots & \ddots & \vdots \\ -a_{m1} e^{-s\tau_{m1}} & -a_{m2} e^{-s\tau_{m2}} & \dots & s^{\alpha_m} - a_{mm} e^{-s\tau_{mm}} \end{bmatrix} \tag{11.6}$$

and

$$\begin{aligned}
b_1(s) &= s^{\alpha_1-1} \psi_1(0) + a_{11} e^{-s\tau_{11}} \int_{-\tau_{11}}^0 e^{-st} \psi_1(t) dt + a_{12} e^{-s\tau_{12}} \int_{-\tau_{12}}^0 e^{-st} \psi_2(t) dt \\
&\quad + \cdots + a_{1m} e^{-s\tau_{1m}} \int_{-\tau_{1m}}^0 e^{-st} \psi_m(t) dt \\
b_2(s) &= s^{\alpha_2-1} \psi_2(0) + a_{21} e^{-s\tau_{21}} \int_{-\tau_{21}}^0 e^{-st} \psi_1(t) dt + a_{22} e^{-s\tau_{22}} \int_{-\tau_{22}}^0 e^{-st} \psi_2(t) dt \\
&\quad + \cdots + a_{2m} e^{-s\tau_{2m}} \int_{-\tau_{2m}}^0 e^{-st} \psi_m(t) dt \\
&\vdots \\
b_m(s) &= s^{\alpha_m-1} \psi_m(0) + a_{m1} e^{-s\tau_{m1}} \int_{-\tau_{m1}}^0 e^{-st} \psi_1(t) dt + a_{m2} e^{-s\tau_{m2}} \int_{-\tau_{m2}}^0 e^{-st} \psi_2(t) dt \\
&\quad + \cdots + a_{mm} e^{-s\tau_{mm}} \int_{-\tau_{mm}}^0 e^{-st} \psi_m(t) dt.
\end{aligned}$$

Remark 11.2 Zero solution of system (11.3) is Lyapunov asymptotically stable if all the roots of $\det(\Delta(s)) = 0$ have negative real parts.

11.2 Fractional Delayed Predator-Prey Model

Lotka [41] in 1925 and Volterra [42] in 1926 introduced the first PP model. After that, many more complicated but realistic PP models, with various forms of “functional responses,” have been formulated by ecologists and mathematicians. One of the most popular PP models was introduced by Freedman [43] in 1980, which has the Michaelis-Menten type or Holling type-II functional response $\frac{\beta x(t)y(t)}{1 + \sigma x(t)}$, where $x(t)$ and $y(t)$ are the population densities of the prey and predator, respectively. β (units: 1/time) is the feeding rate, or the maximal predator per-capita consumption rate, i.e., the maximum number of preys that can be eaten by a predator in each time unit, while σ (units: 1/prey) is a positive constant that describes the effects of capture rate. The prey host population is assumed to have logistic growth $rx(t)\left(1 - \frac{x(t)}{K}\right)$ with carrying capacity K (in a closed community) and a specific growth rate constant r . Then, the interactions between prey and predator with time-delay τ in the saturation term takes the form

$$\begin{aligned} Dx(t) &= rx(t)\left(1 - \frac{x(t)}{K}\right) - \frac{\beta x(t)y(t - \tau)}{1 + \sigma x(t)}, \\ Dy(t) &= \frac{\beta x(t)y(t - \tau)}{1 + \sigma x(t)} - ay(t), \end{aligned} \quad (11.7)$$

where τ is regarded as reaction time of the predations and a is a positive real number. In system (11.7), it is assumed that each individual predator has the same ability to feed on prey.

In this chapter, we extend the derivatives of (11.7) to an arbitrary order to investigate the combination of both fractional-order formulation and time-delay in the same model. Therefore, the model becomes

$$\begin{aligned} D^\alpha x(t) &= rx(t)\left(1 - \frac{x(t)}{K}\right) - \frac{\beta x(t)y(t - \tau)}{1 + \sigma x(t)} \\ D^\alpha y(t) &= \frac{\beta x(t)y(t - \tau)}{1 + \sigma x(t)} - ay(t), \quad 0 < \alpha \leq 1, \quad t \geq 0 \end{aligned} \quad (11.8)$$

with initial conditions $x(0) > 0$ and $y(t) = \psi(t) > 0$ when $t \in [-\tau, 0]$, where $\psi(t)$ is a smooth function. Next, we study the impact of the fractional-order and time-delay τ in the dynamics of the model.

By choosing the delay τ as a bifurcation parameter, when it crosses some critical values τ^* , a Hopf bifurcation about the stability of interior equilibrium in (11.8) can

occur, as we shall discuss in the next section. The fractional order grants the model a greater degree of freedom and consistency with real interactions due to its ability to provide an exact description of the non-linear phenomena.

11.3 Local Stability Analysis and Hopf Bifurcation

Consider the fractional-order systems of the form

$$\begin{aligned} D^\alpha x(t) &= f_1(x, y), \quad D^\alpha y(t) = f_2(x, y), \quad \alpha \in (0, 1], \\ x(0) &= x_0, \quad y(0) = y_0 \end{aligned} \tag{11.9}$$

with an equilibrium point (x_e, y_e) . Therefore,

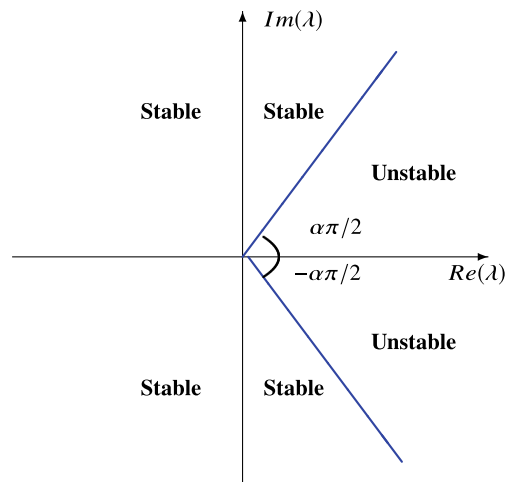
Lemma 11.1 *The equilibrium point (x_e, y_e) of the fractional differential system (11.9) is locally asymptotically stable if and only if all eigenvalues λ_i of the Jacobian matrix*

$$J = \begin{pmatrix} \partial f_1 / \partial x & \partial f_1 / \partial y \\ \partial f_2 / \partial x & \partial f_2 / \partial y \end{pmatrix},$$

evaluated at the equilibrium point (x_e, y_e) , satisfy the condition that $|\arg(\lambda_i)| > \frac{\alpha\pi}{2}$ [44] (see Fig. 11.1).

Since it is known that systems with memory are typically more stable than their memoryless counterparts, we expect that “*fractional-order differential equations are, at least, as stable as their integer-order counterpart.*”

Fig. 11.1 Stability region of the fractional-order system (11.9) when $0 < \alpha \leq 1$



The equilibria of (11.8) are the points of intersections at which $D^\alpha x(t) = 0$ and $D^\alpha y(t) = 0$. Thus, we arrive at the following proposition: For the model system (11.8), there always exist trivial equilibrium $\mathcal{E}_0 = (0, 0)$ and semi-trivial equilibrium $\mathcal{E}_1 = (K, 0)$. However, if the threshold parameter

$$\mathcal{R}_0 = \frac{K[\beta - \sigma a]}{a} > 1, \quad (11.10)$$

there also exists an interior equilibrium $\mathcal{E}_+ = (x^*, y^*)$, where

$$\mathcal{E}_+ = (x^*, y^*) = \left(\frac{a}{\beta - \sigma a}, \frac{rx^{*2}}{Ka}(\mathcal{R}_0 - 1) \right). \quad (11.11)$$

11.3.1 Trivial and Semi-trivial Equilibria and Their Stabilities

The theorem matrix of the linearized system of model (11.8) is

$$J = \begin{pmatrix} r - \frac{2rx^*}{K} - \frac{\beta y^*}{(1 + \sigma x^*)^2} & -\frac{\beta x^*}{1 + \sigma x^*} e^{-\lambda\tau} \\ \frac{\beta y^*}{(1 + \sigma x^*)^2} & \frac{\beta x^*}{1 + \sigma x^*} e^{-\lambda\tau} - a \end{pmatrix} \quad (11.12)$$

Using (11.12), the characteristic equation¹ at the trivial equilibrium point $\mathcal{E}_0 = (0, 0)$ reduces to

$$(\lambda^\alpha - r)(\lambda^\alpha + a) = 0. \quad (11.13)$$

Clearly, Eq. (11.13) has a positive root $\lambda^\alpha = r$ ($0 < \alpha \leq 1$). Then, the trivial equilibrium \mathcal{E}_0 of system (11.8) is always unstable (saddle point). However, at the semi-trivial equilibrium $\mathcal{E}_1 = (K, 0)$, the Jacobian matrix (11.12) reduces to

$$J_{\text{semi-trivial}} = \begin{pmatrix} -r & -\frac{\beta K}{1 + \sigma K} e^{-\lambda\tau} \\ 0 & \frac{\beta K}{1 + \sigma K} e^{-\lambda\tau} - a \end{pmatrix} \quad (11.14)$$

with characteristic equation

$$(\lambda^\alpha + r) \left(\lambda^\alpha + a \left[1 - \frac{\mathcal{R}_0 + \sigma K}{1 + \sigma K} e^{-\lambda\tau} \right] \right) = 0. \quad (11.15)$$

¹ We may note that the characteristic equation of a system with delay has infinite roots.

It is obvious from Eq. (11.15) that the two roots are real and negative if $\mathcal{R}_0 < 1$ (when $\tau = 0$) and the equilibrium \mathcal{E}_1 is then asymptotically stable. In case of $\tau > 0$, we assume that the root of (11.15) $\lambda = \xi i$ must satisfy

$$\xi^{2\alpha} = a^2 \left[\frac{\mathcal{R}_0 + \sigma K}{1 + \sigma K} - 1 \right] < 0.$$

Then, when $\mathcal{R}_0 < 1$, there are no positive real roots ξ . Hence, according to Lemma 11.1, we can get the following theorem to indicate the stability of \mathcal{E}_1 :

Theorem 11.1 *If \mathcal{R}_0 is defined by (11.10), then semi-trivial equilibrium $\mathcal{E}_1 = (K, 0)$ of system (11.8) is asymptotically stable when $\mathcal{R}_0 < 1$ (for all values of $\tau > 0$), unstable when $\mathcal{R}_0 > 1$, and linearly neutrally stable if $\mathcal{R}_0 = 1$.*

11.3.2 Interior Equilibrium and Its Stability

Here, we investigate the linear stability of (11.8) at the interior equilibrium $\mathcal{E}_+ = (x^*, y^*)$ defined in (11.11). $x^* = \frac{a}{\beta - \sigma a} \implies \frac{\beta x^*}{1 + \sigma x^*} = a$, and $y^* = \frac{rx^{*2}}{Ka}(\mathcal{R}_0 - 1) \implies \frac{\beta y^*}{1 + \sigma x^*} = r \left(1 - \frac{1}{\mathcal{R}_0}\right)$. We also have $\mathcal{R}_0 = \frac{K}{x^*}$. Therefore, the corresponding Jacobian matrix at the interior equilibrium \mathcal{E}_+ can be easily expressed in terms of the reproduction number \mathcal{R}_0 , as follows:

$$J_{\text{interior}} = \begin{pmatrix} \eta_{11} & -ae^{-\lambda\tau} \\ \frac{r}{1 + \sigma x^*} \left(1 - \frac{1}{\mathcal{R}_0}\right) & ae^{-\lambda\tau} - a \end{pmatrix}, \quad (11.16)$$

where $\eta_{11} = r \left(1 - \frac{2}{\mathcal{R}_0}\right) - \frac{r}{1 + \sigma x^*} \left(1 - \frac{1}{\mathcal{R}_0}\right)$. The characteristic equation of (11.16) for the interior equilibrium is

$$\begin{aligned} \lambda^{2\alpha} + \lambda^\alpha &\left[-r \left(1 - \frac{2}{\mathcal{R}_0}\right) + a(1 - e^{-\lambda\tau}) \right. \\ &\left. + \frac{r}{1 + \sigma x^*} \left(1 - \frac{1}{\mathcal{R}_0}\right) \right] + a \left[-r \left(1 - \frac{2}{\mathcal{R}_0}\right) (1 - e^{-\lambda\tau}) \right. \\ &\left. + \frac{r}{1 + \sigma x^*} \left(1 - \frac{1}{\mathcal{R}_0}\right) \right] = 0. \end{aligned} \quad (11.17)$$

We need to find the necessary and sufficient condition for every root of the characteristic Eq. (11.17) having negative real part. Introducing

$$\varrho_1 = r \left(1 - \frac{2}{\mathcal{R}_0}\right), \quad \varrho_2 = \frac{r}{1 + \sigma x^*} \left(1 - \frac{1}{\mathcal{R}_0}\right), \quad \varrho_3 = a. \quad (11.18)$$

Then, the characteristic Equation (11.17) can be rewritten in the form

$$\lambda^{2\alpha} + \lambda^\alpha(-\varrho_1 + \varrho_2 + \varrho_3) + \varrho_3(-\varrho_1 + \varrho_2) + e^{-\lambda\tau}(-\varrho_3\lambda + \varrho_1\varrho_3) = 0.$$

For simplicity, let us also assume that

$$\begin{aligned} A_1 &= (-\varrho_1 + \varrho_2 + \varrho_3), \quad A_2 = \varrho_3(-\varrho_1 + \varrho_2), \\ A_3 &= \varrho_3, \quad A_4 = \varrho_1\varrho_3. \end{aligned} \quad (11.19)$$

Then, Eq. (11.19) takes the form

$$\lambda^{2\alpha} + A_1\lambda^\alpha + A_2 + e^{-\lambda\tau}(-A_3\lambda + A_4) = 0. \quad (11.20)$$

We establish the existence of the parameter value τ^* for which the equilibrium solution undergoes two simultaneous Hopf bifurcations.

Theorem 11.2 Assume that $\mathcal{R}_c = 2 + 1/(1 + 2\sigma x^*)$. Then,

- (1) the interior equilibrium \mathcal{E}_+ of system (11.8) is feasible and locally asymptotically stable for all $\tau \geq 0$ if $1 < \mathcal{R}_0 \leq \mathcal{R}_c$ holds;
- (2) if $\mathcal{R}_0 > \mathcal{R}_c > 1$, then there exist $\tau^* > 0$, such that $\tau \in [0, \tau^*)$ the interior equilibrium \mathcal{E}_+ is asymptotically stable, and unstable when $\tau > \tau^*$. When $\tau = \tau^*$, the characteristic equation (11.20) has a pair of purely imaginary roots $\pm i\xi_0^\alpha$ with

$$\xi_0^{2\alpha} = \frac{1}{2}(2A_2 + A_3^2 - A_1^2) + \frac{1}{2}\sqrt{(2A_2 + A_3^2 - A_1^2)^2 - 4(A_2^2 - A_4^2)},$$

and

$$\tau^* = \frac{1}{\xi_0} \arccos \left(\frac{(A_4 + A_1 A_3)\xi_0^2 - A_2 A_4}{A_3^2 \xi_0^2 + A_4^2} \right) + \frac{2j\alpha\pi}{\xi_0^\alpha},$$

where A_1, A_2, A_3 and A_4 are defined in (11.19).

Proof If $\lambda = \xi i$ is a root of (11.19). After substitution and separation of the real and imaginary parts, we have

$$\begin{aligned} -\xi^{2\alpha} + \varrho_3(-\varrho_1 + \varrho_2) &= \xi^\alpha \varrho_3 \sin \xi\tau - \varrho_1 \varrho_3 \cos \xi\tau, \\ \xi^\alpha(-\varrho_1 + \varrho_2 + \varrho_3) &= \varrho_1 \varrho_3 \sin \xi\tau + \xi \varrho_3 \cos \xi\tau, \end{aligned} \quad (11.21)$$

which are equivalent to

$$\begin{aligned} -\xi^{2\alpha} + A_2 &= \xi^\alpha A_3 \sin \xi\tau - A_4 \cos \xi\tau, \\ \xi^\alpha A_1 &= A_4 \sin \xi\tau + \xi A_3 \cos \xi\tau. \end{aligned} \quad (11.22)$$

Squaring and adding both equations yields

$$\xi^{4\alpha} + \xi^{2\alpha}(-\varrho_1 + \varrho_2)^2 + \varrho_2\varrho_3^2(-2\varrho_1 + \varrho_2) = 0, \quad (11.23)$$

which is equivalent to

$$\xi^{4\alpha} - (2A_2 + A_3^2 - A_1^2)\xi^{2\alpha} + (A_2^2 - A_4^2) = 0. \quad (11.24)$$

Equation (11.23) can also be re-written in the form

$$\xi^{4\alpha} + \xi^{2\alpha}[\varrho_1^2 + \varrho_2(-2\varrho_1 + \varrho_2)] + \varrho_2\varrho_3^2(-2\varrho_1 + \varrho_2) = 0. \quad (11.25)$$

Therefore, if $-2\varrho_1 + \varrho_2 \geq 0$ (when $\mathcal{R}_0 > 1$), then there is no positive real ξ satisfying (11.23). According to the definitions given in (11.18), the inequality $-2\varrho_1 + \varrho_2 \geq 0$, which is equivalent to $\mathcal{R}_0 \leq 2 + 1/(1 + 2\sigma x^*)$ so that all the roots ($\lambda = \xi_i$) of (11.17) are negative.

However, if $-2\varrho_1 + \varrho_2 < 0$, then (11.25) has one and only one positive root denoted by ξ_0 , and the characteristic equation (11.20) has a pair of purely imaginary roots $\pm i\xi_0$. Let $\lambda(\tau) = \sigma(\tau) + i\xi(\tau)$ be the eigenvalue of (11.20), such that $\sigma(\tau^*) = 0$ and $\xi(\tau^*) = \xi_0$. From (11.22), we have

$$\tau^* = \frac{1}{\xi_0^\alpha} \arccos \left(\frac{(A_4 + A_1 A_3)\xi_0^2 - A_2 A_4}{A_3^2 \xi_0^2 + A_4^2} \right) + \frac{2j\alpha\pi}{\xi_0^\alpha} \quad (11.26)$$

and from (11.24)

$$\xi_0^{2\alpha} = \frac{1}{2}(2A_2 + A_3^2 - A_1^2) + \frac{1}{2}\sqrt{(2A_2 + A_3^2 - A_1^2)^2 - 4(A_2^2 - A_4^2)} < 0.$$

Hence, according to Lemma 11.1, the interior equilibrium \mathcal{E}_+ of system (11.8) is locally asymptotically stable with $0 < \alpha \leq 1$. The proof is, thus, complete. \square

11.4 Global Stability Analysis

In this section, we extend the analysis to study the global stability conditions [45, 46] for the fractional-order delay differential system. To study the global stability of the equilibrium points of (11.8), we linearize the system into the form

$$\begin{aligned} D^\alpha x(t) &= m_1x(t) + m_2y(t - \tau) \\ D^\alpha y(t) &= n_1x(t) + n_2y(t) + n_3y(t - \tau) \end{aligned} \quad 0 < \alpha \leq 1. \quad (11.27)$$

where

$$\begin{aligned} m_1 &= r - \frac{2x^*}{K} - \frac{\beta y^*}{1 + \sigma x^*} + \frac{\sigma \beta x^* y^*}{(1 + \sigma x^*)^2}, \\ m_2 &= -\frac{\beta x^*}{1 + \sigma x^*}, \quad n_1 = \frac{\beta y^*}{1 + \sigma x^*} - \frac{\sigma \beta x^* y^*}{(1 + \sigma x^*)^2}, \\ n_2 &= -a, \quad n_3 = \frac{\beta x^*}{1 + \sigma x^*}. \end{aligned}$$

If the linear fractional differential equation has non-zero equilibrium point, we can shift equilibrium point to the origin. Put $\bar{x}(t) = x(t) - x^*$, $\bar{y}(t) = y(t) - y^*$, then the Eqs. (11.27) become

$$\begin{aligned} D^\alpha \bar{x}(t) &= m_1 \bar{x}(t) + m_2 \bar{y}(t - \tau) \\ D^\alpha \bar{y}(t) &= n_1 \bar{x}(t) + n_2 \bar{y}(t) + n_3 \bar{y}(t - \tau) \quad 0 < \alpha \leq 1. \end{aligned} \quad (11.28)$$

To study the stability of system (11.8), we take a Laplace transform [47] on both sides of (11.28). Then, we have

$$\begin{aligned} s^\alpha X_1(s) &= m_1 X_1(s) + s^{\alpha-1} \varphi_1(0) \\ &\quad + m_2 e^{-s\tau} \left(X_2(s) + \int_{-\tau}^0 e^{-st} \varphi_2(t) dt \right) \\ s^\alpha X_2(s) &= n_1 X_1(s) + n_2 X_2(s) + s^{\alpha-1} \varphi_2(0) \\ &\quad + n_3 e^{-s\tau} \left(X_2(s) + \int_{-\tau}^0 e^{-st} \varphi_2(t) dt \right). \end{aligned} \quad (11.29)$$

Here, it should be mentioned that the initial values $\bar{x}(t) = \varphi_1(t)$ and $\bar{y}(t) = \varphi_2(t)$ with $t \in [-\tau, 0]$. Additionally, $X_1(s)$ and $X_2(s)$ are Laplace transforms of $\bar{x}(t)$ and $\bar{y}(t)$ with $X_1(s) = L(\bar{x}(t))$ and $X_2(s) = L(\bar{y}(t))$. The system (11.29) can be rewritten as follows:

$$\Delta(s) \begin{pmatrix} X_1(s) \\ X_2(s) \end{pmatrix} = \begin{pmatrix} k_1(s) \\ k_2(s) \end{pmatrix} \quad (11.30)$$

in which

$$\Delta(s) = \begin{pmatrix} s^\alpha - m_1 & -m_2 e^{-s\tau} \\ -n_1 & s^\alpha - n_2 - n_3 e^{-s\tau} \end{pmatrix}$$

and

$$\begin{aligned} k_1(s) &= s^{\alpha-1} \varphi_1(0) + m_2 e^{-s\tau} \int_{-\tau}^0 e^{-st} \varphi_2(t) dt \\ k_2(s) &= s^{\alpha-1} \varphi_2(0) + n_3 e^{-s\tau} \int_{-\tau}^0 e^{-st} \varphi_2(t) dt. \end{aligned}$$

$\Delta(s)$ is considered as characteristic matrix of system (11.8) and $\det \Delta(s)$ as its characteristic polynomial. Therefore, the distribution of the eigenvalues of the characteristic polynomial determines the stability of the system (11.8). In other words, if all roots of the characteristic equation have negative parts, then the equilibrium of the above fractional-order PP system is Lyapunov globally asymptotically stable if the equilibrium exists [45]. If we multiply both sides of (11.30) by s , we have

$$\Delta(s) \begin{pmatrix} sX_1(s) \\ sX_2(s) \end{pmatrix} = \begin{pmatrix} sk_1(s) \\ sk_2(s) \end{pmatrix} \quad (11.31)$$

Therefore, if all roots of the transcendental equation $\det \Delta(s) = 0$ lie in the open left complex plane, i.e., $\text{Re}(s) < 0$, then we consider (11.31) in $\text{Re}(s) \geq 0$. In this restricted area, system (11.31) has a unique solution $(sX_1(s), sX_2(s))$, so that

$$\lim_{s \rightarrow 0, \text{Re}(s) \geq 0} sX_i(s) = 0, \quad i = 1, 2.$$

From the assumption of all roots of the characteristic equation $\det \Delta(s) = 0$ and the final-value theorem of the Laplace transform [47], we get

$$\begin{aligned} \lim_{t \rightarrow +\infty} \bar{x}(t) &\equiv \lim_{s \rightarrow 0, \text{Re}(s) \geq 0} sX_1(s) = 0, \\ \text{and } \lim_{t \rightarrow +\infty} \bar{y}(t) &\equiv \lim_{s \rightarrow 0, \text{Re}(s) \geq 0} sX_2(s) = 0. \end{aligned}$$

It implies that the zero solution of the fractional-order PP system is Lyapunov globally asymptotically stable. Therefore, we arrive at the following result:

Theorem 11.3 *If all the roots of the characteristic equation $\det \Delta(s) = 0$ have negative real parts, then the positive equilibrium points (x^*, y^*) of system (11.8) is Lyapunov globally asymptotically stable.*

11.5 Implicit Euler's Scheme for FODDEs

Since most FODEs do not have exact analytical solutions, approximation and numerical techniques must be used. In addition, most of the resulting biological systems are stiff.² The stiffness often appears due to the differences in speed between the fastest and slowest components of the solutions and due to stability constraints. In addition, the state variables of these types of models are very sensitive to small perturbations (or changes) in the parameters that occur in the model. Therefore, efficient use of a reliable numerical method for dealing with stiff problems is necessary.

Consider the following FODDEs:

² One definition of stiffness is that the global accuracy of the numerical solution is determined by stability rather than local error and implicit methods are more appropriate for it.

$$\begin{aligned} D^\alpha y(t) &= f(t, y(t), y(t - \tau)), \quad t \in J = [0, T], \\ y(t) &= \psi(t), \quad t \in [-\tau, 0], \quad 0 < \alpha \leq 1. \end{aligned} \tag{11.32}$$

Here $y(t) = [y_1(t), y_2(t), \dots, y_n(t)]^T$, $f : J \times \mathbb{R}^n \times \mathbb{R}^n \rightarrow \mathbb{R}^n$ satisfies the Lipschitz condition, and there exists a positive constant $K > 0$ such that

$$\begin{aligned} &\|f(t, y(t), y(t - \tau)) - f(t, x(t), x(t - \tau))\| \\ &\leq K\{\|y(t) - x(t)\| + \|y(t - \tau) - x(t - \tau)\|\}. \end{aligned} \tag{11.33}$$

Theorem 11.4 Problem (11.32) has a unique solution provided that the Lipschitz condition (11.33) is satisfied and $\bar{M} = \frac{2KT^\alpha}{\Gamma(\alpha + 1)} < 1$.

Proof We can apply a fractional integral operator to the differential equation (11.32) and incorporate the initial conditions, thus converting the equation into the equivalent equation

$$y(t) = \psi(0) + \frac{1}{\Gamma(\alpha)} \int_0^t (t-s)^{\alpha-1} f(s, y(s), y(s-\tau)) ds, \tag{11.34}$$

which is also a Volterra equation of the second kind. Define the operator $\mathcal{L} : C(J, \mathbb{R}^n) \rightarrow C(J, \mathbb{R}^n)$, such that

$$\mathcal{L}y(t) = \psi(0) + \frac{1}{\Gamma(\alpha)} \int_0^t (t-s)^{\alpha-1} f(s, y(s), y(s-\tau)) ds. \tag{11.35}$$

Then, we have

$$\begin{aligned} &\|\mathcal{L}y(t) - \mathcal{L}x(t)\| \\ &\leq \frac{1}{\Gamma(\alpha)} \int_0^t (t-s)^{\alpha-1} \times \|f(s, y(s), y(s-\tau)) - f(s, x(s), x(s-\tau))\| ds \\ &\leq \frac{K}{\Gamma(\alpha)} \int_0^t (t-s)^{\alpha-1} \{\|y(s) - x(s)\| + \|y(s-\tau) - x(s-\tau)\|\} ds \\ &\leq \frac{K}{\Gamma(\alpha)} \int_0^t (t-s)^{\alpha-1} \left\{ \sup_{s \in J} \|y(s) - x(s)\| + \sup_{s \in [-\tau, 0]} \|y(s) - x(s)\| + \sup_{s \in J} \|y(s) - x(s)\| \right\} ds \\ &\leq \frac{2K}{\Gamma(\alpha)} \int_0^t (t-s)^{\alpha-1} \sup_{s \in J} \|y(s) - x(s)\| ds \\ &\leq \frac{2K}{\Gamma(\alpha+1)} \|y - x\| T^\alpha. \end{aligned}$$

Therefore, we obtain

$$\|\mathcal{L}y(t) - \mathcal{L}x(t)\| \leq \bar{M} \|y - x\|.$$

Using Banach contraction principle [48], we can deduce that \mathcal{L} has a unique fixed point; this implies that our problem has a unique solution. \square

Several numerical methods have been proposed to solve fractional-order differential equations (FODEs) [36, 49]. The predictor-corrector algorithm is an efficient and powerful technique for solving FODEs, which is a generalization of the Adams-Bashforth-Moulton method. The modification of the Adams-Bashforth-Moulton algorithm is proposed by Diethelm [50] to approximate the fractional-order derivative (See Appendix B). However, the converted Volterra integral equation (11.34) has a weakly singular kernel, such that regularization is not necessary anymore. It appears that there exists only a very small number of software packages for non-linear Volterra equations. In our case, the kernel may not be continuous and, therefore, the classical numerical algorithms for the integral part of (11.34) are unable to handle the solution of Equation (11.32). Therefore, we implement the implicit Euler's scheme to approximate the fractional-order derivative.

Given the delay fractional-order model (11.32) and mesh points $\mathcal{T} = \{t_0, t_1, \dots, t_N\}$, such that $t_0 = 0$ and $t_N = T$ with stepsize $h = \tau/m$. If $\psi(t)$ is a continuous function, then the solution $y(t)$ for $0 \leq t \leq \tau$ (τ is bounded) satisfies the fractional-order ordinary differential equation

$$\begin{aligned} D^\alpha y'(t) &= f(t, y(t), \psi(t - \tau)), \quad 0 \leq t \leq \tau, \\ y(0) &= \psi(0) \quad 0 < \alpha \leq 1. \end{aligned} \tag{11.36}$$

This equation has a unique solution, where f satisfies Lipschitz conditions and the solution of (11.36) on $[0, \tau]$ coincides with the solution of (11.32) on $[0, \tau]$. Once the solution y is known on $[0, \tau]$, we can repeat the same procedure, starting with the solution on $[0, \tau]$, to find the solution for $\tau \leq t \leq 2\tau$, etc. This procedure is called *method of steps*,³ and yields a unique defined solution of the resulting system of FODDEs (11.32), given the initial function $\psi(t)$ on $[0, \tau]$. Therefore, FODDEs (11.32) can be numerically solved by a step-by-step fractional-order ODE integrator provided that the solution is known up to the current integration point.

Next, we will approximate the fractional derivative by a simple quadrature formula, using the Caputo fractional derivative (11.1) of order α , $0 < \alpha \leq 1$, and using *implicit Euler's* approximation as follows (see [37]):

$$\begin{aligned} D_*^\alpha x_i(t_n) &= \frac{1}{\Gamma(1-\alpha)} \int_0^t \frac{dx_i(s)}{ds} (t_n - s)^{-\alpha} ds \\ &\approx \frac{1}{\Gamma(1-\alpha)} \sum_{j=1}^n \int_{(j-1)h}^{jh} \left[\frac{x_i^j - x_i^{j-1}}{h} + O(h) \right] (nh - s)^{-\alpha} ds \\ &= \frac{1}{(1-\alpha)\Gamma(1-\alpha)} \sum_{j=1}^n \left\{ \left[\frac{x_i^j - x_i^{j-1}}{h} + O(h) \right] \times [(n-j+1)^{1-\alpha} - (n-j)^{1-\alpha}] \right\} h^{1-\alpha} \end{aligned}$$

³ Method of steps is not universal, as it cannot be applied with time-varying delays, which vanish in some points.

$$\begin{aligned}
&= \frac{1}{(1-\alpha)\Gamma(1-\alpha)} \frac{1}{h^\alpha} \sum_{j=1}^n \left[x_i^j - x_i^{j-1} \right] \times \left[(n-j+1)^{1-\alpha} - (n-j)^{1-\alpha} \right] \\
&\quad + \frac{1}{(1-\alpha)\Gamma(1-\alpha)} \sum_{j=1}^n \left[x_i^j - x_i^{j-1} \right] \times \left[(n-j+1)^{1-\alpha} - (n-j)^{1-\alpha} \right] O(h^{2-\alpha}).
\end{aligned}$$

Setting

$$\begin{aligned}
\mathcal{G}(\alpha, h) &= \frac{1}{(1-\alpha)\Gamma(1-\alpha)} \frac{1}{h^\alpha}, \\
\text{and } \omega_j^\alpha &= j^{1-\alpha} - (j-1)^{1-\alpha}, \quad (\text{where } \omega_1^\alpha = 1),
\end{aligned} \tag{11.37}$$

then the first-order approximation method for the computation of Caputo's fractional derivative is given by the expression

$$D_*^\alpha x_i(t_n) = \mathcal{G}(\alpha, h) \sum_{j=1}^n \omega_j^\alpha \left(x_i^{n-j+1} - x_i^{n-j} \right) + O(h). \tag{11.38}$$

From the analysis and numerical approximation, we also arrive at the following proposition:

Proposition 11.1 *The presence of a fractional differential order in a differential equation can lead to a notable increase in the complexity of the observed behavior, and the solution continuously depends on all previous states.*

11.5.1 Stability and Convergence of Implicit Scheme for FODDEs

In this section, we prove that the fractional-order implicit difference approximation (11.38) is unconditionally stable. It then follows that the numerical solution converges to the exact solution as $h \rightarrow 0$. To study the stability of the numerical method, let us consider a test problem of a linear scalar fractional differential equation

$$\begin{aligned}
D_*^\alpha u(t) &= \rho_0 u(t) + \rho_1 u(t-\tau), \quad t \geq 0, \quad 0 < \alpha \leq 1 \\
u(t) &= \psi(t), \quad t \in [-\tau, 0], \quad u(0) = u_0
\end{aligned} \tag{11.39}$$

such that $\rho_0 < 0$, $|\rho_1| < \rho_0$ and $\psi(t)$ is a continuous and bounded function.

Theorem 11.5 *The fully implicit numerical approximation (11.38), to test problem (11.39) for all $t \geq 0$, is consistent and unconditionally stable.*

Proof We assume that $\tau = mh$ and the approximate solution of (11.39) is of the form $u(t_n) \approx U^n \equiv \zeta_n$, and $u(t_n - \tau) \approx \zeta_{n-m}$; then, the Eq. (11.39) can be reduced to

$$\left(1 - \frac{\rho_0}{\mathcal{G}_{\alpha,h}}\right) \zeta_n = \zeta_{n-1} + \sum_{j=2}^n \omega_j^{(\alpha)} (\zeta_{n-j} - \zeta_{n-j+1}) + \rho_1 \zeta_{n-m}/\mathcal{G}_{\alpha,h}, \quad n \geq m \quad (11.40)$$

and

$$\begin{aligned} \left(1 - \frac{\rho_0}{\mathcal{G}_{\alpha,h}}\right) \zeta_n &= \zeta_{n-1} + \sum_{j=2}^n \omega_j^{(\alpha)} (\zeta_{n-j} - \zeta_{n-j+1}) \\ &\quad + \rho_1 \psi(t_{n-m})/\mathcal{G}_{\alpha,h}, \quad n = 2, \dots, m. \end{aligned} \quad (11.41)$$

Therefore,

$$\zeta_n = \frac{\zeta_{n-1} + \sum_{j=2}^n \omega_j^{(\alpha)} (\zeta_{n-j} - \zeta_{n-j+1}) + \rho_1 \zeta_{n-m}/\mathcal{G}_{\alpha,h}}{\left(1 - \frac{\rho_0}{\mathcal{G}_{\alpha,h}}\right)}, \quad n \geq 2. \quad (11.42)$$

Since $\left(1 - \frac{\rho_0}{\mathcal{G}_{\alpha,h}}\right) \geq 1$ for all $\mathcal{G}_{\alpha,h}$, then

$$\zeta_1 \leq \zeta_0, \quad (11.43)$$

$$\zeta_n \leq \zeta_{n-1} + \sum_{j=2}^n \omega_j^{(\alpha)} (\zeta_{n-j} - \zeta_{n-j+1}), \quad n \geq 2. \quad (11.44)$$

Thus, for $n = 2$, the above inequality implies

$$\zeta_2 \leq \zeta_1 + \omega_2^{(\alpha)} (\zeta_0 - \zeta_1).$$

Using the relation (11.43) and the positivity of the coefficients ω_2 , we get

$$\zeta_2 \leq \zeta_1.$$

Repeating the process, we have from (11.44)

$$\zeta_n \leq \zeta_{n-1} + \sum_{j=2}^n \omega_j^{(\alpha)} (\zeta_{n-j} - \zeta_{n-j+1}) \leq \zeta_{n-1},$$

since each term in the summation is negative. Thus, $\zeta_n \leq \zeta_{n-1} \leq \zeta_{n-2} \leq \dots \leq \zeta_0$. With the assumption that $\zeta_n = |U^n| \leq \zeta_0 = |U^0|$, which entails $\|U^n\| \leq \|\psi(t_0)\|$ and we have stability. \square

Of course, this numerical technique can be used both for linear and for non-linear problems, and it may be extended to multi-term FODDEs as well.

11.5.2 Numerical Simulations

In this subsection, to verify the effectiveness of the obtained results, some numerical simulations for the fractional-order PP system (11.8) have been conducted. All the differential equations are solved using the method proposed in this chapter. In all numerical runs, the solution has been approximated using the parameter values given in the captions of the figures. Figures 11.2, 11.3 and 11.4 show the numerical simulations of model (11.8), with different values of the model parameters given in the corresponding captions. According to the obtained analysis, Fig. 11.2 shows that the numerical simulations of the model, for particular values of the parameters, admit limit cycles, whereas Fig. 11.3 shows that periodic solutions arise due to Hopf bifurcation. When the reproduction number $\mathcal{R}_0 < 1$, the semi-trivial equilibrium is stable (see Fig. 11.4); however, when $\mathcal{R}_0 > 1$, the semi-trivial equilibrium is unstable and interior equilibrium exists. The interior equilibrium is stable if $1 < \mathcal{R}_0 \leq \mathcal{R}_c$ and a sustained periodic solution is obtained when $\mathcal{R}_0 > \mathcal{R}_c$.

It has been seen that the fractional derivative damps the oscillation behavior of the model (see Figs. 11.5, 11.6, 11.7 and 11.8).

Remark 11.3 For $\alpha \in (0, 1]$ the fractional order is defined by Caputo sense (11.1) so that introducing a convolution integral with a power-law memory kernel is useful to describe memory effects in dynamical systems. The decay rate of the memory kernel (a time correlation function) depends on α . A lower value of α corresponds to more slowly decaying time-correlation functions (long memory) [51]. Therefore, as $\alpha \rightarrow 1$, the influence of memory decreases. Therefore, in the above figures, we observe that the phase portrait gets stretched as the order of the derivative is reduced.

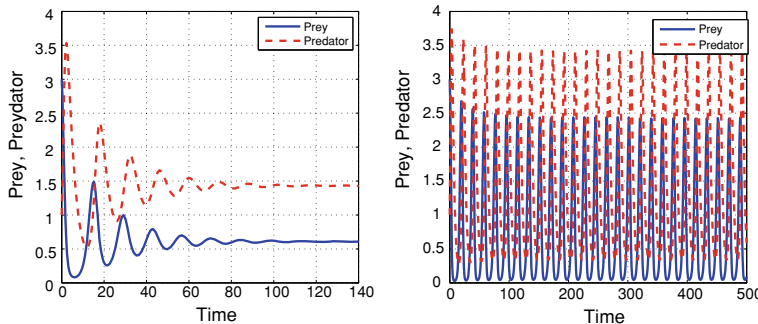


Fig. 11.2 Solution of PP model (11.8) when $r = 0.8, k = 5, \sigma = 0.01, \beta = 0.5; a = 0.3$, and $\mathcal{R}_0 > \mathcal{R}_c > 1$ with time-lag $\tau = 0.1 < \tau^*$ (top) and $\tau = \tau^* = 0.86$ (bottom), which display periodic outbreak of the disease due to a Hopf bifurcation when $\tau = \tau^*$

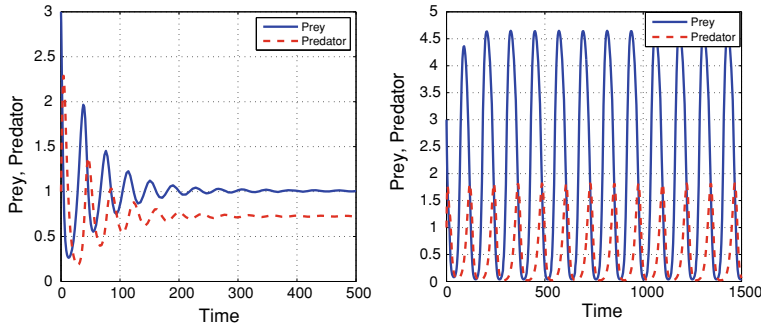


Fig. 11.3 Solution of PP model (11.8), when $r = 0.2$, $k = 5$, $\sigma = 0.01$, $\beta = 0.2$; $a = 0.2$, and $\mathcal{R}_0 = 4.7 > \mathcal{R}_c = 3$ with time-lag $\tau = 0.01 < \tau^*$ (top) and $\tau = 12$ (bottom), which display periodic outbreak of the disease due to a Hopf bifurcation when $\tau = \tau^*$

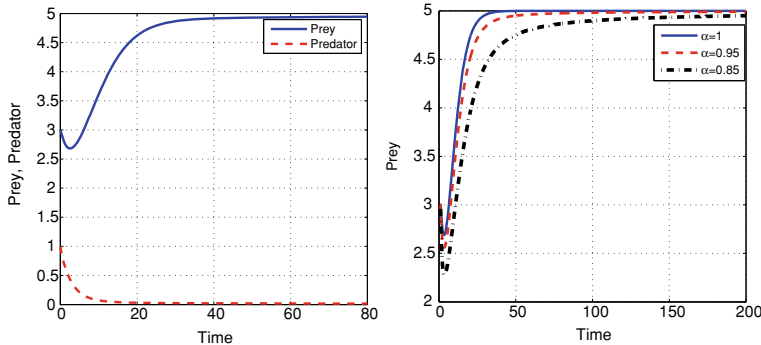


Fig. 11.4 Solution of delayed PP model (11.8). We have asymptotically stable semi-trivial equilibrium $\mathcal{E}_1 = (K, 0)$ when $\mathcal{R}_0 < 1$, with $r = 0.2$, $K = 5$, $\sigma = 0.01$, $\beta = 0.2$, $a = 1$; and $\tau = 1$

11.6 Concluding Remarks

In this chapter, we have introduced a fractional-order PP model with time-delay in the response function. We have also studied local stability and global stability behaviors of all the feasible equilibrium states of the system. It has been found that Hopf bifurcation occurs when the delay passes through a sequence of critical values τ^* , with fractional order $0 < \alpha \leq 1$. We derived the conditions in terms of the threshold parameter \mathcal{R}_0 , which guarantees the asymptotic stability of the semi-trivial and interior equilibria. When $\mathcal{R}_0 < 1$, the semi-trivial equilibrium \mathcal{E}_1 is asymptotically stable for all values of $\tau > 0$ and unstable when $\mathcal{R}_0 > 1$. If all roots of the characteristic equation have negative parts, then the zero solution of the fractional-order delay PP system is Lyapunov globally asymptotical stable. If $\mathcal{R}_0 > \mathcal{R}_c > 1$, then there exists $\tau^* > 0$ such that $\tau \in [0, \tau^*)$ the interior equilibrium \mathcal{E}_+ is asymptotically stable, and unstable when $\tau > \tau^*$.

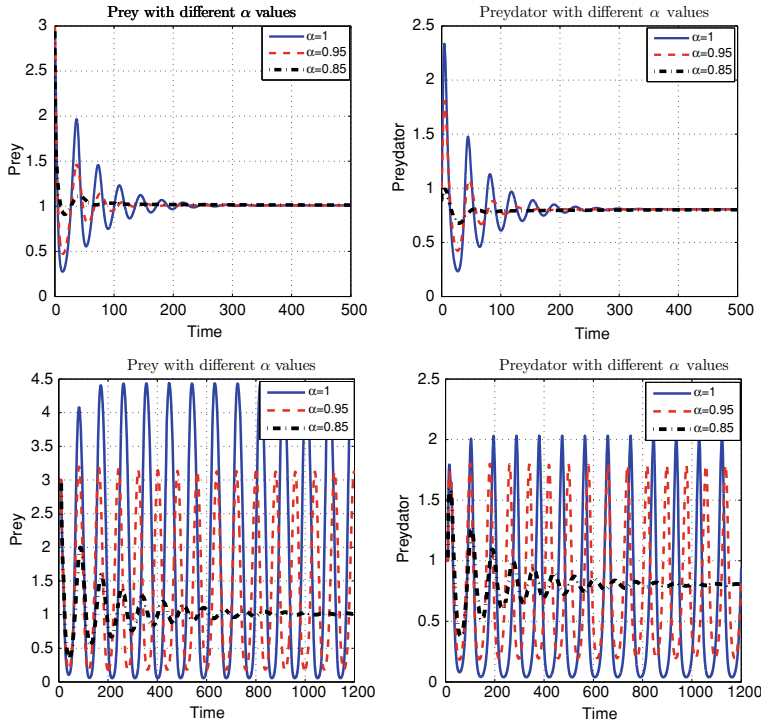


Fig. 11.5 Solution of PP model (11.8) when $r = 0.2$, $k = 5$, $\sigma = 0.01$, $\beta = 0.2$; $a = 0.2$, and $\mathcal{R}_0 = 4.7 > \mathcal{R}_c = 3$ with time-lag $\tau = 0.01 < \tau^*$ (top) and $\tau = 12$ (bottom), which display periodic outbreak of the disease due to a Hopf bifurcation when $\tau = \tau^*$

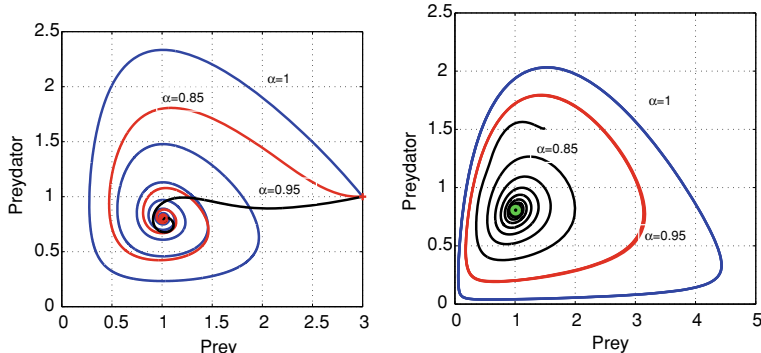


Fig. 11.6 The behavior of the PP model (11.8) with different fractional-order $0 < \alpha \leq 1$, with the same parameter values of Fig. 11.5. The fractional derivative damps the oscillation behavior

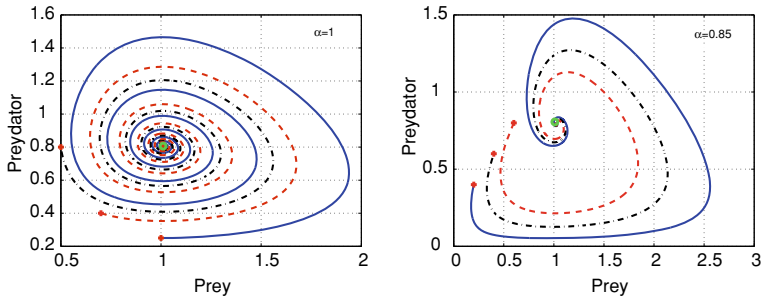


Fig. 11.7 The behavior of the PP model (11.8) with different initial conditions $\tau = 0.2 < \tau^*$. The fractional derivative damps the oscillation behavior

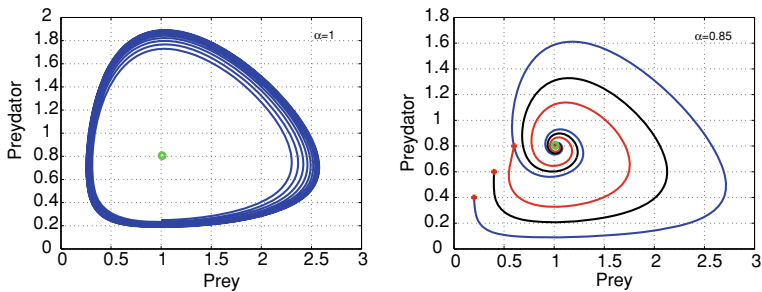


Fig. 11.8 The behavior of the PP model (11.8) with different initial conditions and $\tau = 1 > \tau^*$. The fractional derivative damps the oscillation behavior

We also introduced a suitable numerical method based on an implicit scheme for FODDEs. The numerical simulations demonstrate the accuracy and efficiency of the numerical scheme. Fractional-order models with time-delay are consistent with the dynamics of real PP interactions. We have seen from the numerical simulations that the fractional derivative improves the stability of the solutions and sometimes dampens the oscillation behavior of the solutions.

In the next chapter, we extend the analysis to investigate the dynamics of HCV infection using FODDEs.

References

1. Ahmed, E., Hashish, A., Rihan, F.A.: On fractional order cancer model. *J. Frac. Cal. Appl.* **3**(2), 1–6 (2012)
2. Edelman, M.: Fractional maps as maps with power-law memory. In: Afraimovich, A., Luo, A.C.J., Fu, X. (eds.) *Nonlinear Dynamics and Complexity*, pp. 79–120. Springer, New York (2014)
3. Rihan, F.A., Abdelrahman, D.H.: Delay differential model for tumor-immune dynamics with HIV infection of CD4+ T-cells. *Int. J. Comput. Math.* **90**(3), 594–614 (2013)

4. Tarasov, V.E.: Discrete map with memory from fractional differential equation of arbitrary positive order. *J. Math. Phys.* **50**, 122703 (2009)
5. Laskin, N., Zaslavsky, G.M.: Nonlinear fractional dynamics on a lattice with long-range interactions. *Physica A* **368**, 38–54 (2006)
6. Luo, A.C., Afraimovich, V. (eds.): *Long-Range Interaction, Stochasticity and Fractional Dynamics*. Springer, New York (2010)
7. Zaslavsky, G.M., Edelman, M., Tarasov, V.E.: Dynamics of the chain of forced oscillators with long-range interaction: from synchronization to chaos. *Chaos* **17**(4), 043124 (2007)
8. Cole, K.S.: Electric conductance of biological systems. In: *Cold Spring Harbor Symposia on Quantitative Biology*, pp. 107–116 (1993)
9. El-Sayed, A.M.A., El-Mesiry, A.E.M., El-Saka, H.A.A.: On the fractional-order logistic equation. *Appl. Math. Lett.* **20**(7), 817–823 (2007)
10. Rihan, F.A., Abdelrahman, D.H., Lakshmanan, S.: A time delay model of tumour-immune system interactions: Global dynamics, parameter estimation, sensitivity analysis. *Appl. Math. Comput.* **232**, 606–623 (2014)
11. Xu, H.: Analytical approximations for a population growth model with fractional order. *Commun. Nonlinear Sci. Numer. Simul.* **14**, 1978–1983 (2009)
12. Debnath, L.: Recent applications of fractional calculus to science and engineering. *Int. J. Math. Math. Sci.* **54**, 3413–3442 (2003)
13. El-Sayed, A.M.A.: Nonlinear functional differential equations of arbitrary orders. *Nonlinear Anal.: Theory Methods Appl.* **33**(2), 181–186 (1998)
14. Hilfer, R. (ed.): *Applications of Fractional Calculus in Physics*. World Scientific, River Edge (2000)
15. Zaslavsky, G.M.: Chaos, fractional kinetics, and anomalous transport. *Phys. Rep.* **371**, 461580 (2002)
16. Yuste, S.B., Acedo, L., Lindenberg, K.: Subdiffusion-limited A+B → C reaction-subdiffusion process. *Phys. Rev. E* **69**(3), 036126 (2004)
17. Lin, W.: Global existence theory and chaos control of fractional differential equations. *J. Math. Anal. Appl.* **332**, 709–726 (2007)
18. Sheng, H., Chen, Y.Q., Qiu, T.S.: *Fractional Processes and Fractional-Order Signal Processing*. Springer, New York (2012)
19. Sheng, H.: Entropy analysis of integer and fractional dynamical systems. *Nonlinear Dyn.* **62**(1–2), 371–378 (2010)
20. Machado, J.A.T., Galhano, A.M.S.F.: Fractional order inductive phenomena based on the skin effect. *Nonlinear Dyn.* **68**(1–2), 107–115 (2012)
21. Assaleh, K., Ahmad, W.M.: Modeling of speech signals using fractional calculus. In: *9th International Symposium on Signal Processing and Its Applications (ISSPA 2007)* (2007)
22. Ferdri, Y.: Some applications of fractional order calculus to design digital filters for biomedical signal processing. *J. Mech. Med. Biol.* **12**(2) (2012), 13 p.
23. Grahovac, N.M., Zicic, M.M.: Modelling of the hamstring muscle group by use of fractional derivatives. *Comput. Math. Appl.* **59**, 1695–1700 (2010)
24. Chen, W.-C.: Nonlinear dynamics and chaos in a fractional-order financial system. *Chaos Solitons Fractals* **36**(5), 1305–1314 (2008)
25. Caponetto, R., Dongola, G., Fortuna, L.: *Fractional Order Systems: Modeling and Control Applications*. World Scientific, London (2010)
26. Machado, J.A.T.: Analysis and design of fractional-order digital control systems. *Syst. Anal. Model. Simul.* **27**, 107–122 (1997)
27. Machado, J.A.T.: Fractional-order derivative approximations in discrete-time control systems. *Syst. Anal. Model. Simul.* **34**, 419–434 (1999)
28. Li, L., Wang, Z.-J.: Global stability of periodic solutions for a discrete predator-prey system with functional response. *Nonlinear Dyn.* **72**, 507–516 (2013)
29. Meng, X., Jiao, J., Chen, L.: The dynamics of an age structured predator-prey model with disturbing pulse and time delays. *Nonlinear Anal.: Real World Appl.* **9**, 547–561 (2008)

30. Tang, G., Tang, S., Cheke, R.A.: Global analysis of a Holling type II predator-prey model with a constant prey refuge. *Nonlinear Dyn.* **76**, 635–664 (2014)
31. Xia, Y., Cao, J., Cheng, S.S.: Multiple periodic solutions of a delayed stage-structured predator-prey model with non-monotone functional responses. *Appl. Math. Model.* **31**, 1947–1959 (2007)
32. Zhang, J.-F.: Bifurcation analysis of a modified Holling-Tanner predator-prey model with time delay. *Appl. Math. Model.* **36**, 1219–1231 (2012)
33. Javidi, M., Nyamoradi, N.: Dynamic analysis of a fractional order prey-predator interaction with harvesting. *Appl. Math. Model.* **37**, 8946–8956 (2013)
34. Rivero, M., Trujillo, J.J., Vazquez, L., Velasco, M.P.: Fractional dynamics of populations. *Appl. Math. Comput.* **218**, 1089–1095 (2011)
35. Baleanu, D., Diethelm, K., Scalas, E., Trujillo, J.J.: *Fractional Calculus Models and Numerical Methods*. World Scientific, Singapore (2012)
36. Diethelm, K., Ford, N.J., Freed, A.D.: A predictor-corrector approach for the numerical solution of fractional differential equations. *Nonlinear Dyn.* **29**, 3–22 (2002)
37. Diethelm, K., Ford, N.J., Freed, A.D.: Computational methods for delay parabolic and time fractional partial differential equations. *Numer. Methods Part. Differ. Equ.* **26**(6), 1556–1571 (2010)
38. Das, S., Gupta, P.K.: A mathematical model on fractional Lotka-Volterra equations. *J. Theor. Biol.* **277**, 16 (2011)
39. Rihan, F.A., Baleanu, D., Lakshmanan, S., Rakkiyappan, R.: On fractional SIRC model with salmonella bacterial infection. *Abst. Appl. Anal.* **2014** (2014), 9 p.
40. Podlubny, I.: *Fractional Differential Equations*. Academic, Cambridge (1999)
41. Lotka, A.: *Elements of Physical Biology*. Williams and Wilkins, Baltimore (1925)
42. Volterra, V.: Fluctuations in the abundance of a species considered mathematically. *Nature* **118**, 558–560 (1926)
43. Freedman, H.I.: *Deterministic Mathematical Models in Population Ecology*. Marcel Dekker, New York (1980)
44. Petras, I.: *Fractional-Order Nonlinear Systems: Modeling, Analysis and Simulation*. Springer, London; HEP, Beijing (2011)
45. Deng, W., Li, C., Lu, J.: Stability analysis of linear fractional differential system with multiple time delays. *Nonlinear Dyn.* **48**, 409–416 (2007)
46. Li, C.P., Zhang, F.R.: A survey on the stability of fractional differential equations. *Eur. Phys. J. Spec. Top.* **193**, 27–47 (2011)
47. Muth, E.J.: *Transform Methods with Applications to Engineering and Operations Research*. Prentice-Hall, New Jersey (1977)
48. Suzuki, T.: A generalized Banach contraction principle that characterizes metric completeness. *Proc. Am. Math. Soc.* **136**(5), 1861–1869 (2008)
49. Anguelov, R., Lubuma, J.M.-S.: Nonstandard finite difference method by nonlocal approximation. *Math. Comput. Simul.* **61**, 465–475 (2003)
50. Diethelm, K.: An algorithm for the numerical solution of differential equations of fractional order. *Electron. Trans. Numer. Anal.* **5**, 1–6 (1997)
51. Rihan, F.A., Al-Mdallal, Q., Al-Sakaji, H.J., Hashish, A.: A fractional-order epidemic model with time-delay and nonlinear incidence rate. *Chaos Solitons Fractals* **126**, 97–105 (2019)

Chapter 12

Fractional-Order Delay Differential Equations of Hepatitis C Virus



12.1 Introduction

In this chapter, we investigate a fractional-order delay differential model reflecting the dynamics of Hepatitis C virus (HCV) replication in the presence of interferon- α treatment. We consider a fractional order in the model to represent the intermediate cellular interactions and intracellular delay of the viral life cycle and incorporate a discrete time-delay to justify the short-run memory. The fractional order is also considered with existing model parameters to unify the units of the differential equations. We analyze the steady states and dynamical behavior of the model. We deduce a threshold parameter \mathcal{R}_0 (average number of newly infected cells produced by a single infected cell) in terms of the treatment efficacy parameter $0 \leq \varepsilon < 1$ and other parameters. The numerical simulations confirm that the suggested model with fractional order and time-delay can provide accurate description of non-linear biological systems with memory. The analyses presented here will give the reader an insight into the dynamics of HCV infection.

HCV is an infectious disease that spreads through blood contact. It is estimated that about 200 million individuals have been infected by HCV worldwide [1]. About 50–80% of HCV infected cases are chronic in nature [2]. Of these chronic cases, about 10–20% develop into liver cirrhosis of which, about 5% develop hepatocellular carcinoma. The extent of prevalence of HCV varies widely across geographical locations. In most countries, the transmission of HCV occurs primarily through *injecting drug use* (IDU), which is mainly associated with the sharing of contaminated syringes/needles. Moreover, the absence of reliable screening for HCV among blood donors remains a major challenge in combating the spread of the disease in Eastern countries [3]. Geographically, HCV genotypes 1, 2, and 3 occur globally, whereas infection with HCV genotypes 4 and 5 occurs mainly in Africa, and HCV genotype 6 appears mainly in Asia [4]. Many mathematical epidemic models quantify the transmission of HCV among IDUs in the population. These models provide alternative means to define the problems, organize our thoughts, understand the data,

communicate, test our understanding, and help in making predictions among groups [5]. Currently, there is a motivation for further study of the dynamics and mathematical modeling of HCV on a cellular level; see [6] and references therein.

Mathematical models using ODEs with integer order have proved valuable in understanding the dynamics of HCV infections on a cellular level or in one host [7, 8]. Most of these models have been restricted to the short-term dynamics of the systems. One of the earliest models was proposed by Neumann et al. [9], who examined the dynamics of HCV in the presence of interferon- α treatment. They found that the primary role of interferon- α is in blocking the production of virions from the infected hepatocytes. Dahari et al. [7], in a subsequent and improved model, considered the homeostatic mechanisms for the liver by incorporating a growth function.

However, classical mathematical models with integer orders ignore the intermediate cellular interactions and memory effects. For example, the kinetics of the viral decline in patients responding to interferon- α is characterized by bi-phase shape following a delay of approximately 8–9 h, likely to be the sum of interferon- α pharmacokinetics and pharmacodynamics as well as the intracellular delay of the viral life cycle [10]. Therefore, modeling of the biological systems using fractional-order differential equations is more advantageous than classical integer-order mathematical modeling, in which such effects are neglected [11–13].

Fractional-order differential equations are naturally related to systems with memory, which are found in most biological systems [14–16]. Moreover, all biological models have long-range historical memory or after-effects (such as delay due to incubation time for vectors to become infectious). A fractional-order optimal control problem for HIV-immune system is proposed in [17]. Rihan and Velmurugan, in [18], proposed a delay differential model with fractional order for tumor immune systems with external treatment. They investigated the necessary and sufficient conditions for stability of the steady states and Hopf bifurcation, with respect to two different tumor time-delays. A fractional-order model of cytotoxic T lymphocyte response with long-term behavior of tumor growth and with tumor elimination was investigated in [19]. In [12], a fractional dynamical system of predator-prey with Holling type-II functional response and time-delay was studied. It was deduced in [20] that the membranes of cells of a biological organism have fractional-order electrical conductance, and they were then classified into groups of non-integer order models.

In this chapter, we propose a system of *fractional-order delay differential equations* (FODDEs) for modeling the dynamics of HCV to capture, as accurately as possible, the dynamics of the target cell population: uninfected target cells, infected cells, and viral load in presence of antiviral interferon- α drugs. We assume here that the target cells of the model are hepatocytes. The organization of the chapter is as follows: In Sect. 12.2, we propose a fractional-order delay model of HCV. In Sect. 12.3, we investigate the local stability of the steady states. Section 12.4 discusses the global asymptotic stability of infection-free steady state. In Sect. 12.5, we provide some numerical simulations and investigate the validity of the model by fitting

the model to available data for HCV RNA production For a decay profile case and a chronically infected case during treatment with interferon- α using least-squares approach. We then conclude the chapter in Sect. 12.6.

12.2 Mathematical Model of HCV

The model that we consider for HCV infection is based on a three-dimensional model given by Dahari et al. [7] and the model by Neumann et al. [9]. They assumed a simplified view of HCV infection and described the response to interferon therapy through the coupled evolution of three populations: the uninfected hepatocytes, the productively infected hepatocytes, and the free HCV virions, with the following ODEs:

$$\begin{aligned} DH &= s - \mu_1 H - k_1 V H, \\ DI &= k_2 V H - \mu_2 I, \\ DV &= \mu_3^\alpha I - \mu_4 V. \end{aligned} \quad (12.1)$$

Here, $D \equiv \frac{d}{dt}$, $H = H(t)$ represents the concentration of uninfected (healthy) hepatocytes, $I = I(t)$ is the concentration of infected hepatocytes, and $V = V(t)$ is the concentration of free HCV at time t . The model assumes that uninfected hepatocytes are produced at a constant rate of s , die at rate of μ_1^α per cell, and are infected at a constant rate k_1 . Infected hepatocytes are lost at a rate of μ_2^α per cell. The HCV V is assumed to infect the hepatocytes at a rate k_1 ; thereby, producing infected hepatocytes I . k_2^α is the rate at which infected cells become actively infected. Viral particles (virions) are produced at a rate μ_3^α per infected hepatocyte and cleared at a rate of μ_4^α per virion.

The literature reveals that most mathematical models of viral-immune interactions are based either on ODEs or DDEs with integer order. Indeed, combining both time-delays and fractional-order in the biological systems gives it more degree of freedom and consistency [18, 21]. Herein, we modify the above standard model to include a time-delay to describe the time between an HCV or infected cell contacting an uninfected hepatocyte and the emission of new active HCV. We also replace the integer order by a fractional-order α ($0.5 < \alpha \leq 1$) to the system to naturally relate the system with memory that exists in viral life cycle and to describe long-range interaction of the disease [22]. Moreover, the parameters of the modified model will also depend on the fractional-order to unify the units of the differential equations. The modified model with logistic proliferation of uninfected hepatocytes takes the form

$$\begin{aligned} D^\alpha H(t) &= s^\alpha - \mu_1^\alpha H(t) + r^\alpha H(t) \left(1 - \frac{H(t) + I(t)}{H_{max}} \right) - k_1^\alpha V(t)H(t), \\ D^\alpha I(t) &= k_2^\alpha e^{-\mu_1^\alpha \tau} V(t - \tau)H(t - \tau) - \mu_2^\alpha I(t), \\ D^\alpha V(t) &= (1 - \varepsilon)\mu_3^\alpha M I(t) - k_1^\alpha V(t)H(t) - \mu_4^\alpha V(t). \end{aligned} \quad (12.2)$$

with initial conditions $H(t) = \psi_1(t)$ for $t < 0$ and $H(0) = H_0 > 0$, $V(t) = \psi_2(t)$ for $t < 0$ and $I(0) = I_0 > 0$, and $V(0) = V_0 > 0$. It should be mentioned that the left sides of all equations of the system have dimension $\text{time}^{-\alpha}$. To make the system more consistent with reality, we must ensure that the right-hand sides of these equations have the same dimensions. Therefore, we need to modify the right-hand sides to make the dimensions match. We assume that the uninfected hepatocytes H are being produced at a rate s^α and proliferate logistically $\left(1 - \frac{H + I}{H_{max}}\right)$ at a rate r^α , accompanied by a natural death rate of μ_1^α , and that H_{max} is the maximum hepatocyte count in the liver. We assume that the proliferation of infected cells is neglected and that physiological conditions $\mu_1^\alpha H_{max} > s$, $r > \mu_1^\alpha$. In the absence of any kind of treatment, the infected hepatocytes produce HCV at a rate μ_3^α , which has a clearance rate of μ_4^α . In this model, the impact of antiviral interferon- α drugs on the dynamics of the viral infection is considered by the coefficients $(1 - \varepsilon)$, where ε is the efficacy of interferon- α . The viral production rate is then lowered by a fraction ε . μ_2^α is a blanket death term for infected cells to reflect the assumption that we do not initially know whether the cells die naturally or by bursting. The time-delay τ represents an intracellular delay that is between initial infection of a cell by HCV and the release of new virions, and only a fraction of $e^{-\mu_1^\alpha \tau}$ can survive after the interval τ . The term $e^{-\mu_1^\alpha \tau}$ represents the proportion of latently infected cells becoming actively infected after τ period of time. Since M viral particles are released by each lysing cell, this term is multiplied by the parameter M to represent the source of free virus (assuming a one-time initial infection); see Fig. 12.1.

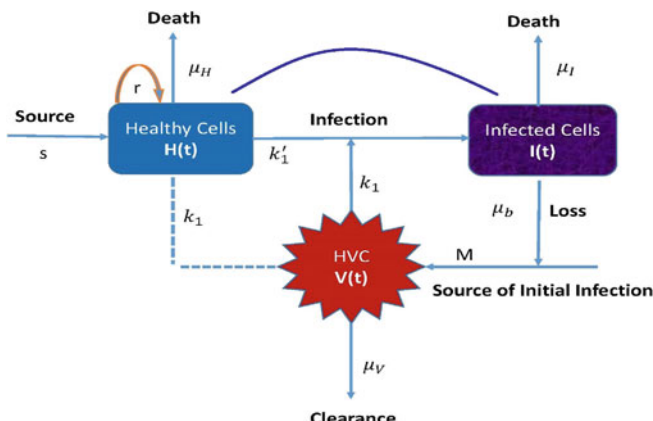


Fig. 12.1 Schematic diagram showing the key players in HCV infection models. $H(t)$ and $I(t)$ represent target and infected cells, respectively, and $V(t)$ represents free virus

Table 12.1 Parameter definitions and values used in the model

| Parameter | Description | Units | Value | Source |
|---------------|---|--|--------------------------|--------|
| s | Production rate of uninfected hepatocytes | cell $\text{ml}^{-1}\text{day}^{-1}$ | 0.1 | [7] |
| μ_1 | Natural death rate of rate of effector cells | day^{-1} | 0.6 | [7] |
| r | Proliferation rate of uninfected hepatocytes | day^{-1} | 0.05 | |
| H_{max} | Maximum hepatocyte count in the liver | cells ml^{-1} | 2×10^6 | [7] |
| k_1 | Infection rate of hepatocytes | $\text{ml day}^{-1} \text{virions}^{-1}$ | 0.08 | [10] |
| k_2 | Rate of infected cells become actively infected | $\text{ml day}^{-1} \text{virions}^{-1}$ | 0.45 | |
| μ_2 | Natural death rate of infected cells | day^{-1} | 0.28 | [10] |
| μ_3 | Production rate of HCV by the infected cells | $\text{cell}^{-1} \text{day}^{-1}$ | 1×10^{-4} | |
| μ_4 | Clearance rate of HCV | $\text{virions virions day}^{-1}$ | 2×10^{-2} | [7] |
| M | Source of free virus in the initial infection | virion | 200 | [10] |
| ε | The efficacy of IFN | — | $0 \leq \varepsilon < 1$ | — |

When Hepatitis C virus first infects a person, the ensuing dynamics depend on the relative parameter values (see Table 12.1). Since newly infected individuals do not know that they are infected, we assume there is initially no treatment ($\varepsilon = 0$). We might expect several different scenarios: infection may fade out without becoming established, infection may spread with limited success and infect only part of the liver, or infection may spread rapidly and infect the whole liver. For untreated chronically infected patients with HCV, the mean serum viral load is approximately $3.5 \times 10^6 \text{ IU/ml}$ according to the WHO HCV RNA standard [23].

To understand the dynamics of system under acute infection corresponding to each of these situations, it is helpful to walk through the stability of the steady states. The boundedness of the solutions is guaranteed by the following theorem:

Theorem 12.1 *The system (12.2) has a unique solution $(H, I, V)^T$ that remains in \mathbb{R}_+^3 and is bounded by H_{max} ; see [24].*

12.3 Local Stability of Infection-Free and Infected Steady States

To evaluate the equilibrium points of system (12.2), we put $D^\alpha H(t) = D^\alpha I(t) = D^\alpha V(t) = 0$. This model admits two steady states, namely, the infection-free steady

state $\mathcal{E}_0 = (H_0, 0, 0)$, where

$$H_0 = \{r^\alpha - \mu_1^\alpha + [(r^\alpha - \mu_1^\alpha)^2 + 4r^\alpha s^\alpha H_{max}^{-1}]^{1/2}\}/2r^\alpha H_{max}^{-1}, \quad (12.3)$$

and the infected state, $\mathcal{E}_+ = (H^*, I^*, V^*)$, where

$$\begin{aligned} H^* &= \frac{\mu_4^\alpha \mu_2^\alpha}{k_2^\alpha M(1-\varepsilon)e^{-\mu_1^\alpha \tau} \mu_3^\alpha - k_1^\alpha \mu_2^\alpha}, \\ I^* &= \frac{k_2^\alpha e^{-\mu_1^\alpha \tau} H^* V^*}{\mu_2^\alpha}, \\ V^* &= \frac{\mu_2^\alpha [(s^\alpha + (r^\alpha - \mu_1^\alpha)H^*)H_{max} - r^\alpha H^{*2}]}{H^*[k_2^\alpha e^{-\mu_1^\alpha \tau} r^\alpha H^* - k_1^\alpha \mu_2^\alpha H_{max}]} . \end{aligned} \quad (12.4)$$

Let us introduce the following definition and assumption to ease the analysis.

Definition 12.1 The basic reproductive number of the virus \mathcal{R}_0 is defined as the average number of newly infected cells produced by a single infected cell at the beginning of the infection. The threshold parameter \mathcal{R}_0 has the property that if $\mathcal{R}_0 < 1$, then the endemic infected state does not exist, whereas if $\mathcal{R}_0 > 1$, the endemic infected state persists, where

$$\mathcal{R}_0 = \frac{k_2^\alpha e^{-\mu_1^\alpha \tau} \mu_3^\alpha (1-\varepsilon) M H_0}{\mu_2^\alpha (\mu_4^\alpha + k_1^\alpha H_0)} . \quad (12.5)$$

The Jacobian matrix $J(\mathcal{E}_0)$ for system (12.2) evaluated at the uninfected steady state \mathcal{E}_0 is then given by

$$J(\mathcal{E}_0) = \begin{pmatrix} -\mu_1^\alpha + r^\alpha - \frac{2rH_0}{H_{max}} - \lambda & -\frac{rH_0}{H_{max}} & -k_1^\alpha H_0 \\ 0 & -\mu_2^\alpha - \lambda & k_2^\alpha e^{-(\mu_1^\alpha + \lambda)\tau} H_0 \\ 0 & (1-\varepsilon)\mu_3^\alpha M & -(k_1 H_0 + \mu_4^\alpha + \lambda) \end{pmatrix} . \quad (12.6)$$

However, Jacobian matrix $J(\mathcal{E}_+)$ for system (12.2) evaluated at the infected steady state \mathcal{E}_+ is

$$J(\mathcal{E}_+) = \begin{pmatrix} -(L^* + \lambda) & -r^\alpha H^*/H_{max} & -k_1^\alpha H^* \\ k_2^\alpha e^{-(\mu_1^\alpha + \lambda)\tau} V^* & -(\mu_2^\alpha + \lambda) & k_2^\alpha e^{-(\mu_1^\alpha + \lambda)\tau} H^* \\ -k_1^\alpha V^* & (1-\varepsilon)M\mu_3^\alpha & -(k_1^\alpha H^* + \mu_4^\alpha + \lambda) \end{pmatrix} . \quad (12.7)$$

Here:

$$L^* = [\mu_1^\alpha - r^\alpha + k_1^\alpha V^* + r^\alpha(2H^* + I^*)/H_{max}] .$$

Then, the characteristic equation of the linearized system is

$$p(\lambda, \tau) = \lambda^3 + a_2 \lambda^2 + a_1 \lambda + a_0 + (b_1 \lambda + b_0) e^{-\lambda \tau} = 0, \quad (12.8)$$

$$\begin{aligned}
a_2 &= \mu_2^\alpha + \mu_4^\alpha + k_1^\alpha H^* + L^*, \\
a_1 &= L^*(\mu_2^\alpha + \mu_4^\alpha + k_1^\alpha H^*) + \mu_2^\alpha(\mu_4^\alpha + k_1^\alpha H^*) - k_1^\alpha e^{-\mu_1^\alpha \tau} H^* \left((1-\varepsilon)M\mu_3^\alpha - \frac{rV^*}{H_{max}} \right), \\
a_0 &= L^*\mu_2^\alpha(k_1^\alpha H^* + \mu_4^\alpha) - \mu_2^\alpha k_1^{\alpha 2} H^* V^* + k_2^\alpha e^{-\mu_1^\alpha \tau} H^* \left(\frac{r\mu_4^\alpha V^*}{H_{max}} + (1-\varepsilon)M\mu_3^\alpha(k_1 V^* - L^*) \right), \\
b_1 &= k_2^\alpha H^* \left(\frac{rV^*}{H_{max}} - (1-\varepsilon)M\mu_3^\alpha \right), \\
b_0 &= \frac{k_2^\alpha H^*}{H_{max}}(rV^* \mu_4^\alpha + (1-\varepsilon)M\mu_3^\alpha H_{max}(k_1 V^* - L^*)).
\end{aligned}$$

Here, a_k ($k = 0, 1, 2$) and b_j ($j = 0, 1$) are non-linear functions of τ . The general form of Eq.(12.8) can be written as

$$p(\lambda, \tau) = p_0(\lambda, \tau) + p_1(\lambda, \tau)e^{-\lambda\tau}, \quad (12.9)$$

where

$$\begin{aligned}
p_0(\lambda, \tau) &= \lambda^3 + a_2(\tau)\lambda^2 + a_1(\tau)\lambda + a_0(\tau), \\
p_1(\lambda, \tau) &= b_1(\tau)\lambda + b_0(\tau).
\end{aligned} \quad (12.10)$$

Case I: $\tau = 0$

For $\tau = 0$, the uninfected steady state is asymptotically stable if all of the eigenvalues λ of the Jacobian matrix $J(\mathcal{E}_0)$, given by (12.6), have negative real parts. The characteristic equation $\det(J(\mathcal{E}_0) - I) = 0$ becomes

$$\lambda^3 + A\lambda^2 + B\lambda + C = 0, \quad (12.11)$$

where $A = k_1^\alpha H_0 + \mu_4^\alpha + \mu_2^\alpha + L_0^*$, $B = L_0^*(\mu_2^\alpha + k_1^\alpha H_0 + \mu_4^\alpha) + \mu_2^\alpha(k_1^\alpha H_0 + \mu_4^\alpha) - (1-\varepsilon)M\mu_3^\alpha k_2^\alpha H_0$, $C = L_0^*(\mu_2^\alpha(k_1^\alpha H_0 + \mu_4^\alpha) - (1-\varepsilon)M\mu_3^\alpha k_2^\alpha H_0)$, and $L_0^* = [\mu_1^\alpha - r^\alpha + \frac{2r^\alpha H^*}{H_{max}}]$.

Proposition 12.1 If $\mathcal{R}_0 \equiv \frac{k_2^\alpha \mu_3^\alpha (1-\varepsilon) M H_0}{\mu_2^\alpha (\mu_4^\alpha + k_1^\alpha H_0)} < 1$, then $A > 0$, $C > 0$, $AB > C$, and the three roots of the characteristic equation (12.11) will have negative real parts.

Assume that

$$\mathcal{R}_0^* = \frac{k_2^\alpha \mu_3^\alpha M H_0}{\mu_2^\alpha (\mu_4^\alpha + k_1^\alpha H_0)} > 1 \geq \mathcal{R}_0. \quad (12.12)$$

Then, under the physiological conditions, $\mu_1^\alpha H_{max} > s$ and $r > \mu_1^\alpha$, we arrive at the following remark.

Remark 12.1 In case of uninfected steady state \mathcal{E}_0 , we have three cases:

- (1) If $\mathcal{R}_0 < 1$, the uninfected state is asymptotically stable and the infected steady-state \mathcal{E}_+ does not exist (unphysical). The efficacy of the drug ε should exceed $\left(1 - \frac{1}{\mathcal{R}_0^*}\right)$ to eradicate the virus.

- (2) If $\mathcal{R}_0 = 1$, then $C = 0$; combined with (12.11), this implies that one eigenvalue must be zero and the remaining two eigenvalues have negative real parts. The uninfected and infected steady states collide and there is a transcritical bifurcation, and the efficacy threshold is $\varepsilon^* = \left(1 - \frac{1}{\mathcal{R}_0^*}\right)$.
- (3) If $\mathcal{R}_0 > 1$, then $C < 0$ and, thus, at least one eigenvalue will be positive real root. Thus, the uninfected state \mathcal{E}_0 is unstable and the endemically infected state \mathcal{E}_+ emerges. The efficacy ε does not exceed $\left(1 - \frac{1}{\mathcal{R}_0^*}\right)$.

For $\tau = 0$, the infected steady-state \mathcal{E}_+ is asymptotically stable if all of the eigenvalues have negative real parts. This occurs if and only if the Routh-Hurwitz conditions are satisfied

$$a_2(0) > 0, \quad a_0(0) + b_0(0) > 0, \quad [a_1(0) + b_1(0)]a_2(0) > a_0(0) + b_0(0).$$

Case II: $\tau \neq 0$

Equation (12.9) can be written as

$$G(\lambda, \tau) = -\frac{p_0(\lambda, \tau)}{p_1(\lambda, \tau)}e^{\lambda\tau}, \quad (12.13)$$

with

$$p_1(\lambda, \tau) \neq 0. \quad (12.14)$$

For $\lambda = i\omega (\omega \in \mathbb{R})$, we get

$$G(i\omega, \tau) = \mu(\omega, \tau)e^{i\theta(\omega, \tau)}, \quad (12.15)$$

where

$$\begin{aligned} \mu(\omega, \tau) &= \left| \frac{p_0(i\omega, \tau)}{p_1(i\omega, \tau)} \right|, \\ \theta(\omega, \tau) &= \angle p_0(i\omega, \tau) - \angle p_1(i\omega, \tau) + \omega\tau + \pi. \end{aligned} \quad (12.16)$$

Clearly, the existence of purely imaginary roots $\lambda = i\omega$ of Eq. (12.9) is equivalent to the following two conditions:

$$\begin{aligned} \mu(\omega, \tau) &= 1, \\ \theta(\omega, \tau) &= 2\pi h, \quad h \text{ is integer.} \end{aligned} \quad (12.17)$$

To establish the existence of purely imaginary roots of Eq. (12.9), the criterion due to Jin et al. [25, 26] is applied. To apply this method, the following assumptions must be achieved for all $\tau \in \Lambda$, where $\Lambda = [0, \tau_{\max}]$ is the range of delay parameters τ of interest:

(A1) $\forall \tau \in \Lambda :$

$$\lim_{\omega \rightarrow \infty} \left| \frac{p_1(i\omega, \tau)}{p_0(i\omega, \tau)} \right| < 1. \quad (12.18)$$

(A2) The following equations are not fulfilled together for any values of the pair (ω, τ) :

$$\begin{aligned} p_0(i\omega, \tau) &= 0, \\ p_1(i\omega, \tau) &= 0. \end{aligned} \quad (12.19)$$

(A3) The following equations have a finite number of pairs (ω, τ) that satisfies it

$$\begin{aligned} \Delta(\omega, \tau) &= 0, \\ \frac{\partial}{\partial \omega} \Delta(\omega, \tau) &= \partial_\omega \Delta(\omega, \tau) = 0, \end{aligned} \quad (12.20)$$

where

$$\Delta(\omega, \tau) = |p_0(i\omega, \tau)|^2 - |p_1(i\omega, \tau)|^2 \quad (12.21)$$

(A4) \forall critical pair (ω^*, τ^*) that satisfies

$$p(i\omega, \tau) = 0, \quad (12.22)$$

then

$$\Re \left. \frac{d\lambda}{d\tau} \right|_{\lambda=i\omega^*, \tau=\tau^*} \neq 0, \quad (12.23)$$

Furthermore, there are a finite number of solutions for (ω, τ) that satisfy (12.22). Note that if ω is a root of $\Delta(\omega, \tau)$, then $-\omega$ is also a root of it.

We first need to find the positive root $\omega = \omega(\tau)$ that satisfies Eq.(12.21) and then identify the critical values (ω^*, τ^*) at which the switch stability has occurred on it. To find the root, we suppose that $\tau_j, j = 1, 2, \dots, m-1$ is the set of all $\tau \in \Lambda$ that satisfies assumption (A3). Then we ascend these τ_j as

$$\tau_1 < \tau_2 < \dots < \tau_{m-1}.$$

Then, Λ is divided into m subintervals as

$$\Lambda_j = [\tau_{j-1}, \tau_j], j = 1, 2, \dots, m,$$

where $\tau_0 = 0$ and $\tau_m = \tau_{\max}$. The following proposition characterizes the positive roots in each portion Λ_j [25, 26].

Proposition 12.2 *For each $\tau \in [\tau_{j-1}, \tau_j]$, the number of real roots of $\Delta(\omega, \tau)$ are the same and simple. These roots are continuous functions of τ and may be expressed as $\pm \omega_{jk}(\tau)$, $k = 1, 2, \dots, q$, $q \leq m$.*

Therefore, the phase angle functions in each subinterval Λ_j can be defined as

$$\theta_{jk}(\omega(\tau), \tau) = \angle p_0(i\omega_{jk}(\tau), \tau) - \angle p_1(i\omega_{jk}(\tau), \tau) + \omega_{jk}(\tau)\tau + \pi. \quad (12.24)$$

To identify the critical delay $\tau = \tau^*$, one goes through each interval Λ_j and each curve $\omega_{jk}(\tau)$ and then finds the values of τ at which the following equation is satisfying

$$\theta_{jk}(\tau^*) = 2\pi h, \quad h \text{ is integer.}$$

Hence, one gets the critical values (ω^*, τ^*) at which the stability switches occur. Next, the direction stability of these critical values is investigated. In other words, we need to know in which direction these critical values cross the imaginary axis. To do that, the sign of the real part of the differentiation of λ with respect to τ must be determined, i.e.,

$$\operatorname{sign} \left[\Re \left(\frac{d\lambda}{d\tau} \right) \Big|_{\lambda=i\omega^*, \tau=\tau^*} \right]. \quad (12.25)$$

If the sign is negative (positive), it means the roots are crossing the imaginary axis from the right (left) to left (right), which indicates that the system is stable (unstable). The following theorem is used for determining the sign of the real part of the derivative of λ with respect to τ [25, 26].

Theorem 12.2 *Let (ω^*, τ^*) satisfy Eqs. (12.22) and (12.23). Then,*

$$\operatorname{sign} \left[\Re \left(\frac{d\lambda}{d\tau} \right) \Big|_{\lambda=i\omega^*, \tau=\tau^*} \right] = \operatorname{sign} [\partial_\omega \Delta(\omega, \tau)]_{\omega=\omega^*, \tau=\tau^*} \times \operatorname{sign} \left[\frac{d\theta(\omega(\tau), \tau)}{d\tau} \right]_{\omega=\omega^*, \tau=\tau^*}. \quad (12.26)$$

12.4 Global Stability of Infection-Free Steady State \mathcal{E}_0

Lemma 12.1 ([27]) *Let $x(t) \in \mathbb{R}^+$ be a continuous and derivative function. Then, for any time $t \geq t_0$,*

$${}_{t_0} D_t^\alpha \left[x(t) - x^* - x^* \ln \frac{x(t)}{x^*} \right] \leq \left(1 - \frac{x^*}{x(t)} \right) {}_{t_0} D_t^\alpha x(t), \quad \forall \alpha \in (0, 1), x^* \in \mathbb{R}^+.$$

Theorem 12.3 *Assume that $k_2^\alpha w_1 e^{-\mu_1^\alpha \tau} < k_1^\alpha w_2$, $w_2(1 - \varepsilon) \mu_3^\alpha M < w_1 \mu_2^\alpha$; then, the fractional-order HCV model (12.2) is globally asymptotically stable at an infection-free steady-state \mathcal{E}_0 .*

Proof We define the following positive definite Lyapunov function:

$$\mathcal{V}(t) = \left(H(t) - H^* - H^* \ln \frac{H(t)}{H^*} \right) + w_1 I(t) + w_2 V(t),$$

where w_1 and w_2 are non-negative constants. Take fractional derivative of \mathcal{V} with respect to time t , yielding

$$\begin{aligned}
& D^\alpha \mathcal{V}(t) \\
& \leq \frac{(H(t) - H^*)}{H(t)} \left(s^\alpha - \mu_1^\alpha H(t) + r^\alpha H(t) \left(1 - \frac{H(t) + I(t)}{H_{max}} \right) - k_1^\alpha V(t) H(t) \right) \\
& \quad + w_1 \left(k_2^\alpha e^{-\mu_1^\alpha \tau} V(t - \tau) H(t - \tau) - \mu_2^\alpha I(t) \right) + w_2 \left((1 - \varepsilon) \mu_3^\alpha M I(t) - k_1^\alpha V(t) H(t) - \mu_4^\alpha V(t) \right), \\
& \leq (H - H^*) \left(\frac{-s^\alpha(H - H^*)}{HH^*} - \frac{r^\alpha}{H_{max}}(H - H^*) - \frac{rI}{H_{max}} - k_1^\alpha V \right) \\
& \quad + w_1 k_2^\alpha e^{-\mu_1^\alpha \tau} VH - w_1 \mu_2^\alpha I + w_2 (1 - \varepsilon) \mu_3^\alpha MI - w_2 k_1^\alpha VH - w_2 \mu_4^\alpha V, \\
& \leq - \left(s + \frac{r^\alpha}{H_{max}} \right) (H - H^*)^2 - \frac{rI}{H_{max}} (H - H^*) - k_1^\alpha V (H - H^*) - (k_1^\alpha w_2 - k_2^\alpha w_1 e^{-\mu_1^\alpha \tau}) VH \\
& \quad - (w_1 \mu_2^\alpha - w_2 (1 - \varepsilon) \mu_3^\alpha M) I - w_2 \mu_4^\alpha V
\end{aligned}$$

Based on the assumption that $k_2^\alpha w_1 e^{-\mu_1^\alpha \tau} < k_1^\alpha w_2$, $w_2 (1 - \varepsilon) \mu_3^\alpha M < w_1 \mu_2^\alpha$, we can obtain

$$D^\alpha \mathcal{V}(t) \leq 0.$$

Hence, the theorem is proved.

12.5 Numerical Simulations and Validity of Model

In this section, we carry out numerical simulations to show the qualitative behavior of model (12.2) and verify it by fitting the model (12.2) to experimental data of HCV RNA replications. The numerical simulations confirm the theoretical results obtained in the above sections. The simulations have been obtained by using the Adams-Bashforth-Moulton predictor-corrector scheme, discussed in [13], with step size $h = 0.005$ and $0.5 < \alpha \leq 1$.

For $s = 10$, $\mu_1 = 0.02$, $r = 0.03$, $H_{max} = 1500$, $k_1 = 2.42 \times 10^{-5}$, $k_2 = 2 \times 10^{-5}$, $\mu_2 = 0.26$, $M = 800$, $\mu_3 = 0.26$, and $\mu_4 = 2.4$, the infection-free steady state is $\mathcal{E}_0 = (1000, 0, 0)$ and the infected steady-state \mathcal{E}_+ is

$$\begin{aligned}
H^* &= -99173.6 + \frac{10^8 e^{-0.26\tau}}{100833e^{-0.26\tau} - 1.6522}, \\
I^* &= \frac{1.18393 \times 10^7 e^{-0.26\tau} + 1.88509 \times 10^6 - 628384e^{0.26\tau}}{376312 - 1226.9e^{0.26\tau} + e^{0.52\tau}}, \\
V^* &= 82370.7 + 251691e^{-0.26\tau} + \frac{10^8 e^{-0.26\tau}}{1.9786 - 122002e^{-0.26\tau}}.
\end{aligned}$$

This steady state exists if $\tau \leq 6.95017$.

We first investigate the stability of the infection-free steady-state \mathcal{E}_0 . The corresponding characteristic equation (12.9) at this point can be written as

$$p(\lambda, \tau) = \lambda^3 + 2.7142\lambda^2 + 0.710818\lambda + 0.0189088 + \left(-3.84e^{-0.26\tau}\lambda - 0.1152e^{-0.26\tau}\right)e^{-\lambda\tau}. \quad (12.27)$$

Then,

$$\Delta(\omega, \tau) = \omega^6 + a\omega^4 + b\omega + c, \quad (12.28)$$

where $a = 5.94525$, $b = 0.402618 - 14.7456e^{-0.52\tau}$, and $c = 357541 \times 10^{-9} - 0.013271e^{-0.52\tau}$.

For $\tau = 0$, the roots of Eq. (12.27) are

$$\lambda_1 = -3.58061, \lambda_2 = -0.03, \lambda_3 = 0.896413,$$

which means that \mathcal{E}_0 is unstable.

However, to ensure the stability of \mathcal{E}_0 for $\tau > 0$, we must check the validity of assumptions (A1)–(A4):

- Obviously, from Eq. (12.27), assumption (A1) is satisfied. It is achieved for any value of the parameters.
- Suppose that

$$p_1(i\omega, \tau) = -3.84e^{-0.26\tau}i\omega - 0.1152e^{-0.26\tau} = 0.$$

Therefore, from Eq. (12.5), we obtain

$$\omega = 0.03i \notin \mathbb{R}.$$

Thus, there is no value of (ω, τ) that satisfies $p_1(i\omega, \tau) = 0$. Therefore, (A2) is satisfied.

- Solving Eqs. (12.20) together, we find that $\Lambda \equiv [0, \tau_{max}]$ can be decomposed into two subintervals $\Lambda_1 \cup \Lambda_2$, where

$$\Lambda_1 = [\tau_0, \tau_1], \Lambda_2 = [\tau_1, \tau_2],$$

$\tau_0 = 0$, $\tau_1 = 6.95017$, and $\tau_2 = \tau_{max} \rightarrow \infty$. The polynomial $\Delta(\omega, \tau)$ has one real positive root $\omega_{11}(\tau)$ in Λ_1 and does not have any real solution in Λ_2 . Thus, assumption (A3) is satisfied.

- From Eq. (12.26), it is easy to get

$$\Re\left(\frac{d\lambda}{d\tau}\right)_{\lambda=i\omega_1^*, \tau=\tau_1^*} = 6.16123 > 0, \quad \Re\left(\frac{d\lambda}{d\tau}\right)_{\lambda=i\omega_2^*, \tau=\tau_2^*} = -0.451645 < 0.$$

Therefore, assumption (A4) is satisfied.

From the above discussion, we arrive at the following theorem:

Theorem 12.4 *The infection-free steady state is locally asymptotically stable for $\tau \in (\tau_2^*, \infty)$ and unstable for $\tau \in [0, \tau_2^*]$.*

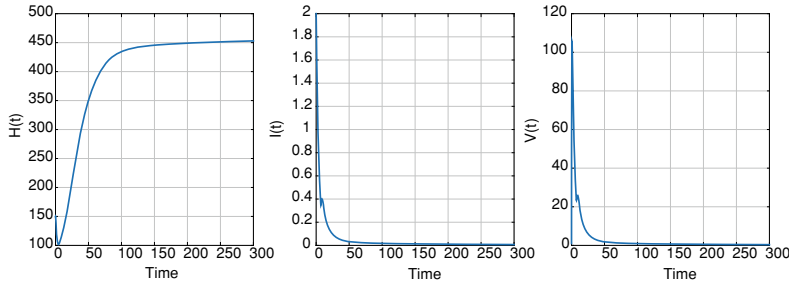


Fig. 12.2 Infection-free steady-state \mathcal{E}_0 of model (12.2) when $\tau = 7 \in (\tau_2^*, \infty)$ with $\mathcal{R}_0 < 1$ and $\alpha = 1$

Regarding the infected steady-state \mathcal{E}_+ , the roots of Eq. (12.27) for $\tau = 0$ are

$$\lambda_1 = -2.67009, \lambda_{2,3} = -0.0292724 \pm 0.12279i,$$

which means that the infected steady-state \mathcal{E}_+ is stable when $\tau = 0$.

To investigate the stability of \mathcal{E}_+ for $\tau > 0$, we must check the validity of assumptions (A1)–(A4).

Figure 12.2 shows that the infection-free steady-state \mathcal{E}_0 is stable when $\tau = 7 \in (\tau_2^*, \infty)$ with $\mathcal{R}_0 < 1$. Moreover, the infected steady-state \mathcal{E}_+ is stable when $\tau = 1 \in [0, \tau_2^*)$; see Fig. 12.3. Figure 12.4 displays an oscillating behavior of model (12.2) when $\tau = \tau^*$.

Figure 12.5 shows an asymptotically stable infected steady-state \mathcal{E}_+ for different values of the fractional-order α , when $\mathcal{R}_0 > 1$. Figure 12.6 shows an infection-free steady-state \mathcal{E}_0 when $\mathcal{R}_0 < 1$. A complete recovery is obtained when $\mathcal{R}_0 < 1$. Before treatment $\varepsilon = 0$, a steady state exists where viral production is balanced by viral clearance and the production of infected cells is balanced by their loss. Uninfected hepatocytes are also in steady state determined by the balance between their production, death, and loss due to infection. We notice that the smaller value of the fractional-order α , the longer is incubational period of the virus in the beginning stage.

12.5.1 Parameter Estimation and Validity of Model

To check the reality of the underlying model, we use non-linear least squares regression, discussed in Chap. 5, to fit the model to real observations. Given the parameterized biological system (12.2), with right-hand side depending on the constant vector of parameters:

$$\mathbf{P} = [s^\alpha, \mu_1^\alpha, r, k_1^\alpha, k_2^\alpha, \mu_2^\alpha, \mu_3^\alpha, \mu_4^\alpha].$$

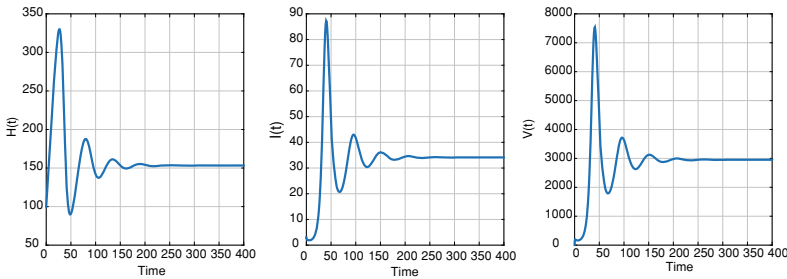


Fig. 12.3 Endemic (infected) steady-state \mathcal{E}_+ of model (12.2) when $\tau = 1 \in [0, \tau_2^*)$ with $\mathcal{R}_0 > 1$ and $\alpha = 1$

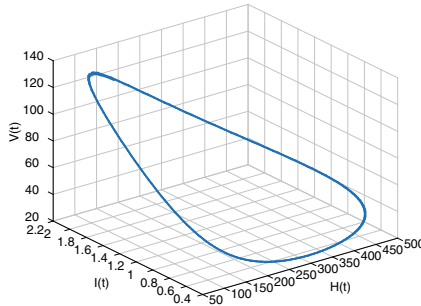


Fig. 12.4 Oscillating behavior of model (12.2) when $\tau = \tau^*$

Let \mathbf{X}_i ($i = 1, 2, \dots, m$) denote a set of observed data vectors with component X_{ij} ($j = 1, 2, 3$), where m is the amount of data. Let $\mathbf{x}(t_i; \tilde{\mathbf{p}}) \equiv [H(t_i), I(t_i), V(t_i)]^T$ denote the “true” solution of the system at time t_i and exact value of parameter $\tilde{\mathbf{p}}$. We assume that data \mathbf{X}_i satisfy the following observation equation:

$$X_{ij} = x_j(t_i) + \sigma_j \varepsilon_{ij} \quad (12.29)$$

where $\sigma_j > 0$ measures the variance of the noise associated with the j th component and is related to the scale of the expected magnitude of the j th component, $|X_j(t)|$. The ε_{ij} are independent and standard Gaussian distributed random variables. The principle of maximum-likelihood yields an appropriate cost function that should be minimized with respect to the parameters \mathbf{p} to yield an approximation $\hat{\mathbf{p}}$ of the true value. We define the cost function or objective function by

$$\Phi(\mathbf{P}) = \sum_{i=1}^m \varepsilon_i^T \omega_i(\sigma) \varepsilon_i \equiv \frac{1}{n} \sum_{i=1}^m \sum_{j=1}^n \frac{[x_j(t_i; \mathbf{p}) - X_{ij}]^2}{2\sigma_j^2}, \quad (12.30)$$

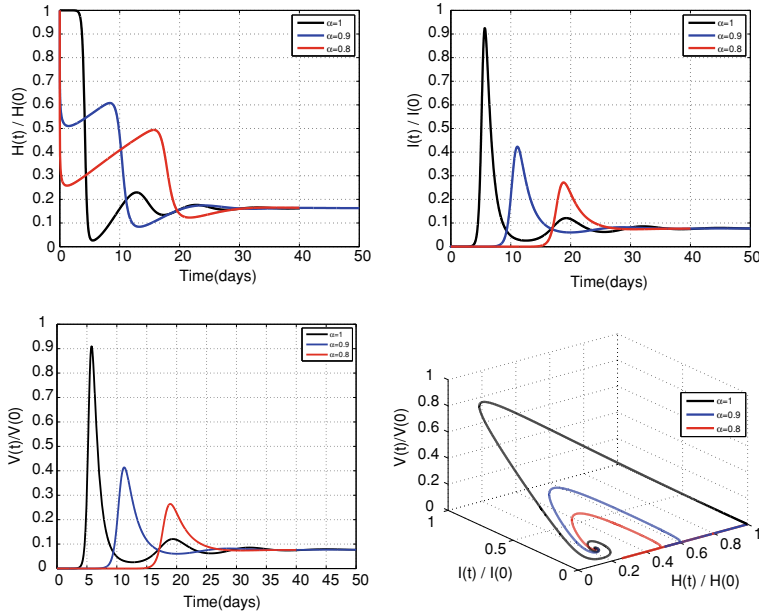


Fig. 12.5 Numerical simulations of the HCV model (12.2) that show a stable infected steady state \mathcal{E}_+ with different fractional order α , with parameter values given in Table 12.1, and with $\varepsilon = 0.0$ ($\mathcal{R}_0 > 1$). The fractional order plays the role of memory and heredity

We seek $\hat{\mathbf{p}}$ that satisfies

$$\Phi(\hat{\mathbf{p}}) =: \min_{\mathbf{p}} \Phi(\mathbf{p}) \equiv \max_{\mathbf{p}} \mathcal{L}(\mathbf{p}). \quad (12.31)$$

where $\mathcal{L}(\mathbf{p}) = [\exp(-\varepsilon_{ij}^2/2\sigma_j^2)]/\sqrt{2\pi\sigma_j^2}$ is the likelihood function; see [28].

Estimation of the parameters that occur in model (12.2), for given data, is considered as an optimization problem that should include the following steps [29]:

1. Provide an initial guess \mathbf{p}_0 for the parameter estimates;
2. Solve the model equations with the current values of the parameters using the scheme in Sect. 12.4;
3. Adjust the parameter values by a minimization routine such as OPTIMTOOL in MATLAB;
4. Check stopping conditions; if satisfied, stop;
5. Otherwise, choose a better value for \mathbf{p} and return to step 2.

The underlying FODEs model is non-linear; thus, the selection of local minima should be based on meaningful biological parameters. To examine the underlying model (12.2), we have used the generated experimental data given in Table 12.2. The dataset taken from Neumann et al. [9] was used to find estimates of the parameters.

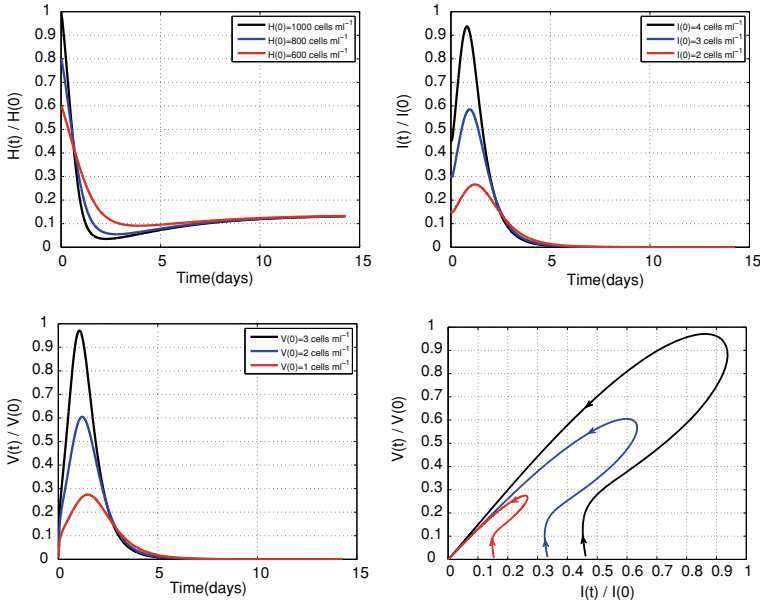


Fig. 12.6 Numerical simulations of the HCV model (12.2) that show a stable infection-free steady-state \mathcal{E}_0 with the same parameter values of Fig. 12.5 but with $r = 0.1$ (increasing proliferation rate of the uninfected hepatocytes) and $k_1 = 0.01$ (decreasing the infection rate of hepatocytes). A complete recovery is obtained when $\mathcal{R}_0 < 1$

Table 12.2 Hepatitis C viremia within 14 days of treatment with interferon- α in a patient [9] (Case I)

| Time (days) | 1 | 2 | 3 | 4 | 5 | 6 | 7 |
|-------------------------------------|-----|-----|-----|------|------|-----|-----|
| $\log_{10} \bar{V}(t)/\text{liver}$ | 8.5 | 8.6 | 8.5 | 10.7 | 10.5 | 7.2 | 4.1 |
| Time (days) | 8 | 9 | 10 | 11 | 12 | 13 | 14 |
| $\log_{10} \bar{V}(t)/\text{liver}$ | 3.5 | 2.6 | 1.6 | 0.7 | 0.6 | 0.4 | 0.3 |

The data was produced to better understand the dynamics of HCV and the antiviral effect of interferon- α . The major initial effect of interferon- α is to block virion production or release, with blocking efficacies of 81, 95, and 96% for daily doses of 5, 10, and 15 million international units, respectively. The estimated virion half-life ($t_{1/2} = 1/2$) was, on average, 2.7 h, with pretreatment production and clearance of 10^{12} virions per day. The estimated infected cell death rate exhibited large interpatient variation (corresponding $t_{1/2} = 1.7 - 7$ days), was inversely correlated with baseline viral load, and was positively correlated with alanine aminotransferase levels; see [10, 30].

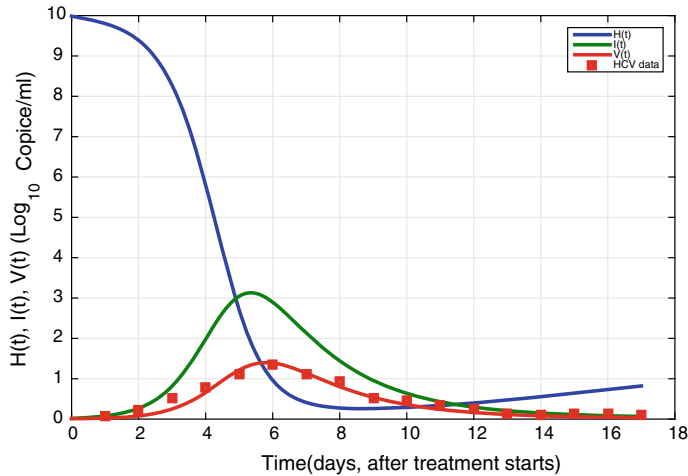


Fig. 12.7 Comparison of viral load data (squares) with model predictions (12.2) for a case of HCV RNA decay profile during antiviral therapy, INF- α [31]. The treatment efficacy, as an estimate, is $\varepsilon = 0.950$. Other parameter values and estimates are given in the text

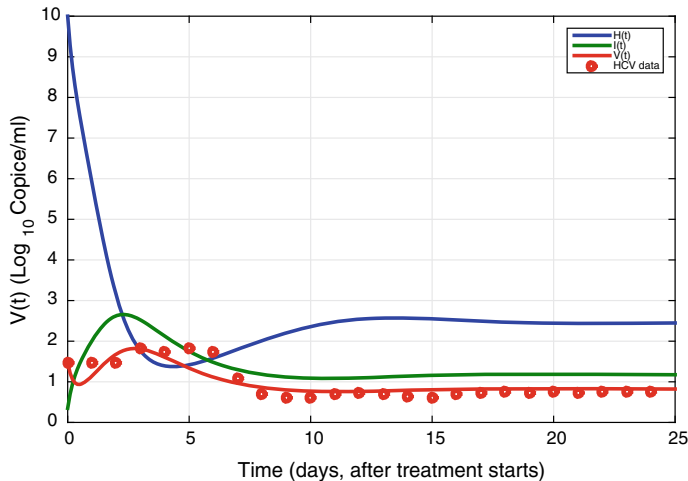


Fig. 12.8 Comparison of viral load data with model predictions for a case of HCV RNA persist (endemic) steady state during INF- α therapy [31]. The treatment efficacy, as an estimate, $\varepsilon = 0.701$

Table 12.3 Hepatitis C viremia within 25 days of treatment with interferon- α in a patient [9] (Case II)

| Time (days) | 1 | 2 | 3 | 4 | 5 | 6 | 7 | 8 | 9 | 10 | 11 | 12 | 13 | 14 |
|-------------------------------------|-----|------|-----|------|------|-----|-----|-----|-----|-----|-----|-----|-----|-----|
| $\log_{10} \bar{V}(t)/\text{liver}$ | 9.6 | 10.2 | 8.5 | 10.1 | 10.2 | 8.2 | 6.2 | 4.5 | 3.6 | 3.6 | 4.0 | 3.8 | 4.2 | 4.1 |
| Time (days) | 15 | 16 | 17 | 18 | 19 | 20 | 21 | 22 | 23 | 24 | 25 | | | |
| $\log_{10} \bar{V}(t)/\text{liver}$ | 3.7 | 3.5 | 4.0 | 4.2 | 4.3 | 4.2 | 4.3 | 4.2 | 4.4 | 4.4 | 4.3 | | | |

In Fig. 12.7, we fit the model (12.2) to the experimental data of Table 12.2 during antiviral therapy ($0 < \varepsilon < 1$) for HCV-infected patients. We fixed all the parameters except $P = [r, k_1, \mu_4^\alpha, \varepsilon]$. The rest of the parameters take the values $s = 0.1 \times 10^2$, $k_2^\alpha = 0.0103$, $M = 800$, $H_{max} = 1.4 \times 10^3$, $\mu_1^\alpha = 0.0107$, and $\mu_2^\alpha = 0.31$. Using least squares approach, the unknown parameters are $\hat{P} = [0.0401, 0.017, 0.731, 0.601]$. The reproductive number for the best estimate and infection-free steady state is $\mathcal{R}_0 = 0.7654 < 1$. The decay occurs rapidly during the treatment and the efficacy of treatment in blocking virion production $\varepsilon = 0.950$. The simulation matches the viral-free steady-state \mathcal{E}_0 . Figure 12.8 shows the fitting of the model (12.2) to the real data of Table 12.3 for chronically infected patients during treatment. The parameter estimates with such data are $\hat{P} = [0.004, 0.021, 1.701, 0.502]$.

12.6 Concluding Remarks

In this chapter, we have developed a mathematical model for HCV dynamics to describe the interactions between healthy liver cells H , infected liver cells I , and virus load V . The model is governed by a system of fractional-order delay differential equations. While the model is overly simple in that it does not account for the immune response to HCV infection, it reflects the complex dynamics sufficiently due to the fractional-order derivative (which considers the longer term behavior) and time-delay (which considers the short memory of the HCV kinetics). The basic reproductive number of the virus \mathcal{R}_0 has been deduced in understanding the persistence of viral infections. If $\mathcal{R}_0 < 1$, the level of virus load and infected cells will monotonically decrease and ultimately be eliminated. However, for $\mathcal{R}_0 > 1$, there will be a chronic HCV infection. The higher the reproductive number \mathcal{R}_0^* , the higher treatment efficacy ε is required to eradicate the virus. When $\mathcal{R}_0 < 1$, the treatment efficacy ε greater than $(1 - 1/\mathcal{R}_0^*)$ leads to complete clearance of infection. We also deduced a threshold parameter τ^* so that the infection-free steady-state \mathcal{E}_0 is locally asymptotically stable for $\tau \in (\tau^*, \infty)$ and unstable when $\tau \in [0, \tau^*)$, whereas the infected steady state \mathcal{E}_+ is stable when $\tau \in [0, \tau^*)$ and unstable when $\tau \in (\tau^*, \infty)$.

The model prediction is validated by fitting the model to available data for HCV RNA production for a decay profile case and a chronic infected case during treatment with interferon- α . When $\mathcal{R}_0 < 1$, the decay of the virion occurs rapidly during the

treatment and the estimated efficacy of the drug (in blocking virion production) is $\varepsilon = 0.950$. While for the chronic state $\mathcal{R}_0 > 1$, the estimated efficacy parameter is $\varepsilon = 0.701$. In this case of the infected steady state, the higher value of ε will not have enough of an effect to reduce the viral load and keep the threshold parameter $\mathcal{R}_0 < 1$.

Our findings show that the combination of fractional-order derivative and time-delay in the model improves the dynamics and increases the complexity of the model. Matching the dimensions of both sides of the differential equations improves the consistency of the model with the real data/observations.

References

- WHO.: Fact sheet No. 164: Hepatitis C. www.who.int/gate2.inist.fr/mediacentre/factsheets/fs164/en/. Accessed 31 Jan 2014
- Mainardi, F., Gorenflo, R.: On Mittag-Leffler-type functions in fractional evolution processes. *J. Comput. Appl. Math.* **118**, 283–299 (2000)
- Mukhopadhyay, A.: Hepatitis C in India. *J. Biosci.* **33**(4), 465–473 (2008)
- Afdhal, H.N.: The natural history of hepatitis C. *Semin. Liver Dis.* **24**(2), 3–8, 5, 6 (2004)
- Wasley, A., Alter, M.J.: Epidemiology of hepatitis C: geographic differences and temporal trends. *Semin. Liver Dis.* **20**(1), 1–16 (2000)
- Ramirez, I.: Mathematical modeling of immune responses to hepatitis C virus infection. Ph.D. thesis, East Tennessee State University (2014)
- Dahari, H., Lo, A., Ribeiro, R.M., Perelson, A.S.: Modeling hepatitis C virus dynamics: liver regeneration and critical drug efficacy. *J. Theor. Biol.* **47**, 371–381 (2007)
- Perelson, A.S.: Modelling viral and immune system dynamics. *Nat. Rev. Immunol.* 28–36 (2002)
- Tanner, J.T.: The stability and intrinsic growth rates of prey and predator populations. *Ecology* **56**, 855–867 (1975)
- Zeuzem, S., Herrmann, E.: Dynamics of hepatitis C virus infection. *Ann. Hepatol.* **1**(2), 56–63 (2002)
- Rihan, F.A., Abdelrahman, D.H.: Delay differential model for tumor-immune dynamics with HIV infection of CD4+ T-cells. *Int. J. Comput. Math.* **90**(3), 594–614 (2013)
- Rihan, F.A., Lakshmanan, S., Hashish, A.H., Rakkiyappan, R., Ahmed, E.: Fractional order delayed predator-prey systems with Holling type-ii functional response. *Nonlinear Dyn.* **80**(1), 777–789 (2015)
- Rihan, F.A., Al-Mdallal, Q., AlSakaji, H.J., Hashish, A.: A fractional-order epidemic model with time-delay and nonlinear incidence rate. *Chaos Solitons Fractals* **126**, 97–105 (2019)
- Chinnathamb, R., Rihan, F.A., Alsakaji, H.J.: A fractional-order model with time delay for tuberculosis with endogenous reactivation and exogenous reinfections. *Math. Methods Appl. Sci.* 1–20 (2019)
- Rakkiyappan, R., Latha, V.P., Rihan, F.A.: A fractional-order model for zika virus infection with multiple delays. *Complexity* **2019**, 1–15 (2019)
- Magin, R.L.: Fractional calculus models of complex dynamics in biological tissues. *Comput. Math. Appl.* **59**, 1586–1593 (2010)
- Ding, Y., Wang, Z., Ye, H.: Optimal control of a fractional-order HIV-immune system with memory. *IEEE Trans. Control Syst. Tech.* **20**(3), 763–769 (2012)
- Rihan, F.A., Velmurugan, G.: Dynamics of fractional-order delay differential model for tumor-immune system. *Chaos Solitons Fractals* **132**, 1–14 (2020)
- Arshad, S., Baleanu, D., Huang, J., Tang, Y., Al Qurashi, M.M.: Dynamical analysis of fractional order model of immunogenic tumors. *Adv. Mech. Eng.* **8**(7), 1687814016656704 (2016)

20. Cole, K.S.: Electric conductance of biological systems. In: Spring Harbor Symposia on Quantitative Biology, pp. 107–116 (1993)
21. Rakkiyappan, R., Latha, V.P., Rihan, F.A.: A fractional-order model for zika virus infection with multiple delays. Complexity (2019), 20 p
22. Ahmed, E., El-Saka, H.A.: On fractional order models for hepatitis C. Nonlinear Biomed. Phys. **4**(1), 1–4 (2010)
23. Pawlotsky, J.M., Bouvier-Alias, M., Hezode, C., Darthuy, F., Remire, J., Dhumeaux, D.: Standardization of hepatitis C virus RNA quantification. Hepatology **32**(3), 654–9 (2000)
24. Lin, W.: Global existence theory and chaos control of fractional differential equations. J. Math. Anal. Appl. **332**, 709–726 (2007)
25. Jin, C., Gu, K., Boussaada, I., Niculescu, S.I.: Stability analysis of a more general class of systems with delay-dependent coefficients. IEEE Trans. Autom. Control **64**(5), 1989–1998 (2018)
26. Jin, C., Gu, K., Niculescu, S.I., Boussaada, I.: Stability analysis of systems with delay-dependent coefficients: an overview. IEEE Access **6**, 27392–27407 (2018)
27. Li, H.L., Zhang, L., Hu, C., Jiang, Y.L., Teng, Z.: Dynamical analysis of a fractional-order prey-predator model incorporating a prey refuge. J. Appl. Math. Comput.
28. Bard, Y.: Nonlinear Parameter Estimation. Academic, New York (1974)
29. Marchuk, G.I., Romanyukha, A.A., Bocharov, G.A.: Mathematical model of antiviral immune response ii: parameter identification for acute viral hepatitis-B. J. Theor. Biol. **151**, 41–70 (1991)
30. Yasui, K., Okanoue, T., Murakami, Y., Itoh, Y., Minami, M., Sakamoto, S., Sakamoto, M., Nishioji, K.: Dynamics of hepatitis C viremia following interferon- α administration. J. Infect. Dis. **177**, 1475–1479 (1998)
31. Dahari, H., Major, M., Zhang, X., Mihalik, K., Rice, C.M., Perelson, A.S., Feinstone, S.M., Neumann, A.U.: Mathematical modeling of primary hepatitis C infection: noncytolytic clearance and early blockage of virion production. Gastroenterology **128**, 1056–1066 (2005)

Chapter 13

Stochastic Delay Differential Model for Coronavirus Infection COVID-19



13.1 Introduction

Environmental factors, such as humidity, precipitation, and temperature, have significant impacts on the spread of coronavirus COVID-19 to humans. In this chapter, we use a stochastic epidemic SIRC model, with cross-immune class and time-delay in transmission terms, for the spread of COVID-19. We analyze the model and prove the existence and uniqueness of positive global solution. We deduce the basic reproduction number \mathcal{R}_0^s for the stochastic model which is smaller than \mathcal{R}_0 of the corresponding deterministic model. Sufficient conditions that guarantee the existence of a unique ergodic stationary distribution, using the stochastic Lyapunov function, and conditions for the extinction of the disease are obtained. We provide a stochastic SIRC model with time delay in Sect. 13.2. In Sect. 13.3, we study the existence and uniqueness of a global positive solution for the stochastic delayed SIRC model. In Sects. 13.4 and 13.5, a stationary distribution and extinction analysis of the underlying model are investigated. Some virtual numerical examples are presented in Sect. 13.6. Finally, concluding remarks are provided in Sect. 13.7.

The ongoing pandemic Coronavirus Disease (COVID-19) is spreading fast, endangering large number of people health, and thus needs immediate actions and intensive studies to control the disease in communities [1]. COVID-19 is the seventh member of the coronavirus (CoV) family, such as MERS-CoV and SARS-CoV [2]. Although SARS-CoV was more deadly, it was much less infectious than COVID-19. There have been no outbreaks of SARS anywhere in the world since 2003. The symptoms of COVID-19 infection include cough, fever, tiredness, diarrhea, and shortness of breath. Mostly in severe cases, COVID-19 causes pneumonia and death [3]. The primary studies show that the incubation period of COVID-19 is between 3 and 14 days or longer [4]. Additionally, the average of basic reproduction number \mathcal{R}_0 for COVID-19 is about 2–2.8. The disease may still be infectious in the latent infection period. Studies to date suggest that the virus is very serious and spreads fast from

Table 13.1 Incubation period of several common infectious diseases

| Disease | Range | Ref. |
|-------------|-------------------------------|------|
| COVID-19 | 3–14 days | [4] |
| Cholera | 0.5–4.5 days | [23] |
| Common cold | 1–3 days | [24] |
| Ebola | 1–21 days | [25] |
| HIV | 2–3 weeks to months or longer | [26] |
| Influenza | 1–3 days | [27] |
| MERS | 2–14 days | [28] |
| SARS | 1–10 days | [29] |

person to person through close contact and respiratory droplets rather than through the air [4]. Table 13.1 shows the incubation period of several common infectious diseases.

Mathematical modeling of infectious diseases has an important role in the epidemiological aspect of disease control [5]. Several epidemic models, with various characteristics, have been described and investigated in the literature. Most of these models are based on the susceptible-infected-removed (SIR) model. Casagrandi et al. [6] introduced the SIRC model to describe the dynamical behavior of influenza A by inserting a new compartment, namely the Cross-Immunity (C) component¹ of people who have recovered after being infected by different strains of the same viral subtype in previous years. Component C describes an intermediate state between susceptible S and recovered R. Rihan et al. [7] investigated the qualitative behavior of the fractional-order SIRC model for Salmonella bacterial infection. Recently, in [8], the authors provided a deterministic SEIR epidemic model of fractional order to describe the dynamics of COVID-19. In other descriptions, quarantine state (Q) may be included in the presence of subjects, such as SIRQ models [9].

In fact, stochastic perturbation factors such as precipitation, absolute humidity, and temperature have a significant impact on the infection force of all types of viral diseases in humans. Taking this into consideration enables us to introduce randomness into deterministic biological models to expose the environmental variability effect, whether it is an environmental fluctuation in parameters or random noise in the differential systems [10–14]. Moreover, stochastic models give an extra degree of freedom and realism in comparison with their corresponding deterministic models. Stochastic population dynamics perturbed by white noise (or Brownian motion) has been studied extensively by many authors [15–17]. It has been investigated in [18], which revealed that an environmental Brownian noise can suppress explosions in population dynamics. Yuan et al. [19] discussed the results of stochastic viral infection and immune response dynamics and analyzed the human immunodeficiency

¹ Cross-immunity (or cross-reactivity) is a major evolutionary force that affects pathogen diversity (i.e., it drives viruses and microbes to be as distinct as possible from one another in order to avoid immunity detection, memory recognition, and clearance).

virus infection. In [20], the author investigated the existence results of ergodic distribution for stochastic hepatitis B virus model based on Lyapunov function. In [21], the authors explored the dynamics of the SIR epidemic model with environmental fluctuations. Additionally, they calculated a threshold parameter to demonstrate the persistence and extinction of the disease. Recently, Lakshmi et al. [22] identified the environmental factors, such as the geographic location of the countries, the upcoming climate, atmospheric temperature, humidity, sociobiological factors, etc., that influence the global spread of COVID-19.

It has been reported that there are many COVID-19 carriers who are not suffering from the disease. This may be due to cross-immunity in people who have survived and recovered from another virus, such as other stains of coronavirus, H1N1, or influenza A. It has been reported in [2] that “*SARS-CoV-2 immunity has some degree of cross-reactive coronavirus immunity in a fraction of the human population, and this fraction of population has influence susceptibility to COVID-19 disease*” Accordingly, in the present chapter, we investigate a SIRC epidemic model of cross-immune class for the dynamics of transmission of COVID-19 among groups. We include time-delay in the transmission terms to represent the incubation period of the virus (the time between infection and symptom onset). We also incorporate white noise type of perturbations to reveal the effect of environmental fluctuations and variability in parameters. Based on existing literature studies, this is the first work dealing with the persistence and extinction of a stochastic epidemic model for COVID-19. We investigate the impact of small and large values of white noise on the persistence and extinction of the disease. We also derive the existing results of stationary distribution and extinction of the disease, using a novel combination of stochastic Lyapunov functional.

13.2 Stochastic SIRC Epidemic Model

For the spread of COVID-19 disease in humans, we classify the population into four categories: $S(t)$, $I(t)$, $R(t)$, and $C(t)$ represent the proportion of susceptible, infected, recovered, and cross-immune people at time t , respectively. Let $N(t) = S(t) + I(t) + R(t) + C(t)$ be the total population. At this stage, we believe that the SIRC model efficiently describes the mechanism for the spread of the SARS-CoV-2 virus. The classical SIRC model [6, 30] takes the form

$$\begin{aligned}\dot{S}(t) &= \eta(1 - S(t)) - \xi S(t)I(t - \tau) + \beta C(t), \\ \dot{I}(t) &= \xi S(t)I(t - \tau) + \sigma \xi C(t)I(t) - (\eta + \alpha)I(t), \\ \dot{R}(t) &= (1 - \sigma)\xi C(t)I(t) + \alpha I(t) - (\eta + \gamma)R(t), \\ \dot{C}(t) &= \gamma R(t) - \xi C(t)I(t) - (\eta + \beta)C(t).\end{aligned}\tag{13.1}$$

We incorporate a discrete time-delay τ into the SIRC model to represent the incubation period, which is about 3–14 days [4]. All the parameters appearing in the model are nonnegative, see Table 13.2. In the absence of cross-immunity, i.e., $(1 - \sigma = 0)$,

Table 13.2 Description of the model parameters

| Parameters | Description |
|------------|---|
| η | Mortality rate in every compartment and is assumed equal to the rate of newborn in the population [6] |
| β | Rate at which the cross-immune population becomes susceptible again |
| ξ | Contact/transmission rate |
| σ | The average reinfection probability of a cross-immune individual |
| α | Recovery rate of the infected population |
| γ | Rate at which the recovered population becomes the cross-immune population and moves from total to partial immunity |

the SIRC model curtails to the SIRS model, since the two individuals S and C become immunologically indistinguishable. Figure 13.1 shows the scheme of SIRC model.

Time-delay $\tau > 0$ is incorporated in the transmission terms to represent the incubation period of the viral infection, i.e., the time between infection and symptom onset. The current studies show that the average/median of the incubation period of early confirmed cases of COVID-19 is approximately 5.5 days, which is similar to SARS. The presence of time-delay in the model may cause periodic solutions many times for different time-delay values τ . The model (13.1) has a disease-free equilibrium $\mathcal{E}_0 = [1, 0, 0, 0]$, and an endemic equilibrium $\mathcal{E}_+ = [S^*, I^*, R^*, C^*]$, where

$$\begin{aligned} S^* &= \frac{\eta + \alpha}{\xi} - \frac{\beta \gamma \alpha I^*}{[(\eta + \gamma) - (1 - \sigma)\gamma]\xi I^* + (\eta + \beta)(\eta + \gamma)}, \\ R^* &= \frac{\alpha I^*(\xi I^* + \eta + \beta)}{[(\eta + \gamma) - (1 - \sigma)\gamma]\xi I^* + (\eta + \beta)(\eta + \gamma)}, \\ C^* &= \frac{\gamma \alpha I^*}{[(\eta + \gamma) - (1 - \sigma)\gamma]\xi I^* + (\eta + \beta)(\eta + \gamma)}, \end{aligned}$$

and I^* is a root of quadratic equation $pI^2 + qI + r = 0$, where

$$\begin{aligned} p &= \eta\xi(\eta + \alpha + \sigma\gamma), \\ q &= \eta\xi [\alpha(2\eta + \gamma + \beta) + (\eta + \beta)(\eta + \gamma) + (\eta + \sigma\gamma)(\eta - \xi)], \\ r &= \eta(\eta + \beta)(\eta + \gamma)(\eta + \alpha)(1 - \mathcal{R}_0). \end{aligned}$$

Here, $\mathcal{R}_0 = \frac{\xi}{\eta + \alpha}$ is known as the *basic reproduction number* of the deterministic model.

In fact, there is an increasing indication that superior consistency with some phenomena can be achieved if the effects of environmental noises in the system are taken into account [31]. The epidemic model (13.1) assumes that the observed dynamics are driven exclusively by internal deterministic cases. We ignore that the environmental variability in the modeling may affect the dynamics of the model and

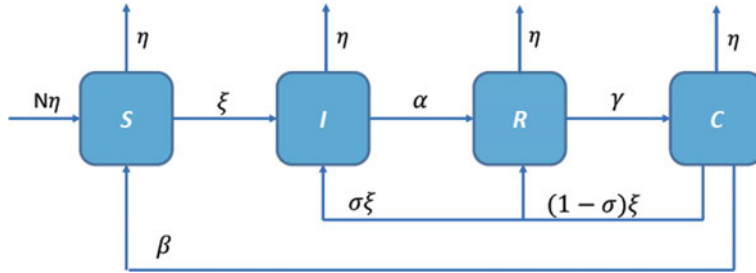


Fig. 13.1 Scheme of SIRC model (13.1), assuming that the total population $N = 1$

transmission of the disease. Accordingly, there is a need to extend the deterministic systems described by differential equations into *stochastic differential equations* (SDEs), where related parameters are modeled as suitable stochastic processes, added to the driving system equations.

From the mathematical and biological point of view, there are some assumptions to incorporate stochastic perturbations into the epidemiological model, such as Markov chain process, parameter perturbations, white noise type, etc. Here, we incorporate white noise type perturbation into model (13.1), which is proportional to S, I, R, and C classes, so that

$$\begin{aligned} dS(t) &= [\eta(1 - S(t)) - \xi S(t)I(t - \tau) + \beta C(t)]dt + v_1 S(t)dW_1(t), \\ dI(t) &= [\xi S(t)I(t - \tau) + \sigma\xi C(t)I(t) - (\eta + \alpha)I(t)]dt + v_2 I(t)dW_2(t), \\ dR(t) &= [(1 - \sigma)\xi C(t)I(t) + \alpha I(t) - (\eta + \gamma)R(t)]dt + v_3 R(t)dW_3(t), \\ dC(t) &= [\gamma R(t) - \xi C(t)I(t) - (\eta + \beta)C(t)]dt + v_4 C(t)dW_4(t), \end{aligned} \quad (13.2)$$

where $W_1(t)$, $W_2(t)$, $W_3(t)$, and $W_4(t)$ denote the independent Brownian motions. v_1^2 , v_2^2 , v_3^2 , and v_4^2 represent the intensity of the environmental white noises, $v_i > 0$ ($i = 1, 2, 3, 4$), subject to the following initial conditions:

$$\begin{aligned} S(\theta) &= \phi_1(\theta), & I(\theta) &= \phi_2(\theta), \\ R(\theta) &= \phi_3(\theta), & C(\theta) &= \phi_4(\theta), & \theta \in [-\tau, 0] \\ \phi_i(\theta) &\in C, & i &= 1, 2, 3, 4, \end{aligned} \quad (13.3)$$

such that C is the family of Lebesgue integrable functions from $[-\tau, 0]$ into \mathbb{R}_+^4 .

13.3 Existence and Uniqueness of Positive Solution

To investigate the dynamical characteristics of SDDEs (13.2), the first consideration is to verify that system (13.2) has a unique global positive solution. As the coefficients of system (13.2) satisfy the local Lipschitz condition together with the linear growth

condition [32], there exists a unique local solution. Now, we need to prove that the solution is positive and global using the Lyapunov analysis method [33].

Theorem 13.1 *System (13.2) has a unique positive solution $(S(t), I(t), R(t), C(t))$ on $t \geq -\tau$, and the solution will remain in \mathbb{R}_+^4 for the given initial condition (13.3) with probability one.*

Proof For any initial value (13.3), as the coefficients of system (13.2) satisfy the local Lipschitz condition, so system (13.2) has a unique local solution $(S(t), I(t), R(t), C(t))$ on $t \in [-\tau, \tau_e]$, a.s., where τ_e represents the explosion time [33].

Our aim is to show that this solution is global, i.e., $\tau_e = \infty$, a.s. Assume $n_0 \geq 1$ is sufficiently large such that $S(\theta), I(\theta), R(\theta)$, and $C(\theta)$ ($\theta \in [-\tau, 0]$) are lying in the interval $\left[\frac{1}{n_0}, n_0\right]$. For each $n \geq n_0$, $n \in \mathbb{N}$, the stopping time is defined as

$$\tau_n = \inf \left\{ t \in [-\tau, \tau_e] : \min\{S(t), I(t), R(t), C(t)\} \leq \frac{1}{n} \quad \text{or} \quad \max\{S(t), I(t), R(t), C(t)\} \geq n \right\},$$

We fix $\inf \phi = \infty$ (ϕ be the empty set). Apparently, τ_n is increasing as $n \rightarrow \infty$. Assume $\tau_\infty = \lim_{n \rightarrow \infty} \tau_n$, then $\tau_\infty \leq \tau_e$ a.s. Therefore, we need to show that $\tau_\infty = \infty$ a.s.; then, $\tau_e = \infty$ a.s. and $(S(t), I(t), R(t), C(t)) \in \mathbb{R}_+^4$ a.s. for all $t \geq -\tau$. If it is erroneous, there is a pair $\epsilon \in (0, 1)$ and $\tilde{T} > 0$ such that $P\{\tau_\infty \leq \tilde{T}\} > \epsilon$. Then, there is an integer $n_1 \geq n_0$ such that

$$P\{\tau_n \leq \tilde{T}\} \geq \epsilon, \forall n \geq n_1. \quad (13.4)$$

We define a C^2 function $\mathcal{V} : \mathbb{R}_+^4 \rightarrow \mathbb{R}_+$ as

$$\begin{aligned} \mathcal{V}(S, I, R, C) = & \left(S - \kappa - \kappa \frac{\ln S}{\kappa} \right) + (I - 1 - \ln I) + (R - 1 - \ln R) + (C - 1 - \ln C) + \\ & \int_t^{t+\tau} \kappa \xi I(s-\tau) ds, \end{aligned}$$

where $\kappa > 0$ is a constant to be determined. By Ito's formula, we can obtain

$$d\mathcal{V} = \mathcal{L}\mathcal{V} dt + v_1(S - \kappa) dW_1(t) + v_2(I - 1) dW_2(t) + v_3(R - 1) dW_3(t) + v_4(C - 1) dW_4(t),$$

where

$$\begin{aligned} \mathcal{L}\mathcal{V} = & \left(1 - \frac{\kappa}{S} \right) (\eta - \eta S - \xi SI(t-\tau) + \beta C) + \left(1 - \frac{1}{I} \right) (\xi SI(t-\tau) + \sigma \xi CI - (\eta + \alpha) I) \\ & + \left(1 - \frac{1}{R} \right) (\xi CI - \sigma \xi CI + \alpha I - \eta R - \gamma R) + \left(1 - \frac{1}{C} \right) (\gamma R - \xi CI) \\ & - (\eta + \beta) C + \frac{\kappa v_1^2 + v_2^2 + v_3^2 + v_4^2}{2} + \kappa \xi I(t) - \kappa \xi I(t-\tau), \\ \leq & 4\eta + \kappa \eta + \alpha + \beta + \gamma - \eta C - \eta R + (\xi(1 + \kappa) - \alpha) I - \eta I - \eta S + \\ & \frac{\kappa v_1^2 + v_2^2 + v_3^2 + v_4^2}{2}. \end{aligned}$$

Let $\kappa = \frac{\alpha - \xi}{\xi}$, then we have

$$\begin{aligned}\mathcal{L}\mathcal{V} &\leq 4\eta + \kappa\eta + \alpha + \beta + \gamma + \frac{\kappa v_1^2 + v_2^2 + v_3^2 + v_4^2}{2} \\ &\leq \mathcal{M},\end{aligned}\tag{13.5}$$

where $\mathcal{M} > 0$ is a constant that is independent of $S(t)$, $I(t)$, $R(t)$, and $C(t)$. Therefore,

$$\begin{aligned}d\mathcal{V}(S, I, R, C) &\leq \mathcal{M}dt + v_1(S - \kappa)dW_1(t) + v_2(I - 1)dW_2(t) \\ &\quad + v_3(R - 1)dW_3(t) + v_4(C - 1)dW_4(t).\end{aligned}\tag{13.6}$$

Integrating (13.6) from 0 to $\tau_n \wedge \tilde{T} = \min\{\tau_n, \tilde{T}\}$ and then taking the expectation E on both sides, we have

$$E[\mathcal{V}(S(\tau_n \wedge \tilde{T}), I(\tau_n \wedge \tilde{T}), R(\tau_n \wedge \tilde{T}), C(\tau_n \wedge \tilde{T}))] \leq E[\mathcal{V}(S(0), I(0), R(0), C(0))] + \mathcal{M}\tilde{T}.\tag{13.7}$$

Let $\Omega_n = \{\tau_n \leq \tilde{T}\}$, for $n \geq n_1$ and in view of (13.4), we obtain $P(\Omega_n) \geq \epsilon$. Such that, for every $\omega \in \Omega_n$, there is at least one of $S(\tau_n, \omega)$, $I(\tau_n, \omega)$, $R(\tau_n, \omega)$, or $C(\tau_n, \omega)$ equaling either to n or $\frac{1}{n}$ and then we obtain

$$\mathcal{V}(S(\tau_n \wedge \tilde{T}), I(\tau_n \wedge \tilde{T}), R(\tau_n \wedge \tilde{T}), C(\tau_n \wedge \tilde{T})) \geq (n - 1 - \ln n) \wedge \left(\frac{1}{n} - 1 - \ln \frac{1}{n}\right).\tag{13.8}$$

According to (13.7), we get

$$\begin{aligned}E\mathcal{V}(S(0), I(0), R(0), C(0)) + \mathcal{M}\tilde{T} &\geq E[1_{\Omega_n(\omega)}\mathcal{V}(S(\tau_n, \omega), I(\tau_n, \omega), R(\tau_n, \omega), C(\tau_n, \omega))] \\ &\geq \epsilon(n - 1 - \ln n) \wedge \left(\frac{1}{n} - 1 - \ln \frac{1}{n}\right),\end{aligned}\tag{13.9}$$

where 1_{Ω_n} represents the indicator function of Ω_n . Letting $n \rightarrow \infty$ yields

$$\infty > E\mathcal{V}(S(0), I(0), R(0), C(0)) + \mathcal{M}\tilde{T} = \infty,\tag{13.10}$$

which leads to a contradiction. It can be concluded that $\tau_\infty = \infty$ a.s., which proves the theorem. \square

13.4 Existence of Ergodic Stationary Distribution

In this section, we construct a suitable stochastic Lyapunov function to study the existence of a unique ergodic stationary distribution of the positive solutions to system (13.2). First, let assume that $X(t)$ is a regular time-homogenous Markov process in \mathbb{R}^d , illustrated by the SDDE

$$dX(t) = f(X(t), X(t - \tau), t)dt + \sum_{r=1}^d g_r(X(t), t)dB_r(t). \quad (13.11)$$

The diffusion matrix of the process $X(t)$ is

$$\Lambda(x) = (\lambda_{ij}(x)), \quad \lambda_{ij}(x) = \sum_{r=1}^d g_r^i(x)g_r^j(x)$$

Lemma 13.1 ([17]) *The Markov process $X(t)$ has a unique ergodic stationary distribution $\pi(\cdot)$ if there exists a bounded domain $\mathcal{U} \subset \mathbb{R}^d$ with regular boundary Γ and*

- (1): *there is a positive number M such that $\sum_{i,j=1}^d \lambda_{ij}(x)\xi_i\xi_j \geq M|\xi|^2$, $x \in \mathcal{U}$, $\xi \in \mathbb{R}^d$.*
- (2): *there exists a non-negative C^2 -function V such that $\mathcal{L}V$ is negative for any $\mathbb{R}^d \setminus \mathcal{U}$.*

Define the reproduction number of the stochastic model as follows:

$$\mathcal{R}_0^s = \frac{\eta\gamma\xi^2(1-\sigma)}{\hat{\eta}\hat{\alpha}\hat{\gamma}\hat{\beta}}, \quad (13.12)$$

where $\hat{\eta} = \eta + \frac{v_1^2}{2}$, $\hat{\alpha} = \eta + \alpha + \frac{v_2^2}{2}$, $\hat{\gamma} = \eta + \gamma + \frac{v_3^2}{2}$, and $\hat{\beta} = \eta + \beta + \frac{v_4^2}{2}$.

Theorem 13.2 *Assume that $\mathcal{R}_0^s > 1$, and $\eta - \frac{v_1^2 \vee v_2^2 \vee v_3^2 \vee v_4^2}{2} > 0$; then, for any initial value $(S(0), I(0), R(0), C(0)) \in \mathbb{R}_+^4$, system (13.2) has a unique ergodic stationary distribution $\pi(\cdot)$.*

Proof First, we need to validate conditions (1) and (2) of Lemma 13.1. To prove condition (1), the diffusion matrix of model (13.2) is described as

$$\Lambda = \begin{pmatrix} v_1^2 S^2 & 0 & 0 & 0 \\ 0 & v_2^2 I^2 & 0 & 0 \\ 0 & 0 & v_3^2 R^2 & 0 \\ 0 & 0 & 0 & v_4^2 C^2 \end{pmatrix}.$$

Then, the matrix Λ is positive definite for any compact subset of \mathbb{R}_+^4 , then condition (1) of Lemma 13.1 is satisfied.

Next, we prove condition (2). To this end, define the C^2 function $\mathcal{V}: \mathbb{R}_+^4 \rightarrow \mathbb{R}$ as follows

$$\begin{aligned} \mathcal{V}(S, I, R, C) &= Q \left(-\ln S - c_1 \ln I - c_2 \ln R - c_3 \ln C + \xi \int_t^{t+\tau} I(s - \tau)ds \right) \\ &\quad - \ln S + \xi \int_t^{t+\tau} I(s - \tau)ds - \ln R - \ln C + \frac{1}{\rho + 1} (S + I + R + C)^{\rho + 1}, \\ &= Q\mathcal{V}_1 + \mathcal{V}_2 + \mathcal{V}_3 + \mathcal{V}_4 + \mathcal{V}_5, \end{aligned}$$

where $c_1 = \frac{\eta\gamma\xi^2(1-\sigma)}{\hat{\alpha}^2\hat{\gamma}\hat{\beta}}$, $c_2 = \frac{\eta\gamma\xi^2(1-\sigma)}{\hat{\alpha}\hat{\gamma}^2\hat{\beta}}$, and $c_3 = \frac{\eta\gamma\xi^2(1-\sigma)}{\hat{\alpha}\hat{\gamma}\hat{\beta}^2}$. Note that $\mathcal{V}(S, I, R, C)$ is not only continuous but also tends to $+\infty$ as (S, I, R, C) approaches the boundary of \mathbb{R}_+^4 and $\|(S, I, R, C)\| \rightarrow \infty$. Therefore, \mathcal{V} must have a minimum point $(S(0), I(0), R(0), C(0))$ in the interior of \mathbb{R}_+^4 . We define a C^2 -function $\tilde{V} : \mathbb{R}_+^4 \rightarrow \mathbb{R}_+$ as

$$\begin{aligned}\tilde{V}(S, I, R, C) &= Q \left(-\ln S - c_1 \ln I - c_2 \ln R - c_3 \ln C + \xi \int_t^{t+\tau} I(s-\tau) ds \right) \\ &\quad - \ln S + \xi \int_t^{t+\tau} I(s-\tau) ds - \ln R - \ln C + \frac{1}{\rho+1} (S + I + R + C)^{\rho+1} \\ &\quad - \mathcal{V}(S(0), I(0), R(0), C(0)), \\ &:= Q\mathcal{V}_1 + \mathcal{V}_2 + \mathcal{V}_3 + \mathcal{V}_4 + \mathcal{V}_5 - \mathcal{V}(S(0), I(0), R(0), C(0))\end{aligned}\tag{13.13}$$

where $(S, I, R, C) \in (\frac{1}{n}, n) \times (\frac{1}{n}, n) \times (\frac{1}{n}, n) \times (\frac{1}{n}, n)$ and $n > 1$ is a sufficiently large integer, $\mathcal{V}_1 = -\ln S - c_1 \ln I - c_2 \ln R - c_3 \ln C + \xi \int_t^{t+\tau} I(s-\tau) ds$, $\mathcal{V}_2 = -\ln S + \xi \int_t^{t+\tau} I(s-\tau) ds$, $\mathcal{V}_3 = -\ln R$, $\mathcal{V}_4 = -\ln C$, and $\mathcal{V}_5 = \frac{1}{\rho+1} (S + I + R + C)^{\rho+1}$. $\rho > 1$ is a constant satisfying

$$\eta - \frac{\rho}{2}(\nu_1^2 \vee \nu_2^2 \vee \nu_3^2 \vee \nu_4^2) > 0,$$

and $Q > 0$ is a sufficiently large number satisfying the following condition:

$$-Q\mu + w \leq -2,\tag{13.14}$$

where $\mu = \frac{\eta\gamma\xi^2(1-\sigma)}{\hat{\alpha}\hat{\gamma}\hat{\beta}} - (\eta + \frac{\nu_1^2}{2}) > 0$, since $\mathcal{R}_0^s > 1$.

$$\begin{aligned}w &= \sup_{(S, I, R, C) \in \mathbb{R}_+^4} \left\{ -\frac{1}{4} \left[\eta - \frac{\rho}{2}(\nu_1^2 \vee \nu_2^2 \vee \nu_3^2 \vee \nu_4^2) \right] I^{\rho+1} \right. \\ &\quad \left. + 3\eta + \gamma + \beta + 2\xi I + A + \frac{\nu_1^2}{2} + \frac{\nu_3^2}{2} + \frac{\nu_4^2}{2} \right\}\end{aligned}\tag{13.15}$$

and

$$\begin{aligned}A &= \sup_{(S, I, R, C) \in \mathbb{R}_+^4} \left\{ \eta(S + I + R + C)^\rho \right. \\ &\quad \left. - \frac{1}{2} \left[\eta - \frac{\rho}{2}(\nu_1^2 \vee \nu_2^2 \vee \nu_3^2 \vee \nu_4^2) \right] (S + I + R + C)^{\rho+1} \right\} < \infty.\end{aligned}\tag{13.16}$$

Applying Itô's formula to \mathcal{V}_1 , we obtain

$$\begin{aligned}
\mathcal{L}\mathcal{V}_1 &= -\frac{\eta}{S} + \eta + \xi I - \frac{\beta C}{S} - \frac{c_1 \xi S I(t-\tau)}{I} - c_1 \sigma \xi C + c_1 (\eta + \alpha) - \frac{c_2 (1-\sigma) \xi C I}{R} \\
&\quad - \frac{c_2 \alpha I}{R} + c_2 (\eta + \gamma) - \frac{c_3 \gamma R}{C} + c_3 \xi I + c_3 (\eta + \beta) + \frac{v_1^2}{2} + \frac{c_1 v_2^2}{2} + \frac{c_2 v_3^2}{2} + \frac{c_3 v_4^2}{2} \\
&\leq -4\sqrt[4]{\eta \gamma \xi^2 (1-\sigma) c_1 c_2 c_3} + \eta + \frac{v_1^2}{2} + c_1 \left(\eta + \alpha + \frac{v_2^2}{2} \right) + c_2 \left(\eta + \gamma + \frac{v_3^2}{2} \right) \\
&\quad + c_3 \left(\eta + \beta + \frac{v_4^2}{2} \right) + \xi (1 + c_3) I \\
&\leq -\frac{\eta \gamma \xi^2 (1-\sigma)}{\hat{\alpha} \hat{\gamma} \hat{\beta}} + \eta + \frac{v_1^2}{2} + \xi (1 + c_3) I = -\mu + \xi (1 + c_3) I,
\end{aligned} \tag{13.17}$$

Similarly, we can get

$$\mathcal{L}\mathcal{V}_2 = -\frac{\eta}{S} + \eta + \xi I - \frac{\beta C}{S} + \frac{v_1^2}{2}, \tag{13.18}$$

$$\mathcal{L}\mathcal{V}_3 = -\frac{(1-\sigma) \xi C I}{R} - \frac{\alpha I}{R} + \eta + \gamma + \frac{v_3^2}{2}, \tag{13.19}$$

$$\mathcal{L}\mathcal{V}_4 = -\frac{\gamma R}{C} + \xi I + \eta + \beta + \frac{v_4^2}{2}, \tag{13.20}$$

$$\begin{aligned}
\mathcal{L}\mathcal{V}_5 &= (S + I + R + C)^\rho [\eta - \eta(S + I + R + C)] + \frac{\rho}{2} (S + I + R + C)^{\rho-1} \\
&\quad \times [v_1^2 S^2 + v_2^2 I^2 + v_3^2 R^2 + v_4^2 C^2], \\
&\leq (S + I + R + C)^\rho [\eta - \eta(S + I + R + C)] + \frac{\rho}{2} (S + I + R + C)^{\rho+1} (v_1^2 \vee v_2^2 \vee v_3^2 \vee v_4^2), \\
&\leq \eta (S + I + R + C)^\rho - (S + I + R + C)^{\rho+1} \left[\eta - \frac{\rho}{2} (v_1^2 \vee v_2^2 \vee v_3^2 \vee v_4^2) \right], \tag{13.21} \\
&\leq A - \frac{1}{2} \left[\eta - \frac{\rho}{2} (v_1^2 \vee v_2^2 \vee v_3^2 \vee v_4^2) \right] (S + I + R + C)^{\rho+1} \\
&\leq A - \frac{1}{2} \left[\eta - \frac{\rho}{2} (v_1^2 \vee v_2^2 \vee v_3^2 \vee v_4^2) \right] (S^{\rho+1} + I^{\rho+1} + R^{\rho+1} + C^{\rho+1}),
\end{aligned}$$

where A is defined by (13.16). From the Eqs. (13.17)–(13.21), we have

$$\begin{aligned}
\mathcal{L}\tilde{V} &\leq -Q\mu + Q\xi(1+c_3)I - \frac{1}{2} \left[\eta - \frac{\rho}{2} (v_1^2 \vee v_2^2 \vee v_3^2 \vee v_4^2) \right] (S^{\rho+1} + I^{\rho+1} + R^{\rho+1} + C^{\rho+1}) \\
&\quad - \frac{\eta}{S} + 3\eta - \frac{\beta C}{S} + \frac{v_1^2}{2} - \frac{\alpha I}{R} + \gamma + \frac{v_3^2}{2} - \frac{\gamma R}{C} + 2\xi I + A + \beta + \frac{v_4^2}{2}, \\
&\leq -Q\mu + Q\xi(1+c_3)I - \frac{1}{4} \left[\eta - \frac{\rho}{2} (v_1^2 \vee v_2^2 \vee v_3^2 \vee v_4^2) \right] (S^{\rho+1} + I^{\rho+1} + R^{\rho+1} + C^{\rho+1}) \\
&\quad - \frac{\eta}{S} - \frac{1}{4} \left[\eta - \frac{\rho}{2} (v_1^2 \vee v_2^2 \vee v_3^2 \vee v_4^2) \right] I^{\rho+1} + 3\eta - \frac{\beta C}{S} + \frac{v_1^2}{2} - \frac{\alpha I}{R} + \gamma \\
&\quad + \frac{v_3^2}{2} - \frac{\gamma R}{C} + 2\xi I + A + \beta + \frac{v_4^2}{2}.
\end{aligned}$$

For $\epsilon > 0$, define a bounded closed set

$$\mathcal{D} = \left\{ (S, I, R, C) \in \mathbb{R}_+^4 : \epsilon \leq S \leq \frac{1}{\epsilon}, \epsilon \leq I \leq \frac{1}{\epsilon}, \epsilon^2 \leq R \leq \frac{1}{\epsilon^2}, \epsilon^3 \leq C \leq \frac{1}{\epsilon^3} \right\}.$$

In the set $\mathbb{R}_+^4 \setminus \mathcal{D}$, let us choose ϵ satisfying the following conditions:

$$-\frac{\eta}{\epsilon} + H \leq -1, \quad (13.22)$$

$$-Q\mu + Q\xi(1 + c_3)\epsilon + w \leq -1, \quad (13.23)$$

$$-\frac{\alpha}{\epsilon} + H \leq -1, \quad (13.24)$$

$$-\frac{\gamma}{\epsilon} + H \leq -1, \quad (13.25)$$

$$-\frac{1}{4} \left[\eta - \frac{\rho}{2} (\nu_1^2 \vee \nu_2^2 \vee \nu_3^2 \vee \nu_4^2) \right] \frac{1}{\epsilon^{\rho+1}} + H \leq -1, \quad (13.26)$$

$$-\frac{1}{4} \left[\eta - \frac{\rho}{2} (\nu_1^2 \vee \nu_2^2 \vee \nu_3^2 \vee \nu_4^2) \right] \frac{1}{\epsilon^{2(\rho+1)}} + H \leq -1, \quad (13.27)$$

$$-\frac{1}{4} \left[\eta - \frac{\rho}{2} (\nu_1^2 \vee \nu_2^2 \vee \nu_3^2 \vee \nu_4^2) \right] \frac{1}{\epsilon^{3(\rho+1)}} + H \leq -1, \quad (13.28)$$

where

$$H = \sup_{(S, I, R, C) \in \mathbb{R}_+^4} \left\{ Q(c_3 + 1)\xi I - \frac{1}{4} \left[\eta - \frac{\rho}{2} (\nu_1^2 \vee \nu_2^2 \vee \nu_3^2 \vee \nu_4^2) \right] I^{\rho+1} + 3\eta + \gamma + \beta + 2\xi I + A + \frac{\nu_1^2}{2} + \frac{\nu_3^2}{2} + \frac{\nu_4^2}{2} \right\}.$$

We need to show that $\mathcal{L}\tilde{V} \leq -1$ for any $(S, I, R, C) \in \mathbb{R}_+^4 \setminus \mathcal{D}$, and $\mathbb{R}_+^4 \setminus \mathcal{D} = \bigcup_{i=1}^8 \mathcal{D}_i$, where

$$\mathcal{D}_1 = \{(S, I, R, C) \in \mathbb{R}_+^4; 0 < S < \epsilon\}, \quad \mathcal{D}_2 = \{(S, I, R, C) \in \mathbb{R}_+^4; 0 < I < \epsilon\},$$

$$\mathcal{D}_3 = \{(S, I, R, C) \in \mathbb{R}_+^4; 0 < R < \epsilon^2, I \geq \epsilon\}, \quad \mathcal{D}_4 = \{(S, I, R, C) \in \mathbb{R}_+^4; 0 < C < \epsilon^3, R \geq \epsilon^2\},$$

$$\mathcal{D}_5 = \left\{ (S, I, R, C) \in \mathbb{R}_+^4; S > \frac{1}{\epsilon} \right\}, \quad \mathcal{D}_6 = \left\{ (S, I, R, C) \in \mathbb{R}_+^4; I > \frac{1}{\epsilon} \right\},$$

$$\mathcal{D}_7 = \left\{ (S, I, R, C) \in \mathbb{R}_+^4; R > \frac{1}{\epsilon^2} \right\}, \quad \mathcal{D}_8 = \left\{ (S, I, R, C) \in \mathbb{R}_+^4; C > \frac{1}{\epsilon^3} \right\}.$$

Case 1. For any $(S, I, R, C) \in \mathcal{D}_1$, we obtain

$$\begin{aligned}
\mathcal{L}\tilde{V} &\leq -\frac{\eta}{S} + Q(c_3 + 1)\xi I - \frac{1}{4}\left[\eta - \frac{\rho}{2}(v_1^2 \vee v_2^2 \vee v_3^2 \vee v_4^2)\right]I^{\rho+1} + 3\eta + \gamma + \beta \\
&\quad + 2\xi I + A + \frac{v_1^2}{2} + \frac{v_3^2}{2} + \frac{v_4^2}{2} \\
&\leq -\frac{\eta}{S} + H, \\
&\leq -\frac{\eta}{\epsilon} + H \leq -1,
\end{aligned}$$

which is obtained from (13.22). Therefore, $\mathcal{L}\mathcal{V} \leq -1$ for any $(S, I, R, C) \in D_1$.

Case 2. For any $(S, I, R, C) \in \mathcal{D}_2$, we have

$$\begin{aligned}
\mathcal{L}\tilde{V} &\leq -Q\mu + Q\xi(1 + c_3)I - \frac{1}{4}\left[\eta - \frac{\rho}{2}(v_1^2 \vee v_2^2 \vee v_3^2 \vee v_4^2)\right]I^{\rho+1} + 3\eta \\
&\quad + \gamma + \beta + 2\xi I + A + \frac{v_1^2}{2} + \frac{v_3^2}{2} + \frac{v_4^2}{2}, \\
&\leq -Q\mu + Q\xi(1 + c_3)I + w \\
&\leq -Q\mu + Q\xi(1 + c_3)\epsilon + w < -1,
\end{aligned}$$

which follows from (13.23) and (13.14). Thus, $\mathcal{L}\mathcal{V} \leq -1$ for any $(S, I, R, C) \in D_2$.

Case 3. For any $(S, I, R, C) \in \mathcal{D}_3$, we can get

$$\begin{aligned}
\mathcal{L}\tilde{V} &\leq -\frac{\alpha I}{R} + Q(c_3 + 1)\xi I - \frac{1}{4}\left[\eta - \frac{\rho}{2}(v_1^2 \vee v_2^2 \vee v_3^2 \vee v_4^2)\right]I^{\rho+1} + 3\eta + \gamma + \beta \\
&\quad + 2\xi I + A + \frac{v_1^2}{2} + \frac{v_3^2}{2} + \frac{v_4^2}{2} \\
&\leq -\frac{\alpha\epsilon}{\epsilon^2} + H \leq -1,
\end{aligned}$$

which follows from (13.24). Consequently, $\mathcal{L}\mathcal{V} \leq -1$ for any $(S, I, R, C) \in D_3$.

Case 4. For any $(S, I, R, C) \in \mathcal{D}_4$, it yields

$$\begin{aligned}
\mathcal{L}\tilde{V} &\leq -\frac{\gamma R}{C} + Q(c_3 + 1)\xi I - \frac{1}{4}\left[\eta - \frac{\rho}{2}(v_1^2 \vee v_2^2 \vee v_3^2 \vee v_4^2)\right]I^{\rho+1} + 3\eta + \gamma + \beta \\
&\quad + 2\xi I + A + \frac{v_1^2}{2} + \frac{v_3^2}{2} + \frac{v_4^2}{2} \\
&\leq -\frac{\gamma\epsilon^2}{\epsilon^3} + H \leq -1,
\end{aligned}$$

which is obtained from (13.25). Thus, $\mathcal{L}\mathcal{V} \leq -1$ for any $(S, I, R, C) \in D_4$.

Case 5. If $(S, I, R, C) \in \mathcal{D}_5$, we have

$$\begin{aligned}\mathcal{L}\tilde{V} &\leq -\frac{1}{4}\left[\eta - \frac{\rho}{2}(v_1^2 \vee v_2^2 \vee v_3^2 \vee v_4^2)\right]S^{\rho+1} + Q(c_3 + 1)\xi I \\ &\quad - \frac{1}{4}\left[\eta - \frac{\rho}{2}(v_1^2 \vee v_2^2 \vee v_3^2 \vee v_4^2)\right]I^{\rho+1} + 3\eta \\ &\quad + \gamma + \beta + 2\xi I + A + \frac{v_1^2}{2} + \frac{v_3^2}{2} + \frac{v_4^2}{2} \\ &\leq -\frac{1}{4}\left[\eta - \frac{\rho}{2}(v_1^2 \vee v_2^2 \vee v_3^2 \vee v_4^2)\right]\frac{1}{\epsilon^{\rho+1}} + H \leq -1,\end{aligned}$$

which is obtained from (13.26). Therefore, we obtain $\mathcal{L}V \leq -1$ for any $(S, I, R, C) \in D_5$.

Case 6 If $(S, I, R, C) \in \mathcal{D}_6$, we get

$$\begin{aligned}\mathcal{L}\tilde{V} &\leq -\frac{1}{4}\left[\eta - \frac{\rho}{2}(v_1^2 \vee v_2^2 \vee v_3^2 \vee v_4^2)\right]I^{\rho+1} + Q(c_3 + 1)\xi I \\ &\quad - \frac{1}{4}\left[\eta - \frac{\rho}{2}(v_1^2 \vee v_2^2 \vee v_3^2 \vee v_4^2)\right]I^{\rho+1} + 3\eta \\ &\quad + \gamma + \beta + 2\xi I + A + \frac{v_1^2}{2} + \frac{v_3^2}{2} + \frac{v_4^2}{2} \\ &\leq -\frac{1}{4}\left[\eta - \frac{\rho}{2}(v_1^2 \vee v_2^2 \vee v_3^2 \vee v_4^2)\right]\frac{1}{\epsilon^{\rho+1}} + H \leq -1,\end{aligned}$$

which is obtained from (13.26). Hence, $\mathcal{L}V \leq -1$ for any $(S, I, R, C) \in D_6$.

Case 7. If $(S, I, R, C) \in \mathcal{D}_7$, then

$$\begin{aligned}\mathcal{L}\tilde{V} &\leq -\frac{1}{4}\left[\eta - \frac{\rho}{2}(v_1^2 \vee v_2^2 \vee v_3^2 \vee v_4^2)\right]R^{\rho+1} + Q(c_3 + 1)\xi I \\ &\quad - \frac{1}{4}\left[\eta - \frac{\rho}{2}(v_1^2 \vee v_2^2 \vee v_3^2 \vee v_4^2)\right]I^{\rho+1} + 3\eta \\ &\quad + \gamma + \beta + 2\xi I + A + \frac{v_1^2}{2} + \frac{v_3^2}{2} + \frac{v_4^2}{2} \\ &\leq -\frac{1}{4}\left[\eta - \frac{\rho}{2}(v_1^2 \vee v_2^2 \vee v_3^2 \vee v_4^2)\right]\frac{1}{\epsilon^{2\rho+2}} + H \leq -1,\end{aligned}$$

which is obtained from (13.27). Hence, $\mathcal{L}V \leq -1$ for any $(S, I, R, C) \in D_7$.

Case 8. If $(S, I, R, C) \in \mathcal{D}_8$, we can see that

$$\begin{aligned}
\mathcal{L}\tilde{V} &\leq -\frac{1}{4}\left[\eta - \frac{\rho}{2}(v_1^2 \vee v_2^2 \vee v_3^2 \vee v_4^2)\right]C^{\rho+1} + Q(c_3 + 1)\xi I \\
&\quad - \frac{1}{4}\left[\eta - \frac{\rho}{2}(v_1^2 \vee v_2^2 \vee v_3^2 \vee v_4^2)\right]I^{\rho+1} + 3\eta \\
&\quad + \gamma + \beta + 2\xi I + A + \frac{v_1^2}{2} + \frac{v_3^2}{2} + \frac{v_4^2}{2} \\
&\leq -\frac{1}{4}\left[\eta - \frac{\rho}{2}(v_1^2 \vee v_2^2 \vee v_3^2 \vee v_4^2)\right]\frac{1}{\epsilon^{3\rho+3}} + H \leq -1,
\end{aligned}$$

which is obtained from (13.28). Therefore, $\mathcal{L}V \leq -1$ for any $(S, I, R, C) \in D_8$. Clearly, condition (2) of Lemma 13.1 holds. Therefore, we conclude that system (13.2) identifies a unique stationary distribution $\pi(\cdot)$. \square

13.5 Extinction

To show the extinction of the disease, we go through the following lemma:

Lemma 13.2 (See Lemmas 2.1 and 2.2 in [34]) *Let $(S(t), I(t), R(t), C(t))$ be the solution of (13.2) with any $(S(0), I(0), R(0), C(0)) \in \mathbb{R}_+^4$, then*

$$\lim_{t \rightarrow \infty} \frac{S(t)}{t} = 0, \quad \lim_{t \rightarrow \infty} \frac{I(t)}{t} = 0, \quad \lim_{t \rightarrow \infty} \frac{R(t)}{t} = 0, \quad \lim_{t \rightarrow \infty} \frac{C(t)}{t} = 0, \quad a.s.$$

Furthermore, if $\eta > \frac{v_1^2 \vee v_2^2 \vee v_3^2 \vee v_4^2}{2}$, then

$$\begin{aligned}
\lim_{t \rightarrow \infty} \frac{\int_0^t S(s)dW_1(s)}{t} &= 0, \quad \lim_{t \rightarrow \infty} \frac{\int_0^t I(s)dW_2(s)}{t} = 0, \quad \lim_{t \rightarrow \infty} \frac{\int_0^t R(s)dW_3(s)}{t} = 0, \\
\lim_{t \rightarrow \infty} \frac{\int_0^t C(s)dW_4(s)}{t} &= 0, \quad a.s.
\end{aligned}$$

Theorem 13.3 *If $\mathcal{R}_0^s < 1$ and $\eta > \frac{v_1^2 \vee v_2^2 \vee v_3^2 \vee v_4^2}{2}$, then the solution of (13.2) satisfies the following: $\limsup_{t \rightarrow \infty} \frac{1}{t} \ln(\alpha(I(t) + C(t)) + (\eta + \alpha)R(t)) \leq \xi - \frac{1}{2(\alpha)^2} \left\{ \alpha^2 \frac{v_2^2}{2} \wedge (\eta(\eta + \alpha + \gamma) + (\eta + \alpha)^2 \frac{v_3^2}{2}) \wedge \alpha^2(\eta + \beta + \frac{v_4^2}{2}) \right\} < 0$ and $\lim_{t \rightarrow \infty} \langle S \rangle = 1$ a.s.*

Proof Define $U(t) = \alpha(I(t) + C(t)) + (\eta + \alpha)R(t)$, taking Ito's formula, we can get

$$\begin{aligned}
d \ln U(t) &= \left\{ \frac{1}{\alpha(I + C) + (\eta + \alpha)R} \left[\alpha\xi SI(t - \tau) - \alpha(\eta + \beta)C - (\eta^2 + \eta\alpha + \eta\gamma)R \right] \right. \\
&\quad \left. - \frac{\left[\alpha^2 v_2^2 I^2 + (\eta + \alpha)^2 v_3^2 R^2 + \alpha^2 v_4^2 C^2 \right]}{2(\alpha(I + C) + (\eta + \alpha)R)^2} \right\} dt + \frac{\alpha v_2 I}{\alpha(I + C) + (\eta + \alpha)R} dW_2(t) \\
&\quad + \frac{(\eta + \alpha)v_3 R}{\alpha(I + C) + (\eta + \alpha)R} dW_3(t) + \frac{\alpha v_4 C}{\alpha(I + C) + (\eta + \alpha)R} dW_4(t),
\end{aligned}$$

$$\begin{aligned}
&\leq \xi S dt - \frac{1}{(\alpha(I+C) + (\eta+\alpha)R)^2} \left\{ \alpha^2 \frac{\nu_2^2}{2} I^2 + \alpha^2 \left(\eta + \beta + \frac{\nu_4^2}{2} \right) C^2 + \left(\eta(\eta + \alpha + \gamma) \right. \right. \\
&\quad \left. \left. + (\eta + \alpha)^2 \frac{\nu_3^2}{2} \right) R^2 \right\} dt + \frac{\alpha \nu_2 I}{\alpha(I+C) + (\eta+\alpha)R} dW_2(t) \\
&\quad + \frac{(\eta + \alpha) \nu_3 R}{\alpha(I+C) + (\eta+\alpha)R} dW_3(t) + \frac{\alpha \nu_4 C}{\alpha(I+C) + (\eta+\alpha)R} dW_4(t), \\
&\leq \xi S dt - \frac{1}{2(\alpha)^2} \left\{ \alpha^2 \frac{\nu_2^2}{2} \wedge \left(\eta(\eta + \alpha + \gamma) + (\eta + \alpha)^2 \frac{\nu_3^2}{2} \right) \wedge \alpha^2 \left(\eta + \beta + \frac{\nu_4^2}{2} \right) \right\} dt \\
&\quad + \frac{\alpha \nu_2 I}{\alpha(I+C) + (\eta+\alpha)R} dW_2(t) + \frac{(\eta + \alpha) \nu_3 R}{\alpha(I+C) + (\eta+\alpha)R} dW_3(t) \\
&\quad + \frac{\alpha \nu_4 C}{\alpha(I+C) + (\eta+\alpha)R} dW_4(t). \tag{13.29}
\end{aligned}$$

From model (13.2), we have

$$\begin{aligned}
d(S(t) + I(t) + R(t) + C(t)) &= \left[\eta - \eta(S(t) + I(t) + R(t) + C(t)) \right] dt + \nu_1 S(t) dW_1(t) \\
&\quad + \nu_2 I(t) dW_2(t) + \nu_3 R(t) dW_3(t) + \nu_4 C(t) dW_4(t). \tag{13.30}
\end{aligned}$$

Integrating (13.30) from 0 to t , we obtain

$$\langle S(t) + I(t) + R(t) + C(t) \rangle = 1 + \psi_1(t), \tag{13.31}$$

where

$$\begin{aligned}
\psi_1(t) &= \frac{1}{\eta} \left[\frac{1}{t} (S(0) + I(0) + R(0) + C(0)) - \frac{1}{t} (S(t) + I(t) + R(t) + C(t)) + \frac{\nu_1 \int_0^t S(s) dW_1(s)}{t} \right. \\
&\quad \left. + \frac{\nu_2 \int_0^t I(s) dW_2(s)}{t} + \frac{\nu_3 \int_0^t R(s) dW_3(s)}{t} + \frac{\nu_4 \int_0^t C(s) dW_4(s)}{t} \right]. \tag{13.32}
\end{aligned}$$

By Lemma 13.2, we can easily obtain

$$\lim_{t \rightarrow \infty} \psi_1(t) = 0 \quad a.s.$$

Therefore, by taking the superior limit on both sides of (13.31), we have

$$\lim_{t \rightarrow \infty} \sup \langle S(t) + I(t) + R(t) + C(t) \rangle = 1 \quad a.s. \tag{13.33}$$

Integrating (13.29) from 0 to t , we obtain

$$\frac{\ln U(t)}{t} \leq \xi - \frac{1}{2(\alpha)^2} \left\{ \alpha^2 \frac{\nu_2^2}{2} \wedge \left(\eta(\eta + \alpha + \gamma) + (\eta + \alpha)^2 \frac{\nu_3^2}{2} \right) \wedge \alpha^2 \left(\eta + \beta + \frac{\nu_4^2}{2} \right) \right\} + \psi_2(t), \tag{13.34}$$

where

$$\begin{aligned}\psi_2(t) &= \frac{\ln U(0)}{t} + \frac{\alpha v_2}{t} \int_0^t \left(\frac{I(s)}{\alpha(I(s) + C(s)) + (\eta + \alpha)R(s)} dW_2(s) \right) \\ &\quad + \frac{(\eta + \alpha)v_3}{t} \int_0^t \left(\frac{R(s)}{\alpha(I(s) + C(s)) + (\eta + \alpha)R(s)} dW_3(s) \right) \\ &\quad + \frac{\alpha v_4}{t} \int_0^t \left(\frac{C(s)}{\alpha(I(s) + C(s)) + (\eta + \alpha)R(s)} dW_4(s) \right).\end{aligned}$$

In the same manner; by Lemma 13.2, we have

$$\lim_{t \rightarrow \infty} \psi_2(t) = 0 \quad a.s.$$

Since $\mathcal{R}_0^s < 1$, therefore, by taking the superior limit of both sides of (13.34), we have

$$\lim_{t \rightarrow \infty} \sup \frac{\ln U(t)}{t} \leq \xi - \frac{1}{2(\alpha)^2} \left\{ \alpha^2 \frac{v_2^2}{2} \wedge (\eta(\eta + \alpha + \gamma) + (\eta + \alpha)^2 \frac{v_3^2}{2}) \wedge \alpha^2(\eta + \beta + \frac{v_4^2}{2}) \right\} < 0, \quad (13.35)$$

which implies that $\lim_{t \rightarrow \infty} I(t) = 0$, $\lim_{t \rightarrow \infty} R(t) = 0$, $\lim_{t \rightarrow \infty} C(t) = 0$. a.s., which confirms that the disease I can die out with probability one.

By using (13.33) and (13.35), it is easy to show that $\lim_{t \rightarrow \infty} \langle S \rangle = 1$ a.s. \square

13.6 Numerical Simulations and Discussions

In this section, numerical simulations are provided to validate our theoretical results using Milstein's Scheme for SDDEs, discussed in Chap. 7, to numerically solve SDDEs (13.2); See Appendix C.

The discretization transformation takes the form

$$\begin{aligned}S_{j+1} &= S_j + [\eta(1 - S_j) - \xi S_j I_{j-m} + \beta C_j] \Delta t + v_1 S_j \sqrt{\Delta t} \zeta_{1,j}, \\ I_{j+1} &= I_j + [\xi S_j I_{j-m} + \sigma \xi C_j I_j - (\eta + \alpha) I_j] \Delta t + v_2 I_j \sqrt{\Delta t} \zeta_{2,j}, \\ R_{j+1} &= R_j + [(1 - \sigma) \xi C_j I_j + \alpha I_j - (\eta + \gamma) R_j] \Delta t + v_3 R_j \sqrt{\Delta t} \zeta_{3,j}, \\ C_{j+1} &= C_j + [\gamma R_j - \xi C_j I_j - (\eta + \beta) C_j] \Delta t + v_4 C_j \sqrt{\Delta t} \zeta_{4,j}.\end{aligned} \quad (13.36)$$

The independent Gaussian random variables denoted as $\zeta_{i,j}$, ($i = 1, 2, 3, 4$), which follow the distribution $N(0, 1)$, the time-delay is defined as $\tau = m\Delta t$, m is an integer and the step size is Δt . Let $v_i > 0$, ($i = 1, 2, 3, 4$) be the white noise values.

Example 13.1 Consider model (13.2), with white noise values of $v_1 = 0.1$, $v_2 = 0.09$, $v_3 = 0.09$, $v_4 = 0.07$ and parameter values Of $\eta = 0.09$, $\xi = 1.3$, $\beta = 0.05$, $\sigma = 0.9$, $\gamma = 0.1$, $\alpha = 0.36$, $\tau = 1.2$. Simple calculation leads to $\mathcal{R}_0^s = \frac{\eta\gamma\xi^2(1-\sigma)}{\hat{\eta}\hat{\alpha}\hat{\gamma}\hat{\beta}} =$

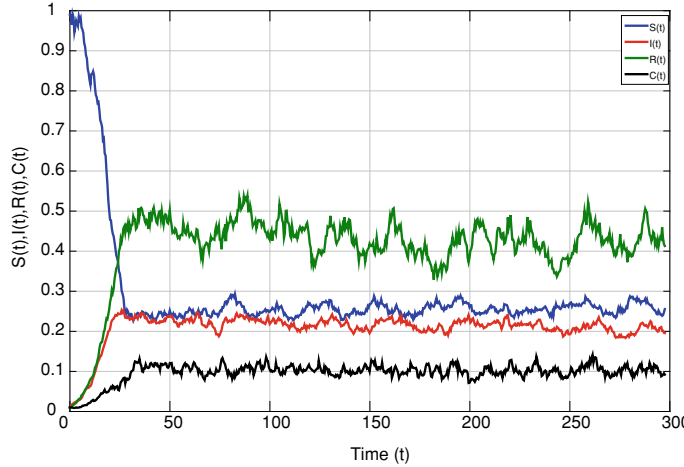


Fig. 13.2 Numerical simulations of stochastic model (13.2), when $\mathcal{R}_0^s = 1.3 > 1$, with $\eta = 0.09$, $\xi = 1.3$, $\beta = 0.05$, $\sigma = 0.9$, $\alpha = 0.36$, $\gamma = 0.1$; $\tau = 1$ and white noises $v_1 = 0.1$, $v_2 = 0.09$, $v_3 = 0.09$, $v_4 = 0.07$. The model has a unique ergodic stationary distribution and the infection is persistent

$1.3 > 1$ and $\eta - \frac{v_1^2 \vee v_2^2 \vee v_3^2 \vee v_4^2}{2} = 0.087 > 0$. Therefore, the conditions of Theorem 13.2 hold. Based on Theorem 13.2, there is a unique ergodic stationary distribution $\pi(\cdot)$ of model (13.2). Thus, the disease I is persistent; see Fig. 13.2.

Example 13.2 Given the model (13.2), with parameters values of $\eta = 0.0005$; $\xi = 0.6$; $\beta = 0.01$; $\sigma = 0.12$; $\alpha = 0.3$; $\gamma = 0.02$, $\tau = 1.4$ and white noises of $v_1 = 0.02$, $v_2 = 0.02$, $v_3 = 0.01$, $v_4 = 0.2$. We obtain $\mathcal{R}_0^s = \frac{\eta\gamma\xi^2(1-\sigma)}{\hat{\eta}\hat{\alpha}\hat{\gamma}\hat{\beta}} = 0.38 < 1$ and $\eta - \frac{v_1^2 \vee v_2^2 \vee v_3^2 \vee v_4^2}{2} = -0.0195 < 0$. In this case, the conditions of Theorem 13.2 are not satisfied. From Fig. 13.3, we can clearly find that the disease goes to extinction. In Fig. 13.4, time-delay is increased to $\tau = 2.5$, with white noises $v_1 = 0.01$, $v_2 = 0.2$, $v_3 = 0.02$, and $v_4 = 0.03$; other parameter values are the same as in Fig. 13.3. Therefore, $\mathcal{R}_0^s < 1$ and $\eta - \frac{v_1^2 \vee v_2^2 \vee v_3^2 \vee v_4^2}{2} = -0.0445 < 0$. The conditions of Theorem 13.2 are not satisfied. Figure 13.5 shows a periodic outbreak due to the time-delay τ . However, the infection dies out with time as white noise increases.

Example 13.3 To further explain the impact of time-delay and white noises on system (13.2) we choose $\tau = 2.5$ and parameter values $\eta = 0.0005$; $\xi = 0.6$; $\beta = 0.01$; $\sigma = 0.12$; $\alpha = 0.3$; $\gamma = 0.02$ and white noises $v_1 = 0.2$, $v_2 = 0.2$, $v_3 = 0.1$, $v_4 = 0.3$, such that $\mathcal{R}_0^s = \frac{\eta\gamma\xi^2(1-\sigma)}{\hat{\eta}\hat{\alpha}\hat{\gamma}\hat{\beta}} = 0.38 < 1$, and $\eta - \frac{v_1^2 \vee v_2^2 \vee v_3^2 \vee v_4^2}{2} = -0.045 < 0$. Thus, the conditions of Theorem 13.2 are not satisfied. Figure 13.5 shows a periodic outbreak due to the time-delay τ ; when the white noise increased, the periodicity of the outbreak decreased. The infection dies out with time as white noise increases.

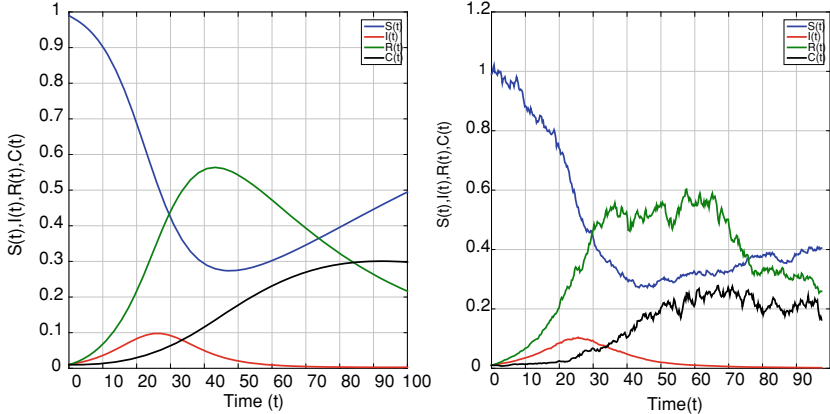


Fig. 13.3 Time domain behaviors of solutions of SDDEs model (13.2) (right) and the corresponding deterministic model (13.1) (left), when $\mathcal{R}_0^s = 0.38 < 1$, with $\eta = 0.0005$, $\xi = 0.6$, $\beta = 0.01$, $\sigma = 0.12$, $\alpha = 0.3$, $\gamma = 0.02$; $\tau = 1.4$ and white noises $v_1 = v_2 = 0.02$, $v_3 = 0.01$, and $v_4 = 0.02$. The infection dies out with probability one

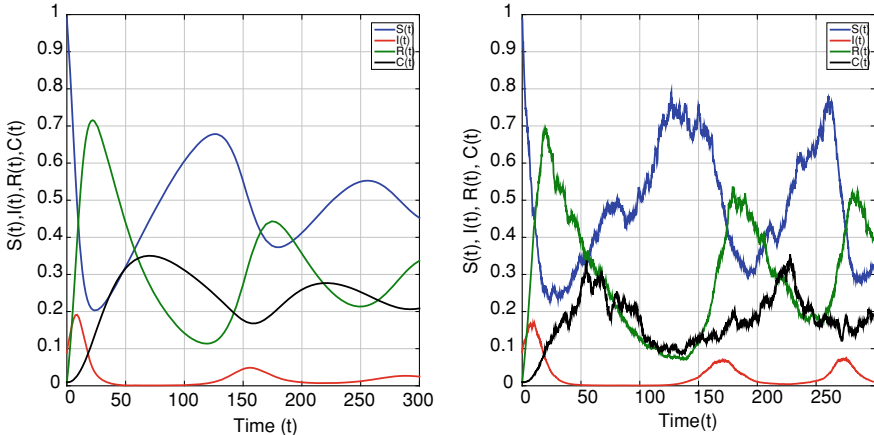


Fig. 13.4 Time domain behavior of SDDE model (13.2) (right) and the corresponding deterministic model (13.1) (left), when $\mathcal{R}_0^s = 0.38 < 1$, with $\eta = 0.0005$, $\xi = 0.6$, $\beta = 0.01$, $\sigma = 0.12$, $\alpha = 0.3$, $\gamma = 0.02$; $\tau = 2.5$ and white noises $v_1 = 0.02$, $v_2 = 0.2$, $v_3 = 0.02$, and $v_4 = 0.2$. The figure shows a periodic outbreak due to the time-delay τ

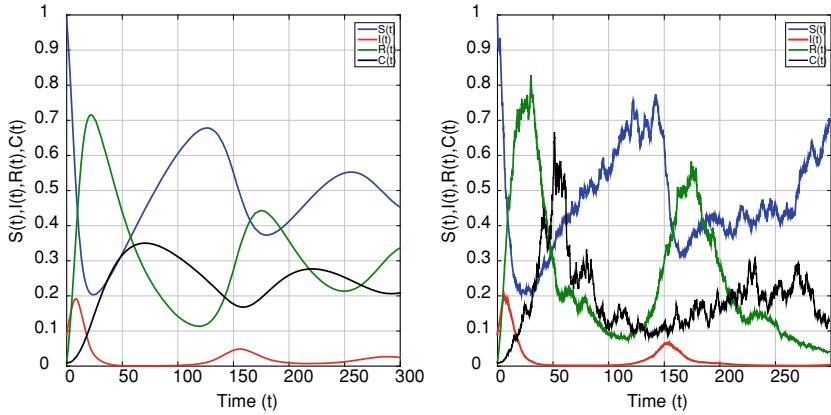


Fig. 13.5 Simulations of the stochastic model (13.2) (right) and the corresponding deterministic model (13.1) (left), when $\mathcal{R}_0^s = 0.38 < 1$, with $\eta = 0.0005$, $\xi = 0.6$, $\beta = 0.01$, $\sigma = 0.12$, $\alpha = 0.3$, $\gamma = 0.02$; $\tau = 2.5$ and white noises $v_1 = 0.2$, $v_2 = 0.2$, $v_3 = 0.1$, and $v_4 = 0.2$. The deterministic model shows a periodic outbreak due to the time-delay τ . The infection dies out with time when white noise is large

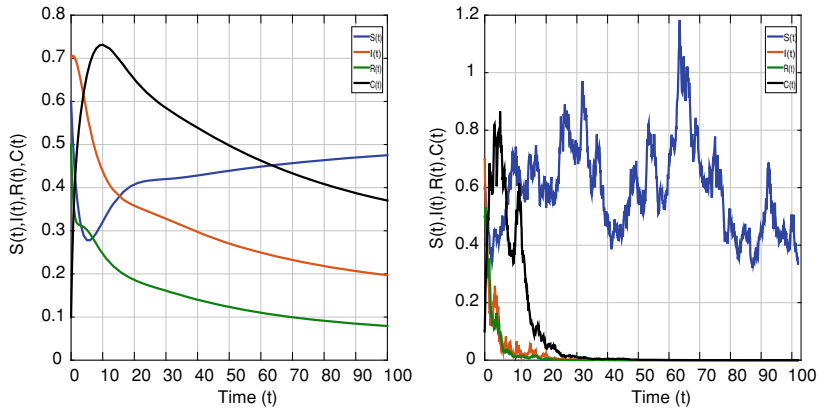


Fig. 13.6 Time domain behavior of SDDE model (13.2) (right) and the corresponding deterministic model (13.1) (left) where $\tau = 1$; when $\mathcal{R}_0 = 1.78 > 1$, the infection persists in the deterministic model; when $\mathcal{R}_0^s = 0.75 < 1$, the infection dies out in the stochastic model. With parameter values $\eta = 0.02$, $\xi = 0.5$, $\beta = 0.1$, $\sigma = 0.2$, $\alpha = 0.26$, $\gamma = 1$ and white noises $v_1 = 0.13$, $v_2 = 0.54$, $v_3 = 0.26$, and $v_4 = 0.75$

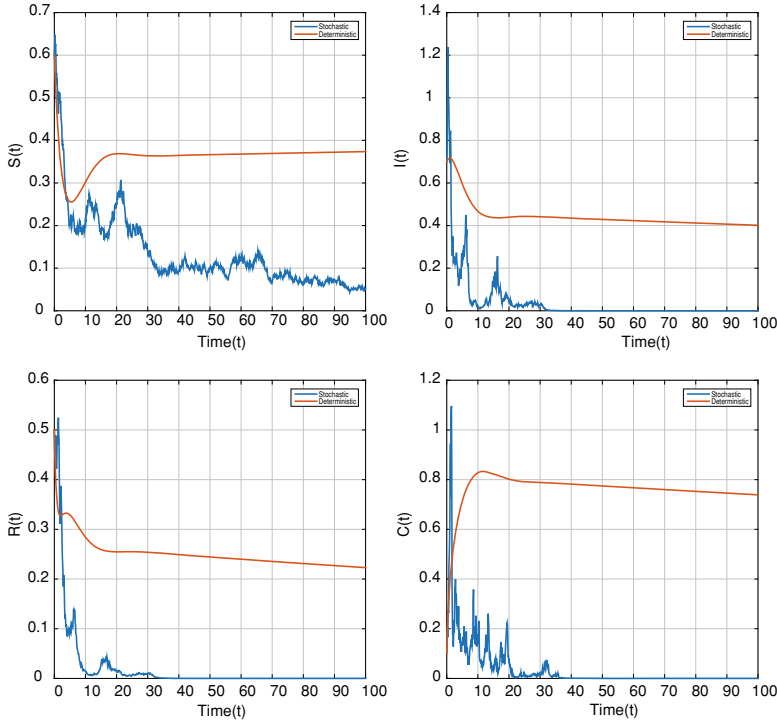


Fig. 13.7 Time response of solutions for model (13.2) (right) and the corresponding deterministic model (13.1) (left); when $\mathcal{R}_0 = 1.78 > 1$, the infection persists in the deterministic model; when $\mathcal{R}_0^s = 0.75 < 1$, the infection dies out in the stochastic model. With parameter values $\eta = 0.02$, $\xi = 0.5$, $\beta = 0.1$, $\sigma = 0.2$, $\alpha = 0.26$, $\gamma = 1$ and white noises $v_1 = 0.13$, $v_2 = 0.54$, $v_3 = 0.26$, and $v_4 = 0.75$

Example 13.4 To show the impact of random perturbation, with $\tau = 1$, we increase the white noise values $v_1 = 0.13$, $v_2 = 0.54$, $v_3 = 0.26$, and $v_4 = 0.75$ with parameter values $\eta = 0.02$; $\xi = 0.5$; $\beta = 0.1$; $\sigma = 0.2$; $\alpha = 0.26$; $\gamma = 1$. Thus, $\mathcal{R}_0^s = \frac{\eta\gamma\xi^2(1-\sigma)}{\hat{\eta}\hat{\alpha}\hat{\gamma}\hat{\beta}} = 0.75 < 1 < 1.78 = \frac{\xi}{\alpha+\eta} = \mathcal{R}_0$ and $\eta - \frac{v_1^2 \vee v_2^2 \vee v_3^2 \vee v_4^2}{2} = 0.0115 > 0$. Therefore, the conditions of Theorem 13.3 hold, and the disease dies out exponentially with probability one. However, the disease persists with the deterministic model; see Fig. 13.6.

Example 13.5 Consider the same parameter values of Example 6.6.4, but with time-delay $\tau = 0$. Thus, according to Theorem 13.3, the disease dies out exponentially with probability one; see Fig. 13.7. Therefore, the smaller values of white noise ensure the existence of unique stationary distribution, which gives the persistence of the disease, while larger values of white noise can lead to disease extinction.

Remark 13.1 Given the deterministic SIRC model (13.1), if the basic reproduction number $\mathcal{R}_0 = \frac{\xi}{\alpha + \eta} < 1$, then the disease-free equilibrium point is globally asymptotically stable. Whereas if $\mathcal{R}_0 > 1$, the unique endemic equilibrium point is globally asymptotically stable. Repeated outbreaks of the infection can occur due to the time-delay in the transmission terms. In our stochastic SIRC model (13.2), if $\mathcal{R}_0^s = \frac{\eta\gamma\xi^2(1-\sigma)}{\hat{\eta}\hat{\alpha}\hat{\gamma}\hat{\beta}} < 1 < \mathcal{R}_0$ and $\eta > \frac{\nu_1^2 \vee \nu_2^2 \vee \nu_3^2 \vee \nu_4^2}{2}$, the stochastic model (13.2) has disease extinction with probability one, and for $\mathcal{R}_0^s > 1$, the stochastic model (13.2) has a unique ergodic stationary distribution. See Figs. 13.6 and 13.7.

13.7 Concluding Remarks

In this chapter, we have provided a stochastic SIRC epidemic model with time-delay for SARS-CoV-2. The stochastic components, due to environmental variability, are incorporated in the model as Gaussian white noise. We established some sufficient conditions for persistence and extinction in the mean of the disease. The model has a unique stationary distribution that is ergodic if the intensity of white noise is small. Introduction of noise in the deterministic SIRC model modifies the basic reproductive number \mathcal{R}_0 , giving rise to a new threshold quantity \mathcal{R}_0^s . It has been proved that the disease dies out if $\mathcal{R}_0^s < 1 < \mathcal{R}_0$. On the other hand, if $\mathcal{R}_0^s > 1$ and $\mathcal{R}_0 > 1$, the disease persists with both models but with different behavior. In other words, extinction of the infection possibly occurs when $\mathcal{R}_0^s < 1 < \mathcal{R}_0$, along with the intensity of white noise being large. This would not happen in the deterministic models. The potential of using stochastic SIRC model for COVID-19 is to consider the environmental fluctuation that affects the spread of the virus. The parameters of the model are stochastically perturbed with a normal distribution to handle the uncertainty in the estimates of COVID-19 prevalence and to simulate the difficulty in detecting patients, different confinement measures taken by different countries, as well as changes in the virus characteristics. Periodicity of the outbreaks is possible due to the presence of time-delay (memory) in the transmission terms.

The author believes that the stochastic SIRC model is an attempt to understand epidemiological characteristics of COVID-19. The model provides new insights into epidemiological situations when environmental noise (perturbations) and cross-immunity are considered in the COVID-19 epidemic models. The combination of white noise and time-delay, in the epidemic model, has a considerable impact on the persistence and extinction of the infection and enriches the dynamics of the model. This work can be extended to include control variables for a vaccination, treatment, and/or quarantine actions. A more sophisticated model is also required to investigate the dynamics of COVID-19 with the immune system at the cell level [35].

References

1. Hui, D.: The continuing 2019-ncov epidemic threat of novel coronavirus to global health - the latest 2019 novel coronavirus outbreak in Wuhan, China. *Int. J. Infect. Dis.* **91**, 264–266 (2020)
2. Grifoni, A., Weiskopf, D., et al.: Targets of T cell responses to SARS-CoV-2 coronavirus in humans with COVID-19 disease and unexposed individuals. *Cell* **181**, 1–13 (2020)
3. Grifoni, A., Weiskopf, D., et al.: Advice for public (2020). <https://www.who.int/emergencies/diseases/novel-coronavirus-2019/advice-for-public>
4. Grifoni, A., Weiskopf, D., et al.: Report of the WHO-China joint mission on coronavirus disease 2019 (COVID-19). World Health Organization (2020)
5. Wu, G.C., Baleanu, D.: Discrete fractional logistic map and its chaos. *Nonlinear Dyn.* **75**, 283–287 (2014)
6. Casagrandi, R., Bolzoni, L., Levin, S., Andreasen, V.: The SIRC model and influenza A. *Math. Biosci.* **200**, 152–169 (2006)
7. Rihan, F.A., Baleanu, D., Lakshmanan, S., Rakkiyappan, R.: On fractional SIRC model with salmonella bacterial infection. *Abst. Appl. Anal.* **2014** (2014), 9 p.
8. Khan, M.A., Atangana, A.: Modeling the dynamics of novel coronavirus (2019-nCov) with fractional derivative. *Alex. Eng. J.* (2020), I11 p.
9. Hethcote, H., Zhien, M., Shengbing, L.: Effects of quarantine in six endemic models for infectious diseases. *Math. Biosci.* **180**, 141–160 (2002)
10. Lahrouz, A., Settati, A.: Necessary and sufficient condition for extinction and persistence of SIRS system with random perturbation. *Appl. Math. Comput.* **233**, 10–19 (2014)
11. Liu, Q., Jiang, D., Hayat, T., Alsaedi, A.: Dynamics of a stochastic tuberculosis model with antibiotic resistance. *Chaos Solitons Fractals* **109**, 223–230 (2018)
12. Martin, A., Ruan, S.: Predator-prey models with delay and prey harvesting. *J. Math. Biol.* **43**(3), 247–267 (2001)
13. Wei, F., Xue, R.: Stability and extinction of SEIR epidemic models with generalized nonlinear incidence. *Math. Comput. Simul.* **170**, 1–15 (2020)
14. Zhao, X., Zeng, Z.: Stationary distribution and extinction of a stochastic ratio-dependent predator-prey system with stage structure for the predator. *Physica A* (2019)
15. Bahar, A., Mao, X.: Stochastic delay Lotka-Volterra model. *J. Math. Anal. Appl.* **292**, 364–380 (2004)
16. Mao, X., Sabanis, S., Renshaw, E.: Asymptotic behaviour of the stochastic Lotka-Volterra model. *J. Math. Anal. Appl.* **287**, 141–156 (2003)
17. Mao, X., Yuan, C., Zou, J.: Stochastic differential delay equations of population dynamics. *J. Math. Anal. Appl.* **304**, 296–320 (2005)
18. Mao, X., Marion, G., Renshaw, E.: Environmental Brownian noise suppresses explosions in population dynamics. *Stoch. Process. Their Appl.* **97**(1), 95–110 (2002)
19. Yuan, Y., Allen, L.J.S.: Stochastic models for virus and immune system dynamics. *Math. Biosci.* **234**, 84–94 (2011)
20. Ji, C.: The stationary distribution of hepatitis B virus with stochastic perturbation. *Appl. Math. Lett.* **100** (2020)
21. Ji, C., Jiang, D.: Threshold behaviour of a stochastic SIR model. *Appl. Math. Model.* **38**(21–22), 5067–5079 (2014)
22. Lakshmi, P., Suresh, M.: Factors influencing the epidemiological characteristics of pandemic COVID-19: a TISM approach. *Int. J. Healthc. Manag.* 1–10 (2020)
23. Azman, A., Rudolph, K., Cummings, D., Lessler, J.: The incubation period of Cholera: a systematic review. *J. Infect.* **66**(5), 432–438 (2013)
24. Lessler, J., Reich, N., Brookmeyer, R., Perl, T., Nelson, K., Cummings, D.: Incubation periods of acute respiratory viral infections: a systematic review. *Lancet Infect. Dis.* **9**(5), 291–300 (2009)
25. WHO.: Are the Ebola outbreaks in Nigeria and Senegal over (2014). <http://www.who.int/mediacentre/news/ebola/14-october-2014/en>

26. Kahn, J., Walker, B.: Acute human immunodeficiency virus type 1 infection. *N. Engl. J. Med.* **339**(1), 33–39 (1998)
27. Rihan, F.A., Alsakaji, H.J., Rajivganthi, C.: Stochastic SIRC epidemic model with time-delay for COVID-19. *Adv. Differ. Equ.* **502**, 1–20 (2020)
28. Al-Jasser, F., Nouh, R., Youssef, R.: Epidemiology and predictors of survival of MERS-CoV infections in Riyadh region, 2014–2015. *J. Infect. Public Health* **12**(2), 171–177 (2019)
29. Seto, W.H., Tsang, D., Yung, R.W., Ching, T.Y., Ng, T.K., Ho, M., Ho, L.M., Peiris, J.S.M., Advisors of Expert SARS group of Hospital Authority, et al.: Effectiveness of precautions against droplets and contact in prevention of nosocomial transmission of severe acute respiratory syndrome (SARS). *The Lancet* **361**(9368), 1519–1520 (2003)
30. Jodar, L., Villanueva, R.J., Arenas, A.J., Gonzalez, G.C.: Nonstandard numerical methods for a mathematical model for influenza disease. *Math. Comput. Simul.* **79**, 622–633 (2008)
31. Rihan, F.A., Alsakaji, H.J.: Persistence and extinction for stochastic delay differential model of prey predator system with hunting cooperation in predators. *Adv. Differ. Equ.* **124**(1), 1–22 (2020)
32. Buckwar, E.: Introduction to the numerical analysis of stochastic delay differential equations. *J. Comput. Appl. Math.* **125**(1–2), 297–307 (2000)
33. Buckwar, E.: Stochastic Differential Equations and Their Applications. Horwood, Chichester (1997)
34. Zhao, Y., Jiang, D.: The threshold of a stochastic SIS epidemic model with vaccination. *Appl. Math. Comput.* **243**, 718–727 (2014)
35. Zhao, Y., Jiang, D.: Dynamics and sensitivity analysis of fractional-order delay differential model for coronavirus infection. *Prog. Fract. Differ. Appl. (PFDA)* **7**, 43–61 (2021)

Chapter 14

Remarks and Current Challenges



The main focus of this book was to analyze the qualitative and quantitative features of *delay differential equations (DDEs)* (with integer- and fractional-order derivatives) and their applications in biological systems with memory. This book covers valuable topics related to DDEs, including its theory and numerical methods; stability; control; biological models; inverse problems; parameter estimations; sensitivity analysis with DDEs; deterministic and stochastic DDEs; numerical method based on extended one-step schemes for optimal control problem with time-lags; applications of DDEs in immunology, epidemiology, and ecology; DDEs of tumor-immune dynamics with chemo-immunotherapy and optimal control; Pontryagins maximum (or minimum) principle and incorporation of optimal control parameters into a delay differential model to describe the interactions of the disease response cells with external therapy; dynamical analysis of biological systems; dynamics of HIV, HCV, and COVID-19 using delay differential models; and local and global stability analysis and Hopf bifurcation.

Several remarks need to be noted:

- Physical and biological systems have a complex non-linear dynamic behavior. Studying the qualitative behavior of all stability and bifurcation properties is essential for ensuring safe application in the real world.
- Time-delays have been considered as an important factor that directly affects system performance; Hopf bifurcation also occurs when the delay passes through a sequence of critical values.
- Delay differential models of real-life phenomena have potentially more interesting dynamics than equations that lack memory effects: They are more qualitatively and quantitatively consistent with cell proliferation phenomena than comparable ODE models.
- Time-delays have been incorporated into biological systems to describe resource regeneration times, maturation periods, reaction times, feeding times, gestation periods, etc.

- Fractional-order derivatives are incorporated to represent long-run memory, while time-delays are considered to represent short-run memory in a model. The presence of fractional-order in the delayed differential model improves the stability of the solutions and enriches the dynamics of the model.
- Sensitivity analysis is an important tool for understanding a particular model, which is considered as an issue of stability with respect to structural perturbations of the model parameters.
- Optimal control results represent the efficiency of drug treatment in inhibiting viral production and preventing new infections.
- The obtained results provide insights to biologists to improve the properties of the models and experimental data.
- Stiff problems can occur in the field of applications of biomathematics; implicit or semi-implicit numerical methods are more suitable for this type of models than explicit methods. Non-linearity, sensitivity to small perturbations in the parameters (or noisy data), identifiability, and model selection are also challenges facing numerical modeling for biosciences.
- The presence of a fractional-order differential in a model can lead to a notable increase in the complexity of the observed behavior. It enriches the dynamics of the model and grants the model a greater degree of freedom and consistency with real interactions.
- A combination of time-delay and fractional-order derivatives enriches the dynamics and improves the stability of the solutions. In addition, fractional-order models are, at least, as stable as their integer-order counterparts.
- Environmental factors, such as humidity, precipitation, and temperature, have a significant impact on the spread of disease among humans, especially COVID-19.
- A combination of white noise and time-delay in an epidemic model has a considerable impact on the persistence and extinction of the infection and enriches the dynamics of the model.

This monograph significantly contributes to the theory and applications of DDEs in biosciences, dynamical systems, and medicine. However, from a mathematical perspective, several challenging issues that remain deserve further analyses, both analytically and numerically. Thus, there are many future directions for this work:

1. Study DDEs with a variety of delay differential models with variable and state-dependent delays and then estimate numerically the unknown lag parameters.
2. Physical and biological phenomena are non-linear in nature, and therefore, are better described by non-linear delay differential models.
3. More sophisticated DDEs of disease dynamics are required to consider control variables in order to determine the best strategy of treatment, control, and elimination.
4. Sensitivity analysis with respect to the parameters of the model is desirable. It is useful to investigate how a small shift (change) in the input parameters would change the stability of the tumor-free equilibrium and detect the most significant parameter that has a major impact on the model dynamics.

5. Stiff problems can occur in biomathematics, immune response models, etc., due to the existence of greatly differing time constants. Reasonable candidate methods for treating stiff DDEs, such as implicit or singly implicit Runge-Kutta methods, are necessary to treat the stiffness, particularly in a large system of equations.
6. Further analyses of interdisciplinary applications from the fields of physics, mechanics, economics, and control theory are also required.
7. More sophisticated DDEs models, with multi-scale effects, different types of stochastic processes, and spatial representation need to be studied and investigated.

To conclude, we expect that mathematical modeling with DDEs is entering the phase of genuine mutual inspiration of biological systems with memory, immunology, physiology, epidemiology, ecology, neural networks, and the dynamics of viral infections. Exciting research involving DDEs with integer and fractional-order derivatives, and stochastic DDEs with spatial state variables will be observed in future work.

Appendix A

Fifth-Order Dormand and Prince RK Method

Butcher tableau for explicit fifth-order Dormand and Prince RK method (that has seven stages) [1] is as follows:

$$\begin{array}{c|ccccc} \mathbf{c} & 0 & 0 & 0 & 0 & 0 \\ \hline \mathbf{A} & \frac{1}{5} & \frac{1}{5} & 0 & 0 & 0 \\ & \frac{3}{5} & \frac{3}{5} & \frac{9}{40} & 0 & 0 \\ & \frac{10}{4} & \frac{40}{44} & \frac{-56}{40} & \frac{32}{9} & 0 \\ \hline \mathbf{b}^T & \frac{8}{9} & \frac{45}{19372} & \frac{15}{25360} & \frac{64448}{6561} & \frac{-212}{46732} \\ & \frac{9}{9} & \frac{6561}{9017} & \frac{2187}{-355} & \frac{6561}{46732} & \frac{729}{49} \\ & 1 & \frac{3168}{35} & \frac{33}{500} & \frac{5247}{125} & \frac{18656}{-2187} \\ & 1 & \frac{384}{384} & 0 & \frac{1113}{1113} & \frac{192}{192} \\ \hline & \frac{5179}{57600} & 0 & \frac{7571}{16695} & \frac{393}{640} & \frac{-92097}{339200} \\ & \frac{35}{384} & 0 & \frac{1113}{1113} & \frac{192}{192} & \frac{187}{6784} \end{array} \quad (A.1)$$

In order to obtain fifth-order Hermite approximation,¹ to get, e.g., $\tilde{y}_{n+1/2}$, we require extra RK stages to be added to (A.1). The following formulae are by Shampine [2]:

$$\begin{array}{c|cccccc} 1 & -33728713 & 2 & -30167461 & 7739027 & -194162737 & 0 & -26949 \\ \hline 2 & \frac{104693760}{7157} & 0 & \frac{21674880}{70925} & \frac{17448960}{10825} & \frac{-123305984}{-220887} & \frac{80069}{4016128} & \frac{-363520}{3530688} \\ & \frac{75776}{75776} & & \frac{164724}{113664} & & \frac{4016128}{4016128} & \frac{5254}{5254} & \frac{-5}{74} \end{array}$$

The Hermite interpolation process (as shown in Sect. 2.4.3) can be converted into the form of continuous extension with polynomials:

¹ The best choice of fixed Hermite support points is $\{0, \frac{1}{2}, 1\}$; see [2].

$$\begin{aligned}
b_1(\theta) &= \frac{29}{16}\theta^5 - \frac{81685}{14208}\theta^4 + \frac{24433}{3552}\theta^3 - \frac{6839}{1776}\theta^2 + \theta, \\
b_2(\theta) &= 0 \\
b_3(\theta) &= -\frac{4000}{371}\theta^5 + \frac{1245700}{41181}\theta^4 - \frac{398800}{13727}\theta^3 + \frac{413200}{41181}\theta^2, \\
b_4(\theta) &= -\frac{125}{8}\theta^5 + \frac{83775}{2368}\theta^4 - \frac{44725}{1776}\theta^3 + \frac{225}{37}\theta^2, \\
b_5(\theta) &= \frac{6561}{848}\theta^5 - \frac{4428675}{251008}\theta^4 + \frac{798255}{62752}\theta^3 - \frac{98415}{31376}\theta^2, \\
b_6(\theta) &= -\frac{22}{7}\theta^5 + \frac{527571}{73556}\theta^4 - \frac{285659}{55167}\theta^3 + \frac{23529}{18389}\theta^2, \\
b_7(\theta) &= 4\theta^5 - \frac{21872}{2627}\theta^4 + \frac{14847}{2627}\theta^3 - \frac{3483}{2627}\theta^2, \\
b_8(\theta) &= -\frac{40}{37}\theta^4 + \frac{80}{37}\theta^3 - \frac{40}{37}\theta^2, \\
b_9(\theta) &= 16\theta^5 - 40\theta^4 + 32\theta^3 - 8\theta^2.
\end{aligned}$$

Appendix B

Adams-Bashforth-Moulton Method for Fractional-Order Delay Differential Equations

The Adams-Bashforth-Moulton method [3] has been proven to be an efficient and powerful technique for finding the solution of fractional-order ODEs. In addition, the authors of [4] discussed the modified Adams-Bashforth-Moulton predictor-corrector scheme [5] to solve fractional-order DDEs. Herein, we have again highlighted the main steps of this algorithm to solve the following fractional-order DDEs of the form:

$$\begin{aligned} D^\alpha y(t) &= f(t, y(t), y(t - \tau)), \quad t \in J = [0, T], \\ y(t) &= \psi(t), \quad t \in [-\tau, 0], \quad 0 < \alpha \leq 1 \end{aligned} \quad (\text{B.1})$$

where $y(t) = [y_1(t), y_2(t), \dots, y_n(t)]^T$, $f : J \times \mathbb{R}^n \times \mathbb{R}^n \rightarrow \mathbb{R}^n$ and for $M > 0$ satisfies the Lipschitz condition:

$$\|f(t, y(t), y(t - \tau)) - f(t, z(t), z(t - \tau))\| \leq M[\|y(t) - z(t)\| + \|y(t - \tau) - z(t - \tau)\|]. \quad (\text{B.2})$$

It is known that the satisfaction of condition (B.2) with $\bar{M} = \frac{2MT^\alpha}{\Gamma(\alpha + 1)} < 1$ ensures the uniqueness of the solution of problem (B.1).

We know that the delay IVP (B.1) for $0 < \alpha \leq 1$ is equivalent to the Volterra-integral equation

$$y(t) = \psi(0) + \frac{1}{\Gamma(\alpha)} \int_0^t (t-s)^{\alpha-1} f(s, y(s), y(s-\tau)) ds. \quad (\text{B.3})$$

Given mesh points $\mathcal{T} = \{t_{-m}, t_{-m+1}, \dots, t_{-1}, t_0, t_1, \dots, t_N\}$, such that $t_0 = 0$ and $t_N = T$ with stepsize $h = \tau/m$. Let $y_h(t_j) = \psi(t_j)$, $j = -m, -m+1, \dots, -1, 0$ and $y_h(t_j - \tau) = y_h(t_j h - mh)$, $j = 0, 1, \dots, N$. Suppose $y_h(t_j) \approx y(t_j)$ (for $j = -m, -m+1, \dots, -1, 0, 1, \dots, n$) are already calculated; then, the numerical scheme of (B.3) is

$$y_h(t_{n+1}) = \psi(0) + \frac{1}{\Gamma(\alpha)} \int_0^{t_{n+1}} (t_{n+1} - s)^{\alpha-1} f(s, y(s), y(s-\tau)) ds. \quad (\text{B.4})$$

Using the product trapezoidal quadrature formula to evaluate the right-hand side integral of (B.4) in which the nodes t_j , ($j = 0, 1, \dots, n+1$) are considered with respect to the weight function $(t_{n+1} - s)^{\alpha-1}$. The integral on the right-hand side of (B.4) can be written by the use of the standard technique of quadrature theory

$$\int_0^{t_{n+1}} (t_{n+1} - s)^{\alpha-1} f(s, y(s), y(s-\tau)) ds \approx \frac{h^\alpha}{\alpha(\alpha+1)} \sum_{j=0}^{n+1} r_{j,n+1} f(t_j, y_h(t_j), y_h(t_j - \tau)),$$

where $r_{j,n+1}$ are given by

$$r_{j,n+1} = \begin{cases} n^{\alpha+1} - (n-\alpha)(n+1)\alpha, & \text{if } j = 0, \\ (n-j+2)^{\alpha+1} - (n-\alpha)(n+1)^\alpha - 2(n-j+1)^{\alpha+1}, & \text{if } 1 \leq j \leq n; \\ 1, & \text{if } j = n+1. \end{cases} \quad (\text{B.5})$$

Therefore, the numerical scheme of the fractional-order DDE (B.1) can be formulated as

$$\begin{aligned} y_h(t_{n+1}) &= \psi(0) + \frac{h^\alpha}{\Gamma(\alpha+2)} f(t_{n+1}, y_h(t_{n+1}), y_h(t_{n+1}-\tau)) + \frac{h^\alpha}{\Gamma(\alpha+2)} \sum_{j=0}^n r_{j,n+1} f(t_j, y_h(t_j), y_h(t_j - \tau)) \\ &= \psi(0) + \frac{h^\alpha}{\Gamma(\alpha+2)} f(t_{n+1}, y_h(t_{n+1}), y_h(t_{n+1-k})) + \frac{h^\alpha}{\Gamma(\alpha+2)} \sum_{j=0}^n r_{j,n+1} f(t_j, y_h(t_j), y_h(t_{j-k})). \end{aligned} \quad (\text{B.6})$$

Then, the term $y_h(t_{n+1})$ in the right-hand side of (B.6) is replaced by an approximation $y_h^P(t_{n+1})$ (called predictor), which is evaluated via the product rectangle rule in Eq. (B.4) to evaluate the predictor term

$$y_h^P(t_{n+1}) = \psi(0) + \frac{1}{\Gamma(\alpha)} \sum_{j=0}^n a_{j,n+1} f(t_j, y_h(t_j), y_h(t_j - \tau)) = \psi(0) + \frac{1}{\Gamma(\alpha)} \sum_{j=0}^n a_{j,n+1} f(t_j, y_h(t_j), y_h(t_{j-k})),$$

where $a_{j,n+1}$ is given by

$$a_{j,n+1} = \frac{h^\alpha}{\alpha} ((n+1-j)^\alpha - (n-j)^\alpha). \quad (\text{B.7})$$

Appendix C

Matlab Program for Stochastic Delay Differential Equations Using Milstein Scheme

Here, a sample of Matlab program for solving SDDEs (13.2) is provided, Fig. 13.2.

%This program to solve Stochastic SIRC Epidemic model with time-delay using
%Milstein Scheme

%The stochastic DDEs model takes the form

```
%dS(t)=[eta*(1-S(t))-xi*S(t)*I(t-tau)+beta*C(t)]dt+sig1*dW1,  
%dI(t)=[xi*S(t)I(t-tau)+sig*xi*C(t)*I(t)-(eta+alpha)I(t)]+sig2*dW2,  
%dR(t)=[(1-sig)*xi*C(t)*I(t)+alpha*I(t)-(eta+gamma)R(t)]dt+sig3*dW3,  
%dC(t)=[gamma*R(t)-xi*C(t)*I(t)-(eta+beta)C(t)]dt+sig4*dW4.
```

```
function SIRC  
clear all;  
clc;  
clear all;  
clc;  
tau = 1;  
M = 10;  
st = 0;  
et = 300;  
h = tau/M;  
t = st:h:et;  
M = tau/h;  
N_0 = round(st/h);  
N_1 = round(et/h);  
N = N_0 + N_1;  
  
global eta xi beta sig alpha gamma  
eta=0.09; xi=1.3; beta=0.05; sig=0.9; alpha=0.36; gamma=0.1;  
sig1=0.1; sig2=.09; sig3=0.09; sig4=0.07;
```

```
for i=1:N + 1  
if i<=M + 1  
x(i)=0.99; y(i)=0.09; z(i)=0.01; r(i)=0.01;  
else  
bt=randn(4, N_1)*sqrt(h);
```

```

x(i)=x(i-1)+h*(eta*(1-x(i-1))-xi*y(i-M-1)*x(i-1)+beta*r(i-1))+...
    sig1*x(i-1)*randn*sqrt(h)+sig1^2*0.5*x(i-1)*(randn^2-1)*h;
y(i)=y(i-1)+h*(xi*y(i-M-1)*x(i-1)+sig*x*i*r(i-1)*y(i-1)-(eta+alpha)*y(i-1))+...
    sig2*y(i-1)*randn*sqrt(h)+sig2^2*0.5*y(i-1)*(randn^2-1)*h;
z(i)=z(i-1)+h*((1-sig)*xi*y(i-1)*r(i-1)+alpha*y(i-1)-(eta+gamma)*z(i-1))+...
    sig3*z(i-1)*randn*sqrt(h)+sig2^2*0.5*z(i-1)*(randn^2-1)*h;
r(i)=r(i-1)+h*(gamma*z(i-1)-xi*r(i-1)*y(i-1)-(eta+beta)*r(i-1))+...
    sig4*r(i-1)*randn*sqrt(h)+sig4^2*0.5*x(i-1)*(randn^2-1)*h;
end
end

figure(1)
plot(t-tau,x,t-tau,y,t-tau,z,t-tau,r,'LineWidth',2)
xlabel('Time (t)', 'FontSize',14)
ylabel('S(t),I(t),R(t),C(t)', 'FontSize',14)
xlim([0,et]);
legend({'S(t)', 'I(t)', 'R(t)', 'C(t)'}, 'FontSize',14)
grid on;

end

```

References

1. Dormand, J.R., Prince, P.J.: Family of embedded Runge-Kutta formulae. *J. Coump. Appl. Math.* **6**, 19–26 (1980)
2. Dormand, J.R., Prince, P.J.: Some practical Runge-Kutta formulas. *Math. Comput.* **46**, 135–150 (1986)
3. Diethelm, K., Ford, N.J., Freed, A.D.: A predictor-corrector approach for the numerical solution of fractional differential equations. *Nonlinear Dyn.* **29**, 3–22 (2002)
4. Bai, J., Wen, G., Rahmani, A., Yu, Y.: Distributed formation control of fractional-order multi-agent systems with absolute damping and communication delay. *Int. J. Syst. Sci.* **46**(13), 2380–92 (2015)
5. Lambert, J.D.: Numerical Methods for Ordinary Differential Systems. Wiley, Chichester (1991)